

Charles University

Faculty of Mathematics and Physics

HABILITATION THESIS



Petr Dohnal

State Selectivity in Recombination of Molecular Ions with Electrons

Department of Surface and Plasma Science

Prague 2022

*“If you can meet with Triumph and Disaster
And treat those two impostors just the same”*

Kipling

Acknowledgements

I would like to thank to all the people without whom I would not be able to finish this thesis. I had privilege to collaborate with Juraj Glosík, Dieter Gerlich, Rainer Johnsen and many, many other excellent scientists.

I am grateful to my family, my beautiful and clever wife and especially to my small daughter who was always there to put a smile on my face

I would like to thank Czech Republic for financial support through Ministry of Education, Youth and Sports, GACR and to the COST association for supporting my stays at foreign research institutions.

Děkuji svým rodičům.

Contents

Introduction	6
Theoretical background	7
Recombination of positive ions with electrons.....	7
Radiative and dielectronic recombination.....	7
Dissociative recombination	8
Recombination assisted by third particle	10
Absorption spectroscopy	13
Basic concepts	13
Spectral line broadening.....	14
Cavity Ring-Down Spectroscopy	16
Langmuir probe diagnostics	18
Microwave diagnostics.....	20
Experimental techniques	22
Cryo-FALP II.....	22
Stationary afterglow with Cavity Ring-Down spectrometer	23
Data analysis	26
Results.....	30
Recombination of H_3^+ with electrons – third-body assisted recombination and the effect of nuclear spin.....	30
Recombination of H_2D^+ and HD_2^+ with electrons	38
Recombination of D_3^+ with electrons.....	42
Recombination of N_2H^+ with electrons.....	46
Recombination of N_2^+ ions with electrons – dependence on vibrational excitation	52
Selected experiments in 22-pole radiofrequency ion trap.....	57
Conclusions	61

References	62
List of publications	75
Publications in journals with impact factor	75
Publications in proceedings of scientific conferences listed in WOS.....	81
Other publications	82
List of attached publications	83
Attached publications	86
Nuclear Spin Effect on Recombination of H_3^+ Ions with Electrons at 77 K.....	87
Binary and ternary recombination of D_3^+ ions at 80–130 K: Application of laser absorption spectroscopy	92
Binary and ternary recombination of para- H_3^+ and ortho- H_3^+ with electrons: State selective study at 77–200 K.....	101
Ternary Recombination of H_3^+ and D_3^+ with Electrons in He- H_2 (D_2) Plasmas at Temperatures from 50 to 300 K.....	116
Binary Recombination of H_3^+ and D_3^+ Ions with Electrons in Plasma at 50–230 K	126
Collisional-radiative recombination of Ar^+ ions with electrons in ambient helium at temperatures from 50 K to 100 K.....	134
H_2 -assisted ternary recombination of H_3^+ with electrons at 300 K.....	144
Flowing-afterglow study of electron-ion recombination of para- H_3^+ and ortho- H_3^+ ions at temperatures from 60 K to 300 K	151
Recombination of H_3^+ ions with electrons in He/ H_2 ambient gas at temperatures from 240 K to 340 K	162
Monitoring the removal of excited particles in He/Ar/ H_2 low temperature afterglow plasma at 80–300 K.....	173
Binary and ternary recombination of H_2D^+ and HD_2^+ ions with electrons at 80 K	181

Stationary afterglow measurements of the temperature dependence of the electron–ion recombination rate coefficients of H_2D^+ and HD_2^+ in He/Ar/ H_2 / D_2 gas mixtures at $T = 80\text{--}145$ K.....	187
Overtone spectroscopy of N_2H^+ molecular ions—application of cavity ring-down spectroscopy	200
Stationary afterglow apparatus with CRDS for study of processes in plasmas from 300 K down to 30 K.....	211
Towards state selective recombination of H_3^+ under astrophysically relevant conditions.....	223
Dissociative recombination of N_2H^+ ions with electrons in the temperature range of 80–350 K	239
Cavity ring-down spectroscopy study of neon assisted recombination of H_3^+ ions with electrons.....	251
Recombination of vibrationally cold N_2^+ ions with electrons	259

Introduction

This thesis summarizes many years of experimental studies focused on recombination of atomic and molecular ions with electrons. Gradually, my scientific interest shifted from binary and third-body assisted recombination processes to question of different reactivity of different quantum states of molecular ions.

The presented experiments were performed using various modifications of stationary afterglow (SA-CRDS, Cryo-SA-CRDS) and flowing afterglow with Langmuir probe (Cryo-FALP II) techniques.

The thesis consists of several chapters. The first chapter (Theoretical background) introduces various recombination processes and covers basics of used absorption spectroscopy, Langmuir probe and microwave diagnostics. The second chapter (Experimental techniques) gives overview of instrumentation used for electron – ion recombination studies and the third chapter (Results) covers the most important results of my studies. The last chapter summarizes the thesis and is followed by a list of publications with me as author or co-author. Attached to this thesis are some of my publications that provide detailed information on the topics discussed in the text.

I have also collaborated on several experiments focused on the study of reactions of ions with molecules in 22-pole radiofrequency ion trap apparatus. As I was not, with some exceptions, main investigator in these studies, I decided to include into this thesis only two examples of how the trapping technique can be effectively utilized to distinguish between two isomers of the same mass or to probe internal excitation of trapped ions.

Theoretical background

Recombination of positive ions with electrons

Mutual neutralization of electron – positive ion system in cold plasmas can be governed by several mechanisms. These will be covered in the following sections. An important distinguishing factor is if the collision involves only electron and the cation – binary processes (radiative and dielectronic recombination, dissociative recombination) or if a collision with another particle is necessary to finish the recombination (third-body assisted recombination). The former processes will be important in low density environments such as the interstellar gas clouds whereas the latter will dominate at high ambient gas or electron number densities, especially at very low temperatures.

Radiative and dielectronic recombination

In low density environments the atomic ions A^+ can recombine with electrons e^- by radiative recombination. In this case, the stabilization of the neutral excited complex formed in recombination proceeds via emission of radiation:



here h is the Planck constant and ν is the frequency of emitted radiation.

Another possible process at such conditions is dielectronic recombination [Schippers *et al.*, 2010], where the excess energy is taken away by excitation of one of the bounded electrons of the ion to another bounded orbit. This is then followed a photon emission. Due to the discrete electronic energies this is a strongly energy dependent resonant process. The typical recombination rate coefficients are on the order of $10^{-9} \text{ cm}^3 \text{ s}^{-1}$ or less at 300 K.

Dissociative recombination

For molecular ions, the electron – positive ion system formed during recombination can get rid of the excess energy by dissociating in to neutral fragments. Dissociative recombination, first proposed by Bates [*Bates et al.*, 1947] as an effective loss process for electrons in Earth’s ionosphere, can proceed via different mechanisms and may involve many highly excited Rydberg states of the neutral molecule.

Motivated by contemporary afterglow studies on plasma deionization [*Biondi et al.*, 1949a; *Biondi et al.*, 1949b], Bates has shown in his seminal paper [*Bates*, 1950] that recombination of molecular ions with electrons can proceed very fast with rate coefficients on the order of $10^{-7} \text{ cm}^3\text{s}^{-1}$. According to Bates [*Bates*, 1950], the electron colliding with the ion is captured into a neutral dissociating state (the state is doubly excited with respect to the original ion – electron system) and this is followed by dissociation of the molecule in to neutral fragments. The described process is now known as direct dissociative recombination and its schematic representation is shown in Figure 1.

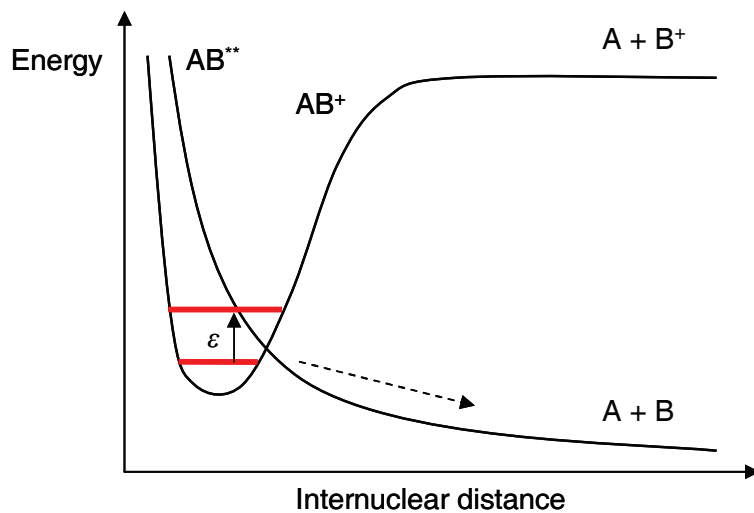


Figure 1. Adapted from refs. [*Larsson et al.*, 2008; *Dohnal*, 2013]. The potential energy curve of the ion, denoted AB^+ , is crossed by the dissociative resonant state AB^{**} . In the direct process of dissociative recombination, the capture of the incoming electron (with kinetic energy ϵ) in the resonant state is followed by dissociation on the potential energy curve.

In the direct dissociative recombination, the favourable curve crossing between the ionic and the resonant state is a necessary prerequisite for fast recombination process. Later, Bardsley [Bardsley, 1968] proposed a modification of Bates' mechanism, for cases in which the incoming electron cannot be directly captured into the resonant dissociating state. Instead, it is captured into a vibrational state of one of the infinite series of Rydberg states of the neutral converging to the ionic state. After that, it couples to the resonant dissociating state and finally the dissociation of the molecule occurs. This indirect process of dissociative recombination is depicted in Figure 2.

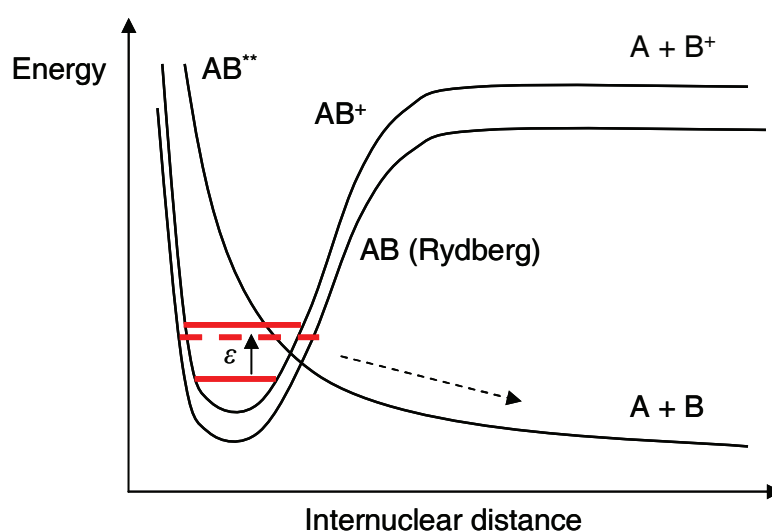


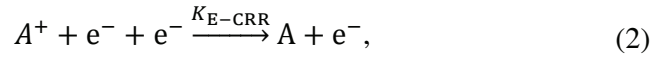
Figure 2. Adapted from refs. [Larsson *et al.*, 2008; Dohnal, 2013]. Indirect dissociative recombination process.

Other mechanisms were proposed such as recombination involving core-excited resonances [Guberman, 1995] or direct predissociation [Guberman, 1994]. For further details I refer the reader to the excellent book on dissociative recombination by Larsson and Orel [Larsson *et al.*, 2008].

Recombination assisted by third particle

At conditions typical for low temperature afterglow recombination studies (electron temperature close to 300 K, electron number density below 10^{10} cm^{-3} with buffer gas number densities on the order of 10^{17} cm^{-3} or below) the influence of third bodies on the overall measured recombination rate coefficient can be usually neglected. At enhanced gas or electron number densities or at very low temperature, the third body assisted processes can substantially contribute to plasma deionization.

In electron assisted collisional recombination (E-CRR) the excess energy of the formed electron – ion metastable neutral complex is taken away in collision(s) with electron(s):



Where K_{E-CRR} is the ternary recombination rate coefficient of E-CRR. According to semi-classical theoretical studies [*Bates et al.*, 1962; *Mansbach et al.*, 1969; *Stevelfelt et al.*, 1975], multiple collisions are necessary for stabilisation of ion – electron collisional complex. An analytical formula for the effective binary recombination rate coefficient α_{E-CRR} as a result of E-CRR of atomic ions was derived by Stevefelt [*Stevelfelt et al.*, 1975]:

$$\alpha_{E-CRR} = 3.8 \times 10^{-9} T_e^{-4.5} n_e + 1.55 \times 10^{-10} T_e^{-0.63} + 6 \times 10^{-9} T_e^{-2.18} n_e^{0.37} \text{ cm}^3 \text{ s}^{-1}, \quad (3)$$

where electron number density n_e is in units of cm^{-3} and electron temperature T_e is in Kelvins. According to ref. [*Stevelfelt et al.*, 1975] the first term in equation (3) accounts for collisional recombination, the radiative processes give rise to the second term and the third term describes coupling between collisional and radiative recombination. Due to its steep temperature dependence, the first term in equation (3) dominates at low temperatures. The corresponding ternary recombination rate coefficient K_{E-CRR} is then:

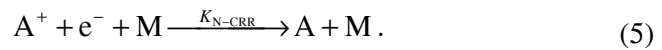
$$K_{E-CRR} = \frac{\alpha_{E-CRR}}{n_e} \cong 3.8 \times 10^{-9} T_e^{-4.5} \text{ cm}^6 \text{ s}^{-1}, \quad (4)$$

where n_e and T_e are in units of cm^{-3} and K, respectively.

Later theoretical treatment by Pohl [Pohl *et al.*, 2008] suggested slightly lower value of the pre-factor in equation (4) – $2.77 \times 10^{-9} \text{ K}^{4.5} \text{ cm}^6 \text{ s}^{-1}$. The values of $K_{\text{E-CRR}}$ that me and my co-workers obtained for Ar^+ ions in the temperature range of 60 – 150 K [Kotrík *et al.*, 2011a; Kotrík *et al.*, 2011b; Dohnal *et al.*, 2013] are within error of the measurement in agreement with both of these predictions [Stevelfelt *et al.*, 1975; Pohl *et al.*, 2008] but closer to the values given by equation (3).

E-CRR is considered an important process in formation of antihydrogen [Killian *et al.*, 1999; Pohl *et al.*, 2008; Wolz *et al.*, 2020] and it was discussed in connection with cold and ultracold plasmas [Rennick *et al.*, 2011]. There are many theoretical and numerical simulation studies [Bannash *et al.*, 2011; Vorob'ev, 2017; Gerber, 2018; Jiang *et al.*, 2020] with emphasis on low temperature E-CRR but the vast majority of available experimental data was obtained at electron temperature of 300 K or higher [Mansbach *et al.*, 1969; Berlande *et al.*, 1970; Curry, 1970; Skrzypkowski *et al.*, 2004]. To the best of my knowledge, the only direct measurement of E-CRR recombination rate coefficient in plasma for electron temperatures below 300 K are the CRYO-FALP II studies focused on Ar^+ ions [Kotrík *et al.*, 2011a; Kotrík *et al.*, 2011b; Dohnal *et al.*, 2013]. There is no experimental or theoretical study concerning E-CRR of molecular ions. Recent experiments [Hejduk *et al.*, 2015] suggest that for some molecular ions the value of the E-CRR rate coefficient may be substantially lower than for atomic ones.

If the particle that carries away the excess energy of recombination is neutral we will call this process neutral assisted collisional radiative recombination (N-CRR):



N-CRR of atomic ions has been studied theoretically from early 20th century [Thomson, 1924; Pitaevskii, 1962; Flannery, 1991; Wojcik *et al.*, 1999; Wojcik *et al.*, 2000]. The recombination rate coefficient is predicted to depend steeply on temperature as $\sim T^{2.5}$ [Thomson, 1924; Pitaevskii, 1962] or $\sim T^{2.9}$ [Bates *et al.*, 1965].

The experimental studies of N-CRR performed for atomic ions or He_2^+ largely agree with theoretical predictions [Berlande *et al.*, 1970; Deloche *et al.*, 1976; Gousset *et al.*, 1978; Sonsbeek *et al.*, 1992; Schregel *et al.*, 2016]. There are only very few

studies performed for temperatures below 300 K. Cao et al. [Cao et al., 1991] studied N-CRR for mixture of atmospheric ions in helium obtaining good agreement with theory. Me and my co-workers have investigated the recombination of Ar^+ with electrons in ambient helium [Dohnal et al., 2013] with results very close to theoretical predictions [Bates et al., 1965].

In 2008 Glosik et al. [Glosik et al., 2008] discovered a very fast helium assisted recombination of H_3^+ ions with ternary recombination rate coefficient on the order of $10^{-25} \text{ cm}^6 \text{ s}^{-1}$, i. e. more than hundred times higher than what would have been expected based on the theory of Bates and Khare [Bates et al., 1965]. We later observed similar behaviour for the deuterated isotopologues of H_3^+ [Dohnal et al., 2012c; Dohnal et al., 2016; Plašil et al., 2017].

The explanation suggested in ref. [Glosik et al., 2009] assumed that after collision of H_3^+ ions with electrons a Rydberg state with a long life-time is formed. The Rydberg state then lives long enough to experience l -changing collision with helium facilitating the recombination process. This was supported by calculations by C. Greene and V. Kokoouline of lifetimes of Rydberg states formed in H_3^+ recombination. The explanation was successful in predicting the order of magnitude of the ternary recombination rate coefficient but rested on some crude assumptions especially for the rate of l -changing collisions between H_3 Rydberg states and helium. Moreover, similar mechanism could be expected also for other molecular ions recombining via indirect recombination process involving Rydberg states. Our studies on HCO^+ [Korolov et al., 2009] and N_2H^+ [Shapko et al., 2020] recombination in helium buffer gas have shown that the values of the corresponding ternary recombination rate coefficients are at least order of magnitude lower than those for H_3^+ ions.

Absorption spectroscopy

Basic concepts

Absorption of radiation by a quantum system is connected with a transition between two energy levels. The decrease of the intensity I of monochromatic light passing through homogenous absorbing medium is given by the Lambert-Beer law [Beer, 1852]:

$$\frac{dI(x, \nu)}{dx} = -\alpha(\nu)I(x, \nu), \quad (6)$$

where x is the position in the absorbing medium, ν is the frequency of the radiation and $\alpha(\nu)$ is absorption coefficient. In homogenous absorbing medium, α does not depend on x and the solution of equation (6) is:

$$I(L, \nu) = I_0 \exp(-\alpha(\nu)L), \quad (7)$$

where L is the distance traversed in the absorbing medium and I_0 is the initial light intensity. Absorption coefficient depends on the number density of the absorbing medium $N(x)$ and on the photo-absorption cross-section $\sigma(\nu)$:

$$\alpha(x, \nu) = N(x)\sigma(\nu). \quad (8)$$

The shape of the absorption line is given by the line-shape function $g(\nu)$:

$$\sigma(\nu) = Sg(\nu), \quad (9)$$

where S stands for integral absorption coefficient (line intensity).

Absorbance:

$$A(\nu) = -\ln\left(\frac{I(\nu)}{I_0(\nu)}\right), \quad (10)$$

connects measured quantities with absorption coefficient. By substituting (7) in to equation (10) we get:

$$A(\nu) = \alpha(\nu)L. \quad (11)$$

In a more general case of non-homogenous absorbing medium containing more than one absorbing specie, the absorbance is given by:

$$A(\nu) = \sum_j \sigma_j(\nu) \int_0^L N_j(x) dx, \quad (12)$$

Where σ_j is the phot-absorption cross section of a specie with number density $N_j(x)$.

Spectral line broadening

Several processes can influence the line-shape function $g(\nu)$ of measured absorption line. At experimental conditions for studies covered in this thesis, the most important are: lifetime broadening, collisional broadening and Doppler broadening.

The finite lifetime of the states involved in the transition together with Heisenberg uncertainty principle results in lifetime broadening with a Lorentzian line-shape function [*Bernath, 2005*]:

$$g(\nu) = \frac{\frac{\Delta\nu}{2\pi}}{(\nu - \nu_{nm})^2 + \left(\frac{\Delta\nu}{2}\right)^2}, \quad (13)$$

where ν_{nm} is the transition frequency and quantity

$$\Delta\nu = \frac{1}{2\pi} \left(\frac{1}{\tau_n} + \frac{1}{\tau_m} \right), \quad (14)$$

is proportional to the full width at half maximum (FWHM) of the line. τ_n and τ_m are the lifetimes of the corresponding states. For transitions between bound states at conditions present in plasmatic experiments this type of broadening can be usually neglected. It can be important if the transition involves weakly bound or resonant states or in an ultra-cold regime when other types of broadening disappear [*McGuyer et al., 2015*].

Collisions of the studied system with other particles give raise to the collisional broadening with Lorentzian line-shape function, where

$$\Delta\nu = \frac{f_{col}}{2\pi}, \quad (15)$$

f_{col} being the collision frequency. The values of pressure broadening are on the order of 10 MHz per 100 Pa [Bernath, 2005]. An example of the pressure broadening coefficients measured for the P(6) transition in the (200) ← (000) vibrational band of N_2H^+ in the helium buffer gas [Shapko *et al.*, 2020] are shown in Table I.

Table I. Pressure broadening coefficients B_p obtained by Shapko *et al.* [2020] for the P(6) transition in the (200) ← (000) vibrational band of N_2H^+ in the helium buffer gas.

T (K)	B_p ($10^{-21} \text{ cm}^{-1} \text{ cm}^3$)
78	6.2 ± 0.5
140	7.7 ± 0.6
200	8.9 ± 0.3
300	9.4 ± 0.5

The thermal movement of particles with respect to the radiation source results in Doppler broadening of the absorption line with gaussian line-shape function:

$$g(\nu) = \frac{1}{\sqrt{2\pi}\sigma_D} \exp\left(-\frac{(\nu - \nu_{nm})^2}{2\sigma_D^2}\right), \quad (16)$$

With

$$\sigma_D = \nu_{nm} \sqrt{\frac{k_B T_{kin}}{Mc^2}}, \quad (17)$$

where k_B is the Boltzmann constant, T_{kin} is the kinetic temperature of the measured specie, M is its mass and c is the speed of light.

At 300 K and pressure of several hundred Pa, the Doppler broadening is dominant mechanism for very light ions such as H_3^+ . If the mass of the studied ions is higher or the temperature is lower, the collisional broadening cannot be neglected and has

to be taken into account in the data analysis by fitting the data by a Voigt profile [Shapko *et al.*, 2020].

Cavity Ring-Down Spectroscopy

Originally developed for measuring the reflectivity of dielectrically coated mirrors [Herbelin *et al.*, 1980; Anderson *et al.*, 1984], Cavity Ring-Down Spectroscopy (CRDS) has been since then utilized in many spectroscopic applications [O'Keefe *et al.*, 1988; Berden *et al.*, 2009].

In principle, two highly reflective mirrors form stable optical cavity and light trapped in the optical resonator leaks through the mirrors. The resulting signal on the photodetector (ring-down) decays exponentially with time [Berden *et al.*, 2009]:

$$I(\nu, t) = I(\nu, 0) \exp\left(-\frac{t}{\tau(\nu)}\right), \quad (18)$$

where:

$$\tau(\nu) = \frac{d}{c[A(\nu) - \ln R(\nu)]} \quad (19)$$

d is the distance between the mirrors, c is speed of light and R is the reflectivity of the mirrors. By measuring the ring-down time constant $\tau(\nu)$ with and without absorbing medium present, one can directly obtain the absolute value of the absorbance A . A big advantage of this setup is no need to calibrate the light source for the wavelength dependence of the emitted power.

There are various implementations of the CRDS technique, here only pulsed and continuous wave variants will be discussed.

The reflectivity of the mirrors forming optical cavity of CRDS is very high ($R \sim 0.999$ to 0.9999), therefore the majority of the incoming light is reflected. The transmission of the resonator is also influenced by the interference of the light circulating in the resonator. In the pulsed CRDS technique [O'Keefe *et al.*, 1988] a short high power laser pulse with a duration shorter than the time needed for the photons to transverse the distance between the mirrors is used. The disadvantage of

this method is the necessity to utilize pulsed lasers that have typically broad bandwidth unsuitable for high resolution spectroscopy.

The continuous wave CRDS (cw-CRDS) is a technique developed originally by Romanini [Romanini *et al.*, 1997]. He used continuous wave laser source coupled to the cavity modes of the optical resonator and utilized resonant build-up of intensity to inject enough power through the highly reflective mirrors. The process can be illustrated on ideal Fabry-Perot resonator formed by parallel plane mirrors of infinite dimensions. In such case, the steady state transmission I for incident light propagating in a direction perpendicular to the entry mirror is given by [Yariv, 1997]:

$$I = I_0 \frac{(1 - R)^2}{(1 - R)^2 + 4R \sin^2 \left(\frac{2\pi d}{\lambda} \right)}, \quad (20)$$

where λ is the wavelength. For some values of d/λ the resonant condition is fulfilled and $I/I_0 = 1$. The corresponding standing waves are called modes of the resonator. Similar result can be obtained for non-planar mirrors, for details see refs. [Lehmann *et al.*, 1996; Morville, 2001]. The planar configuration of mirrors is unstable due to finite mirror dimensions [Yariv, 1997] and optical cavity of the CRDS is usually formed by spherical mirrors. In such case the radii of the curvature of the mirrors, r_1 and r_2 have to fulfil equation:

$$0 \leq \left(1 - \frac{d}{r_1} \right) \left(1 - \frac{d}{r_2} \right) \leq 1, \quad (21)$$

The mode structure of such optical cavity is more complicated than for ideal Fabry-Perot resonator. The solution of Maxwell equations with appropriate boundary conditions involves standing waves with longitudinal modes (analogous to modes in Fabry-Perot resonator, the fundamental mode is denoted TEM_{00}) and transverse modes labelled TEM_{mn} with m and n being integers. For details see ref. [Yariv, 1997].

To ascertain that the resonant condition for equation (20) is fulfilled, Romanini *et al.* [1997] put one of the mirrors on a piezo element that changed the distance of the mirrors by a value larger than the wavelength of the used light. The resonant

condition is then fulfilled at least twice per cavity sweep. This approach is also utilised in our experimental setup (see in the corresponding section).

Langmuir probe diagnostics

Langmuir Probe, a metal electrode immersed in plasma, is one of the oldest techniques of plasma diagnostics [Langmuir, 1923; Mott-Smith *et al.*, 1926]. In principle, the current-voltage characteristic of the probe is utilized to obtain various plasma parameters such as electron number density n_e , electron temperature or distribution function (EEDF). This section will introduce several equations connecting current-voltage characteristic of single cylindrical probe with plasma parameters. If not stated otherwise, it is assumed that following conditions are fulfilled:

- 1) The probe does not emit electrons
- 2) Plasma is not disturbed outside a thin layer around the probe
- 3) The charged particles in plasma consist of singly charged ions and electrons. Negative ions are not present.
- 4) The velocity distribution of charged particles in plasma is Maxwellian
- 5) The mean free paths of electrons and ions are substantially longer than the Debye length λ_D .
- 6) Independence of electron and ion currents.

An example of current voltage characteristic of single probe is plotted in Figure 3. The characteristic can be divided in to three regions depending on the probe voltage U . At plasma potential (U_{pl} , inflexion point of the current-voltage characteristic [Smith *et al.*, 1979]) the probe is neither attractive nor repulsive for charged particles. If $U > U_{pl}$, electrons are attracted to the probe, while the ions are repulsed (saturated electron current region). The electron current i_- collected by the probe is then [Hutchinson, 2002]:

$$i_- = \sqrt{\frac{2}{m_e} \frac{A_{\text{probe}} e n_e}{\pi}} \sqrt{eU_S + k_B T_e}, \quad (22)$$

where A_{probe} is the collecting surface of the probe, m_e electron mass, e is the elementary charge, $U_S = U_p - U$ and k_B is the Boltzmann constant. The electron density can be obtained from the slope of the dependence of the second power of i_- on U_S (i-square method [Mott-Smith *et al.*, 1926]).

If $U < U_p$, the probe attracts ions and electrons are repulsed. Some of the electrons have still enough kinetic energy to overcome the repulsive voltage and fall on the probe. The more is the probe negative with respect to the plasma potential, the fewer electrons are collected by the probe resulting in rapid decrease of the measured probe current with decreasing voltage (retarding region). For Maxwellian electron velocity distribution the electron current can be described in this region as [Pfau *et al.*, 2001]:

$$i_- = -en_e A_{\text{probe}} \sqrt{\frac{k_B T_e}{2\pi m_e}} \exp\left(-\frac{eU_S}{k_B T_e}\right). \quad (23)$$

Electron temperature can be determined from the natural logarithm of electron current given by equation (23) or its second derivative. The second derivative of the probe current in the retarding region can be also used to obtain the electron energy distribution function f (EEDF):

$$f(eU_S) = \frac{2\sqrt{2m_e U_S}}{n_e e^3 A_{\text{probe}}} \frac{d^2 i_-}{dU^2}, \quad (24)$$

where f is normalized to unity:

$$\int_0^{\infty} f(x) dx = 1. \quad (25)$$

Equation (24) derived by Druyvesteyn [Druyvesteyn, 1930] is valid also for non-maxwellian EEDF.

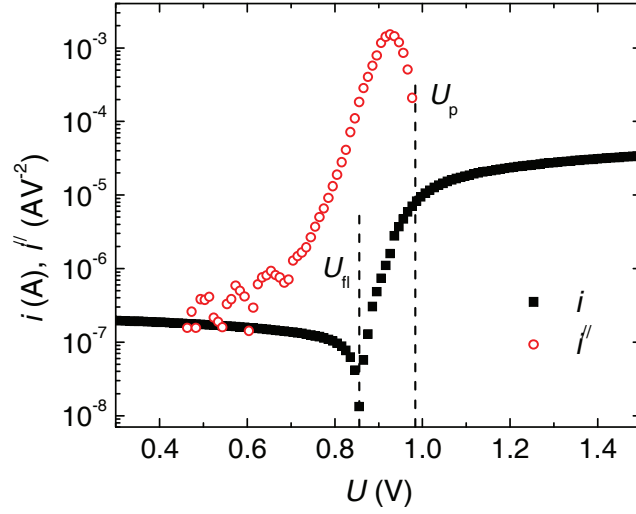


Figure 3. Adapted from ref. [Dohnal, 2013]. Absolute value of the current voltage characteristic (full squares) and its second derivative (circles). Positions of floating potential (U_{fl}) and of plasma potential (U_p) are denoted by vertical dashed lines. The characteristic was obtained in Cryo-FALP II experiment in Ar^+ dominated helium buffered plasma at $T = 250$ K and $P = 800$ Pa.

The region of the current-voltage characteristic where $U \ll U_p$ is denoted as saturated ion current region. If the electron and ion currents collected by the probe are the same, the overall current is zero and the corresponding voltage is called floating potential U_{fl} .

Microwave diagnostics

The microwaves have been used for plasma parameters determination for over seventy years [Brown *et al.*, 1952; Larsson *et al.*, 2008] and many experimental techniques were developed [Brown *et al.*, 1952; Torrisi *et al.*, 2022]. In some of the presented studies we employed a method based on tracing the changes of the resonance frequency of the cylindrical resonator in dependence on electron number density in the resonator [Shapko *et al.*, 2021]. The shift Δf_r of the resonance frequency f_r is proportional to the electron number density n_e [Šiřcha *et al.*, 1966]:

$$n_e = \Delta f_r f_r \frac{2\pi m_e}{e_0^2} \frac{\int_V E^2 dV}{\int_{V'} J_0\left(\frac{2.405}{r_0}\right) E^2 dV}, \quad (26)$$

where E is the intensity of the field in the resonator, V and V' are the volume of the resonator and of the plasma column, respectively, J_0 is the Bessel function of the zeroth order, m_e and e_0 are the electron mass and charge and r_0 is the radius (inner) of the discharge tube containing the plasma with r being distance from the axis of the resonator.

Experimental techniques

The results presented in this thesis were obtained using two modifications of the stationary afterglow technique (SA-CRDS and Cryo-SA-CRDS) and of the flowing afterglow technique (Cryo-FALP II). A short overview of the experimental setup will be given here.

Cryo-FALP II

Cryogenic Flowing Afterglow with Langmuir Probe is a low temperature modification of the flowing afterglow technique [Fehsenfeld *et al.*, 1966; Ferguson *et al.*, 1969] combined with axially movable Langmuir probe [Mahdavi *et al.*, 1971]. A detailed description of the experimental apparatus can be found e. g. in ref. [Kotrik, 2013]. A scheme of the Cryo-FALP II setup is shown in Figure 4.

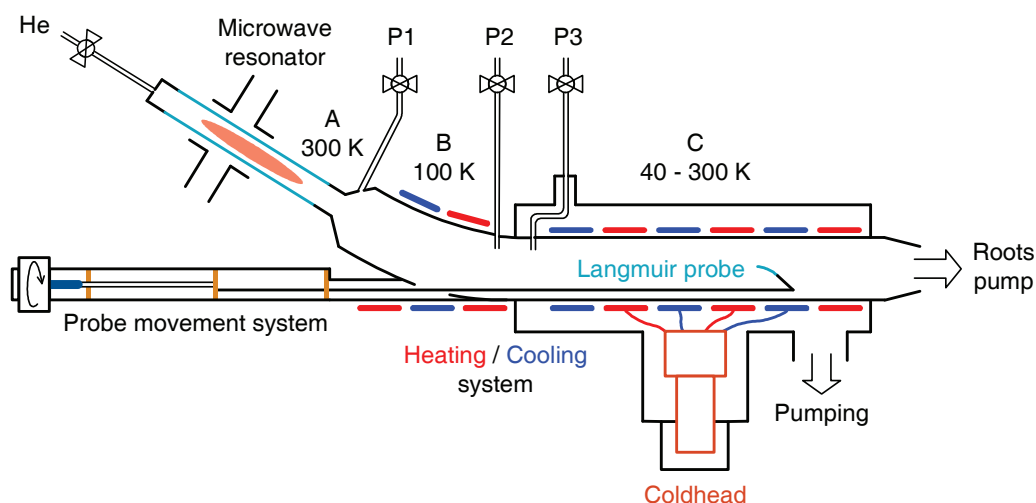


Figure 4. Adapted from ref. [Kotrik, 2013]. A scheme of the Cryo-FALP II apparatus.

Helium buffer gas flows through the glass discharge tube where it is ionized by a microwave discharge ignited in a Evenson cavity [Kotrik, 2013] and plasma containing electrons, He^+ , He_2^+ and helium metastable atoms (2^1S and 2^3S states of helium) is formed. It is then driven to the stainless-steel flow tube with inner

diameter of 5 cm. There are several entry ports for reactants positioned along the flow tube. In this way, the plasma formation and the actual chemistry can be separated as the reactant gases are not subject to the discharge and the reactants can be added at specific position corresponding to the time in the afterglow. The electron number density along the flow tube is probed by a Langmuir probe. At the end of the flow tube, the gas is pumped by a Roots type pump ensuring buffer gas flow on the order of thousands of sccm ($\sim 1 - 10 \text{ Pa m}^3\text{s}^{-1}$). In some experiments the setup can be modified by addition of a differentially pumped chamber and of a mass spectrometer.

As denoted by capital letters in Figure 4, the flow tube is divided in to three sections with different temperature. Section A, containing discharge tube, is kept at room temperature. Section B is cooled by liquid nitrogen to approximately 100 K. The port at the beginning of this section is usually used to add argon for effective removal of helium metastable atoms. Section C is connected to the cold-head of the closed cycle helium refrigerator enabling measurements in the range of 40 – 300 K. The flow tube itself is positioned inside a vacuum chamber to minimize heat losses. The temperature along the tube is monitored by type T thermocouples and DT-471-CU silicon diodes.

Prior entering the apparatus, the helium buffer gas is purified by passing through molecular sieves kept at liquid nitrogen temperature. Similarly, all the reactant gases are purified using cold traps with liquid nitrogen or precooled ethanol.

The gas handling/mixing system of the apparatus (not shown in Figure 4) enables using reactant number densities as low as $10^{10} \text{ cm}^3\text{s}^{-1}$.

Stationary afterglow with Cavity Ring-Down spectrometer

Two modifications of the stationary afterglow setup equipped with Cavity Ring-Down spectrometer were used in presented studies – SA-CRDS and Cryo-SA-CRDS. Both experiments share the gas handling and mixing system with the Cryo-FALP II apparatus.

SA-CRDS is an acronym for Stationary Afterglow apparatus with Cavity Ring-Down Spectrometer. Detailed description can be found e. g. in refs. [Macko *et al.*, 2004; Dohnal, 2013] so only short overview will be given here.

The optical system consists of laser source, optical isolator to protect the laser from back reflections, acousto-optic modulator (AOM) for fast switching off the laser beam and spatial filter consisting of two lenses and a pinhole between them. The optical cavity is formed by two mirrors positioned on the optical axis of the apparatus 75 cm apart. The light exiting the cavity is then collected by a detector based on avalanche photodiode and amplifier. The signal is then processed and stored by the data acquisition system.

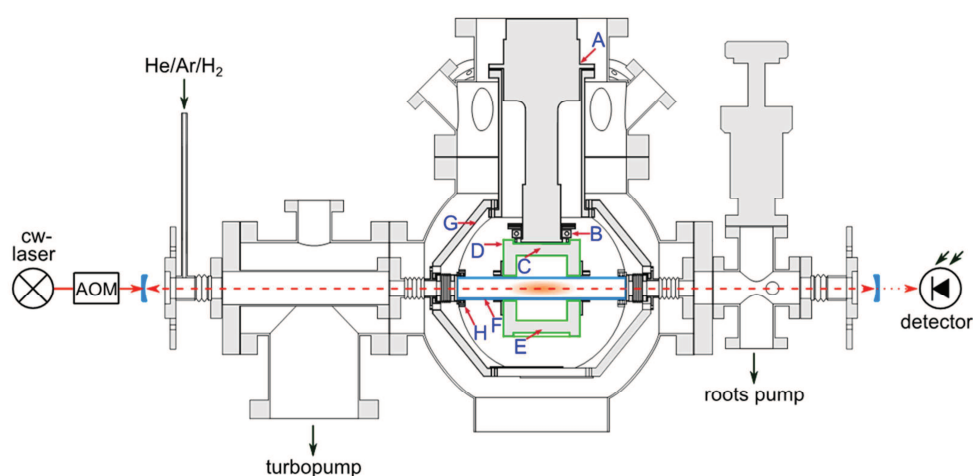


Figure 5. Adapted from ref. [Shapko *et al.*, 2021]. A scheme of the Cryo-SA-CRDS apparatus.

The fused silica discharge tube of the SA-CRDS apparatus is placed inside a microwave resonator cavity enabling discharge ignition. The tube is cooled by liquid nitrogen or liquid nitrogen vapours enabling operation in the temperature range 80 – 300 K. In some experiments, heating elements were placed at both ends of the discharge tube, outside of the microwave resonator, to heat up the tube to approximately 350 K [Shapko *et al.*, 2020].

During the experiments, discharge is periodically ignited in a mixture of gases and then switched off after set time. The time evolution of the ion number density in discharge and afterglow plasma is then probed by cavity ring-down spectrometer.

The Cryogenic Stationary Afterglow apparatus with Cavity Ring-Down Spectrometer (Cryo-SA-CRDS) is a low temperature modification of the SA-CRDS setup [Plašil *et al.*, 2018]. A scheme of the apparatus is shown in Figure 5. It shares many properties of the SA-CRDS setup (gas handling system, similar optical setup) but there are important alterations highly enhancing its capabilities.

The cold head of the closed cycle helium refrigerator is connected to the microwave resonator (green in Figure 5) and it is in turn attached by copper braids to the discharge tube made of monocrystalline sapphire. This enables to prepare ions with kinetic temperatures (evaluated from the Doppler broadening of the absorption lines) as low as 30 K [Plašil *et al.*, 2018]. The discharge tube and cold-head are inside a vacuum chamber to ensure thermal insulation.

As the microwave resonator has no movable parts, to ensure the effective coupling of the microwaves to the resonator, it is necessary to tune the frequency of the microwaves to the resonant frequency of the microwave resonator. I have designed a microwave source based on solid state microwave synthesiser (SLSM5 from Luff Research Inc) that can produce microwaves in the range of 2.4 – 2.6 GHz. The low power (~ 10 mW) microwave radiation can then be switched on and off very fast (rise and fall time of less than 1 μ s) by a PIN switch. The microwave signal is then amplified by an amplifier to 10 – 20 W that is enough to ignite the discharge.

In addition to the cavity ring-down spectroscopy, Cryo-SA-CRDS apparatus is equipped by microwave diagnostics, based on tracing the shift of the resonant frequency of the microwave cavity, for electron number density determination. As a source of probing microwaves, I used the same setup as for plasma ignition but without the amplifier stage. In connection with the data acquisition system, this enables measurements of the evolution of the electron number density in afterglow plasma with an effective time resolution of 2.5 μ s. The detailed description of the setup can be found in ref. [Shapko *et al.*, 2021].

The ability of the Cryo-SA-CRDS apparatus to probe at the same time electron number density and the number density of the ions of interest is crucial for reliable recombination rate coefficient determination even at conditions when the studied ions are not dominant ionic species in the afterglow [Shapko *et al.*, 2021].

Data analysis

In quasineutral afterglow plasma containing singly charged ionic specie A^+ the time evolution of the electron number density can be described by differential equation:

$$\frac{dn_A}{dt} = -\alpha n_A n_e - \frac{n_A}{\tau}, \quad (27)$$

where n_A and n_e are number densities of ions A^+ and of electrons, α is the recombination rate coefficient and τ denotes the losses of ions by ambipolar diffusion and by reactions (ion-molecule reaction, three-body association reaction, etc.):

$$\frac{1}{\tau} = \frac{1}{\tau_D} + \frac{1}{\tau_R}, \quad (28)$$

here τ_D stands for ambipolar diffusion losses (assuming only fundamental diffusion mode) and τ_R denotes reaction losses.

If A^+ is dominant ionic specie in afterglow plasma, then $n_A = n_e$ and equation (27) has an analytical solution:

$$n_e(t) = \frac{1}{\alpha\tau \left(\exp\left(\frac{t-t_0}{\tau}\right) - 1 \right) + \frac{1}{n_0} \exp\left(\frac{t-t_0}{\tau}\right)}, \quad (29)$$

that can be used to determine the recombination rate coefficient by directly fitting the data. Here n_0 is the electron number density at time $t = t_0$.

If A^+ is not dominant ionic specie at the beginning of the afterglow but gradually becomes dominant a technique called “Integral analysis” can be employed [Korolov *et al.*, 2008]. Let’s define the fraction of ions A^+ with respect to all ions as $\zeta(t) = n_A(t)/n_e(t)$. Fraction $\zeta(t)$ varies with time and becomes unity when A^+ is a dominant ion in the afterglow. The time evolution of the electron number density in afterglow can then be rewritten as:

$$\frac{dn_e}{dt} = -\alpha\zeta(t)n_e^2 - \frac{n_e}{\tau}, \quad (30)$$

which after integration gives:

$$\ln \left[\frac{n_e(t_b)}{n_e(t_a)} \right] + \frac{(t_b - t_a)}{\tau} = -\alpha \int_{t_a}^{t_b} \xi(t) n_e dt, \quad (31)$$

Where t_a and t_b are integration limits. When the studied ion becomes dominant, $\xi(t) = 1$ and the plot of the left-hand side of equation (31) in dependence on the integral on the right-hand side gives a straight line with a slope $-\alpha$. In this procedure, τ is a variable parameter determined by minimizing the χ^2 of a given fit.

If the plasma deionisation is dominated by recombination assisted by collisions with electrons as third particles (as in the case of $\text{Ar}^+ + e^- + e^- \rightarrow \text{Ar} + e^-$ recombination studied in ref. [Dohnal *et al.*, 2013]), α in equation (30) depends on n_e :

$$\alpha = K_{E-CRR} n_e, \quad (32)$$

where K_{E-CRR} is the ternary coefficient for electron assisted collisional radiative recombination and for $\zeta = 1$ is the analytical solution of equation (30):

$$n_e(t) = \frac{1}{\left(\alpha \tau \left(\exp \left(2 \frac{t - t_0}{\tau} \right) - 1 \right) + \frac{1}{n_0^2} \exp \left(2 \frac{t - t_0}{\tau} \right) \right)^{1/2}}, \quad (33)$$

while the ‘‘Integral analysis’’ has the form [Dohnal *et al.*, 2013]:

$$\ln \left[\frac{n_e(t_b)}{n_e(t_a)} \right] + \frac{(t_b - t_a)}{\tau} = -K_{E-CRR} \int_{t_a}^{t_b} \xi(t) n_e^2 dt. \quad (34)$$

Let’s assume a more general case when ions A^+ are not necessarily dominant in the afterglow but they are no longer formed. In SA-CRDS or Cryo-FALP II experiment based either on ion or on electron number density determination the mentioned data analysis techniques would lead to erroneous results. The Cryo-SA-CRDS apparatus enables simultaneous determination of the time evolutions of both electron and ion number densities so all the time dependent quantities in equation (27) are known and it can be solved by direct integration [Shapko *et al.*, 2021]:

$$n_A(t_i) = n_A(t_0) e^{-\alpha X(t_i) - \frac{1}{\tau} Y(t_i)}, \quad (35)$$

where

$$X(t_i) = \int_{t_0}^{t_i} n_e(t) dt, \quad (36)$$

and

$$Y(t_i) = t_i - t_0. \quad (37)$$

Note that n_A , $X(t_i)$ and $Y(t_i)$ are measured in Cryo-SA-CRDS experiment (or can be calculated from measured quantities), so we can find the parameters $n_A(t_0)$, α and τ that fulfil the equation (35) in the least square sense.

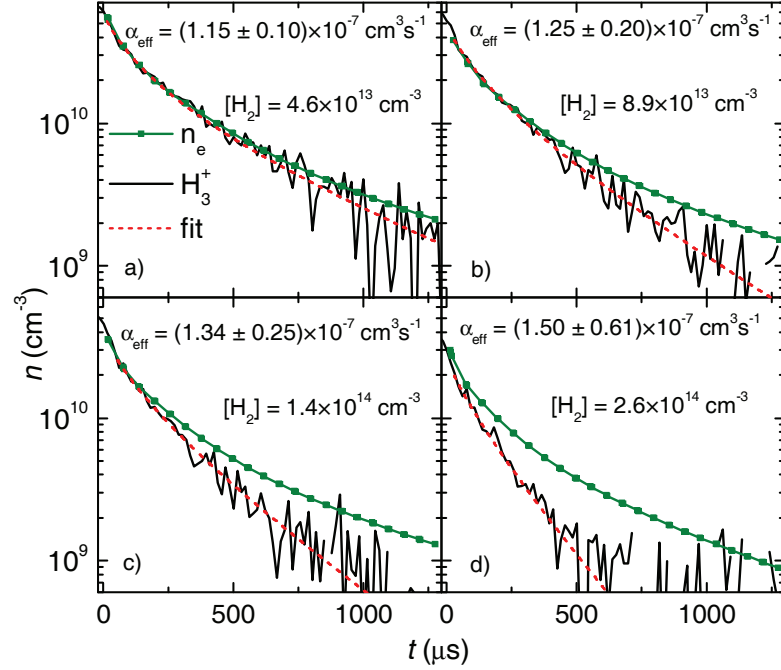


Figure 6. Adapted from ref. [Shapko *et al.*, 2021]. The time evolutions of electron (squares) and H_3^+ (full line) number densities obtained in Cryo-SA-CRDS experiment in helium buffered afterglow plasma at different number densities of H_2 . The dashed line is a fit to the data by equation (35). The corresponding effective recombination rate coefficients are written in each panel, the displayed error being the statistical error of the fit. The conditions of the experiments were: $T = 200$ K, $[He] = 3 \times 10^{17} \text{ cm}^{-3}$, $[Ar] = 2 \times 10^{14} \text{ cm}^{-3}$ and $[H_2]$ in the range of 4.6×10^{13} to $2.6 \times 10^{14} \text{ cm}^{-3}$.

Examples of the time evolutions of H_3^+ and electron number densities measured in the Cryo-SA-CRDS experiment are plotted in Figure 6. In panel a) of Figure 6 the H_3^+ ions are dominant ions in the afterglow plasma. As the number density of H_2 increases, H_5^+ ions are formed in the three-body association reaction of H_3^+ with H_2 and helium. In panel d) the H_3^+ ions are no longer dominant in later afterglow but the recombination rate coefficient evaluated by fitting the data by equation (35) is within the error of the measurement the same as in panel a) of Figure 6.

We also tested the data analysis procedure on a case of H_3^+ ions in neon buffer gas. Here, due to unfavourable chemistry, the fraction of H_3^+ ions in the afterglow was less than one half of all ions the rest being mainly NeH^+ (the formation of H_3^+ from the reaction of NeH^+ with H_2 is very slow). Nevertheless, the evaluated effective recombination rate coefficient for H_3^+ ions was within error of the measurement the same as for H_3^+ ions in helium gas of the same number density. For details see ref. [Shapko *et al.*, 2021].

As a side note, as the left and right-hand side of equation (27) depends on the same order of n_A , the result of the fitting by equation (35) is largely insensitive to systematic errors in n_A determination (e. g. uncertainty in transition line strength or the length of absorbing medium).

Results

Recombination of H_3^+ with electrons – third-body assisted recombination and the effect of nuclear spin

H_3^+ , the simplest polyatomic ion and the most abundantly produced molecular ion in interstellar medium [Oka, 2006] is considered to play a key role in reaction chains leading to formation of complex molecules in interstellar space [Oka, 2006; Millar, 2015]. In fact, the importance of H_3^+ ions for interstellar chemistry was established [Herbst *et al.*, 1973] long before its actual detection [Geballe *et al.*, 1996].

The dissociative recombination is the main destruction process for H_3^+ ions in interstellar medium [Larsson *et al.*, 2008] and as such has been studied for over 70 years. The actual value of the recombination rate coefficient has been subject of controversies with the results of various experimental groups differing by orders of magnitude. Table II summarizes values of the recombination rate coefficient for recombination of H_3^+ ions with electrons obtained starting in the late forties.

Some of the inconsistencies in afterglow experiments were resolved by discovery of surprisingly fast third-body assisted recombination of H_3^+ ion in helium buffer gas by Glosík and co-workers [Glosík *et al.*, 2008] who showed that when the H_3^+ recombination rate coefficients are plotted with respect to helium number density, they can be fitted by a straight line: $\alpha_{\text{eff}} = \alpha_{\text{bin}} + K_{\text{He}}[\text{He}]$. The inferred binary recombination rate coefficient α_{bin} was then in a good agreement with the results of the latest ion storage ring study performed with vibrationally cold ions [McCall *et al.*, 2004]. A third-body assisted recombination process of magnitude similar to that of H_3^+ was later observed for its deuterated isotopologues [Kotřík *et al.*, 2010; Dohnal *et al.*, 2012c; Dohnal *et al.*, 2016; Plašil *et al.*, 2017]. When the helium buffer gas is exchanged for neon, the measured H_3^+ recombination rate coefficients are within the error of the measurement the same as in ambient helium [Shapko *et al.*, 2021] while we observed a substantially larger ternary recombination rate coefficient for hydrogen buffer gas [Dohnal *et al.*, 2014; Glosík *et al.*, 2015]. The ternary recombination rate coefficients K_{He} and K_{H_2} for H_3^+ ions obtained in our various studies are plotted in Figure 7.

Table II. Recombination rate coefficient as measured for H_3^+ ions in different experiments using normal H_2 (ortho to para nuclear spin state ratio of 3:1). Adapted from refs. [Plašil *et al.*, 2002; Dohnal 2013]. SA – stationary afterglow, μw – microwave diagnostics, IB – inclined beam, MB – merged electron-ion beam, IT – ion trap, FALP – flowing afterglow with Langmuir probe, IR – infrared spectroscopy in stationary afterglow setup, SR – ion storage ring, C1, C2 – compilations of multiple experiments.

Year	α ($10^{-7} \text{ cm}^3 \text{ s}^{-1}$)	Method	Comment	Reference
1949	25	SA/ μw		[Biondi <i>et al.</i> , 1949b]
1951	20 and 60	SA/ μw	1 and 7 torr, H_2	[Richardson <i>et al.</i> , 1951]
1951	3 and 25	SA/ μw	3 and 30 torr, H_2	[Varnerin <i>et al.</i> , 1951]
1955	<0.3	SA/ μw		[Persson <i>et al.</i> , 1955]
1973	2.3	SA/ μw	300 K	[Leu <i>et al.</i> , 1973]
1974	2.5	IB		[Peart <i>et al.</i> , 1974]
1977	2.1	MB		[Auerbach <i>et al.</i> , 1977]
1978	1.5	IT		[Mathur <i>et al.</i> , 1978]
1979	2.1	MB		[McGowan <i>et al.</i> , 1979]
1984	<0.2	FALP		[Adams <i>et al.</i> , 1984]
1984	1.5	SA		[MacDonald <i>et al.</i> , 1984]
1988	0.2	MB		[Hus <i>et al.</i> , 1988]
1989	<0.0001	FALP	Estimate	[Adams <i>et al.</i> , 1989]
1990	1.8	IR	273 K	[Amano, 1990]
1992	1.5	FALP-MS	300 K	[Canosa <i>et al.</i> , 1992]
1993	0.1-0.2	FALP		[Smith <i>et al.</i> , 1993]
1994	<2	IR		[Feher <i>et al.</i> , 1994]

Table II. Continued from previous page.

Year	α ($10^{-7} \text{ cm}^3 \text{ s}^{-1}$)	Method	Comment	Reference
1994	1.15	SR	CRYRING	[<i>Sundstrom et al.</i> , 1994]
1995	1.4-2	FALP		[<i>Gougousi et al.</i> , 1995]
1998	0.78	FALP-MS		[<i>Laubé et al.</i> , 1998]
1999	0.7	SR	TARN II	[<i>Tanabe et al.</i> , 1999]
2000	<0.13	SA	[H ₂] < 10 ¹¹ cm ⁻³	[<i>Glosík et al.</i> , 2000]
2001	1	SR	ASTRID	[<i>Jensen et al.</i> , 2001]
2003	1.7	FALP	250 K	[<i>Glosík et al.</i> , 2003]
2004	0.68	SR	CRYRING	[<i>McCall et al.</i> , 2004]
2004	1.6	IR	330 K	[<i>Macko et al.</i> , 2004]
2008	0.75	FALP, C1	260 K	[<i>Glosík et al.</i> , 2008]
2013	0.6	FALP, C2	300 K	[<i>Rubovič et al.</i> , 2013]
2015	0.6	FALP, IR	300 K	[<i>Hejduk et al.</i> , 2015]

Some of the values of the recombination rate coefficients obtained in afterglow experiments are very low and cannot be explained by third-body assisted recombination (see refs. [*Adams et al.*, 1984; *Adams et al.*, 1989; *Smith et al.*, 1993; *Glosík et al.*, 2000]). *Smith et al.* [*Smith et al.*, 1993] in fact observed a fast decay of electron number density in early afterglow and argued that vibrationally excited H₃⁺ ions are responsible and H₃⁺(*v* = 0) recombination is a slow process. *Glosík et al.* [*Glosík et al.*, 2000] reported a very low value of the recombination rate coefficient for low number densities of reactant hydrogen while for [H₂] > 10¹² cm⁻³ the value of the recombination rate coefficient saturates at $\alpha_{\text{eff}} \approx 10^{-7} \text{ cm}^3 \text{ s}^{-1}$. Note that at low H₂ number densities the H₃⁺ ions have on average less than one collision with hydrogen prior recombination so their internal states populations could have been far from equilibrium.

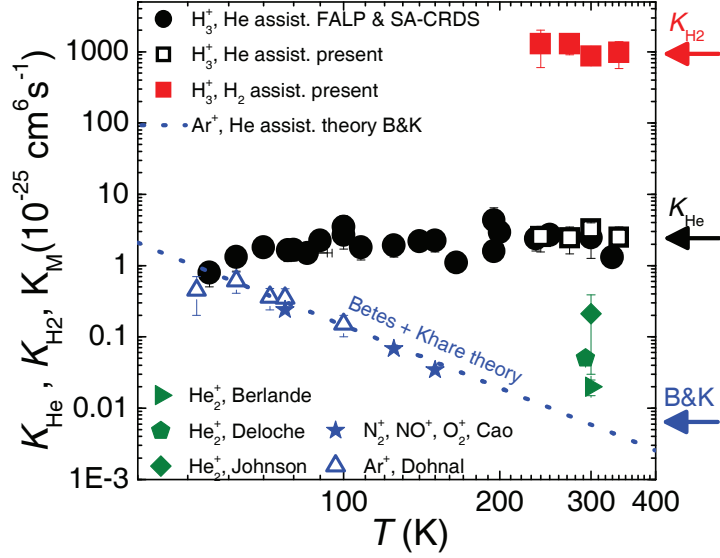


Figure 7. Adapted from ref. [Glosík *et al.*, 2015]. The dependence of the values of ternary recombination rate coefficients on temperature for helium (open squares and full circles [Glosík *et al.*, 2009; Varju *et al.*, 2011; Dohnal *et al.*, 2012a; Johnsen *et al.*, 2013]) and hydrogen (full squares [Glosík *et al.*, 2015]) buffer gas. The values of K_{He} obtained by us for Ar^+ ions [Dohnal *et al.*, 2013] and by other groups for He_2^+ [Berlande *et al.*, 1970; Johnson 1971; Deloche *et al.*, 1976] and a mixture of atmospheric ions in helium [Cao *et al.*, 1991] are plotted for comparison. Theoretical value scaled for Ar^+ ions in helium [Bates *et al.*, 1965] is plotted as dotted line.

In the last ten years I and my co-workers used improvements in instrumentation to characterize the H_3^+ dominated afterglow plasma used for recombination rate coefficient determination. We have shown that at conditions under which the values of the H_3^+ recombination rate coefficient were reported in refs. [Glosík *et al.*, 2008; Rubovič *et al.*, 2013; Hejduk *et al.*, 2015], the rotational and nuclear spin state populations of the recombining ions are in accordance with thermal equilibrium at given temperature, the electron temperature is close to the temperature of the buffer gas (with a rather large systematic error of $40 - 70$ K [Dohnal *et al.*, 2013; Hejduk *et al.*, 2015; Kálosi *et al.*, 2016]) and that the H_3^+ ions are dominant ions in the afterglow and predominantly in their ground vibrational state (see panel a) of Figure 6 and ref. [Shapko *et al.*, 2021]). The same can be stated for our studies focused on determination of the nuclear spin state selective recombination rate coefficients for

H_3^+ ions that will be described below, with an exception of the nuclear spin state populations that are given by the nuclear spin state population of the used hydrogen gas.

For a long time, the theoretical predictions suggested that the recombination of H_3^+ ions with electrons will be very slow at low collisional energies due to lack of favourable potential curve crossings. The inclusion of the Jahn-Teller mechanism into the calculations [Kokoouline *et al.*, 2001] led to the increase of the calculated recombination rate coefficient by orders of magnitude and after some refinement [Fonseca dos Santos *et al.*, 2007; Pagani *et al.*, 2009; Jungen *et al.*, 2009] to a very good agreement with afterglow and ion storage ring data at 300 K.

The most recent theory [Pagani *et al.*, 2009] predicts that at low, astrophysically relevant, temperatures the recombination rate coefficients for ortho and para nuclear spin states of H_3^+ differ by a factor of four or more. The groups based around TSR and CRYRING ion storage rings confirmed that para- H_3^+ ions recombine faster than ortho- H_3^+ but only small enhancement was observed at low collisional energies [Tom *et al.*, 2009; Kreckel *et al.*, 2010]. Note that the rotational temperature of the H_3^+ ions in the ion storage ring experiment was probably 300 K or higher [Petrigiani *et al.*, 2011].

We have studied the recombination of ortho- and para- H_3^+ ions utilizing the ability of our SA-CRDS experimental setup to probe in situ the time evolutions of different quantum states of H_3^+ ions. The recombination rate coefficient was first measured using normal hydrogen (thermal nuclear spin state ortho to para ratio of 3:1 at 300 K) and then the measurement was repeated using the same experimental conditions but with H_2 gas passing through paramagnetic catalyst leading to ortho to para ratio of 90:10 or better [Zymak *et al.*, 2013]. In this way we were able to obtain the nuclear spin state specific recombination rate coefficients for H_3^+ ions in the temperature range of 80 – 300 K [Varju *et al.*, 2011; Dohnal *et al.*, 2012a; Dohnal *et al.*, 2012b]. Later, we used the ortho- H_3^+ and para- H_3^+ populations determined in SA-CRDS to extend these measurements to 60 K using the Cryo-FALP II setup where the direct determination of nuclear spin state populations of recombining ions is not possible [Hejduk *et al.*, 2015].

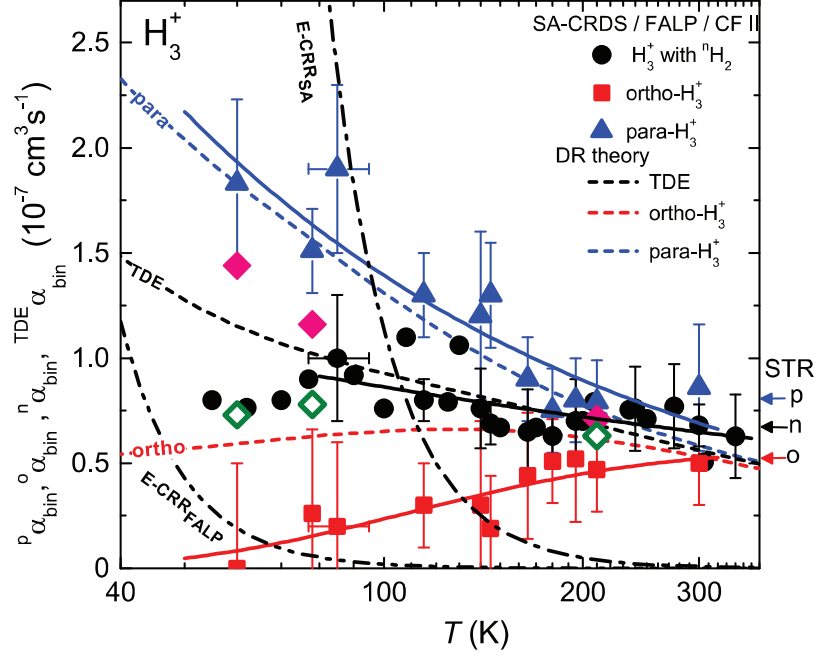


Figure 8. Adapted from ref. [Hejduk et al., 2015]. A compilation of nuclear spin state specific binary recombination rate coefficients obtained in Cryo-FALP II [Hejduk et al., 2015] and SA-CRDS experiments [Varju et al., 2011; Dohnal et al., 2012a]. The values for para- H_3^+ and ortho- H_3^+ ions are plotted as triangles and squares, respectively. The open and full diamonds denote values of binary recombination rate coefficient measured in Cryo-FALP II experiment in normal or para enriched hydrogen gas, respectively, while the full circles are values of binary recombination rate coefficient for H_3^+ ions obtained using normal hydrogen in our previous studies [Dohnal et al., 2012a; Rubovič et al., 2013]. Full lines are fits to the corresponding recombination rate coefficients (for details see ref. [Hejduk et al., 2015]). The dashed lines labelled “ortho”, “para” and “TDE” denote theoretical predictions by Pagani et al. [Pagani et al., 2009] for ortho- H_3^+ , para- H_3^+ and H_3^+ ions with thermal populations of states, respectively. The arrows on the right-hand side of the figure denote values of the corresponding recombination rate coefficients measured at 300 K in ion storage ring experiment CRYRING [Tom et al., 2009].

The binary recombination rate coefficients obtained for ortho- H_3^+ , para- H_3^+ and H_3^+ with thermal population of nuclear spin states are shown in Figure 8. As can be seen from the figure, at 300 K the recombination rate coefficients for ortho- H_3^+ and para-

H_3^+ are the same within the error of the measurement and very close to the values reported in CRYRING experiment for 300 K [Tom *et al.*, 2009]. As the temperature decreases the difference between the measured recombination rate coefficients for ortho and para nuclear spin states of H_3^+ increases in excellent confirmation of theoretical predictions [Pagani *et al.*, 2009].

It is necessary to note that the models of diffuse interstellar gas clouds are unable to get agreement with astronomical observations when our or theoretical recombination rate coefficients for ortho- and para- H_3^+ ions are used [Albertsson *et al.*, 2014]. The best fit between calculations and observations was achieved when ortho- and para- H_3^+ ions recombined with the same recombination rate coefficient with a value two times higher than that reported in CRYRING experiment [McCall *et al.*, 2004]. Some piece of the puzzle is evidently missing – the production (cosmic rate ionisation), the destruction (dissociative recombination) or the nuclear spin state specific reactions between ortho/para- H_3^+ and ortho/para- H_2 . Clearly more experimental work is needed to solve this conundrum. I hope that the new ion storage ring in Heidelberg [von Hahn *et al.*, 2016] will address this issue.

In order to extend our recombination studies to lower temperatures, we developed the Cryo-SA-CRDS apparatus enabling operation in the temperature range of 30 – 300 K. A detailed description of this apparatus can be found in corresponding section of this thesis or in ref. [Plašil *et al.*, 2018].

One of the first tests of the new experimental setup was preparation of cold H_3^+ ions with kinetic temperature around 30 K. At such temperature, almost all H_3^+ ions are in the lowest ortho state (1,0) or in the lowest para state (1,1) of H_3^+ . Changing the nuclear spin populations of H_3^+ using procedure described above then results in different population of these two rotational states of H_3^+ [Dohnal *et al.*, 2019]. An example of absorption line profiles obtained with normal H_2 (ortho to para ratio of 3:1) and almost pure para hydrogen gas is shown in Figure 9. Thus, we can change the population of the lowest rotational state (1,1) from 46 % up to 83 % of all H_3^+ ions, the remainder being mainly in the (1,0) state. This opens way to recombination study focused on reactivity of particular low-lying rotational states of H_3^+ .

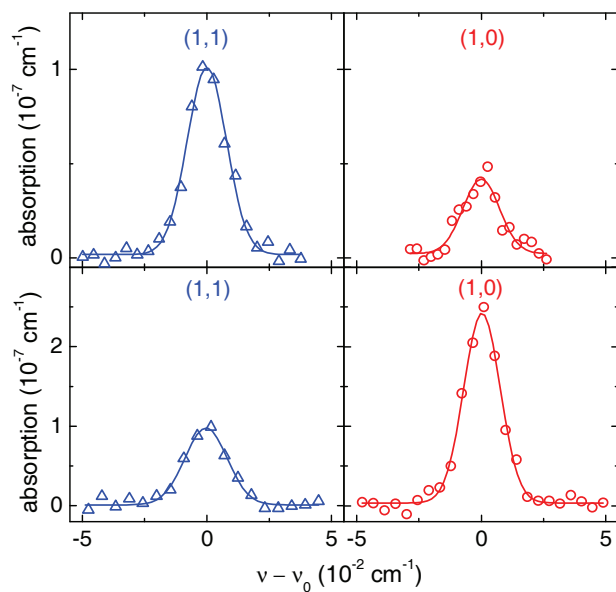


Figure 9. Adapted from ref. [Dohnal *et al.*, 2019]. The absorption line profiles obtained in Cryo-SA-CRDS experiment at 35 K for the two lowest rotational states of H_3^+ : ortho- $\text{H}_3^+(1,0)$ and para- $\text{H}_3^+(1,1)$. Upper panels: fraction of para- H_2 in used hydrogen gas was $p_{f_2} = 0.995 \pm 0.005$. Lower panels: the same as in upper panels, $p_{f_2} = 0.25$.

Recombination of H_2D^+ and HD_2^+ with electrons

The deuterated isotopologues of H_3^+ – H_2D^+ , HD_2^+ and D_3^+ – are produced in interstellar medium in a reaction chain starting with collision of H_3^+ with HD molecule [Hugo *et al.*, 2009]. H_2D^+ and HD_2^+ were detected in interstellar medium [Tennyson *et al.*, 2001; Millar, 2005; Parise *et al.*, 2011] and all four isotopologues play an important part in present chemical models of interstellar molecular clouds [Albertsson *et al.*, 2013; Sipilä *et al.*, 2013; Das *et al.*, 2015]. The dissociative recombination with electrons is an important loss process for these ions in interstellar medium and one of the pathways for production of D atoms [Roberts *et al.*, 2004; Sipilä *et al.*, 2013].

Theoretical calculations by Pagani *et al.* [Pagani *et al.*, 2009] suggest that H_2D^+ should recombine with electrons faster than HD_2^+ by a factor of three at low temperatures prevalent in molecular gas clouds while only small isotopic effect is predicted by Jungen *et al.* [Jungen *et al.*, 2009].

In contrast to the breadth of experimental data focused on H_3^+ recombination with electrons there are only few studies concerning H_2D^+ and HD_2^+ . The recombination cross sections for HD_2^+ ions were measured in merged-beam experiment by Mitchell *et al.* [Mitchell *et al.*, 1984] and the cross sections and recombination rate coefficients for H_2D^+ and HD_2^+ ions were also obtained by ion storage ring CRYRING [Datz *et al.*, 1995; Zhaunerchyk *et al.*, 2008], while the relative cross sections and product branching ratios were measured in ion storage ring TSR [Lammich *et al.*, 2003; Strasser *et al.*, 2004].

Unfortunately, the rotational populations of the ions in ion storage ring experiments were probably pertaining to the temperature of 300 K [Petrignani *et al.*, 2011] so the applicability of these results for cold interstellar medium is questionable.

Until 2016, there were no studies of dissociative recombination of H_2D^+ and HD_2^+ in plasma afterglows. This is not surprising as it is extremely difficult to prepare afterglow plasma with either H_2D^+ or HD_2^+ as dominant ions. An example of the dependence of the fractional populations of H_3^+ and its deuterated isotopologues on

the relative fraction of deuterium in hydrogen/deuterium mixture used in a stationary afterglow experiment SA-CRDS is shown in Figure 10.

As can be seen from Figure 10 we were unable to produce plasma with fractional populations of H_2D^+ or HD_2^+ substantially higher than 0.3. A similar behaviour was observed also at 80 K and 125 K. To surmount these obstacles, I decided to utilize the properties of the SA-CRDS setup – the ability to probe in situ number densities of particular ionic states. Light from several DFB (distributed feedback) laser diodes and an external cavity diode laser covering overtone transitions of H_3^+ , H_2D^+ , HD_2^+ and D_3^+ was directed on the same optical path and then coupled in to the optical cavity of the SA-CRDS apparatus. In this way, we were able to probe the time evolutions of number densities of all isotopomers of H_3^+ in discharge and afterglow plasma.

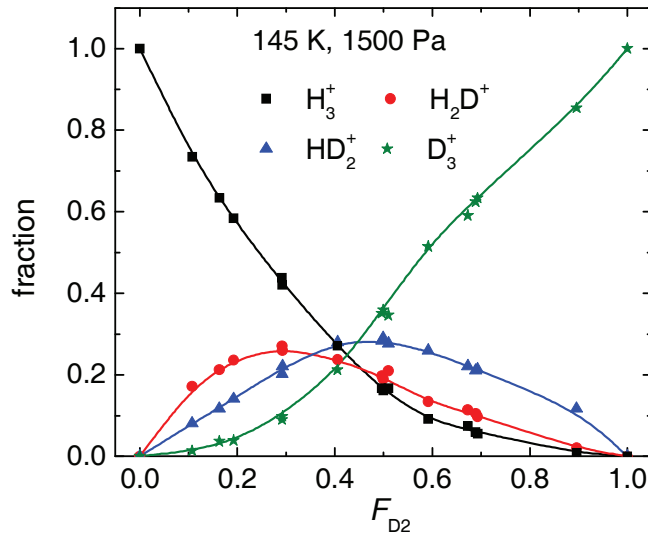


Figure 10. Adapted from ref. [Plašil *et al.*, 2017]. The dependences of the fractional populations of H_3^+ , H_2D^+ , HD_2^+ and D_3^+ on $F_{\text{D}_2} = [\text{D}_2]/([\text{H}_2] + [\text{D}_2])$ obtained in SA-CRDS experiment at 145 K with helium buffer gas pressure of 1500 Pa and $[\text{H}_2] + [\text{D}_2] = 1 \times 10^{14} \text{ cm}^{-3}$. The full lines are for eye guiding only. The data were obtained using known absorption lines of particular ions. For details see in refs. [Dohnal *et al.*, 2016; Plašil *et al.*, 2017].

Assuming plasma quasineutrality and that the H_3^+ isotopomers are dominant ionic species in the afterglow, the measured effective recombination rate coefficient can be written as:

$$\alpha_{\text{eff}} = \alpha_{\text{H}_3^+} f_{\text{H}_3^+} + \alpha_{\text{H}_2\text{D}^+} f_{\text{H}_2\text{D}^+} + \alpha_{\text{HD}_2^+} f_{\text{HD}_2^+} + \alpha_{\text{D}_3^+} f_{\text{HD}_3^+}, \quad (38)$$

where α_i and f_i are the recombination rate coefficient and the relative fraction of respective isotopomer. Fortunately, f_i did not significantly change in the afterglow plasma and were considered constant in the data analysis. Similarly to H_3^+ and D_3^+ recombination, the $\alpha_{\text{H}_2\text{D}^+}$ and $\alpha_{\text{HD}_2^+}$ depended on buffer gas pressure due to helium assisted three-body recombination. At given temperature and buffer gas pressure we measured the dependence of the effective recombination rate coefficient (obtained from the time evolution of the sum of number densities of all isotopomers) on $F_{\text{D}_2} = [\text{D}_2]/([\text{H}_2] + [\text{D}_2])$. We utilized the binary and ternary recombination rate coefficients for H_3^+ and D_3^+ measured in our previous studies using the same or similar experimental setup [Dohnal *et al.*, 2012a; Dohnal *et al.*, 2012b; Dohnal *et al.*, 2012c; Hejduk *et al.*, 2015] and the probed fractions f_i to evaluate binary and ternary recombination rate coefficients for H_2D^+ and HD_2^+ . The binary recombination rate coefficients obtained at three different temperatures are plotted in Figure 11.

As can be seen from Figure 11, the error of the obtained binary recombination rate coefficients is quite high but the disagreement with theoretical calculations by Pagani *et al.* [Pagani *et al.*, 2009] for H_2D^+ ions is evident, especially at low temperatures. It is important to note, that these values are the only low temperature recombination rate coefficients available for H_2D^+ and HD_2^+ ions, where the rotational populations of recombining ions were measured in situ. I am looking forward to the new generation of ion storage rings (for example CSR in Heidelberg [von Hahn *et al.*, 2016]) to bring forth rotationally resolved recombination rate coefficients and confirm (or refute) our results.

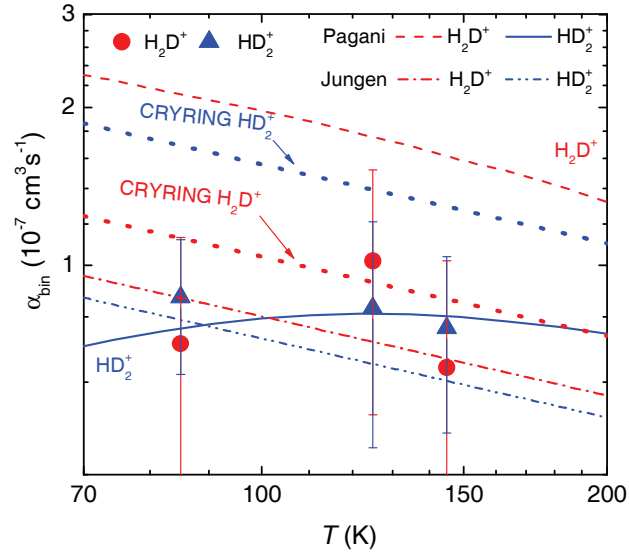


Figure 11. Adapted from ref. [Plašil *et al.*, 2017]. Temperature dependence of the binary recombination rate coefficients for H_2D^+ and HD_2^+ ions. Quantum mechanical calculations by Jungen and Pratt [Jungen *et al.*, 2009; Pratt *et al.*, 2011] (H_2D^+ - dot-dashed line, HD_2^+ - double-dot-dashed line) and by Pagani *et al.* [Pagani *et al.*, 2009;] (H_2D^+ - dashed line, HD_2^+ - full line) are plotted for comparison. Dotted lines denoted by label “CRYRING” show the values obtained in ion storage ring experiment CRYRING [Datz *et al.*, 1995; Zhaunerchyk *et al.*, 2008] at 300 K and extrapolated to lower temperatures by using $T^{-0.5}$ dependence.

The measured recombination rate coefficients were dependent on helium buffer gas number density with the corresponding values of ternary recombination rate coefficients on the order of $10^{-25} \text{ cm}^6 \text{ s}^{-1}$ i.e. similar to those observed for H_3^+ and D_3^+ ions. For more details on the H_2D^+ and HD_2^+ recombination experiments see refs. [Dohnal *et al.*, 2016; Plašil *et al.*, 2017].

Recombination of D_3^+ with electrons

Although part of models of interstellar chemistry, and so far, not yet observed in interstellar medium, the recombination of D_3^+ with electrons has not enjoyed such spotlight as that of H_3^+ . Nevertheless, there are several afterglow [*Smith et al.*, 1993; *Laube et al.*, 1998; *Poterya et al.*, 2002; *Novotny et al.*, 2006], merged electron – ion beam [*van der Donk et al.*, 1991] and ion storage ring [*Larsson et al.*, 1997; *Le Padellec et al.*, 1998] studies focused on this ion mainly by groups that also studied the dissociative recombination of H_3^+ with electrons.

For a long time, the theoretical predictions insisted that D_3^+ ions will recombine only very slowly with electrons [*Larsson et al.*, 2008]. Mirroring the theoretical advances in H_3^+ recombination, the inclusion of Jahn-Teller coupling mechanism led to substantial increase of the calculated recombination rate coefficients [*Pagani et al.*, 2009; *Pratt et al.*, 2011] and to good agreement with the most recent afterglow [*Dohnal et al.*, 2012c] and ion storage ring [*Le Padellec et al.*, 1998] data.

Unsurprisingly, the same disagreements between data obtained by different groups as was observed for H_3^+ recombination take place also for its fully deuterated isotopologue. In case of H_3^+ ions, some of these disagreements were resolved when *Glosik et al.* [*Glosik et al.*, 2008] discovered surprisingly fast helium assisted three body recombination process for H_3^+ ions. Me and my co-workers then focused on D_3^+ recombination using cryogenic modification of FALP technique (Cryo-FALP II) and stationary afterglow with cavity ring-down spectrometer (SA-CRDS).

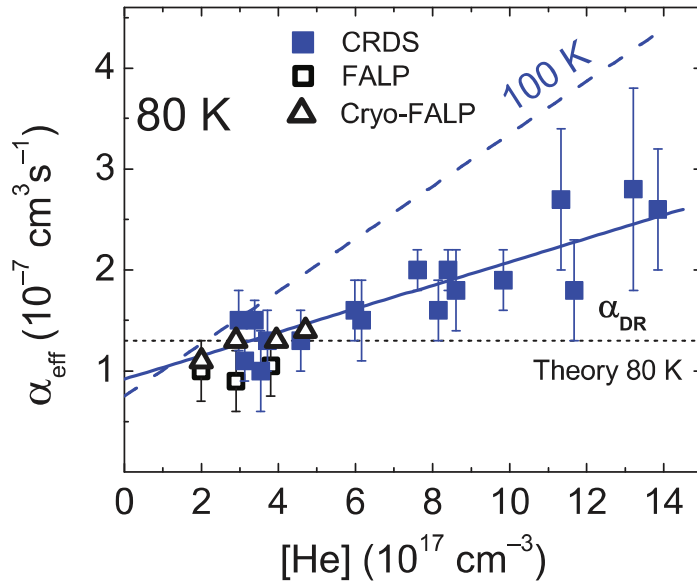


Figure 12. Adapted from ref. [Dohnal *et al.*, 2012c]. Dependence of the effective recombination rate coefficient for D_3^+ ions on helium number density at 80 K. The data were obtained in the SA-CRDS experiment (full squares) [Dohnal *et al.*, 2012c] and using various modifications of the FALP technique (triangles and open squares [Kotrík *et al.*, 2010; Dohnal *et al.*, 2012c]). The full and the dashed line are fits to the data at 80 K and 100 K, respectively. The horizontal dotted line is the theoretical prediction for binary recombination rate coefficient from ref. [Pagani *et al.*, 2009].

Our results confirmed existence of helium assisted three body recombination process with values of the ternary recombination rate coefficients comparable to those of H_3^+ [Kotrík *et al.*, 2010; Dohnal *et al.*, 2012c]. An example of the dependence of the measured effective recombination rate coefficient on helium number density obtained for D_3^+ ions at 80 K is shown in Figure 12. The value of the effective recombination rate coefficient linearly increases with increasing helium number density and its extrapolation to $[He] = 0$ is in reasonable agreement with theoretical predictions. The linear fit of the data plotted in Figure 12 ($\alpha_{\text{eff}} = \alpha_{\text{bin}} + K_{\text{He}}[He]$) yields the binary (α_{bin}) and the ternary (K_{He}) recombination rate coefficients. These are plotted in Figure 13 and Figure 14, respectively.

The measured values of the binary recombination rate coefficient for D_3^+ ions are in a good agreement with theoretical predictions by Pratt and Jungen [Pratt *et al.*,

2011] while the values calculated by Kokoouline and Greene [Pagani et al., 2009] are slightly larger than our data. According to private communication with V. Kokoouline [Kokoouline, 2012], Pratt et al. [Pratt et al., 2011] used experimental data for the Jahn-Teller coupling while in the ref. [Pagani et al., 2009] the couplings were theoretically calculated – the theoretical Jahn-Teller coupling constant is about 10% larger than the experimental one, which makes the recombination rate coefficient larger by about 20%.

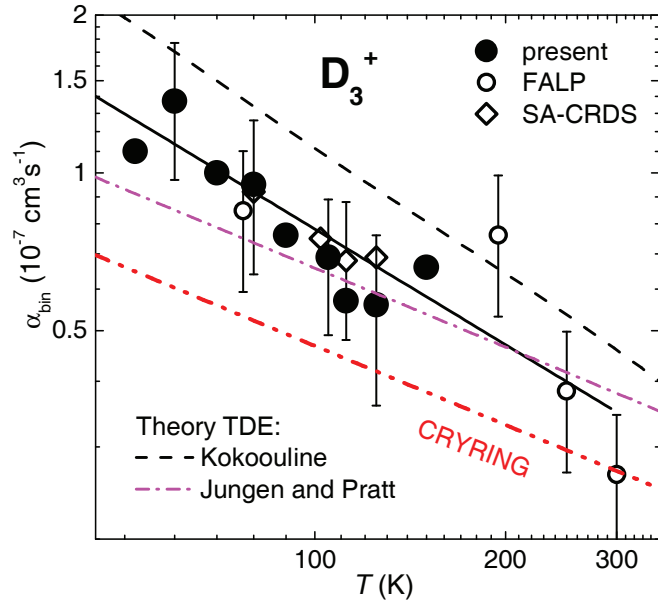


Figure 13. Adapted from ref. [Rubovič et al., 2013]. Temperature dependence of the binary recombination rate coefficients for D_3^+ ions. The values obtained in SA-CRDS (rhomboids [Dohnal et al., 2012c]) and FALP (full and open circles [Kotřík et al., 2010; Rubovič et al., 2013]) experiments are compared to the data from ion storage ring CRYRING (double-dotted-dashed line [Le Padellec et al., 1998]) and to the theoretical predictions by Kokoouline [Pagani et al., 2009] and by Pratt and Jungen [Pratt et al., 2011]. The full line is a fit to our FALP and SA-CRDS data.

Of particular note is the temperature dependence of the ternary recombination rate coefficient K_{He} for D_3^+ ions. It's value changes only very slowly between 100 K and 300 K but around 100 K drops significantly and then slowly increases with

decreasing temperature. We have not observed similar behaviour for H_3^+ ions (compare with data in Figure 7).

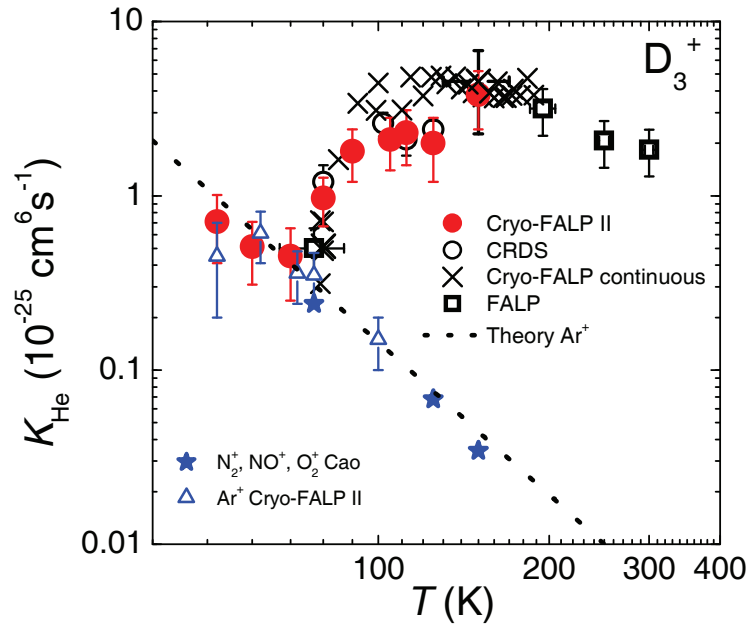


Figure 14. Adapted from ref. [Johnsen *et al.*, 2013]. Dependence of the ternary recombination rate coefficients for D_3^+ ions in helium on temperature. The data were obtained in our SA-CRDS (open circles, [Dohnal *et al.*, 2012c]) and FALP experiments (full circles, squares, crosses, see ref. [Kotrík *et al.*, 2010] and references therein). The triangles denote values of ternary recombination rate coefficient measured for Ar^+ ions in helium [Dohnal *et al.*, 2013], while the stars are ternary recombination rate coefficients reported by Cao *et al.* [Cao *et al.*, 1991] for a mixture of atmospheric ions in helium. Theoretical value scaled for Ar^+ ions in helium [Bates *et al.*, 1965] is plotted as dotted line.

Recombination of N_2H^+ with electrons

N_2H^+ is one of the key ions in the chemistry of interstellar medium and has been observed in a variety of environments such as translucent and dark clouds, protoplanetary disks or protostellar cores and it is used as a tracer for N_2 in dark clouds [Turner *et al.*, 1974; Turner *et al.*, 1995; Caselli *et al.*, 2002; Anderson *et al.*, 2019]. N_2H^+ is also supposed to play a role in chemistry of Titan's atmosphere [Vuitton *et al.*, 2007].

The main production pathway for N_2H^+ ions in interstellar medium is proton transfer in reaction of H_3^+ with N_2 while it is mainly destroyed in collisions with electrons (dissociative recombination) or CO molecules (proton transfer reaction).

Owing to its importance to interstellar chemistry, the dissociative recombination of N_2H^+ ions with electrons has been studied for over 40 years [Larsson *et al.*, 2008] with the results of various theoretical and experimental studies differing by almost an order of magnitude. The early merged beam study by Mul and McGowan [Mul *et al.*, 1979a] reported value of recombination rate coefficient for N_2H^+ ions at 300 K to be $\alpha = 7.5 \times 10^{-7} \text{ cm}^3 \text{ s}^{-1}$ but this value should be probably divided by two due to calibration error [Larsson *et al.*, 2008]. Flowing Afterglow with Langmuir Probe (FALP) experiments obtained values ranging from $1.7 \times 10^{-7} \text{ cm}^3 \text{ s}^{-1}$ to $2.8 \times 10^{-7} \text{ cm}^3 \text{ s}^{-1}$ at 300 K [Smith *et al.*, 1984; Adams *et al.*, 1984; Smith *et al.*, 1993; Rosati *et al.*, 2004; Poterya *et al.*, 2005] while the ion storage ring CRYRING first reported the value of recombination rate coefficient at 300 K to be $1.0 \times 10^{-7} \text{ cm}^3 \text{ s}^{-1}$ [Geppert *et al.*, 2004] later refined upwards to $2.7 \times 10^{-7} \text{ cm}^3 \text{ s}^{-1}$ [Vigren *et al.*, 2012]. At lower temperatures, relevant for astrochemistry, the FALP and ion storage ring data differ by a factor of two or more. It can be expected that the rotational and vibrational populations of N_2H^+ ions in FALP experiments were in accordance with thermal equilibrium at given temperature. The rotational temperature of ions in ion storage ring was probably 300 K or higher [Pettrignani *et al.*, 2011]. The only experiment with in situ identification of recombining ions was performed by Amano [Amano, 1990] using absorption spectroscopy with $\alpha = 7 \times 10^{-7} \text{ cm}^3 \text{ s}^{-1}$ at 273 K, a value substantially higher than in other mentioned studies.

Only few theoretical studies focused on dissociative recombination of N_2H^+ ions with electrons. The direct process of dissociative recombination is highly inefficient at low energies as shown by Talbi [Talbi, 2007] and by Hickman et al. [Hickman et al., 2011]. The indirect process was studied by Fonseca dos Santos et al. [Fonseca dos Santos et al., 2014; Fonseca dos Santos et al., 2016] but their results are by up to factor of two lower than the FALP or ion storage ring results and by almost order of magnitude lower than the results of Amano's experiment [Amano, 1990].

To resolve these discrepancies, I opted to utilize the SA-CRDS setup to probe the time evolutions of number densities of several rovibrational states of N_2H^+ ions in recombination dominated afterglow plasma to ensure that the studied ions are rotationally and vibrationally cold and the measured quantity is really thermal recombination rate coefficient.

In contrast to our previous studies on recombination of isotopomers of H_3^+ with electrons, where usable transitions were known, in case of N_2H^+ we had to find the transitions originating from the low laying rotational states in the ground and the first excited vibrational state of N_2H^+ ions. The corresponding spectroscopic study is described in ref. [Kálosi et al., 2017]. Another complication has arisen due to the higher mass of N_2H^+ ion with respect to H_3^+ resulting in lower Doppler broadening and thus relatively more pronounced effect of collisional broadening. This had to be taken into account especially at higher buffer gas pressures used to estimate the influence of third bodies on measured recombination rate coefficient.

An example of measured time evolutions of number densities of several rotational states of N_2H^+ ions in the ground vibrational state is shown in Figure 15. As can be seen from Figure 15, the relative populations of different states of N_2H^+ are constant in afterglow plasma and are very close to those expected for thermal population of states. A similar picture was observed also for the first vibrationally excited state of $\text{N}_2\text{H}^+(v_1 = 0, v_2 = 1, v_3=0)$ with the average vibrational temperature slightly higher than the kinetic temperature of the ion T_{kin} . For details see ref. [Shapko et al., 2020]. It can be thus safely assumed that the measured recombination rate coefficients correspond to N_2H^+ ions with thermal populations of rotational and vibrational states.

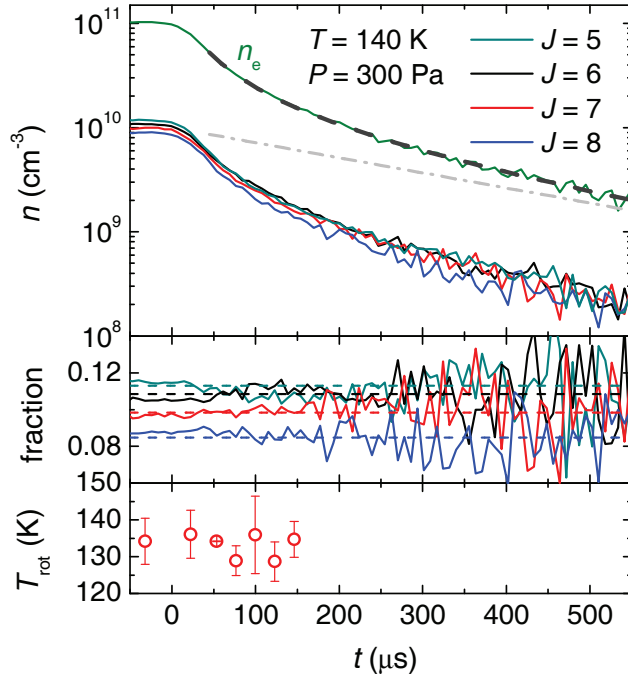
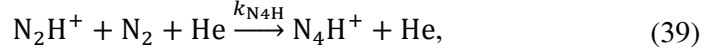


Figure 15. Adapted from ref. [Shapko *et al.*, 2020]. Upper panel: Measured time evolution of number densities of several rotational states of $\text{N}_2\text{H}^+(v_1 = 0, v_2 = 0, v_3=0)$ at 140 K, $T_{\text{kin}} = 139 \pm 6$ K, $[\text{He}] = 1.5 \times 10^{17} \text{ cm}^{-3}$, $[\text{Ar}] = 2.5 \times 10^{14} \text{ cm}^{-3}$, $[\text{H}_2] = 5 \times 10^{14} \text{ cm}^{-3}$ and $[\text{N}_2] = 4 \times 10^{13} \text{ cm}^{-3}$. The electron number density, not measured in presented experiments, was calculated from the ion number densities under assumption of quasineutrality of plasma and thermal population of states. Middle panel: Time evolution of relative populations of rotational states from upper panel. Thermal populations of states are denoted by dashed lines. Lower panel: Time evolution of rotational temperature of the N_2H^+ ions in discharge and afterglow plasma.

As is the case in every experiment reported in this thesis, prior the actual measurement we employed a model of chemical kinetics to ascertain the best conditions for planned experiment. For example, at high number densities of nitrogen reactant gas the N_4H^+ ions can be formed in three body association reaction of N_2H^+ ions with N_2 and He:



where $k_{\text{N}_4\text{H}} = 2.8 \times 10^{-29} \text{ cm}^3 \text{ s}^{-1}$ as measured at 80 K in SIFT experiment [Adams *et al.*, 1984]. Reaction (39) gives upper limit for number densities of helium and nitrogen that can be used in the experiment. This is demonstrated in Figure 16 where the measured effective recombination rate coefficient increases with increasing number density of N_2 in accordance with the prediction of the model of chemical kinetics. Note that the electron number density was not measured in these experiments. As other ions than N_2^+ are produced in the afterglow, the data evaluation procedure (see section on data analysis, equation (29)), that assumes $[\text{N}_2^+] = n_e$, gives proportionally higher value of the effective recombination rate coefficient.

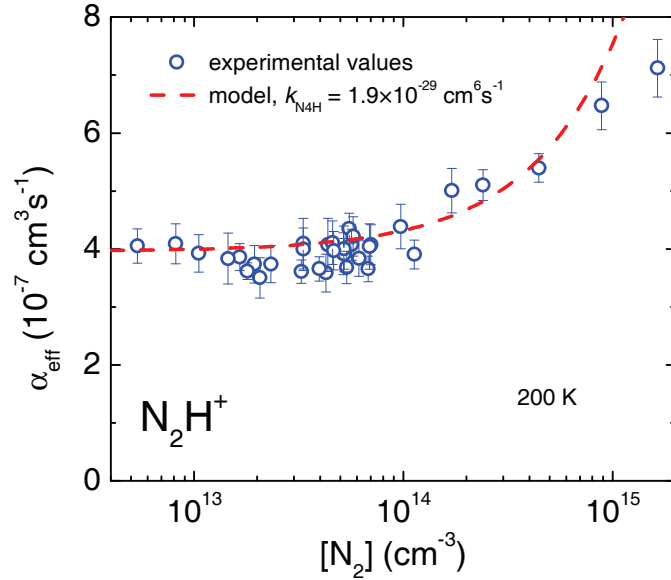


Figure 16. Adapted from ref. [Shapko *et al.*, 2020]. The dependence of the measured effective recombination rate coefficient on number density of molecular nitrogen at $T = 200 \pm 5 \text{ K}$, $[\text{He}] = (1 - 5) \times 10^{17} \text{ cm}^{-3}$, $[\text{H}_2] = (3 - 7) \times 10^{14} \text{ cm}^{-3}$, $[\text{Ar}] \approx 5 \times 10^{14} \text{ cm}^{-3}$. The dashed line denotes recombination rate coefficients obtained from the model of chemical kinetics (for details see ref. [Shapko *et al.*, 2020]).

We have seen no dependence of the measured effective recombination rate coefficient on number density of hydrogen or helium. As N_2H^+ recombines with electrons via indirect mechanism of dissociative recombination [Fonseca dos Santos *et al.*, 2014] we were interested if the ternary recombination rate coefficients for helium assisted recombination of N_2H^+ ions with electrons will be of similar magnitude as those for H_3^+ ions (and its deuterated isotopologues). As we have seen no dependence of the measured effective recombination rate coefficient on helium number density, we were only able to estimate an upper limit for N_2H^+ ternary recombination rate coefficient.

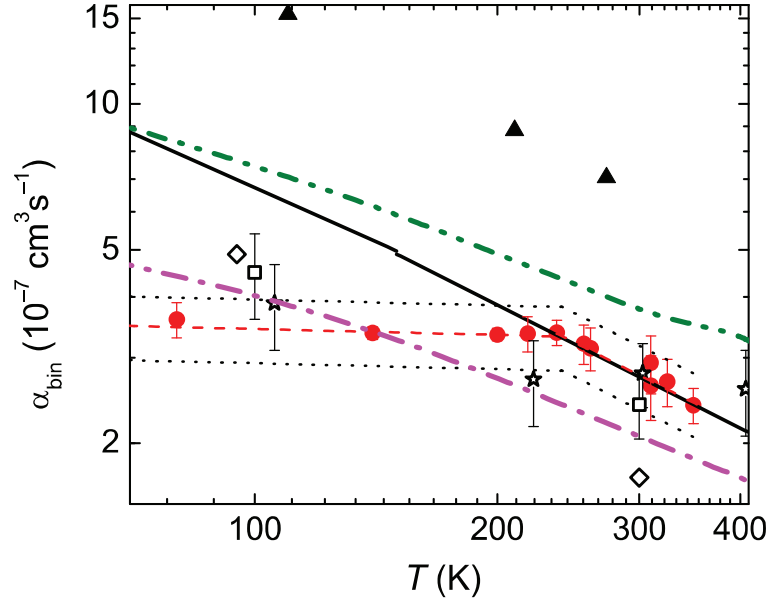


Figure 17. Adapted from ref. [Shapko *et al.*, 2020]. The dependence of the measured recombination rate coefficient for N_2H^+ on temperature. The data were obtained in helium buffer gas with exception of the value at 350 K that was measured in hydrogen buffer gas. The recombination rate coefficients obtained in previous experiments are shown as rhomboids [Adams *et al.*, 1984], squares [Smith *et al.*, 1993], stars [Poterya *et al.*, 2005], triangles [Amano, 1990], double-dot-dashed line [Mul *et al.*, 1979a] and full line [Vigren *et al.*, 2012], respectively. Recent quantum mechanical predictions are plotted as dotted-dashed line [Fonseca dos Santos *et al.*, 2016]. The estimated systematic error of our data is denoted by dotted lines.

The obtained values of binary recombination rate coefficients for N_2H^+ ions are plotted in Figure 17 together with the data from experiments of other groups [Mul *et al.*, 1979a; Adams *et al.*, 1984; Amano, 1990; Smith *et al.*, 1993; Poterya *et al.*, 2005; Vigren *et al.*, 2012] and theoretical predictions [Fonseca dos Santos *et al.*, 2016].

As can be seen from Figure 17, there is a very good agreement between the values obtained in our SA-CRDS experiment [Shapko *et al.*, 2020] (full circles) and those from ion storage ring CRYRING [Vigren *et al.*, 2012] (full line) at 300 K but around 100 K the CRYRING values are by more than factor of two higher than the SA-CRDS data. Here it is necessary to point out one of the differences between these two experiments. In our case, the ionic rotational and vibrational populations are very close to the buffer gas temperature, in ion storage ring, the ion rotational temperature was probably 300 K [Petrignani *et al.*, 2011] even at low collisional energies. The difference between our thermal recombination rate coefficients and those from the CRYRING experiment could be an indication of higher reactivity of rotationally excited states with respect to the lower lying states. A similar effect was recently observed in recombination of HeH^+ ions with electrons [Novotny *et al.*, 2019].

Recombination of N_2^+ ions with electrons – dependence on vibrational excitation

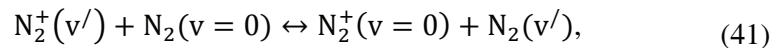
The abilities of the Cryo-SA-CRDS setup are nicely demonstrated in our recent experiments focused on recombination of N_2^+ ions with electrons.

Molecular nitrogen is the most abundant gas in the atmosphere of the Earth and also important component of atmospheres of other large objects in solar system [Elliot *et al.*, 2000; Krasnopolsky, 2014; Krasnopolsky, 2020]. It is considered to be prevalent in ices on surfaces of trans-Neptunian objects [Young *et al.*, 2020]. This results in N_2^+ being one of the main ions in the Earth atmosphere [Min *et al.*, 2022] and in atmospheres of other solar system bodies such as Titan [Lammer *et al.*, 2020] and Triton [Yung *et al.*, 1990].

The dissociative recombination of N_2^+ ions with electrons,

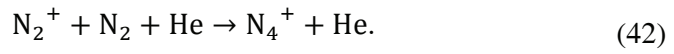


is an important process in modelling of planetary ionospheres [Fox *et al.*, 1985; Sheehan *et al.*, 2004; Fox, 2005] and as such has been studied for more than 70 years both theoretically and experimentally [Sheehan *et al.*, 2004; Larsson *et al.*, 2008]. The recombination rate coefficients obtained in afterglow studies [Kasner *et al.*, 1965; Mehr *et al.*, 1969; Zipf, 1980; Mahdavi *et al.*, 1971; Canosa *et al.*, 1991; Geoghegan *et al.*, 1991] were limited to the temperatures of 300 K or higher with values in the range of $1.8 - 2.9 \times 10^{-7} \text{ cm}^3 \text{ s}^{-1}$. A particular issue was observed by Zipf [Zipf *et al.*, 1980] in his stationary afterglow experiment who reported that only 87 % of N_2^+ ions were in their ground vibrational state the rest populating mainly $v = 1$ and $v = 2$ states. Johnsen [Johnsen, 1987] and later Bates and Mitchell [Bates *et al.*, 1991] pointed out that at conditions present in Zipf's experiment a strong resonant charge transfer process between N_2^+ ions and nitrogen molecules will take place:



resulting in high vibrational temperature of the N_2^+ ions. Bates' reanalysis of these data also indicated that the value of the recombination rate coefficient for higher vibrational states should be lower than for the ground state [*Bates et al.*, 1991].

The results of the flowing afterglow studies [*Mahdavi et al.*, 1971; *Canosa et al.*, 1991; *Geoghegan et al.*, 1991], although performed without identification of the vibrational state of the recombining ions, are likely pertaining to the ground vibrational state due to way how the ions are prepared in such experiments. Nevertheless, these studies were limited to 300 K partially because of fast formation of N_4^+ ions in three body association reaction of N_2^+ with helium and N_2 at low temperatures:



The value of the rate coefficient for reaction (42) is higher than $2 \times 10^{-29} \text{ cm}^3 \text{ s}^{-1}$ at 300 K [*Anicich et al.*, 2000].

Mul et al. [*Mul et al.*, 1979b] obtained in their merged electron – ion beam experiment value of the recombination rate coefficient $\alpha_{N_2^+} = 3.6 \times 10^{-7} (T_e/300)^{-0.5} \text{ cm}^3 \text{ s}^{-1}$ valid for electron temperatures in the range of 100 – 20 000 K (according to discussion in ref. [*Larsson et al.*, 2008] this value should be divided by a factor of two due to calibration error). Later merged electron – ion beam study by Noren et al. [*Noren et al.*, 1989] reported for vibrationally cold ions a substantially lower value of $\alpha_{N_2^+} = 0.4 \times 10^{-7} \text{ cm}^3 \text{ s}^{-1}$ at 300 K and the value of the measured recombination coefficient increased with increasing vibrational excitation.

Ion storage ring experiment CRYRING [*Peterson et al.*, 1998] and another merged electron – ion beam study by Sheehan et al. [*Sheehan et al.*, 2004] reported practically identical cross sections in a broad energy range with inferred values of the recombination rate coefficient at 300 K of $1.75 \times 10^{-7} \text{ cm}^3 \text{ s}^{-1}$ and $1.50 \times 10^{-7} \text{ cm}^3 \text{ s}^{-1}$, respectively. The vibrational populations of recombining ions reported by Peterson et al. [*Peterson et al.*, 1998] were 46% percent of all N_2^+ ions in the $v = 0$ state, 27% in $v = 1$, 10% in $v = 2$, and 16% in $v = 3$ state.

There are no experimental data on recombination of vibrationally cold N_2^+ ions with electrons for temperatures below 300 K.

Guberman extensively studied the collisions of N_2^+ ions with electrons using multichannel quantum defect theory [Guberman, 1991; Guberman, 2012; Guberman, 2014]. He predicted that at high temperatures the $v = 0$ state will recombine with electrons substantially faster than the vibrationally excited states. At 300 K the ratio between the recombination rate coefficients for $v = 0$ and $v = 1$ states is less than 1.5 and decreases with decreasing temperature.

Little [Little *et al.*, 2014] calculated the recombination rate coefficients for different vibrational states of N_2^+ using R matrix theory. His approach was recently refined by Abdoulanziz [Abdoulanziz *et al.*, 2021] who included in the calculation higher kinetic energies of incoming electrons and more vibrational levels of the target molecular ion. These calculations were in agreement with Guberman's predictions [Guberman, 2014] that the recombination process is more effective for $v = 0$ state of N_2^+ than for $v = 1$ state. On the other hand, the calculated ratio between the recombination rate coefficients for $v = 0$ and $v = 1$ states is more than 4 and does not significantly decrease with decreasing temperature. The actual value of the $v = 0$ recombination rate coefficient at 300 K predicted by Abdoulanziz *et al.* [Abdoulanziz *et al.*, 2021] is higher than that of Guberman [Guberman 2014], while the value for $v = 1$ state is substantially lower.

Based on this lengthy overview, it is clear that in order to obtain the recombination rate coefficient for N_2^+ ions in the ground vibrational state in an afterglow study, several conditions have to be fulfilled: 1) It is necessary to probe in situ the rotational and vibrational populations of the recombining ions to ensure that majority of the N_2^+ ions are in the $v = 0$ state. 2) Used experimental technique together with data analysis have to be able to provide reliable recombination rate coefficients even at conditions when N_2^+ ion will not be dominant ions in the afterglow due to formation of N_4^+ ions at low temperatures.

We addressed the first point by using cavity ring-down spectroscopy to probe the number densities of different rovibrational states of N_2^+ utilizing transitions originating in the ground and the first excited vibrational state ($X^2\Sigma_g^+(v = 0) - A^2\Pi_u(v = 2)$ and $X^2\Sigma_g^+(v = 1) - A^2\Pi_u(v = 3)$) around 785 nm and 812 nm, respectively. Our results have shown that within the error of the measurement the rotational temperature of N_2^+ ions was very close to the wall temperature. Less than

1.5 % of all N_2^+ ions were in the $v = 1$ state ensuring that the measured results were pertaining to the ground vibrational state.

For the second point, the simultaneous measurement of time evolutions of N_2^+ and electron number densities enabled us to determine the recombination rate coefficients for N_2^+ (for more details on recombination rate coefficient determination at conditions when the studied ions are not dominant in afterglow plasma see discussion in Data analysis section of this thesis). An example of measured data is shown in Figure 18. The data were fitted by equation (35).

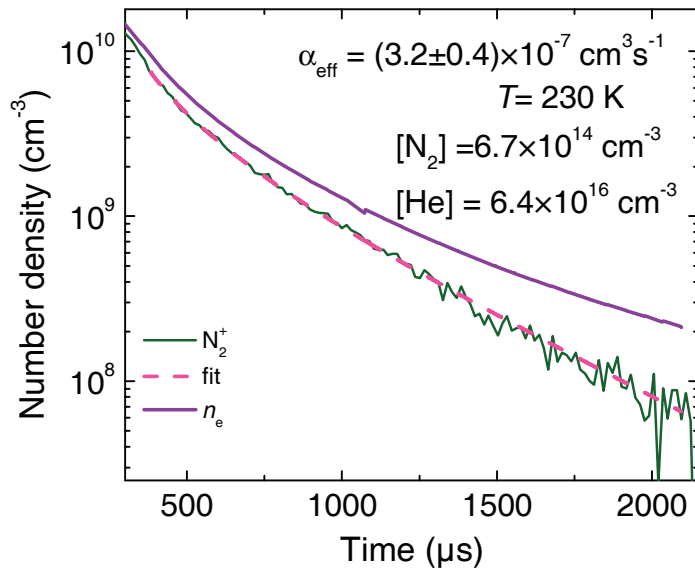


Figure 18. Adapted from ref. [Uvarova *et al.*, 2022]. Time evolutions of measured electron and N_2^+ number densities in afterglow plasma at 230 K, $[He] = 6.4 \times 10^{16} \text{ cm}^3 \text{ s}^{-1}$ and $[N_2] = 6.7 \times 10^{14} \text{ cm}^3 \text{ s}^{-1}$. The dashed line is fit to the data using equation (35). The N_2^+ number density was calculated under assumption of thermal population of states from the absorption at the centre of the $Q_{22}(9.5)$ line of the $^2\Sigma_g^+ - ^2\Pi_u(0 - 2)$ Meinel band of N_2^+ .

Similar data sets as in Figure 18 were obtained for different number densities of helium and nitrogen in the temperature range of 140 – 250 K. The resulting recombination rate coefficients are plotted in Figure 19 together with values obtained in previous studies. Of particular interest is the comparison to experiments in which

the actual vibrational population of recombining ions was probed. The ion storage ring study by Peterson et al. [Peterson et al., 1998] reported that more than half of the N_2^+ ions were in excited vibrational states with the corresponding recombination rate coefficient of about half of our value. The values of the recombination rate coefficient for N_2^+ ions obtained in stationary afterglow experiment by Zipf [Zipf, 1988], with 13 % of N_2^+ ions in excited vibrational states, are between those measured by us and by Petersen et al. [Peterson et al., 1998]. Based on these data we estimated that the recombination rate coefficient for N_2^+ ions in $v = 1$ state at 250 K is $\alpha_{N_2+(v=1)} = (4 \pm 4) \times 10^{-8} \text{ cm}^3 \text{ s}^{-1}$. For more details see ref. [Uvarova et al., 2022].

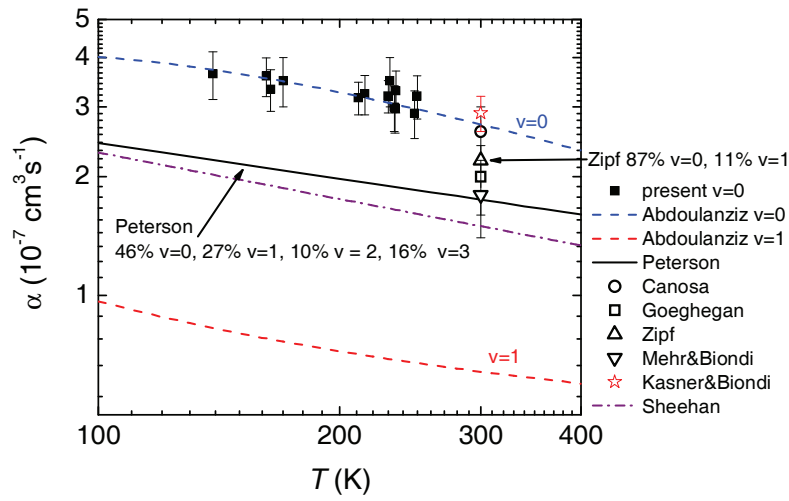


Figure 19. Adapted from ref. [Uvarova et al., 2022]. Dependence of the binary recombination rate coefficient for N_2^+ ions on temperature. The values from the Cryo-SA-CRDS experiment (full squares [Uvarova et al., 2022]) are compared to the data obtained in previous experimental [Kasner et al., 1965; Mehr et al., 1969; Zipf, 1988; Canosa et al., 1991; Goeghan et al., 1991; Peterson et al., 1998; Sheehan et al., 2004] and theoretical [Abdoulanziz et al., 2021] studies.

Both the measured recombination rate coefficient for the vibrational ground state and the estimated value for $v = 1$ state are in a very good agreement with the most recent quantum mechanical calculations by Abdoulanziz et al. [Abdoulanziz et al., 2021].

Dissociative recombination of N_2^+ ions with electrons is a nice example that the measured value of recombination rate coefficient can profoundly depend on the internal excitation of recombining ions.

Selected experiments in 22-pole radiofrequency ion trap

The 22-pole radiofrequency ion trap technique was developed by Dieter Gerlich in the late 20th century [Gerlich, 1992] and was successfully utilized for determination of reaction rate coefficients for temperatures ranging from room temperature down to below 10 K [Gerlich, 1995; Gerlich *et al.*, 2011; Plašil *et al.*, 2011; Zymak *et al.*, 2013; Kumar *et al.*, 2018; Plašil *et al.*, 2021].

I was lucky to work with late Dieter Gerlich during my stay in Chemnitz, Germany and then in Prague. He was a unique person both on professional and personal level.

The description of the 22-pole radiofrequency ion trap apparatus at the Department of surface and plasma science, Faculty of Mathematics and Physics of Charles University can be found e. g. in ref. [Zymak *et al.*, 2013] so only short summary will be given here. The ions are produced in a storage ion source (SIS) by electron bombardment then mass selected by passing through quadrupole mass spectrometer (QMS) and guided by ion optics to the 22-pole ion trap. After set time the trapped ions are released and after mass selection in second QMS detected using multichannel plate detector (MCP). The trap itself is connected to cold-head of a closed cycle helium refrigerator enabling operation in the range of 10 – 300 K.

The trapped ions cooled by collisions with buffer gas (usually helium) can react with added reactant gas. Reaction rate coefficients for ion – molecule reactions and product branching ratios can be determined.

I have participated on several studies involving this apparatus [Plašil *et al.*, 2011; Plašil *et al.*, 2017; Kovalenko *et al.*, 2018; Tran *et al.*, 2018; Roučka *et al.*, 2018; Rednyk *et al.*, 2019; Rednyk *et al.*, 2021; Kovalenko *et al.*, 2021; Plašil *et al.*, 2021] but I have decided to focus here on some advanced abilities of the 22-pole ion trap setup, namely to probe the internal excitation of trapped ions and to study isomer specific reaction rate coefficients and branching ratios.

The radiofrequency traps have been utilized for molecular spectroscopy for almost twenty years using schemes like laser induced reactions [Schlemmer *et al.*, 1999], laser inhibited cluster growth [Savic *et al.*, 2015] and others [Roithová *et al.*, 2019].

In our case we followed approach in ref. [Otto *et al.*, 2012] to determine the rotational temperature of OH⁻ ions in the trap using photodetachment spectroscopy. Light from a diode laser passed through 22-pole ion trap and the wavelength dependent rate of the decay of OH⁻ ions (proportional to the photodetachment cross section) was observed. An example of measured data is shown in Figure 20. The sudden increases of the photodetachment rate correspond to threshold energies for photodetachment from various rotational states of OH⁻ ions.

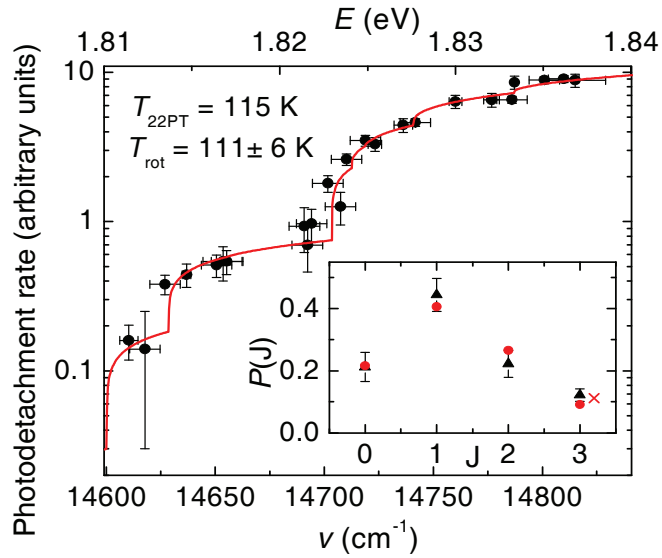


Figure 20. Adapted from ref. [Plašil *et al.*, 2022]. Photodetachment rate at trap temperature $T_{22PT} = 115$ K and $[\text{He}] = 5.5 \times 10^{13} \text{ cm}^{-3}$. The obtained rotational temperature is $T_{\text{rot}} = 111 \pm 6$ K. The full line denotes the fit of the data under assumption of the thermal population of states with temperature as a free parameter **Insert:** The relative populations of the lowest rotational states of OH⁻ anion (triangles) determined from the plotted data with the populations of rotational states up to $J = 3$ as free parameters. The circles denote the calculated thermal populations at 115 K. The value measured for $J = 3$ is given by indistinguishable contributions from states with $J = 3, 4,$ and 5 (because of the position of the corresponding photodetachment thresholds and probed wavelength range). The cross denotes the sum of the calculated relative thermal populations of these states.

The analysis of the data like those plotted in Figure 20 enables not only the calculation of the rotational temperature of trapped ions but also determination of actual populations of corresponding rotational states (see insert in Figure 20). We have shown [Uvarova *et al.*, 2021; Plašil *et al.*, 2022] that for rotational temperature measurement as few as five or six data points are sufficient. These experiments enabled us to prove that the rotational population of the ions reacting in the trap is in accordance with thermal equilibrium at given temperature in the range of 50 – 200 K. For reliable rate coefficients determination it is crucial to ensure that the reacting ions are in a well-defined state.

The second experiment, I would like to focus on, was in fact not performed in Prague but during my stay at MPE in Garching, Germany. The experimental setup is similar to that in Prague experiments differing slightly in construction of the 22-pole trap itself and in detection system (Daly detector instead of MCP). The data acquisition is based on mass selection using QMS that is not sensitive enough to distinguish between two isomers (HCN^+ and HNC^+ in this case) but can be utilized, using clever scheme, to determine the reaction rate coefficients for these ions.

A mixture of $\text{HCN}^+/\text{HNC}^+$ ions was prepared in storage ion source from acetonitrile or $\text{BrCN}/\text{H}_2\text{O}$ precursors, then mass selected and trapped in the 22-pole radiofrequency ion trap. The actual ionic composition was monitored by reactions with SF_6 or O_2 that have different products for HCN^+ or HNC^+ [Petrie *et al.*, 1990]. The trapped ions then reacted with added H_2 gas and the reaction products were, after set trapping time, analysed by detection system consisting of QMS and Daly detector. Approximately 90 % of the trapped ions corresponding to mass 27 Dalton were HCN^+ . To transform the HCN^+ to its low energy isomer HNC^+ we utilized the isomerisation reaction with CO_2 that was added to the trap [Hansel *et al.*, 1998] resulting in more than 90 % of ions at mass 27 Dalton being HNC^+ .

The rate coefficients for reaction of HCN^+ with H_2 were obtained in the temperature range of 17 – 250 K and were close to Langevin reaction rate. The rate coefficients for the reaction of HNC^+ with H_2 were measured in the temperature range of 70 – 250 K (limited by freeze out of CO_2) and increased with decreasing temperature from half of Langevin reaction rate coefficient at 250 K to slightly below Langevin rate at 70 K. for both ions the product of the reaction is HCNH^+ .

Similar approach was used for the determination of the reaction rate coefficient for the reaction of CN^+ ions with H_2 and its product branching ratios. The CN^+ ions produced in the storage ion source from $\text{BrCN}/\text{H}_2\text{O}$ were mass selected and trapped in the 22-pole radiofrequency ion trap. A short pulse of helium with H_2 admixture resulted in production of HCN^+ and HNC^+ at the beginning of the trapping period. The reaction of the produced HCN^+ and HNC^+ with SF_6 was utilized to determine the product branching ratios. The reaction rate coefficient for reaction of CN^+ with H_2 was determined in the range of 17 – 250 K, while the branching ratios were measured only for temperatures above 90 K (due to freeze out of SF_6).

The results are summarized in Figure 21 and are prepared for publication.

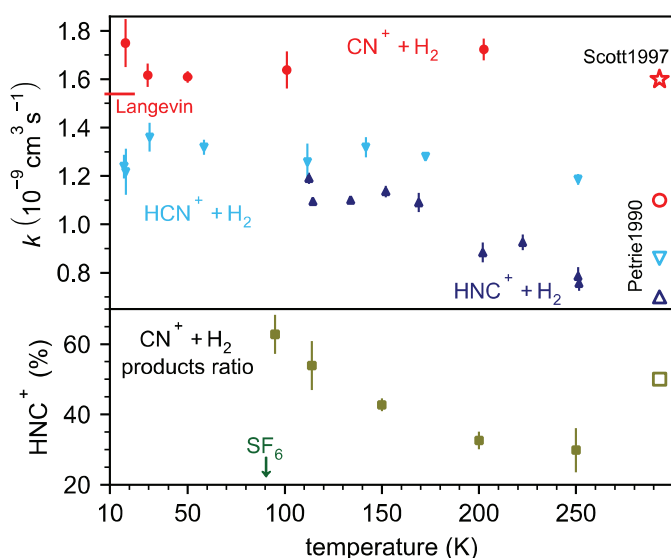


Figure 21. Adapted from ref. [Dohnal *et al.*, 2022]. Reaction rate coefficients for reactions of CN^+ (red), HCN^+ (cyan) and HNC^+ (dark blue) ions with H_2 (top) and branching ratio for the $\text{CN}^+ + \text{H}_2$ reaction (bottom). Open symbols denote values from previous studies (star [Scott *et al.*, 1997], the rest from ref. [Petrie *et al.*, 1991]). The Langevin reaction rate coefficient for reaction of CN^+ ions with H_2 is $1.54 \times 10^{-9} \text{ cm}^3 \text{ s}^{-1}$. Green down arrow points to the freezeout temperature of SF_6 that was used for branching ratio determination.

Conclusions

This thesis summarized years of studies of recombination of atomic and molecular ions with electrons performed in afterglow plasma using several experimental techniques. I focused on the influence of collisions with third bodies on the recombination process and on the possible different reactivity of different quantum states of ions.

I gradually realized that in order to obtain reliable recombination rate coefficients it is necessary to characterize in detail the recombining ions – their internal excitation – and also the environment in which the recombination takes place. This is of course very time consuming – it took approximately two years to obtain data on N_2H^+ recombination with electrons [Shapko *et al.*, 2020]. The determination of H_2D^+ and HD_2^+ [Dohnal *et al.*, 2016; Plašil *et al.*, 2017] recombination rate coefficients was even more demanding. But it is a necessary sacrifice as otherwise we would be blind to possible effects of for example vibrational excitation of recombining ions as was the case in many previous experiments on N_2^+ recombination [Uvarova *et al.*, 2022].

This meticulous approach to recombination studies is supported by advances in instrumentation. After several low temperature FALP modifications, we developed a cryogenic stationary afterglow apparatus (Cryo-SA-CRDS) enabling recombination studies in the range of 30 – 300 K with different diagnostic techniques [Plašil *et al.*, 2018; Shapko *et al.*, 2021].

We are now in a unique position. Our present experimental equipment and years of experience in recombination studies are coming to fruit as now we are able to study recombination of a large scale of ions not limited by the necessity of them being dominant species in afterglow plasma and with resolution of particular quantum states (see discussion in section on N_2^+ recombination and in refs. [Shapko *et al.*, 2021; Uvarova *et al.*, 2022]).

As stated in a famous misquote of Shakespeare, the future is the undiscovered country.

References

- Abdoulanziz A., Argentin C., Laporta V., Chakrabarti K., Bultel A., Tennyson J., Schneider I. F., Mezei J. Zs.: *J. Appl. Phys.* **129**, 053303, 2021.
- Adams N. G., Smith D., Alge E.: *J. Chem. Phys.* **81**, 1778, 1984.
- Adams N. G., Smith D.: in *Dissociative Recombination, Theory, Experiment and Application*, ed. by J. B. A. Mitchell, S. L. Guberman, World Scientific, Singapore, 29, 1989.
- Albertsson T., Semenov D. A., Vasyunin A. I., Henning T. Herbst E.: *Astrophys. J. Suppl. Ser.* **207**, 27, 2013.
- Albertsson T., Indriolo N., Kreckel H., Semenov D., Crabtree K. N., Henning T.: *Astrophys. J.* **787**, 44, 2014.
- Amano T.: *J. Chem. Phys.* **92**, 6492, 1990.
- Anderson D. Z., Frisch J. C., Masser C. S.: *Appl. Opt.* **23**, 1238, 1984.
- Anderson D. E., Blake G. A., Bergin E. A., Zhang K., Carpenter J. M., Schwartz K. R., Huang J., Oberg K. I.: *Astrophys. J.* **881**, 127, 2019.
- Anicich V. G., Milligan D. B., Fairley D. A., McEwan M. J.: *Icarus* **146**, 118-124, 2000.
- Auerbach D., Cacak R., Caudano R., Gaily T. D., Keyser C. J., McGowan J. W., Mitchell J. B. A., Wilk S. F. J.: *J. Phys. B* **10**, 3797, 1977.
- Bannasch G., Pohl T.: *Phys. Rev. A* **84**, 052710, 2011.
- Bates D. R., Massey H. S. W.: *Proc. Roy. Soc. A* **192**, 1, 1947.
- Bates D. R.: *Phys. Rev.* **78**, 492, 1950.
- Bates D. R., Kingston A. E., McWhirter R. W. P.: *Proc. R. Soc. A* **267**, 297, 1962.
- Bates D. R., Khare S. P.: *Proc. Phys. Soc.* **85**, 231, 1965.
- Bates D. R., Mitchell J. B. A.: *Planet. Space. Sci.* **39**, 1297, 1991.
- Beer A.: *Annalen der Physik und Chemie* **86**, 78, 1852.

- Berden G., Engeln R. (editors): *Cavity Ring-Down Spectroscopy: Techniques and Applications*. Wiley-Blackwell, 2009.
- Berlande J., Cheret M., Deloche R., Gonfalone A., Manus C.: *Phys. Rev. A* **1**, 887, 1970.
- Bernath P. F.: *Spectra of Atoms and Molecules*. Oxford University Press, Oxford, 2005.
- Biondi M. A., Brown S. C.: *Phys. Rev.* **75**, 1700, 1949a.
- Biondi M. A., Brown S. C.: *Phys. Rev.* **76**, 1697, 1949b.
- Brown S. C., Rose D. J.: *J. Appl. Phys.* **23**, 711, 1952.
- Canosa A., Gomet J. C., Rowe B. R., Queffelec J. L.: *J. Chem. Phys.* **94**, 7150, 1991.
- Canosa A., Gomet J. C., Rowe B. R., Mitchell J. B. A., Queffelec J. L., *J. Chem. Phys.* **97**, 1028, 1992.
- Cao Y. S., Johnsen R.: *J. Chem. Phys.* **94**, 5443, 1991.
- Caselli P., Walmsley C. M., Zucconi A., Tafalla M., Dore L., Myers P. C.: *Astrophys. J.* **565**, 344, 2002.
- Curry B. P.: *Phys. Rev. A* **1**, 166, 1970.
- Das A., Majumdar L., Chakrabarti S. K., Sahu D.: *New Astron.* **35**, 53, 2015.
- Datz S., Larsson M., Stromholm C., Sundstrom H., Zengin V., Danared H., Kallberg A., Ugglas M.: *Phys. Rev. A* **52**, 2901, 1995.
- Deloche R., Monchicourt P., Cheret M., Lambert F.: *Phys. Rev. A* **13**, 1140, 1976.
- Dohnal P., Hejduk M., Varju J., Rubovič P., Roučka Š., Kotrík T., Plašil R., Glosík J., Johnsen R.: *J. Chem. Phys.* **136**, 244304, 2012a.
- Dohnal P., Hejduk M., Varju J., Rubovič P., Roučka Š., Kotrík T., Plašil R., Johnsen R., Glosík J.: *Philos. Trans. R. Soc. A – Math. Phys. Eng. Sci.* **370**, 5101, 2012b.
- Dohnal P., Hejduk M., Rubovič P., Varju J., Roučka Š., Plašil R., Glosík J.: *J. Chem. Phys.* **137**, 194320, 2012c.

- Dohnal P.: *Ph.D. Thesis*, Charles University, Prague, 2013.
- Dohnal P., Rubovič P., Kotrík T., Hejduk M., Plašil R., Johnsen R., Glosík J.: *Phys. Rev. A* **87**, 052716, 2013.
- Dohnal P., Rubovič P., Kálosi Á., Hejduk M., Plašil R., Johnsen R., Glosík J.: *Phys. Rev. A* **90**, 042708, 2014.
- Dohnal P., Kálosi Á., Plašil R., Roučka Š., Kovalenko A., Rednyk S., Johnsen R., Glosík J.: *Phys. Chem. Chem. Phys.* **18**, 23549, 2016.
- Dohnal P., Shapko D., Kálosi Á., Kassayová M., Roučka Š., Rednyk S., Plašil R., Hejduk M., Glosík J.: *Faraday Discuss.* **217**, 220, 2019.
- Dohnal P., Jusko P., Jimenez-Redondo M., Caselli P.: Isomer specific reactions of CN^+ , HCN^+ and HNC^+ with H_2 , *manuscript is being prepared for publication*.
- van der Donk P., Yousif F. B., Mitchell J. B. A.: *Phys. Rev. A* **43**, 5971, 1991.
- Elliot J. L., Strobel D. F., Zhu X., Stansberry J. A., Wasserman L. H., Franz O. G.: *Icarus* **143**, 425, 2000.
- Feher M., Rohrbacher A., Maier J. P.: *Chem. Phys.* **185**, 357, 1994.
- Fehsenfeld F. C., Ferguson E. E., Schmeltekopf A. L.: *J. Chem Phys.* **44(8)**, 3022, 1966.
- Ferguson E. E., Fehsenfeld F. C., Schmeltekopf A. L.: *Adv. At. Mol. Phys.* **5**, 1, 1969.
- Flannery M. R.: *J. Chem. Phys.* **95**, 8205, 1991.
- Fonseca dos Santos S., Kokoouline V., Greene C. H.: *J. Chem. Phys.* **127**, 124309, 2007.
- Fonseca dos Santos S., Douguet N., Kokoouline V., Orel A. E.: *J. Chem. Phys.* **140**, 164308, 2014.
- Fonseca dos Santos S., Ngassam V., Orel A. E., Larson A.: *Phys. Rev. A* **94**, 022702, 2016.
- Fox J. L., Dalgarno A.: *J. Geophys. Res.: Space Phys.* **90**, 7557, 1985.

- Fox, J. L.: *J. Phys.: Conf. Ser.* **4**, 32, 2005.
- Geballe T. R., Oka T., *Nature* **384**, 334, 1996.
- Geppert W., Thomas R., Semaniak J., Ehlerding A., Millar T. J., Osterdahl F., af Ugglas M., Djuric N., Paal A., Larsson M.: *Astrophys. J.* **609**, 459, 2004.
- Gerbev S.: *J. Phys. B: At. Mol. Opt. Phys.* **51**, 035008, 2018.
- Gerlich D.: *Adv. Chem. Phys.* **82**, 594, 1992.
- Gerlich D.: *Phys. Scr.* **1995**, 256, 1995.
- Gerlich D., Borodi G., Luca A., Mogo C., Smith M. A.: *Z. Für Phys. Chem.* **225**, 475, 2011.
- Glosík J., Plašil R., Poterya V., Kudrna P., Tichý M.: *Chem. Phys. Lett.* **331**, 209, 2000.
- Glosík J., Novotný O., Pysanenko A., Zakouřil P., Plašil R., Kudrna P., Poterya V.: *Plasma Sources Sci. Technol.* **12**, S117, 2003.
- Glosík J., Korolov I., Plašil R., Novotný O., Kotřík, T., Hlavenka P., Varju J., Mikhailov I. A., Kokoouline V., Greene C. H.: *J. Phys. B-At. Mol. Opt. Phys.* **41**, 191001, 2008.
- Glosík J., Plašil R., Korolov I., Kotřík T., Novotný O., Hlavenka P., Dohnal P., Varju J., Kokoouline V., Greene C. H.: *Phys. Rev. A* **79**, 052707, 2009.
- Glosik J., Dohnal P., Rubovič P., Kálosi Á., Plašil R., Roučka Š., Johnsen R.: *Plasma Sources Sci. Technol.* **24**, 065017, 2015.
- Goeghegan M., Adams N. G., Smith D.: *J. Phys. B At. Mol. Opt. Phys.* **24**, 2589, 1991.
- Gougousi T., Johnsen R., Golde M. F.: *Int. J. Mass Spectrom.* **149-150**, 131, 1995.
- Guberman, S. L.: *Geophys. Res. Lett.* **18**, 1051, 1991.
- Guberman, S. L.: *J. Chem. Phys.* **137**, 074309, 2012.
- Guberman, S. L.: *J. Chem. Phys.* **141**, 204307, 2014.
- von Hahn R., Becker A., Berg F., et al.: *Rev. Sci. Instrum.* **87**, 063115, 2016.

- Hansel A., Glantschnig M., Scheiring C., Lindinger W., Ferguson E. E.: *J. Chem. Phys.* **109**, 1743, 1998.
- Hejduk M., Dohnal P., Rubovič P., Kálosi Á., Plašil R., Johnsen R., Glosík J.: *J. Chem. Phys.* **143**, 044303, 2015.
- Herbelin J. M., McKay J. A., Kwok M. A., Ueunten R. H., Urevig D. S., Spencer D. J., Benard D. J.: *Appl. Opt.* **19**, 144, 1980.
- Herbst E., Klemperer W.: *Astrophys. J.* **185**, 505, 1973.
- Hickman A. P., Kashinski D. O., Malenda R. F., Gatti F., Talbi D.: *J. Phys. Conf. Ser.* **300**, 012016, 2011.
- Hugo, E., Asvany O., Schlemmer S.: *J. Chem. Phys.* **130**, 164302, 2009.
- Hus H., Yousif F., Sen A., Mitchell J. B. A.: *Phys. Rev. A* **38**, 658, 1988.
- Hutchinson I. H.: *Principles of Plasma Diagnostics*, Cambridge University Press, Cambridge, 2002.
- Jensen M. J., Pedersen H. B., Safvan C. P., Seiersen K., Urbain X., Andersen L. H.: *Phys. Rev. A* **63**, 052701, 2001.
- Jiang P., Guthrie J., Roberts J. L.: *Phys. Plasmas* **27**, 012109, 2020.
- Johnsen R.: *Int. J. Mass Spectrosc. Ion Processes* **81**, 67, 1987.
- Johnsen R., Rubovič P., Dohnal P., Hejduk M., Plašil R., Glosík J.: *J. Phys. Chem. A* **117**, 9477, 2013.
- Johnson A. W., Gerardo J. B.: *Phys. Rev. Lett.* **27**, 835, 1971.
- Jungen C., Pratt S. T.: *Phys. Rev. Lett.* **102**, 023201, 2009.
- Kálosi Á., Dohnal P., Augustovičová L., Roučka Š., Plašil R., Glosík J.: *Eur. Phys. J.-Appl. Phys.* **75**, 24707, 2016.
- Kálosi Á., Dohnal P., Shapko D., Roučka Š., Plašil R., Johnsen R., Glosík J.: *J. Instrum.* **12**, C10010, 2017.
- Kasner W. H., Biondi M. A.: *Phys. Rev.* **137**, A317, 1965.

- Killian T. C., Kulin S., Bergeson S. D., Orozco L. A., Orzel C., Rolston S. L.: *Phys. Rev. Lett.* **83**, 4776, 1999.
- Kokoouline V., Greene C. H., Esry B. D.: *Nature* **412**, 891, 2001.
- Kokoouline V.: Private communication, 2012.
- Korolov I., Kotřík T., Plašil R., Varju J., Hejduk M., Glosík J.: *Contrib. Plasma Phys.* **48**, 521, 2008.
- Korolov I., Plašil R., Kotřík T., Dohnal P., Glosík J.: *Int. J. Mass Spectrom.* **280**, 144, 2009.
- Kotřík T., Dohnal P., Korolov I., Plašil R., Roučka Š., Glosík J., Greene C. H., Kokoouline V.: *J. Chem. Phys.* **133**, 034305, 2010.
- Kotřík T., Dohnal P., Roučka Š., Jusko P., Plašil R., Glosík J., Johnsen R.: *Phys. Rev. A* **83**, 032720, 2011a.
- Kotřík T., Dohnal P., Rubovič P., Plašil R., Roučka Š., Opanasiuk S., Glosík J.: *Eur. Phys. J. Appl. Phys.* **56**, 24011, 2011b.
- Kotřík T.: Electron-Ion Recombination at Temperatures below 300 K: *Ph.D. Thesis*, Charles University in Prague, Czech Republic, 2013.
- Kovalenko A., Tran T. D., Rednyk S., Roučka Š., Dohnal P., Plašil R., Gerlich D., Glosík J.: *Astrophys. J.* **856**, 100, 2018.
- Kovalenko A., Roučka Š., Tran T. D., Rednyk S., Plašil R., Dohnal P., Glosík J.: *J. Chem. Phys.* **154**, 094301, 2021.
- Krasnopolsky V. A.: *Icarus* **236**, 83, 2014.
- Krasnopolsky V. A.: *Icarus* **335**, 113374, 2020.
- Kreckel H., Novotný O., Crabtree K. N., Buhr H. et al.: *Phys. Rev. A* **82**, 042715, 2010.
- Kumar S. S., Grussie F., Suleimanov Y. V., Guo H., Kreckel H. *Sci. Adv.* **4**, eaar3417, 2018.
- Lammer H., Stumptner W., Molina-Cuberos G., Bauer S., Owen T.: *Planet. Space Sci.* **48**, 529, 2000.

- Lammich L., Strasser D., Kreckel H., Lange M., Pedersen H. B., Altevogt S., Andrianarijaona V., Buhr H., Heber O., Witte P., Schwalm, D., Wolf A., Zajfman D.: *Phys. Rev. Lett.* **91**, 143201, 2003.
- Langmuir I.: *J. Franklin Inst.* **196**, 751, 1923.
- Larsson M., Danared H., Larson A., Le Padellec A., Peterson J. R., Rosén S., Semaniak J., Stromholm C.: *Phys. Rev. Lett.* **79**, 395, 1997.
- Larsson M., Orel A. E.: *Dissociative Recombination of Molecular Ions*. Cambridge University Press, Cambridge, 2008.
- Laube S., Padellec A. L., Sidko O., Rebrion-Rowe C., Mitchell J. B. A., Rowe B. R.: *J. Phys. B* **31**, 2111, 1998.
- Lehmann K. K., Romanini D.: *J. Chem. Phys.* **105**, 10263, 1996.
- Le Padellec A., Larsson M., Danared H., Larson A., Peterson J. R., Semaniak J., Stromholm C.: *Phys. Scr.* **57**, 215, 1998.
- Leu M., Biondi M. A., Johnsen R.: *Phys. Rev. A* **8**, 413, 1973.
- Little D. A., Chakrabarti K., Mezei Zs., Schneider I. F., Tennyson, J.: *Phys. Rev. A* **90**, 052705, 2014.
- MacDonald J. A., Biondi M. A., Johnsen R.: *Planet. Space Sci.* **32**, 651, 1984.
- Macko P., Bano G., Hlavenka P., Plašil R., Poterya V., Pysanenko A., Votava O., Johnsen R., Glosík J.: *Int. J. Mass Spectrom.* **233**, 299, 2004.
- Mahdavi M. R., Hasted J. B., Nakshbandi M. M.: *J. Phys. B: At. Mol. Phys.* **4**, 1726, 1971.
- Mansbach P., Keck J.: *Phys. Rev.* **181**, 275, 1969.
- Mathur D., Khan S. U., Hasted J. B.: *J. Phys. B* **11**, 3615, 1978.
- McCall B. J., Honeycutt A. J., Saykally R. J., Djuric N., Dunn G. H., Semaniak J., Novotný O., Al-Khalili A., Ehlerding A., Hellberg F., Kalhori S., Neau A., Thomas R. D., Paal A., Osterdahl F., Larsson M.: *Phys. Rev. A* **70**, 052716, 2004.

- McGowan J. W., Mul P. M., D'Angelo V. S., Mitchell J. B. A., Defrance P., Froelich H. R.: *Phys. Rev. Lett.* **42**, 373, 1979.
- McGuyer B. H., McDonald M., Iwata G. Z., Tarollo M. G., Grier A. T., Apfelbeck F., Zelevinsky T.: *New J. Phys.* **17**, 055004, 2015.
- Mehr F. J., Biondi M. F.: *Phys. Rev.* **181**, 264, 1969.
- Millar T. J.: *Astron. Geophys.* **46**, 2.29, 2005.
- Millar T. J.: *Plasma Sources Sci. Technol.* **24**, 043001, 2015.
- Min M.-Y., Ilie R.: *Front. Astron. Space Sci.* **8**, 745357, 2022.
- Mitchell J. B. A., Ng C. T., Janssen F. L., McGowan J. W.: *J. Phys. B: At. Mol. Phys.* **17**, L909, 1984.
- Morville J.: Injection des cavités optiques de haute finesse par laser à diode – Application à la CW-CRDS et à la détection de traces atmosphériques, *Ph.D. Thesis*, L'Université Joseph Fourier – Grenoble I, France, 2001.
- Mott-Smith H. M., Langmuir I.: *Phys. Rev.* **28**, 727, 1926.
- Mul P. M., McGowan J. W.: *Astrophys. J. Lett.* **227**, L157, 1979a.
- Mul P. M., McGowan J. W.: *J. Phys. B At. Mol. Opt. Phys.* **12**, 1591, 1979b.
- Noren C., Yousif F. B., Mitchell J. B. A.: *J. Chem. Soc. Faraday Trans.* **2**, 85, 1697, 1989.
- Novotný O., Plašil R., Pysanenko A., Korolov I., Glosík J.: *J. Phys. B* **39**, 2561, 2006.
- Novotný O., Wilhelm P., Paul D., Kálosi Á., Saurabh S., Becker A., Blaum K., George S., Gock J., Wolf A.: *Science* **365**, 676, 2019.
- Oka T.: *Proc. Natl. Acad. Sci. U. S. A.* **103**, 12235, 2006.
- O'Keefe A., Deacon D. A. G.: *Rev. Sci. Instrum.* **59**, 2544, 1988.
- Otto R., von Zastrow A., Best T., Wester R.: *Phys. Chem. Chem. Phys.* **15**, 612, 2013.

- Pagani L., Vastel C., Hugo E., Kokoouline V., Greene C. H., Bacmann A., Bayet E., Ceccarelli C., Peng R., Schlemmer S.: *Astron. Astrophys.* **494**, 623, 2009.
- Parise B., Belloche A., Du F., Gunsten R., Menten K. M.: *Astron. Astrophys.* 526, A31, 2011.
- Peart B., Dolder K. T.: *J. Phys. B* **7**, 1948, 1974.
- Persson K. B., Brown S.: *Phys. Rev.* **100**, 729, 1955.
- Peterson J. R., Le Padellec A., Danared H., et al.: *J. Chem. Phys.* **108**, 1978, 1998.
- Petrie S., Freeman C. G., Meot-Ner M., McEwan M. J., Ferguson E. E., *J. Am. Chem. Soc.* **112**, 7121, 1990.
- Petrie S., Freeman G., McEwan M. J., Ferguson E. E.: *Mon. Notices Royal Astron. Soc.* 248, 272, 1991.
- Petrignani A., Altevogt S., Berg M. H., et al., *Phys. Rev. A* **83**, 032711, 2011.
- Pfau S., Tichý M.: in *Low Temperature Plasma Physics*, ed. by R. Hippler, Wiley-VCH, 131, 2001.
- Pitaevskii L. P.: *Sov. Phys.-JETP* **1**, 919, 1962.
- Plašil R., Glosík J., Poterya V., Kudrna P., Ruzs J., Tichý M., Pysanenko A.: *Int. J. Mass Spectrom.* **218**, 105, 2002.
- Plašil R., Mehner T., Dohnal P., Kotrčík T., Glosík J., Gerlich D.: *Astrophys. J.* **737**, 60, 2011.
- Plašil R., Dohnal P., Kálosi Á., Roučka Š., Johnsen R., Glosík J.: *Plasma Sources Sci. Technol.* **26**, 035006, 2017.
- Plašil R., Tran T. D., Roučka Š., Jusko P., Mulin D., Zymak I., Rednyk S., Kovalenko A., Dohnal P., Glosík J., Houfek K., Táborský J., Čížek M.: *Phys. Rev. A* **96**, 062703, 2017.
- Plašil R., Dohnal P., Kálosi Á., Roučka Š., Shapko D., Rednyk S., Johnsen R., Glosík J.: *Rev. Sci. Instrum.* **89**, 063116, 2018.
- Plašil R., Rednyk S., Kovalenko A., Tran T. D., Roučka Š., Dohnal P., Novotný O., Glosík J.: *Astrophys. J.* **910**, 155, 2021.

- Plašil R., Rednyk S., Roučka Š., Uvarova L., Vanko E., Dohnal P., Glosík J.: The temperature dependence of the rate coefficient of reaction of OH⁻ anion with HD at temperatures from 20 K up to 300 K. Experimental study using RF 22-Pole Ion Trap, *manuscript is being prepared for publication*.
- Pohl T., Vrinceanu D., Sadeghpour H. R.: *Phys. Rev. Lett.* **100**, 223201, 2008.
- Poterya V., Glosik J., Plasil R., Tichy M., Kudrna P., Pysanenko A.: *Phys. Rev. Lett.* **88**, 044802, 2002.
- Poterya V., McLain J. L., Adams N. G., Babcock L. M.: *J. Phys. Chem. A* **109**, 7181, 2005.
- Pratt S. T., Jungen C.: *J. Phys.: Conf. Ser.* **300**, 012019, 2011.
- Rednyk S., Roučka Š., Kovalenko A., Tran T. D., Dohnal P., Plašil R., Glosík J.: *Astron. Astrophys.* **625**, A74, 2019.
- Rednyk S., Roučka Š., Dohnal P., Hejduk M., Glosík J., Plašil R.: *Phys. Rev. A* **104**, 062803, 2021.
- Rennick C. J., Saquet N., Morrison J. P., Ortega-Arroyo J., Godin P., Fu L., Schulz-Weiling M., Grant E. R.: *J. Phys.: Conf. Ser.* **300**, 012005, 2011.
- Richardson J. M., Holt R. B.: *Phys. Rev.* **81**, 153, 1951.
- Roberts H., Herbst E., Millar T. J.: *Astron. Astrophys.* **424**, 16, 2004.
- Roithova J., Jašík J., Del Pozo Mellado J., Gerlich D.: *Faraday Discuss.* **217**, 98, 2019.
- Romanini D., Kachanov A. A., Stoeckel F.: *Chem. Phys. Lett.* **270**, 546, 1997.
- Rosati R. E., Johnsen R., Golde M. F.: *J. Chem. Phys.* **120**, 8025, 2004.
- Roučka Š., Rednyk S., Kovalenko A., Tran T. D., Plašil R., Kálosi Á., Dohnal P., Gerlich D., Glosík J.: *Astron. Astrophys.* **615**, L6, 2018.
- Rubovič P., Dohnal P., Hejduk M., Plašil R., Glosík J.: *J. Phys. Chem. A* **117**, 9626, 2013.
- Savic I., Gerlich D., Asvany O., Jusko P., Schlemmer S.: *Mol. Phys.* **113**, 2320, 2015.

- Schippers S., Lestinsky M., Muller A., Savin D. W., Schmidt E. W., Wolf A.: *International Review of Atomic and Molecular Physics (IRAMP)* **1**, 109, 2010.
- Schlemmer S., Kuhn T., Lescop E., Gerlich D.: *Int. J. Mass Spectrom.* **185**, 589, 1999.
- Schregel C. G., Carbone E. A. D., Luggenholscher D., Czarnetzki U.: *Plasma Sources Sci. Technol.* **25**, 054003, 2016.
- Scott G. B., Fairley D. A., Freeman C. G., McEwan M. J., Spanel P., Smith D.: *J. Chem. Phys.* **106**, 3982, 1997.
- Shapko D., Dohnal P., Kassayová M., Kálosi Á., Rednyk S., Roučka Š., Plašil R., Augustovičová L. D., Johnsen R., Špirko V., Glosík J.: *J. Chem. Phys.* **152(2)**, 024301, 2020.
- Shapko D., Dohnal P., Roučka Š., Uvarova L., Kassayová M., Plašil R., Glosík J.: *J. Mol. Spectrosc.* **378**, 111450, 2021.
- Sheehan C. H., St.-Maurice J. P.: *J. Geophys. Res.* **109**, A03302, 2004.
- Sipila O., Caselli P., Harju J.: *Astron. Astrophys.* **554**, A92, 2013.
- Skrzypkowski M. P., Johnsen R., Rosati R. E., Golde M. F.: *Chem. Phys.* **296(1)**, 23, 2004.
- Smith J. R., Hershkowitz N., Coakley P.: *Rev. Sci. Instrum.* **50**, 210, 1979.
- Smith D., Adams N. G.: *Astrophys. J. Lett.* **284**, L13, 1984.
- Smith D., Španěl P.: *Int. J. Mass Spectrom. Ion Processes* **129**, 163, 1993.
- Strasser D., Lammich L., Kreckel H., Lange M., Krohn S., Schwalm D., Zajfman D.: *Phys. Rev. A* **69**, 064702, 2004.
- Stevelfelt J., Boulmer J., Delpech J.: *Phys. Rev. A* **12**, 1246, 1975.
- Sundstrom G., Mowat J. R., Danared H., Datz S., Brostrom L., Filevich A., Kallberg A., Mannervik S., Rensfel K. G., Sigraý P., af Ugglas M., Larsson M.: *Science* **263**, 785, 1994.
- Šícha M., Gajdůšek J., Vepřek Š.: *Br. J. Appl. Phys.* **17**, 1511, 1966.

- Talbi D.: *Chem. Phys.* **332**, 298, 2007.
- Tanabe T., Chida K., Watanabe T., Arakaki Y., Takagi H., Katayama I., Haruyama Y., Saito M., Nomura I., Honma T., Noda K., Hoson K.: in *Dissociative Recombination, Theory, Experiment and Applications IV*, ed. by M. Larsson, J. B. A. Mitchell, I. F. Schneider, World Scientific, Singapore, 170, 1999.
- Tennyson J., Miller S.: *Spectrochim. Acta A* **57**, 661, 2001.
- Thomson J. J.: *Phil. Mag.* **47**, 337, 1924.
- Tom B. A., Zhaunerchyk V., Wiczer M. B., et al.: *J. Chem. Phys.* **130**, 031101, 2009.
- Torrìsi G., Naselli E., Donato L. D., Mauro G. S., Mazzaglia M., Mishra B., Pìdatella A., Sorbello G., Mascali D.: *J. Instrum.* **17**, C01050, 2022.
- Tran T. D., Rednyk S., Kovalenko A., Roučka Š., Dohnal P., Plašìl R., Gerlich D., Glosík J.: *Astrophys. J.* **854**, 25, 2018.
- Turner B. E.: *Astrophys. J. Lett.* **193**, L83, 1974.
- Turner B. E.: *Astrophys. J.* **449**, 635, 1995.
- Uvarova L., Dohnal P., Kasayová M., Rednyk S., Roučka Š., Plašìl R., Glosík J.: Recombination of vibrationally cold N_2^+ ions with electrons, *prepared for publication in J. Geophys. Res. (Atmos)*.
- Varnerin, Jr. L. J.: *Phys. Rev.* **84**, 563, 1951.
- Vìgren E., Zhaunerchyk V., Hamberg M., Kaminska M., Semaniak J., af Ugglas M., Larsson M., Thomas R. D., Geppert W. D.: *Astrophys. J.* **757**, 34, 2012.
- Vorob'ev V. S.: *Phys. Plasmas* **24**, 073513, 2017.
- Vuitton V., Yelle R. V., McEwan M. J.: *Icarus* **191**, 722, 2007.
- Wojcik M., Tachiya M.: *J. Chem. Phys.* **110**, 10016, 1999.
- Wojcik M., Tachiya M.: *J. Chem. Phys.* **112**, 3845, 2000.
- Wolz T., Malbrunot C., Vieille-Grosjean M., Comparat D.: *Phys. Rev. A* **101**, 043412, 2020.

Yariv A.: *Optical Electronics in Modern Communications*, 5rd ed., Oxford University Press, Oxford, 1997.

Yung Y. L., Lyons J. R.: *Geophys. Res. Lett.* **17**, 1717, 1990.

Young L. A., Braga-Ribas F., Johnson R. E.: Volatile evolution of atmospheres of trans-neptunian objects”, in *The Trans-Neptunian Solar System*, ed. by D. Prialnik, M. A. Barucci, L. A. Young, Elsevier, The Netherlands, 2020, Chapter 6, p. 127.

Zhaunerchyk V., Thomas R. D., Geppert W. D., Hamberg M., Kaminska M., Vignen E., Larsson M.: *Phys. Rev. A* **77**, 034701, 2008.

Zipf E. C.: *Geophys. Res. Lett.* **7**, 645, 1980.

Zymak I., Hejduk M., Mulin D., Plasil R., Glosik J., Gerlich D.: *Astrophys. J.* **768**, 86, 2013.

List of publications

Publications in journals with impact factor

- 1) Cavity ring-down spectroscopy study of neon assisted recombination of H_3^+ ions with electrons**
Shapko, D., Dohnal, P., Roučka, Š., Uvarova, L., Kassayová, M., Plašil, R.,
Glosík, J.,
J. Mol. Spectrosc. **378**, 111450, 2021.
- 2) Reaction of carbon dication C_2^+ with O_2 , N_2 , CO , and HD at low temperatures: Experimental study using a 22-pole ion trap**
Rednyk, S., Roučka, Š., Dohnal, P., Hejduk, M., Glosík, J., Plašil, R.,
Phys. Rev. A **104(6)**, 062803, 2021.
- 3) The reaction of $\text{O}^+(4\text{S})$ ions with H_2 , HD , and D_2 at low temperatures: Experimental study of the isotope effect**
Kovalenko, A., Roučka, Š., Tran, T. D., Rednyk, S., Plašil, R., Dohnal, P.,
Glosík, J.,
J. Chem. Phys. **154(9)**, 094301, 2021.
- 4) Experimental Study on CH^+ Formation from Doubly Charged Carbon and Molecular Hydrogen**
Plašil, R., Rednyk, S., Kovalenko, A., Tran, T. D., Roučka, Š., Dohnal, P.,
Novotný, O., Glosík, J.,
Astrophys. J. **910(2)**, 155, 2021.
- 5) Dissociative recombination of N_2H^+ ions with electrons in the temperature range of 80–350 K**
Shapko, D., Dohnal, P., Kassayová, M., Kálosi, Á., Rednyk, S., Roučka, Š.,
Plašil, R., Augustovičová, L. D., Johnsen, R., Špirko, V., Glosík, J.,
J. Chem. Phys. **152(2)**, 024301, 2020.

- 6) **Towards state selective recombination of H_3^+ under astrophysically relevant conditions**
Dohnal, P., Shapko, D., Kálosi, Á., Kassayová, M., Roučka, Š., Rednyk, S., Plašil, R., Hejduk, M., Glosík, J.,
Faraday Discuss. **217**, 220–234, 2019.
- 7) **Reaction of NH^+ , NH_2^+ , and NH_3^+ ions with H_2 at low temperatures**
Rednyk, S., Roučka, Š., Kovalenko, A., Tran, T. D., Dohnal, P., Plašil, R., Glosík, J.,
Astron. Astrophys. **625**, A74, 2019.
- 8) **Stationary afterglow apparatus with CRDS for study of processes in plasmas from 300 K down to 30 K**
Plašil, R., Dohnal, P., Kálosi, Á., Roučka, Š., Shapko, D., Rednyk, S., Johnsen, R., Glosík, J.,
Rev. Sci. Instrum. **89**, 063116, 2018.
- 9) **OH^+ Formation in the Low-temperature $\text{O}^+(4S) + \text{H}_2$ Reaction**
Kovalenko, A., Tran, T. D., Rednyk, S., Roučka, Š., Dohnal, P., Plašil, R., Gerlich, D., Glosík, J.,
Astrophys. J. **856(2)**, 100, 2018.
- 10) **Formation of H_2O^+ and H_3O^+ Cations in Reactions of OH^+ and H_2O^+ with H_2 : Experimental Studies of the Reaction Rate Coefficients from $T = 15$ to 300 K**
Tran, T. D., Rednyk, S., Kovalenko, A., Roučka, Š., Dohnal, P., Plašil, R., Gerlich, D., Glosík, J.,
Astrophys. J. **854(1)**, 25, 2018.
- 11) **Effect of rotational excitation of H_2 on isotopic exchange reaction with OD^- at low temperatures**
Roučka, Š., Rednyk, S., Kovalenko, A., Tran, T. D., Plašil, R., Kálosi, Á., Dohnal, P., Gerlich, D., Glosík, J.,
Astron. Astrophys. **615**, L6, 2018.

12) Stationary afterglow measurements of the temperature dependence of the electron-ion recombination rate coefficients of H_2D^+ and HD_2^+ in He/Ar/ H_2 / D_2 gas mixtures at $T = 80\text{--}145\text{ K}$

Plašil, R., Dohnal, P., Kálosi, Á., Roučka, Š., Johnsen, R., Glosík, J.,
Plasma Sources Sci. Technol. **26(3)**, 035006, 2017.

13) Electron-ion recombination in low temperature hydrogen/deuterium plasma

Glosík, J., Dohnal, P., Kálosi, Á., Augustovičová, L. D., Shapko, D.,
Roučka, Š., Plašil, R.,
Eur. Phys. J.-Appl. Phys. **80(3)**, 30801, 2017.

14) Overtone spectroscopy of N_2H^+ molecular ions—application of cavity ring-down spectroscopy

Kálosi, A., Dohnal, P., Shapko, D., Roučka, Š., Plašil, R., Johnsen, R.,
Glosík, J.,
J. Instrum. **12**, C10010, 2017.

15) Isotopic effects in the interaction of O^- with D_2 and H_2 at low temperatures

Plašil, R., Tran, T. D., Roučka, Š., Jusko, P., Mulin, D., Zymak, I., Rednyk, S.,
Kovalenko, A., Dohnal, P., Glosík, J., Houfek, K., Táborský, J., Cížek, M.,
Phys. Rev. A **96(6)**, 062703, 2017.

16) Binary and ternary recombination of H_2D^+ and HD_2^+ ions with electrons at 80 K

Dohnal, P., Kálosi, Á., Plašil, R., Roučka, Š., Kovalenko, A., Rednyk, S.,
Johnsen, R., Glosík, J.,
Phys. Chem. Chem. Phys. **18(34)**, 23549–23553, 2016.

17) Monitoring the removal of excited particles in He/Ar/ H_2 low temperature afterglow plasma at 80–300 K

Kálosi, Á., Dohnal, P., Augustovičová, L., Roučka, Š., Plašil, R., Glosík, J.,

Eur. Phys. J.-Appl. Phys. **75(2)**, 24707, 2016.

18) Recombination of H_3^+ ions with electrons in He/ H_2 ambient gas at temperatures from 240 K to 340 K

Glosik, J; Dohnal, P; Rubovic, P; Kalosi, A; Plasil, R; Roucka, S; Johnsen, R
Plasma Sources Sci. Technol. **24(6)**, 065017, 2015.

19) Flowing-afterglow study of electron-ion recombination of para- H_3^+ and ortho- H_3^+ ions at temperatures from 60 K to 300 K

Hejduk, M., Dohnal, P., Rubovic, P., Kalosi, A., Plasil, R., Johnsen, R., Glosik, J.,
J. Chem. Phys. **143(4)**, 044303, 2015.

20) H_2 -assisted ternary recombination of H_3^+ with electrons at 300 K

Dohnal, P., Rubovic, P., Kalosi, A., Hejduk, M., Plasil, R., Johnsen, R., Glosik, J.,
Phys. Rev. A **90**, 042708, 2014.

21) Collisional-radiative recombination of Ar^+ ions with electrons in ambient helium at temperatures from 50 K to 100 K

Dohnal, P., Rubovic, P., Kotrik, T., Hejduk, M., Plasil, R., Johnsen, R., Glosik, J.,
Phys. Rev. A **87**, 052716, 2013.

22) Binary Recombination of H_3^+ and D_3^+ Ions with Electrons in Plasma at 50–230 K

Rubovic, P., Dohnal, P., Hejduk, M., Plasil, R., Glosik, J.,
J. Phys. Chem. A **117(39)**, 9626–9632, 2013.

23) Ternary Recombination of H_3^+ and D_3^+ with Electrons in He- H_2 (D_2) Plasmas at Temperatures from 50 to 300 K

Johnsen, R., Rubovic, P., Dohnal, P., Hejduk, M., Plasil, R., Glosik, J.,
J. Phys. Chem. A **117(39)**, 9477–9485, 2013.

24) Binary recombination of para- and ortho-H₃⁺ with electrons at low temperatures

Dohnal, P., Hejduk, M., Varju, J., Rubovic, P., Roucka, S., Kotrik, T., Plasil, R., Johnsen, R., Glosik, J.,

Philos. Trans. R. Soc. A-Math. Phys. Eng. Sci. **370(1978)**, 5101–5108, 2012.

25) Binary and ternary recombination of para-H₃⁺ and ortho-H₃⁺ with electrons: State selective study at 77–200 K

Dohnal, P., Hejduk, M., Varju, J., Rubovic, P., Roucka, S., Kotrik, T., Plasil, R., Glosik, J., Johnsen, R.,

J. Chem. Phys. **136(24)**, 244304, 2012.

26) Binary and ternary recombination of D₃⁺ ions at 80–130 K: Application of laser absorption spectroscopy

Dohnal, P., Hejduk, M., Rubovic, P., Varju, J., Roucka, S., Plasil, R., Glosik, J.,

J. Chem. Phys. **137(19)**, 194320, 2012.

27) Nuclear spin state-resolved cavity ring-down spectroscopy diagnostics of a low-temperature H₃⁺-dominated plasma

Hejduk, M., Dohnal, P., Varju, J., Rubovic, P., Plasil, R., Glosik, J.,

Plasma Sources Sci. Technol. **21(2)**, 024002, 2012.

28) Cryo-FALP study of collisional-radiative recombination of Ar⁺ ions at 40–200 K

Kotrik, T., Dohnal, P., Rubovic, P., Plasil, R., Roucka, S., Opanasiuk, S., Glosik, J.,

Eur. Phys. J.-Appl. Phys. **56(2)**, 24011, 2011.

29) Collisional-radiative recombination Ar⁺ + e + e: Experimental study at 77–180 K

Kotrik, T., Dohnal, P., Roucka, S., Jusko, P., Plasil, R., Glosik, J., Johnsen, R.,

Phys. Rev. A **83(3)**, 032720, 2011.

30) Reactions of Cold Trapped CH⁺ Ions with Slow H Atoms

Plasil, R., Mehner, T., Dohnal, P., Kotrik, T., Glosik, J., Gerlich, D.,
Astrophys. J. **737(2)**, 60, 2011.

31) Nuclear Spin Effect on Recombination of H₃⁺ Ions with Electrons at 77 K

Varju, J., Hejduk, M., Dohnal, P., Jilek, M., Kotrik, T., Plasil, R., Gerlich, D.,
Glosik, J.,
Phys. Rev. Lett. **106(20)**, 203201, 2011.

32) Temperature dependence of binary and ternary recombination of D₃⁺ ions with electrons

Kotrik, T., Dohnal, P., Korolov, I., Plasil, R., Roucka, S., Glosik, J.,
Greene, C. H., Kokoouline, V.,
J. Chem. Phys. **133(3)**, 034305, 2010.

33) Binary and ternary recombination of H₃⁺ and D₃⁺ ions with electrons in low temperature plasma

Glosik, J., Plasil, R., Kotrik, T., Dohnal, P., Varju, J., Hejduk, M., Korolov,
I., Roucka, S., Kokoouline, V.,
Mol. Phys. **108(17)**, 2253–2264, 2010.

34) Recombination of HCO⁺ and DCO⁺ ions with electrons

Korolov, I., Plasil, R., Kotrik, T., Dohnal, P., Glosik, J.,
Int. J. Mass Spectrom. **280(1-3)**, 144–148, 2009.

35) Non-Maxwellian electron energy distribution function in He, He/Ar, He/Xe/H₂ and He/Xe/D₂ low temperature afterglow plasma

Plasil, R., Korolov, I., Kotrik, T., Dohnal, P., Bano, G., Donko, Z., Glosik, J.,
Eur. Phys. J. D **54(2)**, 391–398, 2009.

36) Binary and ternary recombination of D_3^+ ions with electrons in He- D_2 plasma

Glosik, J., Korolov, I., Plasil, R., Kotrik, T., Dohnal, P., Novotny, O., Varju, J., Roucka, S., Greene, C. H., Kokoouline, V.,
Phys. Rev. A **80(4)**, 042706, 2009.

37) Temperature dependence of binary and ternary recombination of H_3^+ ions with electrons

Glosik, J., Plasil, R., Korolov, I., Kotrik, T., Novotny, O., Hlavenka, P., Dohnal, P., Varju, J., Kokoouline, V., Greene, C. H.,
Phys. Rev. A **79(5)**, 052707, 2009.

38) Measurements of EEDF in Helium Flowing Afterglow at Pressures 500 – 2000 Pa

Korolov, I., Plasil, R., Kotrik, T., Dohnal, P., Novotny, O., Glosik, J.,
Contrib. Plasma Phys. **48(5-7)**, 461–466, 2008.

Publications in proceedings of scientific conferences listed in WOS

1) Reactions of O^- with D_2 at temperatures below 300 K

Plašil, R., Tran, T. D., Roučka, Š., Rednyk, S., Kovalenko, A., Jusko, P., Mulin, D., Zymak, I., Dohnal, P., Glosík, J.,
J. Phys.: Conf. Ser. **875(1)**, 012015, 2017.

2) State selective study of H_3^+ recombination in Cryo-FALP and SA-CRDS experiments at 77 K

Glosik, J., Hejduk, M., Dohnal, P., Rubovic, P., Kalosi, A., Plasil, R.,
EPJ Web of Conferences **84**, 01002, 2015.

3) Recombination in low temperature Ar^+ dominated plasmas

Dohnal, P., Kotrik, T., Plasil, R., Korolov, I., Glosik, J.,
J. Phys.: Conf. Ser. **300(1)**, 012021, 2011.

- 4) **Experimental study of para- and ortho- H_3^+ recombination**
Plasil, R., Varju, J., Hejduk, M., Dohnal, P., Kotrik, T., Glosik, J.,
J. Phys.: Conf. Ser. **300(1)**, 012023, 2011.

- 5) **Measurements of EEDF in recombination dominated afterglow plasma**
Plasil, R., Korolov, I., Kotrik, T., Varju, J., Dohnal, P., Donko, Z., Bano, G.,
Glosik, J.,
J. Phys.: Conf. Ser. **192**, 012023, 2009.

- 6) **Recombination of KrD^+ and KrH^+ ions in afterglow plasma**
Korolov, I., Kotrik, T., Plasil, R., Hejduk, M., Varju, J., Dohnal, P., Glosik,
J.,
J. Phys.: Conf. Ser. **192**, 012018, 2009.

- 7) **Recombination of D_3^+ Ions with Electrons in Low Temperature Plasma**
Korolov, I., Kotrik, T., Dohnal, P., Plasil, R., Glosik, J.,
Publ. Astron. Obs. Belgrade **84**, 39–44, 2008

Other publications

- 1) **Equilibrium in Low Temperature H_3^+ -dominated Plasma, Application of Cavity Ring-Down Spectroscopy**
Hejduk, M., Dohnal, P., Rubovic, P., Varju, J., Opanasiuk, S., Plasil, R.,
Glosik, J.,
Acta Univ. Carolin. Math. Phys. **53(1)**, 51–59, 2012

List of attached publications

Varju J., Hejduk M., Dohnal P., Jilek M., Kotrík T., Plašil R., Gerlich D., Glosík J.: Nuclear Spin Effect on Recombination of H_3^+ Ions with Electrons at 77 K, *Phys. Rev. Lett.* **106(20)**, 203201, 2011. doi:10.1103/PhysRevLett.106.203201

Dohnal P., Hejduk M., Rubovič P., Varju J., Roučka Š., Plašil R., Glosík J.: Binary and ternary recombination of D_3^+ ions at 80–130 K: Application of laser absorption spectroscopy, *J. Chem. Phys.* **137(19)**, 194320, 2012. doi:10.1063/1.4767396

Dohnal P., Hejduk M., Varju J., Rubovič P., Roučka Š., Kotrík T., Plašil R., Glosík J., Johnsen R.: Binary and ternary recombination of para- H_3^+ and ortho- H_3^+ with electrons: State selective study at 77–200 K, *J. Chem. Phys.* **136(24)**, 244304, 2012. doi:10.1063/1.4730162

Johnsen R., Rubovič P., Dohnal P., Hejduk M., Plašil R., Glosík J.: Ternary Recombination of H_3^+ and D_3^+ with Electrons in He- H_2 (D_2) Plasmas at Temperatures from 50 to 300 K, *J. Phys. Chem. A* **117(39)**, 9477–9485, 2013. doi:10.1021/jp311978n

Rubovič P., Dohnal P., Hejduk M., Plašil R., Glosík J.: Binary Recombination of H_3^+ and D_3^+ Ions with Electrons in Plasma at 50–230 K, *J. Phys. Chem. A* **117(39)**, 9626–9632, 2013. doi:10.1021/jp3123192

Dohnal P., Rubovič P., Kotrík T., Hejduk M., Plašil R., Johnsen R., Glosík J.: Collisional-radiative recombination of Ar^+ ions with electrons in ambient helium at temperatures from 50 K to 100 K, *Phys. Rev. A* **87**, 052716, 2013. doi:10.1103/PhysRevA.87.052716

Dohnal P., Rubovič P., Kálosi A., Hejduk M., Plašil R., Johnsen R., Glosík J.: H_2 -assisted ternary recombination of H_3^+ with electrons at 300 K, *Phys. Rev. A* **90**, 042708, 2014. doi:10.1103/PhysRevA.90.042708

Hejduk M., Dohnal P., Rubovic P., Kálosi Á., Plašil R., Johnsen R., Glosík J.: Flowing-afterglow study of electron-ion recombination of para- H_3^+ and ortho- H_3^+ ions at temperatures from 60 K to 300 K, *J. Chem. Phys.* **143(4)**, 044303, 2015. doi:10.1063/1.4927094

Glosík J., Dohnal P., Rubovič P., Kálosi Á., Plašil R., Roučka S., Johnsen R.: Recombination of H_3^+ ions with electrons in He/ H_2 ambient gas at temperatures from 240 K to 340 K, *Plasma Sources Sci. Technol.* **24**(6), 065017, 2015. doi:10.1088/0963-0252/24/6/065017

Kálosi Á., Dohnal P., Augustovičová L., Roučka Š., Plašil R., Glosík J.: Monitoring the removal of excited particles in He/Ar/ H_2 low temperature afterglow plasma at 80–300 K, *Eur. Phys. J.-Appl. Phys.* **75**(2), 24707, 2016. doi:10.1051/epjap/2016150587

Dohnal P., Kálosi Á., Plašil R., Roučka Š., Kovalenko A., Rednyk S., Johnsen R., Glosík J.: Binary and ternary recombination of H_2D^+ and HD_2^+ ions with electrons at 80 K, *Phys. Chem. Chem. Phys.* **18**(34), 23549, 2016. doi:10.1039/C6CP04152C

Plašil R., Dohnal P., Kálosi Á., Roučka Š., Johnsen R., Glosík J.: Stationary afterglow measurements of the temperature dependence of the electron–ion recombination rate coefficients of H_2D^+ and HD_2^+ in He/Ar/ H_2 / D_2 gas mixtures at $T = 80\text{--}145$ K, *Plasma Sources Sci. Technol.* **26**(3), 035006, 2017. doi:10.1088/1361-6595/aa5916

Kálosi A., Dohnal P., Shapko D., Roučka Š., Plašil R., Johnsen R., Glosík J.: Overtone spectroscopy of N_2H^+ molecular ions—application of cavity ring-down spectroscopy, *J. Instrum.* **12**, C10010, 2017. doi:10.1088/1748-0221/12/10/C10010

Plašil R., Dohnal P., Kálosi Á., Roučka Š., Shapko D., Rednyk S., Johnsen R., Glosík J.: Stationary afterglow apparatus with CRDS for study of processes in plasmas from 300 K down to 30 K, *Rev. Sci. Instrum.* **89**, 063116, 2018. doi:10.1063/1.5036834

Dohnal P., Shapko D., Kálosi Á., Kassayová M., Roučka Š., Rednyk S., Plašil R., Hejduk M., Glosík J.: Towards state selective recombination of H_3^+ under astrophysically relevant conditions, *Faraday Discuss.* **217**, 220–234, 2019. doi:10.1039/C8FD00214B

Shapko D., Dohnal P., Kassayová M., Kálosi Á., Rednyk S., Roučka Š., Plašil R., Augustovičová L. D., Johnsen R., Špirko V., Glosík J.: Dissociative recombination of N_2H^+ ions with electrons in the temperature range of 80–350 K, *J. Chem. Phys.* **152**(2), 024301, 2020. doi:10.1063/1.5128330

Shapko D., Dohnal P., Roučka Š., Uvarova L., Kassayová M., Plašil R., Glosík J.: Cavity ring-down spectroscopy study of neon assisted recombination of H_3^+ ions with electrons, *J. Mol. Spectrosc.* **378**, 111450, 2021. doi:10.1016/j.jms.2021.111450

Uvarova L., Dohnal P., Kassayová M., Saito S., Rednyk S., Roučka Š., Plašil R., Glosík J.: Recombination of vibrationally cold N_2^+ ions with electrons, Prepared for publication in *J. Geophys. Res. Atmos.*

Attached publications

**Nuclear Spin Effect on Recombination of H_3^+ Ions with Electrons
at 77 K**

Varju J., Hejduk M., Dohnal P., Jilek M., Kotrík T., Plašil R., Gerlich D., Glosík J.

Phys. Rev. Lett. **106(20)**, 203201, 2011.

Nuclear Spin Effect on Recombination of H_3^+ Ions with Electrons at 77 K

J. Varju, M. Hejduk, P. Dohnal, M. Jílek, T. Kotrčík, R. Plašil, D. Gerlich, and J. Glošík

Charles University, Faculty of Mathematics and Physics, Prague, Czech Republic

(Received 13 September 2010; published 17 May 2011)

Utilizing different ratios of para to ortho H_2 in normal and para enriched hydrogen, we varied the population of para- H_3^+ in an H_3^+ dominated plasma at 77 K. Absorption spectroscopy was used to measure the densities of the two lowest rotational states of H_3^+ . Monitoring plasma decays at different populations of para- H_3^+ allowed us to determine the rate coefficients for binary recombination of para- H_3^+ and ortho- H_3^+ ions: ${}^p\alpha_{\text{bin}}(77\text{ K}) = (1.9 \pm 0.4) \times 10^{-7} \text{ cm}^3 \text{ s}^{-1}$ and ${}^o\alpha_{\text{bin}}(77\text{ K}) = (0.2 \pm 0.2) \times 10^{-7} \text{ cm}^3 \text{ s}^{-1}$.

DOI: 10.1103/PhysRevLett.106.203201

PACS numbers: 34.80.Lx, 34.80.Nz, 52.72.+v, 95.30.Ft

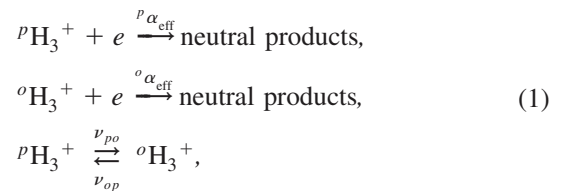
Introduction.— H_3^+ is the dominant ion in many types of hydrogen-containing plasmas including astrophysically relevant plasmas [1,2]. It is the simplest polyatomic ion; its properties are well known [3,4]. The recombination of H_3^+ has been studied for over 50 years [5,6]. Only recently, the process of binary dissociative recombination (DR) of H_3^+ was described by going beyond the Born-Oppenheimer approximation and accounting for Jahn-Teller coupling [7]. The calculated cross sections [8,9] and the cross sections measured recently in storage ring experiments are approaching each other [10,11]. Presently, no reliable rate coefficient measured with storage rings below 300 K exists [12,13]. Only two years ago, it was demonstrated that the recombination rate coefficients (effective α_{eff}) determined from plasma decay during an afterglow are composed of the binary and ternary process [14]. Taking this into the account, an agreement between experimental and calculated (DR) rate coefficients has been achieved for 77–300 K [15–19].

For temperatures below 300 K, the theory [9] of DR of H_3^+ predicts different values of recombination rate coefficients for different nuclear spin states of H_3^+ (${}^p\alpha_{\text{DR}}$ and ${}^o\alpha_{\text{DR}}$ for para- H_3^+ with a total nuclear spin quantum number $I = 1/2$ and ortho- H_3^+ with $I = 3/2$, respectively). The qualitative reason is that at small collisional energies there are more Rydberg resonances of the neutral para- H_3 that can be populated during the electron-ion collisions. It is because there are more low energy rotational states of the ground vibrational state of para- H_3^+ , for example, $(J, K) = (2, 2)$ and $(2, 1)$ (corresponding to energy of ~ 151 and 249 K). For ortho- H_3^+ , the lowest rotational states of the ground vibrational state have relatively higher energies [for example, $(3, 0)$ corresponds to ~ 650 K]. More Rydberg resonances in para- H_3 enhances DR cross sections in para- H_3^+ more than in ortho- H_3^+ at low temperatures (< 200 K). The difference between ${}^p\alpha_{\text{DR}}$ and ${}^o\alpha_{\text{DR}}$ was partly confirmed by storage ring experiments [10].

The recent observations made towards several diffuse molecular clouds showed a large difference between excitation temperatures $T_{10}(\text{H}_2)$ and $T(\text{H}_3^+)$ derived from

the relative intensities of lowest rotational levels of H_2 and H_3^+ , respectively (for details, see Ref. [20]). These observations lead to the conclusion that in a reliable chemical model the nuclear spin dependences of the reactions, including recombination of para- and ortho- H_3^+ , have to be considered. The dependences on spin, rotational excitation, and temperature have to be measured.

In this Letter, we report results of our pursuit of measuring the recombination rate coefficients ${}^p\alpha$ and ${}^o\alpha$ of pure para- H_3^+ and pure ortho- H_3^+ . This is achieved by *in situ* determination of para- H_3^+ and ortho- H_3^+ densities in an H_3^+ dominated and recombination governed plasma in a He-Ar- H_2 mixture at 77 K. In the following, we will use upper left index p , o , n , and e to indicate “para,” “ortho,” “normal,” and “para enriched,” respectively, e.g., ${}^p\text{H}_2$, ${}^o\text{H}_2$, ${}^n\text{H}_2$, and ${}^e\text{H}_2$. For para- H_3^+ and ortho- H_3^+ ions we use ${}^p\text{H}_3^+$ and ${}^o\text{H}_3^+$. Symbols pf and of denote relative populations (fractions, ${}^pf + {}^of = 1$) of H_3^+ ions in the para and ortho state, respectively (i.e., ${}^pf = [{}^p\text{H}_3^+]/[\text{H}_3^+]$ and ${}^of = [{}^o\text{H}_3^+]/[\text{H}_3^+]$). Normal (${}^n\text{H}_2$) and para enriched (${}^e\text{H}_2$) hydrogen were used in the experiments. In ${}^n\text{H}_2$, 1/4 of the H_2 molecules are in para and 3/4 in ortho states. In a low temperature hydrogen afterglow plasma, the main processes determining the density of ${}^p\text{H}_3^+$ and ${}^o\text{H}_3^+$ are diffusion and the following processes:



where ${}^p\alpha_{\text{eff}}$ and ${}^o\alpha_{\text{eff}}$ are the effective rate coefficients of the overall recombination of ${}^p\text{H}_3^+$ and ${}^o\text{H}_3^+$, respectively. ν_{po} and ν_{op} are frequencies of ${}^p\text{H}_3^+$ to ${}^o\text{H}_3^+$ transitions and vice versa. If collisions with ${}^p\text{H}_2$ and ${}^o\text{H}_2$ dominate such processes, then ν_{po} and ν_{op} can be expressed as $\nu = k[{}^p,{}^o\text{H}_2]$ where k is a rate coefficient of the corresponding

nuclear spin changing reaction. The balance equations for ${}^p\text{H}_3^+$ and ${}^o\text{H}_3^+$ are

$$\frac{d[{}^p\text{H}_3^+]}{dt} = -{}^p\alpha_{\text{eff}}[{}^p\text{H}_3^+]n_e - \frac{[{}^p\text{H}_3^+]}{\tau_D} - \nu_{\text{po}}[{}^p\text{H}_3^+] + \nu_{\text{op}}[{}^o\text{H}_3^+], \quad (2)$$

$$\frac{d[{}^o\text{H}_3^+]}{dt} = -{}^o\alpha_{\text{eff}}[{}^o\text{H}_3^+]n_e - \frac{[{}^o\text{H}_3^+]}{\tau_D} - \nu_{\text{op}}[{}^o\text{H}_3^+] + \nu_{\text{po}}[{}^p\text{H}_3^+], \quad (3)$$

where τ_D is the time constant of ambipolar diffusion. If $[{}^p\text{H}_3^+] + [{}^o\text{H}_3^+] = n_e$, then we obtain by summing Eqs. (2) and (3)

$$\frac{dn_e}{dt} = -({}^p\alpha_{\text{eff}}{}^p f + {}^o\alpha_{\text{eff}}{}^o f)n_e^2 - \frac{n_e}{\tau_D} = -\alpha_{\text{eff}}n_e^2 - \frac{n_e}{\tau_D}. \quad (4)$$

We see that α_{eff} determined from the decay of n_e [21] depends on ${}^p f$, ${}^o f$, ${}^p\alpha_{\text{eff}}$, and ${}^o\alpha_{\text{eff}}$. If ${}^p f$ and ${}^o f$ are constant during the afterglow, the decay can be described by an effective recombination rate coefficient $\alpha_{\text{eff}} = {}^p\alpha_{\text{eff}}{}^p f + {}^o\alpha_{\text{eff}}{}^o f$. If α_{eff} is measured at least for two different values of ${}^p f$, one can derive ${}^p\alpha_{\text{eff}}$ and ${}^o\alpha_{\text{eff}}$. The overall recombination includes a binary and a ternary helium assisted recombination [15–18]. In the first approximation we can write

$$\alpha_{\text{eff}}(T, [\text{He}]) = \alpha_{\text{bin}}(T) + K_{\text{He}}(T)[\text{He}], \quad (5)$$

where α_{bin} and K_{He} are the corresponding rate coefficients; a similar relation can be written for ${}^p\alpha_{\text{eff}}$ and ${}^o\alpha_{\text{eff}}$.

Because of the weak coupling of the nuclear spin to the remaining degrees of freedom in H_3^+ and H_2 , the probability of changing the nuclear spin by radiation is very low. In the present experiment, the main nuclear spin scrambling process is the reaction with H_2 via the formation of an $(\text{H}_5^+)^\#$ reaction complex [20,22–27]. This reaction allows efficient scrambling of the protons. Besides the dynamical details, rather stringent nuclear spin selection rules affect the ratio of $[{}^p\text{H}_3^+]$ and $[{}^o\text{H}_3^+]$ in the plasma [20,22–28]. Therefore the change in ${}^p f$ can be achieved by using ${}^e\text{H}_2$ instead of ${}^n\text{H}_2$ [20,23,29]. By performing the measurements with different $[\text{He}]$, the values α_{bin} and K_{He} for the individual spin states have been obtained. For a detailed discussion of experiments with ${}^n\text{H}_2$, see Refs. [14,15,19].

Experiment.—In the experiment, the plasma is formed in a pulsed microwave discharge in a fused silica tube cooled by liquid nitrogen to 77 K. The discharge was ignited in a mixture of He-Ar- H_2 (a typical composition 10^{18} , 10^{14} , 10^{13} cm^{-3} [30]). Para enriched ${}^e\text{H}_2$ was produced from ${}^n\text{H}_2$ by using a Fe_2O_3 catalytic converter cooled below 20 K. Nuclear magnetic resonance spectroscopy was used to determine the fraction of ${}^p\text{H}_2$ [$> (87 \pm 5)\%$].

The ion density was measured with a near infrared cavity ring down absorption spectrometer [31,32]. The densities of the two lowest rotational states of the ground vibrational state of H_3^+ were measured by using the transition $3\nu_2^1(2,0) \leftarrow 0\nu_2^0(1,0)$ for ${}^o\text{H}_3^+$ and $3\nu_2^1(2,1) \leftarrow 0\nu_2^0(1,1)$ for ${}^p\text{H}_3^+$; for notation and details, see Refs. [31,32]. In a thermodynamic equilibrium at 77 K, these two lowest rotational states contain $\approx 86\%$ of the population of H_3^+ . The Doppler broadening of the absorption lines was measured to obtain the kinetic temperature of H_3^+ . The measured kinetic temperature of ions in the active discharge was (80 ± 15) K. Because of the high helium density [$[\text{He}] = (2\text{--}18) \times 10^{17} \text{ cm}^{-3}$], the relaxation time for the electron temperature is below $1 \mu\text{s}$. In the early afterglow, the electron and ion temperatures relax, and in the later afterglow ($\geq 50 \mu\text{s}$), we can expect that the temperature of electrons and ions is 77 K.

Because of high $[\text{He}]$, $[\text{H}_2]$, and n_e , any ion has on average 10^5 collisions with He, 10 collisions with electrons [33], and more than 10 collisions with H_2 prior to its recombination. This is why it is safe to assume that during the afterglow the population of states within the ${}^p\text{H}_3^+$ and

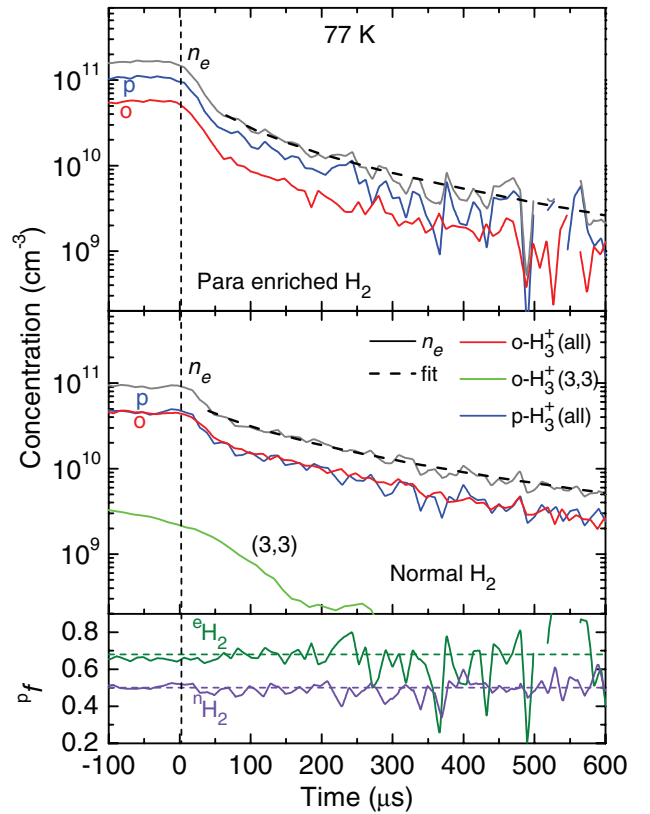


FIG. 1 (color online). The decay curves measured for ${}^p\text{H}_3^+$ and ${}^o\text{H}_3^+$ using para enriched ${}^e\text{H}_2$ (${}^e\text{H}_2$, top panel) and normal ${}^n\text{H}_2$ (${}^n\text{H}_2$, middle panel). Obtained n_e are also plotted. The line indicated as (3,3) in the middle panel is a decay curve for H_3^+ in the eponymous state. The fractions ${}^p f$ of ${}^p\text{H}_3^+$ measured in experiments with ${}^n\text{H}_2$ and ${}^e\text{H}_2$ are plotted in the lower panel.

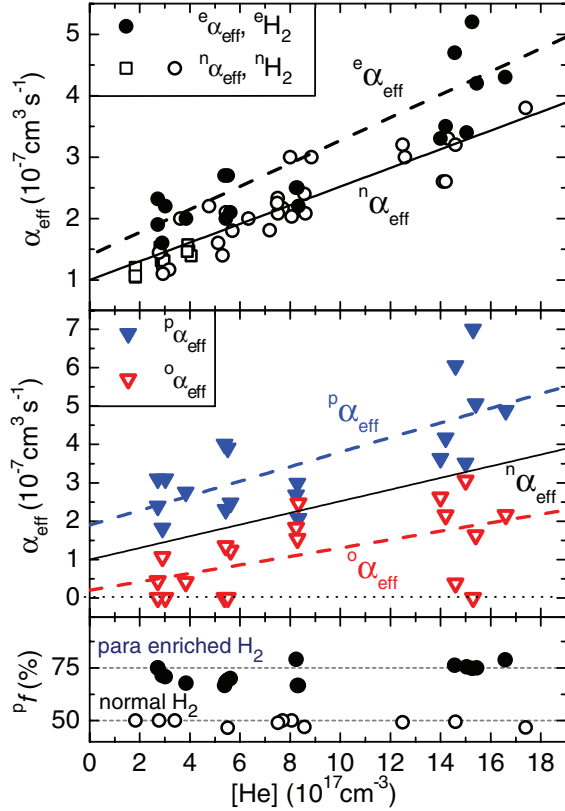


FIG. 2 (color online). Dependencies of effective recombination rate coefficients on He density. Upper panel: Data from experiments with ${}^n\text{H}_2$ and ${}^e\text{H}_2$ (${}^n\alpha_{\text{eff}}$ and ${}^e\alpha_{\text{eff}}$). Included are data obtained in the FALP experiment using ${}^n\text{H}_2$ (at 82 ± 5 K, open squares). Lower panel: Relative populations of ${}^p\text{H}_3^+$ (fraction pf) measured in experiments using ${}^n\text{H}_2$ and ${}^e\text{H}_2$. Middle panel: The effective recombination rate coefficients ${}^p\alpha_{\text{eff}}$ and ${}^o\alpha_{\text{eff}}$ for ${}^p\text{H}_3^+$ and ${}^o\text{H}_3^+$ calculated from measured ${}^e\alpha_{\text{eff}}$, ${}^n\alpha_{\text{eff}}$, and pf .

${}^o\text{H}_3^+$ manifold is thermalized to 77 K and it is sufficient to measure densities of H_3^+ in the lowest rotational states, i.e., (1, 1) of ${}^p\text{H}_3^+$ and (1, 0) of ${}^o\text{H}_3^+$. This assumption was confirmed also by the measurement of a population distribution among (3, 3) metastable ortho state [24] and two aforementioned states in the ${}^n\text{H}_2$ discharge for temperatures in the 77–200 K range.

Results and discussion.—When using ${}^n\text{H}_2$ as precursor, we observed ${}^pf \approx {}^of \approx 0.5$; see Figs. 1 and 2. That holds for the whole H_2 density range used in the present experiments [$(0.5\text{--}5) \times 10^{14} \text{ cm}^{-3}$].

For each set of experimental conditions, the evolutions of $[{}^p\text{H}_3^+]$ and $[{}^o\text{H}_3^+]$ were measured and n_e were calculated (Fig. 1). From these evolutions, we extracted α_{eff} and pf . The first 50–100 μs of the decay are excepted from the analysis to exclude the formation-relaxation region. In Fig. 2 (upper panel), rate coefficients measured with ${}^n\text{H}_2$ at 77 K are plotted as a function of $[\text{He}]$. The data were fitted by using Eq. (5), and the recombination rate

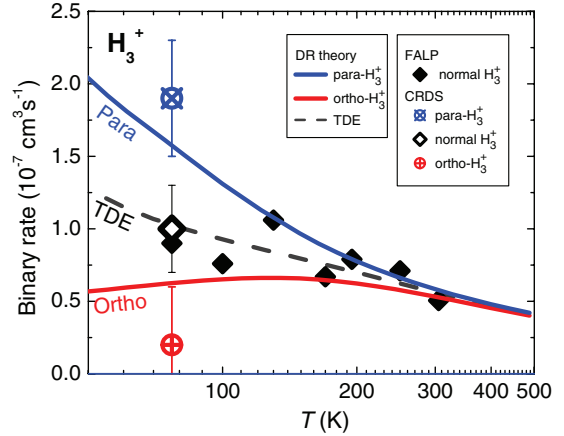


FIG. 3 (color online). Measured binary recombination rate coefficients for normal H_3^+ , ortho- H_3^+ , and para- H_3^+ in comparison with FALP data for normal H_3^+ [14,15,19] and theoretical predictions [9]. Normal H_3^+ indicates data measured with normal H_2 . TDE stands for thermodynamic equilibrium.

coefficients of H_3^+ with ${}^pf \approx {}^of \approx 0.5$ were obtained: ${}^n\alpha_{\text{bin}}(77 \text{ K}) = (1.0 \pm 0.2) \times 10^{-7} \text{ cm}^3 \text{ s}^{-1}$ for the binary and ${}^nK_{\text{He}}(77 \text{ K}) = (1.5 \pm 0.2) \times 10^{-25} \text{ cm}^6 \text{ s}^{-1}$ for the ternary process. Earlier data obtained with a Langmuir probe in the flowing afterglow experiment (FALP) at $(82 \pm 5) \text{ K}$ are also plotted for comparison [15].

Using ${}^e\text{H}_2$ as a precursor, we increased the fraction of ${}^p\text{H}_3^+$. The obtained ${}^e\alpha_{\text{eff}}$ and pf are plotted in Fig. 2. It is evident already from these plots that the recombination of ${}^p\text{H}_3^+$ is faster. From ${}^e\alpha_{\text{eff}}$ and pf , measured with ${}^e\text{H}_2$, the values ${}^p\alpha_{\text{eff}}$ and ${}^o\alpha_{\text{eff}}$ for ${}^p\text{H}_3^+$ and ${}^o\text{H}_3^+$ were calculated. In these calculations, the dependence fitted through data measured with ${}^n\text{H}_2$ was used as a reference (full lines in Fig. 2 indicated as ${}^n\alpha_{\text{eff}}$). By fitting the data ${}^p\alpha_{\text{eff}}$ and ${}^o\alpha_{\text{eff}}$ with a linear dependence [Eq. (5)], we obtained corresponding binary and ternary recombination rate coefficients. For ${}^p\text{H}_3^+$, ${}^p\alpha_{\text{bin}} = (1.9 \pm 0.4) \times 10^{-7} \text{ cm}^3 \text{ s}^{-1}$ and ${}^pK_{\text{He}} = (1.9 \pm 0.4) \times 10^{-25} \text{ cm}^6 \text{ s}^{-1}$. For ${}^o\text{H}_3^+$, ${}^o\alpha_{\text{bin}} = (0.2 \pm 0.2) \times 10^{-7} \text{ cm}^3 \text{ s}^{-1}$ and ${}^oK_{\text{He}} < (1.1 \pm 0.4) \times 10^{-25} \text{ cm}^6 \text{ s}^{-1}$. The results are summarized in Fig. 3—the agreement with FALP experiments [15,19] and with the theory [9] is excellent.

Summary.—By using a cavity ring down absorption spectrometer, the evolution of ortho- H_3^+ and para- H_3^+ densities has been monitored *in situ* during the afterglow. From such measurements, effective rate coefficients of recombination of H_3^+ , for a particular para- H_3^+ /ortho- H_3^+ ratio at 77 K, have been determined and the effective recombination rate coefficients of both spin modifications (${}^p\alpha_{\text{eff}}$ and ${}^o\alpha_{\text{eff}}$) were obtained. The rate coefficients of the binary recombination of para- H_3^+ and ortho- H_3^+ (${}^p\alpha_{\text{bin}}$ and ${}^o\alpha_{\text{bin}}$) were determined by measuring at different $[\text{He}]$.

To our knowledge, this is the first study of H_3^+ recombination with *in situ* determination of the composition of the decaying plasma with respect to para and ortho states of

H_3^+ . Since the majority of the ions is in the lowest rotational states of para and ortho modifications [(1, 1) and (1, 0)] at 77 K, it is the first time that binary recombination rate coefficients were obtained for ions in the ground vibrational, specific nuclear, and rotational states. The theoretical prediction made for binary DR [9] is in excellent agreement with our data. No reliable storage ring data below 300 K exists [13].

This work is a part of the research plan MSM 0021620834 and Grant No. OC10046 financed by the Ministry of Education of the Czech Republic and was partly supported by GACR (202/07/0495, 202/08/H057, 205/09/1183, and 202/09/0642), by GAUK 92410, GAUK 353811, and GAUK 54010, and by COST Action CM0805 (The Chemical Cosmos).

-
- [1] S. Miller *et al.*, *Phil. Trans. R. Soc. A* **358**, 2485 (2000).
 - [2] E. Herbst, *Phil. Trans. R. Soc. A* **358**, 2523 (2000).
 - [3] C.P. Morong, J.L. Gottfried, and T. Oka, *J. Mol. Spectrosc.* **255**, 13 (2009).
 - [4] O.L. Polyansky and J. Tennyson, *J. Chem. Phys.* **110**, 5056 (1999).
 - [5] M. Larsson and A. Orel, *Dissociative Recombination of Molecular Ions* (Cambridge University Press, Cambridge, England, 2008).
 - [6] R. Plašil *et al.*, *Int. J. Mass Spectrom.* **218**, 105 (2002).
 - [7] V. Kokoouline, C.H. Greene, and B.D. Esry, *Nature (London)* **412**, 891 (2001).
 - [8] V. Kokoouline and C. H. Greene, *Phys. Rev. A* **68**, 012703 (2003).
 - [9] S.F. dos Santos, V. Kokoouline, and C.H. Greene, *J. Chem. Phys.* **127**, 124309 (2007).
 - [10] H. Kreckel *et al.*, *Phys. Rev. Lett.* **95**, 263201 (2005).
 - [11] B.J. McCall *et al.*, *Nature (London)* **422**, 500 (2003).
 - [12] H. Kreckel *et al.*, *Phys. Rev. A* **82**, 042715 (2010).
 - [13] A. Petrigani *et al.*, *Phys. Rev. A* **83**, 032711 (2011).
 - [14] J. Glosík *et al.*, *J. Phys. B* **41**, 191001 (2008).
 - [15] J. Glosík *et al.*, *Phys. Rev. A* **79**, 052707 (2009).
 - [16] J. Glosík *et al.*, *Phys. Rev. A* **80**, 042706 (2009).
 - [17] J. Glosík *et al.*, *J. Phys. Conf. Ser.* **192**, 012005 (2009).
 - [18] T. Kotrík *et al.*, *J. Chem. Phys.* **133**, 034305 (2010).
 - [19] J. Glosík *et al.*, *Mol. Phys.* **108**, 2253 (2010).
 - [20] K.N. Crabtree, N. Indriolo, H. Kreckel, B.A. Tom, and B.J. McCall, *Astrophys. J.* **729**, 15 (2011).
 - [21] I. Korolov *et al.*, *Contrib. Plasma Phys.* **48**, 521 (2008).
 - [22] M. Quack, *Mol. Phys.* **34**, 477 (1977).
 - [23] M. Cordonnier *et al.*, *J. Chem. Phys.* **113**, 3181 (2000).
 - [24] T. Oka and E. Epp, *Astrophys. J.* **613**, 349 (2004).
 - [25] D. Gerlich *et al.*, *Phil. Trans. R. Soc. A* **364**, 3007 (2006).
 - [26] K. Park and J.C. Light, *J. Chem. Phys.* **126**, 044305 (2007).
 - [27] E. Hugo, O. Asvany, and S. Schlemmer, *J. Chem. Phys.* **130**, 164302 (2009).
 - [28] T. Oka, *J. Mol. Spectrosc.* **228**, 635 (2004).
 - [29] B.A. Tom *et al.*, *J. Chem. Phys.* **132**, 081103 (2010).
 - [30] J. Varju *et al.*, *J. Phys. Conf. Ser.* **227**, 012026 (2010).
 - [31] P. Macko *et al.*, *Int. J. Mass Spectrom.* **233**, 299 (2004).
 - [32] P. Hlavenka *et al.*, *Int. J. Mass Spectrom.* **255–256**, 170 (2006).
 - [33] V. Kokoouline *et al.*, *Mon. Not. R. Astron. Soc.* **405**, 1195 (2010).

**Binary and ternary recombination of D_3^+ ions at 80–130 K:
Application of laser absorption spectroscopy**

Dohnal P., Hejduk M., Rubovič P., Varju J., Roučka Š., Plašil R., Glosík J.

J. Chem. Phys. **137(19)**, 194320, 2012.

Binary and ternary recombination of D_3^+ ions at 80–130 K: Application of laser absorption spectroscopy

Petr Dohnal, Michal Hejduk, Peter Rubovič, Jozef Varju, Štěpán Roučka, Radek Plašil, and Juraj Glosík

Department of Surface and Plasma Science, Faculty of Mathematics and Physics, Charles University, Prague, Czech Republic

(Received 14 August 2012; accepted 24 October 2012; published online 20 November 2012)

Recombination of D_3^+ ions with electrons at low temperatures (80–130 K) was studied using spectroscopic determination of D_3^+ ions density in afterglow plasmas. The use of cavity ring-down absorption spectroscopy enabled an *in situ* determination of the abundances of the ions in plasma and the translational and the rotational temperatures of the recombining ions. Two near infrared transitions at $(5792.70 \pm 0.01) \text{ cm}^{-1}$ and at $(5793.90 \pm 0.01) \text{ cm}^{-1}$ were used to probe the number densities of the lowest ortho state and of one higher lying rotational state of the vibrational ground state of D_3^+ ion. The results show that D_3^+ recombination with electrons consists of the binary and the third-body (helium) assisted process. The obtained binary recombination rate coefficients are in agreement with a recent theoretical prediction for electron-ion plasma in thermodynamic equilibrium with $\alpha_{\text{bin}}(80 \text{ K}) = (9.2 \pm 2.0) \times 10^{-8} \text{ cm}^3 \text{ s}^{-1}$. The measured helium assisted ternary rate coefficients K_{He} are in agreement with our previously measured flowing afterglow data giving a value of $K_{\text{He}}(80 \text{ K}) = (1.2 \pm 0.3) \times 10^{-25} \text{ cm}^6 \text{ s}^{-1}$. © 2012 American Institute of Physics. [<http://dx.doi.org/10.1063/1.4767396>]

I. INTRODUCTION

The astronomical importance of trihydrogen cation H_3^+ has been driving research in many areas of both physics and chemistry¹ for a long time. This simplest of all polyatomic ions and its isotopologues are also very important for theory, because their properties including interactions with electrons, can be calculated. Processes leading to formation and destruction of H_3^+ ions and similar processes in which deuterated isotopologues are formed or destroyed are important for astronomy and fundamental physics. Deuteration of H_3^+ and formation of H_2D^+ , HD_2^+ , and D_3^+ are important processes that enable us to characterize the environment in which the deuteration takes place.² This also includes interstellar plasma and plasmas under physical conditions believed to be appropriate for pre-protostellar cores.^{2,3} The particular importance of H_3^+ , but also of H_2D^+ and HD_2^+ , was recognized and they were detected in interstellar plasma.^{4–7} These detections confirm expectations that multiple deuterated ions play a key role in the chemistry of the early universe.² The inclusion of HD_2^+ and D_3^+ in the models leads to predictions of higher values of the D/H ratio in the gas phase.⁴ Unfortunately, D_3^+ has not been directly observed in the interstellar medium or in other astronomical object up to now.

Because of its fundamental character, the recombination of H_3^+ and D_3^+ ions with electrons has been studied for over 60 years with emphasis on H_3^+ (see, e.g., the book by Larsson and Ore⁸). For details on recombination studies of the D_3^+ ion, see Refs. 9–19. For both H_3^+ and D_3^+ significant differences between recombination rate coefficients were obtained in different types of experiments^{10,12–15,19,20} over many years and the differences between the experimental values and the

theoretical ones were very large.²¹ Moreover, recombination studies of H_2D^+ and HD_2^+ ions are very rare.^{22–25}

Only in the early 2000s the modern theory of binary dissociative recombination (DR) of these ions was formulated.^{24–28} Agreement between this theory and experiments achieved in the late 1990s and in the years 2000–2003 was only partial. The remaining discrepancies were assumed to be in internal excitation of recombining ions, which can play a role at low collision energies. Because of this assumption ion storage rings were equipped with “cold ion sources” and better agreement was obtained for H_3^+ recombination.^{29–31} In these experiments, it had been assumed that the “cold” rotational distributions measured in the ion source, survived the injection and storage in the ring. Recent high-resolution storage ring experiments indicate that these assumptions were not necessarily correct.^{32,33} At this moment, there are no reliable storage ring data for H_3^+ recombination below 300 K (see discussion in Refs. 32 and 33). We assume that the situation with D_3^+ is similar to H_3^+ (i.e., no reliable data from storage ring experiments exist for low temperature recombination of the D_3^+ ion).

In our laboratory, we have studied D_3^+ recombination using stationary afterglow (AISA experiment^{14,34}) and also flowing afterglow (FALP).¹⁵ In our recent studies, we discovered a fast ternary neutral assisted recombination of H_3^+ and D_3^+ ions in plasma.^{16–18,35–37} At temperatures between 77 and 300 K in helium buffer gas, the losses due to this ternary process are comparable with the losses due to binary dissociative recombination already at a buffer gas pressure of few hundred Pa. When this process is accounted for, then the rate coefficient of binary process can be obtained from afterglow experiments. In H_3^+ experiments, we obtained very good agreement

of the measured binary recombination rate coefficients with the ones theoretically predicted for thermodynamic equilibrium (TDE) and for pure para- and pure ortho- H_3^+ .^{38–41}

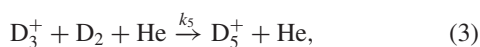
Among the H_3^+ studies only few were made using spectroscopic identification of the recombining ions (e.g., Refs. 42–46). The study by Amano done in pure hydrogen^{42,43} is well known. Nevertheless, his value of the recombination rate coefficient is up to three times larger than other measured values.^{30,37,41} We can speculate that in his experiments the H_3^+ recombination was enhanced by the ternary H_2 assisted process.

The situation with D_3^+ is different. To our knowledge, there was no spectroscopic study of D_3^+ recombination up to now. Only few studies were made using afterglow experiments^{9,10,12,14,15} and storage ring experiments.^{13,19} There are few storage ring experiments²² and no afterglow experiments with H_2D^+ and HD_2^+ . Usable, near infrared (NIR) absorption frequencies are known^{47,48} and we have made spectroscopic investigation of plasma containing a mixture of these ions.⁴⁷ Recombination study of these ions using cavity ring down spectroscopy (CRDS) in the afterglow experiment is possible, but it would be very complicated. As was already mentioned, there are no recent storage ring studies of these ions and none at all with “cold ion source”. The recent theory predicts the rate coefficients for DR of these ions to be smaller than the one of H_3^+ at temperatures ~ 300 K.^{27,49,50}

In the present study, we formed D_3^+ dominated plasma in local thermodynamic equilibrium and we measured the binary recombination rate coefficient α_{bin} and the helium assisted ternary recombination rate coefficient K_{He} of D_3^+ recombination with electrons. To our knowledge, this is the first spectroscopic study concerning recombination of D_3^+ ions with electrons.

II. EXPERIMENTAL METHODS

The method of measuring the recombination rate coefficients in stationary afterglow plasma is well known, so only a very short description will be given here (see, e.g., Refs. 14 and 34). In pulsed discharge, quasi-neutral D_3^+ dominated plasma is formed and when the discharge is switched off a decrease of the ion number density is monitored during the afterglow. At these conditions the decay of the afterglow plasma is governed by ambipolar diffusion to the walls and by electron-ion recombination. Here, in addition to the mentioned processes, we also consider the conversion of D_3^+ ions to D_5^+ in ternary helium assisted association reaction.¹⁵ The main processes are



where α_{bin} is the binary recombination rate coefficient of D_3^+ ions, K_{He} is the ternary recombination rate coefficient of He

assisted recombination, k_5 is the ternary rate coefficient of He assisted association, and α_5 is the binary recombination rate coefficient of D_5^+ ions with electrons.^{15,51} If the recombination of D_5^+ is fast and the ternary association (3) is the rate determining reaction in the sequence of processes (3) and (4), then the balance equation can be written in the form

$$\frac{d[\text{D}_3^+]}{dt} = -\alpha_{\text{bin}}[\text{D}_3^+]n_{\text{e}} - K_{\text{He}}[\text{He}][\text{D}_3^+]n_{\text{e}} - \frac{n_{\text{e}}}{\tau_{\text{D}}} - \frac{n_{\text{e}}}{\tau_{\text{R}}}, \quad (5)$$

where τ_{D} is the characteristic diffusion time, τ_{R} the time constant characterizing losses due to ternary association followed by a rapid recombination of D_5^+ . If we assume quasineutrality and if we introduce the time constant τ_{L} for “linear losses” by equation $1/\tau_{\text{L}} = 1/\tau_{\text{D}} + 1/\tau_{\text{R}}$, then the balance equation can be rewritten as

$$\frac{dn_{\text{e}}}{dt} = -\alpha_{\text{eff}}n_{\text{e}}^2 - \frac{n_{\text{e}}}{\tau_{\text{L}}}, \quad (6)$$

where we introduced the effective binary recombination rate coefficient α_{eff} which can be written in the form

$$\alpha_{\text{eff}}(T, [\text{He}]) = \alpha_{\text{bin}}(T) + K_{\text{He}}(T)[\text{He}]. \quad (7)$$

We have demonstrated in our previous studies^{16–18} and here we will demonstrate again, that the overall recombination of D_3^+ in afterglow plasma can be described in this way. To obtain α_{bin} and K_{He} one has to measure the dependence of α_{eff} on $[\text{He}]$ at fixed temperature T .

III. EXPERIMENT

The plasma is generated in a pulsed microwave discharge in a fused silica tube (inner diameter ~ 1.5 cm). The tube is cooled to 80 K by liquid nitrogen or by pre-cooled nitrogen vapors for measurements in the temperature range of 80–220 K. To form a D_3^+ dominated plasma a mixture of He/Ar/ D_2 with a typical composition $10^{17}/10^{14}/10^{14}$ cm^{-3} is flowing through the discharge tube. The D_3^+ ions are formed in a sequence of ion molecule reactions. The details of the kinetics of the ion formation are well known (see Refs. 14, 15, 18, 34, and 52). The microwave generator ($f = 2.45$ GHz) is equipped with an external fast high-voltage switch to cut off the HV power to the magnetron. The switch off transient time is less than 30 μs . This was indirectly confirmed by monitoring the spontaneous emission of the plasma.⁴⁵ A fairly low microwave power in the range 5–15 W, with $\sim 50\%$ duty cycle, was used to avoid excessive heating of the gas during the discharge. A NIR-CRDS was used as the main diagnostic tool, the principal layout is shown in Figure 1. The discharge tube, equipped with an optical resonator (not in scale), forms the main part of the continuous wave modification of CRDS. Because the apparatus was described elsewhere (see Refs. 38–41, 45, and 46) only a short description will be given here.

A distributed feedback laser diode covering the spectral range of 5788–5798 cm^{-1} was used in the present study. During the measurement the laser current was kept constant and wavelength change was done by means of computer controlled temperature change. An interference signal from the Fabry-Perot etalon was used to linearize the wavenumber

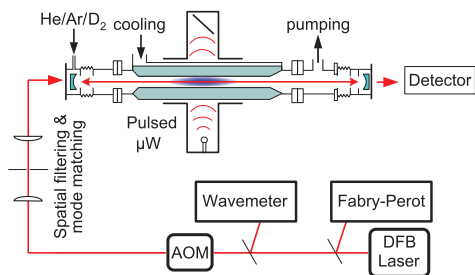


FIG. 1. Stationary afterglow with the CRDS absorption spectrometer. A discharge is periodically ignited in the microwave resonator (μW) in the middle part of the discharge tube. A He/Ar/D₂ gas mixture is used to form a D₃⁺ dominated afterglow plasma. The laser light modulated by the acousto-optic modulator (AOM) is injected through the mirror on one side and photons exiting the cavity through the mirror on the other side are detected by an In-GaAs avalanche photodiode. The absolute wavelength is measured using a Michelson wavemeter and relatively by a Fabry-Perot etalon.

scale. Two H₂O lines at 5789.65 cm⁻¹ and 5793.03 cm⁻¹ (line positions taken from HITRAN database⁵³) were used to transform the relative value given by Fabry-Perot etalon to absolute wavelength. The resulting precision of wavelength determination is better than 0.01 cm⁻¹. At conditions used in the present experiment, where D₃⁺ was the dominant ion, only two absorption lines (5792.70 ± 0.01) cm⁻¹ and (5793.90 ± 0.01) cm⁻¹ were visible during the discharge and early afterglow. The difference between the measured line positions and those predicted by quantum mechanical calculations is less than 0.02 cm⁻¹.⁵⁴ Given this fact and that those two absorption lines were only in plasma with D₂ present, we concluded that they belong to D₃⁺ ion. The conclusion was also supported by measuring the temperature dependence of the intensities of both lines. The examples of measured profiles of absorption lines are shown in Figure 2. In this study we used the transitions, which we assigned (after discussion with Tennyson⁵⁴) as 3ν₂¹(1, 0) ← 0ν₂⁰(0, 0) and 3ν₂¹(3, 2) ← 0ν₂⁰(4, 2) for ortho-D₃⁺ (0,0) and meta-D₃⁺ (4,2), respec-

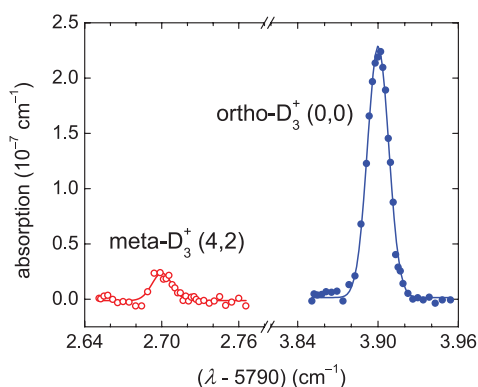


FIG. 2. Example of absorption line profiles of D₃⁺ ions measured at the wall temperature of $T_{\text{wall}} = 112 \text{ K}$ and $P = 560 \text{ Pa}$ of He. The kinetic temperature $T_{\text{kin}} = (112 \pm 10) \text{ K}$ was obtained from the Doppler broadening of the absorption lines. The line center positions are: (5793.90 ± 0.01) cm⁻¹ and (5792.70 ± 0.01) cm⁻¹ for ortho-D₃⁺ (0,0) and meta-D₃⁺ (4,2), respectively. The calculated values are 5793.92 cm⁻¹ for 3ν₂¹(1, 0) ← 0ν₂⁰(0, 0) and 5792.68 cm⁻¹ for 3ν₂¹(3, 2) ← 0ν₂⁰(4, 2) for ortho-D₃⁺ (0,0) and meta-D₃⁺ (4,2), respectively.^{54,55}

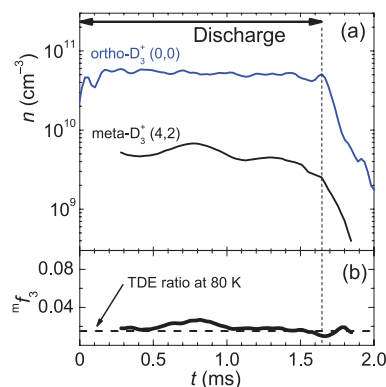


FIG. 3. Panel (a) Measured number densities of the ions in ortho (0,0) and meta (4,2) states of D₃⁺ during the discharge and early afterglow. Panel (b) Measured fraction ${}^m f_3$ of meta-D₃⁺ (4,2), ${}^m f_3 = [\text{meta-D}_3^+(4,2)]/[\text{D}_3^+]$. The value of the ratio corresponding to the TDE at 80 K is indicated by the dashed horizontal line. Used conditions are $T_{\text{He}} = 80 \text{ K}$, $P = 400 \text{ Pa}$ of He, $[\text{D}_2] = 4 \times 10^{14} \text{ cm}^{-3}$ and $[\text{Ar}] = 2 \times 10^{14} \text{ cm}^{-3}$.

tively. The rotational levels are labeled by corresponding quantum numbers (J,G), for details on notation and calculations of transitions frequencies see Ref. 55.

An example of measured ion number density evolutions in discharge and early afterglow is shown in panel (a) of Figure 3. The dashed vertical line indicates the end of the discharge and the beginning of the afterglow. The measured evolution of the fraction ${}^m f_3$ of the number density of the meta-D₃⁺ (4,2) to the number density of D₃⁺ is shown in the lower panel of Figure 3. The horizontal dashed line indicates the calculated ratio corresponding to the TDE at 80 K.

IV. TEMPERATURE IN THE D₃⁺ DOMINATED AFTERGLOW PLASMA

In general, in an afterglow plasma the different particles and their internal degrees of freedom are not necessarily in complete thermal equilibrium with each other and with the walls of the plasma container. For instance, the electron temperature T_e can significantly exceed the kinetic temperature of the ions T_{kin} and the buffer gas atoms temperature T_{He} because the transfer of kinetic energy in electron collisions with heavy particles is less efficient than the kinetic energy transfer in collisions of ions and gas atoms. Also, the ions' rotational temperature T_{rot} and vibrational temperature T_{vib} do not have to be equal to the ions' translational temperature if the corresponding relaxation times are long in comparison with the characteristic time of the ion density decay. We have discussed this problem for H₃⁺ dominated plasma in Refs. 40, 41, and 56. In the present studies, we determine kinetic temperature (T_{kin}) of ions from the Doppler broadening of measured absorption lines. In Figure 4 an example of the evolution of T_{kin} measured at a wall temperature of $T_{\text{wall}} = (112 \pm 1) \text{ K}$ is plotted. The obtained equality $T_{\text{wall}} = T_{\text{kin}}$ means also $T_{\text{wall}} = T_{\text{He}}$. We have made such measurements for the whole range of pressures and temperatures used in the present study with the same conclusion.

The electron temperature T_e in the afterglow was not measured in these experiments. The time constant for

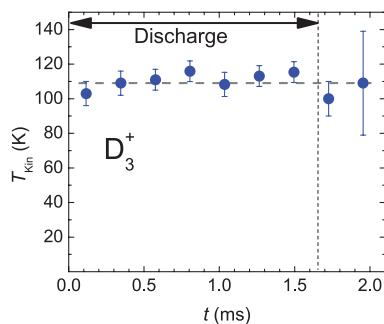


FIG. 4. The measured evolution of the kinetic temperature of the ions (T_{Kin}) during the discharge and during the early afterglow, while a wall temperature was $T_{\text{Wall}} = (112 \pm 1)$ K and rotational temperature was $T_{\text{Rot}} = (112 \pm 3)$ K. Used helium buffer gas concentration was $[\text{He}] = 3.6 \times 10^{17} \text{ cm}^{-3}$. The mean value of the measured T_{Kin} is indicated by a horizontal dashed line.

electron cooling at a typical helium density used in the experiment can be estimated from the electron-helium collision frequency (>1 GHz) and the mass ratio $2m_e/m_{\text{He}}$. The calculated time constant for electron cooling is $\tau_e < 10 \mu\text{s}$. In previous FALP experiments, we measured the electron energy distribution function (EEDF) in He and He/Ar buffered afterglow plasmas under conditions similar to those in the present study.^{57–59} It was found that EEDF is close to a Maxwellian distribution with a temperature close to the buffer gas temperature.⁶⁰ In stationary afterglow with CRDS, we indirectly observed fast cooling of electrons after switching off the discharge by monitoring visible light emissions from the discharge and very early afterglow. Using analogy with H_3^+ , we also expect that all excited vibrational states of D_3^+ are quenched in multiple collisions with He, Ar, and D_2 (see discussion for H_3^+ in Ref. 41).

Using FALP, we also studied the collisional radiative recombination (CRR) in an Ar^+ dominated plasma in a He/Ar gas mixture and we measured the corresponding ternary recombination rate coefficient K_{CRR} which has a very pronounced temperature dependence, $K_{\text{CRR}} \sim T_e^{-9/2}$.^{61–63} In this study, we also measured the temperature dependence of ambipolar diffusion. In both cases, we obtained very good agreement with theory for temperatures of 77–300 K.^{62,63} This is an excellent confirmation that at the given experimental conditions $T_e = T_{\text{He}} = T_{\text{Wall}}$. These estimates need to be refined when the plasma contains energy sources that can lead to heating of the electron gas. One such source can be He metastables.^{59,60} In the present experiments, metastables are destroyed in reaction with Ar (by Penning ionization^{58,60}). At low temperatures and high electron densities the electron heating can be caused by CRR; we will discuss this possibility later. In our previous studies of H_3^+ recombination,⁴¹ we showed that at the used electron densities, the CRR can elevate the electron temperature only slightly in the early afterglow at gas temperatures near 77 K, but becomes unimportant at higher gas temperatures and lower electron densities.

From the measured relative population of the ions in the two monitored states we determined the rotational temperature T_{Rot} . The rotational temperature T_{Rot} was measured not only during the discharge but also during the early afterglow

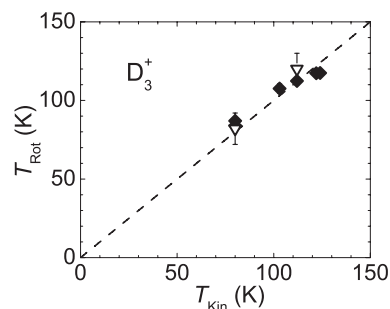


FIG. 5. The measured rotational temperature T_{Rot} of the D_3^+ ions versus the measured kinetic temperature T_{Kin} . The dashed straight line indicates the equality $T_{\text{Rot}} = T_{\text{Kin}}$. The open triangles and filled rhomboids indicate data measured during the early afterglow and during the discharge, respectively.

when the signal from meta- D_3^+ (J, G) = (4,2) was still sufficient. The measured dependence of T_{Rot} on T_{Kin} is shown in Figure 5.

Recently, we studied relaxation processes and equilibrium in H_3^+ dominated plasma using very similar experimental conditions, the only difference being that now we use D_2 instead of H_2 .^{38–41,56} In H_3^+ studies, we monitored the population of two ortho states and one para state and the used transitions were more suitable for measurements of rotational temperatures at He buffer gas temperatures in the range of 80–200 K. We were also able to monitor the para to ortho ratio, $[\text{para-H}_3^+]/[\text{ortho-H}_3^+]$. In addition, in the H_3^+ experiments we used normal and para enriched hydrogen to manipulate the fraction of para- H_3^+ in the plasma. From the obtained results we also concluded that $T_{\text{Rot}} = T_{\text{Kin}} = T_{\text{He}} = T_{\text{Wall}}$ for H_3^+ . Later on, for present experiments we will use temperature measured from the Doppler broadening of the absorption lines (mean value from several measurements at the same wall temperature). For previous FALP data, we will use the measured temperature of the flow tube. On the basis of the present experiments and using comparison and analogy with the results obtained in H_3^+ experiments, we concluded that the plasma in the afterglow is in the thermodynamic equilibrium at a temperature given by the wall of the discharge tube.

V. RESULTS AND DISCUSSION

We measured the variation of light absorption in afterglow plasma using CRDS. Under the assumption that the plasma is in thermal equilibrium and D_3^+ is the dominant ion we calculated the electron density decay. Examples of data measured at 112 K are plotted in Figure 6. The measured number densities of the ions in ortho (0,0) and meta (4,2) states of D_3^+ , the calculated electron density and the partial density of ions in (4,2) state (fraction ${}^m f_3$ of meta- D_3^+ (4,2), ${}^m f_3 = [\text{meta-D}_3^+(4,2)]/[\text{D}_3^+]$) are plotted.

We studied plasma decay at temperatures of 80–130 K over a wide range of He pressures. The decay curves were analyzed using “integral analysis” (for details see Refs. 57 and 64). This analysis can separate α_{eff} from τ_L (see Eqs. (5) and (6)) and minimize the influence of D_3^+ formation followed by a rapid recombination on the determination of α_{eff} . The first 50–150 μs of the afterglow decay were not taken into

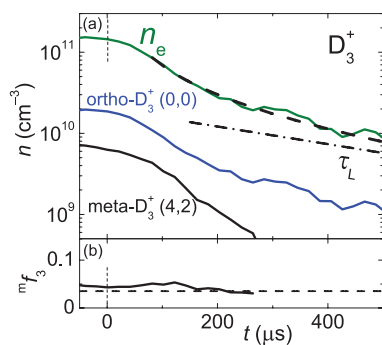


FIG. 6. Panel (a) Example of the decay of densities of ions in ortho (0,0) and meta (4,2) states of D_3^+ , measured during the afterglow in a He/Ar/ D_2 gas mixture at 112 K, 550 Pa of He, $[D_2] = 1.7 \times 10^{14} \text{ cm}^{-3}$ and $[\text{Ar}] = 8.4 \times 10^{13} \text{ cm}^{-3}$. Time is set to zero at the beginning of the afterglow (indicated by vertical dashed line). The electron density (n_e) is obtained from the partial density of ions in the (0,0) state under assumption of TDE. The dashed-dotted line indicates losses due to diffusion and reactions with the time constant τ_L , the dashed line indicates the fit of the electron number density decay, see Eqs. (5) and (6). Panel (b) Measured fraction ${}^m f_3$ of meta- D_3^+ (4,2), ${}^m f_3 = [\text{meta-}D_3^+(4,2)]/[D_3^+]$.

account from the analysis to exclude eventual formation of D_3^+ in very early afterglow (for details see Refs. 18, 39, and 65). Dependencies of the effective recombination rate coefficient α_{eff} on $[\text{He}]$, measured at 80 and 100 K are shown in panels (a) and (b) of Figure 7, respectively. Linear dependence of α_{eff} on $[\text{He}]$ is obvious. Similar dependencies were measured also at 112 and 125 K. The data from previous FALP experiment are plotted in Figure 7 as open squares.¹⁷ In addition, we performed series of experiments using new Cryo-FALP II apparatus (for details on experimental setup see Ref. 63) at

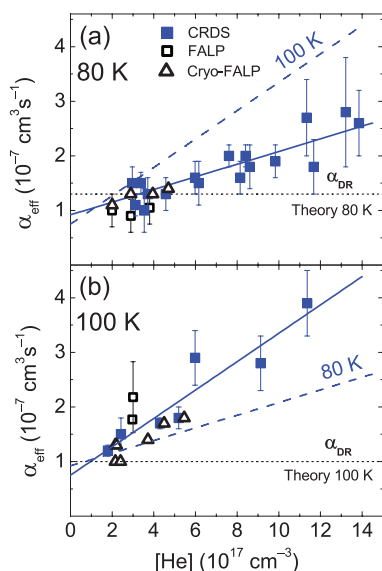


FIG. 7. Measured dependence of the effective recombination rate coefficients on $[\text{He}]$ at 80 K - panel (a) and 100 K - panel (b). The data indicated by filled squares were measured in present experiments using CRDS and the data indicated by open squares were measured using a Langmuir probe in previous FALP experiment (see compilation in Ref. 17). The data indicated by open triangles were measured in this study using a new Cryo-FALP II apparatus. For comparison straight lines obtained by a fit of CRDS data at indicated temperatures are plotted in both panels. The horizontal dotted lines indicate theoretical values of α_{DR} at corresponding temperatures.^{27,50}

the same conditions (temperature, number density of Ar and D_2) as in the already mentioned FALP experiment but in a broader pressure range and with better temperature control. These data are plotted in Figure 7 as open triangles.

Special attention was paid to the analysis of the decay curves measured at 80 and 100 K because of a possible influence of CRR process described by Bates.^{66,67} To demonstrate and evaluate the effect of CRR we used the fact that the overall binary rate coefficient α_{CRR} of the ternary CRR process is dependent on the electron density, $\alpha_{\text{CRR}} = K_{\text{CRR}} \cdot n_e$, where K_{CRR} is the ternary rate coefficient, only dependent on the temperature. We measured α_{eff} in two types of experiments, in FALP with a typical initial electron density of $n_{e0} = 2 \times 10^9 \text{ cm}^{-3}$ and in SA-CRDS with a typical initial electron density $n_{e0} = 3 \times 10^{10} \text{ cm}^{-3}$. The measured α_{eff} are plotted in Figure 7. Within experimental accuracy, the data measured at the same temperature but with very different electron densities give the same value of α_{eff} . From this we concluded that CRR contribution, which should be dependent on n_{e0} is small in comparison with the contribution from processes with their rate coefficients independent of electron density. This conclusion can be surprising, but it agrees with conclusions from more detailed studies of this phenomenon made for recombination of H_3^+ ions, for details see Ref. 41. For comparison if one uses the classical Stevefelt formula for calculation of α_{CRR} at $T = 77 \text{ K}$ and $n_e = 3 \times 10^{10} \text{ cm}^{-3}$ then the value of $\alpha_{\text{CRR}} \sim 3 \times 10^{-7} \text{ cm}^3 \text{ s}^{-1}$ is obtained (for details see Refs. 41 and 61). From the data plotted in Figure 7 it is clear that Stevefelt's calculated value of α_{CRR} ⁶¹ is three times higher than the measured overall recombination rate coefficient α_{eff} at low $[\text{He}]$. We experimentally verified the validity of Stevefelt formula for atomic ions by measuring α_{CRR} in Ar^+ dominated plasma at temperature range of 60–300 K and we obtained a good agreement.^{62,63} Up to now we do not have an explanation for not observing CRR for H_3^+ nor D_3^+ molecular ions while we can observe it for atomic Ar^+ (bearing in mind the differences between both the experiments).

We calculated binary and ternary recombination rate coefficients α_{bin} and K_{He} from the measured dependencies of α_{eff} on $[\text{He}]$ (see Eq. (7)). Present measurements are made over a broad range of $[\text{He}]$, so the accuracy of obtained α_{bin} and K_{He} is higher in comparison with previous FALP and AISA studies.¹⁷ The obtained values of α_{bin} and K_{He} are plotted in Figures 8 and 9 as a function of the temperature and summarized in Table I. The thermal rate coefficients α_{DR} calculated for binary dissociative recombination^{27,28,50} are also plotted in Figure 8 (recombination rate coefficient plotted in Figure 8 as theory of Pratt and Jungen was calculated from the dependence of the recombination rate on energy published in Ref. 28). We also included several values of rate coefficients measured in previous afterglow experiments at 300 K.^{10–12} These rate coefficients were corrected by taking the He density into account in particular experiments and the actual values of ternary rate coefficients as measured in the FALP experiment.¹⁷ We also plotted the rate coefficients calculated from the corresponding cross section measured in storage ring experiment CRYRING.^{13,19} For comparison of the measured α_{bin} with α_{CRR} , we also plotted expected

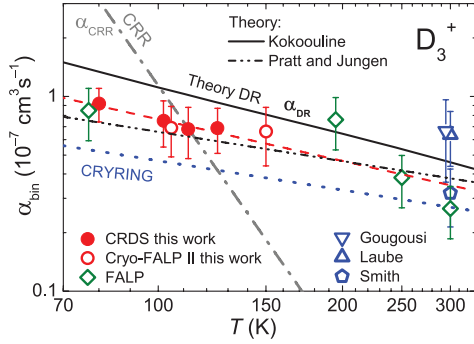


FIG. 8. D_3^+ binary recombination rate coefficients. The solid line and the dashed double dotted line indicate the values for the binary dissociative recombination (α_{DR}) at a thermal population of the para-/ortho-/meta-states of D_3^+ calculated by Kokouline^{27,30} and by Pratt and Jungen,²⁸ respectively. The values α_{bin} indicated by filled circles were obtained in present study from the dependencies of α_{eff} on [He] at particular T . The open circles denote the data obtained in this study using Cryo-FALP II apparatus. The values indicated by open diamonds were obtained in previous FALP experiments from dependencies of α_{eff} on [He] at fixed T .^{16–18} The dotted line indicates the rate coefficients measured in storage ring experiment CRYRING.^{13,19} Previous FALP data obtained in other laboratories are indicated as Gougousi,¹¹ Laube,¹⁰ and Smith;¹² these data were corrected (see text). The steep dashed-dotted line labeled CRR is the effective binary rate coefficient α_{CRR} of CRR calculated using Stevefelt formula (see Refs. 41 and 61) for electron density $n_e = 3 \times 10^{10} \text{ cm}^{-3}$. The dashed line is a fit to FALP, Cryo-FALP II, and CRDS data.

α_{CRR} in Figure 8 calculated for $n_e = 3 \times 10^{10} \text{ cm}^{-3}$ using the Stevefelt formula.^{41,61}

The measured ternary recombination rate coefficients K_{He} are in good agreement with previous data measured in FALP experiments. In our previous studies, we discussed the ternary helium assisted recombination in terms of the lifetimes of excited Rydberg states D_3^* formed in the collision of D_3^+ ions with electrons.^{16–18} Because of long life-time of D_3^* (up to several hundreds of picoseconds) the process can be, depending on the temperature, hundred times more effective

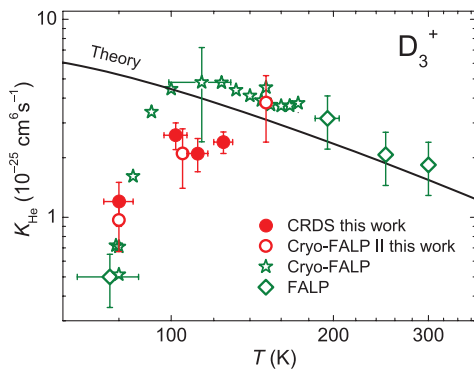


FIG. 9. The ternary recombination rate coefficient, $K_{He}(T)$, for He assisted ternary recombination of D_3^+ ions. The filled circles indicate the present values obtained from the measured linear dependencies of α_{eff} on [He] at fixed T , see full lines in Figure 7. The open circles were obtained in present study with Cryo-FALP II apparatus from the dependence of α_{eff} on [He]. The open diamonds indicate data obtained from dependence of α_{eff} on [He] measured in FALP experiment (for more details see Refs. 16–18). The data measured using Cryo-FALP with the continuously increasing temperature are labeled by stars.^{17,18} The full line indicates theoretical ternary rate coefficients calculated for D_3^+ ions in thermal equilibrium.^{16–18}

TABLE I. Measured binary α_{bin} and ternary K_{He} recombination rate coefficients of D_3^+ . The displayed temperature T is the temperature obtained from Doppler broadening of absorption lines in the present study and temperature of the metal wall of the flow tube in FALP experiments.¹⁷

T [K]	α_{bin} ($10^{-8} \text{ cm}^3 \text{ s}^{-1}$)	K_{He} ($10^{-25} \text{ cm}^6 \text{ s}^{-1}$)	Reference
77	8.5 ± 2.5	0.5 ± 0.2	FALP ¹⁷
80	9.2 ± 2.0	1.2 ± 0.3	This study
100	7.5 ± 2.0	2.6 ± 0.4	This study
112	6.5 ± 2.0	2.1 ± 0.4	This study
125	6.9 ± 1.8	2.4 ± 0.3	This study
300	2.7 ± 0.8	1.8 ± 0.6	FALP ¹⁷

than classical neutral assisted ternary recombination predicted by Thomson⁶⁸ and by Bates and Khare.⁶⁹ The process is essentially different from the process considered by Thomson. The present studies confirmed the previously measured strong increase of K_{He} with temperatures starting from 80 K.

VI. CONCLUDING REMARKS

We studied electron-ion recombination in D_3^+ dominated afterglow plasma in He/Ar/ D_2 gas mixture using CRDS for measuring ion density decays during the afterglow and for characterizing kinetic and rotational temperature of ions. From this measurements and using similarity with H_3^+ dominated afterglow plasma^{39,41,56} we concluded that at used conditions D_3^+ dominated afterglow plasma is in thermal equilibrium with He buffer gas. The study confirmed that the decay of D_3^+ dominated afterglow plasma is controlled by the binary recombination and in parallel by the three body helium assisted recombination process. The magnitude and temperature dependence of rate coefficients of these processes as measured with CRDS are in agreement with our previous flowing afterglow studies using Langmuir probe.^{16–18} The binary and the ternary recombination rate coefficients were obtained in the temperature range of 80–130 K yielding $\alpha_{bin}(80 \text{ K}) = (9.2 \pm 2.0) \times 10^{-8} \text{ cm}^3 \text{ s}^{-1}$, $\alpha_{bin}(125 \text{ K}) = (6.9 \pm 1.8) \times 10^{-8} \text{ cm}^3 \text{ s}^{-1}$, $K_{He}(80 \text{ K}) = (1.2 \pm 0.3) \times 10^{-26} \text{ cm}^6 \text{ s}^{-1}$ and $K_{He}(125 \text{ K}) = (2.4 \pm 0.3) \times 10^{-26} \text{ cm}^6 \text{ s}^{-1}$.

As in our previous recombination study of H_3^+ dominated plasma, neither for recombination of D_3^+ ions we have seen any substantial dependence of recombination rate coefficient on electron number density as predicted by theory of collisional radiative recombination.⁶¹ This rather surprising result is supported by comparison of effective recombination rate coefficients obtained at the temperature of 80 K in this study and in previous flowing afterglow measurement¹⁷ (see Figure 7 for details) at electron number densities different by an order of magnitude.

This is the first study on the recombination of D_3^+ ions with electrons with spectroscopically resolved abundances of the recombining ions. The results support theoretical predictions and are in agreement with previous flowing afterglow measurements^{16–18} and with storage ring data.^{13,19}

ACKNOWLEDGMENTS

This work was partly financed by the research grant OC10046 from the Ministry of Education of the Czech Republic and was partly supported by GACR (205/09/1183, P209/12/0233), by SV 265 302, by GAUK 92410, GAUK 353811, GAUK 54010, and by COST Action CM0805 (The Chemical Cosmos).

- ¹T. R. Geballe and T. Oka, *Science* **312**, 1610 (2006).
- ²C. D. Gay, P. C. Stancil, S. Lepp, and A. Dalgarno, *Astrophys. J.* **737**, 44 (2011).
- ³D. R. Flower, G. P. des Forets, and C. M. Walmsley, *Astron. Astrophys.* **427**, 887 (2004).
- ⁴C. Vastel, T. G. Phillips, and H. Yoshida, *Astrophys. J.* **606**, L127 (2004).
- ⁵R. Stark, F. F. S. van der Tak, and E. F. van Dishoeck, *Astrophys. J.* **521**, L67 (1999).
- ⁶R. Stark, G. Sandell, S. C. Beck, M. R. Hogerheijde, E. F. van Dishoeck, P. van der Wal, F. F. S. van der Tak, F. Schafer, G. J. Melnick, M. L. N. Ashby, and G. de Lange, *Astrophys. J.* **608**, 341 (2004).
- ⁷E. Roueff, *J. Phys.: Conf. Ser.* **4**, 1 (2005).
- ⁸M. Larsson and A. Orel, *Dissociative Recombination of Molecular Ions* (Cambridge University Press, Cambridge, 2008).
- ⁹P. van der Donk, F. B. Yousif, and J. B. A. Mitchell, *Phys. Rev. A* **43**, 5971 (1991).
- ¹⁰S. Laube, A. L. Padellec, O. Sidko, C. Rebrion-Rowe, J. B. A. Mitchell, and B. R. Rowe, *J. Phys. B* **31**, 2111 (1998).
- ¹¹T. Gougousi, R. Johnsen, and M. F. Golde, *Int. J. Mass Spectrom.* **149-150**, 131 (1995).
- ¹²D. Smith and P. Spanel, *Int. J. Mass Spectrom.* **129**, 163 (1993).
- ¹³M. Larsson, H. Danared, A. Larson, A. L. Padellec, J. R. Peterson, S. Rosen, J. Semaniak, and C. Stromholm, *Phys. Rev. Lett.* **79**, 395 (1997).
- ¹⁴V. Poterya, J. Glosik, R. Plasil, M. Tichy, P. Kudrna, and A. Pysanenko, *Phys. Rev. Lett.* **88**, 044802 (2002).
- ¹⁵O. Novotny, R. Plasil, A. Pysanenko, I. Korolov, and J. Glosik, *J. Phys. B* **39**, 2561 (2006).
- ¹⁶J. Glosik, I. Korolov, R. Plasil, T. Kotrik, P. Dohnal, O. Novotny, J. Varju, S. Roucka, C. Greene, and V. Kokoouline, *Phys. Rev. A* **80**, 042706 (2009).
- ¹⁷T. Kotrik, P. Dohnal, I. Korolov, R. Plasil, S. Roucka, J. Glosik, C. Greene, and V. Kokoouline, *J. Chem. Phys.* **133**, 034305 (2010).
- ¹⁸J. Glosik, R. Plasil, T. Kotrik, P. Dohnal, J. Varju, M. Hejduk, I. Korlov, S. Roucka, and V. Kokoouline, *Mol. Phys.* **108**, 2253 (2010).
- ¹⁹A. L. Padellec, M. Larsson, H. Danared, A. Larson, J. R. Peterson, S. Rosen, J. Semaniak, and C. Stromholm, *Phys. Scr.* **57**, 215 (1998).
- ²⁰T. Tanabe, I. Katayama, and H. Kamegaya, *Dissociative Recombination: Theory, Experiments and Applications III* (World Scientific, Singapore, 1996), pp. 84–93.
- ²¹A. E. Orel, I. F. Schneider, and A. Suzor-Weiner, *Philos. Trans. R. Soc. London, Ser. A* **358**, 1445 (2000).
- ²²J. B. A. Mitchell, C. T. Ng, L. Forand, R. Janseen, and J. W. McGowan, *J. Phys. B* **17**, L909 (1984).
- ²³V. Zhaunerchyk, R. D. Thomas, W. D. Geppert, M. Hamberg, M. Kaminska, E. Vigren, and M. Larsson, *Phys. Rev. A* **77**, 034701 (2008).
- ²⁴V. Kokoouline and C. H. Greene, *Phys. Rev. A* **72**, 022712 (2005).
- ²⁵C. Jungen and S. T. Pratt, *Phys. Rev. Lett.* **102**(1), 023201 (2009).
- ²⁶V. Kokoouline, C. H. Greene, and B. D. Esry, *Nature (London)* **412**, 891 (2001).
- ²⁷V. Kokoouline and C. H. Greene, *Phys. Rev. A* **68**, 012703 (2003).
- ²⁸S. T. Pratt and C. Jungen, *J. Phys.: Conf. Ser.* **300**, 012019 (2011).
- ²⁹B. J. McCall, A. J. Honeycutt, R. J. Saykally, T. R. Geballe, N. Djuric, G. H. Dunn, J. Semaniak, O. Novotny, A. Al-Khalili, A. Ehlerding, F. Hellberg, S. Kalhori, A. Neau, R. Thomas, F. Osterdahl, and M. Larsson, *Nature (London)* **422**, 500 (2003).
- ³⁰H. Kreckel, M. Motsch, J. Mikosch, J. Glosik, R. Plasil, S. Altevogt, V. Andrianarijaona, H. Buhr, J. Hoffmann, L. Lammich, M. Lestinsky, I. Nevo, S. Novotny, D. A. Orlov, H. B. Pedersen, F. Sprenger, A. S. Terekhov, J. Toker, R. Wester, D. Gerlich, D. Schwalm, A. Wolf, and D. Zajfman, *Phys. Rev. Lett.* **95**, 263201 (2005).
- ³¹B. J. McCall, A. J. Honeycutt, R. J. Saykally, N. Djuric, G. H. Dunn, J. Semaniak, O. Novotny, A. Al-Khalili, A. Ehlerding, F. Hellberg, S. Kalhori, A. Neau, R. Thomas, A. Paal, F. Osterdahl, and M. Larsson, *Phys. Rev. A* **70**, 052716 (2004).
- ³²H. Kreckel, O. Novotny, K. N. Crabtree, H. Buhr, A. Petrigani, B. A. Tom, R. D. Thomas, M. H. Berg, D. Bing, M. Grieser, C. Krantz, M. Lestinsky, M. B. Mendes, C. Nordhorn, R. Repnow, J. Stutzel, A. Wolf, and B. J. McCall, *Phys. Rev. A* **82**, 042715 (2010).
- ³³A. Petrigani, S. Altevogt, M. H. Berg, D. Bing, M. Grieser, J. Hoffmann, B. Jordon-Thaden, C. Krantz, M. B. Mendes, O. Novotny, S. Novotny, D. A. Orlov, R. Repnow, T. Sorg, J. Stutzel, A. Wolf, H. Buhr, H. Kreckel, V. Kokoouline, and C. H. Greene, *Phys. Rev. A* **83**, 032711 (2011).
- ³⁴R. Plasil, J. Glosik, V. Poterya, P. Kudrna, J. Ruzs, M. Tichy, and A. Pysanenko, *Int. J. Mass Spectrom.* **218**(2), 105 (2002).
- ³⁵J. Glosik, R. Plasil, I. Korolov, O. Novotny, and T. Kotrik, *J. Phys.: Conf. Ser.* **192**, 012005 (2009).
- ³⁶J. Glosik, I. Korolov, R. Plasil, O. Novotny, T. Kotrik, P. Hlavenka, J. Varju, I. A. Mikhailov, V. Kokoouline, and C. H. Greene, *J. Phys. B* **41**, 191001 (2008).
- ³⁷J. Glosik, R. Plasil, I. Korolov, T. Kotrik, O. Novotny, P. Hlavenka, P. Dohnal, J. Varju, V. Kokoouline, and C. Greene, *Phys. Rev. A* **79**, 052707 (2009).
- ³⁸J. Varju, S. Roucka, T. Kotrik, R. Plasil, and J. Glosik, *J. Phys.: Conf. Ser.* **227**, 012026 (2010).
- ³⁹J. Varju, M. Hejduk, P. Dohnal, M. Jilek, T. Kotrik, R. Plasil, D. Gerlich, and J. Glosik, *Phys. Rev. Lett.* **106**, 203201 (2011).
- ⁴⁰M. Hejduk, P. Dohnal, J. Varju, P. Rubovic, T. Kotrik, R. Plasil, and J. Glosik, *Plasma Sources Sci. Technol.* **21**, 024002 (2012).
- ⁴¹P. Dohnal, M. Hejduk, J. Varju, P. Rubovic, S. Roucka, T. Kotrik, R. Plasil, J. Glosik, and R. Johnsen, *J. Chem. Phys.* **136**, 244304 (2012).
- ⁴²T. Amano, *J. Chem. Phys.* **92**, 6492 (1990).
- ⁴³T. Amano, *Astrophys. J.* **329**, L121 (1988).
- ⁴⁴M. Feher, A. Rohrbacher, and J. P. Maier, *Chem. Phys.* **185**, 357 (1994).
- ⁴⁵P. Macko, G. Bano, P. Hlavenka, R. Plasil, V. Poterya, A. Pysanenko, O. Votava, R. Johnsen, and J. Glosik, *Int. J. Mass Spectrom.* **233**, 299 (2004).
- ⁴⁶P. Macko, R. Plasil, P. Kudrna, P. Hlavenka, V. Poterya, A. Pysanenko, G. Bano, and J. Glosik, *Czech. J. Phys.* **52**, 695 (2002).
- ⁴⁷P. Hlavenka, R. Plasil, G. Bano, I. Korolov, D. Gerlich, J. Ramanlal, J. Tennyson, and J. Glosik, *Int. J. Mass Spectrom.* **255**, 170 (2006).
- ⁴⁸J. Glosik, P. Hlavenka, R. Plasil, F. Windisch, D. Gerlich, A. Wolf, and H. Kreckel, *Philos. Trans. R. Soc. London, Ser. A* **364**(1848), 2931 (2006).
- ⁴⁹S. F. dos Santos, V. Kokoouline, and C. H. Greene, *J. Chem. Phys.* **127**, 124309 (2007).
- ⁵⁰L. Pagani, C. Vastel, E. Hugo, V. Kokoouline, C. H. Greene, A. Bacmann, E. Bayet, C. Ceccarelli, R. Peng, and S. Schlemmer, *Astron. Astrophys.* **494**, 623 (2009).
- ⁵¹M. T. Leu, M. A. Biondi, and R. Johnsen, *Phys. Rev. A* **8**, 413 (1973).
- ⁵²J. Glosik, R. Plasil, V. Poterya, P. Kudrna, M. Tichy, and A. Pysanenko, *J. Phys. B* **34**(15), L485 (2001).
- ⁵³L. S. Rothman, I. E. Gordon, A. Barbe, D. C. Benner, P. F. Bernath, M. Borik, V. Boudon, L. R. Brown, A. Campargue, J.-P. Champion, K. Chance, L. H. Coudert, V. Dana, V. M. Devi, S. Fally, J.-M. Flaud, R. R. Gamache, A. Goldman, D. Jacquemart, I. Kleiner, N. Lacome, W. J. Lafferty, J.-Y. Mandin, S. T. Massie, S. N. Mikhailenko, C. E. Miller, N. Moazzen-Ahmadi, O. V. Naumenko, A. V. Nikitin, J. Orphai, V. I. Perevalov, A. Perrin, A. Predoi-Cross, C. P. Rinsland, M. Rotger, M. Simeckova, M. A. H. Smith, K. Sung, S. A. Tashkun, J. Tennyson, R. A. Toth, A. C. Vandaele, and J. V. Auwera, *J. Quant. Spectrosc. Radiat. Transf.* **110**, 533 (2009).
- ⁵⁴J. Tennyson, private communication (2012).
- ⁵⁵J. Ramanlal and J. Tennyson, *Mon. Not. R. Astron. Soc.* **354**, 161 (2004).
- ⁵⁶P. Dohnal, M. Hejduk, J. Varju, P. Rubovic, S. Roucka, T. Kotrik, R. Plasil, R. Johnsen, and J. Glosik, *Philos. Trans. R. Soc. London, Ser. A* **370**, 5101 (2012).
- ⁵⁷I. Korolov, T. Kotrik, R. Plasil, J. Varju, M. Hejduk, and J. Glosik, *Contrib. Plasma Phys.* **48**(5–7), 521 (2008).
- ⁵⁸R. Plasil, I. Korolov, T. Kotrik, J. Varju, P. Dohnal, Z. Donko, G. Bano, and J. Glosik, *J. Phys.: Conf. Ser.* **192**, 012023 (2009).
- ⁵⁹R. Plasil, I. Korolov, T. Kotrik, P. Dohnal, G. Bano, Z. Donko, and J. Glosik, *Eur. Phys. J. D* **54**, 391 (2009).
- ⁶⁰J. Glosik, G. Bano, R. Plasil, A. Luca, and P. Zakouril, *Int. J. Mass Spectrom.* **189**, 103 (1999).
- ⁶¹J. Stevefelt, J. Boulmer, and J. Delpech, *Phys. Rev. A* **12**, 1246 (1975).
- ⁶²T. Kotrik, P. Dohnal, S. Roucka, P. Jusko, R. Plasil, J. Glosik, and R. Johnsen, *Phys. Rev. A* **83**, 032720 (2011).
- ⁶³T. Kotrik, P. Dohnal, P. Rubovic, R. Plasil, S. Roucka, S. Opanasiuk, and J. Glosik, *Eur. Phys. J.: Appl. Phys.* **56**, 24011 (2011).
- ⁶⁴R. Plasil, I. Korolov, T. Kotrik, and J. Glosik, *Int. J. Mass Spectrom.* **275**, 80 (2008).

- ⁶⁵R. Plasil, J. Varju, M. Hejduk, P. Dohnal, T. Kotrik, and J. Glosik, *J. Phys.: Conf. Ser.* **300**(1), 012023 (2011).
- ⁶⁶D. R. Bates, A. E. Kingston, and W. P. McWhirter, *Philos. Trans. R. Soc. London, Ser. A* **267**, 297 (1962).

- ⁶⁷E. W. McDaniel, J. B. A. Mitchell, and M. E. Rudd, *Atomic Collisions, Heavy Particle Projectiles* (Wiley Interscience, New York, 1993).
- ⁶⁸J. J. Thomson, *Philos. Mag.* **47**, 337 (1924).
- ⁶⁹D. Bates and S. Khare, *Proc. Phys. Soc. London* **85**, 231 (1965).

Binary and ternary recombination of para- H_3^+ and ortho- H_3^+ with electrons: State selective study at 77–200 K

Dohnal P., Hejduk M., Varju J., Rubovič P., Roučka Š., Kotrík T., Plašil R.,
Glosík J., Johnsen R.

J. Chem. Phys. **136(24)**, 244304, 2012.

Binary and ternary recombination of para- H_3^+ and ortho- H_3^+ with electrons: State selective study at 77–200 K

Petr Dohnal,¹ Michal Hejduk,¹ Jozef Varju,¹ Peter Rubovič,¹ Štěpán Roučka,¹ Tomáš Kotřík,¹ Radek Plašil,¹ Juraj Glosík,¹ and Rainer Johnsen²

¹Department of Surface and Plasma Science, Faculty of Mathematics and Physics, Charles University, Prague 18000, Czech Republic

²Department of Physics and Astronomy, University of Pittsburgh, Pittsburgh, Pennsylvania 15260, USA

(Received 13 April 2012; accepted 1 June 2012; published online 26 June 2012)

Measurements in H_3^+ afterglow plasmas with spectroscopically determined relative abundances of H_3^+ ions in the para-nuclear and ortho-nuclear spin states provide clear evidence that at low temperatures (77–200 K) para- H_3^+ ions recombine significantly faster with electrons than ions in the ortho state, in agreement with a recent theoretical prediction. The cavity ring-down absorption spectroscopy used here provides an *in situ* determination of the para/ortho abundance ratio and yields additional information on the translational and rotational temperatures of the recombining ions. The results show that H_3^+ recombination with electrons occurs by both binary recombination and third-body (helium) assisted recombination, and that both the two-body and three-body rate coefficients depend on the nuclear spin states. Electron-stabilized (collisional-radiative) recombination appears to make only a small contribution. © 2012 American Institute of Physics. [<http://dx.doi.org/10.1063/1.4730162>]

I. INTRODUCTION

The present experiments were motivated by the fundamental character of the recombination of H_3^+ ions,¹ its relevance to modeling of astrophysical diffuse clouds,² and electrical discharges in hydrogen. In cold diffuse clouds (temperatures from 50 to 100 K), H_3^+ ions are formed by cosmic-ray ionization of H_2 , followed by the reaction $\text{H}_2^+ + \text{H}_2 \rightarrow \text{H}_3^+ + \text{H}$.³ The H_3^+ ions subsequently either recombine by dissociative recombination (DR) with electrons or transfer protons to other atoms or molecules.⁴ The recombination of H_3^+ ions competes with the rate of molecule formation in diffuse clouds and plays a pivotal role in the chemical evolution. Even though H_3^+ is the “simplest” triatomic ion, its recombination is a rather subtle process that has challenged theorists and experimentalists for many years. It has become clear in recent years that the ortho-modifications and para-modifications of H_3^+ , distinguished by their nuclear spins and allowed rotational states, may recombine differently at low temperatures. The experiments described in this paper focus on this question. Unlike other previous experiments, they incorporate *in situ* spectroscopic identification of the recombining ion species in the recombining medium.

The spin dependence of H_3^+ recombination also plays a role in the interpretation of spectra observed in astrophysical clouds. For instance, a recent analysis by Crabtree *et al.*⁵ of several diffuse molecular clouds suggests that the observed differences between the rotational excitation temperatures of H_2 and H_3^+ (denoted as $T_{(01)}(\text{H}_2)$ and $T(\text{H}_3^+)$) can be explained by a kinetic model that includes both reactive collisions of H_3^+ or para- H_3^+ with H_2 and recombination with electrons. The model makes specific allowance for the dependence of all relevant reaction rates on the ortho/para states of both

H_2 and H_3^+ . Surprisingly, reasonable agreement between observed and calculated excitation temperatures was found only when the DR rate coefficients of para- H_3^+ (nuclear spin $I = 1/2$) and H_3^+ (nuclear spin $I = 3/2$) were assumed to be nearly equal, which, however, is in conflict with the theoretical prediction⁶ that the low-temperature DR rate coefficient of para- H_3^+ is considerably larger than that of H_3^+ .

The history of H_3^+ recombination studies has been extensively covered in a number of reviews^{7–12} and in the book by Larsson and Ore.¹³ Many of the once puzzling disagreements among measured recombination coefficients have either been resolved or can be rationalized by invoking third-body stabilized recombination processes that occur in plasmas but not in beam-type experiments. Also, earlier serious discrepancies between experimental results and theory were largely resolved in 2001 when it was shown that the Jahn–Teller mechanism can account for the observed magnitude of dissociative recombination rates of H_3^+ ions.¹⁴ Subsequent improvements of the theory¹⁵ yielded a thermal rate coefficient of the dissociative recombination at 300 K of $\alpha_{\text{DR}} = 5.6 \times 10^{-8} \text{ cm}^3 \text{ s}^{-1}$ which comes close to the magnitude of many experimental values. Theoretical predictions also agree quite well with the temperature dependence of the thermal rate coefficients inferred from ion-storage-rings (ISR) experiments. The more recent ISR studies employed ion sources specifically designed to produce rotationally cold ions (“cold ion sources”)^{16–18} and the results supported the theoretical thermal rate coefficients.¹⁹ At that time it appeared that a satisfactory solution to the “ H_3^+ enigma,” the often-cited term coined by Bates *et al.* in 1993,²⁰ had been found. However, it proved difficult to verify experimentally that the H_3^+ ions circulating in the storage rings were truly rotationally cold

and this problem has not been entirely solved. It had been assumed that the “cold” rotational distributions inferred from spectroscopic observations in the ion source survived extraction into the storage ring and were not altered further in the ring, but recent experiments using high-resolution storage-rings indicate that these assumptions were not necessarily correct.^{21,22} The problem awaits clarification by further experiments. Also, high-resolution storage rings data exhibit resonances at particular collision energies that have not been clearly assigned to specific recombination paths and are not predicted by theory.²² Thus, a truly satisfactory convergence of theory and experiment has not been achieved. Petrigani *et al.*²² summed up the current situation of storage-ring experiments: “*Presently no rate coefficient measurement with a confirmed temperature below 300 K exists.*” Plasma afterglow measurements at reduced temperatures have been made, but those, as will be discussed later, have their own set of complications. Paraphrasing Bates *et al.*²⁰ and Larsson *et al.*,¹⁹ we can sum up the state of the art today in the words: “... *the saga of the H₃⁺ enigma continues...*”

Recent theoretical calculations⁶ predict that the low-temperature DR rate coefficients for para-H₃⁺ are larger than those for H₃⁺ ions, by a factor of about ten at temperatures below 10 K. This prediction has been qualitatively confirmed at low electron-ion collision energies in storage-ring experiments using para-enriched H₃⁺,^{17,23} but, as has been mentioned before, the actual para/ortho abundance ratio of the recombining ions was not experimentally verified. This problem, of course, is closely linked to that of the rotational populations. Further progress will require direct *in situ* determination of the para/ortho ratio and rotational excitation of the stored H₃⁺ ions. Experimental photodissociation measurements on H₃⁺ ions in the ring may be one feasible approach (see discussion in Refs. 24 and 25).

The experiments described here make use of the plasma afterglow technique but add spectroscopic capabilities. Here, the ion densities are many orders of magnitude larger than those in storage rings which enables *in situ* spectroscopic absorption measurements of rotational populations of H₃⁺ ions under recombination-controlled conditions. The feasibility of such experiments was demonstrated by us in a recent study in which we measured binary recombination rate coefficients for para-H₃⁺ and ortho-H₃⁺ ions (^pα_{bin} and ^oα_{bin}) at buffer gas temperature ~77 K.^{26,27} The present study extends this work and provides recombination rate coefficients for pure para-H₃⁺ and pure ortho-H₃⁺ over a wider range of temperatures from 77 K to 200 K. As before, the experiments were carried out in a stationary afterglow (SA) in conjunction with a near-infrared cavity-ring-down absorption spectrometer (NIR-CRDS) for direct *in situ* determination of the kinetic temperature, the rotational temperature, and the spin states of the ions.

In a SA experiment²⁸ electrons and ions undergo multiple collisions with buffer gas atoms (here He and Ar) and reagent molecules (here H₂) prior to their recombination. The early phase of the afterglow is dominated by ion-formation and ion-conversion reactions, electron thermalization, and equilibration of internal degrees of freedom of the ions. Ideally, this early phase should be completed rapidly so that the only

relevant processes during the recombination phase are binary electron-ion recombination and ambipolar diffusion of ions and electrons. However, the neutral constituents (He, H₂, and Ar in our case) and ambient electrons and ions can affect the overall recombination process as well as the para/ortho ratio and this requires careful consideration. There are two known ternary recombination processes that contribute to the plasma decay, ternary neutral-assisted recombination (largely due to the helium buffer),²⁹ and ternary electron-assisted collisional radiative recombination (CRR).^{30–32} We have recently studied the ternary helium-assisted recombination of H₃⁺ and D₃⁺ ions with electrons at conditions similar to those of the present experiments^{8,33–37} and found that H₃⁺ ions recombine by both the binary process with rate coefficient α_{bin} and by ternary (“He-assisted”) process with ternary rate coefficient K_{He}. The observed plasma decay yields an “effective” rate coefficient α_{eff} given by the sum α_{eff} = α_{bin} + K_{He}[He] that can be decomposed into its parts by measuring the dependence of α_{eff} on helium density [He].

The role of electron-assisted CRR is less clear because experimental data and theoretical calculations exist only for atomic ions but not for molecular ions. For atomic ions the predicted very strong negative temperature dependence, α_{CRR} ~ n_eT^{-4.5}, of the CRR rate coefficient, has been confirmed for temperatures above 300 K,^{30,38,39} and recently also for Ar⁺ ions at temperatures below 300 K.^{32,40} In low-temperature plasmas most molecular ions are removed by fast dissociative recombination (see, e.g., book by Larsson and Orei¹³) and the contribution from collisional radiative recombination is usually negligible. However, at temperatures approaching 77 K the effective binary rate of CRR (Refs. 38 and 39) becomes comparable to typical DR rate coefficients for electron densities >10¹⁰ cm⁻³. Somewhat surprisingly, the H₃⁺ afterglow studies of Amano^{41,42} at gas temperatures near 77 K and electron densities >10¹¹ cm⁻³ seemed to indicate that CRR did not play a significant role. However, as Bates²⁰ pointed out, the occurrence of CRR is “inevitable,” and to make matters worse, the observed plasma decay due to CRR can give the appearance of binary recombination since the energy released by CRR can lead to a time-dependent electron temperature. A quantitative re-analysis of Amano’s experiments is beyond the scope of this paper. It is far from obvious that CRR made only a negligible contribution. It is also difficult to accept the author’s conclusion that clustering of H₃⁺ to form fast recombining H₅⁺ ions was entirely absent.

In our flowing afterglow (FA, FALP (Ref. 34)) and stationary afterglow (SA (Refs. 26 and 43)) experiments we can measure at gas temperatures close to 77 K and cover a wide range of electron and ion densities, from 10⁸ to 10¹¹ cm⁻³. This makes it possible to separate binary and helium-assisted ternary recombination of H₃⁺ ions from CRR. We will conclude (see Appendix) that CRR may have a slight effect at the lowest temperature (77 K), but most likely it is completely negligible at higher temperatures.

II. EXPERIMENTAL METHODS

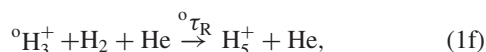
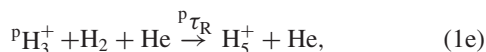
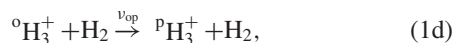
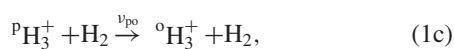
The basic methods of measuring recombination rates in afterglow plasmas are well known and will not be

discussed here in great detail. This section focuses on the interconversion processes between para- H_3^+ and ortho- H_3^+ ions, and their recombination. Technical details of the experiments will be presented in Sec. III.

A. Afterglow processes in para- H_3^+ and ortho- H_3^+ dominated plasma

In the following upper left indices p, o, n, and e denote “para,” “ortho,” “normal,” and “para-enriched” hydrogen (e.g., ${}^p\text{H}_2$, ${}^o\text{H}_2$, ${}^n\text{H}_2$, and ${}^e\text{H}_2$) and ${}^p f_2$ and ${}^o f_2$ denote their fractions. Para- H_3^+ and ortho- H_3^+ ions denote ${}^p\text{H}_3^+$ and ${}^o\text{H}_3^+$, while ${}^p f_3$ and ${}^o f_3$ stand for their fractions (i.e., ${}^p f_3 = [{}^p\text{H}_3^+]/[\text{H}_3^+]$ and ${}^o f_3 = [{}^o\text{H}_3^+]/[\text{H}_3^+]$ with ${}^p f_3 + {}^o f_3 = 1$). Absence of an index implies that the spin modification is not specified.

In a low-temperature afterglow plasma in a gas mixture of helium (the “buffer gas”) with small additions of argon and hydrogen the principal processes affecting the densities of ${}^p\text{H}_3^+$ and ${}^o\text{H}_3^+$ are recombination, ambipolar diffusion, para/ortho conversion in reactions with H_2 , and formation of H_5^+ in ternary association, i.e.:



where ${}^p\alpha_{\text{eff}}$ and ${}^o\alpha_{\text{eff}}$ stand for effective (apparent binary) recombination rate coefficients of pure para- H_3^+ and pure ortho- H_3^+ ions, respectively. ν_{po} and ν_{op} are the frequencies of para- H_3^+ /ortho- H_3^+ conversion due to reactions with H_2 . The spin state of the neutral hydrogen molecule in reactions (1c) and (1d) will change also, but because the neutral hydrogen is far more abundant than the ions, the resulting change in ${}^p f_2$ can be neglected. ${}^p\tau_{\text{R}}$ and ${}^o\tau_{\text{R}}$ are time constants for ternary association, later we will assume that ${}^p\tau_{\text{R}} = {}^o\tau_{\text{R}}$ for simplification. The continuity equations for the ion densities $[{}^p\text{H}_3^+]$ and $[{}^o\text{H}_3^+]$ during the afterglow are:

$$\frac{d[{}^p\text{H}_3^+]}{dt} = -{}^p\alpha_{\text{eff}}[{}^p\text{H}_3^+]n_e - \frac{[{}^p\text{H}_3^+]}{\tau_{\text{D}}} - \nu_{po}[{}^p\text{H}_3^+] + \nu_{op}[{}^o\text{H}_3^+] - \frac{[{}^p\text{H}_3^+]}{{}^p\tau_{\text{R}}}, \quad (2)$$

$$\frac{d[{}^o\text{H}_3^+]}{dt} = -{}^o\alpha_{\text{eff}}[{}^o\text{H}_3^+]n_e - \frac{[{}^o\text{H}_3^+]}{\tau_{\text{D}}} + \nu_{po}[{}^p\text{H}_3^+] - \nu_{op}[{}^o\text{H}_3^+] - \frac{[{}^o\text{H}_3^+]}{{}^o\tau_{\text{R}}}, \quad (3)$$

where n_e is electron density and τ_{D} is the time constant for ambipolar diffusion, assumed to be equal for both spin modification of H_3^+ . Three-body association of H_3^+ with H_2 to form H_5^+ is at the hydrogen and helium densities used in the present experiments relatively slow in comparison with the rate of the recombination (for details see Refs. 9, 34, and 44) and we can conclude $[\text{H}_5^+] \ll [\text{H}_3^+]$. Assuming that the plasma is quasineutral and that it contains no ions other than H_3^+ (i.e., $n_e = [{}^p\text{H}_3^+] + [{}^o\text{H}_3^+]$), the continuity equation for the electron density (obtained by summing Eqs. (2) and (3)) becomes

$$\frac{dn_e}{dt} = -({}^p f_3 {}^p\alpha_{\text{eff}} + {}^o f_3 {}^o\alpha_{\text{eff}})n_e^2 - \frac{n_e}{\tau_{\text{D}}} - \frac{n_e}{\tau_{\text{R}}}. \quad (4a)$$

The experimental data (see Sec. V) show that the fractions ${}^p f_3$ and ${}^o f_3$ are nearly constant during the afterglow. This implies that the para/ortho ratio is maintained by reactions (1c) and (1d) on a time scale that is short compared to the recombination time scale. In that case, one can define an overall effective (apparent binary) recombination rate coefficient for a given mixture of ortho and para ions by $\alpha_{\text{eff}} = {}^p f_3 {}^p\alpha_{\text{eff}} + {}^o f_3 {}^o\alpha_{\text{eff}}$. Equation (4a) then simplifies to

$$\frac{dn_e}{dt} = -\alpha_{\text{eff}}n_e^2 - \frac{n_e}{\tau_{\text{L}}}, \quad (4b)$$

where $1/\tau_{\text{L}} = 1/\tau_{\text{D}} + 1/\tau_{\text{R}}$. The time constant τ_{L} characterizes losses due to diffusion and reactions (1e) and (1f).

A measurement of α_{eff} for two or more different values of ${}^p f_3$, but under otherwise identical conditions (temperature and density of He and H_2), then permits a determination of the individual recombination rate coefficients ${}^p\alpha_{\text{eff}}$ and ${}^o\alpha_{\text{eff}}$. These rate coefficients still do not necessarily represent purely binary recombination. In earlier work we observed that H_3^+ recombination in low-temperature (<300 K) helium-buffered afterglows occurs not only by binary recombination but also by ternary helium-assisted recombination.^{8,33,34,36} In those studies ${}^n\text{H}_2$ was used as a precursor gas to form H_3^+ . It was then found that the effective recombination coefficient α_{eff} varies linearly with helium density $[\text{He}]$, i.e.,

$$\alpha_{\text{eff}}(T, [\text{He}]) = \alpha_{\text{bin}}(T) + K_{\text{He}}[\text{He}], \quad (5)$$

where α_{bin} and K_{He} are the binary and ternary recombination rate coefficients. Previous experiments at 77 K (Ref. 27) showed that the same linear relation holds for the state-selected effective recombination rate coefficients ${}^p\alpha_{\text{eff}}$ and ${}^o\alpha_{\text{eff}}$. Hence, least-square fits to data of α_{eff} as a function of the helium density for two different values of ${}^p f_3$ can be analyzed to obtain α_{bin} and K_{He} for each of the two spin states of H_3^+ .

In experiment, ${}^p f_3$ can be enhanced from about 0.5 to 0.8 by substituting para-enriched hydrogen for normal hydrogen. This was tested by a preliminary set of experiments, to be discussed next. Technical details of the para H_2 generator and the optical absorption measurements will be presented in Sec. III.

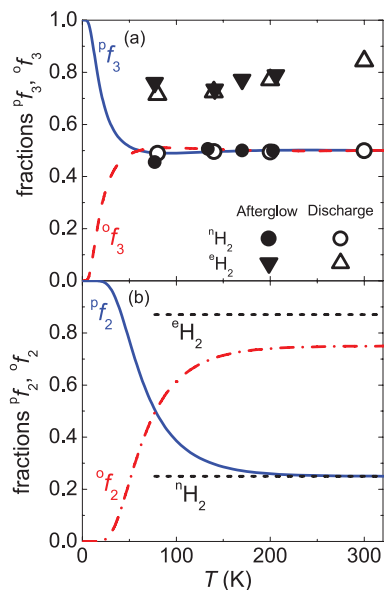


FIG. 1. Panel (a): Calculated temperature variation of the fractions ${}^p f_3$ and ${}^o f_3$ in thermal equilibrium, compared to measured values of ${}^p f_3$ during the discharge phase (open triangles) and during the afterglow (closed circles and triangles) in experiments with either ${}^n\text{H}_2$ or ${}^e\text{H}_2$. Panel (b): Calculated thermal-equilibrium fractions ${}^p f_2$ and ${}^o f_2$. The dashed horizontal lines indicate the values of ${}^p f_2$ in experiments with either ${}^n\text{H}_2$ or ${}^e\text{H}_2$ (measured by NMR).

B. Method of controlling the relative abundance of para- H_3^+ and ortho- H_3^+

In the experiment, normal ${}^n\text{H}_2$ is obtained by cooling normal hydrogen from 300 K to lower temperatures without ortho–para conversion, i.e., in a container without a catalyst. Hence, ${}^n\text{H}_2$ will have fraction ${}^p f_2 = 1/4$ and ${}^o f_2 = 3/4$. Para-enriched H_2 is produced by cooling normal hydrogen to cryogenic temperatures in the presence of a catalyst and then letting it warm up without the catalyst to the desired temperature. Our experiments confirmed earlier findings that an increase of ${}^p f_3$ in hydrogen discharges can be achieved by using ${}^e\text{H}_2$ instead of ${}^n\text{H}_2$ (see, e.g., Refs. 45 and 46), and that the increase of ${}^p f_3$ observed during the microwave discharge persists into afterglow phase.^{26,27,43}

Figure 1 shows the equilibrium values ${}^p f_3$ and ${}^o f_3$ and ${}^p f_2$ and ${}^o f_2$ for temperatures from 0 to 300 K, calculated using published energy levels.^{47,48} The same graph shows our experimental values of ${}^p f_3$ and ${}^o f_3$. In normal H_2 measured ${}^p f_3$ approach 0.5 at temperatures above ~ 77 K, this is the value corresponding to thermal equilibrium at these temperatures. When para-enriched H_2 is used, measured ${}^p f_3$ becomes significantly larger (~ 0.8).

III. EXPERIMENTAL APPARATUS

A. Stationary afterglow

The plasma is generated in a pulsed microwave discharge in a fused silica tube (inner diameter ~ 1.5 cm) cooled by liquid nitrogen to nearly 77 K or by pre-cooled nitrogen gas for measurements in the range 80–220 K. The tube contains a mixture of He/Ar/ H_2 with a typical composition

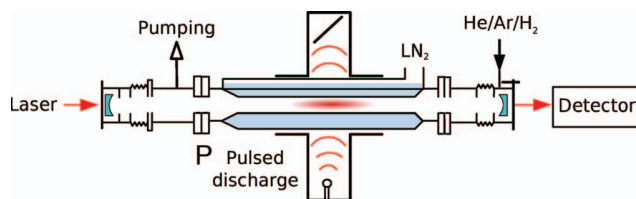


FIG. 2. Schematic diagram (not to scale) of the discharge tube and the optical resonator (cw-CRDS). The discharge tube at the center (containing a He/Ar/ H_2 gas mixture) is immersed in liquid or pre-cooled gaseous nitrogen. The light signal exiting the optical cavity is measured by a photodetector (InGaAs avalanche photodiode).

$10^{17}/10^{14}/10^{14}$ cm^{-3} (details of the ion formation reactions are given in Refs. 8, 9, 34, 37, 44, and 49). The gas handling system includes a “para H_2 generator,” used to prepare samples of para-enriched H_2 , indicated here as ${}^e\text{H}_2$.⁴³ The microwave generator 2.45 GHz is equipped with an external fast high voltage switch to cut off the power to the magnetron within a fall time of < 30 μs . A fairly low microwave power in the range 5–15 W, with $\sim 50\%$ duty cycle, was used to avoid excessive heating of the gas during the discharge.

B. CRDS spectroscopy

The principal diagnostic technique employs cavity ring down absorption spectroscopy in the continuous wave modification (cw-CRDS), based on the configuration described by Romanini *et al.*⁵⁰ The instrument used here was fabricated in our laboratory for spectroscopic time-resolved studies of elementary processes in plasmas, such as ion–electron recombination (see, e.g., Refs. 43 and 51–54). The light source is a fiber-coupled distributed feedback (DFB) laser diode with a central wavelength of 1381.55 nm, linewidth < 2 MHz, and maximum output optical power of 20 mW. The wavelengths are measured by a wavemeter and a Fabry–Perot etalon. The ring-down signal exiting the optical cavity is detected by an InGaAs avalanche photodiode. A schematic picture of the apparatus is shown in Fig. 2.

The cw-CRDS instrument in conjunction with associated data processing electronics records the time-dependent optical absorption signals during the discharge and the afterglow. The observed absorption strengths are then converted to ion concentrations. By tuning the wavelength of the laser diode one can also determine the kinetic temperatures of the H_3^+ ions from the Doppler-broadened absorption line profiles, and their evolution during the discharge and in the early afterglow.

All spectroscopic absorption measurements were performed on the second overtone transitions originating from the ground vibrational level of H_3^+ . The lowest rotational levels (1,0) (ortho) and (1,1) (para) of the vibrational ground state were monitored routinely, but the higher lying level (3,3) (ortho) was probed only occasionally. These first two transitions were chosen for routine scanning because they have closely spaced frequencies that can be covered by a single DFB laser. This made it possible to switch quickly from observing one to the other H_3^+ spin state. Figure 3 shows the relevant rotational levels and Table I lists the transitions. The

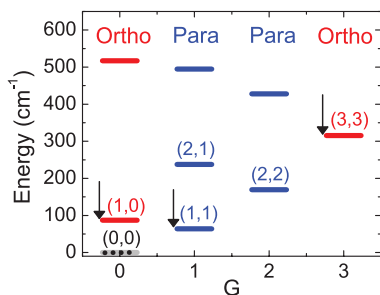


FIG. 3. Rotational energy levels of the ground vibrational state of H_3^+ . The energy levels (J,G) are labeled by quantum numbers J and G.⁵⁵ The zero of the energy scale is taken at the forbidden (0,0) level, indicated by a dashed line. The rotational states, (1,0), (1,1), and (3,3) observed in the present study are indicated by arrows. Compiled from the data in Ref. 56.

energy levels are labeled (J,G) by their quantum numbers J and G.⁵⁵

C. Para H_2 generator

Normal hydrogen gas at 300 K is a mixture of 1/4 para-hydrogen and 3/4 ortho-hydrogen (i.e., $^p f_2 = 0.25$ and $^o f_2 = 0.75$, see Fig. 1). It is well known that the composition changes extremely slowly when the hydrogen is cooled or heated, unless the gas is in contact with a suitable paramagnetic catalyst that facilitates re-alignment of the proton spins. By using a catalyst and cooling to low temperatures, nearly pure samples of para-hydrogen in the lowest rotational state ($J = 0, \nu = 0$) can be produced. When the catalyst is then removed and the gas is reheated, the hydrogen retains its low-temperature para/ortho composition for a sufficiently long time to carry out experiments with para-enriched hydrogen.

We produced para-enriched hydrogen in a closed-cycle helium cryostat that cools hydrogen in a conversion chamber⁵⁷ filled with the catalyst Fe_2O_3 . Nuclear magnetic resonance (NMR) was used to check the actual para/ortho ratio in the enriched para-hydrogen $^e\text{H}_2$. The experimental setup for measurement of para-hydrogen enrichment was similar to the one used in study by Tom.⁵⁸ The NMR measurements indicated $(87 \pm 5)\%$ content of para-hydrogen, i.e., $^p f_2 = 0.87$,⁵⁹ which is adequate for our experiments. In the following text we will use this value of $^p f_2$ without explicitly mentioning its error. It suffices to enrich the hydrogen to a level where the fraction of para- H_3^+ significantly exceeds the value $^p f_3 = 0.5$ in normal hydrogen. Figure 1 shows experimental data on the para-enrichment of H_3^+ measured in the discharge and in the afterglow for $^e\text{H}_2$ and for $^n\text{H}_2$.

IV. TEMPERATURES IN THE H_3^+ AFTERGLOW PLASMA

The different particles in a plasma afterglow and their internal degrees of freedom are not necessarily in complete thermal equilibrium with each other and with the walls of the plasma container. For instance, the electron temperature T_e can significantly exceed that of the ions T_{Kin} and gas atoms T_G because the energy transfer in electron collisions with heavy particles is inefficient. Also, the ion's rotational temperature T_{Rot} and vibrational temperature T_{Vib} do not have to be equal to the ion's translational temperature.

A. Ion and neutral gas kinetic temperatures

Since the exchange of translational energy between ions and neutral gas atoms is very efficient, the kinetic temperature of the H_3^+ ions during the afterglow should be nearly the same as the gas temperature, provided that the plasma is free of macroscopic electric fields that, in principle, can heat the ions. The ambipolar electric field is too weak to cause a significant heating. This expectation was confirmed by time-resolved scans of the Doppler-broadened absorption lines of H_3^+ ions over the experimental temperature range from 77 K to 220 K. The inferred temperatures of the H_3^+ ions during the discharge and the afterglow were equal to the wall temperature within ~ 10 K (see also Figs. 3 and 4 in Ref. 43). This also confirmed that the gas temperature in the discharge region approaches that of the walls. Previous afterglow studies in this lab performed under similar conditions,⁶⁰ but using absorption lines of H_2O rather than of H_3^+ , led to the same conclusion.

B. Electron temperature T_e

The electron temperature T_e was not measured in these experiments. In previous FALP experiments^{61–63} we used Langmuir probes to determine the electron energy distribution function in He and He/Ar buffered afterglow plasmas under conditions similar to those in the present study. It was found that the electrons gained a Maxwellian distribution with the gas temperature very quickly after the metastable helium atoms from the microwave discharge had been depleted by Penning ionization of argon atoms.⁶⁴ The electron cooling time constant at typical helium densities can also be estimated as the product of the electron-helium collision frequency (> 1 GHz) and the mass ratio $2m_e/m_{\text{He}}$, which yields a cooling time of $\tau_e < 10 \mu\text{s}$.⁶⁵ We indirectly observed fast cooling of electrons by monitoring visible light emissions from the discharge and in the very early afterglow.⁵¹ These estimates

TABLE I. Transitions monitored in the present study. For details on the spectroscopic notation see Ref. 55. Energy levels were taken from Ref. 56.

Wavenumber (cm^{-1})	Spin	Low. lvl. (cm^{-1})	Up. lvl. (cm^{-1})	Transition
7234.957	o	315.349	7550.316	$3\nu_2^1(4, 3) \leftarrow 0\nu_2^0(3, 3)$
7237.285	p	64.1234	7301.4084	$3\nu_2^1(2, 1) \leftarrow 0\nu_2^0(1, 1)$
7241.245	o	86.9591	7328.2041	$3\nu_2^1(2, 0) \leftarrow 0\nu_2^0(1, 0)$

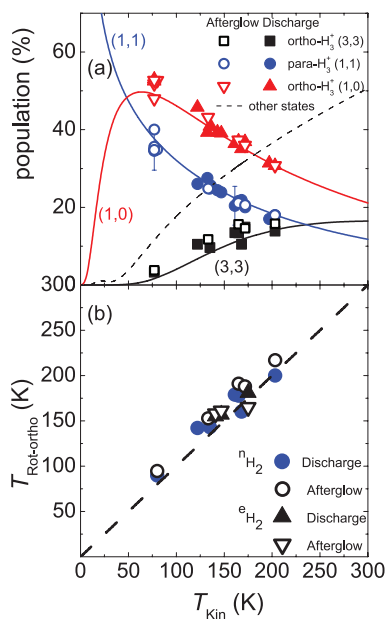


FIG. 4. Rotational temperatures of H_3^+ ions. Panel (a): Relative populations of H_3^+ ions in ortho (1,0) and (3,3) and para (1,1) states versus kinetic temperature of the ions measured in the experiments with normal H_2 . The data obtained during the discharge (before switching it off) and during the afterglow (at $\sim 150 \mu\text{s}$) are indicated by the filled and the open symbols, respectively. The full lines indicate the calculated populations of the indicated states for ions in thermal equilibrium at temperatures equal to T_{Kin} . The dashed line indicates joint population of all other states. Panel (b): The measured rotational temperature of ortho manifold ($T_{\text{Rot-ortho}}$) versus measured kinetic temperature (T_{Kin}). The data were obtained in experiments with $^n\text{H}_2$ and with $^e\text{H}_2$. The dashed straight line indicates equality $T_{\text{Rot-ortho}} = T_{\text{Kin}}$.

need to be refined when the plasma contains energy sources that heat the electron gas, for instance, recombination of ions by collisional radiative recombination. It is shown in Appendix that this heating mechanism at used electron densities can elevate the electron temperature slightly in the early afterglow at gas temperatures near 77 K, but becomes unimportant at higher gas temperatures and lower electron densities.

C. Vibrational excitation of the H_3^+ ions

We expect that all excited vibrational states of H_3^+ are quenched in collisions with He, Ar, and H_2 . The reaction $\text{H}_2^+ + \text{H}_2$ can produce H_3^+ ions with vibrational excitation up to $v = 5$ but the ions with internal energies above 0.57 eV are rapidly destroyed by proton transfer with Ar, leaving only ions in $v \leq 2$ (for details see Refs. 23 and 53). There is also a high probability that the vibrational excitation of H_3^+ will be quenched in collision with H_2 . Kim *et al.*⁶⁶ obtained a rate coefficient $3 \times 10^{-10} \text{ cm}^3 \text{ s}^{-1}$ for vibrational relaxation of H_3^+ ions in H_2 . At $[\text{H}_2] \sim 10^{14} \text{ cm}^{-3}$ this leads to vibrational relaxation within 30 μs (see also discussion and references in Ref. 67). We conclude that at Ar and H_2 densities of the order of $\sim 10^{14} \text{ cm}^{-3}$ vibrational excitation will be quenched within 30 μs after ion formation. Collisions with He atoms are more frequent by at least by three orders of magnitude, but vibrational quenching by helium can be very low, as it is, e.g., in collisions of He with vibrationally excited N_2^+ ions

(see, e.g., Ref. 68). To estimate the rate of formation of H_3^+ ions (in reactions with H_2 , Ar, and He) we studied the processes at very early afterglow at several He densities and at low H_2 and Ar densities ($[\text{H}_2]$, $[\text{Ar}] \sim 10^{12} \text{ cm}^{-3}$) in our previous study⁶⁹ and we found qualitative agreement with results obtained from kinetic model.

D. Rotational and nuclear spin states of the H_3^+ ions

The determination of the spin-dependent recombination rate coefficients of H_3^+ ions relies on accurate knowledge of the relative abundance of ions in the ortho-states and para-states and corresponding rotational states. In this experiment these quantities were measured by optical absorption, rather than by modeling the kinetic processes, but we will briefly describe the reactions of relevance.

The probability of changing the nuclear spin alignment by radiation is very low and likewise collisions with He or Ar atoms are inefficient in causing spin changes. The principal rotational equilibration and spin scrambling process is the proton-hopping or exchange reaction of H_3^+ with H_2 that proceeds via a short-lived $(\text{H}_3^+)^*$ reaction complex. The reaction has been studied in great detail.^{5,27,70–75} It has been found that the ratio of $[\text{pH}_3^+]/[\text{oH}_3^+]$ in plasmas containing H_2 is constrained by nuclear spin selection rules and depends on the relative concentrations of $^p\text{H}_2$ and $^o\text{H}_2$ (Refs. 70–75) and on temperature. Rotational-state changes without changing the nuclear spin state, i.e., within the para or ortho manifold, are possible by radiation and in collisions with He or Ar. Electron collisions can change the rotational states within the para or the ortho manifold with rates approximately ten times faster than the rate of the dissociative recombination (for details see Ref. 76) which means that on average an H_3^+ ion has ten thermalizing collisions with electrons prior to its recombination at our conditions. For this reason, we expect that ions are rotationally thermalized within the para and ortho manifolds.

Rotational temperatures of the ions were inferred from measurements of absolute densities of ions in three rotational states. Panel (a) of Fig. 4 shows the populations of two ortho-states and one para-state, measured during the discharge and during the afterglow in experiments with normal H_2 at temperatures 77–200 K. The relative populations of the ortho- and para-states were computed by dividing the measured absolute ion densities in a given state by the density of all H_3^+ ions, assuming a thermal rotational state distribution. At temperatures where two H_3^+ absorption lines were observable, the rotational temperature $T_{\text{Rot-ortho}}$ within the ortho manifold was obtained also. The relation between the rotational temperature ($T_{\text{Rot-ortho}}$) and the kinetic temperature (T_{Kin}) of the ions is shown in panel (b) of Fig. 4. The data plotted in panel (b) were obtained in experiments with $^n\text{H}_2$ and with $^e\text{H}_2$. The agreement between $T_{\text{Rot-ortho}}$ and T_{Kin} is very good ($|T_{\text{Rot-ortho}} - T_{\text{Kin}}| < 15 \text{ K}$). During the discharge, a slightly higher rotational temperature $T_{\text{Rot-ortho}}$ compared to the kinetic temperature T_{Kin} is expected since the ions are produced with higher rotational excitation and then relax by collisions to lower states. During the afterglow, the lifetime of the H_3^+ ions is longer (because ambipolar diffusion is slower) and

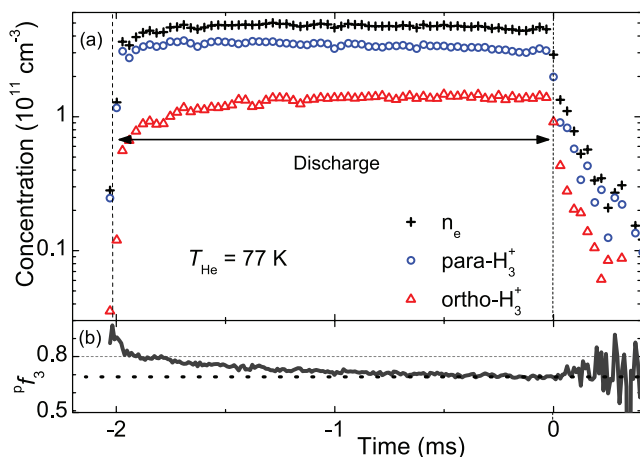


FIG. 5. Panel (a): Evolution of $[^p\text{H}_3^+]$, $[^o\text{H}_3^+]$, and n_e measured in experiments with enriched hydrogen, $^e\text{H}_2$, at $T_{\text{He}} \sim 77 \text{ K}$ and $[\text{He}] = 4 \times 10^{17} \text{ cm}^{-3}$, $[^e\text{H}_2] = 3 \times 10^{14} \text{ cm}^{-3}$, $[\text{Ar}] = 6 \times 10^{13} \text{ cm}^{-3}$. The decay in the early afterglow is caused by recombination. Panel (b): Evolution of $^p f_3$. The final value of $^p f_3 \sim 0.7$ during the late discharge and in the early afterglow exceeds the equilibrium value of $^p f_3 \sim 0.5$ in normal hydrogen.

more time is available for rotational relaxation. Some production of rotationally excited H_3^+ ions may occur in very early afterglow. Therefore, in the determination of $T_{\text{Rot-ortho}}$ we excluded data obtained during the first $\sim 150 \mu\text{s}$ after switching off the discharge.

We concluded that the ions under study were kinetically and internally thermalized in plasmas containing $^n\text{H}_2$, within the experimental uncertainties of $T_{\text{Rot-ortho}}$, T_{Kin} , and $^p f_3$ (see Figs. 1 and 4). In plasmas containing $^e\text{H}_2$, we also found that $T_{\text{Rot-ortho}} \sim T_{\text{Kin}} \sim T_{\text{He}}$ (see panel (b) of Fig. 4), but in this case the relative abundances of para- H_3^+ and ortho- H_3^+ ($^p f_3$ and $^o f_3$) are not in thermal equilibrium (see panel (a) of Fig. 1). The enrichment of para- H_3^+ will be discussed next.

E. H_3^+ para to ortho ratio

We measured absolute densities $[^p\text{H}_3^+]$ and $[^o\text{H}_3^+]$ during the discharge and during the afterglow to determine the dependence of the para- H_3^+ and ortho- H_3^+ fractions on experimental conditions. The time resolution in our experiment suffices to record the temporal evolution during the discharge and during the early afterglow. Typical evolutions of $[^p\text{H}_3^+]$, $[^o\text{H}_3^+]$ and electron densities are plotted in panel (a) of Fig. 5 for the case where $^e\text{H}_2$ was the precursor gas. The electron density n_e is taken as the sum $[^p\text{H}_3^+] + [^o\text{H}_3^+]$. Panel (b) of Fig. 5 shows the measured fraction $^p f_3$ of $[^p\text{H}_3^+]$. After the rapid change in the early discharge the variation during the discharge becomes slow. The faster change of $^p f_3$ at the beginning reflects the transition from the nascent H_3^+ , formed by proton transfer from ArH^+ or H_2^+ to H_2 , to the steady state established in subsequent reactions with H_2 . A thorough discussion of the reactions is contained in two recent papers by Crabtree *et al.*^{45,46}). During the discharge, the para/ortho composition of H_2 ($^p f_2$) changes slowly as a consequence of H_2 dissociation and recombination and hence $^p f_3$ also changes during the discharge. When we refer to values (e.g., $T_{\text{Rot-ortho}}$, T_{Kin}) measured “during the discharge” we mean

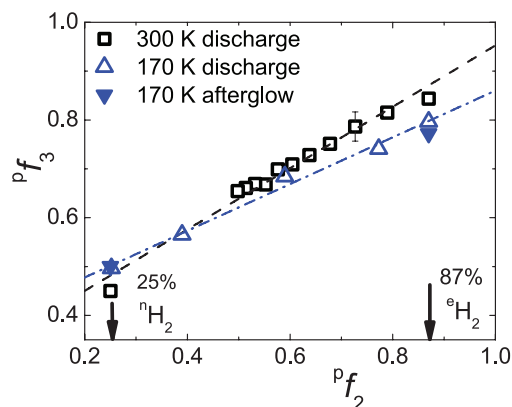


FIG. 6. Dependence of $^p f_3$ on $^p f_2$ measured in a He/Ar/ H_2 mixture at 300 K (discharge) and 170 K (discharge and afterglow). Arrows point to the values of $^p f_2$ in $^n\text{H}_2$ and $^e\text{H}_2$ that were used in the recombination studies. Open symbols: Values in the discharge ($\tau_{\text{Disch}} \sim 2 \text{ ms}$). Filled symbols: Values during the afterglow ($\tau_{\text{Afterglow}} \sim 150 \mu\text{s}$).

values measured shortly before switching off the discharge ($\tau_{\text{Disch}} \sim 2 \text{ ms}$), unless stated otherwise (see also discussion in Ref. 43).

Our systematic measurements of the evolution of the para/ortho composition show that, under the conditions of this set of experiments, the fraction $^p f_3$ remains nearly constant during the afterglow, and that it can be varied by using normal or para enriched hydrogen. We also measured the dependence of $^p f_3$ on $^p f_2$ which was varied from $^p f_2 = 0.25$ to ~ 0.87 by mixing $^n\text{H}_2$ with $^e\text{H}_2$, while keeping the overall hydrogen density ($[^n\text{H}_2] + [^e\text{H}_2]$) constant. The dependence of $^p f_3$ on $^p f_2$ measured at 300 K and at 170 K (see Fig. 6) is linear and the same was found to be true at other temperatures (for details see Ref. 43). The linearity is a consequence of the spin-scrambling reaction with hydrogen.^{70–73} Crabtree *et al.*^{45,46} have recently discussed in great detail the general dependence of $^p f_3$ on $^p f_2$ and other experimental conditions. For the present study of H_3^+ recombination a quantitative understanding of the reaction kinetics is not required; it is only important that $^p f_3$ is known and can be varied over a significant range.

V. EXPERIMENTAL RESULTS – STATE SELECTIVE RECOMBINATION

The measured electron-density decay curves were analyzed to obtain apparent binary recombination rate coefficients for two particular values of $^p f_3$ (see Eqs. (2)–(4)). Further details can also be found in Ref. 27. We carried out a systematic set of measurements which differed only in the value of $^p f_2$, but employed otherwise very similar conditions. The densities of para (1,1), ortho (1,0), and ortho (3,3) states of H_3^+ were monitored. Examples of data measured at 170 K with $^n\text{H}_2$ and with $^e\text{H}_2$ are plotted in Figs. 7 and 8, respectively. Note the large difference in measured populations of particular rotational states of H_3^+ in both experiments (see panels (b) of both figures). In this set of experiments we obtained $^p f_3 \sim 0.5$ for $^n\text{H}_2$ and $^p f_3 \sim 0.7–0.8$ for $^e\text{H}_2$ (see panels (c) of both figures). Note also that in both experiments the values of $^p f_3$ are nearly constant during the afterglow.

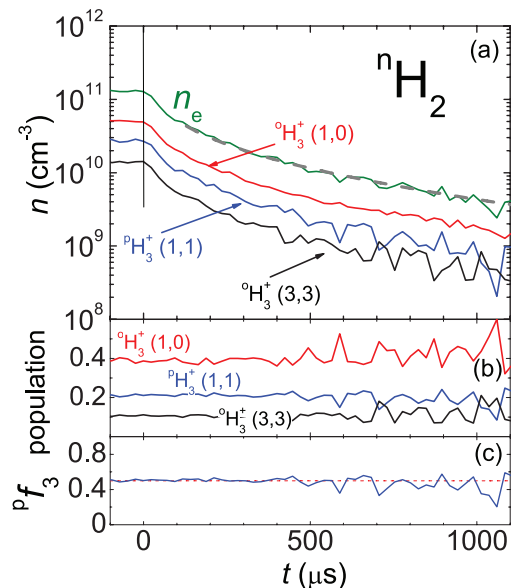


FIG. 7. Panel (a): Example of decay curves of densities of ions in para (1,1), ortho (1,0), and ortho (3,3) states of H_3^+ , measured during the afterglow in a He/Ar/ $^n\text{H}_2$ gas mixture at 170 K, 1440 Pa of He, $[\text{H}_2] = 1 \times 10^{14} \text{ cm}^{-3}$, and $[\text{Ar}] = 2 \times 10^{14} \text{ cm}^{-3}$. Time is set to zero at the beginning of the afterglow. The vertical bar shows the end of the discharge period and the beginning of the afterglow. Electron density is obtained as a sum of ion densities. Panel (b): The measured relative populations of para (1,1), ortho (1,0), and ortho (3,3) states of H_3^+ , note the nearly constant values during whole afterglow. Panel (c): Measured fraction $^p f_3$ of para- H_3^+ .

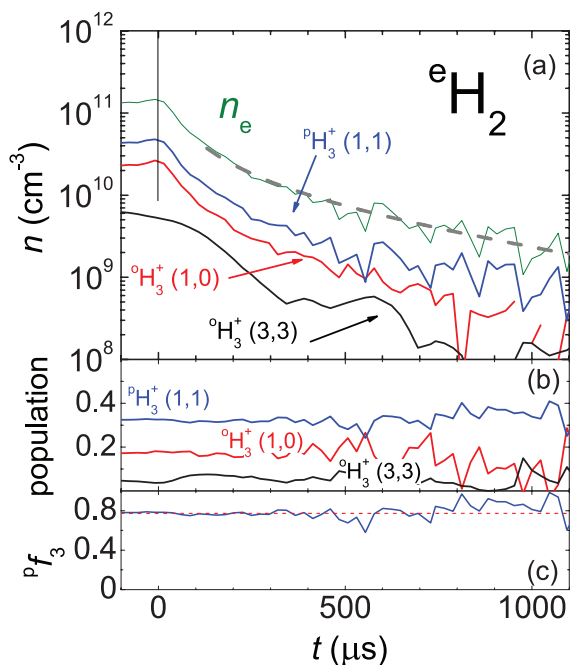


FIG. 8. Panel (a): Example of decay curves of densities of ions in para (1,1), ortho (1,0), and ortho (3,3) states of H_3^+ , measured during the afterglow in a He/Ar/ $^e\text{H}_2$ gas mixture at 170 K, 1550 Pa of He, $[\text{H}_2] = 1 \times 10^{14} \text{ cm}^{-3}$, and $[\text{Ar}] = 2 \times 10^{14} \text{ cm}^{-3}$. The vertical bar shows the end of the discharge period and the beginning of the afterglow. Panel (b): The measured relative populations of para (1,1), ortho (1,0), and ortho (3,3) states of H_3^+ . Panel (c): Measured fraction $^p f_3$ of para- H_3^+ .

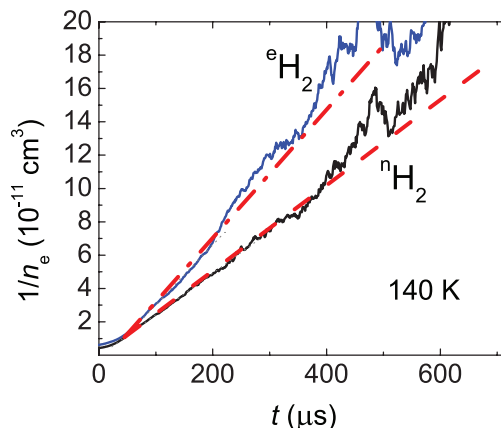


FIG. 9. Examples of the evolutions of the reciprocal number density $1/n_e$ during the afterglow when using normal $^n\text{H}_2$ or para-enriched $^e\text{H}_2$ at otherwise identical conditions. The effective (apparent) binary recombination rate coefficient is given by the slope of the linear part of the plot.

From the densities of the ions in (1,1) and (1,0) states we calculated, assuming thermal equilibrium (TDE) within the para-manifolds and ortho-manifolds, the total densities $[\text{H}_3^+]$ and $[\text{H}_3^+]$ and their sum, i.e., the electron density. The electron-density decay curves can be approximately analyzed by graphing $1/n_e$ versus decay time. The slope of the linear part of the plot yields the effective (apparent) binary recombination rate (for details see Ref. 61). Examples of such graphs of data obtained with $^n\text{H}_2$ and $^e\text{H}_2$ are shown in Fig. 9.

This simple form of analysis demonstrates that recombination in afterglows containing para-enriched hydrogen $^e\text{H}_2$, i.e., with higher relative population of para- H_3^+ , is faster than when normal hydrogen is used. However, it neglects ambipolar diffusion and eventual reactive losses characterized in Eqs. (2) and (3). Hence, we used the more advanced “integral analysis” of the measured electron density decay curves (for details of “integral analysis” see Refs. 61 and 77). This analysis can separate α_{eff} from τ_L and minimize influence of ternary association (1e) and (1f) on determination of α_{eff} . The first 50–150 μs of the afterglow decay were excluded because probably new ions were still being formed (for details see Refs. 8, 27, 43, and 69). At 77 K special attention was paid to analysis of the decay curves because of a possible influence of the CRR process, which is discussed in Appendix.

The dependences of $^n\alpha_{\text{eff}}$ and $^e\alpha_{\text{eff}}$ on He density measured at 170 K are shown in panel (a) of Fig. 10. Panel (c) shows values of the corresponding fractions $^p f_3$. Note that the fractions $^p f_3$ are different in $^n\text{H}_2$ and in $^e\text{H}_2$, but are independent on helium density $[\text{He}]$. Both, $^n\alpha_{\text{eff}}$ and $^e\alpha_{\text{eff}}$ increase linearly with increasing $[\text{He}]$. Therefore (see Eq. (5)), we can obtain separate binary and ternary recombination rate coefficients for known para/ortho ratios. The values obtained with normal hydrogen refer to the thermal equilibrium H_3^+ with $^p f_3 \sim 0.5$. In our previous FALP experiments using $^n\text{H}_2$ we assumed but did not prove that $^p f_3 = 0.5$. The present experiments with $^n\text{H}_2$ confirmed that $^p f_3 = 0.5$ and $T_{\text{Rot-ortho}} = T_{\text{Kin}}$. In other words, the values of α_{bin} and K_{He} recombination rate coefficients obtained in our previous FALP experiments were the values appropriate for thermal equilibrium.^{8,33–37}

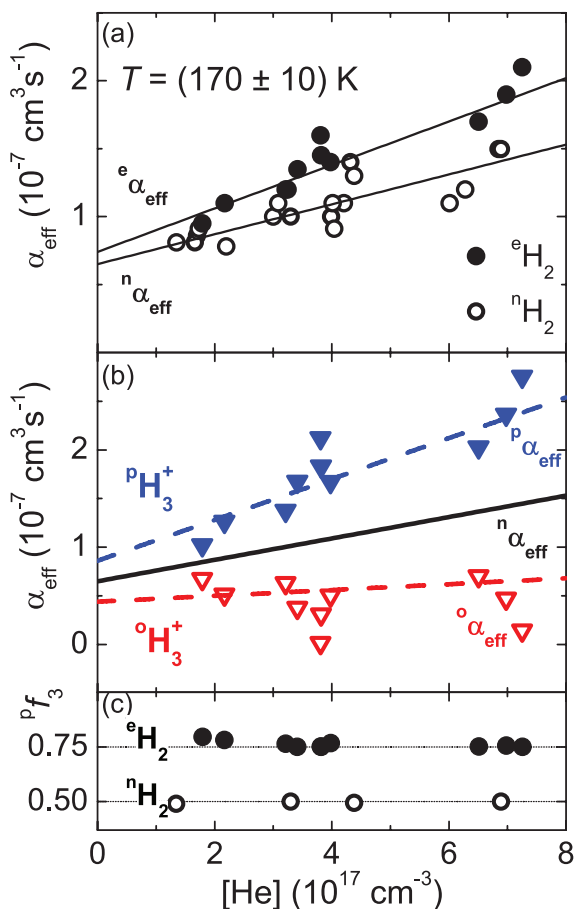


FIG. 10. Measured dependence of effective recombination rate coefficients α_{eff} on He density at 170 K. Panel (a): The values α_{eff} measured using ${}^n\text{H}_2$ as the precursor gas (${}^n\alpha_{\text{eff}}$, open circles) and the values measured using ${}^e\text{H}_2$ (${}^e\alpha_{\text{eff}}$, filled circles). Panel (b): The calculated values ${}^p\alpha_{\text{eff}}$ and ${}^o\alpha_{\text{eff}}$ for pure para- H_3^+ (filled triangles) and pure H_3^+ (open triangles), respectively. For comparison straight line obtained by fit of values ${}^n\alpha_{\text{eff}}$ in panel (a) is also plotted. Panel (c): The ${}^p f_3$ fractions of para- H_3^+ measured in the experiments with ${}^n\text{H}_2$ and ${}^e\text{H}_2$.

We measured the dependences of ${}^n\alpha_{\text{eff}}$ and ${}^e\alpha_{\text{eff}}$ on $[\text{He}]$ for temperatures in the range 77–200 K. From the dependences of ${}^n\alpha_{\text{eff}}$ and ${}^e\alpha_{\text{eff}}$ on $[\text{He}]$ and the corresponding values of ${}^p f_3$ we calculated values ${}^p\alpha_{\text{eff}}$ and ${}^o\alpha_{\text{eff}}$ for pure para- H_3^+ and for pure ortho- H_3^+ , respectively. In these calculations, linear fits to the data measured with ${}^n\text{H}_2$ were used as a reference (the full lines in panels (a) and (b) of the Fig. 10 indicated as ${}^n\alpha_{\text{eff}}$). The obtained negative values of ${}^o\alpha_{\text{eff}}$ were truncated to zero and the corresponding values of ${}^p\alpha_{\text{eff}}$ were corrected accordingly. By fitting the data ${}^p\alpha_{\text{eff}}$ and ${}^o\alpha_{\text{eff}}$ (panel (b) of Fig. 10) with a linear dependence (Eq. (5)) we obtained the corresponding binary (${}^p\alpha_{\text{bin}}$ and ${}^o\alpha_{\text{bin}}$) and ternary (${}^p K_{\text{He}}$ and ${}^o K_{\text{He}}$) recombination rate coefficients for pure para- H_3^+ and for pure ortho- H_3^+ . This form of data analysis is also described in Ref. 27.

VI. RESULTS—TERNARY HE ASSISTED RECOMBINATION OF PARA- H_3^+ AND ORTHO- H_3^+

The present SA-CRDS experiments cover a range of pressures from 200 to 1600 Pa, corresponding to max-

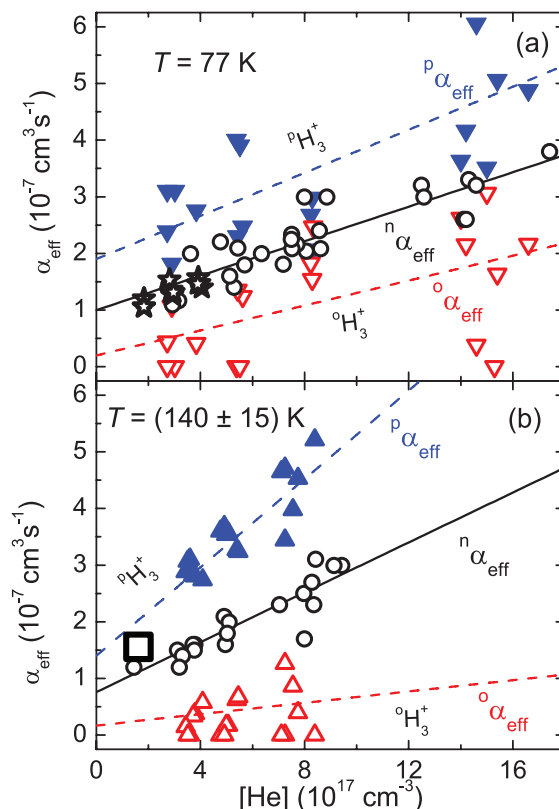


FIG. 11. Measured effective recombination rate coefficients ${}^p\alpha_{\text{eff}}$ and ${}^o\alpha_{\text{eff}}$ (closed and open triangles, respectively) as a function of He density at 77 K (panel (a), for details see also Ref. 27) and at 140 K (panel (b)). The full lines indicate ${}^n\alpha_{\text{eff}}$. The stars in panel (a) are data measured in previous FALP experiment at 77 K (Ref. 34) and the large square in panel (b) represents data measured in previous FALP and stationary afterglow experiments at 130 K.^{34,79} The slopes of the straight-line fits yield the corresponding ternary recombination rate coefficients (K_{He}) while the intercept for $[\text{He}] \rightarrow 0$ gives the corresponding α_{bin} .

imum He densities of $1.6 \times 10^{18} \text{ cm}^{-3}$ at 77 K and $\sim 6 \times 10^{17} \text{ cm}^{-3}$ at 200 K. The ability to vary the He density over a large range of nearly a factor of 10 improves the accuracy of the inferred ternary rate coefficients. The dependences of α_{eff} on $[\text{He}]$ were measured at four temperatures (77, 140, 170, and 200 K) using ${}^n\text{H}_2$ and ${}^e\text{H}_2$. The dependences of ${}^p\alpha_{\text{eff}}$ and ${}^o\alpha_{\text{eff}}$ on helium density obtained for 170 K are shown in panel (b) of Fig. 10 and dependences obtained for 77 K and for 140 K can be found in our previous papers^{27,78} and are shown in Fig. 11 (the values of ${}^p\alpha_{\text{eff}}$ were omitted in Fig. 11 for better clarity). From the dependences of ${}^p\alpha_{\text{eff}}$ and ${}^o\alpha_{\text{eff}}$ on $[\text{He}]$ we obtained (using Eq. (5)) the corresponding binary and ternary recombination rate coefficients α_{bin} and K_{He} . In spite of the fairly large scatter in the data it is clear that ternary recombination depends on the spin state of recombining ions (on ${}^p f_3$). This large scatter is mirrored in error bars of the values shown in Figs. 12 and 13. As can be seen from Fig. 11, zero values of extrapolated ${}^o\alpha_{\text{bin}}$ cannot be excluded at the lowest temperatures. For all three temperatures the ternary helium-assisted recombination of para- H_3^+ is faster than the recombination of H_3^+ .

Figure 12 shows the ternary recombination rate coefficients ${}^p K_{\text{He}}$ and ${}^o K_{\text{He}}$ as a function of temperature, as

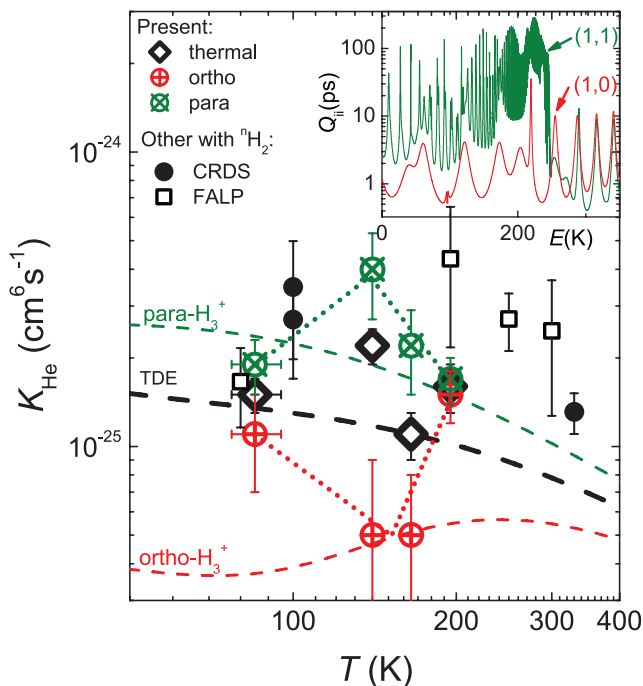


FIG. 12. Ternary recombination rate coefficients ${}^p K_{\text{He}}$, ${}^o K_{\text{He}}$, and ${}^n K_{\text{He}}$. The data obtained in previous CRDS (closed circles) and FALP/SA (open squares) experiments^{33,34} are also shown. The dotted lines drawn through the para and ortho data are only meant to guide the eye. In the insert diagonal elements Q_{ii} of lifetime Matrix \mathbf{Q} for the two lowest initial rotational states of H_3^+ are plotted. Each curve is labeled with the corresponding quantum numbers (J,G) .^{8,34}

obtained from the slopes of graphs of the kind shown in Figs. 10 and 11. The values ${}^n K_{\text{He}}$ corresponding to thermal equilibrium at 77, 140, 170, and 200 K (open rhomboids in Fig. 12) were obtained in the same way from ${}^n \alpha_{\text{eff}}$ (see Figs. 10 and 11). Particular attention was paid to experiments at 77 and 140 K (see Fig. 11) where we obtained high accuracy by measuring at larger helium density range (when comparing current CRDS data to FALP data, see Fig. 11). The CRDS data at 100 and 330 K (closed circles in Fig. 12) and FALP data at 200 K were measured in previous experiments and were obtained from the measured dependences of ${}^n \alpha_{\text{eff}}$ on hydrogen number density in the “saturated region.” For details see Ref. 34. Values of K_{He} at 250 K and 300 K were obtained from the slopes of the linear dependence on helium number density from the data collection of SA and FALP data.³⁴ Because of the lower electron density in FALP experiment plasma decay is longer and formation of H_5^+ can influence the decay at higher helium densities. We have taken this effect into the account by enlarging error bars of the FALP data. Having in mind high He density and low temperature we used kinetic models to verify our assumptions on influence of H_5^+ formation on plasma decay and on determination of α_{eff} . Note that H_5^+ formed in association (1e) and (1f) is in used experimental conditions removed from plasma within $\sim 10 \mu\text{s}$ and the association is loss determining process. Possible error caused by H_5^+ formation is within statistical error of the data, as was confirmed by the chemical kinetics model. In Fig. 12 we did not include the data previously measured in “continuous regime” where FALP was first cooled to 77 K and after

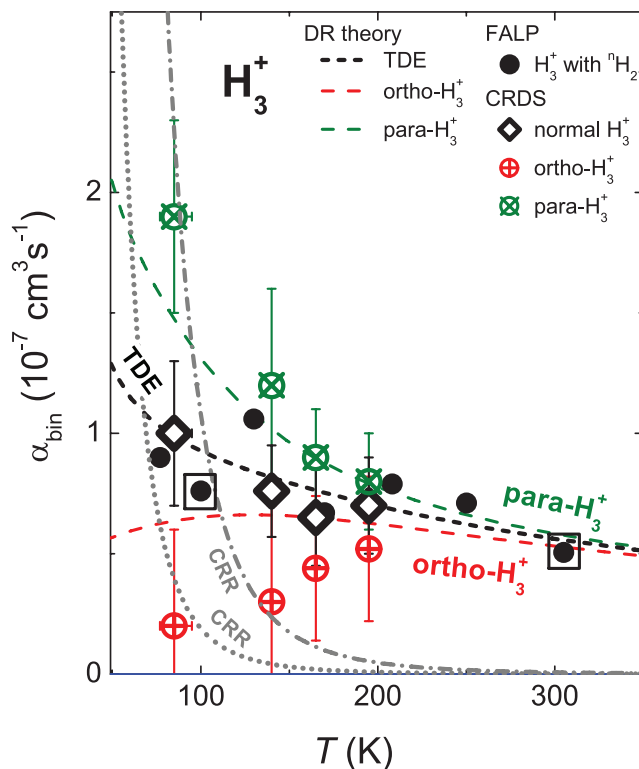


FIG. 13. Measured temperature dependences of the binary recombination rate coefficients ${}^n \alpha_{\text{bin}}$, ${}^o \alpha_{\text{bin}}$, and ${}^p \alpha_{\text{bin}}$ for normal- H_3^+ (measured in experiments with ${}^n \text{H}_2$), para- H_3^+ , and ortho- H_3^+ , respectively (see also Ref. 78). Previous FALP data^{8,33,34} measured with ${}^n \text{H}_2$ are indicated by full circles. Combined SA–CRDS/FALP data at 100 K and 305 K (Refs. 8 and 34) are indicated by a full circle in a square. The temperature T in the SA–CRDS experiments is given by T_{kin} , while in the FALP it is the temperature of the flow tube. That is why we use $T = 82 \text{ K}$ for data obtained in experiment made with discharge tube (SA–CRDS) immersed in liquid nitrogen, otherwise we indicate it as 77 K (e.g., in Fig. 5). Error bars (present CRDS data) represent statistical errors (see linear fits in Figs. 10 and 11). The dashed lines indicate the theoretical rate coefficients for para- H_3^+ , ortho- H_3^+ , and for H_3^+ ions in the thermal equilibrium (TDE).⁶ The curves labeled CRR are the effective binary rate coefficients of collisional radiative recombination (CRR) calculated from the Stevefelt formula (see Refs. 31, 32, and 38) for electron densities $n_e = 5 \times 10^9 \text{ cm}^{-3}$ (dotted line) and $n_e = 3 \times 10^{10} \text{ cm}^{-3}$ (dash-dotted line). For details see the Appendix.

stopping cooling effective rate coefficients were measured at continuously increasing temperature (for details see Ref. 8). The accuracy of data obtained in “continuous regime” is lower when comparing with accuracy of present data obtained from dependences on helium density (Figs. 10 and 11).

In our previous studies^{8,33,34} of recombination of H_3^+ with electrons we discussed the ternary recombination rate coefficient K_{He} in terms of the lifetimes of excited metastable Rydberg states H_3^* formed in collision of H_3^+ ion with electron.^{8,33,34} At low collision energies the calculated values of the lifetimes depend on the spin state of the recombining ions and on collision energy. In the inset in Fig. 12 the calculated diagonal elements Q_{ii} of the lifetime Matrix \mathbf{Q} for the two lowest initial rotational states of H_3^+ are plotted. The calculated lifetimes are long enough to enable l -changing collision of H_3^* molecule with helium buffer gas atom. The calculated ternary recombination rate coefficients³⁴ for para- H_3^+ and ortho- H_3^+ , shown as dashed lines in Fig. 12,

are in qualitative agreement with measured values. ${}^p K_{\text{He}}$ is greater than ${}^o K_{\text{He}}$ due to the longer lifetimes of para- H_3^+ Rydberg resonances. Although some rather rough assumptions were made in the theoretical calculations (mainly the independence of the rate coefficient of l -changing collision on temperature) the overall agreement with the measured data is quite good in comparison with older theories of ternary assisted recombination.^{29,80} An alternative explanation of ternary recombination of H_3^+ has been suggested by Johnsen and Guberman.¹²

More accurate theory should address decrease of ternary rate coefficients at temperature decreasing towards 77 K and also observed small difference between ${}^p K_{\text{He}}$ and ${}^o K_{\text{He}}$ at 77 K (see also Ref. 27), which are in contradiction with calculated dependences.

VII. RESULTS—BINARY RECOMBINATION OF PARA- H_3^+ AND ORTHO- H_3^+

The values of ${}^p \alpha_{\text{bin}}$ and ${}^o \alpha_{\text{bin}}$ for pure para- H_3^+ and pure ortho- H_3^+ and values of ${}^n \alpha_{\text{bin}}$ measured in the present experiment are plotted versus temperature in Fig. 13. Plotted are also values ${}^n \alpha_{\text{bin}}$ for H_3^+ ions in thermal equilibrium obtained in our previous FALP experiments.^{8,33,34} The theoretical rate coefficients for pure para- H_3^+ , pure ortho- H_3^+ , and for H_3^+ ions in thermal equilibrium⁶ are also shown in Fig. 13. The agreement between experimental and theoretical binary recombination rate coefficients ${}^n \alpha_{\text{bin}}$, ${}^p \alpha_{\text{bin}}$, and ${}^o \alpha_{\text{bin}}$ is very good. Also, the agreement between the present ${}^n \alpha_{\text{bin}}$ values and those obtained in our earlier FALP experiments using Langmuir probes is very good over the whole temperature range, even though in the present experiments the electron densities in the early afterglow were higher by at least a factor of 20.³⁴ The agreement at higher temperatures (140, 170, and 200 K) indicates that the measured rate coefficients at 77 K do not depend on electron density (see overlap of FALP and CRDS data plotted in Fig. 11), which means that CRR has little effect on the binary recombination rate coefficients ${}^p \alpha_{\text{bin}}$ and ${}^o \alpha_{\text{bin}}$ (for details see discussion in the Appendix).

VIII. POSSIBLE CONTRIBUTION OF CRR

The afterglow experiments described here had to be performed at high ion and electron densities (approaching 10^{11} cm^{-3}) in order to obtain adequate optical absorption. Hence, we were concerned that electron-stabilized recombination (CRR) might contribute to the recombination loss, especially at the lowest gas temperature of 77 K. The dominant term in the “classical” treatment of CRR for atomic ions by Stevefelt *et al.*^{30,38} yields a three-body CRR rate coefficient $K_{\text{CRR}} = 3.8 \times 10^{-9} T_e^{-4.5} \text{ cm}^6 \text{ s}^{-1}$. The formula (hereinafter referred to as the “Stevefelt formula”) has been experimentally verified for recombination of atomic argon ions at temperatures down to 60 K (Refs. 32 and 40). Its validity for molecular ions seems plausible but has not been tested.

An uncritical application of the commonly used “Stevefelt formula”³⁸ results in an effective binary CRR rate coefficient of $3 \times 10^{-7} \text{ cm}^3 \text{ s}^{-1}$ (at $T_e = 77 \text{ K}$ and an electron density $n_e = 3 \times 10^{10} \text{ cm}^{-3}$, see Fig. 13), larger than the bi-

nary H_3^+ recombination coefficient measured in normal H_2 at the same temperature. At later afterglow times, e.g., when the electron density has dropped below $5 \times 10^9 \text{ cm}^{-3}$, the contribution of CRR becomes much smaller (see Fig. 13). However, the real situation is more complicated because the electrons that are captured by CRR transfer energy to other electrons, thereby raise the temperature of the electron gas, and reduce the rate of the strongly temperature-dependent CRR. The estimates of the electron heat balance described in the Appendix indicate that the electron temperature in the very early afterglow may be as high as 100 K, when the gas temperature is 77 K. This would reduce the contribution of CRR considerably but not make it entirely negligible. The model calculations described in the Appendix suggest that the effect of CRR is negligible, even at 77 K.

The fact that the present data for normal hydrogen are very close to those measured by us in flow tubes (FALP) at ten times smaller electron densities³⁴ supports our conclusion that CRR makes only a small contribution to recombination. While the exact contribution of CRR is difficult to determine, our main conclusion, namely that para- H_3^+ and ortho- H_3^+ recombine with different rates, remains unaffected since CRR should not distinguish between nuclear spin states, however this question is in need of further clarification. Under preparation is the SA-CRDS experiment where wall temperature will be below liquid nitrogen temperature, i.e., below 77 K.

IX. DISCUSSION AND CONCLUSION

Our investigations show that the low-temperature recombination of H_3^+ ions depends strongly on the nuclear spin states of the ions. CRDS proved eminently capable of quantifying the populations of para- H_3^+ and ortho- H_3^+ in the discharge and during the afterglow and to verify that the afterglow plasma was in thermal equilibrium with the He buffer gas. By adding normal and para enriched hydrogen to He buffer gas we were able to form plasmas with different partial populations of para- H_3^+ (fractions, ${}^p f_3$) and ortho- H_3^+ (fractions, ${}^o f_3$) and to deduce both binary and ternary (He-assisted) recombination rate coefficients for pure para- H_3^+ and ortho- H_3^+ ions. The rate coefficients were measured at temperatures from 77 to 200 K. As far as applications to astrophysical clouds are concerned, the binary rate coefficients are the most important. Applications to laboratory hydrogen plasmas will have to include the ternary coefficients as well. It is worth mentioning here that the recent observation of laser lines in hydrogen/rare gas discharge was explained by three-body recombination of H_3^+ .⁸¹

This is the first time that binary and ternary recombination rate coefficients have been determined for H_3^+ ions with *in situ* measured abundances of the para and ortho nuclear spin state and actual kinetic and rotational temperature. The results support theoretical predictions and are compatible with the partial results obtained in storage-ring experiments.

ACKNOWLEDGMENTS

We would like to thank Mgr. Mojmir Jilek for the design of para- H_2 generator and RNDr. Jan Lang, Ph.D. for

TABLE II. Electron processes and corresponding characteristic times calculated for a plasma at $T_{\text{He}} = T_{\text{Kin}} = T_{\text{Rot}} = 77$ K, $T_e = 82$ K, $n_e = 5 \times 10^{10}$ cm $^{-3}$, and $[\text{He}] = 5 \times 10^{17}$ cm $^{-3}$ (~ 500 Pa). Definition of symbols: v : electron velocity; $\sigma_{e/\text{He}}(v)$: tabulated cross section of electron-He elastic scattering; $\langle \dots \rangle$: average over relative velocity distribution; λ_D : Debye length; Λ : impact parameter for 90° coulombic scattering; m_{He} : mass of He atom; m_e : electron mass; λ : coulombic logarithm; $\Delta_{1,2}$: energy difference between rotational states (1,1) and (2,1); n_1, n_2 : number density of H_3^+ ions in rotational states (1,1) and (2,1); α_{21}, α_{12} : rate coefficients for electron (de)excitation between the states $2 \rightarrow 1$ and vice versa; K_{He} : ternary rate coefficient of helium assisted dissociative recombination; α_{bin} : rate coefficient of binary dissociative recombination.

Reactants	Process	τ [μs]	Remark	Reference
e + He	Elastic scattering	0.0008	${}^c\tau_{e/\text{He}} = 1/[\text{He}]\langle\sigma_{e/\text{He}} \cdot v\rangle$	85
e + e	Coulombic scattering	0.004	${}^c\tau_{e/e} = 1/n_e \langle v \pi \Lambda^2 \ln(\lambda_D/\Lambda) \rangle$	83,84
e + He	Elastic cooling	2.9	${}^\varepsilon\tau_{e/\text{He}} = {}^c\tau_{e/\text{He}}(m_{\text{He}}/2m_e)$	65
e + H_3^+	Coulombic cooling	3.4	${}^\varepsilon\tau_{e/i} = \frac{6\sqrt{2}m_e\varepsilon_0^2(\pi k_B T_e)^{3/2}}{n_e e^4 \lambda} \frac{m_i}{2m_e}$	86
e + e + H_3^+	CRR	43	$\tau_{\text{CRR}} = 1/n_e^2 K_{\text{CRR}}$	38
e + H_3^+	Rotational cooling	140	${}^\varepsilon\tau_{\text{Rot}} = \frac{3}{2} \frac{k_B(T_{\text{Rot}} - T_e)}{\Delta_{1,2}(n_2\alpha_{21} - n_1\alpha_{12})}$	76,87
e + H_3^+ + He	Ternary recombination	200	$\tau_{\text{ternary}} = 1/K_{\text{He}}[\text{He}]n_e$	34
e + H_3^+	Binary recombination	250	$\tau_{\text{bin}} = 1/\alpha_{\text{bin}}n_e$	34

NMR measurements of para enrichment of ${}^c\text{H}_2$ gas. This work was partly financed by the research Grant No. OC10046 from the Ministry of Education of the Czech Republic and was partly supported by GACR (205/09/1183, P209/12/0233), SV 265 302, GAUK 92410, GAUK 353811, GAUK 54010, and COST Action CM0805 (The Chemical Cosmos).

APPENDIX A: ELECTRON HEATING AND EFFECT OF COLLISIONAL RADIATIVE RECOMBINATION

In this appendix we consider the heat balance for electrons in low temperature plasma. First we consider the heat balance between the heat released by CRR and heat transfer to ions and neutrals and the resulting increase of the electron temperature. In the second step we consider the effect of electron heating on the afterglow decay.

We denote characteristic times between electron collisions as ${}^c\tau$ (left superscript c) and characteristic times for equipartition of energy as ${}^\varepsilon\tau$ (left superscript ε). Right subscript will be used to denote collision partners. For example, the characteristic time for electron/He collisions is denoted as ${}^c\tau_{e/\text{He}}$ and the electron temperature relaxation time due to electron/He collisions is denoted as ${}^\varepsilon\tau_{e/\text{He}}$. Both quantities are related by the equation: ${}^\varepsilon\tau_{e/\text{He}} = {}^c\tau_{e/\text{He}}(m_{\text{He}}/2m_e)$.⁶⁵

In these calculations we do not distinguish between the para and ortho nuclear spin states of H_3^+ . In this approximation we treat the interactions as spin independent. The relevant collision processes are listed in Table II together with calculated characteristic times for conditions typical in our experiment: $T_{\text{He}} = T_{\text{Kin}} = T_{\text{Rot}} = 77$ K, $T_e = 82$ K, $n_e = 5 \times 10^{10}$ cm $^{-3}$, and $[\text{He}] = 5 \times 10^{17}$ cm $^{-3}$ (~ 500 Pa). Collisional radiative recombination adds ΔE_{CRR} to the internal energy of the electron gas. We assume that this energy is of the order of $\Delta E_{\text{CRR}} = 0.13$ eV per recombined electron. This corresponds to the ionization potential of the lowest Rydberg state recombining predominantly by collisions rather than radiative transitions.^{38,82} Varying the ΔE_{CRR} by a factor of 2 had no qualitative effect on the conclusions of our simulations. The CRR ternary rate coefficient

is taken as $K_{\text{CRR}} = 3.8 \times 10^{-9} T_e^{-4.5}$ cm $^6\text{s}^{-1}$.³⁸ Heat transfer from the electron gas to neutrals (He) and ions occurs via electron/He collisions, electron-ion coulombic collisions, and by rotational excitation of H_3^+ between the rotational levels (1,1) and (2,1). We use recently calculated thermal rates (see Ref. 76) for rotational energy transfer. Electron-electron collisions establish and maintain a maxwellian energy distribution of the electron gas.

The maxwellization of the electron gas by electron-electron coulombic collisions^{83,84} is much faster than the cooling processes under our conditions. Hence, we can define an electron temperature and write a simple equation for the internal energy of the electron gas U :

$$\frac{dU}{dt} = Q_{\text{CRR}} - Q_{\text{elastic}} - Q_{e/i} - Q_{\text{Rot}}, \quad (\text{A1})$$

where the Q_{CRR} , Q_{elastic} , $Q_{e/i}$, and Q_{Rot} terms represent the heating by CRR, cooling by elastic collisions with neutrals, cooling by coulombic collisions with ions, and cooling by rotational excitation of ions, respectively. This equation can be rewritten in terms of relaxation times defined in Table II:

$$\frac{dT_e}{dt} = \frac{2\Delta E_{\text{CRR}}/3k_B}{\tau_{\text{CRR}}} - \frac{T_e - T_G}{{}^\varepsilon\tau_{e/\text{He}}} - \frac{T_e - T_{\text{Kin}}}{{}^\varepsilon\tau_{e/i}} - \frac{T_e - T_{\text{Rot}}}{{}^\varepsilon\tau_{\text{Rot}}}. \quad (\text{A2})$$

In determining the electron temperature, the time derivative term can be neglected, because the relaxation processes are fast enough to maintain the equilibrium temperature at each time during the afterglow. The electron temperature is then obtained by numerically solving Eq. (A2) with zero time derivative.

For the beginning we use the theory of CRR of atomic ions³⁸ to estimate a rate of CRR of H_3^+ ions, then the effective binary rate of CRR should be comparable to the rate of effective binary recombination at 77 K and $n_e > 10^{10}$ cm $^{-3}$ (see plots in Figs. 11 and 13). We deliberately chose conditions where a large influence of CRR can be expected. We then numerically model afterglow recombination in the presence of electron heating by CRR and compare the results to our experimental data. The evolution of electron density on axis of

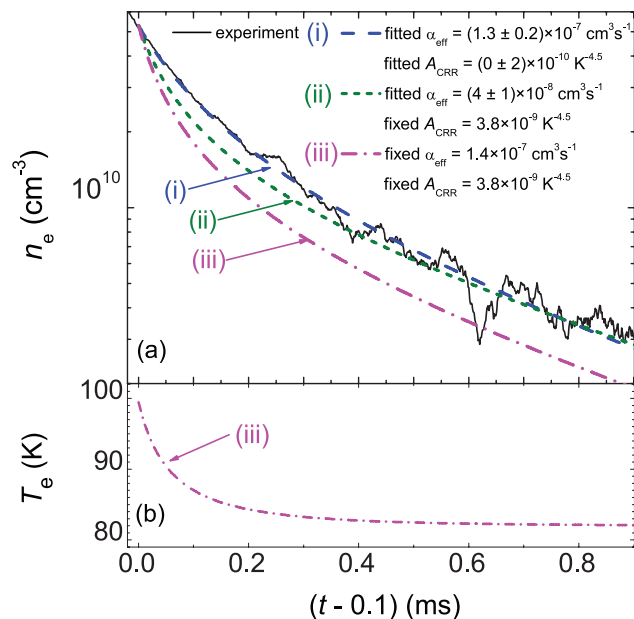


FIG. 14. Model fits of sample data measured in normal hydrogen at 77 K. Panel (a): The dashed line (i) shows the best fit to the data when α_{eff} and A_{CRR} are treated as free parameters. The short dashed line (ii) indicates the best fit when α_{eff} is treated as a free parameter, but A_{CRR} is taken as that given by the Stevefelt formula.³⁸ The dashed-dotted line (iii) shows model results assuming that both the Stevefelt value of A_{CRR} and the FALP values of α_{eff} (Ref. 34) are correct. Panel (b): The corresponding evolution of the electron temperature calculated for conditions corresponding to fit (iii).

the discharge tube is given by the differential equation (4b) augmented with the CRR term

$$\frac{dn_e}{dt} = -K_{\text{CRR}}(T_e)n_e^3 - \alpha_{\text{eff}}n_e^2 - \frac{n_e}{\tau_D}, \quad (\text{A3})$$

where T_e is given by Eq. (A2) and is dependent on n_e . In the numerical models, the value of K_{CRR} was taken as $K_{\text{CRR}} = A_{\text{CRR}}T_e^{-4.5} \text{ cm}^6\text{s}^{-1}$ with either $A_{\text{CRR}} = 3.8 \times 10^{-9} \text{ K}^{4.5}$ or with A_{CRR} as a free fitting parameter.³⁸ The latter choice is permissible since no accurate measurement or theory of CRR for H_3^+ ions is available. Figure 14 compares numerical fits to sample data measured in normal hydrogen at 77 K. As before, the first 100 μs of the afterglow were excluded to eliminate possible effects of ion formation in the early afterglow.

It can be seen in Fig. 14 that the best fit to the data is obtained for a value of the CRR coefficient close to zero (line (i) in Fig. 14). The fit obtained under the constraint that K_{CRR} is given by the Stevefelt formula is noticeably worse, even when α_{eff} is reduced (line (ii)). An even worse agreement is obtained when α_{eff} is taken as the FALP value measured previously³⁴ (see panel (a) of Fig. 11) and the Stevefelt value is used for K_{CRR} (line (iii)). Since the previous FALP measurements were performed at lower electron densities, they should not be affected by CRR even if the Stevefelt value of K_{CRR} is appropriate for H_3^+ .

The same fitting procedures were applied to several of our normal and enriched hydrogen datasets and led to the same conclusion that CRR has only a negligible effect. Hence, we did not correct the measured values of α_{eff} for CRR contributions. The apparent absence of CRR is surprising. It is

known to occur for atomic ions and the high Rydberg states involved in CRR are essentially the same for molecular ions. On the other hand, it is also possible that the electron temperature in the experimental afterglow plasmas was somewhat higher than we estimate. This would greatly reduce the rate of CRR but make only a minor difference in the dissociative recombination coefficient of H_3^+ .

- ¹T. Oka, *Philos. Trans. R. Soc. London, Ser. A* **364**, 2847 (2006).
- ²E. Herbst and W. Klemperer, *Astrophys. J.* **185**, 505 (1973).
- ³N. Indriolo, G. A. Blake, M. Goto, T. Usuda, T. Oka, T. R. Geballe, B. D. Fields, and B. J. McCall, *Astrophys. J.* **724**, 1357 (2010).
- ⁴J. Glosik, *Int. J. Mass Spectrom.* **1369**, 15 (1994).
- ⁵K. N. Crabtree, N. Indriolo, H. Kreckel, B. A. Tom, and B. J. McCall, *Astrophys. J.* **729**, 15 (2011).
- ⁶S. F. dos Santos, V. Kokouline, and C. H. Greene, *J. Chem. Phys.* **127**, 124309 (2007).
- ⁷M. Larsson, *Philos. Trans. R. Soc. London, Ser. A* **358**, 2433 (2000).
- ⁸J. Glosik, R. Plasil, T. Kotrik, P. Dohnal, J. Varju, M. Hejduk, I. Korlov, S. Roucka, and V. Kokouline, *Mol. Phys.* **108**, 2253 (2010).
- ⁹R. Plasil, J. Glosik, V. Poterya, P. Kudrna, J. Ruzs, M. Tichy, and A. Pysanenko, *Int. J. Mass Spectrom.* **218**(2), 105 (2002).
- ¹⁰D. Smith and P. Spanel, *Int. J. Mass Spectrom.* **129**, 163 (1993).
- ¹¹R. Johnsen, *J. Phys.: Conf. Ser.* **4**, 83 (2005).
- ¹²R. Johnsen and S. L. Guberman, *Adv. At., Mol., Opt. Phys.* **59**, 75 (2010).
- ¹³M. Larsson and A. Orel, *Dissociative Recombination of Molecular Ions* (Cambridge University Press, Cambridge, England, 2008).
- ¹⁴V. Kokouline, C. H. Greene, and B. D. Esry, *Nature (London)* **412**, 891 (2001).
- ¹⁵V. Kokouline and C. H. Greene, *Phys. Rev. A* **68**, 012703 (2003).
- ¹⁶B. J. McCall, A. J. Honeycutt, R. J. Saykally, T. R. Geballe, N. Djuric, G. H. Dunn, J. Semaniak, O. Novotny, A. Al-Khalili, A. Ehlerding, F. Hellberg, S. Kalhori, A. Neau, R. Thomas, F. Osterdahl, and M. Larsson, *Nature (London)* **422**, 500 (2003).
- ¹⁷H. Kreckel, M. Motsch, J. Mikosch, J. Glosik, R. Plasil, S. Altevogt, V. Andrianarajaona, H. Buhr, J. Hoffmann, L. Lammich, M. Lestinsky, I. Nevo, S. Novotny, D. A. Orlov, H. B. Pedersen, F. Sprenger, A. S. Terekhov, J. Toker, R. Wester, D. Gerlich, D. Schwalm, A. Wolf, and D. Zajfman, *Phys. Rev. Lett.* **95**, 263201 (2005).
- ¹⁸B. J. McCall, A. J. Honeycutt, R. J. Saykally, N. Djuric, G. H. Dunn, J. Semaniak, O. Novotny, A. Al-Khalili, A. Ehlerding, F. Hellberg, S. Kalhori, A. Neau, R. Thomas, A. Paal, F. Osterdahl, and M. Larsson, *Phys. Rev. A* **70**, 052716 (2004).
- ¹⁹M. Larsson, B. McCall, and A. Orel, *Chem. Phys. Lett.* **462**, 145 (2008).
- ²⁰D. R. Bates, M. F. Guest, and R. A. Kendall, *Planet. Space Sci.* **41**(1), 9 (1993).
- ²¹H. Kreckel, O. Novotny, K. N. Crabtree, H. Buhr, A. Petrigani, B. A. Tom, R. D. Thomas, M. H. Berg, D. Bing, M. Grieser, C. Krantz, M. Lestinsky, M. B. Mendes, C. Nordhorn, R. Repnow, J. Stutzel, A. Wolf, and B. J. McCall, *Phys. Rev. A* **82**, 042715 (2010).
- ²²A. Petrigani, S. Altevogt, M. H. Berg, D. Bing, M. Grieser, J. Hoffmann, B. Jordan-Thaden, C. Krantz, M. B. Mendes, O. Novotny, S. Novotny, D. A. Orlov, R. Repnow, T. Sorg, J. Stutzel, A. Wolf, H. Buhr, H. Kreckel, V. Kokouline, and C. H. Greene, *Phys. Rev. A* **83**, 032711 (2011).
- ²³J. Mikosch, H. Kreckel, R. Wester, J. Glosik, R. Plasil, D. Gerlich, D. Schwalm, and A. Wolf, *J. Chem. Phys.* **121**(22), 11030 (2004).
- ²⁴A. Petrigani, D. Bing, O. Novotny, M. H. Berg, H. Buhr, M. Grieser, B. Jordan-Thaden, C. Krantz, M. B. Mendes, S. Menk, S. Novotny, A. D. A. Orlov, R. Repnow, J. Stutzel, X. Urbain, and A. Wolf, *J. Phys. Chem. A* **114**, 4864 (2010).
- ²⁵U. Hechtischer, Z. Amitay, P. Forck, M. Lange, J. Linkemann, M. Schmitt, U. Schramm, D. Schwalm, R. Wester, D. Zajfman, and A. Wolf, *Phys. Rev. Lett.* **80**, 2809 (1998).
- ²⁶J. Varju, S. Roucka, T. Kotrik, R. Plasil, and J. Glosik, *J. Phys.: Conf. Ser.* **227**, 012026 (2010).
- ²⁷J. Varju, M. Hejduk, P. Dohnal, M. Jilek, T. Kotrik, R. Plasil, D. Gerlich, and J. Glosik, *Phys. Rev. Lett.* **106**, 203201 (2011).
- ²⁸D. Smith and P. Spanel, *Methods Exp. Phys.* **29**(A), 273 (1995).
- ²⁹D. Bates and S. Khare, *Proc. Phys. Soc. Lond.* **85**, 231 (1965).
- ³⁰D. R. Bates, A. E. Kingston, and W. P. McWhirter, *Philos. Trans. R. Soc. London, Ser. A* **267**, 297 (1962).

- ³¹E. W. McDaniel, J. B. A. Mitchell, and M. E. Rudd, *Atomic Collisions, Heavy Particle Projectiles* (Wiley Interscience, New York, 1993).
- ³²T. Kotrik, P. Dohnal, S. Roucka, P. Jusko, R. Plasil, J. Glosik, and R. Johnsen, *Phys. Rev. A* **83**, 032720 (2011).
- ³³J. Glosik, I. Korolov, R. Plasil, O. Novotny, T. Kotrik, P. Hlavenka, J. Varju, I. A. Mikhailov, V. Kokoouline, and C. H. Greene, *J. Phys. B* **41**, 191001 (2008).
- ³⁴J. Glosik, R. Plasil, I. Korolov, T. Kotrik, O. Novotny, P. Hlavenka, P. Dohnal, J. Varju, V. Kokoouline, and C. Greene, *Phys. Rev. A* **79**, 052707 (2009).
- ³⁵J. Glosik, I. Korolov, R. Plasil, T. Kotrik, P. Dohnal, O. Novotny, J. Varju, S. Roucka, C. Greene, and V. Kokoouline, *Phys. Rev. A* **80**, 042706 (2009).
- ³⁶J. Glosik, R. Plasil, I. Korolov, O. Novotny, and T. Kotrik, *J. Phys.: Conf. Ser.* **192**, 012005 (2009).
- ³⁷T. Kotrik, P. Dohnal, I. Korolov, R. Plasil, S. Roucka, J. Glosik, C. Greene, and V. Kokoouline, *J. Chem. Phys.* **133**, 034305 (2010).
- ³⁸J. Stevefelt, J. Boulmer, and J. Delpech, *Phys. Rev. A* **12**, 1246 (1975).
- ³⁹T. Pohl, D. Vrinceanu, and H. R. Sadeghpour, *Phys. Rev. Lett.* **100**, 223201 (2008).
- ⁴⁰T. Kotrik, P. Dohnal, P. Rubovic, R. Plasil, S. Roucka, S. Opanasiuk, and J. Glosik, *Eur. Phys. J. Appl. Phys.* **56**, 24011 (2011).
- ⁴¹T. Amano, *J. Chem. Phys.* **92**, 6492 (1990).
- ⁴²T. Amano, *Astrophys. J.* **329**, L121 (1988).
- ⁴³M. Hejduk, P. Dohnal, J. Varju, P. Rubovic, R. Plasil, and J. Glosik, *Plasma Sources Sci. Technol.* **21**, 024002 (2012).
- ⁴⁴J. Glosik, O. Novotny, A. Pysanenko, P. Zakouril, R. Plasil, P. Kudrna, and V. Poterya, *Plasma Sci. Technol.* **12**, S117 (2003).
- ⁴⁵K. N. Crabtree, B. A. Tom, and B. J. McCall, *J. Chem. Phys.* **134**, 194310 (2011).
- ⁴⁶K. N. Crabtree, C. Kauffman, B. Tom, E. Bečka, B. McGuire, and B. J. McCall, *J. Chem. Phys.* **134**, 194311 (2011).
- ⁴⁷J. Tennyson, see <http://www.tampa.phys.ucl.ac.uk/ftp/astrodata/h3+/> for a list of H₃⁺ transitions (2011).
- ⁴⁸P. F. Goldsmith, T. Velusamy, D. Li, and W. D. Langer, *Astrophys. J.* **715**, 1370 (2010).
- ⁴⁹J. Glosik, R. Plasil, V. Poterya, P. Kudrna, M. Tichy, and A. Pysanenko, *J. Phys. B* **34**(15), L485 (2001).
- ⁵⁰D. Romanini, A. A. Kachanov, N. Sadeghi, and F. Stoeckel, *Chem. Phys. Lett.* **264**(3-4), 316 (1997).
- ⁵¹P. Macko, G. Bano, P. Hlavenka, R. Plasil, V. Poterya, A. Pysanenko, O. Votava, R. Johnsen, and J. Glosik, *Int. J. Mass Spectrom.* **233**, 299 (2004).
- ⁵²P. Hlavenka, R. Plasil, G. Bano, I. Korolov, D. Gerlich, J. Ramanlal, J. Tennyson, and J. Glosik, *Int. J. Mass Spectrom.* **255-256**, 170 (2006).
- ⁵³J. Glosik, P. Hlavenka, R. Plasil, F. Windisch, D. Gerlich, A. Wolf, and H. Kreckel, *Philos. Trans. R. Soc. London, Ser. A* **364**(1848), 2931 (2006).
- ⁵⁴P. Hlavenka, I. Korolov, R. Plasil, J. Varju, T. Kotrik, and J. Glosik, *Czech J. Phys.* **56**, B749 (2006).
- ⁵⁵C. M. Lindsay and B. J. McCall, *J. Mol. Spectrosc.* **210**, 60 (2001).
- ⁵⁶L. Neale, S. Miller, and J. Tennyson, *Astrophys. J.* **464**, 516 (1996).
- ⁵⁷S. Tam and M. Fajardo, *Rev. Sci. Instrum.* **70**, 1926 (1999).
- ⁵⁸B. A. Tom, S. Bashler, Y. Miyamoto, T. Momose, and B. J. McCall, *Rev. Sci. Instrum.* **80**, 016108 (2009).
- ⁵⁹J. Lang, private communication (2011).
- ⁶⁰R. Plasil, P. Hlavenka, P. Macko, G. Bano, A. Pysanenko, and J. Glosik, *J. Phys.: Conf. Ser.* **4**, 118 (2005).
- ⁶¹I. Korolov, T. Kotrik, R. Plasil, J. Varju, M. Hejduk, and J. Glosik, *Contrib. Plasma Phys.* **48**(5-7), 521 (2008).
- ⁶²R. Plasil, I. Korolov, T. Kotrik, J. Varju, P. Dohnal, Z. Donko, G. Bano, and J. Glosik, *J. Phys.: Conf. Ser.* **192**, 012023 (2009).
- ⁶³R. Plasil, I. Korolov, T. Kotrik, P. Dohnal, G. Bano, Z. Donko, and J. Glosik, *Eur. Phys. J. D* **54**, 391 (2009).
- ⁶⁴J. Glosik, G. Bano, R. Plasil, A. Luca, and P. Zakouril, *Int. J. Mass Spectrom.* **189**, 103 (1999).
- ⁶⁵Y. P. Raizer, *Gas Discharge Physics* (Springer-Verlag, Berlin, 1991) p. 14.
- ⁶⁶J. Kim, L. Theard, and W. Hultner, *Int. J. Mass Spectrom.* **15**, 223 (1974).
- ⁶⁷F. B. Yousif, G. Hinojosa, J. de Urquijo, C. Cisneros, and I. Alvarez, *Int. J. Mass Spectrom.* **171**(1-3), 127 (1997).
- ⁶⁸E. Ferguson, *J. Phys. Chem.* **90**, 731 (1986).
- ⁶⁹R. Plasil, J. Varju, M. Hejduk, P. Dohnal, T. Kotrik, and J. Glosik, *J. Phys.: Conf. Ser.* **300**(1), 012023 (2011).
- ⁷⁰M. Quack, *Mol. Phys.* **34**, 477 (1977).
- ⁷¹M. Cordonnier, D. Uy, R. M. Dickson, K. E. Kerr, Y. Zhang, and T. Oka, *J. Chem. Phys.* **113**, 3181 (2000).
- ⁷²T. Oka and E. Epp, *Astrophys. J.* **613**, 349 (2004).
- ⁷³D. Gerlich, F. Windisch, P. Hlavenka, R. Plasil, and J. Glosik, *Philos. Trans. R. Soc. London, Ser. A* **364**, 3007 (2006).
- ⁷⁴K. Park and J. C. Light, *J. Chem. Phys.* **126**, 044305 (2007).
- ⁷⁵E. Hugo, O. Asvany, and S. Schlemmer, *J. Chem. Phys.* **130**, 164302 (2009).
- ⁷⁶V. Kokoouline, A. Faure, J. Tennyson, and C. Greene, *Mon. Not. R. Astron. Soc.* **405**, 1195 (2010).
- ⁷⁷R. Plasil, I. Korolov, T. Kotrik, and J. Glosik, *Int. J. Mass Spectrom.* **275**, 80 (2008).
- ⁷⁸P. Dohnal, M. Hejduk, J. Varju, P. Rubovic, S. Roucka, T. Kotrik, R. Plasil, R. Johnsen, and J. Glosik, "Binary recombination of para and ortho-H₃⁺ with electrons at low temperatures," *Philos. Trans. R. Soc. London, Ser. A* (in press) (Conference Proceeding 2012).
- ⁷⁹J. Glosik, R. Plasil, A. Pysanenko, O. Novotny, P. Hlavenka, P. Macko, and G. Bano, *J. Phys.: Conf. Ser.* **4**, 104 (2005).
- ⁸⁰M. R. Flannery, *J. Chem. Phys.* **95**(11), 8205 (1991).
- ⁸¹R. J. Saykally, E. A. Michael, J. Wang, and C. H. Greene, *J. Chem. Phys.* **133**, 234302 (2010).
- ⁸²S. Byron, R. C. Stabler, and P. I. Bortz, *Phys. Rev. Lett.* **8**, 376 (1962).
- ⁸³F. F. Chen, *Introduction to Plasma Physics* (Plenum, New York, 1974).
- ⁸⁴D. Trunec, P. Spänel, and D. Smith, *Chem. Phys. Lett.* **372**, 728 (2003).
- ⁸⁵A. V. Phelps, see http://jila.colorado.edu/~avp/collision_data/ for compilation of electron cross sections (2011).
- ⁸⁶A. A. Dougal and L. Goldstein, *Phys. Rev.* **109**, 615 (1958).
- ⁸⁷J. Ramanlal and J. Tennyson, *Mon. Not. R. Astron. Soc.* **354**, 161 (2004).

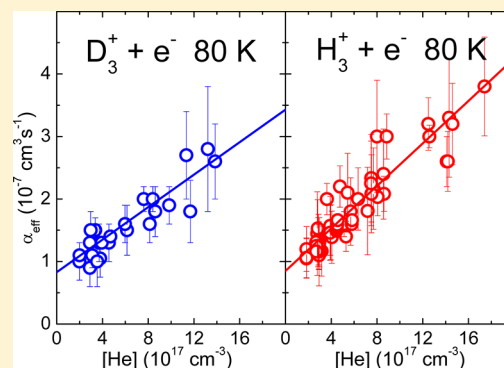
**Ternary Recombination of H_3^+ and D_3^+ with Electrons in He– H_2 (D_2)
Plasmas at Temperatures from 50 to 300 K**

Johnsen R., Rubovič P., Dohnal P., Hejduk M., Plašil R., Glosík J.

J. Phys. Chem. A **117(39)**, 9477–9485, 2013.

Ternary Recombination of H_3^+ and D_3^+ with Electrons in He– H_2 (D_2) Plasmas at Temperatures from 50 to 300 KR. Johnsen,^{*,†} P. Rubovič,[‡] P. Dohnal,[‡] M. Hejduk,[‡] R. Plašil,[‡] and J. Glosík[‡][†]Department of Physics and Astronomy, University of Pittsburgh, Pittsburgh, Pennsylvania 15260, United States[‡]Faculty of Mathematics and Physics, Department of Surface and Plasma Science, Charles University, Prague, Czech Republic

ABSTRACT: We present results of plasma afterglow experiments on ternary electron-ion recombination rate coefficients of H_3^+ and D_3^+ ions at temperatures from 50 to 300 K and compare them to possible three-body reaction mechanisms. Resonant electron capture into H_3^+ Rydberg states is likely to be the first step in the ternary recombination, rather than third-body-assisted capture. Subsequent interactions of the Rydberg molecules with ambient neutral and charged particles provide the rate-limiting step that completes the recombination. A semiquantitative model is proposed that reconciles several previously discrepant experimental observations. A rigorous treatment of the problem will require additional theoretical work and experimental investigations.



1. INTRODUCTION

The recombination of H_3^+ ions and their deuterated analogs with thermal electrons has been studied for more than four decades, motivated largely by its pivotal role in the chemistry and physics of astrophysical clouds and the atmospheres of the outer planets, applications to man-made discharges, and basic interest. However, a true reconciliation of often discrepant experimental data, and a convergence of theory and experiment have not been achieved, as has been pointed out in recent reviews of the subject (see, e.g., Johnsen and Guberman¹). This article focuses on three-body recombination of H_3^+ ions, i.e., the enhancement of recombination by collisions with ambient plasma particles, such as electrons, ions, and neutrals. Theoretical^{2–5} and experimental^{6–8} work on purely binary recombination of H_3^+ has made enormous progress since the advent of storage rings, advanced afterglow techniques, and the modern Jahn–Teller type theories.² At this time, the theory reproduces the experimental values of the thermal (Maxwellian) rate coefficients very well, but discrepancies still exist between the calculated resonances and the structures seen in high-resolution storage-ring data, as has been discussed in great detail by Petrigiani et al.⁹ Some of these resonances may also play a role in the three-body effects discussed here (see section 5).

It is important to realize that third-body assisted recombination does not always lead to experimentally detectable dependences on ambient gas density. We briefly illustrate this point by revisiting the early experiment of Leu et al.^{10,11} Their microwave-afterglow measurements yielded an H_3^+ recombination coefficient ($2.4 \times 10^{-7} \text{ cm}^3/\text{s}$ at 300 K) that is far larger (by a factor of nearly 4) than that obtained later (about $0.6 \times 10^{-7} \text{ cm}^3/\text{s}$) in low-pressure afterglows^{12–14} and storage-ring experiments.^{6–8} Leu et al. employed helium as buffer gas, at

densities from 4.4×10^{17} to $8.6 \times 10^{17} \text{ cm}^{-3}$ at $T = 300 \text{ K}$, and from 4.1×10^{17} to $7.8 \times 10^{17} \text{ cm}^{-3}$ at 205 K. They found that the recombination rates were independent (within about 5%) of density and that they were independent of the experimental electron densities from 5×10^9 to about 1/20 of that density. Over the limited range of temperatures the measured recombination coefficients varied with temperature as $T^{-1/2}$, exactly what was expected for binary recombination, and hence the authors were confident that they had observed binary recombination of H_3^+ , but as we will discuss later, they probably measured a “saturated” three-body reaction that only gives the appearance of binary recombination. A crude estimate of the three-body rate coefficient at 300 K would be given by the ratio $(2.4 \times 10^{-7} - 0.6 \times 10^{-7}) / 4.4 \times 10^{17} = 4 \times 10^{-25} \text{ cm}^6/\text{s}$, a rather large value that cannot be ascribed to known three-body mechanism¹⁵ such as collisional radiative recombination in which atoms act as third bodies. We emphasize that the large body of data for ions other than H_3^+ collected by the microwave technique was confirmed later and that three-body effects are not at all common. The gas phase recombination of H_3^+ , the simplest triatomic ion, clearly has some unusual features!

Systematic measurements of the neutral-assisted recombination have been carried out in the Prague laboratory over a period of about four years and have recently been extended to unprecedented low temperatures (50 K). Both stationary and

Special Issue: Oka Festschrift: Celebrating 45 Years of Astrochemistry

Received: December 5, 2012

Revised: February 6, 2013

Published: February 6, 2013

flowing afterglow apparatus were employed, always in conjunction with mass spectrometric identification of the recombining ions. In some measurements the traditional Langmuir probe technique was used to determine electron densities. Although accurate recombination coefficients can be obtained by this method, the internal state of the ions remains unspecified. Hence, optical absorption (cavity-ring-down-spectroscopy, CRDS) was added to observe the decay of H_3^+ (D_3^+) ions in known vibrational/rotational states and to measure the dependence of the recombination on the nuclear spin modification (para, ortho, meta). Complete descriptions of the earlier experiments can be found in Glosík et al.,^{16–19,22} Varju et al.,^{20,23} Kotřík et al.,²¹ Plašil et al.,²⁹ Rubovič et al.,²⁴ and Dohnal et al.^{25–27}

The earliest such measurements,²⁸ carried out over a small range of helium densities, were consistent with a lack of density dependence. However, as the accuracy of the data improved, and the density range was increased, a dependence of the recombination on neutral (helium) density was invariably observed. The measurements revealed that the three-body coefficients vary with temperature and that they also depend on the nuclear spin states of the H_3^+ (D_3^+) ions (see Varju et al.,^{20,23} Plašil et al.,²⁹ and Dohnal et al.^{25,27}).

We limit the discussion to plasmas in which helium is the dominant neutral gas and ignore possible effects of the minority gases that are often present in afterglow experiments, typically argon and hydrogen. Tests showed that small additions of argon have no significant effect. The hydrogen density is kept small ($<10^{13} \text{ cm}^{-3}$), sufficient to maintain thermal equilibrium among rotational states (within either the para or ortho manifolds) and to convert precursor ions (mainly Ar^+) rapidly to H_3^+ (D_3^+). We digress briefly to discuss one important measurement that was performed in pure hydrogen to assess the possible effect of H_2 .

Amano's³⁰ pioneering and very influential optical absorption measurements in pure hydrogen afterglows yielded a large recombination coefficient of $1.8 \times 10^{-7} \text{ cm}^3/\text{s}$ at 300 K, about 3 times larger than the now accepted binary value. Amano did not observe a dependence of the recombination coefficient on hydrogen density in the range from $3.2 \times 10^{15} \text{ cm}^{-3}$ to 10 times that value, which seems to indicate an absence of a three-body contribution due to hydrogen. However, as was pointed out earlier, the absence of a density dependence is not conclusive proof that three-body effects are not present. If one were to ascribe the larger observed recombination coefficient entirely to H_2 -stabilized recombination (ignoring possible contributions from electrons), the three-body rate would have to be larger than $(1.8 \times 10^{-7} - 0.6 \times 10^{-7})/3.2 \times 10^{15} = 3.75 \times 10^{-23} \text{ cm}^6/\text{s}$, about 100 times faster than the estimate made earlier for He as third body. This estimate is compatible with that obtained in the experiments of Gougousi et al.³¹ In the afterglow experiments described here, the H_2 density was kept below 10^{13} cm^{-3} and hence H_2 -assisted recombination should have been negligible. In later work Amano³² extended his measurements to low temperatures ($\sim 110 \text{ K}$) and found even larger recombination coefficients. Under those conditions, conversion of H_3^+ to H_5^+ is not negligible (see Johnsen³³) and there is the further complication that the electron densities in Amano's studies were unusually high ($\sim 3 \times 10^{11} \text{ cm}^{-3}$).

Neutral particles are probably not the only third bodies that affect H_3^+ recombination. Two afterglow experiments,^{31,34} both performed at low helium densities, indicated that the H_3^+ recombination slowed down in the later afterglow (i.e., at

smaller electron densities), but the same was not observed in recombination studies of O_2^+ ions, the "benchmark" ion often used to test experimental procedures. However, this observation has also been ascribed to vibrationally excited H_3^+ ions.³⁴

In the following, we will present experimental data on the temperature dependence of neutral assisted recombination, followed by a discussion of possible reaction mechanisms. The proposed mechanisms have in common that they invoke high molecular Rydberg states with principal quantum number n , formed either by third-body assisted capture or by resonant capture into autoionizing states. If such states are sufficiently long-lived, their interactions with third bodies may induce dissociation into stable recombination products, thus making the recombination irreversible. In the case of molecular ions, the ionic core may be rotationally (or vibrationally) excited so that several sets of Rydberg states exist that converge to different ionization limits. One should also be aware that the electron "orbits" can be quite large so that many ambient gas particles will be closer to the ion core than the Rydberg electron. For instance, at gas densities of $3 \times 10^{17} \text{ cm}^{-3}$ (~ 10 Torr at 300 K), the spherical volume of an $n = 50$ state contains several thousand atoms. The density of charged particles is typically much lower, but above the Inglis–Teller limit^{35,36} ($n_{\text{max}} \sim 80$ at $n_e = 1 \times 10^9 \text{ cm}^{-3}$, $n_{\text{max}} \sim 60$ at $n_e = 1 \times 10^{10} \text{ cm}^{-3}$) the Stark broadening due to neighboring charged particles is on the same order as the energy difference between adjacent Rydberg states.

2. EXPERIMENTAL DATA ON THE TEMPERATURE DEPENDENCE OF THE HELIUM-ASSISTED RECOMBINATION COEFFICIENT

A comprehensive set of rate coefficients of H_3^+ and D_3^+ has been collected in helium-buffered afterglow plasmas in the Prague laboratory. Some of the data were measured earlier, and some were obtained as part of the present investigation. The instruments used and the methods of analysis are the same as those employed in determinations of the binary recombination coefficients and there is no need to repeat detailed descriptions (see, e.g., Kotřík et al.,³⁷ Dohnal et al.,³⁸ and Rubovič et al.²⁴). In all these measurements the electron and ion temperatures were the same as the gas temperature, the hydrogen and deuterium gases were taken from room-temperature reservoirs, and their nuclear spin states have their "normal" abundances. We will not discuss recent measurements with para-enriched gases (see Varju et al.,²³ Dohnal et al.,^{25–27} and Hejduk et al.³⁹).

As a precaution, a series of measurements was performed (Dohnal et al.³⁸) to rule out the unlikely possibility that the measured dependences on helium density were due to unrecognized systematic errors, for instance in the determinations of electron densities or in the corrections for diffusion losses. In these tests the well-known recombination coefficient of O_2^+ ions was measured at $T = 230 \text{ K}$ for helium densities (in units of cm^{-3}) from 3.8×10^{17} to 5×10^{17} , and at $T = 155 \text{ K}$ from 2.7×10^{17} to 5.6×10^{17} . No detectable variation with density was observed and the absolute values agreed with the known recombination coefficients.

The three-body (ternary) H_3^+ (D_3^+) rate coefficients K_{He} are derived from graphs of the measured "effective" rate coefficient vs the density of helium, assuming that binary recombination (α_{bin}) and ternary recombination simply add, i.e., that

$$\alpha_{\text{eff}} = \alpha_{\text{bin}} + K_{\text{He}}[\text{He}] \quad (1)$$

Experimental values of α_{eff} (Figure 1), collected by the SA-CRDS (stationary afterglow – cavity ring-down spectrometer)

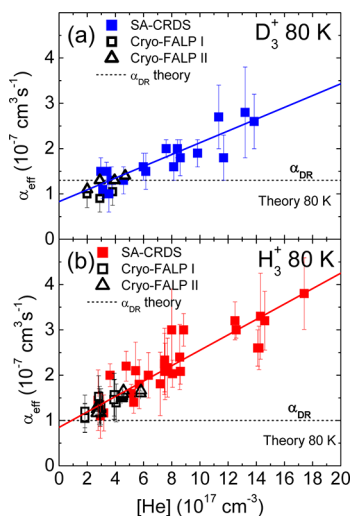


Figure 1. Dependence α_{eff} on helium density at $T = 80 \pm 3$ K, as measured in a stationary afterglow in conjunction with cavity-ring-down spectroscopy (SA-CRDS) and in flowing afterglows (Cryo-FALP I and Cryo-FALP II). (a) D_3^+ data (from Dohnal et al.,²⁶ Kotrík et al.²¹). (b) H_3^+ data (from Glosík et al.,¹⁸ Varju et al.²³). The dashed horizontal lines show theoretical values of the binary coefficients (Pagani et al.,⁴ Fonseca dos Santos et al.³).

and the flowing afterglow (CRYO-FALP I and II), are consistent with a linear dependence over the differing density ranges covered by the experiments. No measurable dependence on electron density was observed, even though the Cryo-FALP I and II data were obtained at low electron densities (typically $n_e = 2 \times 10^9 \text{ cm}^{-3}$) in the afterglow plasma and the SA-CRDS data were obtained at much higher electron densities (typically $3 \times 10^{10} \text{ cm}^{-3}$).

However, the linear addition of binary and ternary recombination implied by eq 1 is valid only when the two recombination mechanisms occur in parallel, but not when binary and ternary recombination share the same “finite resource”, for instance, an intermediate excited state that is formed by electron capture (see section 5). The observations discussed in the Introduction suggest that α_{eff} is more likely to approach a constant value at higher $[\text{He}]$. Hence, the experimental values of K_{He} maybe only approximate first-order values that are valid in the limit of small helium densities.

Figure 2 shows measured K_{He} data for H_3^+ in the temperature range from $T = 50$ K to $T = 350$ K, the first such data ever obtained for molecular ions at temperatures below 77 K.

It has been verified in additional studies (Dohnal et al.,^{25–27,38} Kotrík et al.³⁷) that such plasmas are close to thermal equilibrium ($T_{\text{He}} = T_e = T_{\text{ion}}$). Although the consistency of the present data with those obtained in earlier experiments is not perfect, the overall temperature dependences are similar. The present experiments covered a wider range of densities and have better accuracy. At temperatures below about 100 K the three-body coefficient falls off with decreasing temperature and then approaches the three-body coefficient for neutral-stabilized recombination. For comparison, we have added experimental data points obtained by Dohnal et al.³⁸ in plasmas that contained only atomic Ar^+ ions

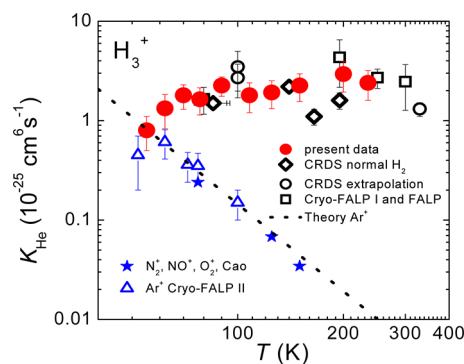


Figure 2. Upper data set: measured variation of K_{He} of H_3^+ ions with gas temperature, obtained when normal hydrogen was used (Varju et al.,²³ Dohnal et al.,²⁵ Glosík et al.¹⁸). Lower data set: measured helium-assisted collisional radiative recombination rate coefficient of Ar^+ ions (Dohnal et al.³⁸), and earlier results of Cao and Johnsen.⁴⁰ Dashed line: theoretical values of the Ar^+ rate coefficient (Bates and Khare¹⁵).

(in the absence of hydrogen) and those agree very well with earlier data⁴⁰ and with theory of neutral assisted collisional radiative recombination (N-CRR, see section 3). At higher temperatures, the latter recombination mechanism makes only a negligible recombination.

Figure 3 shows a similar data set for D_3^+ ions. Here, the rapid decline of the rate coefficient below 100 K is more obvious. In

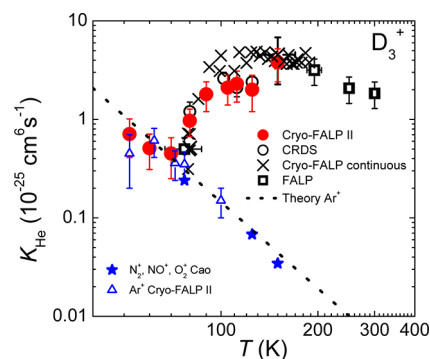


Figure 3. Upper data set: measured variation of K_{He} of D_3^+ ions with gas temperature (Kotřík et al.,²¹ Dohnal et al.²⁶). Lower data set: measured helium-assisted collisional radiative recombination rate coefficient of Ar^+ ions (Dohnal et al.³⁸) and earlier results of Cao and Johnsen.⁴⁰ Dashed line: theoretical values of the Ar^+ rate coefficient (Bates and Khare¹⁵).

these data it is also clear that the D_3^+ ternary rate coefficient rises again below ~ 70 K, exactly as is observed for atomic argon ions, removing all doubt that neutral collisional radiative recombination occurs in both cases.

Although H_3^+ and D_3^+ are similar in many respects, there is no reason to believe that they recombine with the same rates or that the three-body rate coefficients should be identical because their rotational and vibrational levels are different. The three-body coefficients exceed those of collisional radiative recombination in both cases at all but the lowest temperatures. Also, the temperature dependence clearly does not obey a simple inverse power-law dependence on temperature, such as is often seen in three-body reactions such as ion–molecule association reactions. A casual inspection of the data, especially those for D_3^+ , suggests that the three-body recombination

involves an activation energy or a resonance that requires a minimum energy.

3. MODELS OF THREE-BODY ELECTRON-ION RECOMBINATION OF H_3^+ AND D_3^+

Many, if not most, molecular ions recombine by the direct mechanism. Here, the captured electron induces rapid dissociation and there is insufficient time for stabilizing collisions with third bodies. When, as is the case in indirect recombination, the electron is first captured into autoionizing Rydberg states, collisions with third bodies can affect their subsequent evolution, if the lifetime of such states is long enough. The density of third bodies here enters in the “stabilizing” step. It is also possible, though, that the third bodies play a role in the formation of Rydberg states, as in collisional radiative recombination. It is not obvious which of the two mechanisms is more important and whether the capture step or the stabilization step are rate-limiting.

The earliest attempts³¹ to explain the peculiar recombination in H_3^+ containing afterglow plasmas (at low helium densities of $3 \times 10^{16} \text{ cm}^{-3}$ at $T = 300 \text{ K}$) were made at a time when theoretical calculations predicted a very small binary recombination coefficient. Gougousi et al.³¹ observed that the recombination rate coefficient declined in the late afterglow, a finding that was quite similar to that found in earlier afterglow experiments by Smith and Španěl.³⁴ Gougousi et al. proposed a model in which an electron was captured into a long-lived Rydberg state with a vibrationally excited core, followed by electron induced l -mixing (l being the Rydberg electron’s angular momentum) and eventual stabilization by a reaction with ambient hydrogen. In hindsight, the lifetimes used in their model were probably too long, and improved theories² showed that binary recombination was not as slow as earlier theories had suggested. The experimental observations of Gougousi et al. and Smith and Španěl, however, should not be dismissed as “early data”.

When later afterglow experiments (Glosík et al.,^{16–19,22} Kotrík et al.,²¹ Dohnal et al.²⁵) showed that the recombination rate increased with the density of the buffer gas (helium), the authors developed an approximate model in which electrons of low angular momentum ($l = 1$) are captured into rotationally excited Rydberg states, subsequently suffer l -mixing in collisions with helium, and are eventually stabilized. As will be discussed later, rather large l -mixing rates for high Rydberg states have to be invoked to obtain agreement with experiment. An alternate mechanism (Johnsen and Guberman¹) invokes three-body capture into lower Rydberg states that have higher l -mixing rates. This estimate, however, relies on the approximation that states with binding energies less than $-4kT$ (the so-called “bottleneck”) are in thermal Saha equilibrium, which is not necessarily true if those states are subject to stabilization other than by collisional energy loss.

In the following, we will use the following abbreviations: E-CRR and N-CRR denote electron or neutral assisted collisional radiative recombination of atomic ions. We use E-CDR and N-CDR (electron or neutral collisional dissociative recombination) for molecular ions that can be stabilized by dissociation. In reality, all these processes can occur together, do not add in a simple manner, and are difficult to separate.

We begin with a brief introduction to the essential properties of collisional radiative recombination for ions with an atomic core. Though neither of these processes provides an adequate explanation for the three-body effect observed in the case of

recombining H_3^+ plasmas, some aspects of the problem are best understood by first considering atomic ions before examining modifications that should be made in the case of molecular ions. Electron assisted collisional radiative recombination (E-CRR) involves three-body capture of an electron by the ion in the presence of other electrons. One of the electrons is captured into a high Rydberg state whereas the second electron carries away the excess energy. Subsequent collisions with ambient electrons then cause a net downward cascade that eventually makes reionization impossible.

The rate coefficient for E-CRR is given by (see, e.g., Stevefelt et al.⁴¹)

$$\alpha_{\text{E-CRR}} = 2.7 \times 10^{-20} (T_e/300)^{-4.5} n_e \text{ [cm}^3/\text{s]} \quad (2)$$

Here and in the following we will ignore the additional terms that represent radiative effects. The validity of eq 2 at very low temperatures T_e (down to 52 K) was recently verified for Ar^+ ions in a helium-buffered afterglow plasma in a Cryo-FALP II experiment (Kotřík et al.,^{27,42} Dohnal et al.³⁸). Excellent agreement of experimental and theoretical values was obtained.

The capture into high Rydberg states (a few kT below the ionization limit) is much faster than that given by the formula above, but most of the Rydberg atoms will be reionized, rather than recombined. The capture rate coefficient can be calculated from the detailed balance between capture of free electrons and ionization of Rydberg atoms in thermal Saha equilibrium as

$$\alpha_{\text{cap}}(n) = n^2 \lambda_{\text{th}}^3 e^{\epsilon_n} k_{\text{ion}} n_e \text{ [cm}^3/\text{s]} \quad (3)$$

Here λ_{th} is the thermal de Broglie wavelength

$$\lambda_{\text{th}}^3 = (h^2/(2\pi m_e kT))^{3/2} \quad (4)$$

and ϵ_n is the ionization energy of a Rydberg atom ($13.6 \text{ [eV]}/n^2$) with principal quantum number n , divided by $kT_e \text{ [eV]}$, i.e.

$$\epsilon_n = \frac{13.6}{n^2 kT_e} \quad (5)$$

The electron ionization coefficient k_{ion} in eq 3 is quite accurately known. Vriens and Smeets⁴³ derived the semi-empirical analytical formula

$$k_{\text{ion}} = \frac{9.56 \times 10^{-6} (kT_e)^{-1.5} \exp(-\epsilon_n)}{\epsilon_n^{2.33} + 4.38 \epsilon_n^{1.72} + 1.32 \epsilon_n} \text{ [cm}^3/\text{s]} \quad (6)$$

Here, kT_e has to be inserted in units of electronvolts. More elaborate calculations by Pohl et al.⁴⁴ have confirmed the validity of this formula, and Vrinceanu⁴⁵ has shown that the ionization coefficient is only weakly dependent on the electronic angular momentum. If one now makes the simple assumption that low Rydberg states with binding energies above kT cannot be reionized, the capture rate coefficient of eq 3 in conjunction with eq 6 provides a rather good estimate of the E-CRR rate of eq 2 that, however, is somewhat fictitious because it ignores the contribution of downward n -changing collisions. Capture into higher Rydbergs is much faster than α_{CRR} of eq 2. For instance, capture into a range of Rydberg states from $n = 40$ to $n = 80$ at $n_e = 1 \times 10^{10} \text{ cm}^{-3}$ proceeds with an effective binary capture rate coefficients of $\alpha_{\text{cap}} \sim 1 \times 10^{-6} \text{ cm}^3/\text{s}$ at $T_e = 300 \text{ K}$, $\alpha_{\text{cap}} \sim 5 \times 10^{-6} \text{ cm}^3/\text{s}$ at $T_e = 100 \text{ K}$. Note that the equilibrium between capture and collisional ionization will be maintained on a time scale of $1/k_{\text{ion}} n_e$, about 10^{-8} s for $n = 80$ (at 300 K and $n_e = 1 \times 10^{10} \text{ cm}^{-3}$), which is

much shorter than the recombination time scale of afterglow experiments.

In the case of atomic ion cores the capture into high Rydberg states is almost entirely compensated by reionization, but the same need not be true for molecular cores that, at least in principle, can be stabilized by predissociation into fragments that can no longer be ionized. This is the basic idea of the collisional dissociative recombination (E-CDR), first proposed by Collins.⁴⁶ If one assumes that all Rydberg atoms with p from 40 to 80 predissociate rapidly, the effective recombination coefficient approaches the capture coefficient that rises linearly with n_e and is very large, $\sim 1 \times 10^{-6} \text{ cm}^3/\text{s}$ at $T_e = 300 \text{ K}$ and $n_e = 1 \times 10^{10} \text{ cm}^{-3}$, $\sim 5 \times 10^{-6} \text{ cm}^3/\text{s}$ at 100 K. The effective recombination coefficient will rise with n_e until the reionization rate exceeds the predissociation rate and then levels off. However, the assumption that a large fraction of the Rydberg predissociate rapidly is probably not realistic. The capture populates all allowed angular momentum states evenly (because the inverse, ionization, is only weakly l -dependent) but only very few of those, namely those with small l are likely to predissociate (see Chupka⁴⁷). If only ions with low l , e.g., in $l = 1$, are capable of predissociating, the estimates of the E-CDR rate coefficient will be reduced by the factor $(2l + 1)/n^2$, approximately 10^{-3} at $n = 50$. One might presume that l -mixing by electrons would be effective in converting high- l ions to predissociating l -states. The l -mixing rate by electrons from a given l' to a different l is indeed very large (Dutta et al.⁴⁸), but the rate for converting a random l to a given l' is smaller by the factor $(2l' + 1)/[n^2 - (2l' + 1)]$, again a number on the order of 10^{-3} . Thus, it appears unlikely that E-CDR is an important process under the conditions of the afterglow experiments, unless Rydberg molecules in high l -states dissociate rapidly or are destroyed by some other reaction. If E-CDR were important, its rate should increase quite fast with decreasing temperature and lead to a strong dependence on electron density. This, however, is not what is experimentally observed.

Collisional radiative recombination, however, should become noticeable at very low temperatures and high electron densities. For instance, at 100 K and $n_e = 1 \times 10^{10} \text{ cm}^{-3}$ eq 2 gives $\alpha_{\text{CRR}} \sim 4 \times 10^{-8} \text{ cm}^3/\text{s}$.

Similar considerations apply to neutral-assisted recombination processes. The approximation made in the above estimates of the electron-assisted three-body capture is not applicable in the case of neutral-assisted capture. Ionization of Rydberg states by helium atoms as opposed to electrons is slower by about 10 orders of magnitude (see Lebedev⁴⁹). Hence, one would obtain extremely small rates of capture into high Rydberg states. This estimate is inappropriate because those states are populated predominantly by multiple electron-atom collisions that gradually reduce the total energy. A more reasonable estimate can be based on the treatment by Flannery,⁵⁰ who obtained the following rate coefficient for the neutral assisted recombination of atomic ions:

$$\alpha = 8\pi \frac{m_e}{M_{\text{atom}}} R_0 R_e^2 \left(\frac{8kT}{\pi m_e} \right)^{1/2} \sigma_{e,\text{atom}} n_{\text{atom}} \quad (7)$$

Here, m_e and M_{atom} denote the masses of the electron and gas atoms (e.g., helium), $\sigma_{e,\text{atom}}$ is the electron-atom momentum transfer cross section, and $R_e = e^2/kT$ ($= 5 \times 10^{-6} \text{ cm}$ at 300 K). R_0 is the trapping radius. The assumption is made that an electron that collides with an atom inside this radius recombines with unit probability, whereas those colliding

outside that radius will escape recombination. If R_0 is taken as $2R_e/3$, the recombination coefficient decreases with temperature as $T^{-2.5}$ and agrees with the energy-diffusion model of Pitaevskii.⁵¹ In the case of recombination in ambient helium (using $\sigma_{e,\text{atom}} = 5 \times 10^{-16} \text{ cm}^2$), one obtains

$$\alpha(T) = 2.1 \times 10^{-27} (T/300)^{-2.5} n(\text{He}) [\text{cm}^3/\text{s}] \quad (8)$$

A smaller (by about 40%) rate coefficient was obtained by Bates and Khare¹⁵ in their classical treatment of the problem. At temperatures above 100 K, this recombination coefficient is far smaller than what is needed to explain the neutral assisted coefficient in the H_3^+ recombination studies. However, at temperatures below 50 K and $n(\text{He}) = 6 \times 10^{17} \text{ cm}^{-3}$ $\alpha(T)$ of eq 8 exceeds $1 \times 10^{-7} \text{ cm}^3/\text{s}$, which is clearly not negligible.

It is difficult to construct a general theory of third-body assisted recombination of molecular ions because the decay of molecular ions in high Rydberg states depends critically on the specific molecule. However, one can estimate the relative efficiencies of helium and electrons in leading to recombination from the ratio of the rates in eqs 2 and 8. At $T_e = 300 \text{ K}$, one ambient electron has about the same stabilizing effect as 10^7 helium atoms. If one now, as before, assumes that high Rydberg atoms can also be stabilized by predissociation, it seems reasonable to expect that the flux into such states is controlled by helium atoms with an efficiency that is smaller by 10^7 compared to that of electrons. For example, a density of ambient electrons of $n_e = 1 \times 10^{10} \text{ cm}^{-3}$ would have an effect similar to that of helium with density $n(\text{He}) = 1 \times 10^{17} \text{ cm}^{-3}$. Such conditions are fairly typical in experiments. Again, however, the magnitude of N-DRR is expected to be significant only if a very large number of Rydberg states can predissociate, which seems unlikely. Also, the N-DRR rate coefficient would increase as the temperature is reduced, rather than exhibiting a drastic decline, such as that seen in the D_3^+ data below 100 K (Figure 3).

We conclude that neither E-CDR nor N-CDR provides a compelling or even plausible explanation for the experimental findings. However, at very low temperatures collisional radiative recombination, given by eqs 2 and 8, becomes competitive with binary recombination. It may seem surprising that collisional dissociative recombination is less important than collisional radiative recombination. The reason is that dissociation is effective only for states of low l , whereas collisional stabilization also occurs for states with high l and much higher statistical weights.

4. RESONANT CAPTURE AND L-MIXING MODEL

A more promising mechanism of the helium-assisted recombination may be electron capture of a p-electron into an autoionizing resonance with a rotationally excited core, followed by a helium-induced change of the Rydberg electron's angular momentum (l -mixing), and final stabilization by predissociation or perhaps some other stabilizing mechanism. This is the model that has been invoked in several earlier publications.^{16,21} Calculations of the lifetimes (or "time delays") of such resonances show that they can be indeed quite large (100–1000 ps) but the subsequent collisions that lead to irreversible recombination are more difficult to quantify. Essentially, the effective rate coefficient is estimated as

$$\alpha_{\text{eff}} = f \alpha_{\text{cap}} k_i n(\text{He}) / \nu_a [\text{cm}^3/\text{s}] \quad (9)$$

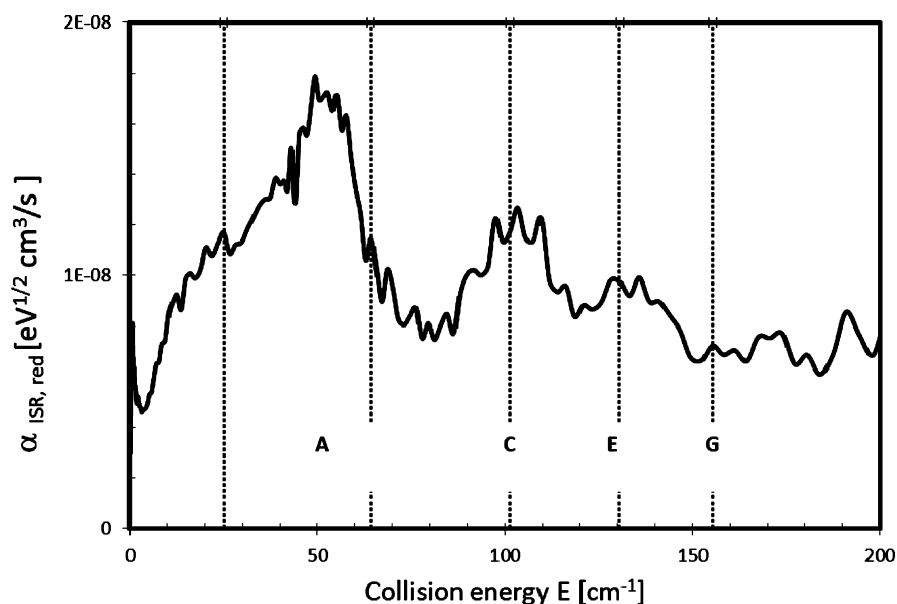


Figure 4. Reduced H_3^+ rate coefficient observed in storage-ring experiments as a function of collision energy, drawn from data supplied by Petrigani.⁵³ Vertical dashed lines indicate the energies at which the calculated lifetimes¹⁶ of (1, 1) to (2, 1) resonances have maxima. The energies C, E, and G correspond to resonant capture into $n = 39$, 50, and 78, respectively.

where $\nu_a = 1/\tau_a$ is the reciprocal of the autoionizing lifetime, α_{cap} denotes the capture coefficient, and k_l is the l -mixing rate from the initial p -state to higher angular momenta. The factor f denotes the fraction of the H_3^+ ions that are capable of capturing electrons, e.g., are in an appropriate rotational state. That number is estimated to be about 0.25. If one uses $\tau_a = 10^{-10}$ s, $\alpha_{\text{cap}} = 3 \times 10^{-7}$ cm^3/s , and $k_l = 3 \times 10^{-8}$ cm^3/s , one obtains a three-body rate coefficient of 2.25×10^{-25} cm^6/s , in good agreement with the experimental value assuming that Rydberg states from $p = 40$ –80 contribute. Equation 9 is valid only in the limit of vanishing helium density. At finite helium densities, l -mixing also depletes the resonant state. Hence, eq 9 should be replaced by

$$\alpha_{\text{eff}} = f\alpha_{\text{cap}} \frac{k_l n(\text{He})}{k_l n(\text{He}) + \nu_a} \quad (10)$$

which agrees with formula 9 in the limit $n(\text{He}) = 0$. At a helium density of 3×10^{17} cm^{-3} , $\alpha(\text{He})$ is now only about 50% of that given by eq 9. At higher helium densities it “saturates” at $f\alpha_{\text{cap}}$ and the differential three-body rate ($d\alpha_{\text{eff}}/dn(\text{He})$) approaches zero. The saturation should be taken into account in comparisons of experimental data to model calculations. We note also that eq 10 only considers l -mixing by helium atoms. If one includes the much faster l -mixing by electrons, the “saturation” would set in at lower helium densities under many experimental conditions.

The assumption that the l -mixing rate coefficient due to helium is given by $k_l = 3 \times 10^{-8}$ cm^3/s , independent of the principal quantum number, is in conflict with the theoretical conclusion of Hickman⁵² that for higher n it should decline as $n^{-2.7}$. Also, the theories of l -mixing consider only mixing from $l \geq 2$. The rates for mixing from $l = 0, 1$ to higher l are actually smaller because the quantum defects are larger. Unfortunately, there are no direct measurements of l -mixing coefficients for high p for molecular ions to reach a clear decision.

The assumption that the autoionizing high- l Rydberg states formed by l -mixing predissociate much faster than they autoionize is also not obvious, and there is no good argument

that rules out the opposite assumption. In the following section we will explore a modification of the resonant-capture model that is, in part, based on experimental observations. In a more rigorous treatment, multiple capture resonances should be considered and their contributions should be added.

5. COMPLEX MODEL

At low electron densities binary rotational capture will always be a faster route to Rydberg states than three-body assisted capture. Hence, we will neglect contributions due to three-body capture. The resonant lifetimes that were used in earlier treatments were calculated from the matrix that describes the rotational capture of p -electrons and their release assuming that the ionic core, except for changing its rotational state, remains unaffected. Other channels, such as predissociation or vibrational excitation were deemed to play no significant role. It seems possible, however, that the rotational resonances lead to more complicated complexes, in which the ionic core becomes highly vibrationally excited and eventually decays into dissociating channels. This conjecture motivated us to examine the energy dependence of the H_3^+ recombination that has been observed in storage-ring experiments

The high-resolution storage-ring data on H_3^+ recombination Petrigani et al.^{9,53} show several recombination peaks at energies from 40 to 160 cm^{-1} (0.005–0.02 eV) that are not predicted by theory. As shown in Figure 4, their positions correlate with the calculated¹⁶ positions of the lifetime maxima for the rotational resonances from the (1, 1) to the (2, 1) (excitation energy of 173 cm^{-1}) rotational states of para- H_3^+ . In Figure 5 of Petrigani et al. the peaks are labeled C and E (we labeled the next higher peak “G”). In this graph, the “raw” (referring to narrow, non-Maxwellian energy distributions) rate coefficients have been reduced by multiplying with the square root of the collision energy to remove the overall energy dependence. It is still not entirely clear whether or not H_3^+ recombination measurements in storage rings are free from possible effects due to electric stray fields.

One could dismiss the correlation as coincidence, but resonant capture by H_3^+ in the (1, 1) state, the rotational ground state of para- H_3^+ , is a natural first step in complex formation. Helium, of course is absent in the storage ring, and the electron density is much lower than in afterglow experiments. Hence, it appears that some of the long-lived rotational resonances actually lead to binary recombination. The largest (very broad) peak in the storage ring data at 50 cm^{-1} (labeled A) has no counterpart in the lifetime graph of (1, 1) to (2, 1) resonances and probably has a different origin. Storage ring data by Kreckel et al.⁵⁴ (see their Figure 8) indicate that the central part of peak “A” remained the same when para-enriched rather than normal hydrogen was fed to the ISR ion source. Peak “A” may reflect a rotational resonance from the para (2, 1) to the (3, 1) rotational state. If this assignment is correct, this resonance could contribute to afterglow recombination at $T = 300 \text{ K}$, but it should not play a role at very low temperatures, because the abundance of the (2, 1) rotational state would be small.

Returning to three-body effects, we now assume that the Rydberg states formed by rotational capture of a p-electron actually interact with the ion core and form an ensemble of complexes with lifetimes that exceed those given by the lifetime matrix. We further assume that the complexes can autoionize, dissociate in the absence of third-body interactions, and that the dissociation rate can be enhanced by third bodies. The resulting recombination rate coefficient in terms of several, however not well-known, rate coefficients has the form

$$\alpha_{\text{eff}}(\text{He}) = \alpha_{\text{cap}} \frac{k_{\text{He}} n(\text{He}) + k_e n_e + \nu_{\text{diss},0}}{k_{\text{He}} n(\text{He}) + k_e n_e + \nu_{\text{diss},0} + \nu_a} \quad (11)$$

The effective recombination coefficient is the product of a capture rate coefficient and the ratio of recombination channels to all decay channels. It is similar to eq 10, but the rate coefficients have different meanings. Here, k_{He} and k_e denote the net rate coefficients for complex stabilization (i.e., leading to predissociation rather than collisional ionization) by helium atoms or electrons, respectively. $\nu_{\text{diss},0}$ is the predissociation rate in the absence of third bodies, and ν_a is the autoionization frequency. We prefer to use decay frequencies rather than lifetimes, because an ensemble of complexes does not necessarily decay with a single exponential time constant.

The coefficients in eq 11 are not known and it is not likely that they can be deduced from simple theoretical arguments. However, it is easy to find values that approximately reproduce the experimental data. Figure 5 shows a fit of eq 11 to data obtained at $T = 300 \text{ K}$ for three different electron densities. The autoionization rate has been chosen as $\nu_a = 8 \times 10^8 \text{ 1/s}$ such that the model agrees with those of the Prague experiments rather than with those of Leu et al.¹⁰

The data by Smith and Španěl³⁴ and by Gougousi et al.³¹ are shown with upward arrows, from the values that they observed at low n_e (late afterglow) to those at high n_e (early afterglow). If one chooses $k_e = 10^7 k_{\text{He}}$, the same “efficiency factor” used in section 3, the model roughly reproduces the range of rate coefficients observed in those experiments at different n_e . A precise fitting of those data is not possible and would be pointless because the accuracy of those data at low n_e is considerably worse than at high electron densities. At high $n(\text{He})$ the model gives a weaker dependence on n_e , in agreement with the findings by both Leu et al.¹⁰ and the Prague experiments. Although a linear extrapolation of the Prague data

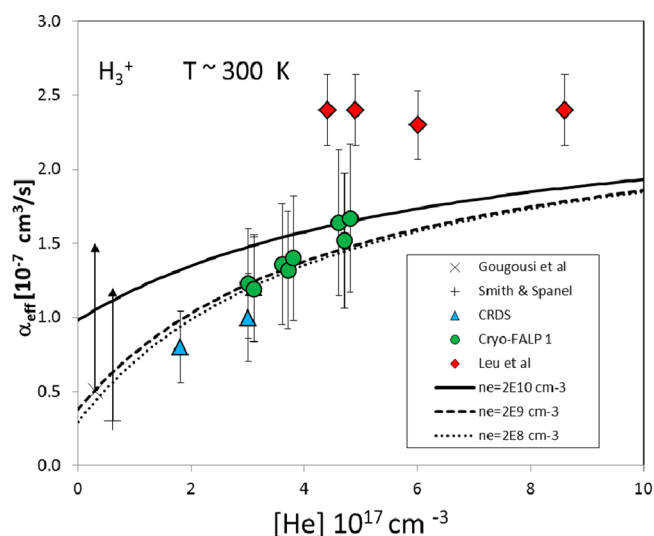


Figure 5. Comparison of eq 11 to experimental data at $T = 300 \text{ K}$. The following values were used for the rate coefficients and decay rates: $\alpha_{\text{cap}} = 2.55 \times 10^{-7} \text{ cm}^3/\text{s}$, $k_{\text{He}} = 2 \times 10^{-9} \text{ cm}^3/\text{s}$, $k_e = 5 \times 10^{-2} \text{ cm}^3/\text{s}$, $\nu_{\text{diss},0} = 1 \times 10^8 \text{ 1/s}$, $\nu_a = 8 \times 10^8 \text{ 1/s}$. See text for additional explanations. Data points from Gougousi et al.,³¹ Smith and Španěl,³⁴ CRDS and Cryo-FALP I from Glosik et al.¹⁸ and Leu et al.¹¹

to $n(\text{He}) = 0$ is not strictly compatible with the model, it results in a binary value that is only slightly too high.

Our exploratory model provides a common framework that makes the apparent discrepancies between experimental data easier to accept. Obviously, the model is crude because it uses the same rate coefficients for all members of the ensemble of complexes. This is unavoidable, given the severe lack of knowledge of the relevant parameters. It is also difficult to estimate how the effective recombination coefficients would vary with temperature. At low electron temperatures resonant capture can only occur into Rydberg states with smaller principal quantum numbers and the spacing between states will increase. Thus, one might expect that three-body effect would become smaller at low temperatures. The changing rotational distribution of H_3^+ is likely to have an effect also.

In the complex model, collisions with third bodies enhance the recombination rate at the expense of the autoionization rate ν_a . If ν_a is vanishingly small, however, then (see eq 11) the recombination rate is limited by electron capture and third-body effects disappear. In the simplified theory of Jungen and Pratt⁵ electrons are captured by vibrational excitation mediated by the linear Jahn–Teller effect and autoionization is assumed to be negligible. Because their theory reproduces the rate coefficients measured in storage rings quite well, the agreement can be seen as a possible argument against the complex model. However, in a later and more detailed paper Jungen and Pratt⁵⁵ conclude that purely rotational capture into autoionizing states should also be considered and that recombination in that case would not be capture limited. It is difficult to go further without knowing the relative efficiencies of the capture mechanisms.

6. CONCLUSIONS

The multiyear efforts to elucidate the ternary recombination of H_3^+ and D_3^+ ions, in particular the novel extension to very low temperatures, have resulted in a rather unique set of data. It is particularly pleasing to see that the traditional three-body reaction (i.e., the Bates and Khare mechanism¹⁵) becomes

detectable at temperatures below 70 K. This observation strongly supports the validity of the afterglow methods used here.

It appears that many of the seeming discrepancies between afterglow recombination data on H_3^+ (D_3^+) can be traced to third-body effects involving both neutral and charged particles. Although these measurements of third-body assisted recombination have narrowed the range of plausible mechanisms, developing a quantitative theoretical model is seriously hampered by the lack of needed data, especially on rates of predissociation, their dependence on angular momentum, and coupling between electronic and core degrees of freedom. The tentative model proposed here presents an attempt to develop a common framework that seeks to reconcile experimental observations.

The data obtained in helium-buffered plasmas are nearly complete, but there is a lack of data in other rare gases. Neon might be a good choice for further work because the momentum transfer between electrons and neon is far smaller than with helium. The only experiment in neon buffer⁵⁶ was done at a single pressure and does not permit any inferences regarding pressure dependences. Hence, we did not discuss this work but note that it resulted in smaller recombination coefficients than those obtained with helium buffer gas.

There remains some doubt about the role that electrons play as stabilizing body because the only two experiments^{34,31} that point to electron-stabilized recombination may have alternate explanations. Additional experiments, especially measurements at very low temperatures, may be worth the effort.

Finally, it would certainly be highly desirable to have more theoretical information on the configuration interaction between electronic and core excitations in H_3^+ Rydberg states, and to identify clearly the origin of the resonance peaks that are seen in storage-ring experiments.

AUTHOR INFORMATION

Corresponding Author

*Phone: 412-624-9285. E-mail: rj@pitt.edu.

Notes

The authors declare no competing financial interest.

ACKNOWLEDGMENTS

This work was partly financed by the research grant OC10046 from the Ministry of Education of the Czech Republic and was partly supported by GACR (205/09/1183, P209/12/0233), by SV 267 302, by GAUK 353811, GAUK 406011, GAUK 659112, and by COST Action CM0805 (The Chemical Cosmos). We thank A. Petrigani for supplying numerical data on the storage ring results

REFERENCES

- (1) Johnsen, R.; Guberman, S. L. Dissociative Recombination of H_3^+ Ions with Electrons: Theory and Experiment. *Adv. At., Mol., Opt. Phys.* **2010**, *59*, 75–127.
- (2) Kokoouline, V.; Greene, C. H. Unified Theoretical Treatment of Dissociative Recombination of D3h Triatomic Ions: Application to H_3^+ and D_3^+ . *Phys. Rev. A: At., Mol., Opt. Phys.* **2003**, *68*, 012703-1–23.
- (3) Fonseca dos Santos, S.; Kokoouline, V.; Greene, C. H. Dissociative Recombination of H_3^+ in the Ground and Excited Vibrational States. *J. Chem. Phys.* **2007**, *127*, 124309-1–8.
- (4) Pagani, L.; Vastel, C.; Hugo, E.; Kokoouline, V.; Greene, C. H.; Bacmann, A.; Bayet, E.; Ceccarelli, C.; Peng, R.; Schlemmer, S.

Chemical Modeling of L183 (L134N): An Estimate of the Ortho/Para H_2 ratio. *Astron. Astrophys.* **2009**, *494*, 623–636.

- (5) Jungen, Ch.; Pratt, S. T. Jahn-Teller Interactions in the Dissociative Recombination of H_3 . *Phys. Rev. Lett.* **2009**, *102*, 023201-1–4.

- (6) McCall, B. J.; Huneycutt, A. J.; Saykally, R. J.; Djuric, N.; Dunn, G. H.; Semaniak, J.; Novotny, O.; Al-Khalili, A.; Ehlerding, A.; Hellberg, F.; et al. Dissociative Recombination of Rotationally Cold H_3^+ . *Phys. Rev. A: At., Mol., Opt. Phys.* **2004**, *70*, 052716-1–12.

- (7) Wolf, A.; Kreckel, H.; Lammich, L.; Strasser, D.; Mikosch, J.; Glosik, J.; Plašil, R.; Altevogt, S.; Andrianarijaona, V.; Buhr, H.; et al. Effects of Molecular Rotation in Low-Energy Electron Collisions of H_3^+ . *Philos. Trans. R. Soc. A.* **2006**, *364*, 2981–2997.

- (8) Kreckel, H.; Motsch, M.; Mikosch, J.; Glosik, J.; Plašil, R.; Altevogt, S.; Andrianarijaona, V.; Buhr, H.; Hoffmann, J.; Lammich, L.; et al. High-Resolution Dissociative Recombination of Cold H_3^+ and First Evidence for Nuclear Spin Effects. *Phys. Rev. Lett.* **2005**, *95*, 263201-1–4.

- (9) Petrigani, A.; Altevogt, S.; Berg, M. H.; Bing, D.; Grieser, M.; Hoffmann, J.; Jordon-Thaden, B.; Krantz, C.; Mendes, M.; Novotny, O.; et al. Resonant Structure of Low-Energy H_3^+ Dissociative Recombination. *Phys. Rev. A: At., Mol., Opt. Phys.* **2011**, *83*, 032711-1–10.

- (10) Leu, M. T.; Biondi, M. A.; Johnsen, R. Measurements of Recombination of Electrons with H_3^+ and H_3^+ Ions. *Phys. Rev. A: At., Mol., Opt. Phys.* **1973**, *8*, 413–419.

- (11) Leu, M. T. *Ph.D. thesis*, University of Pittsburgh, Pittsburgh, PA, USA, 1972.

- (12) Macko, P.; Bánó, G.; Hlavenka, P.; Plašil, R.; Poterya, V.; Pysanenko, A.; Votava, O.; Johnsen, R.; Glosik, J. Afterglow Studies of $\text{H}_3^+(v=0)$ Recombination Using Time Resolved CW-Diode Laser Cavity Ring-Down Spectroscopy. *Int. J. Mass Spectrom.* **2004**, *233*, 299–304.

- (13) Plašil, R.; Glosik, J.; Poterya, V.; Kudrna, P.; Ruzs, J.; Tichý, M.; Pysanenko, A. Advanced Integrated Stationary Afterglow Method for Experimental Study of Recombination processes of H_3^+ and D_3^+ Ions With electrons. *Int. J. Mass Spectrom.* **2002**, *218*, 105–130.

- (14) Laubé, S.; Le Padellec, A.; Sidko, O.; Rebrion-Rowe, C.; Mitchell, J. B. A.; Rowe, B. R. New FALP-MS Measurements of H_3^+ , D_3^+ and HCO^+ Dissociative Recombination. *J. Phys. B: At., Mol. Opt. Phys.* **1998**, *31*, 2111–2128.

- (15) Bates, D. R.; Khare, S. P. Recombination of Positive Ions with Electrons in a Dense Gas. *Proc. Phys. Soc.* **1965**, *85*, 231–243.

- (16) Glosik, J.; Korolov, I.; Plašil, R.; Novotny, O.; Kotrík, T.; Hlavenka, P.; Varju, J.; Mikhailov, I. A.; Kokoouline, V.; Greene, C. H. Recombination of H_3^+ ions in the Afterglow of a He–Ar– H_2 Plasma. *J. Phys. B: At., Mol. Opt. Phys.* **2008**, *41*, 191001–191009.

- (17) Glosik, J.; Plašil, R.; Korolov, I.; Novotny, O.; Kotrík, T. Multicollision Character of Recombination of H_3^+ Ions in Afterglow Plasma. *J. Phys.: Conf. Ser.* **2009**, *192*, 012005 (8 pages).

- (18) Glosik, J.; Plašil, R.; Korolov, I.; Kotrík, T.; Novotny, O.; Hlavenka, P.; Dohnal, P.; Varju, J.; Kokoouline, V.; Greene, C. H. Temperature Dependence of Binary and Ternary Recombination of H_3^+ ions with Electrons. *Phys. Rev. A: At., Mol., Opt. Phys.* **2009**, *79*, 052707-1–10.

- (19) Glosik, J.; Korolov, I.; Plašil, R.; Kotrík, T.; Dohnal, P.; Novotny, O.; Varju, J.; Roučka, Š.; Greene, C. H.; Kokoouline, V. Binary and Ternary Recombination of D_3^+ Ions with Electrons in He– D_2 plasma. *Phys. Rev. A: At., Mol., Opt. Phys.* **2009**, *80*, 042706-1–9.

- (20) Varju, J.; Roučka, Š.; Kotrík, T.; Plašil, R.; Glosik, J. Application of NIR – CRDS for State Selective Study of Recombination of Para and Ortho H_3^+ Ions with Electrons in Low Temperature Plasma. *J. Phys.: Conf. Ser.* **2010**, *227*, 012026 (4 pages).

- (21) Kotrík, T.; Dohnal, P.; Korolov, I.; Plašil, R.; Roučka, S.; Glosik, J.; Greene, C. H.; Kokoouline, V. Temperature Dependence of Binary and Ternary Recombination of D_3^+ Ions with Electrons. *J. Chem. Phys.* **2010**, *133*, 034305–034313.

- (22) Glosik, J.; Plašil, R.; Kotrík, T.; Dohnal, P.; Varju, J.; Hejduk, M.; Korolov, I.; Roučka, Š.; Kokoouline, V. Temperature Dependence of

Binary and Ternary Recombination of D_3^+ ions with Electrons. *Mol. Phys.* **2010**, *108*, 2253–2264.

(23) Varju, J.; Hejduk, M.; Dohnal, P.; Jílek, M.; Kotřík, T.; Plašil, R.; Gerlich, D.; Glosík, J. Nuclear Spin Effect on Recombination of H_3^+ Ions with Electrons at 77 K. *Phys. Rev. Lett.* **2011**, *106*, 203201–203205.

(24) Rubovič, P.; Dohnal, P.; Hejduk, M.; Plašil, R.; Glosík, J. Binary Recombination of H_3^+ and D_3^+ Ions with Electrons in Plasmas at 50–230 K. *J. Phys. Chem. A* **2013**, DOI: 10.1021/jp3123192.

(25) Dohnal, P.; Hejduk, M.; Varju, J.; Rubovič, P.; Roučka, Š.; Kotřík, T.; Plašil, R.; Glosík, J.; Johnsen, R. Binary and Ternary Recombination of Para- H_3^+ and Ortho- H_3^+ with Electrons: State Selective Study at 77–200 K. *J. Chem. Phys.* **2012**, *136*, 244304-1–14.

(26) Dohnal, P.; Hejduk, M.; Rubovič, P.; Varju, J.; Roučka, Š.; Plašil, R.; Glosík, J. Binary and Ternary Recombination of D_3^+ Ions at 80–130 K: Application of Laser Absorption Spectroscopy. *J. Chem. Phys.* **2012**, *137*, 194320-1–8.

(27) Dohnal, P.; Hejduk, M.; Varju, J.; Rubovič, P.; Roučka, S.; Kotřík, T.; Plašil, R.; Johnsen, R.; Glosík, J. Binary Recombination of Para- and Ortho- H_3^+ with Electrons at Low Temperatures. *Philos. Trans. R. Soc. A* **2012**, *370*, 5101–5108.

(28) Glosík, J.; Plašil, R.; Poterya, V.; Tichy, M.; Pysanenko, A. Experimental Study of Recombination of H_3^+ Ions with Electrons Relevant for Interstellar and Planetary Plasmas. *J. Phys. B: At. Mol. Opt. Phys.* **2001**, *34*, L458–L494.

(29) Plašil, R.; Varju, J.; Hejduk, M.; Dohnal, P.; Kotřík, T.; Glosík, J. Experimental Study of Para- and Ortho- H_3^+ Recombination. *J. Phys. Conf. Ser.* **2011**, *300*, 012023 (8 pages).

(30) Amano, T. Is the Dissociative Recombination of H_3^+ Really Slow? A New Spectroscopic Measurement of the Rate Constant. *Astrophys. J., Lett.* **1988**, *329*, L121–L124.

(31) Gougousi, T.; Johnsen, R.; Golde, M. F. Recombination of H_3^+ and D_3^+ Ions in a Flowing Afterglow Plasma. *Int. J. Mass Spectrom.* **1995**, *149–150*, 131–151.

(32) Amano, T. The Dissociative Recombination Rate Coefficients of H_3^+ , HN_2^+ , and HCO . *J. Chem. Phys.* **1990**, *92*, 6492–6501.

(33) Johnsen, R. Kinetic Processes in Recombining H_3^+ Plasmas. *Philos. Trans. R. Soc. A* **2012**, *370*, 5109–5117.

(34) Smith, D.; Španěl, P. Dissociative Recombination of H_3^+ . Experiment and Theory reconciled. *Chem. Phys. Lett.* **1993**, *211*, 454–460.

(35) Inglis, D. R.; Teller, E. Ionic Depression of Series Limits in One-Electron Spectra. *Astrophys. J.* **1939**, *90*, 439–448.

(36) Mitrafanov, A. V. On a Revised Version of the Inglis-Teller Formula. *Soviet Astronomy-AJ* **1973**, *16*, 867–869.

(37) Kotřík, T.; Dohnal, P.; Rubovič, P.; Plašil, R.; Roučka, S.; Opanasiuk, S. Glosík. Cryo-FALP Study of Collisional-Radiative Recombination of Ar^+ Ions at 40–200 K. *Eur. Phys. J.: Appl. Phys.* **2011**, *56*, 24011–24016.

(38) Dohnal, P.; Rubovič, P.; Kotřík, T.; Hejduk, M.; Plašil, R.; Johnsen, R.; Glosík, J. Ternary Recombination of Ar^+ with Electrons in He at Temperatures 50–100 K. To be published.

(39) Hejduk, M.; Dohnal, P.; Varju, J.; Rubovič, P.; Plašil, R.; Glosík, J. Nuclear Spin State-Resolved Cavity Ring-Down Spectroscopy Diagnostics of a Low-Temperature H_3^+ -Dominated Plasma. *Plasma Sources Sci. Technol.* **2012**, *21*, 024002–024011.

(40) Cao, Y. S.; Johnsen, R. Neutral Stabilized Electron-ion Recombination in Ambient Helium Gas. *J. Chem. Phys.* **1991**, *94*, 5443–5446.

(41) Stevefelt, J.; Boulmer, J.; Delpéch, J. Collisional-Radiative Recombination in Cold Plasmas. *Phys. Rev. A: At., Mol., Opt. Phys.* **1975**, *12*, 1246–1251.

(42) Kotřík, T.; Dohnal, P.; Roučka, S.; Jusko, P.; Plašil, R.; Glosík, J.; Johnsen, R. Collisional Radiative Recombination $Ar^+ + e + e$; Experimental Study at 77–180 K. *Phys. Rev. A: At., Mol., Opt. Phys.* **2011**, *83*, 032720-1–032720-8.

(43) Vriens, L.; Smeets, H. M. Cross-section and Rate Formulas for Electron Impact Ionization, Excitation, and Total Population of Excited Atoms. *Phys. Rev. A: At., Mol., Opt. Phys.* **1980**, *22*, 940–951.

(44) Pohl, T.; Vrinceanu, D.; Sadeghepour, H. R. Rydberg Atom Formation in Ultracold Plasmas: Small Energy Transfer with Large Consequences. *Phys. Rev. Lett.* **2008**, *100*, 223201-1–3.

(45) Vrinceanu, D. Electron Impact Ionization of Rydberg Atoms. *Phys. Rev. A: At., Mol., Opt. Phys.* **2005**, *72*, 022722-1–8.

(46) Collins, C. B. Collisional-Dissociative Recombination of Electrons with Molecules. *Phys. Rev. A: At., Mol., Opt. Phys.* **1965**, *140*, 1850–1857.

(47) Chupka, W. A. Factors Affecting Lifetimes and Resolution of Rydberg States Observed in Zero-Electron-Kinetic-Energy Spectroscopy. *J. Chem. Phys.* **1993**, *98*, 4520–4530.

(48) Dutta, S. K.; Feldbaum, D.; Walz-Flannigan, A.; Guest, J. R.; Raithel, G. High-Angular-Momentum States in Cold Rydberg Gases. *Phys. Rev. Lett.* **2001**, *86*, 3993–3996.

(49) Lebedev, V. S. Ionization of Rydberg atoms by neutral particles. I. Mechanism of the Perturber-Quasifree-Electron Scattering. *J. Phys. B: At. Mol. Opt. Phys.* **1991**, *24*, 1977–1991.

(50) Flannery, M. R. Transport Collisional Master Equations for Termolecular Recombination as a Function of Gas Density. *J. Chem. Phys.* **1991**, *95*, 8205–8226.

(51) Pitaevskii, L. P. Electron Recombination in an Atomic Gas. *Sov. Phys. JETP* **1962**, *15*, 919–921.

(52) Hickman, A. P. Theory of Angular Momentum Mixing in Rydberg-Atom-Rare-Gas Collisions. *Phys. Rev. A: At., Mol., Opt. Phys.* **1978**, *18*, 1339–1342.

(53) Petrigiani, A. Private communication. 2012.

(54) Kreckel, H.; Novotny, O.; Crabtree, K. N.; Buhr, H.; Petrigiani, A.; Tom, B. A.; Thomas, R. D.; Berg, M. H.; Bing, D.; Grieser, M.; et al. High-Resolution Storage-Ring Measurements of the Dissociative Recombination of H_3^+ Using a Supersonic Expansion Ion Source. *Phys. Rev. A: At., Mol., Opt. Phys.* **2010**, *82*, 042715-1–11.

(55) Jungen, Ch.; Pratt, S. T. Low-Energy Dissociative Recombination in Small Polyatomic Molecules. *J. Chem. Phys.* **2010**, *133*, 214303-1–9.

(56) Macdonald, J. A.; Biondi, M. A.; Johnsen, R. Recombination of Electrons with H_3^+ and H_5^+ Ions. *Planet. Space Sci.* **1984**, *32*, 651–654.

**Binary Recombination of H_3^+ and D_3^+ Ions with Electrons in Plasma
at 50–230 K**

Rubovič P., Dohnal P., Hejduk M., Plašil R., Glosík J.

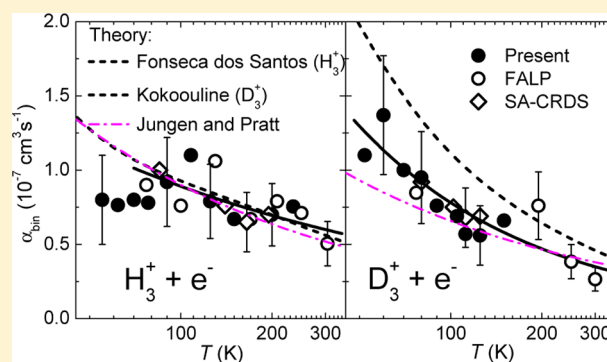
J. Phys. Chem. A **117(39)**, 9626–9632, 2013.

Binary Recombination of H_3^+ and D_3^+ Ions with Electrons in Plasma at 50–230 K

Peter Rubovič, Petr Dohnal, Michal Hejduk, Radek Plašil,* and Juraj Glosík

Department of Surface and Plasma Science, Faculty of Mathematics and Physics, Charles University, Prague 18000, Czech Republic

ABSTRACT: The results of an experimental study of the H_3^+ and D_3^+ ions recombination with electrons in afterglow plasmas in the temperature range 50–230 K are presented. A flowing afterglow apparatus equipped with a Langmuir probe was used to measure the evolution of the electron number density in the decaying plasma. The obtained values of the binary recombination rate coefficient are $\alpha_{\text{binH}_3^+} = (6.0 \pm 1.8) \times 10^{-8} (300/T)^{0.36 \pm 0.09} \text{ cm}^3 \text{ s}^{-1}$ for H_3^+ ions in the temperature range 80–300 K and $\alpha_{\text{binD}_3^+} = (3.5 \pm 1.1) \times 10^{-8} (300/T)^{0.73 \pm 0.09} \text{ cm}^3 \text{ s}^{-1}$ for D_3^+ ions in the temperature range 50–300 K. This is the first measurement of the binary recombination rate coefficient of H_3^+ and D_3^+ ions in a plasma experiment down to 50 K.



I. INTRODUCTION

The recombination of the simplest polyatomic ion H_3^+ (and to some extent of its deuterated isotopologues) with electrons has been the subject of extensive study by both experimental and theoretical physicists during the previous fifty years.¹ This process is fundamental for modeling of astrophysical diffuse clouds² and other hydrogen containing plasmas. The long history of H_3^+ recombination studies has been summarized in a number of reviews^{3–8} and in the thorough book by Larsson and Orel.⁹ The once puzzling disagreements in magnitude of recombination rate coefficients obtained in different types of experiments have been largely resolved by taking into account third-body stabilized recombination processes that can substantially enhance the overall recombination in plasmas over the pure binary recombination rate coefficients measured in beam type experiments.^{10,11} Moreover, the large discrepancy between experimentally obtained recombination rate coefficients and some early quantum mechanical calculations¹² has been successfully resolved by including the role of the Jahn–Teller effect.^{13–16} Theoretical predictions now agree very well with values obtained in ion-storage-rings experiments^{17–20} and in afterglow experiments.^{4,10,11,21,22}

In comparison, the neutral assisted ternary recombination of H_3^+ and D_3^+ ions with electrons as found in helium buffered afterglow experiments is still not fully understood. The recombining H_3^+ and D_3^+ ions form long living metastable Rydberg states^{11,21} with lifetimes in the order of hundreds of picoseconds. At pressures above 100 Pa, this is long enough for several collisions with particles of the buffer gas prior to recombination. Although some mechanisms for these interactions have been proposed,^{8,11} none of them fully explains the experimental data. This topic is thoroughly discussed in another article in this volume²³ together with new experimental data on

the ternary helium assisted recombination of H_3^+ or D_3^+ ions with electrons.

The theory of the dissociative recombination of H_3^+ ions with electrons also predicts a large difference between the recombination of *ortho*- and *para*- H_3^+ (more than 10 times at 10 K, 2.5 times at 80 K and no difference above 300 K).¹⁵ This was partially confirmed by storage ring measurements conducted using normal and *para*-enriched hydrogen (normal hydrogen contains 25% of *para*- H_2 and 75% of *ortho*- H_2 —i.e., the population of the rotational states of H_2 in thermodynamic equilibrium at 300 K).^{18,24–26} Tom et al.²⁵ found that *para*- H_3^+ recombines about twice as fast as *ortho*- H_3^+ at low collisional energies (10 K). The rotational temperature of H_3^+ ions in this experiment was probably higher than 300 K (see discussion in refs 20 and 26). In recent stationary afterglow experiments^{27–29} a cavity ring down spectrometer (CRDS) was used to probe the decay of ions in specific rotational states and to determine the state specific recombination coefficients. According to these experiments at 77 K *para*- H_3^+ ions recombine three to 10 times faster (if the error bars are taken into account) than *ortho*- H_3^+ ions. In these experiments, the H_3^+ ions were in thermodynamic equilibrium (TDE) with the helium buffer gas; i.e., the measured kinetic and rotational temperatures of the H_3^+ ions were close to the wall temperature, $T_{\text{kin}} = T_{\text{rot}} = T_{\text{He}} = T_{\text{wall}}$.

Another afterglow experiment with spectroscopically resolved number densities of the recombining H_3^+ ions was conducted by Amano in pure hydrogen in the early nineties.³⁰

Special Issue: Oka Festschrift: Celebrating 45 Years of Astrochemistry

Received: December 14, 2012

Revised: March 6, 2013

Published: March 27, 2013



His value of recombination rate coefficient $\alpha = 1.8 \times 10^{-7} \text{ cm}^3 \text{ s}^{-1}$ at 273 K and measured at pressure below 100 Pa is rather high and it probably indicates a very effective H_2 assisted ternary recombination.

The recombination of D_3^+ ions with electrons was also studied in storage ring experiments³¹ and in plasmatic experiments.^{4,21,32} Up to now there is only one study in a D_3^+ dominated plasma with spectroscopically resolved recombining ions.³³ In that experiment the measured kinetic and rotational temperatures of the recombining ions was also close to the buffer gas temperature (for details see ref 33).

In addition to the ternary neutral assisted recombination, an entirely different ternary process that can enhance the overall recombination rate in low temperature afterglow plasma is electron assisted ternary recombination (collisional radiative recombination, E-CRR).³⁴ At 80 K and an electron number density of $n_e = 5 \times 10^{10} \text{ cm}^{-3}$ the predicted effective binary recombination rate coefficient due to E-CRR is $5 \times 10^{-7} \text{ cm}^3 \text{ s}^{-1}$ —much larger than the actual values measured in H_3^+ or D_3^+ dominated afterglow plasmas under the same conditions.^{28,33} The thorough analysis of experimental data made by Dohnal et al.²⁸ has shown that the E-CRR contribution to the overall recombination rate in their experiments is more than order of magnitude lower than that predicted by the theory of E-CRR.³⁴ We have recently studied the E-CRR of Ar^+ ions in the temperature range 50–200 K,^{35,36} and we have obtained reasonable agreement with the theory. It is rather puzzling that we can measure value for the recombination rate coefficient close to the calculated one for the atomic ion Ar^+ and not for the molecular ion H_3^+ . Recently, Shuman et al.³⁷ observed the dependence of the mutual neutralization of Ar^+ ions with various molecular anions on electron number density. Although the process they proposed is different than E-CRR (and 10–100 times faster), it is clear that the magnitude of the electron induced enhancement of the recombination rate of more complicated species (e.g., molecular ions) is still an open question (especially given the lack of experimental data on the subject). One of the motivations for the present experiments was to study the role of E-CRR on the overall recombination of $\text{H}_3^+/\text{D}_3^+$ ions in an afterglow plasma.

In this article we will present the results of our study of the recombination of H_3^+ and D_3^+ ions with electrons in the temperature range 50–230 K, extending our previous measurement down to 50 K. The present measurements were performed with better temperature stability and over a broader range of pressures than in our previous flowing afterglow experiments^{10,11,21} to gain better accuracy of obtained binary and ternary recombination rate coefficients. To the best of our knowledge this is the first study of recombination of these molecular ions in an afterglow plasma below 80 K.

II. EXPERIMENT

In this study we used a Cryo-FALP II apparatus—a modification of the standard FALP (Flowing Afterglow with Langmuir Probe) device. The details of the FALP technique may be found in refs 9 and 38. The current experimental setup is described in ref 36 so only a short description will be given here.

The helium buffer gas is ionized in a microwave discharge in the upstream glass section of the flow tube, enters the stainless steel flow tube, and is pumped out by a Roots pump located at the other end of the flow tube. Argon is added a few centimeters downstream from the discharge to remove

metastable helium atoms and to form an Ar^+ dominated plasma. Further downstream, H_2 or D_2 is added to form H_3^+ or D_3^+ dominated plasmas. The sequence of ion–molecule reactions leading to the formation of H_3^+ (D_3^+) dominated plasma is discussed, e.g., in refs 5 and 39. The decrease of the electron number density along the flow tube is measured by means of axially movable Langmuir probe.

In our previous SA-CRDS (stationary afterglow with cavity ring down spectrometer) experiments^{27–29,33,40} conducted under conditions (pressure, temperature, and gas composition) similar to those in the present experiment, the measured kinetic and rotational temperatures of the H_3^+ or D_3^+ ions in the afterglow were close to the buffer gas temperature. Therefore, we have good reason to suppose that the internal temperature of the recombining ions is close to the buffer gas temperature also in the presented study which essentially extends previous measurements down to 50 K. Nevertheless, as discussed below, the actual *para*- H_3^+ to *ortho*- H_3^+ ratio could have been slightly shifted in favor of *ortho*- H_3^+ at temperatures below 80 K.

The electron temperature T_e was not directly measured in these (SA-CRDS and Cryo-FALP II) experiments. Recently, we have studied the collisional radiative recombination of Ar^+ ions with electrons, a process with a steep dependence on electron temperature.^{35,36} The results were in overall agreement with the theory of E-CRR³⁴ indicating that T_e was not significantly higher than the buffer gas temperature. Another indirect measure of the value of T_e is the rate of ambipolar diffusion. Ambipolar diffusion time constants measurements for the Ar^+ ions in helium gas, performed using the same experimental setup as in present study,³⁵ confirmed that in the studied range 80–200 K the measured ambipolar diffusion is close to the expected value, i. e. again that the electron temperature is not higher than the buffer gas temperature (within experimental error of 10%).

III. DETERMINATION OF THE BINARY RECOMBINATION RATE COEFFICIENTS

Here and in the following text we will refer to the recombining ions as H_3^+ , but the same considerations apply to D_3^+ ions unless stated otherwise.

It has been shown in previous afterglow experiments^{4,10,11,21} that the recombination losses due to the ternary helium assisted recombination of H_3^+ or D_3^+ ions can be comparable to that due to the dissociative recombination at buffer gas pressures of a few hundred pascals. Furthermore, at low temperatures and high densities of H_2 and He, H_5^+ cluster ions, which quickly recombine with electrons with a recombination rate coefficient $\alpha_5 \sim 10^{-6} \text{ cm}^3 \text{ s}^{-1}$, are formed in three body association reactions.^{41,42}

The overall losses of charged particles in a H_3^+ dominated plasma with a small fraction of H_5^+ ions, following the derivation in refs 35 and 42 can be described by the equation

$$\begin{aligned} \frac{dn_e}{dt} = & \frac{d[\text{H}_3^+]}{dt} \\ = & -\alpha_{\text{bin}}[\text{H}_3^+]n_e - \alpha_5 R[\text{H}_3^+]n_e - K_{\text{He}}[\text{He}][\text{H}_3^+]n_e \\ & - K_{\text{E-CRR}}[\text{H}_3^+]n_e^2 - \frac{n_e}{\tau_{\text{D}}} - \frac{n_e}{\tau_{\text{R}}} \end{aligned} \quad (3)$$

where n_e is the electron number density, $[\text{H}_3^+]$ is the number density of H_3^+ ions, $[\text{He}]$ is the number density of neutral buffer gas atoms (helium in this experiment), α_{bin} is the binary

recombination rate coefficient of H_3^+ ions, α_5 is the H_5^+ binary recombination rate coefficient, $R = [H_5^+]/[H_3^+] \approx K_C[H_2]$ (K_C is the equilibrium constant, the ratio R is equal to $K_C[H_2]$ if R does not change in time), K_{He} is the ternary recombination rate coefficient of neutral assisted ternary recombination (N-CRR), K_{E-CRR} is the ternary recombination rate coefficient of electron assisted collisional radiative recombination (E-CRR), τ_D is the time constant of ambipolar diffusion, and τ_R is the time constant of losses due to reactions with impurities and consequent fast recombination of formed ions. Assuming that H_3^+ is the dominant ion in the decaying plasma, and that the plasma is quasineutral, eq 3 can be then simplified:

$$\frac{dn_e}{dt} = -\alpha_{\text{eff}} n_e^2 - \frac{n_e}{\tau_L} \quad (4)$$

where

$$\alpha_{\text{eff}} = \alpha_{\text{extrap}} + \alpha_5 K_C [H_2] = \alpha_{\text{eff0}} + K_{He} [He] + \alpha_5 K_C [H_2] \quad (5)$$

is the effective binary recombination rate coefficient, and $1/\tau_L = 1/\tau_D + 1/\tau_R$. The α_{extrap} is part of the effective recombination rate coefficient independent of hydrogen number density. In the limit of vanishing helium and hydrogen densities, $\alpha_{\text{eff}} ([H_2] \rightarrow 0, [He] \rightarrow 0) = \alpha_{\text{eff0}} = (\alpha_{\text{bin}} + K_{E-CRR} n_e)$.

In the previous paragraph we have assumed that losses by N-CRR and E-CRR can be linearly added. This assumption might not be necessarily correct because of competition between both ternary processes.⁴³ At temperatures above 100 K and electron number densities $n_e \sim 10^9 \text{ cm}^{-3}$, the predicted losses due to E-CRR³⁴ are negligible in comparison with the losses due to dissociative recombination of H_3^+ (or D_3^+). At lower temperatures the losses due to E-CRR could be comparable with those from the dissociative recombination reaction. Nevertheless, we decided not to evaluate the K_{E-CRR} from the measured decay of the electron number density. If the E-CRR is present, it would be included in the α_{eff0} term of eq 5, because the H_2 and He dependent terms are evaluated separately (see below).

The "integral data analysis" described in ref 44 enables us to evaluate the effective recombination rate coefficient, α_{eff} and the time constant, τ_L , from the measured evolution of the electron number density.

To correct for the presence of H_5^+ ions, we measured the dependence of the effective recombination rate coefficient, α_{eff} on the H_2 number density at each temperature and pressure. Examples of such dependences are plotted in Figure 1.

The recombination rate coefficients of H_3^+ ions with electrons at a given temperature and pressure $\alpha_{\text{extrap}}(T, [He]) = \alpha_{\text{eff}}(T, [He], [H_2] \rightarrow 0)$, are then obtained by linear extrapolation of the measured α_{eff} to $[H_2] = 0$, as shown in Figure 1. The steepness of the slope fitted to these data increased with helium density and decreasing temperature. The number density of H_2 was always kept above $5 \times 10^{11} \text{ cm}^{-3}$ because it has to be high enough to form H_3^+ rapidly from the Ar^+ precursor ions and to maintain a constant *para*- to *ortho*- H_3^+ ratio. Otherwise, the faster recombining species would be depleted preferentially. We perform calculations of the chemical kinetics to determine the best conditions for the experiment. The discussions in refs 4 and 11 suggest that at conditions similar to the present experiment, the number density of H_2 should be greater than 10^{12} cm^{-3} . In this study $[H_2]$ was in the range 5×10^{11} to $2 \times 10^{13} \text{ cm}^{-3}$, sufficient to maintain the *para*-

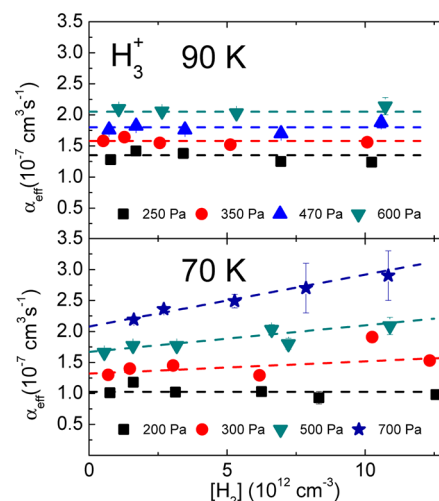


Figure 1. Dependence of the measured effective recombination rate coefficient of recombination of H_3^+ ions with electrons on H_2 number density at 90 K (upper panel) and 70 K (lower panel). Dashed lines are linear fits to the data. The extrapolation of these fits to $[H_2] = 0$ gives the value of $\alpha_{\text{extrap}}(T, [He])$ at the given temperature and pressure.

H_3^+ to *ortho*- H_3^+ ratio at the value appropriate for the *para*/*ortho* composition of the H_2 gas used.^{40,45}

Examples of measured dependences of α_{eff} on the helium number density for H_3^+ and for D_3^+ are plotted in Figure 2.

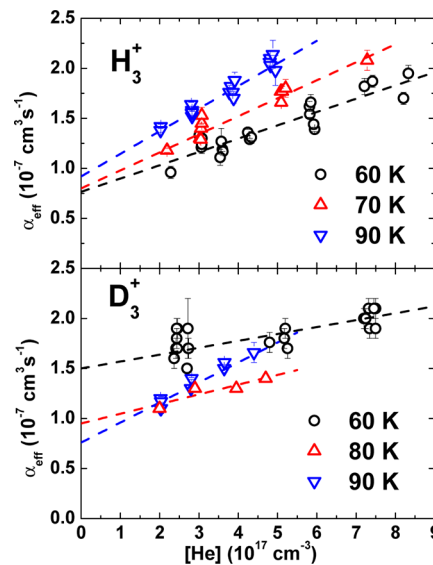


Figure 2. Upper panel: dependence of the effective recombination rate coefficient of recombination of H_3^+ ions with electrons on the helium buffer gas density measured at each of the following temperatures: 60, 70, and 90 K. Lower panel: as in the upper panel but for D_3^+ ions at the temperatures 60, 80, and 90 K. The dashed lines are linear fits to the data. The displayed errors are statistical errors.

These data were obtained at number densities of H_2 in the range 1×10^{12} to $7 \times 10^{12} \text{ cm}^{-3}$. In general, the binary and the ternary recombination rate coefficients can be obtained from the dependences plotted in Figure 2, as is discussed, e.g., in ref 28. At low temperatures (especially at 50 K) and at higher helium densities the formation of H_5^+ (D_5^+) would cause an additional increase in the effective recombination rate

coefficient. The binary α_{eff0} and the ternary K_{He} recombination rate coefficients at a given temperature were thus obtained using eq 5 from the dependence of $\alpha_{\text{extrap}}(T, [\text{He}])$ on the helium number density. The errors displayed in Figures 1 and 2 are statistical errors of the fit to the time decay of electron number density.

IV. RESULTS AND DISCUSSION

The measured dependence of the binary recombination rate coefficient α_{bin} (α_{eff0} , see below) of the recombination of H_3^+ ions with electrons on temperature is plotted in Figure 3. The

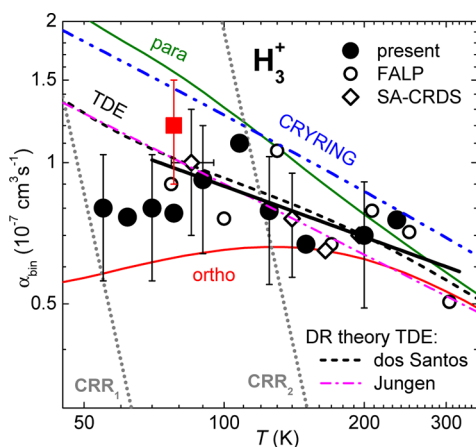


Figure 3. Temperature dependence of the binary recombination rate coefficient for the recombination of H_3^+ ions with electrons. Present Cryo-FALP II data are indicated by full circles. Open rhomboids indicate values measured by Varju et al.²⁷ and Dohnal et al.²⁸ using the SA-CRDS apparatus with spectroscopic identification of the recombining ions. Open circles are binary recombination rate coefficients measured in this laboratory using the FALP technique (see discussion in refs 11 and 28). The dashed double dotted line shows data measured at the storage ring CRYRING.¹⁹ The dashed, and the dot dashed, lines marked TDE are theoretical calculations by Fonseca dos Santos¹⁵ and Pratt and Jungen,⁴⁶ respectively. The dotted lines marked CRR₁ and CRR₂ indicate calculated³⁴ recombination rate coefficient for E-CRR at electron number densities of 10^9 and $5 \times 10^{10} \text{ cm}^{-3}$, respectively. The thick full straight line is a fit to the FALP, Cryo-FALP II, and SA-CRDS data in the range 80–300 K: $\alpha_{\text{binH}_3^+} = (6.0 \pm 1.8) \times 10^{-8} (300/T)^{0.36 \pm 0.09} \text{ cm}^3 \text{ s}^{-1}$. The full lines labeled para and ortho are recombination rate coefficients calculated by Fonseca dos Santos¹⁵ for para- H_3^+ and ortho- H_3^+ ions. The full square is the value of α_{bin} measured using the Cryo-FALP II apparatus with para-enriched H_2 instead of normal H_2 .

present data are plotted as full circles. Values from previous FALP,¹¹ SA-CRDS,^{27,28} and CRYRING¹⁹ experiments are also plotted in Figure 3 together with the thermal dissociative recombination rate coefficients calculated by Fonseca dos Santos et al.¹⁵ and by Pratt and Jungen.^{16,46} We computed the thermal values from the energy dependent recombination rate coefficients published by Pratt and Jungen.⁴⁶ The estimated errors of the measured recombination rate coefficients α_{bin} are $\pm 30\%$.⁴⁷ The main contributions of the systematic errors arise from the electron number density measurement by Langmuir probe and from uncertainties in the determination of pressure and gas flows. The statistical error from the aforementioned fitting steps (less than 10%) is negligible in comparison with the systematic one.

The dotted lines in Figure 3 labeled CRR₁ and CRR₂ are effective binary recombination rate coefficients of E-CRR ($\alpha_{\text{E-CRR}}$) at electron number density of 10^9 cm^{-3} (a typical value for the present Cryo-FALP II experiment) and $5 \times 10^{10} \text{ cm}^{-3}$ (a typical value for the SA-CRDS experiment), calculated from the dependence $\alpha_{\text{E-CRR}} = 3.8 \times 10^{-9} T^{-4.5} n_e \text{ cm}^3 \text{ s}^{-1}$ (see ref 34), respectively. Note that at $T \sim 80 \text{ K}$, the difference between the values of α_{bin} obtained in the present study and in the previous SA-CRDS experiment²⁷ is less than $2 \times 10^{-8} \text{ cm}^3 \text{ s}^{-1}$. This suggests that the effect of E-CRR on the recombination of H_3^+ ions with electrons is at least 20 times lower than predicted by theory of E-CRR.³⁴ A substantial increase of the recombination rate coefficient below 80 K (in accordance with the $T^{-4.5}$ temperature dependence of $\alpha_{\text{E-CRR}}$) was not observed. This leads to the conclusion that under our experimental conditions $\alpha_{\text{eff0}} = \alpha_{\text{bin}}$.

We have previously measured the rate coefficients of E-CRR of Ar^+ ions using the same setup as in current experiment^{35,36} and we have found good agreement with theory of E-CRR.³⁴ We do not have an explanation for the seeming absence of E-CRR in the H_3^+ dominated plasma investigated here.

The thick full straight line plotted in Figure 3 is the fit of the FALP, Cryo-FALP II, and SA-CRDS data in the temperature range 80–300 K giving the value $\alpha_{\text{binH}_3^+} = (6.0 \pm 1.8) \times 10^{-8} (300/T)^{0.36 \pm 0.09} \text{ cm}^3 \text{ s}^{-1}$. We included in the fit only the data for which we have information about the internal state of the recombining ions. The agreement of the present data with our previous afterglow experiments, storage ring values and with the theoretical calculations is very good. Below 80 K the experimental values begin to deviate from the theoretical ones. To form H_3^+ ions, we used normal H_2 from a 300 K reservoir, with a para- to ortho- H_2 ratio of 1:3. The para- to ortho- H_2 equilibrium ratio at 50 K is approximately 3:1. We suspect that this huge difference could shift the population of H_3^+ ions toward ortho- H_3^+ . At 77 K where the para- to ortho- H_2 equilibrium ratio is 1:1, the resulting percentage of para- H_3^+ states was $45 \pm 2\%$ depending on conditions (see Figure 10 in Hejduk et al.⁴⁰). There is a difference in magnitude of the recombination rate coefficients of para- and ortho- H_3^+ below 300 K. para- H_3^+ recombines 2 times faster than ortho- H_3^+ at 10 K as measured in storage ring experiment CRYRING²⁵ or 3–10 times faster at 80 K as measured in our stationary afterglow experiment.²⁷ The theory¹⁵ suggests that para- H_3^+ recombines 2.5 times faster than ortho- H_3^+ at 80 K (Figure 3). This would lead to substantial decrease of measured α_{bin} if the fraction of ortho- H_3^+ ions was enhanced with respect to the equilibrium population of states of the H_3^+ ions.

To see the influence of the different para- to ortho- H_3^+ ratios on the overall recombination in plasma, we used hydrogen with an enriched fraction of para- H_2 at otherwise identical conditions as in presented experiments with normal H_2 . The para-enriched hydrogen was produced using apparatus described in ref 40. According to the measurements of the reaction rate coefficient of the reaction of N^+ with H_2 ,⁴⁸ the produced H_2 gas contained $99.5 \pm 0.5\%$ molecules in para- H_2 states. Using this para- H_2 -enriched gas to form the H_3^+ dominated plasma, the obtained value of the binary recombination rate coefficient was $(1.2 \pm 0.3) \times 10^{-7} \text{ cm}^3 \text{ s}^{-1}$ at 80 K in comparison with the value of $(0.8 \pm 0.3) \times 10^{-7} \text{ cm}^3 \text{ s}^{-1}$ obtained using normal H_2 . The result is plotted in Figure 3 as a full square. Unfortunately, we are not able to measure in situ the para- to ortho- H_3^+ ratio in the present Cryo-

FALP II setup. The fraction of *para*-H₃⁺ ions obtained in SA-CRDS experiment at 80 K when *para*-enriched H₂ was used was 70–75%.⁴⁰ We suppose that the *para*-H₃⁺ fraction in our Cryo-FALP II experiment is similar.

The experiments with D₃⁺ dominated plasmas were similar to those with H₃⁺ dominated plasmas. We measured the dependence of the effective recombination rate coefficient on the D₂ number density at particular temperatures and pressures and obtained the binary α_{bin} and the ternary K_{He} recombination rate coefficients for the recombination of D₃⁺ ions with electrons. The measured binary recombination rate coefficients of recombination of D₃⁺ ions with electrons are plotted in Figure 4 together with values from previous SA-CRDS,³³

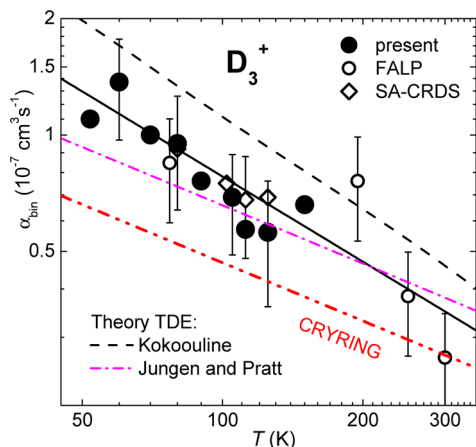


Figure 4. Temperature dependence of the measured binary recombination rate coefficient for the recombination of D₃⁺ ions with electrons. Full circles indicate the present data obtained in the Cryo-FALP II experiment. Open rhomboids are the values obtained in SA-CRDS experiment.³³ Open circles are data from previous FALP²¹ experiments. The dashed double dot line indicates results from the storage ring CRYRING.³¹ The theoretical calculations of Kokouline⁴⁹ and Pratt and Jungen⁴⁶ are plotted as dashed lines and dot dashed lines, respectively. The full straight line is a fit to the FALP, Cryo-FALP II, and SA-CRDS data in the range 50–300 K: $\alpha_{\text{binD}_3^+} = (3.5 \pm 1.1) \times 10^{-8}(300/T)^{0.73 \pm 0.09} \text{ cm}^3 \text{ s}^{-1}$.

FALP,²¹ and CRYRING³¹ experiments. The theoretical dependences calculated by Kokouline⁴⁹ and by Pratt and Jungen⁴⁶ are also plotted in Figure 4. We calculated the recombination rate coefficients labeled Jungen and Pratt in Figure 4 by thermally averaging their energy dependent recombination rates published in ref 46. The full straight line plotted in Figure 4 is the fit to the FALP, Cryo-FALP II, and SA-CRDS data in the range 50–300 K, giving a value for recombination rate coefficient $\alpha_{\text{binD}_3^+} = (3.5 \pm 1.1) \times 10^{-8}(300/T)^{0.73 \pm 0.09} \text{ cm}^3 \text{ s}^{-1}$. The theory⁴⁹ predicts that the difference between the recombination rate coefficients of each nuclear spin state modification of D₃⁺ (*ortho*, *para*, and *meta*) is only small and not so pronounced as in the case of H₃⁺. For example at 50 K *ortho*-D₃⁺ should recombine 1.5 times faster than *meta*-D₃⁺. Moreover, the relative population of nuclear spin modifications in the D₂ gas used in the experiment is close to the equilibrium value even at 60 K due to the closer spacing of the rotational energy levels of D₂ in comparison with H₂. At 300 K the *para*-D₂ to *ortho*-D₂ equilibrium ratio is 2, at 60 K the *para*-D₂ to *ortho*-D₂ equilibrium ratio is 1.8. Therefore, we suppose that the *ortho/para/meta*-D₃⁺ ratio is maintained in the

whole temperature range used in this study. This is probably why the values for the D₃⁺ recombination rate coefficient obtained below 80 K continue to follow the $T^{-0.73}$ dependence (the full line plotted in Figure 4). As in the case of H₃⁺, the results obtained for D₃⁺ are in good agreement with theoretical calculations and with other experiments. No substantial difference between present values and values obtained in SA-CRDS experiment³³ conducted at order of magnitude higher n_e was observed. As in the case of H₃⁺ dominated plasma we have seen no substantial influence of E-CRR on the overall recombination of D₃⁺ ions with electrons over the range of experimental conditions.

Together with binary recombination rate coefficients α_{bin} we also evaluated the ternary recombination rate coefficients K_{He} for the recombination of H₃⁺ and D₃⁺ ions with electrons in the temperature range 50–230 K. These results are published elsewhere²³ together with a thorough discussion of possible ternary recombination processes occurring in low temperature plasmas. The temperature range 80–300 K was already covered in our previous experiments;^{11,21,28,33} the present data were measured over wider temperature and pressure ranges than in the FALP^{11,21} experiments and with better accuracy and temperature stability. The agreement with these previous studies is good.

V. CONCLUSION

We have measured the binary and the ternary recombination rate coefficient for the recombination of H₃⁺ and D₃⁺ ions with electrons in the temperature range 50–230 K. The results are in good agreement with previous afterglow experiments (FALP and SA-CRDS), storage ring data, and theoretical calculations. The obtained binary recombination rate coefficients follow the dependence $\alpha_{\text{binH}_3^+} = (6.0 \pm 1.8) \times 10^{-8}(300/T)^{0.36 \pm 0.09} \text{ cm}^3 \text{ s}^{-1}$ for H₃⁺ in the temperature range 80–300 K and $\alpha_{\text{binD}_3^+} = (3.5 \pm 1.1) \times 10^{-8}(300/T)^{0.73 \pm 0.09} \text{ cm}^3 \text{ s}^{-1}$ for D₃⁺ in the temperature range 50–300 K. We have seen no enhancement of the measured recombination rate coefficient of H₃⁺ and D₃⁺ ions due to E-CRR even at the lowest temperature. This is in agreement with our previous SA-CRDS experiments^{27,33} conducted at higher electron number densities than in present study. The addition of *para*-enriched H₂ instead of normal H₂ led to the increase of the binary recombination rate coefficient at 80 K from $(0.8 \pm 0.3) \times 10^{-7} \text{ cm}^3 \text{ s}^{-1}$ with normal H₂ to $(1.2 \pm 0.3) \times 10^{-7} \text{ cm}^3 \text{ s}^{-1}$ with *para*-enriched H₂. This is the first measurement of the recombination rate coefficient of H₃⁺ and D₃⁺ ions in a plasma experiment down to 50 K.

■ AUTHOR INFORMATION

Corresponding Author

*Phone: +420221912224. E-mail: radek.plasil@mff.cuni.cz.

Author Contributions

The manuscript was written through contributions of all authors. All authors have given approval to the final version of the manuscript.

Notes

The authors declare no competing financial interest.

■ ACKNOWLEDGMENTS

We thank Rainer Johnsen for helpful discussion and comments. This work was partly supported by GACR (205/09/1183, P209/12/0233), SV 267 302, GAUK 353811, GAUK 406011,

GAUK 659112, and COST Action CM0805 (The Chemical Cosmos).

REFERENCES

- (1) Oka, T. in *Dissociative Recombination of Molecular Ions with Electrons*; Guberman, S. L., Ed.; Kluwer Academic/Plenum Publishers: New York, USA, 2003; pp 209–220
- (2) Herbst, E.; Klemperer, W. The Formation and Depletion of Molecules in Dense Interstellar Clouds. *Astrophys. J.* **1973**, *185*, 505–533.
- (3) Larsson, M. Experimental Studies of the Dissociative Recombination of H_3^+ . *Philos. Trans. R. Soc. A* **2000**, *358*, 2433–2444.
- (4) Glosik, J.; Plasil, R.; Kotrik, T.; Dohnal, P.; Varju, J.; Hejduk, M.; Korolov, I.; Roucka, S.; Kokoouline, V. Binary and Ternary Recombination of H_3^+ and D_3^+ Ions with Electrons in Low Temperature Plasma. *Mol. Phys.* **2010**, *108*, 2253–2264.
- (5) Plasil, R.; Glosik, J.; Poterya, V.; Kudrna, P.; Ruz, J.; Tichy, M.; Pysanenko, A. Advanced Integrated Stationary Afterglow Method for Experimental Study of Recombination of Processes of H_3^+ and D_3^+ Ions with Electrons. *Int. J. Mass Spectrom.* **2002**, *218*, 105–130.
- (6) Smith, D.; Spanel, P. Dissociative Recombination of H_3^+ and Some Other Interstellar Ions: a Controversy Resolved. *Int. J. Mass Spectrom.* **1993**, *129*, 163–182.
- (7) Johnsen, R. A Critical Review of H_3^+ Recombination Studies. *J. Phys.: Conf. Ser.* **2005**, *4*, 83–91.
- (8) Johnsen, R.; Guberman, S. L. Dissociative Recombination of H_3^+ Ions with Electrons: Theory and Experiment. *Adv. At., Mol., Opt. Phys.* **2010**, *59*, 75–128.
- (9) Larsson, M.; Orel, A. *Dissociative Recombination of Molecular Ions*; Cambridge University Press: Cambridge, U.K., 1995.
- (10) Glosik, J.; Korolov, I.; Plasil, R.; Novotny, O.; Kotrik, T.; Hlavenka, P.; Varju, J.; Mikhailov, I. A.; Kokoouline, V.; Greene, C. H. Recombination of H_3^+ Ions in the Afterglow of a He-Ar- H_2 Plasma. *J. Phys. B-At. Mol. Opt.* **2008**, *41*, 191001.
- (11) Glosik, J.; Plasil, R.; Korolov, I.; Kotrik, T.; Novotny, O.; Hlavenka, P.; Dohnal, P.; Varju, J.; Kokoouline, V.; Greene, C. H. Temperature Dependence of Binary and Ternary Recombination of H_3^+ Ions with Electrons. *Phys. Rev. A* **2009**, *79*, 052707.
- (12) Michels, H. H.; Hobbs, R. H. Low-Temperature Dissociative Recombination of $e + H_3^+$. *Astrophys. J.* **1984**, *286*, L27–L29.
- (13) Kokoouline, V.; Greene, C. H.; Esry, B. D. Mechanism for the Destruction of H_3^+ Ions by Electron Impact. *Nature* **2001**, *412*, 891–894.
- (14) Kokoouline, V.; Greene, C. H. Unified Theoretical Treatment of Dissociative Recombination of D_{3h} Triatomic Ions: Application to H_3^+ and D_3^+ . *Phys. Rev. A* **2003**, *68*, 012703.
- (15) Fonseca dos Santos, S.; Kokoouline, V.; Greene, C. H. Dissociative Recombination of H_3^+ in the Ground and Excited Vibrational States. *J. Chem. Phys.* **2007**, *127*, 124309.
- (16) Jungen, Ch.; Pratt, S. T. Jahn-Teller Interactions in the Dissociative Recombination of H_3^+ . *Phys. Rev. Lett.* **2009**, *102*, 023201.
- (17) McCall, B. J.; Honeycutt, A. J.; Saykally, R. J.; Geballe, T. R.; Djuric, N.; Dunn, G. H.; Semaniak, J.; Novotny, O.; Al-Khalili, A.; Ehlerding, A.; et al. An Enhanced Cosmic-Ray Flux Towards ζ Persei Inferred from a Laboratory Study of the $H_3^+e^-$ Recombination Rate. *Nature* **2003**, *422*, 500–502.
- (18) Kreckel, H.; Motsch, M.; Mikosch, J.; Glosik, J.; Plasil, R.; Altevogt, S.; Andrianarijaona, V.; Buhr, H.; Hoffman, J.; Lammich, L.; et al. High-Resolution Dissociative Recombination of Cold H_3^+ and First Evidence for Nuclear Spin Effects. *Phys. Rev. Lett.* **2005**, *95*, 263201.
- (19) McCall, B. J.; Honeycutt, A. J.; Saykally, R. J.; Djuric, N.; Dunn, G. H.; Semaniak, J.; Novotny, O.; Al-Khalili, A.; Ehlerding, A.; Hellberg, F.; et al. Dissociative Recombination of Rotationally Cold H_3^+ . *Phys. Rev. A* **2004**, *70*, 052716.
- (20) Petrigani, A.; Altevogt, S.; Berg, M. H.; Bing, D.; Grieser, M.; Hoffman, J.; Jordon-Thaden, B.; Krantz, C.; Mendes, M. B.; Novotny, O.; et al. Resonant Structure of Low-Energy H_3^+ Dissociative Recombination. *Phys. Rev. A* **2011**, *83*, 032711.
- (21) Kotrik, T.; Dohnal, P.; Korolov, I.; Plasil, R.; Roucka, S.; Glosik, J.; Greene, C. H.; Kokoouline, V. Temperature Dependence of Binary and Ternary Recombination of D_3^+ Ions with Electrons. *J. Chem. Phys.* **2010**, *133*, 034305.
- (22) Glosik, J.; Plasil, R.; Korolov, I.; Novotny, O.; Kotrik, T. Multicollision Character of Recombination of H_3^+ Ions in Afterglow Plasma. *J. Phys.: Conf. Ser.* **2009**, *192*, 012005.
- (23) Johnsen, R.; Rubovic, P.; Dohnal, P.; Hejduk, M.; Plasil, R.; Glosik, J. Ternary Recombination of H_3^+ and D_3^+ with Electrons in He- H_2 (D_2) Plasmas at Temperatures from 50 to 300 K. Elsewhere in this volume. *J. Phys. Chem. A* **2013**, DOI: 10.1021/jp311978n.
- (24) Wolf, A.; Kreckel, H.; Lammich, L.; Strasser, D.; Mikosch, J.; Glosik, J.; Plasil, R.; Altevogt, S.; Andrianarijaona, V.; Buhr, H.; et al. Effects of Molecular Rotation in Low-Energy Electron Collisions of H_3^+ . *Philos. Trans. R. Soc. A* **2006**, *364*, 2981–2997.
- (25) Tom, B. A.; Zhaunerchyk, V.; Wiczer, M. B.; Mills, A. A.; Crabtree, K. N.; Kaminska, M.; Geppert, W. D.; Hamberg, M.; af Ugglas, M.; Vigren, E.; et al. Dissociative Recombination of Highly Enriched Para- H_3^+ . *J. Chem. Phys.* **2009**, *130*, 031101.
- (26) Kreckel, H.; Novotny, O.; Crabtree, K. N.; Buhr, H.; Petrigani, A.; Tom, B. A.; Thomas, R. D.; Berg, M. H.; Bing, D.; Grieser, M.; et al. High-Resolution Storage-Ring Measurements of the Dissociative Recombination of H_3^+ Using a Supersonic Expansion Ion Source. *Phys. Rev. A* **2010**, *82*, 042715.
- (27) Varju, J.; Hejduk, M.; Dohnal, P.; Jilek, M.; Kotrik, T.; Plasil, R.; Gerlich, D.; Glosik, J. Nuclear Spin Effect on Recombination of H_3^+ Ions with Electrons at 77 K. *Phys. Rev. Lett.* **2011**, *106*, 203201.
- (28) Dohnal, P.; Hejduk, M.; Varju, J.; Rubovic, P.; Roucka, S.; Kotrik, T.; Plasil, R.; Glosik, J.; Johnsen, R. Binary and Ternary Recombination of Para- H_3^+ and Ortho- H_3^+ with Electrons: State Selective Study at 77–200 K. *J. Chem. Phys.* **2012**, *136*, 244304.
- (29) Dohnal, P.; Hejduk, M.; Varju, J.; Rubovic, P.; Roucka, S.; Kotrik, T.; Plasil, R.; Johnsen, R.; Glosik, J. Binary Recombination of Para- and Ortho- H_3^+ with Electrons at Low Temperatures. *Philos. Trans. R. Soc. A* **2012**, *370*, 5101–5108.
- (30) Amano, T. The Dissociative Recombination Rate Coefficients of H_3^+ , HN_2^+ and HCO^+ . *J. Chem. Phys.* **1990**, *92*, 6492–6501.
- (31) Le Padellec, A.; Larsson, M.; Danared, H.; Larson, A.; Peterson, J. R.; Rosen, S.; Semaniak, J.; Stromholm, C. A Storage Ring Study of Dissociative Excitation and Recombination of D_3^+ . *Phys. Scr.* **1998**, *57*, 215–221.
- (32) Poterya, V.; Glosik, J.; Plasil, R.; Tichy, M.; Kudrna, P.; Pysanenko, A. Recombination of D_3^+ ions in the Afterglow of a He-Ar- D_2 Plasma. *Phys. Rev. Lett.* **2002**, *88*, 044802.
- (33) Dohnal, P.; Hejduk, M.; Rubovic, P.; Varju, J.; Roucka, S.; Plasil, R.; Glosik, J. Binary and Ternary Recombination of D_3^+ Ions at 80–130 K: Application of Laser Absorption Spectroscopy. *J. Chem. Phys.* **2012**, *137*, 194320.
- (34) Stevefelt, J.; Boulmer, J.; Delpech, J. F. Collisional-Radiative Recombination in Cold Plasmas. *Phys. Rev. A* **1975**, *12*, 1246–1251.
- (35) Kotrik, T.; Dohnal, P.; Roucka, S.; Jusko, P.; Plasil, R.; Glosik, J.; Johnsen, R. Collisional-Radiative Recombination $Ar^+ + e + e$: Experimental Study at 77–180 K. *Phys. Rev. A* **2011**, *83* (3), 032720.
- (36) Kotrik, T.; Dohnal, P.; Rubovic, P.; Plasil, R.; Roucka, S.; Opanasiuk, S.; Glosik, J. Cryo-FALP Study of Collisional-Radiative Recombination of Ar^+ Ions at 40–200 K. *Eur. Phys. J. Appl. Phys.* **2011**, *56*, 24011.
- (37) Shuman, S.; Miller, T. M.; Bemish, R. J.; Viggiano, A. A. Electron-Catalyzed Mutual Neutralization of Various Anions with Ar^+ : Evidence of a New Plasma Process. *Phys. Rev. Lett.* **2011**, *106*, 018302.
- (38) Smith, D.; Adams, N. G.; Dean, A. G.; Church, M. J. The Application of the Langmuir Probes to the Study of the Flowing Afterglow Plasmas. *J. Phys. D: Appl. Phys.* **1975**, *8*, 141–152.
- (39) Novotny, O.; Plasil, R.; Pysanenko, A.; Korolov, I.; Glosik, J. The Recombination of D_3^+ and D_5^+ Ions with Electrons in Deuterium Containing Plasma. *J. Phys. B-At. Mol. Opt. Phys.* **2006**, *39*, 2561–2569.
- (40) Hejduk, M.; Dohnal, P.; Varju, J.; Rubovic, P.; Plasil, R.; Glosik, J. Nuclear Spin State-Resolved Cavity Ring-Down Spectroscopy

Diagnostics of a Low-Temperature H_3^+ Dominated Plasma. *Plasma Sources Sci. Technol.* **2012**, *21*, 024002.

(41) Hiraoka, K. A determination of the Stabilities of $\text{H}_3^+(\text{H}_2)_n$ with $n = 1-9$ from Measurements of the Gas Phase Ion Equilibria $\text{H}_3^+(\text{H}_2)_{n-1} + \text{H}_2 = \text{H}_3^+(\text{H}_2)_n$. *J. Chem. Phys.* **1987**, *87*, 4048–4055.

(42) Glosik, J.; Novotny, O.; Pysanenko, A.; Zakouril, P.; Plasil, R.; Kudrna, P.; Poterya, V. The Recombination of H_3^+ and H_5^+ Ions with Electrons in Hydrogen Plasma: Dependence on Temperature and on Pressure of H_2 . *Plasma Sources Sci. Technol.* **2003**, *12*, S117–S122.

(43) Bates, D. R. Recombination and Electrical Networks. *Proc. R. Soc. London A* **1974**, *337*, 15–20.

(44) Korolov, I.; Kotrik, T.; Plasil, R.; Varju, J.; Hejduk, M.; Glosik, J. Application of Langmuir Probe in Recombination Dominated Afterglow Plasma. *Contrib. Plasma Phys.* **2008**, *48*, 521–526.

(45) Grussie, F.; Berg, M. H.; Crabtree, K. N.; Gartner, S.; McCall, B. J.; Schlemmer, S.; Wolf, A.; Kreckel, H. The Low-Temperature Nuclear Spin Equilibrium of H_3^+ in Collisions with H_2 . *Astrophys. J.* **2012**, *759*, 21.

(46) Pratt, T.; Jungen, Ch. Dissociative Recombination of Small Polyatomic Molecules. *J. Phys.: Conf. Ser.* **2011**, *300*, 012019.

(47) Glosik, J.; Bano, G.; Plasil, R.; Luca, A.; Zakouril, P. Study of the Electron Ion Recombination in High Pressure Flowing Afterglow: Recombination of $\text{NH}_4^+(\text{NH}_3)_2$. *Int. J. Mass Spectrom.* **1999**, *189*, 103–113.

(48) Zymak, I.; Hejduk, M.; Mulin, D.; Plasil, R.; Glosik, J.; Gerlich, D. Low Temperature Ion Trap Studies of $\text{N}^+(\text{}^3\text{P}_a) + \text{H}_2(j) \rightarrow \text{NH}^+ + \text{H}$. *Astrophys. J.* **2013**, in press.

(49) Pagani, L.; Vastel, C.; Hugo, E.; Kokoouline, V.; Greene, C. H.; Backmann, A.; Bayet, E.; Ceccarelli, C.; Peng, R.; Schlemmer, S. Chemical Modeling of L183 (L134N): an Estimate of the Ortho/Para H_2 Ratio. *Astron. Astrophys.* **2009**, *494*, 623–636.

**Collisional-radiative recombination of Ar⁺ ions with electrons in
ambient helium at temperatures from 50 K to 100 K**

Dohnal P., Rubovič P., Kotřík T., Hejduk M., Plašil R., Johnsen R., Glosik J.

Phys. Rev. A **87**, 052716, 2013.

Collisional-radiative recombination of Ar⁺ ions with electrons in ambient helium at temperatures from 50 K to 100 K

Petr Dohnal,¹ Peter Rubovič,¹ Tomáš Kotrčík,¹ Michal Hejduk,¹ Radek Plašil,¹ Rainer Johnsen,² and Juraj Glosík¹

¹*Department of Surface and Plasma Science, Faculty of Mathematics and Physics, Charles University in Prague, Czech Republic*

²*Department of Physics and Astronomy, University of Pittsburgh, Pittsburgh, Pennsylvania 15260, USA*

(Received 26 April 2013; published 29 May 2013)

Ternary electron-assisted collisional radiative recombination (E-CRR) and neutral-assisted radiative recombination (N-CRR) have very strong negative temperature dependencies and hence dominate electron recombination in some plasmas at very low temperatures. However, there are only few data for molecular ions and almost none for atomic ions at temperatures much below 300 K. In this experimental study we used a cryogenic afterglow plasma experiment (Cryo-FALP II) at temperatures from 50 K to 100 K to measure ternary recombination rate coefficients for Ar⁺ ions in ambient helium gas. The measured magnitudes and the temperature dependencies of the ternary recombination rate coefficients for electron-assisted and neutral-assisted collisional radiative recombination agree well with theoretical predictions ($K_{\text{E-CRR}} \sim T^{-4.5}$ and $K_{\text{He-CRR}} \sim T^{-2.5}$ to $T^{-2.9}$) over a broad range of electron and He densities.

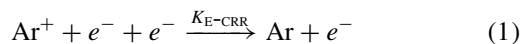
DOI: [10.1103/PhysRevA.87.052716](https://doi.org/10.1103/PhysRevA.87.052716)

PACS number(s): 34.80.Lx, 52.27.Aj, 52.20.-j

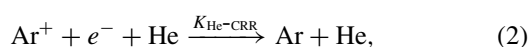
I. INTRODUCTION

Electron-ion recombination in cold plasmas can occur by several mechanisms. When the ions in the plasma are molecular, dissociative recombination (DR) [1] is almost always much faster than third-body-assisted recombination, unless the densities of third particles (electrons, ions, and neutrals) are very high or the temperature is very low. Hence, in many afterglow determinations of DR rate coefficients of molecular ions at temperatures near 300 K, neutral densities below $1 \times 10^{17} \text{ cm}^{-3}$, and electron densities $< 1 \times 10^{10} \text{ cm}^{-3}$, third-body-assisted recombination can usually be neglected. Experimental methods have now been developed that are capable of measuring DR rate coefficients at the very low temperatures (near 50 K) that exist in cold interstellar clouds. At those temperatures, third-body-assisted recombination becomes competitive with DR and must be clearly separated from binary DR. The studies described here test existing theories of ternary recombination at very low temperatures in helium-buffered plasmas containing predominantly atomic argon ions, thus largely eliminating DR. The remaining recombination processes consist of ternary recombination in which electrons and helium atoms act as third bodies and a slow conversion of atomic argon ions to molecular Ar₂⁺ ions that recombine by DR. As will be shown, the relative contributions of the three mechanisms can be separated and the results confirm theoretical calculations.

In the following we will refer to ternary electron-assisted collisional radiative recombination (see, e.g., [2]) as E-CRR and to the ternary neutral-assisted recombination process (see, e.g., [3]) as N-CRR, where N denotes the neutral atom (e.g., He). The overall reaction equations for atomic argon ions in the presence of electrons and helium atoms can be written as



and



where $K_{\text{E-CRR}}$ and $K_{\text{He-CRR}}$ are ternary recombination rate coefficients (in units of $\text{cm}^6 \text{ s}^{-1}$). Writing the reactions in this form is not meant to imply that a single three-particle collision completes the recombination. In general, several energy-reducing collisions are required to render the product atom stable against reionization. Both E-CRR and N-CRR have been extensively treated by semiclassical theories (see, e.g., [2,4]) that solve the coupled equations for three-body electron capture into discrete Rydberg states, ionization, and stepwise collisional and radiative reduction of the electron energy. Results of numerical calculations of E-CRR by Stevefelt *et al.* [2] can be expressed by the following formula for the effective binary rate coefficient:

$$\alpha_{\text{E-CRR}} = 3.8 \times 10^{-9} T_e^{-4.5} n_e + 1.55 \times 10^{-10} T_e^{-0.63} + 6 \times 10^{-9} T_e^{-2.18} n_e^{0.37} \text{ cm}^3 \text{ s}^{-1}, \quad (3)$$

where T_e is the electron temperature in K and n_e is the electron number density in cm^{-3} . At low temperatures the second and third terms on the right-hand side tend to be small in comparison with the first term and one can define a three-body rate coefficient $K_{\text{E-CRR}}$ by dividing E-CRR by the electron density:

$$K_{\text{E-CRR}} = \alpha_{\text{E-CRR}} / n_e \cong 3.8 \times 10^{-9} T_e^{-4.5} \text{ cm}^6 \text{ s}^{-1}. \quad (4)$$

Recently, Pohl *et al.* [5] have revised the rates of electron capture into high Rydberg states and of the energy exchange between high Rydberg states and free electrons. In the limit of small energy transfer the revised rates differ drastically from the earlier rates, however, the steady-state recombination rate is only weakly affected. The numerical coefficient in Eq. (4) is reduced to 2.77×10^{-9} . The only experimental data on E-CRR for temperatures below 300 K are those of our Cryo-FALP I studies of Ar⁺ ions [6] at 77–180 K, and our recent study at temperatures 57–200 K [7]. Those agreed well with theory. However, our studies of the recombination of H₃⁺ and D₃⁺ ions with electrons gave no indication of E-CRR, a rather puzzling result since E-CRR should have been faster than binary dissociative recombination at very low temperatures [8–10]. Those observations motivated us

to conduct the present studies of E-CRR in a range of temperatures that is largely unexplored. Ternary recombination in cold and ultracold plasmas is also of interest in the formation of antihydrogen [5,11].

As a consequence of the small electron-to-neutral mass ratio, transfer of electronic energy to heavy particles is slow and N-CRR is less efficient than E-CRR by many orders of magnitude. A good estimate of the recombination rate coefficient can be derived from the energy-diffusion model [3,12–14] that treats the electron energy states as a continuum, as discussed in great detail by Flannery [3]. Flannery derived the following rate coefficient for the case of atomic ions in their parent gas:

$$\alpha_{\text{N-CRR}} = 8\pi \frac{m_e}{M_{\text{atom}}} R_0 R_e^2 \left(\frac{8k_B T_e}{\pi m_e} \right)^{1/2} \sigma_{e,\text{atom}} n_{\text{atom}}. \quad (5)$$

Here, k_B is the Boltzmann constant, m_e and M_{atom} denote the masses of the electron and gas atoms (e.g., helium), $\sigma_{e,\text{atom}}$ is the electron-atom momentum transfer cross section, and $R_e = e^2/k_B T_e (=5.6 \times 10^{-6} \text{ cm at } 300 \text{ K})$. R_0 is a “trapping radius,” the assumption being made that electrons that collide with an atom inside this radius recombines with unit probability, while those colliding outside that radius will escape recombination. If R_0 is taken as $2R_e/3$, the recombination coefficient decreases with temperature as $T_e^{-2.5}$ and agrees with the energy-diffusion model of Pitaevskii [12].

The more elaborate theory of Bates and Khare [4], in which recombination proceeds by stepwise collisional deexcitation of excited Rydberg states of the ion, yields nearly identical recombination coefficients (for He^+ in He) at temperatures below 125 K, but lower values (by approximately a factor of 2) at 300 K. Much larger values ($\sim 10^{26} \text{ cm}^6 \text{ s}^{-1}$ at 300 K) have been calculated by Whitten *et al.* [15], but, as has been pointed out by Wojcik and Tachiya [13,14], the results of Whitten *et al.* depend sensitively on several assumptions, for instance, that the Rydberg populations of states with binding energies less than $4k_B T$ are in thermal equilibrium.

It is not quite clear how the theoretical results should be modified when the ions and neutrals have different masses, the case of interest in our experiments. Bates and Khare [4] suggest that the recombination rate at low temperatures and densities is approximately proportional to the reciprocal of the ion-atom reduced mass, i.e., that the mass M_{atom} in Eq. (5) should be replaced by $2M_{\text{red}}$, where M_{red} is the reduced mass of the ion and gas atoms. If one adopts that rule, the recombination of Ar^+ ions in helium should be slower by a factor of 0.54 than that for He^+ in helium. This scaling agrees with the conclusion of Wojcik and Tachiya [13,14] that the energy-diffusion model for heavy ions yields smaller rates by a factor of 2 than for ions of the same mass as the gas atoms.

In the case of recombination of atomic argon ions in ambient helium of density $[\text{He}]$ Eq. (5) reduces to

$$\alpha_{\text{He-CRR}}(T_e) = 1.2 \times 10^{-27} (T_e/300)^{-2.5} [\text{He}] \text{ cm}^3 \text{ s}^{-1}. \quad (6)$$

The momentum transfer cross section for electron-helium collisions was taken as $5.4 \times 10^{-16} \text{ cm}^2$ [16], independent of energy.

The ternary rate coefficient $K_{\text{He-CRR}}$ is obtained by dividing $\alpha_{\text{He-CRR}}$ by the helium number density:

$$K_{\text{He-CRR}} = \alpha_{\text{He-CRR}}/[\text{He}] \text{ cm}^6 \text{ s}^{-1}. \quad (7)$$

Experimental data on ternary neutral-assisted recombination N-CRR at temperatures $\geq 300 \text{ K}$ have mostly confirmed theoretical predictions [3,4], including the expected $T^{-2.5}$ temperature dependence. Deloche *et al.* [17] found similar coefficients for both atomic and molecular ions. The only experimental measurements at low temperatures (77–150 K) by Cao and Johnsen [18] yielded rate coefficients close to those expected for atomic ions, even though the ions were most likely simple diatomic ions (N_2^+ , O_2^+ , NO^+). On the other hand, our recent low-temperature studies of recombination of H_3^+ and D_3^+ ions, summarized in [9,10,19–23], gave much faster ternary He-assisted recombination with rate coefficients $K_{\text{He-CRR}}(300 \text{ K}) > 10^{-25} \text{ cm}^6 \text{ s}^{-1}$, indicating that ternary recombination of H_3^+ and D_3^+ ions can also proceed by dissociation of long-lived intermediate rotationally excited H_3^* and D_3^* Rydberg molecules.

In this paper, after describing the Cryo-FALP II apparatus, methods of data analysis, and test measurements on O_2^+ ions, we will discuss the determination of the electron temperature in the afterglow plasma by monitoring the decay of the electron density due to ambipolar diffusion. Finally we will present new data on ternary electron- and helium-assisted recombination of Ar^+ at temperatures down to 50 K.

II. EXPERIMENTS

A. Experimental apparatus

The recombination measurements described here were carried out in a decaying fast-flowing plasma, created by passing helium gas through a continuous microwave discharge and converting the primary active particles (mainly helium metastables) to argon ions by adding argon through a gas inlet downstream from the discharge. When the decay of the electron density is monitored by a Langmuir probe, a thin tungsten wire, the technique is referred to as the flowing afterglow Langmuir probe (FALP) method. Afterglow optical emissions from the decaying plasma, for instance, argon emission lines resulting from recombination, are present but were not analyzed in these experiments. While the FALP method has been used extensively to study recombination in decaying plasmas, the extension to very low temperatures required construction of the Cryo-FALP II apparatus to be described below. Also, additional efforts are needed to characterize the thermal properties of the plasma.

We note in passing that it might have been simpler to construct a cryogenic pulsed “stationary afterglow.” However, the FALP arrangement offers better control of plasma parameters and avoids exposing all reagent gases directly to an intense discharge, which can lead to undesired excitation of atomic or molecular species.

In the Cryo-FALP II apparatus (see Fig. 1) the reaction section of the flow tube can be cooled down to 40 K and recombination processes can be studied down to 50 K. Effective binary recombination rate coefficients above $1 \times 10^{-8} \text{ cm}^3 \text{ s}^{-1}$ can be reliably measured. A very broad range of helium pressures and partial pressures of reactant gases

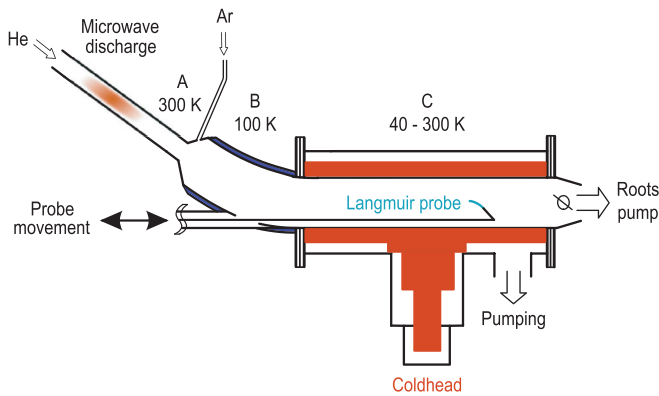


FIG. 1. (Color online) Simplified diagram of the Cryo-FALP II apparatus (not to scale). The three sections A, B, and C have temperatures of 300, 100, and 40–300 K, respectively. The axially movable Langmuir probe measures the decaying electron density along the section C of the flow tube.

can be covered which enables accurate measurements of rate coefficients of binary and ternary recombination processes. Using Cryo-FALP II we recently studied E-CRR of Ar^+ at temperatures 57–200 K and at electron number densities $n_e \sim 10^9\text{--}10^{10}\text{ cm}^{-3}$ [6,7] and we found good agreement with theoretical predictions (see, e.g., [2]). At those electron densities E-CRR of Ar^+ was the dominant loss process during the afterglow. The present work focuses mainly on He-assisted ternary recombination (He-CRR) of Ar^+ ions at very low temperatures and lower electron densities. However, the relative contributions of E-CRR and He-CRR are often of similar magnitude and the data analysis (see Sec. II B) necessarily involves both processes.

A detailed description of the FALP technique can be found in the papers by Mahdavi [24] and by Smith [25] and in the book by Larsson and Orel [1]. The high-pressure version of the FALP and Langmuir probe technique is described in [26]. A short description of Cryo-FALP II is also given in Refs. [7,22,23].

The flow tube of Cryo-FALP II has three sections A, B, and C with different temperatures. The internal diameter of the flow tube is ~ 5 cm and the length is ~ 80 cm. Helium buffer gas flows through the glass section (A, 300 K) where it is partially ionized in a microwave discharge (2.45 GHz, power of 10–30 W). Downstream from the discharge region the plasma contains mainly helium metastables (He^m), He^+ ions, and electrons. At high helium densities ($[\text{He}] \sim (1\text{--}25) \times 10^{17}\text{ cm}^{-3}$) most He^+ ions are converted by ternary association to He_2^+ . The addition of Ar gas ($[\text{Ar}] \sim (0.01\text{--}10) \times 10^{14}\text{ cm}^{-3}$) further downstream from the discharge region at the beginning of the stainless steel section B of the flow tube converts the He_2^+ ions by charge transfer reaction to Ar^+ ions. The metastables He^m are converted to Ar^+ ions by Penning ionization [27,28]. The Ar^+ -dominated plasma is carried along the section B of the flow tube that is cooled to ~ 100 K by liquid nitrogen. In sections A and B at temperatures above 100 K the recombination of He_2^+ and Ar^+ ions is very slow and the plasma decay is caused mainly by ambipolar diffusion to the walls of the flow tube.

After precooling in section B the plasma enters section C, made from stainless steel. This section is connected to the cold head (Sumitomo CH-110) by copper braids, and temperatures of the flow tube wall in the range of 40–300 K can be achieved. To obtain good thermal insulation the whole section C and the cold head are placed in another vacuum chamber. Calculations showed that the buffer gas temperature T_{He} in section C is equal to the wall temperature T_W of the flow tube, and that the ion and electron temperatures (T_{ion} and T_e , respectively) in the afterglow are equal to that of the buffer gas, i.e., $T_{\text{ion}} = T_e = T_{\text{He}} = T_W$. The temperature distribution along the flow tube and the resulting temperature of the He buffer gas was calculated by a computer model (see [7]). The calculated relaxation time constant for the electron temperature is < 0.1 ms, i.e., electron temperature relaxes to the buffer gas temperature immediately after removal of the He metastables (see [26,29]). We verified the electron thermalization by analyzing characteristic times of ambipolar diffusion (see Sec. II D). The results supported the assumption $T_W = T_e$. The ion thermalization is many times faster (with time constant $< 0.1\ \mu\text{s}$) because the masses of ions are similar to those of the neutral atoms. This was also confirmed by spectroscopic measurements in H_3^+ - and D_3^+ -dominated plasma at otherwise very similar conditions (see [8–10]). In the following we will refer to the kinetic temperatures simply as T without subscripts.

The gas handling system and the flow tube itself employ UHV technology and high-purity He and Ar are used. Helium is further purified by passing it through two in-line liquid-nitrogen-cooled molecular sieve traps, resulting in an estimated level of impurities of the order of 10^{-2} ppm. A throttle valve at the downstream end of the flow tube (prior to the Roots pump) adjusts the working pressure and the flow velocity of the buffer gas to the desired values.

The recombination measurements, carried out in section C of the flow tube, rely on the electron density decays as determined by an axially movable Langmuir probe (length 7 mm, diameter 18 μm). To convert positions in the flow tube to afterglow time, the plasma velocity is needed. It is measured by modulating the discharge and observing the time of the Langmuir probe response at certain positions on the flow tube axis. The plasma velocities range from 1 to 20 m s^{-1} , depending on pressure, helium flow rate, and on the flow tube temperature (see Fig. 2 in [7]). The plasma velocity is not constant along the whole flow tube because the wall temperature is different in different sections.

The Langmuir probe characteristics are measured point by point along the flow tube, and the actual values of the electron densities are obtained from the saturated electron current to the probe at positive probe potential [30,31]. The reliability of Langmuir probes used in this mode has been established many times, e.g., by comparing recombination rate coefficients obtained with laser absorption spectroscopy (CRDS technique [32]) to those obtained with Langmuir probes [8–10] or by measuring recombination rate coefficients of well-known recombination processes, e.g., dissociative recombination of O_2^+ ions with electrons (see Sec. II C).

To establish optimal conditions for the measurements of the ternary rate coefficients we developed a kinetic model which includes all significant processes taking place during the

afterglow [33,34]. The temperature evolution along the flow tube was explicitly taken into the account. The calculations show that Ar^+ is the dominant ion at the beginning of the section C, and that the plasma is completely thermalized at that position.

B. Data analysis and conditions of measurement

In a quasineutral afterglow plasma, dominated by a single ion species A^+ in ambient helium gas, the loss rate of electrons and ions is given by

$$\frac{dn_e}{dt} = \frac{d[\text{A}^+]}{dt} = -\alpha_{\text{bin}}[\text{A}^+]n_e - K_{\text{He-CRR}}[\text{He}][\text{A}^+]n_e - K_{\text{E-CRR}}[\text{A}^+]n_e^2 - \frac{n_e}{\tau_{\text{D}}} - \frac{n_e}{\tau_{\text{R}}}, \quad (8)$$

where α_{bin} is the rate coefficient of binary recombination (e.g., DR) and τ_{D} is the time constant of ambipolar diffusion. The additional term containing time constant τ_{R} accounts for a loss due to possible reactions (for details see Sec. IID). By combining the recombination terms into an effective binary rate coefficient α_{eff} and combining the diffusion and reaction loss terms into a linear loss term characterized by a time constant τ_{L} one obtains

$$\frac{dn_e}{dt} = \frac{d[\text{A}^+]}{dt} = -\alpha_{\text{eff}}n_e^2 - \frac{n_e}{\tau_{\text{L}}}, \quad (9)$$

where

$$\alpha_{\text{eff}}(T, [\text{He}], n_e) = \alpha_{\text{bin}} + K_{\text{He-CRR}}[\text{He}] + K_{\text{E-CRR}}n_e \quad (10)$$

and

$$\frac{1}{\tau_{\text{L}}} = \frac{1}{\tau_{\text{D}}} + \frac{1}{\tau_{\text{R}}}. \quad (11)$$

We note that a linear addition of the contributions of He-CRR and E-CRR in Eq. (8) is not necessarily correct, as Bates pointed out [35], since both processes can partly compete for the populations of the same energy levels. Hence, we regard Eq. (10) as a first (linear) approximation that is valid only in the limit when a small fraction of the intermediate levels is stabilized by collision with electrons or neutrals. We will discuss this again in Sec. IV.

The effective binary recombination rate coefficients for ternary processes depend on electron and neutral density. For atomic Ar^+ ions purely binary recombination can be neglected so that the overall effective (measured) binary rate coefficient can be taken as $\alpha_{\text{eff}} = \alpha_{\text{E-CRR}} + \alpha_{\text{He-CRR}} = K_{\text{E-CRR}}n_e + K_{\text{He-CRR}}[\text{He}]$. Different experimental conditions must be chosen to separate the two contributions: To determine $K_{\text{E-CRR}}$, n_e should be large but $[\text{He}]$ should be small. On the other hand, to determine $K_{\text{He-CRR}}$, $[\text{He}]$ should be as high as possible, while n_e should be small. Figure 2 shows decay curves measured at a temperature of 60 K for two different sets of parameters. For the decay curve (i) $[\text{He}]$ was minimized and n_e maximized, so that E-CRR dominates. For the decay curve (ii) $[\text{He}]$ was maximized and n_e minimized, so that He-CRR dominates. The temperature distribution model showed that for both data sets in Fig. 2 the temperature in the recombining plasma is relaxed to 60 ± 2 K. This was confirmed by measuring the plasma velocity along the flow tube [7].

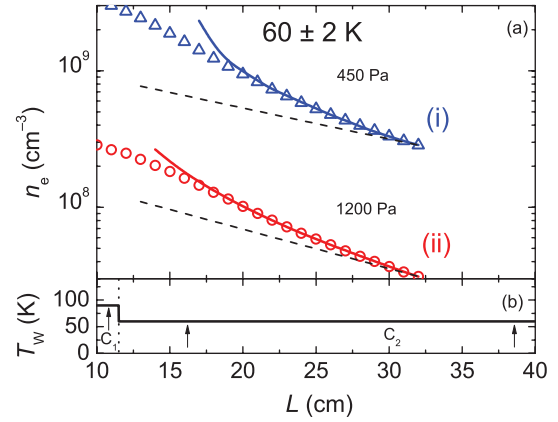


FIG. 2. (Color online) (a) Measured electron density decay in an Ar^+ -dominated afterglow plasma for two helium pressures, 450 (open triangles) and 1200 Pa (open circles). Symbols show measured data, full lines represent fits of these data, and dashed lines indicate diffusion losses. The effective recombination rate coefficients at 1200 and 450 Pa are 1.0×10^{-7} and $3.3 \times 10^{-8} \text{ cm}^3 \text{ s}^{-1}$, respectively. (b) Measured temperatures of the flow tube wall (T_w) at the positions of the temperature sensors (indicated by arrows). Section C is divided into two subsections C_1 and C_2 in the figure indicating different measured temperature.

In a low-temperature Ar^+ -dominated plasma in He buffer gas with a small admixture of Ar gas the reactive loss term in Eq. (8) accounts for the relatively slow ternary association of Ar^+ with atomic argon, i.e., the reaction $\text{Ar}^+ + \text{Ar} + \text{He} \rightarrow \text{Ar}_2^+ + \text{He}$ [36,37]. Since the Ar_2^+ product ions recombine rapidly with electrons [1,38], the rate determining step at low argon concentrations is ternary association. The association reaction essentially constitutes an additional electron loss process that can be represented by a time constant τ_{R} as written in Eq. (8). In this particular case, τ_{R} depends on the ternary association rate coefficient k_a and on Ar and He densities, $\tau_{\text{R}} = 1/(k_a[\text{Ar}][\text{He}])$. The temperature dependence of τ_{R} is given by the temperature dependence of k_a (details will be discussed below). At higher Ar and He densities and lower temperatures the formation of Ar_2^+ is faster and the recombination of Ar_2^+ is the rate determining process. The effect of Ar_2^+ ions on observed effective binary recombination (on α_{eff}) was determined by measuring the effective binary recombination rate coefficient as a function of argon density. Examples of such dependencies are plotted in Fig. 3 for 62 K and He pressure 500 and 1200 Pa. The measured effective binary recombination rate coefficients are constant below $[\text{Ar}] = 1 \times 10^{13} \text{ cm}^{-3}$ but increase above this value, in accordance with our kinetics model that includes the formation of Ar_2^+ . To minimize the influence of Ar_2^+ formation on the measured α_{eff} the typical number density of Ar used in the present experiment was limited to $[\text{Ar}] \sim 3 \times 10^{12} \text{ cm}^{-3}$, which is still sufficient to form an Ar^+ -dominated plasma before entering zone C of the flow tube. The final data were taken under conditions where the effect of Ar_2^+ on measured α_{eff} was negligible.

Figure 4 shows data for α_{eff} as a function of helium density $[\text{He}]$ for three different temperatures. The slopes of the linear dependencies yield $K_{\text{He-CRR}}(T)$ [see Eq. (10)], and the

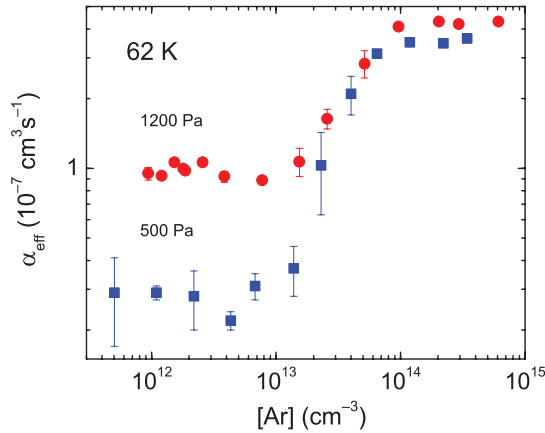


FIG. 3. (Color online) The dependence of measured effective binary recombination rate coefficient α_{eff} on Ar number density at 62 K and indicated pressures of He (full circles for the pressure of 1200 Pa and full squares for 500 Pa). Displayed errors are statistical.

intercept at $[\text{He}] = 0$ gives the sum $\alpha_{\text{bin}} + K_{\text{E-CRR}}n_e$. Since previous work [6] has shown that $\alpha_{\text{bin}} = 0$ (see Fig. 4 and discussion in [6]), we can write $\alpha_{\text{eff}} = K_{\text{E-CRR}}n_e$ at $[\text{He}] = 0$. This is in agreement with the expectation of slow radiative recombination of atomic Ar⁺.

C. Test measurements on recombination of O₂⁺ ions

Some of the present studies were conducted under conditions (helium densities, temperatures, flow velocities, etc.) that have not been used much in earlier work. Also, the data analysis relies on modeling of the temperature distribution and flow velocities. As a precaution, we performed a series of test measurements of the well-known binary recombination rate coefficient of dissociative recombination $\alpha_{\text{bin DR}}$ of O₂⁺ ions, which is much simpler to measure than ternary recombination. Our test results (see Fig. 5) agreed very well with previous data [39–45]. The rate coefficients were measured for three temperatures and over a broad range of He pressures and O₂

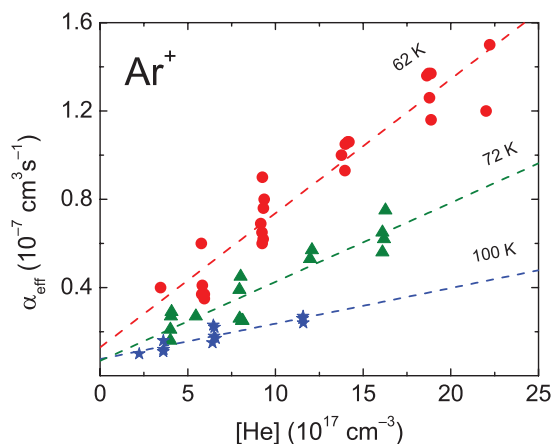


FIG. 4. (Color online) Measured dependence of the effective binary recombination rate coefficient $\alpha_{\text{eff}}(T, [\text{He}], n_e)$ of recombination of Ar⁺ ions with electrons on He number density at 62 (full circles), 72 (full triangles), and 100 K (full stars). The lines represent the linear fits of the data.

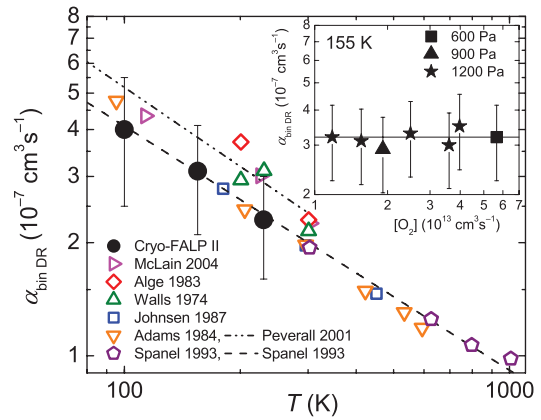


FIG. 5. (Color online) Temperature dependence of the measured recombination rate coefficient $\alpha_{\text{bin DR}}$ of the binary dissociative recombination of O₂⁺ ions with electrons. The present Cryo-FALP II data (large circles) are compared to previous results [39–45]. The dashed line represents a fit given by [43,45]. Inset: Data obtained at different O₂ number densities, measured at 155 K and at several helium pressures. The full line is the mean of the measured values.

number densities. The results of these tests clearly confirm the validity of the methods used in present experiments.

D. Verification of the electron temperature by measuring ambipolar diffusion losses

The strong temperature dependencies of $K_{\text{E-CRR}}$ and $K_{\text{He-CRR}}$ make the electron temperature a crucial parameter that is not directly measured, but within some limitations a precise measurement of ambipolar diffusion losses in the late afterglow can serve as a “diffusion thermometer.” Ambipolar diffusion losses also enter directly [see Eq. (8)] in the determinations of α_{eff} and τ_L . The measured time constant τ_L has two components: one representing ambipolar diffusion (τ_D) and the second representing reactive losses (τ_R) (see Sec. II B). The value of τ_D depends on temperature, helium density, the characteristic diffusion length Λ of the flow tube, and the zero-field reduced mobility K_0 of Ar⁺ ions in He (for details see [6]). For a long flow tube of radius R the characteristic diffusion length is $\Lambda = R/2.405$. Using the relations given by Mason and McDaniel [46] one can show that if electrons, ions, and gas atoms have the same temperature $T_e = T_{\text{ion}} = T_{\text{He}} = T$ then

$$\frac{1}{\tau_D} = 4.63 \times 10^{15} \frac{K_0(T)}{\Lambda^2} \frac{T}{[\text{He}]} \text{ s}^{-1}. \quad (12)$$

The units are $[\text{He}]$ in cm^{-3} , T in K, Λ in cm, and K_0 in $\text{cm}^2 \text{V}^{-1} \text{s}^{-1}$. Since the zero-field reduced mobility of Ar⁺ in He is nearly constant for temperatures below 300 K, a graph of $[\text{He}]/\tau_D$ versus T should yield nearly a straight line, with small deviations when the dependence of K_0 on temperature is included [6]. Measured values of $[\text{He}]/\tau_D$ should be proportional to the temperature thus providing an independent measure of the otherwise difficult to determine electron temperature. Figure 6 shows the theoretical temperature dependence of $[\text{He}]/\tau_D$, where τ_D is calculated using zero-field reduced mobilities of $K_0 = 18.9 \text{ cm}^2 \text{V}^{-1} \text{s}^{-1}$

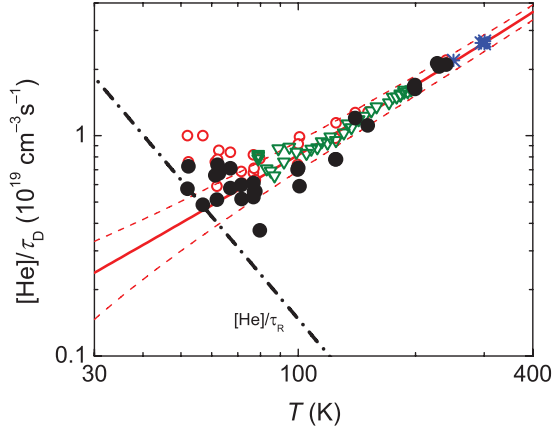


FIG. 6. (Color online) Temperature dependencies of the inverted time constants of diffusion losses $[\text{He}]/\tau_D$ and $[\text{He}]/\tau_R$. Solid line represents the theoretical temperature dependence of $[\text{He}]/\tau_D$ on T , calculated from the zero-field reduced mobility of Ar^+ in He for a thermalized afterglow plasma [47–49]. Dashed lines are calculated for 10 K higher or lower temperatures. The dash-dotted line labeled $[\text{He}]/\tau_R$ shows values corresponding to reactive losses due to Ar_2^+ formation at densities $[\text{Ar}] = 3 \times 10^{12} \text{ cm}^{-3}$ and $[\text{He}] = 7 \times 10^{17} \text{ cm}^{-3}$ (see text). In the calculation we used the formula $[\text{He}]/\tau_R = k_a[\text{Ar}][\text{He}]^2 = 9.5 \times 10^{-32}(300/T)^{2.19}[\text{Ar}][\text{He}]^2$. Data measured with Cryo-FALP I (open triangles) are adapted from [6] as well as data indicated by asterisk symbols measured at 250 and 300 K. Open circles indicate measured $[\text{He}]/\tau_L$ and closed circles indicate corresponding experimental $[\text{He}]/\tau_D$ calculated for particular $[\text{He}]$ and $[\text{Ar}]$ using relation $[\text{He}]/\tau_D = ([\text{He}]/\tau_L - [\text{He}]/\tau_R)$.

at 77 K and $20.5 \text{ cm}^2 \text{ V}^{-1} \text{ s}^{-1}$ at 300 K [47–49] and a linear interpolation at intermediate temperatures.

To show the sensitivity to small errors in temperature, we also include in Fig. 6 calculated values of $[\text{He}]/\tau_D$ for two temperatures that are 10 K higher or lower. As may be seen in Fig. 6, the accuracy of the “diffusion thermometer” deteriorates rapidly below ~ 70 K because the experimental values $[\text{He}]/\tau_L$ include a contribution $[\text{He}]/\tau_R$ due to reactive losses in the late afterglow [see Eq. (11)]. We tried to correct the raw “experimental” values $[\text{He}]/\tau_L$ (open circles) by subtracting an estimated reactive loss term $[\text{He}]/\tau_R$ to obtain the pure diffusion loss rate term $[\text{He}]/\tau_D$ (solid circles). The reactive loss term $[\text{He}]/\tau_R$ was ascribed to conversion of Ar^+ ions to fast recombining Ar_2^+ ions, using the experimental association ternary rate coefficient k_a of Bohme *et al.* [36] and extrapolating it assuming a temperature dependence of the form $k_a \sim T^{-n}$. From the measured values $k_a(82 \text{ K}) = 1.6 \times 10^{-30} \text{ cm}^6 \text{ s}^{-1}$ and $k_a(290 \text{ K}) = 1 \times 10^{-31} \text{ cm}^6 \text{ s}^{-1}$ we calculated $k_a(T) = 9.5 \times 10^{-32}(300/T)^{2.19} \text{ cm}^6 \text{ s}^{-1}$. The size of this correction is included in Fig. 6 (dash-dotted line), the values were calculated for $[\text{Ar}] = 3 \times 10^{12} \text{ cm}^{-3}$ and $[\text{He}] = 7 \times 10^{17} \text{ cm}^{-3}$. Since the reactive losses increase rapidly at lower temperatures, while the diffusion losses become smaller, the accuracy of the diffusion thermometer becomes poor below 70 K and corrections for reactive losses do not improve it by much. For comparison, in Fig. 6 we also show data from our previous FALP and Cryo-FALP I experiments measured at 250 and 300 K [6]. In that case the whole flow tube was cooled

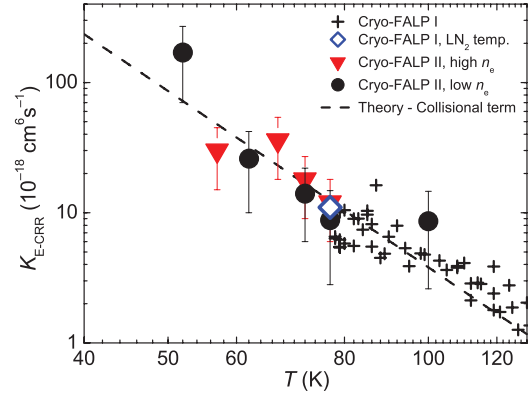


FIG. 7. (Color online) Temperature dependence of the measured ternary recombination rate coefficient $K_{\text{E-CRR}}$ of ternary electron-assisted collisional radiative recombination of Ar^+ ions with electrons. The full circles are the present data measured at lower n_e (10^8 – 10^9 cm^{-3}). The data represented by full triangles are measured in our previous studies at higher n_e (10^9 – 10^{10} cm^{-3}) [7]. Data depicted by the open rhomboid at 77 K is compiled from several measurements on Cryo-FALP I. The crosses indicate previous data measured on Cryo-FALP I at temperatures above 77 K (adopted from [6]). The dashed line indicates $K_{\text{E-CRR}}$ calculated by using Stevefelt’s formula (4), $K_{\text{E-CRR}} \sim T^{-4.5}$.

by liquid nitrogen to the same temperature and there was no doubt about temperature equilibration.

The measurements of the diffusion losses corroborate our calculations of the temperature distribution in the flow tube only for temperatures above ~ 70 K. Nevertheless, this does not necessarily imply a difference between T_W , T_e , and T_{ion} below 70 K. The agreement between experimental data on the rate coefficients for E-CRR and N-CRR and theory (see Secs. III A and III B) also supports the assumption of complete thermalization.

III. RESULTS AND DISCUSSION

A. Temperature dependence of $K_{\text{E-CRR}}$

Figure 7 shows the temperature dependence of $K_{\text{E-CRR}}$ obtained in the present experiment and compares it to previous data measured with the Cryo-FALP I apparatus in the range 77–200 K [6], to previous data measured with the Cryo-FALP II apparatus in the range 57–77 K [7], and to theoretical dependence. The agreement between the experimental data sets is good, even though the electron density n_e in the earlier experiments was much higher (10^9 – 10^{10} cm^{-3}) than in the present experiment (10^8 – 10^9 cm^{-3}) and experimental conditions were different. In the present study $K_{\text{E-CRR}}$ was obtained by extrapolation of α_{eff} to zero helium density, as shown in Fig. 4. The present and previous data agree well with the collisional term of the Stevefelt formula [see Eq. (4)], leaving no doubt that the $K_{\text{E-CRR}} \sim T^{-4.5}$ dependence remains valid for Ar^+ ions down to 50 K.

The agreement of the experimental values of $K_{\text{E-CRR}}$ with theory can be taken also as another confirmation that the electron temperature and the measured temperature of the wall of the flow tube are nearly equal. Note also the good agreement

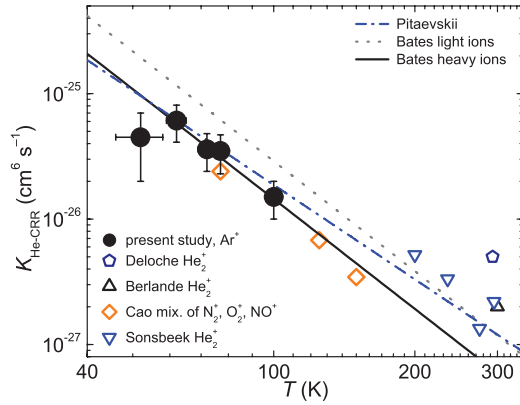


FIG. 8. (Color online) Temperature dependence of the measured ternary recombination rate coefficient $K_{\text{He-CRR}}$ of He-assisted recombination of Ar^+ ions with electrons (full circles). Included are also data from previous experiments [17,18,50,51]. The dotted line follows calculation by Bates [4]; the solid line is scaled for this study using the dependence of the ternary recombination rate coefficient on reduced mass as suggested by Bates [4]. The dash-dotted line indicates theory by Pitaevskii [12].

of data obtained at 77 K at very different experimental conditions (it will be again discussed in Sec. IV).

B. Temperature dependence of $K_{\text{He-CRR}}$

The measured temperature dependence of $K_{\text{He-CRR}}$ of ternary recombination of Ar^+ ions with electrons in helium buffer is depicted in Fig. 8, together with examples of data measured in previous experiments with different ions at higher temperatures, predominantly at 300 K [17,18,50,51]. Our data for Ar^+ ions agree well with the calculations of Bates [4] after scaling by the reduced mass factor. The temperature dependence (approximately $T^{-2.9}$) is somewhat stronger than the $T^{-2.5}$ dependence of Pitaevskii [12], presumably because the energy diffusion model of Pitaevskii ignores the discreteness of the electron energy states.

IV. DISCUSSION AND CONCLUSIONS

We have reported on He-assisted ternary recombination of atomic ions below 300 K and rate coefficients of both ternary recombination processes were clearly separated and measured in a well-characterized afterglow plasma at temperatures below 100 K. Careful attention was paid to verifying electron temperatures by measuring the characteristic time constant of ambipolar diffusion τ_D at fixed pressure and flow tube temperature. It was concluded that the plasma particles have nearly the same temperature as the wall of the flow tube, i.e., that $T = T_e = T_{\text{ion}} = T_{\text{He}} = T_w$. However, at the lowest temperatures the verification was complicated by reactive losses.

The measured magnitudes and the temperature dependencies of both ternary recombination rate coefficients $K_{\text{He-CRR}}$ and $K_{\text{E-CRR}}$ of Ar^+ ions agree with theoretical predictions [3,4,12] ($K_{\text{He-CRR}} \sim T^{-2.9}$) in the temperature range from 50 to 100 K and $K_{\text{E-CRR}} \sim T^{-4.5}$ in the range from 50 to 180 K [2] over a broad range of electron and He densities. This observed agreement is not at all obvious. Recent experimental studies

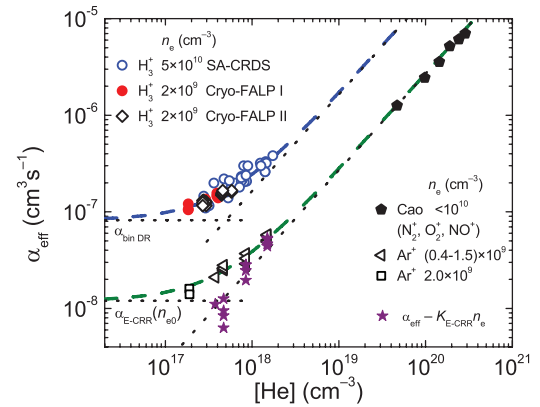


FIG. 9. (Color online) Dependence of the effective recombination rate coefficient α_{eff} on helium number density at 77 K. Present values (open triangles) are plotted together with values obtained by Cao *et al.* [18] (full pentagons) for a mixture of ions, by Varju *et al.* [8], by Dohnal *et al.* [9], and by Glosik *et al.* [19] for H_3^+ and by Kotrik *et al.* [6] for Ar^+ (open squares). The full stars are the present data corrected by subtracting the E-CRR component of α_{eff} . The dashed lines are linear fits to the data (values by Cao were not included in the fit). The dotted lines show the binary and the ternary components of the fitted α_{eff} .

of both ternary recombination processes for H_3^+ and D_3^+ ions at temperatures below 300 K gave drastically different results [9,10,22,23], as is demonstrated in Fig. 9 that summarizes the effective binary recombination rate coefficients α_{eff} measured at 77 K in helium afterglow plasmas dominated by different ions. The data obtained by Cao *et al.* [18] for a mixture of molecular ions at very high helium densities are in agreement with the aforementioned results, giving comparable ternary rate coefficients. At their experimental conditions the ternary E-CRR and the binary dissociative recombination can be neglected and He-CRR is by far the dominant recombination process.

The figure also shows data obtained for atomic Ar^+ ions in the present experiments for electron densities $n_e = (0.4-1.5) \times 10^9 \text{ cm}^{-3}$ and He densities $[\text{He}] = (5-20) \times 10^{17} \text{ cm}^{-3}$. Some earlier data measured at high n_e and low $[\text{He}]$ [6] are also plotted. For atomic Ar^+ ions binary recombination is negligible and both ternary processes He-CRR and E-CRR have comparable rates. The overall rate coefficients can be expressed as $\alpha_{\text{eff}} = \alpha_{\text{He-CRR}} + \alpha_{\text{E-CRR}} = K_{\text{He-CRR}}[\text{He}] + K_{\text{E-CRR}}n_e$. At high $[\text{He}]$ and low n_e (triangles) $\alpha_{\text{He-CRR}}$ dominates, while at low $[\text{He}]$ and high n_e (open squares) $\alpha_{\text{E-CRR}}$ dominates. The fit of the Ar^+ data gives values $K_{\text{He-CRR}}$ and $K_{\text{E-CRR}}$ in agreement with those obtained by precise analyses (see Figs. 7 and 8). At low $[\text{He}]$ the data (triangles) level off due to the contribution from $\alpha_{\text{E-CRR}}$, indicated by a horizontal dashed line (calculated for $n_e = 1 \times 10^9 \text{ cm}^{-3}$). To show the contribution from $K_{\text{He-CRR}}$ alone we plotted the values $\alpha_{\text{He-CRR}}$ (indicated by full stars) obtained by subtracting $\alpha_{\text{E-CRR}}$ from the measured α_{eff} . We used expression (4) for $\alpha_{\text{E-CRR}}$ and the actual n_e . Note that the corrected data $\alpha_{\text{He-CRR}}$ (stars) and data obtained by Cao *et al.* [18] (pentagons) then follow a straight line $\alpha_{\text{He-CRR}} = K_{\text{He-CRR}}[\text{He}]$ over three orders of magnitude of $[\text{He}]$.

The sample of data (upper set of data) obtained in H_3^+ -dominated He buffered afterglow plasma are significantly larger. These data were obtained at electron densities from 2×10^9 up to $5 \times 10^{10} \text{ cm}^{-3}$ in Cryo-FALP I, Cryo-FALP II, and SA-CRDS experiments [8,9,19]. We did not observe any significant dependence of α_{eff} on n_e that would indicate electron-assisted recombination (see discussion in [9,10,22,23]), so we can expect $\alpha_{\text{eff}} = \alpha_{\text{bin DR}} + \alpha_{\text{He}} = \alpha_{\text{bin DR}} + K_{\text{He}}[\text{He}]$, where $\alpha_{\text{bin DR}}$ is the binary rate coefficient of dissociative recombination of H_3^+ and K_{He} ternary rate coefficients of helium-assisted recombination of H_3^+ . The seeming absence of electron-assisted recombination is surprising (see discussion in [9,10]).

Figure 9 strongly suggests that the mechanisms of the ternary helium-assisted processes for Ar^+ and H_3^+ (D_3^+) must be very different. The rate coefficients at low $[\text{He}]$ are also different. They reflect dissociative recombination in the case of H_3^+ ($\alpha_{\text{bin DR}}$) and ternary electron-assisted recombination ($\alpha_{\text{E-CRR}}$) in the case of Ar^+ .

The present study was, in part, undertaken to learn whether our earlier measurements of the ternary recombination rate coefficients of H_3^+ and D_3^+ [9,10,19,20,23,52] were subject to possible systematic errors. This does not seem to be the case.

The good agreement of the helium-assisted ternary channel for Ar^+ with theory [4] strongly corroborates the methods used in the earlier work. We conclude that the very fast helium-assisted ternary recombination of H_3^+ and D_3^+ ions must be due to an entirely different mechanism than that proposed for atomic ions by Bates and Khare [4] and Flannery [3]; for discussion and suggestion of the mechanism see [9,19–21].

The presented experimental results on the ternary electron- and neutral-assisted recombination of atomic Ar^+ ions at temperatures down to 50 K show a remarkable difference in comparison with ternary recombination of H_3^+ and D_3^+ ions. To find differences between ternary recombination of atomic and molecular ions and a possible dependence on type of buffer gas we plan to study ternary recombination of other ions and temperature dependence of recombination processes at temperatures down to 30 K.

ACKNOWLEDGMENTS

This work was partly supported by GACR 205/09/1183, GACR P209/12/0233, SV 267 302, GAUK 353811, GAUK 388811, and GAUK 659112.

-
- [1] M. Larsson and A. Orel, *Dissociative Recombination of Molecular Ions* (Cambridge University Press, Cambridge, 2008).
- [2] J. Stevefelt, J. Boulmer, and J. Delpech, *Phys. Rev. A* **12**, 1246 (1975).
- [3] M. R. Flannery, *J. Chem. Phys.* **95**, 8205 (1991).
- [4] D. Bates and S. Khare, *Proc. Phys. Soc. London* **85**, 231 (1965).
- [5] T. Pohl, D. Vrinceanu, and H. R. Sadeghpour, *Phys. Rev. Lett.* **100**, 223201 (2008).
- [6] T. Kotrik, P. Dohnal, S. Roucka, P. Jusko, R. Plasil, J. Glosik, and R. Johnsen, *Phys. Rev. A* **83**, 032720 (2011).
- [7] T. Kotrik, P. Dohnal, P. Rubovic, R. Plasil, S. Roucka, S. Opanasiuk, and J. Glosik, *Eur. Phys. J. Appl. Phys.* **56**, 24011 (2011).
- [8] J. Varju, M. Hejduk, P. Dohnal, M. Jilek, T. Kotrik, R. Plasil, D. Gerlich, and J. Glosik, *Phys. Rev. Lett.* **106**, 203201 (2011).
- [9] P. Dohnal, M. Hejduk, J. Varju, P. Rubovic, S. Roucka, T. Kotrik, R. Plasil, J. Glosik, and R. Johnsen, *J. Chem. Phys.* **136**, 244304 (2012).
- [10] P. Dohnal, M. Hejduk, P. Rubovic, J. Varju, S. Roucka, R. Plasil, and J. Glosik, *J. Chem. Phys.* **137**, 194320 (2012).
- [11] T. C. Killian, S. Kulin, S. D. Bergeson, L. A. Orozco, C. Orzel, and S. L. Rolston, *Phys. Rev. Lett.* **83**, 4776 (1999).
- [12] L. P. Pitaevskii, *Sov. Phys. JETP* **1**, 919 (1962).
- [13] M. Wojcik and M. Tachiya, *J. Chem. Phys.* **110**, 10016 (1999).
- [14] M. Wojcik and M. Tachiya, *J. Chem. Phys.* **112**, 3845 (2000).
- [15] B. L. Whitten, L. W. Downes, and W. E. Wells, *J. Appl. Phys.* **52**, 1255 (1981).
- [16] R. W. Crompton, M. T. Elford, and R. L. Jory, *Aust. J. Phys.* **20**, 396 (1967).
- [17] R. Deloche, P. Monchicourt, M. Cheret, and F. Lambert, *Phys. Rev. A* **13**, 1140 (1976).
- [18] Y. S. Cao and R. Johnsen, *J. Chem. Phys.* **94**, 5443 (1991).
- [19] J. Glosik, R. Plasil, I. Korolov, T. Kotrik, O. Novotny, P. Hlavenka, P. Dohnal, J. Varju, V. Kokoouline, and C. H. Greene, *Phys. Rev. A* **79**, 052707 (2009).
- [20] J. Glosik, I. Korolov, R. Plasil, T. Kotrik, P. Dohnal, O. Novotny, J. Varju, S. Roucka, C. H. Greene, and V. Kokoouline, *Phys. Rev. A* **80**, 042706 (2009).
- [21] J. Glosik, R. Plasil, T. Kotrik, P. Dohnal, J. Varju, M. Hejduk, I. Korolov, S. Roucka, and V. Kokoouline, *Mol. Phys.* **108**, 2253 (2010).
- [22] P. Rubovič, P. Dohnal, M. Hejduk, R. Plašil, and J. Glosík, *J. Phys. Chem. A* (2013), doi: [10.1021/jp3123192](https://doi.org/10.1021/jp3123192).
- [23] R. Johnsen, P. Rubovič, P. Dohnal, M. Hejduk, R. Plasil, and J. Glosík, *J. Phys. Chem. A* (2013), doi: [10.1021/jp311978n](https://doi.org/10.1021/jp311978n).
- [24] M. R. Mahdavi, J. B. Hasted, and M. M. Nakshbandi, *J. Phys. B* **4**, 1726 (1971).
- [25] D. Smith, N. G. Adams, A. G. Dean, and M. J. Church, *J. Phys. D: Appl. Phys.* **8**, 141 (1975).
- [26] J. Glosik, G. Bano, R. Plasil, A. Luca, and P. Zakouril, *Int. J. Mass Spectrom.* **189**, 103 (1999).
- [27] A. J. Yencha, in *Electron Spectroscopy: Theory, Techniques and Applications*, edited by C. R. Bundle and A. D. Baker (Academic Press, London, 1984), Vol. 5.
- [28] R. Plasil, I. Korolov, T. Kotrik, P. Dohnal, G. Bano, Z. Donko, and J. Glosik, *Eur. Phys. J. D* **54**, 391 (2009).
- [29] I. Korolov, T. Kotrik, R. Plasil, J. Varju, M. Hejduk, and J. Glosik, *Contrib. Plasma Phys.* **48**, 521 (2008).
- [30] J. D. Swift and M. J. R. Schwar, *Electrical Probes for Plasma Diagnostics* (Elsevier, New York, 1969).
- [31] O. Chudacek, P. Kudrna, J. Glosik, M. Sicha, and M. Tichy, *Contrib. Plasma Phys.* **35**, 503 (1995).
- [32] P. Macko, G. Bano, P. Hlavenka, R. Plasil, V. Poterya, A. Pysanenko, O. Votava, R. Johnsen, and J. Glosik, *Int. J. Mass Spectrom.* **233**, 299 (2004).

- [33] O. Novotny, R. Plasil, A. Pysanenko, I. Korolov, and J. Glosik, *J. Phys. B* **39**, 2561 (2006).
- [34] R. Plasil, J. Glosik, V. Poterya, P. Kudrna, J. Ruzs, M. Tichy, and A. Pysanenko, *Int. J. Mass Spectrom.* **218**, 105 (2002).
- [35] D. R. Bates, *Proc. R. Soc. London, Ser. A* **337**, 15 (1974).
- [36] D. K. Bohme, D. B. Dunkin, F. C. Fehsendeld, and E. E. Ferguson, *J. Chem. Phys.* **51**, 863 (1969).
- [37] B. M. Smirnov, *Sov. Phys. Usp.* **20**, 119 (1977).
- [38] J. Royal and A. E. Orel, *Phys. Rev. A* **73**, 042706 (2006).
- [39] J. L. McLain, V. Poterya, C. D. Molek, L. M. Babcock, and N. G. Adams, *J. Phys. Chem. A* **108**, 6704 (2004).
- [40] E. Alge, N. G. Adams, and D. Smith, *J. Phys. B* **16**, 1433 (1983).
- [41] F. L. Walls and G. H. Dunn, *J. Geophys. Res.* **79**, 1911 (1974).
- [42] R. Johnsen, *Int. J. Mass Spectrom. Ion Processes* **81**, 67 (1987).
- [43] N. G. Adams, D. Smith, and E. Alge, *J. Chem. Phys.* **81**, 1778 (1984).
- [44] R. Peverall, S. Rosen, J. R. Peterson, M. Larsson, A. Al-Khalili, L. Viktor, J. Semaniak, R. Bobbenkamp, A. N. Maurellis, and W. J. van der Zande, *J. Chem. Phys.* **114**, 6679 (2001).
- [45] P. Spanel, L. Dittrichova, and D. Smith, *Int. J. Mass Spectrom.* **129**, 183 (1993).
- [46] E. Mason and E. McDaniel, *Transport Properties of Ions in Gases* (Wiley, New York, 1988).
- [47] L. Viehland, A. Viggiano, and E. Mason, *J. Chem. Phys.* **95**, 7286 (1991).
- [48] W. Lindinger and D. Albritton, *J. Chem. Phys.* **62**, 3517 (1975).
- [49] R. Johnsen and M. A. Biondi, *Phys. Rev. A* **20**, 221 (1979).
- [50] J. Berlande, M. Cheret, R. Deloche, A. Gonfalone, and C. Manus, *Phys. Rev. A* **1**, 887 (1970).
- [51] R. J. van Sonsbeek, R. Cooper, and R. N. Bhave, *J. Chem. Phys.* **97**, 1800 (1992).
- [52] T. Kotrik, P. Dohnal, I. Korolov, R. Plasil, S. Roucka, J. Glosik, C. H. Greene, and V. Kokoouline, *J. Chem. Phys.* **133**, 034305 (2010).

H₂-assisted ternary recombination of H₃⁺ with electrons at 300 K

Dohnal P., Rubovič P., Kálosi A., Hejduk M., Plašil R., Johnsen R., Glosík J.

Phys. Rev. A **90**, 042708, 2014.

H₂-assisted ternary recombination of H₃⁺ with electrons at 300 KPetr Dohnal,¹ Peter Rubovič,¹ Ábel Kálosi,¹ Michal Hejduk,¹ Radek Plašil,¹ Rainer Johnsen,² and Juraj Glosík¹¹*Department of Surface and Plasma Science, Faculty of Mathematics and Physics, Charles University in Prague, Prague 18000, Czech Republic*²*Department of Physics and Astronomy, University of Pittsburgh, Pittsburgh, Pennsylvania 15260, USA*

(Received 12 March 2014; revised manuscript received 27 August 2014; published 16 October 2014)

Stationary afterglow measurements in conjunction with near-infrared absorption spectroscopy show that the recombination of the H₃⁺ ion with electrons in ionized gas mixtures of He, Ar, and H₂ at 300 K is strongly enhanced by neutral helium and by molecular hydrogen. The H₂-assisted ternary recombination coefficient $K_{H_2} = (8.7 \pm 1.5) \times 10^{-23} \text{ cm}^6 \text{ s}^{-1}$ substantially exceeds the value measured for H₃⁺ in ambient helium ($K_{He} \sim 10^{-25} \text{ cm}^6 \text{ s}^{-1}$) or predicted by the generally accepted classical theory of Bates and Khare ($\sim 10^{-27} \text{ cm}^6 \text{ s}^{-1}$) for atomic ions. Because of the extremely large value of K_{H_2} in a hydrogen plasma the ternary recombination dominates over binary recombination already at pressures above 3 Pa. This can have consequences in plasma physics, astrophysics, recombination pumped lasers, plasma spectroscopy, plasmatic technologies, etc. The ternary processes provide a plausible explanation for the discrepancies between many earlier experimental results on H₃⁺ recombination. The observation that the ternary process saturates at high He and H₂ densities suggests that recombination proceeds by a two-step process: formation of a long-lived complex [with a rate coefficient $\alpha_F = (1.5 \pm 0.1) \times 10^{-7} \text{ cm}^3 \text{ s}^{-1}$] followed by collisional stabilization.

DOI: [10.1103/PhysRevA.90.042708](https://doi.org/10.1103/PhysRevA.90.042708)

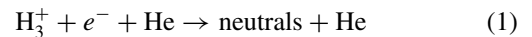
PACS number(s): 34.80.Lx, 42.62.Fi, 52.20.Hv

I. INTRODUCTION

The triatomic hydrogen ion occupies a special position in molecular physics, in physical chemistry, and in astrophysics. This simple ion, whose very existence was once doubted, is now recognized as the most abundantly produced molecular ion in the universe. It not only plays a pivotal role in the molecular evolution of some interstellar clouds but also provides a tool for measuring their temperatures [1]. The recombination of the H₃⁺ ion with electrons is of interest for modeling hydrogen-containing plasmas and, in part for this reason, has been studied experimentally and theoretically for over 60 years [2]. Many extensive laboratory studies have been performed to clarify the formation and destruction processes of H₃⁺, in particular the recombination of H₃⁺ with electrons at low temperatures [2,3]. The word “enigma” appeared frequently in publications [4] because the measured recombination rate coefficients differed by several orders of magnitude (see extended discussion in [2,3]). The principal current motivation for H₃⁺ recombination studies comes from the physics and chemistry of diffuse astrophysical clouds and planetary ionospheres (see discussion in [5–7]). H₃⁺ was observed spectroscopically in the laboratory in 1980 [8], but it took many years until it was detected in emission spectra from Jupiter [9], Saturn, and Uranus (see discussion in [10]), and in interstellar plasmas [11,12].

In 2001 a new theory of H₃⁺ recombination was developed [13,14] and it became clear afterwards that para-H₃⁺ and ortho-H₃⁺ behave differently [15]. Storage rings were used in corresponding state selected studies [2]. For temperatures above 300 K the agreement between theory and the most recent storage ring experiments [16–19] is excellent but data at lower temperatures are still not quite conclusive because internal states of the recombining ions are not necessarily in thermal equilibrium [20]. It is now generally accepted that recombination of H₃⁺ occurs with a binary rate coefficient of $\alpha_{\text{bin}}(300 \text{ K}) \sim 6 \times 10^{-8} \text{ cm}^3 \text{ s}^{-1}$ [21]. For applications to low-density astrophysical clouds it is the binary coefficient that matters.

The fact remains that many well-executed plasma afterglow experiments gave recombination rates that were larger by factors of 3 to 4 than the theoretical and storage ring data. A better understanding was achieved after the discovery of fast helium-assisted ternary recombination of H₃⁺ in afterglow plasma in a He-Ar-H₂ gas mixture [22,23]. It was then found that the ternary He-assisted recombination process



is indeed very effective, exceeding by over two orders of magnitude (at 300 K) the value predicted by the classical treatment of Bates and Khare [24]. The much faster ternary recombination of H₃⁺ has been attributed to formation of long-lived rotationally excited neutral H₃[#] Rydberg molecules and subsequent collisions with helium atoms [22,23] that eventually lead to dissociation into neutral products. We note that the formation of H₃[#] Rydberg states has also been invoked as a mechanism in a recombination-pumped laser in H₃⁺ containing plasma [25].

The recombination of the H₃⁺ ion has been studied in our laboratory for almost 15 years. During those years, several different stationary afterglow (Advanced Integrated Stationary Afterglow (AISA) [26], Stationary Afterglow with Cavity Ring Down Spectrometer (SA-CRDS) [27,28]) and flowing afterglow (Flowing Afterglow with Langmuir Probe (FALP) [29], Cryo-FALP [21,23,30]) experiments were employed to study the H₃⁺ recombination process in low-temperature afterglow plasma in a He-Ar-H₂ gas mixture. The main differences are in the range of covered number densities of He and H₂, in the electron and ion densities, in the covered temperature range, in the time scale of monitored plasma decay, and in applied diagnostics (see, e.g., [23]). A broad range of the measured plasma parameters is necessary to study the dependence of the measured effective recombination rate coefficient α_{eff} on plasma parameters and eventually to determine rate coefficients for binary and ternary recombination of H₃⁺ ions and their temperature dependences. This procedure is necessary

especially in the case of the H_3^+ ion, where long-lived highly excited neutral H_3 can be formed in collision of H_3^+ with electrons [22,23]. Very extensive and systematic studies are required because the afterglow plasmas are influenced also by formation and relaxation processes and also by ambipolar diffusion and these processes depend on the same parameters as the effective recombination rate coefficient.

We should mention here that in early AISA experiments (stationary afterglow with Langmuir probe and mass spectrometer [26]) we observed a rapid fall off of value of measured effective recombination rate coefficient α_{eff} at $[H_2] \ll 10^{12} \text{ cm}^{-3}$, where newly formed H_3^+ ions undergo on average less than one collision with H_2 prior to its recombination. The mass spectra obtained during the experiment showed that H_3^+ was the dominant ion species but the internal state of the ions was not probed in the AISA experiments. We do not have a certain explanation for this observation (see discussion in [23,31]). In later experiments we used $10^{12} < [H_2] < 5 \times 10^{13} \text{ cm}^{-3}$; the measured α_{eff} did not change with $[H_2]$ (in the context of those experiments we called it the “saturated region”, see [23,31]). At these conditions the formed H_3^+ ions have many collisions with H_2 and He prior to their recombination. We found that the measured α_{eff} depends linearly on helium number density; $\alpha_{\text{eff}} = \alpha_{\text{bin}} + K_{\text{He}}[\text{He}]$ in the “saturated region.” The binary rate coefficient was determined from the low-pressure limit as $\alpha_{\text{bin}} = \alpha_{\text{eff}}([\text{He}] \rightarrow 0)$. The obtained binary recombination rate coefficients are very close to the theoretically predicted value [15] and the value reported by storage ion ring CRYRING [18]. Using SA-CRDS we confirmed that H_3^+ ions in recombination dominated afterglow plasmas are in thermal equilibrium with He [32]. All these later studies were performed for $[H_2]$ higher than 10^{12} cm^{-3} but low enough to prevent formation of fast recombining H_5^+ ions.

There are good reasons to believe that hydrogen molecules should be more efficient than inert helium atoms in promoting H_3^+ recombination, and there is some earlier experimental evidence in support of this expectation [29,30,33,34]. However, the effect of H_2 has not been studied systematically and this is the first study dedicated to H_2 -assisted ternary recombination.

II. EXPERIMENT

The technical details of the stationary-afterglow cavity-ring-down-spectroscopy apparatus (SA-CRDS) have been adequately described elsewhere [27]. The plasma is formed in a pulsed microwave discharge in a mixture of He, Ar, and H_2 and the densities of three rotational states of the ground vibrational state of H_3^+ during the afterglow are measured using the transitions $3\nu_2^1(2,0) \leftarrow 0\nu_2^0(1,0)$ and $3\nu_2^1(4,3) \leftarrow 0\nu_2^0(3,3)$ for ortho- H_3^+ and $3\nu_2^1(2,1) \leftarrow 0\nu_2^0(1,1)$ for para- H_3^+ . Details and notation are discussed in [32,35,36]. The kinetic temperature of the ions is obtained by measuring Doppler broadening of the absorption lines and the rotational temperature is obtained from the relative populations of measured states (for details see [32]). A numerical model of the chemical kinetics is used to determine the most appropriate conditions for the experiment. A water transition at 7236.45 cm^{-1} (line position taken from HITRAN database [37]) was routinely scanned to estimate the amount of H_2O impurities in the apparatus. Typically, the

water vapor concentration was at a safe level of less than $5 \times 10^{10} \text{ cm}^{-3}$ (less than 0.1 ppm of buffer gas number density).

The present experimental study focus on H_2 -assisted recombination of H_3^+ ions. Ternary recombination rate coefficients were derived from the measured ion number density decays with an effective recombination rate coefficient $\alpha_{\text{eff-ion}}$ for a wide range of $[\text{He}]$ and $[\text{H}_2]$ densities. For details on the data analysis see [32].

III. COMPLEX MODEL OF TERNARY RECOMBINATION

Ternary contributions in H_3^+ recombination can occur by formation of Rydberg molecules $H_3^\#$ by resonant capture of an electron into a rotationally excited Rydberg state with the formation rate coefficient α_F . The unstable molecule (or “complex”) can decay during its lifetime by autoionization with a time constant τ_a or it can be “stabilized” (rendered incapable of being autoionized or being collisionally reionized) with rate coefficient k_{SM} in a collision with a third particle M of number density $[\text{M}]$. Provided that the lifetime τ_a is much shorter than the time scale of the plasma decay, the number density ratio $[H_3^\#]/[H_3^+]$ can be taken as constant and the effective recombination coefficient for H_3^+ dominated plasma becomes

$$\alpha_{\text{eff-ion}} = \alpha_{\text{bin}} + \alpha_F \frac{k_{\text{SM}}[\text{M}]}{1/\tau_a + k_{\text{SM}}[\text{M}]} \quad (2)$$

This model of ternary recombination is similar to that proposed in our earlier publications [22,23,30]. We introduce the three-body recombination rate coefficient K_M defined as $K_M = \alpha_F k_{\text{SM}} \tau_a$. In the limit of small $[\text{M}]$ (the “linear” regime) the second term of Eq. (2) reduces to $K_M[\text{M}]$. In the limit of large $[\text{M}]$, the second term of Eq. (2) approaches the constant value α_F and the three-body recombination process is then said to “saturate.” This brief discussion hides a great amount of detail. In reality, one should consider an ensemble of many complexes, and more than two steps may be required to stabilize the complexes. In the experiment both He and H_2 can act as neutral third bodies. If one assumes that both gases act on the same complexes, the product $K_M[\text{M}]$ can be replaced by the sum $K_{H_2}[\text{H}_2] + K_{\text{He}}[\text{He}]$. We assume these contributions to be additive. We also assume that binary and ternary recombination are purely additive. This is not necessarily true if both processes share the same initial states.

The proposed simplified recombination mechanism is summarized in Fig. 1, where k_{SHe} and k_{SH_2} are the binary rate coefficients for collisional stabilization of $H_3^\#$ in collisions with He and H_2 , respectively. The ternary recombination rate coefficients for He- and H_2 -assisted recombination

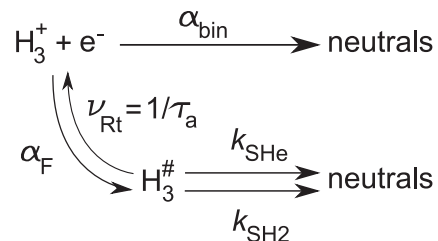


FIG. 1. The scheme of the proposed H_3^+ recombination mechanism. Used symbols are explained in the text.

(K_{He} and K_{H_2} , respectively) are introduced as $K_{\text{He}} = \alpha_{\text{F}} k_{\text{SHe}} \tau_{\text{a}}$ and $K_{\text{H}_2} = \alpha_{\text{F}} k_{\text{SH}_2} \tau_{\text{a}}$.

There is one additional recombination process that can make a contribution at high $[\text{H}_2]$: The H_3^+ ions are known to enter a chemical equilibrium with weakly bound H_5^+ cluster ions that recombine very fast at 300 K ($\alpha_5 \sim 2 \times 10^{-6} \text{ cm}^3 \text{ s}^{-1}$) [38,39]. At 300 K, the clustering equilibrium constant, defined by $[\text{H}_5^+]/[\text{H}_3^+] = K_{\text{C}}[\text{H}_2]$, has a value $K_{\text{C}}(300 \text{ K}) = 6.7 \times 10^{-19} \text{ cm}^3$ [40]. Even at the highest H_2 concentrations ($6 \times 10^{16} \text{ cm}^{-3}$) used in present experiments less than 4% of the H_3^+ ions are clustered.

To a good approximation, the effective recombination rate coefficient can then be written as

$$\alpha_{\text{eff-ion}} = \alpha_{\text{bin}} + \alpha_{\text{F}} \frac{K_{\text{He}}[\text{He}] + K_{\text{H}_2}[\text{H}_2]}{\alpha_{\text{F}} + K_{\text{He}}[\text{He}] + K_{\text{H}_2}[\text{H}_2]} + \alpha_5 K_{\text{C}}[\text{H}_2]. \quad (3)$$

A more rigorous kinetic analysis, that includes recombination of H_5^+ , shows that the relative abundance of H_5^+ in recombining plasmas is smaller by about a factor of 2 than $K_{\text{C}}[\text{H}_2]$ and that it varies with electron density.

Equation (3) implies that $\alpha_{\text{eff-ion}}$ saturates at the value $\alpha_{\text{bin}} + \alpha_{\text{F}}$ if $\alpha_{\text{F}} \ll (K_{\text{He}}[\text{He}] + K_{\text{H}_2}[\text{H}_2])$. While in previous H_3^+ experiments [21–23,31,32] the range of $[\text{He}]$ was too small to detect saturation, the present experiments clearly exhibit saturation (details to be given below). Also, a slight dependence on $[\text{H}_2]$ was observed in the earlier experiments [29,33,38] but it was then thought to arise from formation of fast recombining H_5^+ ions at higher $[\text{H}_2] > 10^{14} \text{ cm}^{-3}$. However, H_5^+ formation at temperatures near 300 K does not suffice to explain the increase of the recombination rate coefficient dependent on $[\text{H}_2]$ at 300 K (with $[\text{H}_2] < 2 \times 10^{15} \text{ cm}^{-3}$) that was also observed by Gougousi *et al.* [33]. On the other hand, Amano's [34] spectroscopic studies in a stationary afterglow experiment in pure hydrogen yielded an H_3^+ recombination rate coefficient that was independent of H_2 density, but three times larger than the currently accepted binary recombination rate coefficient [2].

IV. EXPERIMENTAL DATA AND RESULTS

Figure 2 shows typical H_3^+ decay curves measured by SA-CRDS and the calculated densities of H_3^+ and H_5^+ ions. The rate coefficients $\alpha_{\text{eff-ion}}$ are obtained by fitting the decay of the H_3^+ number densities, taken as the sum of those in the ortho and para states assuming thermal equilibrium (see discussion in [32]), or calculated from the population of the ortho- H_3^+ (1,0) state only. No substantial difference between these two evaluations was observed.

The chemical kinetics calculations solve the set of reactions as described by Plašil *et al.* [26]. Because the composition of the plasma at the end of the microwave pulse is difficult to ascertain, the calculations were performed for many sets of different initial conditions. The results of the model show that at the number densities of He, Ar, and H_2 used in present experiments the H_3^+ ion becomes the dominant ion species within 150 μs after switching off the discharge. An example is displayed in Fig. 2 for the following initial conditions in quasineutral plasma: $[\text{H}_3^+] = n_{\text{e}}$; $[\text{He}^{\text{m}}] = 1 \times 10^{11} \text{ cm}^{-3}$, where $[\text{He}^{\text{m}}]$ is the number density of metastable helium

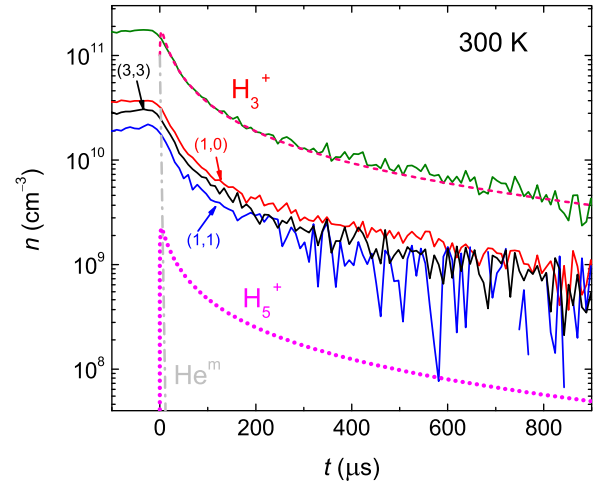


FIG. 2. (Color online) The decay curves measured for (1,0), (1,1), and (3,3) states of H_3^+ at 300 K and number densities $[\text{He}] = 8 \times 10^{17} \text{ cm}^{-3}$, $[\text{H}_2] = 2 \times 10^{16} \text{ cm}^{-3}$, and $[\text{Ar}] = 7 \times 10^{14} \text{ cm}^{-3}$. The total number density of H_3^+ ions, calculated from the measured data under assumption of LTE, is shown as a full line. Calculated evolutions of the number densities of H_3^+ , H_5^+ , and He^{m} are indicated as dashed, dotted, and dash-dotted lines, respectively.

atoms. For illustration of the result of the model, the measured evolutions of the number density of (1,0), (1,1), and (3,3) states of the H_3^+ ion and of the overall number density of the H_3^+ ion are also plotted in Fig. 2. The most important reactions taking place in the formation of H_3^+ are listed in Table II of [26]. A fast decay of helium metastables He^{m} is given by Penning ionization with H_2 and Ar. The H_3^+ recombination rate coefficient was taken from the present data and the H_5^+ recombination rate coefficient at 300 K was taken as $\alpha_5 \sim 2 \times 10^{-6} \text{ cm}^3 \text{ s}^{-1}$ [38,39].

A large set of decay curves at 300 K, similar to those in Fig. 2, were recorded and analyzed for a wide range of $[\text{H}_2]$ and for several $[\text{He}]$. The dependences of $\alpha_{\text{eff-ion}}$ on $[\text{H}_2]$ at particular $[\text{He}]$ are shown in Fig. 3. The value obtained in pure H_2 using the same experimental setup at $(270 \pm 5) \text{ K}$ is also included (full diamond).

The binary rate coefficient, $\alpha_{\text{bin}}(300 \text{ K}) = 6 \times 10^{-8} \text{ cm}^3 \text{ s}^{-1}$, is known from previous SA-CRDS and Cryo-FALP experiments [21]. To emphasize the ternary contribution we subtracted the value of α_{bin} from the measured $\alpha_{\text{eff-ion}}$ and only the difference $\alpha_{\text{eff-ion}} - \alpha_{\text{bin}}$ corresponding to the ternary contribution is shown in Fig. 3. The data clearly show that $\alpha_{\text{eff-ion}} - \alpha_{\text{bin}}$ rises with increasing $[\text{H}_2]$ up to $[\text{H}_2] \sim 10^{16} \text{ cm}^{-3}$ and then saturates, as expected from the complex formation model [see Eq. (3)]. Two estimates of the contribution due to formation and subsequent recombination of H_5^+ ions to the overall measured recombination rate coefficient are displayed in Fig. 3. The line denoted LTE_{H_5} shows the product of $\alpha_5 K_{\text{C}}[\text{H}_2]$, i.e., H_5^+ is assumed to be in thermal equilibrium with H_3^+ and the $[\text{H}_5^+]/[\text{H}_3^+]$ ratio is approximated using an equilibrium constant of $K_{\text{C}}(300 \text{ K}) = 6.7 \times 10^{-19} \text{ cm}^3$ [40]. A considerably smaller and more realistic contribution of H_5^+ (the line marked M_{H_5}) is obtained from our kinetic model that includes the recombination loss of H_5^+ . The comparison

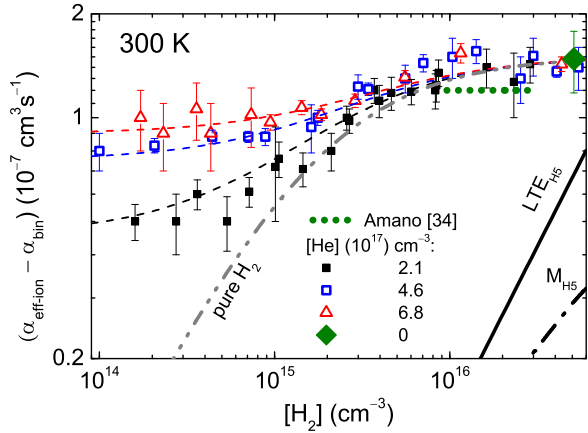


FIG. 3. (Color online) The dependencies of $(\alpha_{\text{eff-ion}} - \alpha_{\text{bin}})$ on $[\text{H}_2]$ measured at indicated $[\text{He}]$. Full diamond: measurements in pure H_2 . Dashed lines: fits of Eq. (3) to the data, using the parameters mentioned in the text. Double-dot-dashed line: three-body recombination in pure H_2 . Solid line (LTE_{H_5}): approximate H_5^+ contribution, $\alpha_5 K_C [\text{H}_2]$. Dash-dotted line (M_{H_5}): H_5^+ contribution obtained from the kinetic model for $[\text{He}] = 2.1 \times 10^{17} \text{ cm}^{-3}$. Dotted horizontal line: data obtained by Amano [34] in pure H_2 at 273 K, after subtracting $\alpha_{\text{bin}} = 6 \times 10^{-8} \text{ cm}^3 \text{ s}^{-1}$.

of the measured $\alpha_{\text{eff-ion}}$ with calculated contributions (LTE_{H_5} and M_{H_5}) indicates that the actual contribution due to H_5^+ formation is negligible at $[\text{H}_2] < 2 \times 10^{16} \text{ cm}^{-3}$. We fitted the measured $\alpha_{\text{eff-ion}}$ by Eq. (3), neglecting contribution from H_5^+ formation and using $\alpha_{\text{bin}} = 6 \times 10^{-8} \text{ cm}^3 \text{ s}^{-1}$; see the dashed lines in the Fig. 3. The inferred rate coefficients are $K_{\text{He}} = (3.3 \pm 0.7) \times 10^{-25} \text{ cm}^6 \text{ s}^{-1}$, $K_{\text{H}_2} = (8.7 \pm 1.5) \times 10^{-23} \text{ cm}^6 \text{ s}^{-1}$, and $\alpha_F = (1.5 \pm 0.1) \times 10^{-7} \text{ cm}^3 \text{ s}^{-1}$. Substituting these rate constants into Eq. (3) we derived $(\alpha_{\text{eff-ion}} - \alpha_{\text{bin}})$ for the ternary recombination in pure H_2 . This gives the double-dot-dashed line labeled “pure H_2 ” in Fig. 3.

For comparison we also include in Fig. 3 the values obtained by Amano [34] in his spectroscopic study of H_3^+ recombination in afterglow plasma in pure H_2 at 273 K. The binary contribution has been subtracted. Amano’s results agree quite well with our data, strongly suggesting that Amano measured in the saturated region.

For consistency and for comparison with previous experiments we remeasured the dependence of $\alpha_{\text{eff-ion}}$ on $[\text{He}]$ up to $[\text{He}] = 8 \times 10^{17} \text{ cm}^{-3}$ at a low hydrogen density, $[\text{H}_2] = 2 \times 10^{14} \text{ cm}^{-3}$, and at 100 times higher density, $[\text{H}_2] = 2 \times 10^{16} \text{ cm}^{-3}$. The obtained values can be seen in Fig. 4. At low $[\text{H}_2]$, $\alpha_{\text{eff-ion}}$ increases with increasing $[\text{He}]$ and approaches saturation at very high $[\text{He}]$. At high $[\text{H}_2]$ $\alpha_{\text{eff-ion}}$ is nearly constant at the value α_F obtained by fitting the data in Fig. 3. The agreement of the present SA-CRDS values with those obtained in the Cryo-FALP experiment [23] is noteworthy since the electron densities in those experiments differed by more than a factor of 10. The errors in Figs. 3 and 4 are statistical errors of the fits to the time decay of $[\text{H}_3^+]$. The systematic error is estimated as 10%.

To show the difference between the helium- and hydrogen-assisted ternary recombination of the H_3^+ ion, the dependences of $\alpha_{\text{eff-ion}}$ on $[\text{He}]$ and $[\text{H}_2]$ are plotted in Fig. 5 together

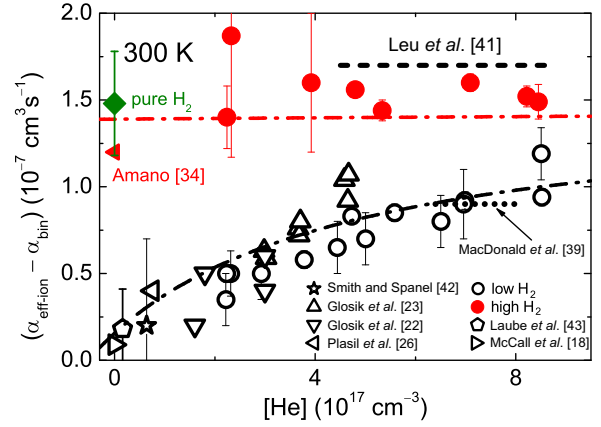


FIG. 4. (Color online) Measured dependence of $(\alpha_{\text{eff-ion}} - \alpha_{\text{bin}})$ on He number density at 300 K for $[\text{H}_2] = 2 \times 10^{14} \text{ cm}^{-3}$ (open circles) and for $[\text{H}_2] = 2 \times 10^{16} \text{ cm}^{-3}$ (closed circles). The values of $(\alpha_{\text{eff-ion}} - \alpha_{\text{bin}})$ measured in pure H_2 at $(270 \pm 5) \text{ K}$ are denoted by full diamonds (see also Fig. 3). The values measured in other experiments [18,22,23,26,34,39,41–43] are plotted for comparison. Values indicated by open symbols were measured for $[\text{H}_2] < 5 \times 10^{14} \text{ cm}^{-3}$. All experiments were performed with helium as a buffer gas with the exception of data in [18,34,39] where no buffer gas, pure H_2 , or neon buffer gas was used, respectively. The dot-dashed lines denote values given by Eq. (3) for $[\text{H}_2] = 2 \times 10^{14}$ and $2 \times 10^{16} \text{ cm}^{-3}$ and with parameters written in the text.

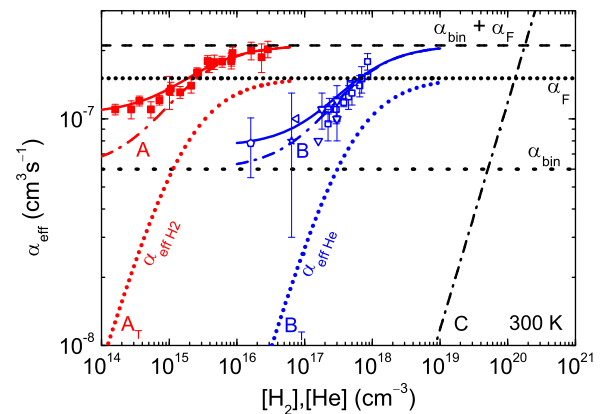


FIG. 5. (Color online) Measured dependence of the effective recombination rate coefficient on H_2 (full squares, with $[\text{He}] = 2 \times 10^{17} \text{ cm}^{-3}$) and He number density (open squares, with $[\text{H}_2] = 2 \times 10^{14} \text{ cm}^{-3}$) measured at 300 K. The full lines are fit to the data from Figs. 3 and 4. The horizontal dotted line shows the value of the binary recombination rate coefficient α_{bin} of H_3^+ ions at 300 K. The dashed line shows the sum $(\alpha_{\text{bin}} + \alpha_F)$, i.e., maximum rate coefficient given by the sum of contributions from binary and saturated ternary recombination. The dot-dashed lines (A, B, and C) denote the sum of α_{bin} and the contribution of the H_2 -assisted process only (A), the sum of α_{bin} and the contribution of the He-assisted process only (B), and the α_{eff} arising from ternary helium-assisted recombination as predicted by the theory of Bates and Khare [24] with the ternary recombination rate coefficient of $1.2 \times 10^{-27} \text{ cm}^6 \text{ s}^{-1}$ (C). The dotted lines denoted A_T and B_T indicate the contributions to the measured α_{eff} arising from the H_2 - and He-assisted ternary process, respectively. Values from other afterglow experiments are plotted using the same notation as in Fig. 4.

with the dependence predicted by classical Bates-Khare theory [24]. Values from other experiments are plotted using the same notation as in Fig. 4. Note the orders-of-magnitude difference between both ternary processes.

It is difficult to explain the third-body effects by accurate theoretical models. In this paper, we rationalize our observations by a highly simplified model that postulates the existence of long-lived H₃[#] complexes, without specifying their detailed nature and the interactions that cause these complexes to eventually decay. The basic ideas are similar to those that we have described in our previous paper [30], in which we also discuss possible other three-body mechanisms.

The lifetimes of the intermediate complexes must be very large: An estimate of the three-body coefficient K_{H_2} due to H₂ is given by the product of the formation rate coefficient α_F , the complex lifetime τ_a , and the rate coefficient of stabilizing collisions $k_{S_{H_2}}$. If one takes the formation rate coefficient as $\alpha_F = 1.5 \times 10^{-7} \text{ cm}^3 \text{ s}^{-1}$, and the stabilization coefficient as $k_{S_{H_2}} = 10^{-9} \text{ cm}^3 \text{ s}^{-1}$ (a typical ion-neutral collision rate coefficient), then one needs a lifetime of $\tau_a \sim 6 \times 10^{-7} \text{ s}$ to reproduce the experimental value $K_{H_2} = (8.7 \pm 1.5) \times 10^{-23} \text{ cm}^6 \text{ s}^{-1}$ which can be obtained as $K_{H_2} = \alpha_F k_{S_{H_2}} \tau_a$. That lifetime exceeds the longest calculated [23] lifetimes of some rotational resonances ($\sim 10^{-10} \text{ s}$) by a wide margin. On the other hand, some experimental studies showed that Rydberg states of the H₃ molecule can have lifetimes exceeding 10^{-6} s [44]. Previous treatments of this problem suggest that l mixing of the Rydberg electrons' angular momentum by either plasma electrons [33] or neutral particles [23,30,31] occurs and that it could enhance the complex lifetimes; l mixing of high Rydberg states with $n \gtrsim 40$ due to ambient plasma electrons is indeed an exceedingly fast process: At electron densities near 10^{11} cm^{-3} mixing would occur in a time on the order of 10^{-11} to 10^{-10} s for an $n = 40$ Rydberg atom [45] and increase the lifetimes by a factor of about n^2 .

The experimental data show that H₂ is a much more efficient third body than helium. This suggests that complex stabilization involves reactions with the ion core, which may be rotationally and perhaps vibrationally excited, rather than with the Rydberg electron. Rydberg reactions are similar to ion-molecule reactions [46,47]. Reactions with H₂ but not He can occur by proton or H-atom exchange that reduces the energy of the complex and eventually leads to dissociation. Uy *et al.* [48] invoke this type of reaction as the principal rotational quenching mechanism in plasmas containing He and H₂.

The principal difference between He-assisted and H₂-assisted recombination can be in the interaction of the Rydberg H₃[#] molecule with atomic He and with molecular H₂. Particularly if we have in mind the possibility of a reactive collision of H₃[#] and H₂ followed by formation of H₃^{*} and its dissociation as it is described by Fermi's independent-collider model. See, e.g., recent studies of reactions of Rydberg atoms with molecules [46,47].

V. SUMMARY AND CONCLUSIONS

The cavity ring down absorption spectrometer was used to monitor *in situ* the evolution of number densities of ortho- and para-H₃⁺ during the afterglow in a He-Ar-H₂ gas mixture at 300 K. From these measurements the effective recombination

rate coefficient and its dependence on [He] and [H₂] were determined.

A very fast H₂-assisted ternary recombination was observed with the value of ternary recombination rate coefficient $K_{H_2} = (8.7 \pm 1.5) \times 10^{-23} \text{ cm}^6 \text{ s}^{-1}$ substantially exceeding those values measured for the same ion in ambient helium ($K_{He} \sim 10^{-25} \text{ cm}^6 \text{ s}^{-1}$) or predicted by the classical theory of Bates and Khare (with rate coefficient $\sim 10^{-27} \text{ cm}^6 \text{ s}^{-1}$) [24]. The disagreement with the Bates and Khare theory for neutral stabilized recombination of atomic ions is not surprising. In their model, the energy of Rydberg states is only reduced by Rydberg electron-atom collisions but stabilization by collision-induced predissociation, of course, is absent. The large effect of H₂ most likely explains one of the remaining discrepancies in H₃⁺ recombination studies, namely, the large recombination rate coefficients measured by Amano [34].

These results are not at all the typical finding in recombination studies. As far as we know, most other molecular ions recombine largely by the binary process and the environment has little effect. The sensitivity of the H₃⁺ recombination to third-body effects seems to account for many of the discrepancies between experimental studies that have been conducted and clearly demonstrates the need of further theoretical work on recombination of this simplest polyatomic ion with electrons with emphasis on formation of long-lived collisional complexes and on the influence of third particles on the overall recombination. An existence of a similar ternary process for D₃⁺ ions with D₂ as the third particle is expected. We are not able to predict to what extent the H₂-assisted ternary process may have influenced recombination rates of other ions measured in plasma afterglows. The required lifetimes of the metastable Rydberg states formed in the proposed recombination process are quite long; therefore the ions recombining via direct mechanism [49] should not be affected. However, the recombination rate coefficients of some ions recombining via the indirect recombination mechanism obtained in the afterglow experiments could have been enhanced by fast ternary He- or H₂-assisted recombination. Possibly affected ions are HCO⁺ and N₂H⁺, as both of them recombine by the indirect mechanism [50] and the reported results of the afterglow experiments differ by almost an order of magnitude (see Fig. 2 in [51]). Moreover, the highest recombination rate coefficients for both of these ions were reported by Amano, who measured in H₂ buffer gas [34].

A fast H₂-assisted ternary recombination may directly impact models describing hydrogen plasmas and it can have consequences in plasma physics including physics of discharges, astrophysics, recombination pumped lasers, plasma spectroscopy, plasmatic technologies, etc. It can also influence processes in ionospheres of large planets with relatively high pressure of H₂, e.g., Jupiter and Jupiter-like planets, and may be important for chemistry of gas giant exoplanets.

Further measurements at different temperatures are in progress.

ACKNOWLEDGMENTS

This work was partly supported by Czech Science Foundation projects GACR P209/12/0233 and GACR 14-14649P, and by Charles University in Prague projects GAUK 659112, GAUK 692214, UNCE 204020/2012 and SVV 260 090.

- [1] K. N. Crabtree *et al.*, *Astrophys. J.* **729**, 15 (2011).
- [2] M. Larsson and A. Orel, *Dissociative Recombination of Molecular Ions* (Cambridge University, Cambridge, 2008).
- [3] R. Johnsen and S. L. Guberman, in *Advances In Atomic, Molecular, and Optical Physics*, edited by E. Arimondo, P. Berman, and C. Lin, Vol. 59 (Academic, New York, 2010), pp. 75–128.
- [4] D. R. Bates, M. F. Guest, and R. A. Kendall, *Planet. Space Sci.* **41**, 9 (1993).
- [5] W. D. Watson, *Astrophys. J.* **183**, L17 (1973).
- [6] E. Herbst and W. Klempner, *Astrophys. J.* **185**, 505 (1973).
- [7] S. C. O. Glover and D. W. Savin, *Mon. Not. R. Astron. Soc.* **393**, 911 (2009).
- [8] T. Oka, *Phys. Rev. Lett.* **45**, 531 (1980).
- [9] P. Drossart *et al.*, *Nature (London)* **340**, 539 (1989).
- [10] S. Miller, T. Stallard, J. Tennyson, and H. Melin, *J. Phys. Chem. A* **117**, 9770 (2013).
- [11] T. R. Geballe and T. Oka, *Nature (London)* **384**, 334 (1996).
- [12] T. Oka, *Proc. Natl. Acad. Sci. USA* **103**, 12235 (2006).
- [13] V. Kokoouline, C. H. Greene, and B. D. Esry, *Nature (London)* **412**, 891 (2001).
- [14] V. Kokoouline and C. H. Greene, *Phys. Rev. A* **68**, 012703 (2003).
- [15] S. Fonseca dos Santos, V. Kokoouline, and C. H. Greene, *J. Chem. Phys.* **127**, 124309 (2007).
- [16] B. J. McCall *et al.*, *Nature (London)* **422**, 500 (2003).
- [17] H. Kreckel *et al.*, *Phys. Rev. Lett.* **95**, 263201 (2005).
- [18] B. J. McCall *et al.*, *Phys. Rev. A* **70**, 052716 (2004).
- [19] A. Wolf *et al.*, *Phil. Trans. R. Soc. A* **364**, 2981 (2006).
- [20] A. Petignani *et al.*, *Phys. Rev. A* **83**, 032711 (2011).
- [21] P. Rubovic *et al.*, *J. Phys. Chem. A* **117**, 9626 (2013).
- [22] J. Glosik *et al.*, *J. Phys. B* **41**, 191001 (2008).
- [23] J. Glosík, R. Plašil, I. Korolov, T. Kotřík, O. Novotný, P. Hlavenka, P. Dohnal, J. Varju, V. Kokoouline, and C. H. Greene, *Phys. Rev. A* **79**, 052707 (2009).
- [24] D. Bates and S. Khare, *Proc. Phys. Soc. Lond.* **85**, 231 (1965).
- [25] R. J. Saykally, E. A. Michael, J. Wang, and C. H. Greene, *J. Chem. Phys.* **133**, 234302 (2010).
- [26] R. Plasil *et al.*, *Int. J. Mass Spectrom.* **218**, 105 (2002).
- [27] P. Macko *et al.*, *Int. J. Mass Spectrom.* **233**, 299 (2004).
- [28] J. Varju, M. Hejduk, P. Dohnal, M. Jilek, T. Kotřík, R. Plasil, D. Gerlich, and J. Glosik, *Phys. Rev. Lett.* **106**, 203201 (2011).
- [29] O. Novotny *et al.*, *J. Phys. B* **39**, 2561 (2006).
- [30] R. Johnsen *et al.*, *J. Phys. Chem. A* **117**, 9477 (2013).
- [31] J. Glosik *et al.*, *Molec. Phys.* **108**, 2253 (2010).
- [32] P. Dohnal *et al.*, *J. Chem. Phys.* **136**, 244304 (2012).
- [33] T. Gougousi, R. Johnsen, and M. F. Golde, *Int. J. Mass Spectrom.* **149–150**, 131 (1995).
- [34] T. Amano, *J. Chem. Phys.* **92**, 6492 (1990).
- [35] P. Hlavenka *et al.*, *Int. J. Mass Spectrom.* **255**, 170 (2006).
- [36] C. M. Lindsay and B. J. McCall, *J. Mol. Spectrosc.* **210**, 60 (2001).
- [37] L. S. Rothman *et al.*, *J. Quant. Spectrosc. Radiat. Transfer* **110**, 533 (2009).
- [38] J. Glosik *et al.*, *Plasma Sci. Technol.* **12**, S117 (2003).
- [39] J. A. MacDonald, M. A. Biondi, and R. Johnsen, *Planet. Space Sci.* **32**, 651 (1984).
- [40] K. Hiraoka, *J. Chem. Phys.* **87**, 4048 (1987).
- [41] M. T. Leu, M. A. Biondi, and R. Johnsen, *Phys. Rev. A* **8**, 413 (1973).
- [42] D. Smith and P. Spanel, *Int. J. Mass Spectrom.* **129**, 163 (1993).
- [43] S. Laube *et al.*, *J. Phys. B* **31**, 2111 (1998).
- [44] C. Bordas and H. Helm, *Phys. Rev. A* **47**, 1209 (1993).
- [45] S. K. Dutta, D. Feldbaum, A. Walz-Flannigan, J. R. Guest, and G. Raithel, *Phys. Rev. Lett.* **86**, 3993 (2001).
- [46] S. Yu *et al.*, *J. Chem. Phys.* **140**, 034310 (2014).
- [47] H. Song *et al.*, *J. Chem. Phys.* **123**, 074314 (2005).
- [48] D. Uy, C. M. Gabrys, M.-F. Jagod, and T. Oka, *J. Chem. Phys.* **100**, 6267 (1994).
- [49] D. R. Bates, *Phys. Rev.* **78**, 492 (1950).
- [50] S. Fonseca dos Santos, N. Douguet, V. Kokoouline, and A. E. Orel, *J. Chem. Phys.* **140**, 164308 (2014).
- [51] V. Poterya, J. L. McLain, N. G. Adams, and L. M. Babcock, *J. Phys. Chem. A* **109**, 7181 (2005).

**Flowing-afterglow study of electron-ion recombination of para- H_3^+
and ortho- H_3^+ ions at temperatures from 60 K to 300 K**

Hejduk M., Dohnal P., Rubovic P., Kálosi Á., Plašil R., Johnsen R., Glosík J.

J. Chem. Phys. **143**(4), 044303, 2015.

Flowing-afterglow study of electron-ion recombination of para- H_3^+ and ortho- H_3^+ ions at temperatures from 60 K to 300 K

Michal Hejduk,¹ Petr Dohnal,^{1,a)} Peter Rubovič,¹ Ábel Kálosi,¹ Radek Plašil,¹
 Rainer Johnsen,² and Juraj Glosík¹

¹Department of Surface and Plasma Science, Faculty of Mathematics and Physics,
 Charles University in Prague, Prague 18000, Czech Republic

²Department of Physics and Astronomy, University of Pittsburgh, Pittsburgh, Pennsylvania 15260, USA

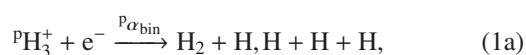
(Received 9 April 2015; accepted 9 July 2015; published online 22 July 2015)

Detailed measurements employing a combination of a cryogenic flowing afterglow with Langmuir probe (Cryo-FALP II) and a stationary afterglow with near-infrared absorption spectroscopy (SA-CRDS) show that binary electron recombination of para- H_3^+ and ortho- H_3^+ ions occurs with significantly different rate coefficients, ${}^p\alpha_{\text{bin}}$ and ${}^o\alpha_{\text{bin}}$, especially at very low temperatures. The measurements cover temperatures from 60 K to 300 K. At the lowest temperature of 60 K, recombination of para- H_3^+ is at least three times faster than that of ortho- H_3^+ (${}^p\alpha_{\text{bin}} = (1.8 \pm 0.4) \times 10^{-7} \text{ cm}^3 \text{ s}^{-1}$ vs. ${}^o\alpha_{\text{bin}} = (0_{-0}^{+5}) \times 10^{-8} \text{ cm}^3 \text{ s}^{-1}$). © 2015 AIP Publishing LLC. [<http://dx.doi.org/10.1063/1.4927094>]

I. INTRODUCTION

H_3^+ ion is the most abundantly produced molecular ion in interstellar space¹ and plays a pivotal role in the reaction chains that form astrophysically important molecules like, e.g., H_2O (Ref. 2) or simple hydrocarbons.³ Dissociative recombination with electrons is one of the competing destruction mechanisms of H_3^+ ions in diffuse interstellar clouds⁴ and, in part for this reason, has been studied experimentally and theoretically for more than 60 years.^{5–7} Although much progress has been made in recent years, a true convergence between observational and laboratory data has not been achieved, and the situation is further complicated by the dependence of the recombination rate coefficient of H_3^+ ions on the nuclear spin configurations (para and ortho). Detailed discussions, preliminary conclusions, and comments on astrophysical relevance have been published (see, e.g., Ref. 8).

The present experiments focus on binary dissociative recombination of H_3^+ ions in specific nuclear spin states, namely,



where the “p” and “o” superscripts distinguish the para- and ortho-nuclear spin states of H_3^+ . The corresponding binary recombination rate coefficients are denoted by ${}^p\alpha_{\text{bin}}$ and ${}^o\alpha_{\text{bin}}$. State-specific coefficients have been measured in storage-ring experiments by feeding para-enriched hydrogen to “cold” ion sources and varying the relative abundances of the two spin states of H_3^+ .^{9–16} Unfortunately, the results are now in doubt, as has been summarized, e.g., in Refs. 15, 17, and 18,

because the abundances of the two spin states in the beam were not exactly known, and the rotational temperature of the ions was not as low as had been thought but was of the order or above 300 K.¹⁵ The state-specific recombination of H_3^+ was studied also in afterglow experiments by monitoring the decay of a low temperature H_3^+ dominated afterglow plasma (predominantly in He/Ar/ H_2 gas mixtures).^{19–21} It is an advantage of the afterglow experiments that the abundances of para- and ortho- H_3^+ ions can be measured using absorption spectroscopy and that the ions are rotationally thermalized by multiple collisions with atoms/molecules of ambient neutral gas (see experimental confirmation and discussion in Refs. 19 and 22). Such afterglow experimental techniques (stationary afterglow (SA) and flowing afterglow with Langmuir probe (FALP)) are well established and relatively simple, have been extensively verified, but they are not entirely free of complications.^{6,23,24} In our recent SA experiments, the density decays of H_3^+ ions in the particular spin state and their rotational thermalization within the para- and ortho-nuclear spin manifolds were monitored by near-infrared (NIR) Cavity Ring Down Spectroscopy (CRDS).^{20,21,25}

One complication of afterglow experiments arises from additional ion loss processes (mainly ternary or third-body assisted recombination) that can contribute to the electron and ion density decays during the afterglow. It took over 50 years to realize that the discrepancies between rate coefficients measured in afterglow experiments were in part due to ternary neutral assisted recombination.²⁶ On the other hand, ternary processes involving neutrals or electrons (see, e.g., Refs. 27–31) are of interest for some applications and the plasma environment makes it possible to study them. For instance, our studies of recombination of H_3^+ ions in He/Ar/ H_2 gas mixture showed that ternary He-assisted recombination of H_3^+ ions,

^{a)}Petr.Dohnal@mff.cuni.cz



is a rather fast process.^{19,20,26,30,32} Here, ${}^pK_{\text{He}}$ and ${}^oK_{\text{He}}$ are ternary recombination rate coefficients for pure para- H_3^+ and pure ortho- H_3^+ . Recently, an even faster ternary H_2 -assisted recombination of H_3^+ at 300 K was reported.³¹ The theory of the ternary processes (2a) and (2b)^{26,30,32} is not sufficiently developed to cleanly decompose experimental data into binary and ternary components. Hence, we are forced to measure recombination as a function of the third-body concentration (number of species in unit volume) and to obtain the binary recombination by extrapolating to zero third-body densities.

The state selective studies of H_3^+ recombination by Varju *et al.*²¹ and Dohnal *et al.*^{19,20} were limited to temperatures from 77 K to 200 K due to design limitations of the SA-CRDS apparatus. The measurements with SA-CRDS at 77 K showed that the binary recombination rate coefficient ${}^p\alpha_{\text{bin}}$ for para- H_3^+ is at 77 K at least three times higher than corresponding ${}^o\alpha_{\text{bin}}$ for ortho- H_3^+ .¹⁹ The ratio decreases with increasing temperature up to ≈ 200 K,¹⁹ where both rate coefficients are comparable. The ternary recombination rate coefficients also showed small nuclear spin specificity at temperatures 140–200 K.¹⁹

The results of recent state selective afterglow (SA-CRDS) experiments^{19–21} are in qualitative agreement with theoretical predictions.^{33,34} However, at temperatures below ≈ 200 K, the difference between the coefficients ${}^p\alpha_{\text{bin}}$ and ${}^o\alpha_{\text{bin}}$ for the two nuclear spin manifolds seems to be increasing with decreasing temperature faster than predicted.^{19,20,35} As mentioned earlier, storage-ring experiments have also produced state-selected cross sections at low collisional energies, but the rotational excitation of stored ions was of the order or above 300 K (see, e.g., discussion in Ref. 15 and in Reviews Refs. 17 and 18). Those experiments may eventually yield improved data but at this time, both the CRYRING (Electron Accelerator and Storage Ring Facility (Stockholm, Sweden))^{10,13,16} and TSR (Test Storage Ring (Heidelberg, Germany))^{9,11,15} facilities are closed and new cryogenic rings are being constructed.

Several authors have stated that the current state of knowledge on H_3^+ recombination is unsatisfactory and pointed out the need for further state-selective experimental studies at low temperatures with well-defined conditions and with several experimental techniques.^{8,12} In astrochemistry, if para- H_3^+ really recombines faster than ortho- H_3^+ at temperatures below 200 K, the current models of rotational thermalization of H_3^+ ions and H_2 molecules in molecular clouds would have to be reformulated.^{8,36} Astronomical observations of diffuse molecular clouds indicate that the population of fast recombining para- H_3^+ ions is higher than thermal.³⁷ This seriously questions generally accepted cosmic ray ionization rate of H_2 molecules.^{8,38} Further experimental studies on nuclear spin specificity of rate coefficients of H_3^+ recombination with electron at temperatures below 200 K are needed and, if they confirm previous experimental results, they may require changes in the quantum-mechanical description of the recombination processes and a reevaluation of fundamental aspects of interstellar gas-phase chemistry.

This article contributes new experimental values of the state selected recombination rate coefficients ${}^p\alpha_{\text{bin}}$ and ${}^o\alpha_{\text{bin}}$ measured using our ‘‘Cryogenic Flowing Afterglow with Langmuir Probe’’ instrument (Cryo-FALP II) in the temperature range from 60 K to 210 K. In addition, we added new data to those of our previous SA-CRDS experiments in the temperature range from 80 K to 300 K. The two methods have different strengths and weaknesses: In the SA-CRDS afterglow, the electron and ion densities are sufficiently high ($\approx 3 \times 10^{10} \text{ cm}^{-3}$ at the onset of the afterglow phase) to infer recombination rates directly from *in situ* determinations of the density decays of para- and ortho- H_3^+ by optical absorption. In the Cryo-FALP II apparatus, the electron and ion densities are much lower ($\approx 5 \times 10^8 \text{ cm}^{-3}$) and optical absorption measurements are not practical. Here, the recombination rates are inferred from the decay of the electron density measured by a Langmuir probe. In combined experiments, the relative concentrations of para- and ortho- H_3^+ ions are taken from the SA-CRDS data, measured at the same temperature and using the same hydrogen gas (either normal or para-enriched).

The higher electron densities in the SA-CRDS afterglow, however, can also enhance recombination by electron-assisted collisional radiative recombination (E-CRR), especially at very low temperatures because E-CRR depends very strongly on electron temperature (as $T_e^{-4.5}$). The SA-CRDS method is subject to a possible further problem: The discharge that produces the plasma can excite molecules (e.g., form vibrationally excited H_2). Some of them can survive into the afterglow phase and then transfer energy to the electron gas. In the Cryo-FALP II apparatus, the discharge region contains only helium and is well separated from the recombination region. These shortcomings of the SA-CRDS method were the main reasons why we decided to check and augment our earlier SA-CRDS measurements by similar measurements using Cryo-FALP II. As we will discuss later, the important conclusions remain the same as those reached earlier, namely, that at low temperatures, para- H_3^+ ions recombine with electrons much faster than ortho- H_3^+ ions.

In Sec. II, we will first describe the Cryo-FALP II apparatus, the para-hydrogen generator, and the SA-CRDS apparatus. After presenting results from SA-CRDS, we will discuss thermalization of H_3^+ ions in He/Ar/ H_2 afterglow plasmas. The thermalization of electrons in the flowing afterglow plasma will be discussed in Sec. III. Determinations of state-specific recombination rate coefficients of H_3^+ ions will be discussed in Sec. IV. The temperature dependence of the recombination rate coefficients ${}^p\alpha_{\text{bin}}$ and ${}^o\alpha_{\text{bin}}$ of the state selected para- H_3^+ and ortho- H_3^+ will be presented in Sec. V.

II. EXPERIMENTAL DETAILS

A. Cryo-FALP II

The Cryo-FALP II (see Fig. 1) is a cryogenic high pressure modification of the FALP instrument,^{6,39,40} whose technical details have been described earlier.^{27,29,30,41} A movable cylindrical Langmuir probe (a 7 mm long tungsten wire, 18 μm in diameter) records the electron density^{23,42,43} along the flow-tube axis (see Fig. 1). The three sections of the flow tube

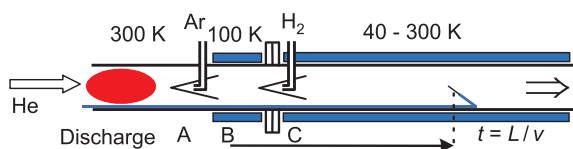


FIG. 1. The Cryo-FALP II apparatus (not to scale). The helium gas first passes through the microwave discharge. Ar and H₂ are added via two inlets located in the upstream part of sections B and C, respectively. The inner diameters of sections B and C are 5 cm. Section C, thermally insulated by a vacuum housing, is cooled by a closed-cycle helium refrigerator to adjustable temperatures down to 40 K. The electron density in section C is measured by the axially movable Langmuir probe.

(A–C) have different wall temperatures. Section A (made from Quartz) contains the microwave discharge and has a temperature of 300 K, section B is cooled to 100 K, while the temperature in the final section C can be varied from 40 K to 300 K, denoted as T_{wall} in the following. The Langmuir probe can measure the electron density from the end of section B (position $L = 0$), passing through the connection of B and C (position $L = 5$ cm) and along section C.

A microwave discharge, ignited in helium buffer gas (with a number density $[\text{He}] \approx 10^{16} - 10^{18} \text{ cm}^{-3}$) at the beginning of the section A of the flow tube, forms a plasma consisting of helium metastable atoms He^m , He^+ , and He_2^+ ions. The plasma is carried by the helium flow downstream to section B where argon is added through an inlet (facing upstream to enhance gas mixing) at a density $[\text{Ar}] \approx 1.5 \times 10^{13} \text{ cm}^{-3}$ in order to convert the He_2^+ ions by charge transfer reactions to Ar^+ ions. The metastables He^m are converted to Ar^+ ions by Penning ionization. This standard method has been described repeatedly (see, e.g., Ref. 23). Under the conditions of the experiment, the destruction of He^m is essentially complete³⁹ in section B, even if the argon gas takes a finite time to blend into the helium flow (the so-called “end-effect”⁴⁴).

The plasma then flows into section C of the flow tube that is cooled by a closed-cycle helium refrigerator to the desired temperature. At the beginning of section C (position $L = 5.5$ cm), either normal H₂ ($^n\text{H}_2$) or para-enriched H₂ ($^e\text{H}_2$) is introduced (at typical densities $[\text{H}_2] \approx 10^{12} - 10^{13} \text{ cm}^{-3}$). The hydrogen mixes with the helium buffer gas and ion molecule reactions of Ar^+ ions with H₂ then form the recombining H_3^+ ions.^{23,43} After the “transition region” (position $L = 5$ to 10 cm), the plasma becomes increasingly dominated by H_3^+ ions. In this region, the gas also cools down to T_{wall} of section C. The thermalization of the gas can be observed by measuring the velocity of the gas (see Ref. 29). The measurements are carried out in the thermally equilibrated plasma.

We routinely employ a numerical model of the kinetic processes in the data analysis and to optimize conditions prior to every experiment (details can be found, e.g., in Refs. 23 and 31).

Our earlier studies^{27–29} of E–CRR of Ar^+ ions proved that electrons and ions are in thermal equilibrium with the neutral gases in the recombination region and the same should be true in the present experiment. The hydrogen in the Cryo-FALP II experiment is never directly exposed to a microwave discharge and delayed heat sources, such as vibrationally excited hydrogen, are absent.

Rotational and vibrational modes of the formed H_3^+ ions are thermalized in subsequent collisions with He and H₂. This was shown in earlier SA-CRDS studies of the kinetic and rotational temperatures of H_3^+ ions under conditions similar to those in section C of the flow tube.^{19,21,22}

B. Para-hydrogen generator

We will denote the relative concentrations of para-H₂ hydrogen ($^p\text{H}_2$) and ortho-H₂ hydrogen ($^o\text{H}_2$) by $^p f_2$ and $^o f_2$, respectively. In normal hydrogen ($^n\text{H}_2$) $^p f_2 = 0.25$ and $^o f_2 = 0.75$. The symbol $^e\text{H}_2$ denotes para-enriched H₂ gas with $^p f_2 \approx 0.995$. The para-enriched hydrogen gas is produced using a “para-hydrogen generator” that converts $^o\text{H}_2$ to $^p\text{H}_2$ on a paramagnetic surface (thermally dehydrated HFeO_2 , CAS number 20344–49–4), cooled down in a cryostat to temperatures 10–18 K.^{45,46} In our experiment, $^n\text{H}_2$ is liquefied in the catalyst container and the saturated vapor of converted gas ($^e\text{H}_2$) is collected through an outlet tube that transfers it to the hydrogen ports of the Cryo-FALP II or the SA-CRDS. The flow of $^e\text{H}_2$ is controlled by varying the temperature of the catalyst container, i.e., by changing its vapor pressure. This configuration has been proved to provide a well-defined and constant value of $^p\text{H}_2$ equaling to $(99.5 \pm 0.5)\%$, which is the value obtained by measurement of the temperature dependence of the $\text{N}^+ + \text{H}_2$ reaction rate coefficient in an ion trap.⁴⁷ Only two flow-limiting valves are placed in the transfer tube to Cryo-FALP II or SA-CRDS to minimize para-to-ortho back conversion. If desired, the value of $^p f_2$ can be reduced by diluting $^e\text{H}_2$ with normal hydrogen $^n\text{H}_2$.⁴⁷

C. SA-CRDS. Measurements of kinetic and rotational temperatures and nuclear spin state of H_3^+ ions in the afterglow plasma

We denote the relative populations of para- H_3^+ ($^p\text{H}_3^+$) and ortho- H_3^+ ($^o\text{H}_3^+$) ions in an ensemble of H_3^+ ions by $^p f_3$ and $^o f_3$ with $^p f_3 + ^o f_3 = 1$. Several studies of $^p f_3$ and $^o f_3$ in low-temperature hydrogen plasmas have been conducted (see, e.g., Refs. 22, 48, and 49). In our recent SA-CRDS experiments, we systematically measured $^p f_3$ fractions during the active discharge and during the afterglow in He/Ar/H₂ mixtures similar to those used in the present work. We used $^n\text{H}_2$ or nearly pure $^p\text{H}_2$ and sometimes mixtures of $^n\text{H}_2$ and $^e\text{H}_2$ in order to obtain the desired value of $^p f_2$. The data measured during the recombination dominated afterglow in SA-CRDS experiments indicated that the values of $^p f_3$ are nearly independent on $[\text{He}]$ and $[\text{H}_2]$ in the density range covered by the experiments (see Figs. 3 and 4 in Ref. 50). The SA-CRDS experiments were carried out at temperatures 77–300 K. The absorption on two para-states and two ortho-states was used to monitor densities of para- H_3^+ and ortho- H_3^+ ions during the discharge and during the afterglow in SA-CRDS. The following second overtone transitions were used: $\text{P}(2,2) : 3v_2^1(1,2) \leftarrow 0v_2^0(2,2)$; $\text{R}(3,3)^1 : 3v_2^1(4,3) \leftarrow 0v_2^0(3,3)$; $\text{R}(1,1)^u : 3v_2^1(2,1) \leftarrow 0v_2^0(1,1)$; $\text{R}(1,0) : 3v_2^1(2,0) \leftarrow 0v_2^0(1,0)$. The levels are labeled by their corresponding quantum numbers (J,G) (see Ref. 51). Further details of the CRDS technique used in recombination studies are given in Refs. 19, 21, 25, and 52.

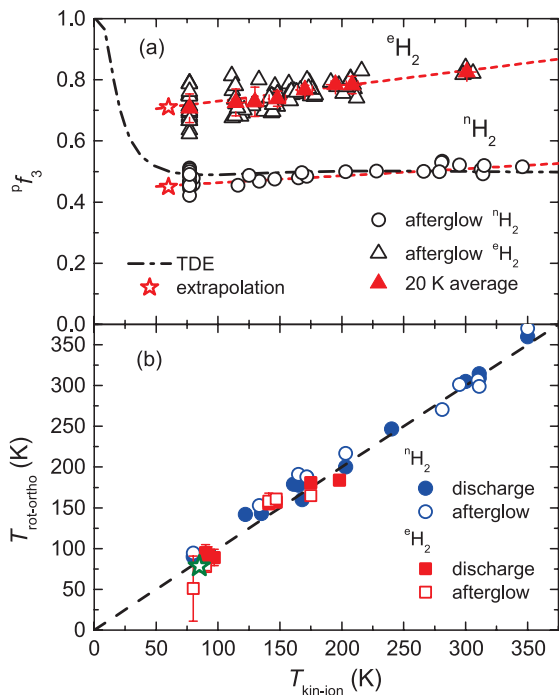


FIG. 2. SA-CRDS data. Panel (a) The temperature dependence of fraction Pf_3 of para- H_3^+ using either nH_2 or eH_2 as a precursor gas. Data were obtained during the early afterglow (empty symbols). To obtain average values, the temperature scale was divided into bins of length of 20 K and the values of Pf_3 measured in eH_2 were averaged within each bin. The resulting 20 K averages are denoted by full triangles. The dashed-dotted line indicates Pf_3 calculated for thermodynamic equilibrium. Linear extrapolation of the Pf_3 data to 60 K along the dashed lines results in the values (star symbols) used in the analysis of Cryo-FALP II data at 60 K. Panel (b) The dependence of the rotational temperature $T_{rot-ortho}$ calculated from measured relative populations of $^oH_3^+$ (1,0) and $^eH_3^+$ (3,3) states of the H_3^+ ion on kinetic temperature of the ions $T_{kin-ion}$. New data were added to the previously measured values.¹⁹ The green star denotes the rotational temperature $T_{rot-para}$ obtained from the measured populations of two para-states ($^pH_3^+$ (1,1) and $^pH_3^+$ (2,2)) in the afterglow plasma at 77 K in experiments with eH_2 . The dashed line indicates equality $T_{rot} = T_{kin-ion}$.

The CRDS absorption data yield the densities of ions in particular states, their kinetic and rotational temperatures and the dependence of the fractions Pf_3 on wall temperature T_{wall} and the para-fraction of hydrogen Pf_2 (see panel (a) of Fig. 2). The kinetic temperature ($T_{kin-ion}$) of H_3^+ ions was determined from the Doppler broadening of the absorption lines. The conclusion from these studies is that in very good approximation $T_{kin-ion} = T_{wall}$, this implies also that $T_{wall} = T_{He}$. The present experiments with SA-CRDS confirm the results of earlier work (see, e.g., Fig. 1 in Ref. 21 and Figs. 5, 7, and 8 in Ref. 19) showing that Pf_3 is nearly time independent during the afterglow phase. Most importantly, it is evident that Pf_3 is enhanced when enriched hydrogen is the precursor gas²² and that Pf_3 depends only weakly on temperature in the range from 77 K to 300 K. Examples of data measured during the afterglow in experiments with nH_2 or eH_2 as a precursor gas are shown in panel (a) of Fig. 2. In the present study, we also confirmed previous result that the values of Pf_3 measured during the discharge and during the afterglow are nearly the same.

The rotational temperature $T_{rot-ortho}$ was determined by measuring densities of ions in two rotational states of the

ortho manifold. In some experiments, the discharge tube was immersed in liquid nitrogen ($T_{wall} = 77$ K) and the rotational temperature for the para-manifold $T_{rot-para}$ was also determined. The dependence of the measured T_{rot} on the measured $T_{kin-ion}$ is plotted in panel (b) of Fig. 2. It is obvious that the two temperatures are essentially the same.

From the experiments with SA-CRDS, we concluded that the H_3^+ ions in the afterglow plasma are very close to thermal equilibrium with the helium buffer gas, which in turn is in good thermal contact with the wall of the discharge tube. Hence, we are justified in assuming that $T = T_{wall} = T_{He} = T_{rot} = T_{kin-ion}$. Because of the relatively high He density and very low microwave power used for plasma generation, the same assumption can be made for the plasma in the discharge just before termination of the microwave pulse. The experimental data confirm this conclusion (see Fig. 2). Although this is not crucial for the recombination measurements, we note that the ion temperature varies slowly during the transition from the active discharge to the afterglow. In contrast, the electron temperature changes rather abruptly.

An experimental verification of the thermal equilibrium assumption is essential in the analysis of the SA-CRDS measurements because otherwise total ion densities and electron densities in SA-CRDS could not be inferred from the measured absorption strengths of particular transitions. Also, the separation of the measured effective recombination coefficient into the components due to para- H_3^+ and ortho- H_3^+ is possible only if the relative fractions of the two species remain constant during the afterglow, even if one species recombines faster than the other.

III. ELECTRON TEMPERATURE IN HE/AR/H₂ AFTERGLOW PLASMA IN CRYO-FALP II

The electron temperature, T_e , is a key plasma parameter but there is no simple direct way of measuring it with good accuracy at low temperatures. Measurements of ambipolar diffusion losses in the late afterglow provide a reasonably accurate “proxy thermometer.” The reciprocal time constant describing the ambipolar diffusion loss in a container with fundamental diffusion length Λ can be derived from the basic relations contained in the book of Mason and McDaniel⁵³ as

$$\frac{1}{\tau_D} = 4.63 \times 10^{15} \frac{K_0(T)}{\Lambda^2} \frac{T}{[He]} \text{ s}^{-1}, \quad (3)$$

where $K_0(T)$ is the reduced mobility of the ion (in units $\text{cm}^2 \text{ V}^{-1} \text{ s}^{-1}$), the fundamental diffusion length Λ is in cm, temperature T in K, and helium number density $[He]$ in cm^{-3} . For cylindrical geometry, the value of Λ can be calculated⁵³ as $1/\Lambda^2 = (J_0/r)^2 + (\pi/l)^2$, where J_0 is the first root of the zeroth order Bessel function, $J_0 \approx 2.405$, r is the radius of the flow tube, and l is the length of the flow tube. In our case, $r = 2.5$ cm, $l \approx 60$ cm, and $\Lambda^2 = 1.1 \text{ cm}^2$. If measurements of τ_D in the late afterglow (after recombination becomes negligible) agree with this formula, then one can conclude that the electron and neutral temperatures are nearly equal.

We have used the same method successfully in our Cryo-FALP II measurements of E-CRR and helium-assisted collisional radiative recombination (He-CRR) of Ar^+ ions.^{27–29} The

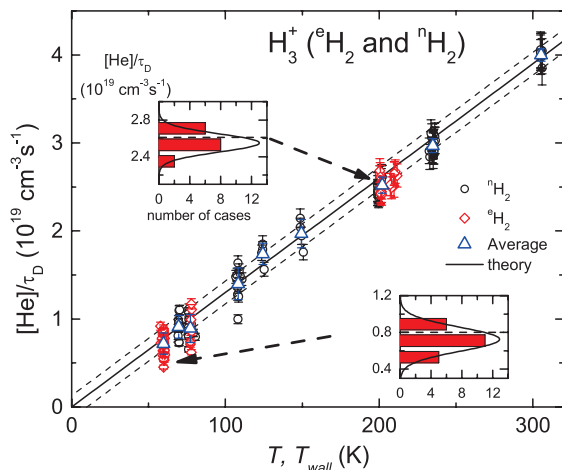


FIG. 3. Cryo-FALP II data. The measured reciprocal time constant of ambipolar diffusion losses $[\text{He}]/\tau_D$ as a function of the wall temperature (T_{wall}). Circle and diamond symbols: data obtained using ${}^{\text{p}}\text{H}_2$ or ${}^{\text{o}}\text{H}_2$, respectively. Triangles: average values at a particular temperature. Solid line: values calculated from Eq. (3) as a function of the temperature $T = T_{\text{wall}}$. Dashed lines: the same as the solid line but calculated for alternate temperatures $T_e = T_{\text{wall}} \pm 20$ K. Insets: frequency distribution of the data at $T_{\text{wall}} = 60$ K and $T_{\text{wall}} = (204 \pm 3)$ K, fitted to a normal distribution. The width of each bin is $1.8 \times 10^{18} \text{ cm}^{-3} \text{ s}^{-1}$. The dashed lines refer to the calculated value of $[\text{He}]/\tau_D$ at a given temperature.

ternary rate coefficients of both processes depend very strongly on electron temperature ($K_{\text{E-CRR}} \propto T_e^{-4.5}$, $K_{\text{He-CRR}} \propto T_e^{-2.5}$) so that measurements of their values provide a sensitive test of the electron-temperature scale.^{19,27–29,54} It was found that the electron temperature was always close to the gas temperature within a few kelvins.

The same type of measurement of diffusion losses in H_3^+ afterglows using Cryo-FALP II yielded the graph in Fig. 3. The data follow the calculated line very well, but the data scatter at the lowest temperatures and high helium densities is noticeably worse. This is a consequence of the fact that the diffusion rate becomes very small and that recombination in the late afterglow is not entirely negligible. The full line is calculated using a zero-field reduced mobility of $K_0(300 \text{ K}) = 30.5 \text{ cm}^2 \text{ V}^{-1} \text{ s}^{-1}$, adopted from Ref. 55. To show the sensitivity to small deviations in temperature, we also calculated alternate values of $[\text{He}]/\tau_D$ for $T_e \pm 20$ K (the dashed lines). There was no detectable difference between experiments with ${}^{\text{p}}\text{H}_2$ and ${}^{\text{o}}\text{H}_2$ that are distinguished by different symbols, circles, and diamonds.

The data presented in Figs. 2 and 3 support the assumption that the various temperatures in the Cryo-FALP II afterglow have a common value, i.e., that $T = T_{\text{wall}} = T_{\text{He}} = T_{\text{rot}} = T_{\text{kin-ion}} = T_e$. The rotational states are in equilibrium within the para- H_3^+ or the ortho- H_3^+ nuclear spin manifolds, but because of nuclear spin restrictions in the reactions of ${}^{\text{p/o}}\text{H}_2$ with ${}^{\text{p/o}}\text{H}_3^+$, the fraction ${}^{\text{p}}f_3$ also depends on the ${}^{\text{p}}f_2$ value of the used hydrogen gas. The value of ${}^{\text{p}}f_3$ corresponds to the thermodynamic equilibrium (TDE) only for experiments with ${}^{\text{p}}\text{H}_2$ and only at temperatures above ≈ 77 K (see panel (a) of Fig. 2 and also Figs. 7 and 8 in Ref. 22). We stress that our experimental verification that $T_e = T_{\text{He}}$ is important. One could reach the same conclusion by considering only elastic energy transfer between electrons and helium atoms,

which is quite efficient at the experimental helium densities, but this leaves out possible electron heating by superelastic collisions with remaining metastable helium atoms and excited argon atoms. Such heat sources do not seem to play a role in the Cryo-FALP II experiments, as we had concluded earlier from our experiments on E-CRR and He-CRR.^{27–29} We should also note, however, that the same may not be true in SA-CRDS measurements (see also the discussion in Sec. V B).

IV. DETERMINATION OF STATE-SPECIFIC RECOMBINATION RATE COEFFICIENTS

The methods of obtaining state-specific recombination rate coefficients are essentially identical in the Cryo-FALP II and in the SA-CRDS studies.^{19–21} In the Cryo-FALP II experiment, we measure the decay of the electron number density n_e by the Langmuir probe but the values of ${}^{\text{p}}f_3 = {}^{\text{p}}f_3({}^{\text{p}}f_2, T)$ are taken from the SA-CRDS studies. The effective recombination rate coefficient α_{eff} is defined by the relation,

$$\frac{dn_e}{dt} = -\alpha_{\text{eff}} n_e^2 - \frac{n_e}{\tau_D}, \quad (4)$$

where τ_D is the characteristic time of ambipolar diffusion. As usual, it is assumed that the afterglow plasma is quasineutral. The measured value of α_{eff} is a weighted sum of the effective recombination rate coefficients of ${}^{\text{p}}\text{H}_3^+$ and ${}^{\text{o}}\text{H}_3^+$ ions, i.e.,

$$\alpha_{\text{eff}} = {}^{\text{p}}f_3 {}^{\text{p}}\alpha_{\text{eff}} + {}^{\text{o}}f_3 {}^{\text{o}}\alpha_{\text{eff}}, \quad (5)$$

where ${}^{\text{p}}\alpha_{\text{eff}}$ and ${}^{\text{o}}\alpha_{\text{eff}}$ are the effective recombination rate coefficients of pure ${}^{\text{p}}\text{H}_3^+$ and pure ${}^{\text{o}}\text{H}_3^+$, respectively. Both ${}^{\text{p}}\alpha_{\text{eff}}$ and ${}^{\text{o}}\alpha_{\text{eff}}$ can then be obtained from measurements of α_{eff} (H_3^+) for two or more different values of ${}^{\text{p}}f_3$. These values are still “effective” values and are not necessarily equal to the corresponding binary recombination coefficients.

Examples of the electron-density decays measured in experiments at $T = 60$ K with ${}^{\text{o}}\text{H}_2$ and ${}^{\text{p}}\text{H}_2$ are shown in Figure 4. The electron densities are plotted as functions of the Langmuir probe position L and the equivalent afterglow time $t = v/L$, where v is the plasma flow velocity.²⁹ All recombination measurements are carried out in the thermally equilibrated plasma where H_3^+ decays mainly by recombination and diffusion to the walls, as is assumed in Eq. (4). Panel (a) of Figure 4 only shows the time evolutions of electron densities in this region. Note that losses due to recombination and due to diffusion are comparable.

The desired binary recombination coefficients are obtained by extrapolating values of α_{eff} measured at different hydrogen and helium densities to zero densities. We have suggested possible mechanisms leading to density dependences earlier (see Refs. 26 and 31) but this is not essential for the present work and we omit the details. Fig. 5 shows an example of the dependence of α_{eff} (observed at 60 K) on hydrogen density at different fixed helium densities, while Fig. 6 shows the dependence of α_{eff} on helium density for fixed hydrogen densities. Linear extrapolations to zero densities of He and H_2 yield binary recombination coefficients at 60 K that are larger when enriched hydrogen is substituted for normal hydrogen. The data sets measured in Cryo-FALP II at higher

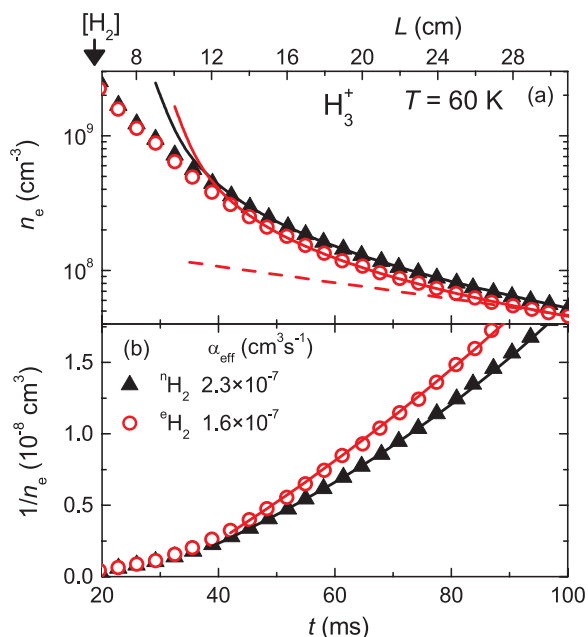


FIG. 4. Cryo-FALP II data. Panel (a) Examples of electron density n_e decays, as measured by the movable Langmuir probe, observed when H_3^+ ions are formed by reactions with either normal (nH_2 , triangles) or para-enriched hydrogen (eH_2 , circles). Time (t , lower axis) and position (L , upper axis) are related by the helium flow velocity.²⁹ The arrow indicates the position of the hydrogen entry port at the beginning of the section C of the flow tube (see Fig. 1). The full lines are fits to the data (for details on data analysis, see Ref. 42). The dashed line indicates the decay due to ambipolar diffusion losses for the experiment with eH_2 . Panel (b) The time evolutions of the reciprocal electron number density ($1/n_e$). The data were obtained at $T = 60$ K, $P_{He} = 480$ Pa, $[Ar] = 1.6 \times 10^{13} \text{ cm}^{-3}$, $[^nH_2] = 1.5 \times 10^{12} \text{ cm}^{-3}$, $[^eH_2] = 1.0 \times 10^{12} \text{ cm}^{-3}$.

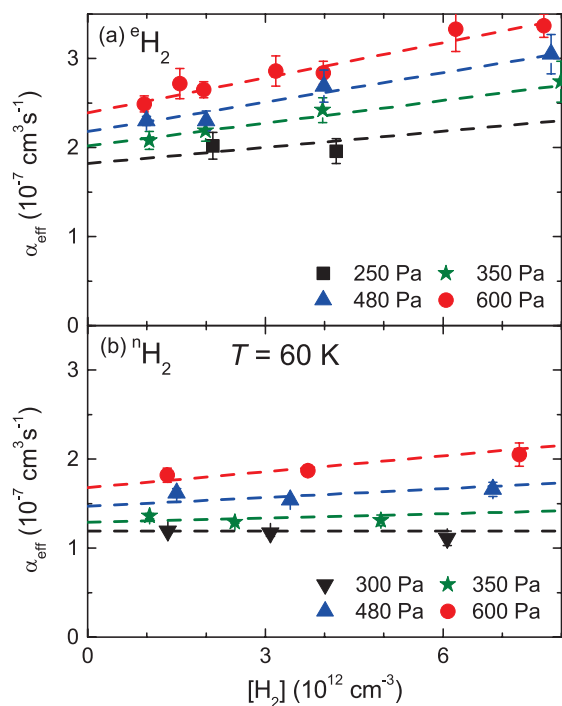


FIG. 5. Cryo-FALP II data. Dependence of α_{eff} on H_2 density measured at 60 K at the indicated pressures of helium. Panels (a) and (b) show data measured in the experiments with eH_2 and nH_2 , respectively.

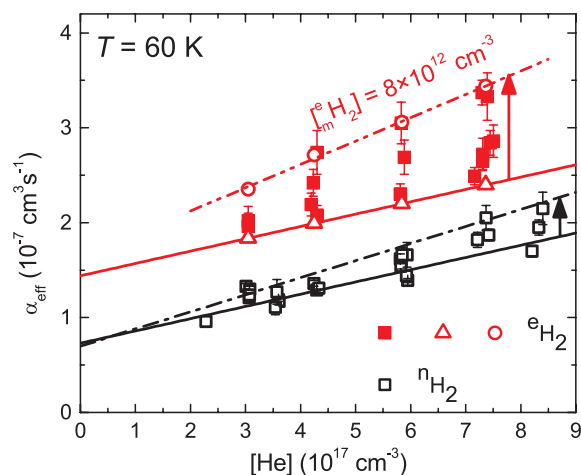


FIG. 6. Cryo-FALP II data. Dependence of α_{eff} at $T = 60$ K on helium density in experiments with eH_2 (full squares) and with nH_2 (open squares). The arrows indicate the increase of α_{eff} with increasing density of H_2 at fixed $[He]$. Open triangles and open circles indicate values obtained at the limits for $[^eH_2] \rightarrow 0$ and $[^eH_2] \rightarrow 8 \times 10^{12} \text{ cm}^{-3}$, respectively. The solid lines are linear fits of the data measured at low hydrogen densities. Dashed-dotted-dotted and dashed-dotted lines are fits of the data at high hydrogen density, in the experiment with eH_2 and nH_2 , respectively.

temperatures (78 K and 210 K) are similar to the 60 K data but the difference between data with normal and enriched hydrogen becomes smaller as T increases.

The dependence of α_{eff} on $[He]$ and on $[H_2]$ shown in Figs. 5 and 6 is actually somewhat more complex than it appears in Figs. 5 and 6. To illustrate this, we also plotted the same data in the form of a 3-dimensional graph, shown in Fig. 7. The data are fitted by the equation

$${}^{e/n}\alpha_{\text{eff}} = {}^{e/n}\alpha_{\text{bin}} + {}^{e/n}\xi_1[He] + {}^{e/n}\xi_2[H_2] + {}^{e/n}\xi_3[He][H_2], \quad (6)$$

where ${}^{e/n}\xi_1$, ${}^{e/n}\xi_2$, and ${}^{e/n}\xi_3$ are constants at a given temperature. The superscripts refer to the type of hydrogen used in the

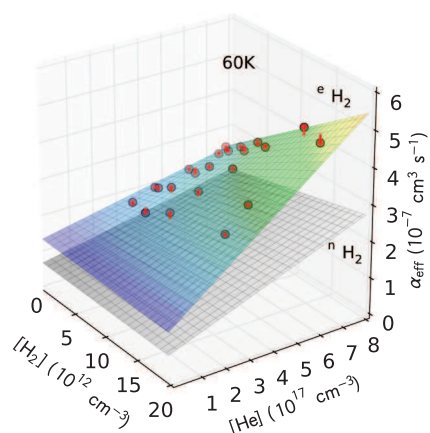


FIG. 7. Cryo-FALP II data. Dependence of ${}^{e/n}\alpha_{\text{eff}}$ and ${}^n\alpha_{\text{eff}}$ on $[He]$ and $[H_2]$ measured at $T = 60$ K in experiments with eH_2 and with nH_2 , respectively. The upper surface is a fit of Eq. (6) to the data (indicated by circles) obtained with eH_2 . The lower surface represents a fit of Eq. (6) to the data obtained from the surfaces by amounts on the order $< 2 \times 10^{-8} \text{ cm}^3 \text{ s}^{-1}$ as is shown by red lines connecting the data points with the plane. The parameters of the fits are listed in Table I.

TABLE I. The fitting parameters ξ_1 , ξ_2 , and ξ_3 for the data obtained at $T = 60$ K in experiments with $^n\text{H}_2$ and $^e\text{H}_2$ hydrogen (see Figure 7). Values ξ_1 , ξ_2 , and ξ_3 are given in format $\xi_{i0}(m)$ indicating $\xi_i = \xi_{i0} \times 10^m$. For comparison, the values $^e/n\alpha_{\text{bin}}$ and contributions from $\xi_1[\text{He}]$, $\xi_2[\text{H}_2]$, and $\xi_3[\text{H}_2][\text{He}]$ terms are given in units $10^{-7} \text{ cm}^3 \text{ s}^{-1}$. The values are deduced from Equation (6) using fitting parameters ξ_1 , ξ_2 , ξ_3 for typical densities of H_2 and He , $[\text{He}] = 5 \times 10^{17} \text{ cm}^{-3}$, $[\text{H}_2] = 5 \times 10^{12} \text{ cm}^{-3}$.

60 K gas	$^e/n\alpha_{\text{bin}}$ ($10^{-7} \text{ cm}^3 \text{ s}^{-1}$)	$\xi_1[\text{He}]$ ($10^{-7} \text{ cm}^3 \text{ s}^{-1}$)	$\xi_2[\text{H}_2]$ ($10^{-7} \text{ cm}^3 \text{ s}^{-1}$)	$\xi_3[\text{H}_2][\text{He}]$ ($10^{-7} \text{ cm}^3 \text{ s}^{-1}$)	ξ_1 ($\text{cm}^6 \text{ s}^{-1}$)	ξ_2 ($\text{cm}^6 \text{ s}^{-1}$)	ξ_3 ($\text{cm}^9 \text{ s}^{-1}$)
$^n\text{H}_2$	0.75	0.65	7.0(-12)	0.15	1.29(-25)	1.4(-31)	5.8(-39)
$^e\text{H}_2$	1.44	0.66	-1.5(-12)	0.45	1.32(-25)	-3.0(-32)	1.8(-38)

experiment. The binary values $^e\alpha_{\text{bin}}$ and $^n\alpha_{\text{bin}}$ are those in the limits $[\text{He}] \rightarrow 0$ and $[\text{H}_2] \rightarrow 0$.

The fitting parameters for the data measured at 60 K with $^n\text{H}_2$ and $^e\text{H}_2$ are given in Table I. Listed are also the contributions from all four terms of function (6) deduced for typical densities of H_2 and He in experiments ($[\text{He}] = 5 \times 10^{17} \text{ cm}^{-3}$, $[\text{H}_2] = 5 \times 10^{12} \text{ cm}^{-3}$). The contributions from the third term $\xi_2[\text{H}_2]$ are very low in comparison with contributions from other terms. The contribution from $\xi_3[\text{H}_2][\text{He}]$ is comparable with $^e/n\alpha_{\text{bin}}$ and with contribution from $\xi_1[\text{He}]$, and hence, the best-fitting surfaces are not planes but are slightly twisted. More twisted is the surface obtained from data measured with $^e\text{H}_2$. This may indicate the existence of a loss process that depends on the product $[\text{He}][\text{H}_2]$ and this process is more effective for $^e\text{H}_2$ (see also Fig. 6). It is possible that part of the observed recombination loss is due to H_5^+ ions that are formed by three-body association involving both helium and hydrogen, but the data do not allow a firm conclusion. The inference of the binary recombination rates is not affected by this ambiguity.

V. RESULTS AND DISCUSSION

A. Temperature dependence of the rate coefficients

Sections III and IV point out the experimental difficulties in measuring state specific binary recombination coefficients for H_3^+ in the two nuclear spin states. One needs large data sets at different gas densities and has little choice but to obtain the final result by extrapolation. In this section, we show that the results obtained by different methods are nevertheless quite consistent.

The results of the Cryo-FALP II measurements of $^p\alpha_{\text{bin}}$ and $^o\alpha_{\text{bin}}$ at different temperatures (60 K, 78 K, and 210 K) are compared to those obtained in the parallel SA-CRDS experiment in Fig. 8. The graph includes new SA-CRDS data of $^n\alpha_{\text{eff}}$ and $^e\alpha_{\text{eff}}$ at 115 K, 145 K, 180 K, and 300 K obtained by *in situ* determination of $^p f_3$ and data obtained in our earlier SA-CRDS experiments^{19-21,50} at temperatures 85 K, 140 K, 165 K, and 195 K. In addition, the graph shows values of $^n\alpha_{\text{eff}}$ measured in FALP, SA-CRDS, and Cryo-FALP II experiments with $^n\text{H}_2$ as precursor gas to form H_3^+ ions (see Ref. 41).

The rate coefficients $^p\alpha_{\text{bin}}$ and $^o\alpha_{\text{bin}}$ obtained in the Cryo-FALP II experiments are in good agreement with the values obtained in SA-CRDS experiments in the covered temperature range. In our previous studies, we also observed

agreement between values of $^n\alpha_{\text{bin}}$ measured by SA-CRDS and by FALP/Cryo-FALP II (see Ref. 41). This is particularly noteworthy because these two experiments differ greatly in the formation of the H_3^+ plasma, in the electron/ion densities, in the time scale of the plasma decay, and in the diagnostics used to determine the parameters of the afterglow plasma. Within the accuracy of the experimental data, there is also good agreement with the storage ring data at 300 K^{9,16} that are indicated by arrows on the right hand side of the graph. The values of $^p\alpha_{\text{bin}}$, $^o\alpha_{\text{bin}}$, and $^n\alpha_{\text{bin}}$ are given in the summarization of CRYRING data for 300 K in Ref. 13. At lower temperatures, there are no accurate data from storage rings to compare.¹⁵ Figure 8 also shows the theoretical temperature dependences of the binary recombination rate coefficients for pure para- H_3^+ , pure

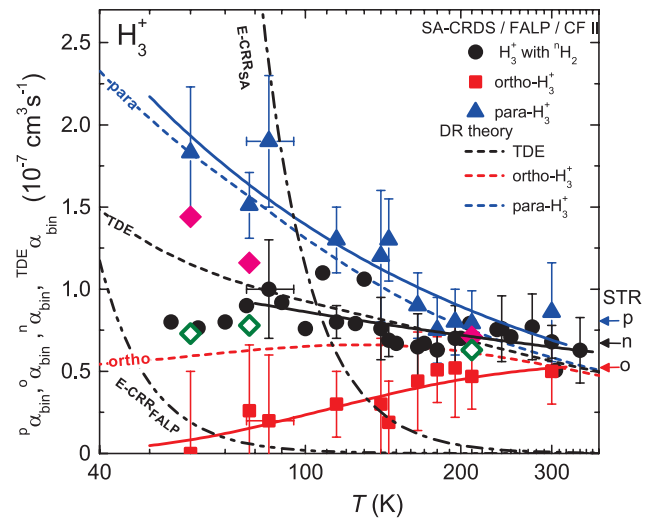


FIG. 8. Cryo-FALP II and SA-CRDS. Nuclear spin state-specific binary recombination rate coefficients measured in Cryo-FALP II, FALP, and SA-CRDS experiments. Triangles and squares indicate $^p\alpha_{\text{bin}}$ and $^o\alpha_{\text{bin}}$, respectively. The values at 85 K, 140 K, 165 K, and 195 K were taken from our previous experiments.¹⁹ The values of $^n\alpha_{\text{bin}}$ (circles) were measured in the Cryo-FALP II, FALP, and SA-CRDS experiments and some data were taken from our previous studies.^{19,41} The diamonds refer to $^n\alpha_{\text{bin}}$ (open diamonds) and $^e\alpha_{\text{bin}}$ (closed diamonds) measured in the present Cryo-FALP II experiment. The full lines are fits to $^p\alpha_{\text{bin}}$, $^o\alpha_{\text{bin}}$, and $^n\alpha_{\text{bin}}$ to the function in Eq. (7) that is used in astrophysical databases. For details and for the parameters of the fits see the text and Table II. The arrows on the right hand side of the figure denoted as p, o, and n indicate the values of $^p\alpha_{\text{bin}}$, $^o\alpha_{\text{bin}}$, and $^n\alpha_{\text{bin}}$ obtained in CRYRING,¹³ respectively. The dashed lines indicated as para, ortho, and thermodynamic equilibrium (TDE) are theoretical dependences for para- H_3^+ , ortho- H_3^+ , and for H_3^+ ions in TDE.^{33,35} The dashed-dotted lines E-CRDSA and E-CRR-FALP are effective binary rate coefficients of ternary E-CRR calculated for electron number densities $n_e(\text{SA-CRDS}) = 3 \times 10^{10} \text{ cm}^{-3}$ and $n_e(\text{Cryo-FALP II}) = 5 \times 10^8 \text{ cm}^{-3}$.^{19,27-29}

TABLE II. Parameters α_{A-K} , β , and γ of the fit by Arrhenius-Kooij formula (7). The values of ${}^p\alpha_{\text{bin}}$ and ${}^o\alpha_{\text{bin}}$ plotted in Fig. 8 were fitted for 60–300 K. The values of ${}^n\alpha_{\text{bin}}$ were fitted for 77–340 K. As it is discussed above (see Fig. 2), in this temperature range, the afterglow plasma with ${}^n\text{H}_2$ is in thermal equilibrium including the para to ortho H_3^+ ratio. The values of ${}^p\alpha_{\text{bin}}$ (300 K), ${}^o\alpha_{\text{bin}}$ (300 K), and ${}^{\text{TDE}}\alpha_{\text{bin}}$ (300 K) were measured in SA-CRDS experiment. The values of ${}^p\alpha_{\text{bin}}$ (60 K) and ${}^o\alpha_{\text{bin}}$ (60 K) for para- H_3^+ and ortho- H_3^+ were obtained from data measured in the Cryo-FALP II experiment. The value ${}^{\text{TDE}}\alpha_{\text{bin}}$ (60 K) for H_3^+ in TDE is calculated from the measured ${}^p\alpha_{\text{bin}}$ and ${}^o\alpha_{\text{bin}}$ and from ${}^p f_3$ calculated for H_3^+ in TDE at $T = 60$ K.

Ion	${}^p/{}^o/{}^{\text{TDE}}\alpha_{\text{bin}}$ (60 K) ($10^{-7} \text{ cm}^3 \text{ s}^{-1}$)	${}^p/{}^o/{}^{\text{TDE}}\alpha_{\text{bin}}$ (300 K) ($10^{-7} \text{ cm}^3 \text{ s}^{-1}$)	α_{A-K} ($10^{-7} \text{ cm}^3 \text{ s}^{-1}$)	β	γ (K)
Para- H_3^+	(1.8 ± 0.4)	(0.86 ± 0.30)	(0.69 ± 0.08)	(-0.64 ± 0.10)	0
Ortho- H_3^+	$(0.0^{+0.5}_{-0.0})$	(0.50 ± 0.20)	(0.97 ± 0.40)	(-0.41 ± 0.91)	(187 ± 143)
H_3^+ (TDE)	$(0.9^{+0.6}_{-0.4})$	(0.68 ± 0.10)	(0.65 ± 0.04)	(-0.26 ± 0.07)	0

ortho- H_3^+ , and for H_3^+ ions in TDE.^{33,35} The theoretical results of ${}^{\text{TDE}}\alpha_{\text{bin}}$ by Ch. Jungen and S. T. Pratt³⁴ are nearly identical and are not shown.

For compatibility of our results with databases used in astrophysics, the measured recombination rate coefficients are fitted by the Arrhenius-Kooij formula as used in the KIDA database,⁵⁶

$$k_{\text{Kooij}}(T) = \alpha_{A-K}(T/300 \text{ K})^\beta \exp(-\gamma/T), \quad (7)$$

where α_{A-K} , β , and γ are free parameters. The values k_{Kooij} and α_{A-K} are in $\text{cm}^3 \text{ s}^{-1}$, β is dimensionless, the temperature and the parameter γ are in K. The parameters of the fit of the values of ${}^p\alpha_{\text{bin}}$ and ${}^o\alpha_{\text{bin}}$ for temperatures 60–300 K and of the values of ${}^n\alpha_{\text{bin}}$ for 77–340 K are given in Table II. Together with actual values of ${}^n\alpha_{\text{bin}}$, ${}^p\alpha_{\text{bin}}$, and ${}^o\alpha_{\text{bin}}$ measured at 60 K and 300 K. Note that parameters α_{A-K} , β , and γ are different for para- H_3^+ , ortho- H_3^+ , and H_3^+ in TDE. The corresponding values of $k_{\text{Kooij}}(T)$ calculated from Eq. (7) are plotted in Fig. 8 as full lines.

B. Possible contribution of E-CRR in recombination of H_3^+

It is well known that recombination in low-temperature plasmas can also occur by E-CRR that proceeds by three-body electron capture into high Rydberg states and subsequent cascading to lower Rydberg states. The effective (apparent) binary rate coefficients, $\alpha_{\text{E-CRR}} \sim 3.8 \times 10^{-9} n_e T_e^{-4.5} \text{ cm}^3 \text{ s}^{-1}$,^{27–29,54} are indicated by the dashed-dotted lines in Fig. 8 for typical electron densities in the SA-CRDS ($n_e(\text{SA-CRDS}) = 3 \times 10^{10} \text{ cm}^{-3}$) and in the Cryo-FALP II ($n_e(\text{Cryo-FALP II}) = 5 \times 10^8 \text{ cm}^{-3}$) experiments. At the higher electron densities in the SA-CRDS experiment, the effective binary E-CRR recombination rate coefficient actually becomes larger than our measured values at temperatures below $T \approx 100$ K, which is peculiar and rather disturbing. In the Cryo-FALP II experiment, the electron densities are smaller by a factor of 60 and E-CRR should be nearly negligible. Both experiments, however, give almost the same values for the H_3^+ recombination rate coefficients. One, however unlikely, explanation might be that the formula for the E-CRR recombination is not valid at low temperatures. This explanation was ruled out by our recent experiments on E-CRR of atomic Ar^+ ions using Cryo-FALP II^{28,29} which

confirmed the standard E-CRR formula at low temperatures down to 50 K. These experiments leave open the possibility that E-CRR of a molecular ion, such as H_3^+ , is much slower than that of atomic ions. To the best of our knowledge, there are no pertinent experiments or theories that support or refute such an *ad hoc* assumption. It is also possible and perhaps more likely that the electron temperatures in the SA-CRDS experiments were higher than the gas temperatures and that E-CRR was hence strongly reduced. In the Cryo-FALP II experiments, E-CRR should be absent and this was one reason why we performed them. We conclude that the main result of the present study is not affected by E-CRR and that ${}^p\alpha_{\text{bin}}$ is much larger than ${}^o\alpha_{\text{bin}}$.

C. Sources of errors

The random errors in the effective recombination rate coefficients measured in SA-CRDS and Cryo-FALP II experiments are less than 5%. In the Cryo-FALP II experiment, the main systematic errors arise from the evaluation of the electron number density by the Langmuir probe that is calibrated by measurements of a well-known rate coefficient of O_2^+ recombination.²⁷ The estimated uncertainty of recombination rate coefficients measured in Cryo-FALP II experiment is 20%. A systematic error of the SA-CRDS experiment arises from the uncertainty of the length of the plasma column and is on the order of 10%. The state specific recombination rate coefficients measured in the Cryo-FALP II experiment are also subject to errors originating from the uncertainty of ${}^p f_3$ which we estimated at 5% (in SA-CRDS experiment, the value of ${}^p f_3$ is measured directly).

VI. CONCLUSION

We measured nuclear spin state-specific H_3^+ recombination rate coefficients ${}^p\alpha_{\text{bin}}$ and ${}^o\alpha_{\text{bin}}$ for para- H_3^+ and ortho- H_3^+ in the temperature range 60–300 K employing Cryo-FALP II and SA-CRDS experiments. This is the first time that state selected recombination rate coefficients have been measured down to 60 K using a FALP type experiment with variable relative population of para- H_3^+ and ortho- H_3^+ . It is gratifying to note that results obtained by two distinct experiments and a combination of them are mutually consistent. As the temperature decreases, the difference between binary ${}^p\alpha_{\text{bin}}$ and

$^o\alpha_{\text{bin}}$ increases: at 60 K, para- H_3^+ recombines with an at least a factor of three higher rate coefficient than ortho- H_3^+ , $^p\alpha_{\text{bin}}(60 \text{ K}) = (1.8 \pm 0.4) \times 10^{-7} \text{ cm}^3 \text{ s}^{-1}$ vs. $^o\alpha_{\text{bin}}(60 \text{ K}) = (0_{-0}^{\pm 5}) \times 10^{-8} \text{ cm}^3 \text{ s}^{-1}$. The measured temperature dependence of $^{\text{TDE}}\alpha_{\text{bin}}$ for ions in TDE and $^p\alpha_{\text{bin}}$ and $^o\alpha_{\text{bin}}$ for pure para- H_3^+ and ortho- H_3^+ agrees well with modern theories.^{33–35} The existence of two groups of H_3^+ ions with very different recombination rate coefficients at low temperatures should be seriously considered in astrochemical models of the interstellar medium. The results presented here depend on an assumption that there are no unrecognized strong pressure dependences below the lowest experimental pressures. The seeming absence of E-CRR of H_3^+ ions in SA-CRDS experiment is also disturbing. Further experiments performed in an environment of lower pressures with negligible influence of three body effects (such as in the merged beams technique), under good control of the H_3^+ rotational temperature and ortho/para-populations, remain desirable as a verification in the future.

ACKNOWLEDGMENTS

This work was partly supported by Czech Science Foundation Project Nos. GACR P209/12/0233, GACR 14-14649P, and GACR 15-15077S and by Charles University in Prague Project Nos. GAUK 659112, GAUK 692214, GAUK 572214, UNCE 204020/2012, and SVV 260 090.

- ¹T. Oka, *Proc. Natl. Acad. Sci. U. S. A.* **103**, 12235 (2006).
- ²A. Dalgarno, in *Advances in Atomic, Molecular, and Optical Physics*, edited by B. Bederson and A. Dalgarno (Academic Press, 1994), Vol. 32, pp. 57–68.
- ³J. Tennyson, in *Handbook of Molecular Physics and Quantum Chemistry*, edited by S. Wilsom (Wiley, Chichester, 2003), Vol. 3, pp. 356–369.
- ⁴T. P. Snow and B. J. McCall, *Annu. Rev. Astron. Astrophys.* **44**, 367 (2006).
- ⁵T. Oka, in *Dissociative Recombination of Molecular Ions with Electrons*, edited by S. L. Guberman (Springer US, 2003), pp. 209–220.
- ⁶M. Larsson and A. E. Orel, *Dissociative Recombination of Molecular Ions* (Cambridge University Press, 2008).
- ⁷R. Johnsen and S. L. Guberman, in *Advances in Atomic, Molecular, and Optical Physics*, edited by P. B. E. Arimondo and C. Lin (Academic Press, 2010), Vol. 59, pp. 75–128.
- ⁸T. Albertsson, N. Indriolo, H. Kreckel, D. Semenov, K. N. Crabtree, and T. Henning, *Astrophys. J.* **787**, 44 (2014).
- ⁹H. Kreckel, M. Motsch, J. Mikosch, J. Glosík, R. Plašil, S. Altevogt, V. Andrianarijaona, H. Buhr, J. Hoffmann, L. Lammich, M. Lestinsky, I. Nevo, S. Novotny, D. A. Orlov, H. B. Pedersen, F. Sprenger, A. S. Terekhov, J. Toker, R. Wester, D. Gerlich, D. Schwalm, A. Wolf, and D. Zajfman, *Phys. Rev. Lett.* **95**, 263201 (2005).
- ¹⁰B. J. McCall, A. J. Huneycutt, R. J. Saykally, T. R. Geballe, N. Djuric, G. H. Dunn, J. Semaniak, O. Novotny, A. Al-Khalili, A. Ehlerding, F. Hellberg, S. Kalhori, A. Neau, R. Thomas, F. Osterdahl, and M. Larsson, *Nature* **422**, 500 (2003).
- ¹¹A. Wolf, H. Kreckel, L. Lammich, D. Strasser, J. Mikosch, J. Glosík, R. Plašil, S. Altevogt, V. Andrianarijaona, H. Buhr, J. Hoffmann, M. Lestinsky, I. Nevo, S. Novotny, D. Orlov, H. Pedersen, A. Terekhov, J. Toker, R. Wester, D. Gerlich, D. Schwalm, and D. Zajfman, *Philos. Trans. R. Soc., A* **364**, 2981 (2006).
- ¹²A. Pettrignani, H. Kreckel, M. H. Berg, S. Altevogt, D. Bing, H. Buhr, M. Froese, M. Grieser, J. Hoffmann, B. Jordon-Thaden, C. Krantz, M. B. Mendes, O. Novotný, S. Novotny, D. A. Orlov, S. Reinhardt, and A. Wolf, *J. Phys.: Conf. Ser.* **192**, 012022 (2009).
- ¹³B. A. Tom, V. Zhaunerchyk, M. B. Wiczer, A. A. Mills, K. N. Crabtree, M. Kaminska, W. D. Geppert, M. Hamberg, M. af Ugglas, E. Vigren, W. J. van der Zande, M. Larsson, R. D. Thomas, and B. J. McCall, *J. Chem. Phys.* **130**, 031101 (2009).
- ¹⁴H. Kreckel, O. Novotný, K. N. Crabtree, H. Buhr, A. Pettrignani, B. A. Tom, R. D. Thomas, M. H. Berg, D. Bing, M. Grieser, C. Krantz, M. Lestinsky, M. B. Mendes, C. Nordhorn, R. Repnow, J. Stützel, A. Wolf, and B. J. McCall, *Phys. Rev. A* **82**, 042715 (2010).
- ¹⁵A. Pettrignani, S. Altevogt, M. H. Berg, D. Bing, M. Grieser, J. Hoffmann, B. Jordon-Thaden, C. Krantz, M. B. Mendes, O. Novotný, S. Novotny, D. A. Orlov, R. Repnow, T. Sorg, J. Stützel, A. Wolf, H. Buhr, H. Kreckel, V. Kokoouline, and C. H. Greene, *Phys. Rev. A* **83**, 032711 (2011).
- ¹⁶B. J. McCall, A. J. Huneycutt, R. J. Saykally, N. Djuric, G. H. Dunn, J. Semaniak, O. Novotný, A. Al-Khalili, A. Ehlerding, F. Hellberg, S. Kalhori, A. Neau, R. D. Thomas, A. Paal, F. Osterdahl, and M. Larsson, *Phys. Rev. A* **70**, 052716 (2004).
- ¹⁷M. Larsson, *Philos. Trans. R. Soc., A* **370**, 5118 (2012).
- ¹⁸H. Kreckel, A. Pettrignani, O. Novotný, K. Crabtree, H. Buhr, B. J. McCall, and A. Wolf, *Philos. Trans. R. Soc., A* **370**, 5088 (2012).
- ¹⁹P. Dohnal, M. Hejduk, J. Varju, P. Rubovič, Š. Roučka, T. Kotřík, R. Plašil, J. Glosík, and R. Johnsen, *J. Chem. Phys.* **136**, 244304 (2012).
- ²⁰P. Dohnal, M. Hejduk, J. Varju, P. Rubovič, Š. Roučka, T. Kotřík, R. Plašil, R. Johnsen, and J. Glosík, *Philos. Trans. R. Soc., A* **370**, 5101 (2012).
- ²¹J. Varju, M. Hejduk, P. Dohnal, M. Jílek, T. Kotřík, R. Plašil, D. Gerlich, and J. Glosík, *Phys. Rev. Lett.* **106**, 203201 (2011).
- ²²M. Hejduk, P. Dohnal, J. Varju, P. Rubovič, R. Plašil, and J. Glosík, *Plasma Sources Sci. Technol.* **21**, 024002 (2012).
- ²³R. Plašil, J. Glosík, V. Poterya, P. Kudrna, J. Ruzs, M. Tichý, and A. Pysanenko, *Int. J. Mass Spectrom.* **218**, 105 (2002).
- ²⁴I. Korolov, R. Plašil, T. Kotřík, P. Dohnal, and J. Glosík, *Int. J. Mass Spectrom.* **280**, 144 (2009).
- ²⁵P. Macko, G. Bánó, P. Hlavenka, R. Plašil, V. Poterya, A. Pysanenko, O. Votava, R. Johnsen, and J. Glosík, *Int. J. Mass Spectrom.* **233**, 299 (2004).
- ²⁶J. Glosík, I. Korolov, R. Plašil, O. Novotný, T. Kotřík, P. Hlavenka, J. Varju, I. A. Mikhailov, V. Kokoouline, and C. H. Greene, *J. Phys. B: At. Mol. Opt.* **41**, 191001 (2008).
- ²⁷P. Dohnal, P. Rubovič, T. Kotřík, M. Hejduk, R. Plašil, R. Johnsen, and J. Glosík, *Phys. Rev. A* **87**, 052716 (2013).
- ²⁸T. Kotřík, P. Dohnal, Š. Roučka, P. Jusko, R. Plašil, J. Glosík, and R. Johnsen, *Phys. Rev. A* **83**, 032720 (2011).
- ²⁹T. Kotřík, P. Dohnal, P. Rubovič, R. Plašil, Š. Roučka, S. Opanasiuk, and J. Glosík, *Eur. Phys. J. Appl. Phys.* **56**, 24011 (2011).
- ³⁰R. Johnsen, P. Rubovič, P. Dohnal, M. Hejduk, R. Plašil, and J. Glosík, *J. Phys. Chem. A* **117**, 9477 (2013).
- ³¹P. Dohnal, P. Rubovič, Á. Kálosi, M. Hejduk, R. Plašil, R. Johnsen, and J. Glosík, *Phys. Rev. A* **90**, 042708 (2014).
- ³²J. Glosík, R. Plašil, I. Korolov, T. Kotřík, O. Novotný, P. Hlavenka, P. Dohnal, J. Varju, V. Kokoouline, and C. H. Greene, *Phys. Rev. A* **79**, 052707 (2009).
- ³³S. Fonseca dos Santos, V. Kokoouline, and C. H. Greene, *J. Chem. Phys.* **127**, 124309 (2007).
- ³⁴C. Jungen and S. T. Pratt, *Phys. Rev. Lett.* **102**, 023201 (2009).
- ³⁵L. Pagani, C. Vastel, E. Hugo, V. Kokoouline, C. H. Greene, A. Bacmann, E. Bayet, C. Ceccarelli, R. Peng, and S. Schlemmer, *Astron. Astrophys.* **494**, 623 (2009).
- ³⁶K. N. Crabtree and B. J. McCall, *Philos. Trans. R. Soc., A* **370**, 5055 (2012).
- ³⁷K. N. Crabtree, N. Indriolo, H. Kreckel, B. A. Tom, and B. J. McCall, *Astrophys. J.* **729**, 15 (2011).
- ³⁸N. Indriolo and B. J. McCall, *Astrophys. J.* **745**, 91 (2012).
- ³⁹J. Glosík, G. Bánó, R. Plašil, A. Luca, and P. Zakouřil, *Int. J. Mass Spectrom.* **189**, 103 (1999).
- ⁴⁰M. R. Mahdavi, J. B. Hasted, and M. M. Nakshbandi, *J. Phys. B: At. Mol. Opt.* **4**, 1726 (1971).
- ⁴¹P. Rubovič, P. Dohnal, M. Hejduk, R. Plašil, and J. Glosík, *J. Phys. Chem. A* **117**, 9626 (2013).
- ⁴²I. Korolov, R. Plašil, T. Kotřík, P. Dohnal, O. Novotný, and J. Glosík, *Contrib. Plasma Phys.* **48**, 461 (2008).
- ⁴³J. Glosík, R. Plašil, T. Kotřík, P. Dohnal, J. Varju, M. Hejduk, I. Korolov, Š. Roučka, and V. Kokoouline, *Mol. Phys.* **108**, 2253 (2010).
- ⁴⁴E. Alge, N. G. Adams, and D. Smith, *J. Phys. B: At. Mol. Opt.* **16**, 1433 (1983).
- ⁴⁵E. Ilişca, *Prog. Surf. Sci.* **41**, 217 (1992).
- ⁴⁶S. Yucel, *Phys. Rev. B* **39**, 3104 (1989).
- ⁴⁷I. Zymak, M. Hejduk, D. Mulin, R. Plašil, J. Glosík, and D. Gerlich, *Astrophys. J.* **768**, 86 (2013).
- ⁴⁸M. Cordonnier, D. Uy, R. M. Dickson, K. E. Kerr, Y. Zhang, and T. Oka, *J. Chem. Phys.* **113**, 3181 (2000).
- ⁴⁹F. Grussie, M. H. Berg, K. N. Crabtree, S. Gärtner, B. J. McCall, S. Schlemmer, A. Wolf, and H. Kreckel, *Astrophys. J.* **759**, 21 (2012).

- ⁵⁰J. Glosík, M. Hejduk, P. Dohnal, P. Rubovič, Á. Kálosi, and R. Plašil, *EPJ Web Conf.* **84**, 01002 (2015).
- ⁵¹C. M. Lindsay and B. J. McCall, *J. Mol. Spectrosc.* **210**, 60 (2001).
- ⁵²P. Dohnal, M. Hejduk, P. Rubovič, J. Varju, Š. Roučka, R. Plašil, and J. Glosík, *J. Chem. Phys.* **137**, 194320 (2012).
- ⁵³E. A. Mason and E. W. McDaniel, *Transport Properties of Ions in Gases* (Wiley, New York, 1988).
- ⁵⁴J. Stevefelt, J. Boulmer, and J. F. Delpech, *Phys. Rev. A* **12**, 1246 (1975).
- ⁵⁵W. Lindinger and D. L. Albritton, *J. Chem. Phys.* **62**, 3517 (1975).
- ⁵⁶V. Wakelam, E. Herbst, J.-C. Loison, I. W. M. Smith, V. Chandrasekaran, B. Pavone, N. G. Adams, M.-C. Bacchus-Montabonel, A. Bergeat, K. Béroff, V. M. Bierbaum, M. Chabot, A. Dalgarno, E. F. van Dishoeck, A. Faure, W. D. Geppert, D. Gerlich, D. Galli, E. Hébrard, F. Hersant, K. M. Hickson, P. Honvault, S. J. Klippenstein, S. L. Picard, G. Nyman, P. Pernot, S. Schlemmer, F. Selsis, I. R. Sims, D. Talbi, J. Tennyson, J. Troe, R. Wester, and L. Wiesenfeld, *Astrophys. J., Suppl. Ser.* **199**, 21 (2012).

Recombination of H_3^+ ions with electrons in He/ H_2 ambient gas at temperatures from 240 K to 340 K

Glosik J., Dohnal P., Rubovič P., Kálosi Á., Plašil R., Roučka S., Johnsen R.

Plasma Sources Sci. Technol. **24(6)**, 065017, 2015.

Recombination of H_3^+ ions with electrons in He/ H_2 ambient gas at temperatures from 240 K to 340 K

J Glosík¹, P Dohnal¹, P Rubovič¹, Á Kálosi¹, R Plašil¹, Š Roučka¹
and R Johnsen²

¹ Department of Surface and Plasma Science, Faculty of Mathematics and Physics, Charles University in Prague, Czech Republic

² Department of Physics and Astronomy, University of Pittsburgh, Pittsburgh, USA

E-mail: juraj.glosik@mff.cuni.cz

Received 13 July 2015, revised 9 October 2015

Accepted for publication 22 October 2015

Published 17 November 2015



CrossMark

Abstract

We have studied the recombination of H_3^+ ions with electrons in a stationary afterglow experiment either in pure hydrogen or in mixtures of helium, hydrogen, and argon. The decay of the ion density during the afterglow was monitored using near-infrared cavity ring-down absorption spectroscopy. The gas temperatures ranged from 240 K to 340 K.

We find that three-body recombination, where molecular hydrogen acts as a third body, increases the recombination rate significantly. However, H_2 assisted three-body recombination saturates at hydrogen densities above $\approx 10^{16} \text{ cm}^{-3}$ and the recombination rate then becomes nearly independent of the neutral gas density. The saturation can lead to the erroneous conclusion that the recombination is purely binary and this appears to be the cause of some inconsistencies between previously reported recombination rate coefficients. At temperatures 240–340 K the obtained three-body recombination rate coefficient is independent on temperature ($K_{H_2} = (9.4 \pm 1.3) \times 10^{-23} \text{ cm}^6 \text{ s}^{-1}$) and it is larger by five orders of magnitude than those expected from the classical theory for atomic ions of Bates and Khare ($K_{BK}(300 \text{ K}) \approx 10^{-27} \text{ cm}^6 \text{ s}^{-1}$). The observed dependences on H_2 density suggest that a substantial fraction of neutral $H_3^{\#}$ complexes formed in capture of electrons by H_3^+ ions do not rapidly predissociate but can be stabilized by interactions with third bodies. Saturation occurs if the capture step is rate limiting rather than stabilization.

Keywords: ion-electron recombination, H_3^+ , H_2 assisted three-body recombination

(Some figures may appear in colour only in the online journal)

1. Introduction

The electron recombination of H_3^+ ion is of special interest for physical chemistry, quantum physics, astrophysics, plasma spectroscopy and the physics of discharges. H_3^+ , the most abundantly produced molecular ion in the universe [1], is deemed to play a crucial role in the formation of molecules in interstellar clouds [2]. Its recombination with electrons has been subject of intensive experimental and theoretical research (see e.g. recent reviews [3–8]) for over 65 years and

the major discrepancies between experimental and theoretical results have now been mostly resolved. For many years theoretical calculations predicted that H_3^+ recombination should be much slower than was observed because favorable crossings [3, 9] between the ionic and dissociating potential curves are absent. This created the often cited enigma of H_3^+ recombination [10]. The large gap between experimental results and theory was largely closed in 2001 by taking into account the Jahn–Teller mechanism [11]. Theoretical results [12, 13] now agree quite well with the ion storage ring results [14–16], but

slight deviations remain at low collisional energies and temperatures below 300 K (see discussion in [17–19]). The binary recombination rate coefficients inferred from recent plasma afterglow experiments by extrapolation to zero gas densities [20–22] also agree. Low-temperature afterglow studies (from 60 K to 300 K) of state-selected recombination of para- H_3^+ and ortho- H_3^+ support the theoretically predicted temperature dependences of recombination rate coefficients for para- H_3^+ and ortho- H_3^+ [23–26].

One of the remaining problems is that the recombination coefficients of H_3^+ ions with electrons inferred from plasma afterglow experiments at 300 K have varied from less than $2 \times 10^{-8} \text{ cm}^3 \text{ s}^{-1}$ [27, 28] to $\approx 2 \times 10^{-7} \text{ cm}^3 \text{ s}^{-1}$ [29, 30]. These discrepancies are not likely to be due to experimental errors because the afterglow techniques generally have yielded consistent results for other molecular ions. Rather, recent experimental results suggest that H_3^+ recombination in plasmas containing neutral atoms (He) or molecules (H_2) is not entirely due to the binary recombination but also proceeds by three-body recombination. Such three-body recombination is the subject of the present experimental work that extends our earlier work performed at a fixed temperature of 300 K [31].

Afterglow recombination experiments are typically carried out in plasmas containing mixtures of helium, hydrogen, and sometimes argon at total pressures in the range of 100–2000 Pa. The function of the helium gas (the buffer gas) is to inhibit diffusive losses of ions and to thermalize the electrons. Hydrogen is the precursor gas for H_3^+ formation, and argon is added to remove undesired He metastable atoms created during the discharge. Some important experiments were carried out in pure hydrogen [30]. In most early work it was tacitly assumed that recombination occurred exclusively by binary recombination and that the neutral particles played no role. An observed lack of pressure dependence was sometimes adduced as evidence for the absence of three-body effects, but, as will be discussed later, three-body recombination saturates at high pressures. For instance, the saturation of the three-body recombination channel at effective binary rate coefficient $\alpha_{\text{eff}} \approx 2 \times 10^{-7} \text{ cm}^3 \text{ s}^{-1}$ explains why Leu *et al* [29] failed to observe a pressure dependence of the recombination rate coefficient in their high-pressure stationary afterglow. Recent systematic studies of recombination of H_3^+ ions have demonstrated that at helium pressures of 100–2000 Pa the assumption of purely binary recombination is not always valid. The measured three-body He assisted recombination rate coefficient was found to be large, $K_{\text{He}} \approx 10^{-25} \text{ cm}^6 \text{ s}^{-1}$, exceeding at 300 K the value expected from the classical three-body mechanism of Bates and Khare [32] by about two orders of magnitude. Hence, the seeming discrepancies between results of afterglow and storage-ring studies of H_3^+ recombination were in part removed (see e.g. Glosik *et al* [20]) by invoking helium assisted three-body recombination [21, 33, 34]. An important exception from this accord is the spectroscopic study performed in a pulsed afterglow of pure hydrogen by Amano, who reported value of the recombination rate coefficient $\alpha(273 \text{ K}) = 1.8 \times 10^{-7} \text{ cm}^3 \text{ s}^{-1}$ independent on H_2

number density [30]. Recently, a very fast three-body H_2 -assisted recombination process was observed [31] with a rate coefficient $K_{\text{H}_2} = (8.7 \pm 1.5) \times 10^{-23} \text{ cm}^6 \text{ s}^{-1}$ at 300 K that is nearly five orders of magnitude larger than the value predicted by the theory of Bates and Khare [32]. The corresponding effective binary recombination rate coefficient at H_2 number densities similar to those used in Amano's experiment [30] is very close to the value reported by Amano.

In the following we will present new experimental results on helium and hydrogen assisted recombination of H_3^+ ions at temperatures from 240 K to 340 K, extending our previous study performed at a single temperature of 300 K [31]. The results clearly indicate that molecular H_2 is much more effective as a third body than atomic He.

2. Experiment

As in our previous work [31], recombination rate coefficients [3, 24, 28] are measured in a stationary afterglow (SA) in conjunction with cavity ring-down spectroscopy (CRDS) to monitor the decay of density of H_3^+ ions. The plasma is generated in a pulsed microwave discharge in a fused silica tube (inner diameter $\approx 1.3 \text{ cm}$). The microwave generator is equipped with an external fast high-voltage switch to cut off the power to the plasma within a fall time of $< 30 \mu\text{s}$. A low microwave power in the range of 5–15 W, with $\approx 40\%$ duty cycle, is used to avoid excessive heating of the gas during the discharge. The temperature of the discharge tube can be adjusted between 80 K and 340 K. The discharge is ignited in a mixture of He/Ar/ H_2 (with a typical composition $10^{17}/10^{14}/10^{14}\text{--}10^{17} \text{ cm}^{-3}$) or in pure H_2 gas (typical density $[\text{H}_2] = 3 \times 10^{16}\text{--}1 \times 10^{17} \text{ cm}^{-3}$). Only normal hydrogen ($^n\text{H}_2$) was used in this set of experiments, i.e. hydrogen gas where para and ortho nuclear spin manifolds are in equilibrium at 300 K and para- H_2 to ortho- H_2 ratio is 1/3. Details of the ion formation reactions, including discussion of para- H_3^+ to ortho- H_3^+ ratio in normal H_2 can be found in [21, 26, 28, 33, 35, 36]. The time constants of processes of relaxation and formation of H_3^+ dominated afterglow plasma are discussed in the appendix.

The main diagnostic technique is the time-resolved cavity ring-down absorption spectroscopy in the continuous wave modification (cw-CRDS), based on the configuration described by Romanini *et al* [37]. For details on the SA-CRDS setup used in our laboratory for studies of electron-ion recombination see e.g. [24, 38–42]. Second overtone transitions originating from the ground vibrational level of H_3^+ were used to probe the number densities of H_3^+ ions in para (1, 1), ortho (1, 0), and ortho (3, 3) states where the numbers in parentheses denote the quantum numbers J and G [43]. A water transition at 7236.447 cm^{-1} (line position taken from HITRAN database [44]) was routinely scanned to estimate the amount of H_2O impurities in the buffer gas. Typically, the water vapor concentration was at a safe level of less than $5 \times 10^{10} \text{ cm}^{-3}$ i.e. less than 0.1 ppm of buffer gas number density.

The time dependent optical absorption signals are recorded during the discharge and during the afterglow. The measured absorbances are then converted to number densities of H_3^+ ions

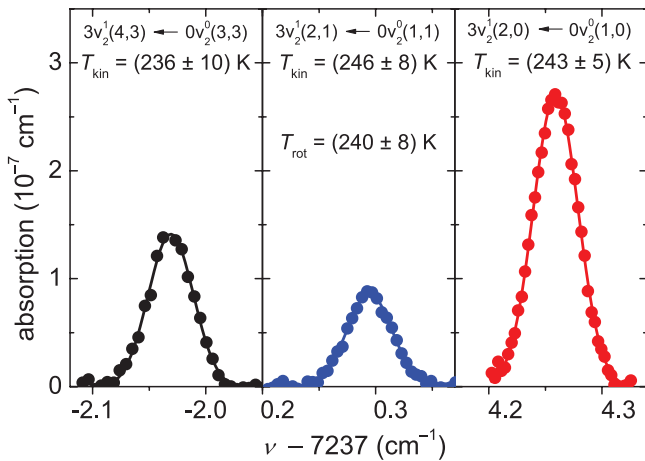


Figure 1. Examples of absorption line profiles measured at 240 K in $5.2 \times 10^{16} \text{ cm}^{-3}$ of pure H_2 . The full lines are Gaussian fits to the data. The corresponding kinetic temperature is listed at each line. The rotational temperature T_{rot} was obtained from populations of (1, 0), (1, 1) and (3, 3) states of H_3^+ .

in particular ionic states. The effective recombination rate coefficients $\alpha_{\text{eff-ion}}$ are obtained by fitting the decay curves of density of H_3^+ ions. Examples of measured decay curves for para (1, 1), ortho (1, 0), and ortho (3, 3) states and one calculated for electrons are shown in panel (a) of figure 2. The measured relative populations (fractions) of para (1, 1), ortho (1, 0), and ortho (3, 3) states are shown in panel (b) of figure 2. If electron-ion recombination was the only ion loss process, $\alpha_{\text{eff-ion}}$ could be directly obtained from the slope of a graph of the reciprocal electron number density ($1/n_e$) as a function of time (see panel (c) of figure 2). A more complex data analysis includes also losses of charged particles due to ambipolar diffusion and losses due to formation of H_5^+ ions and their subsequent recombination. For details on the data analysis see [24].

The kinetic temperature of the H_3^+ ions $T_{\text{kin-ion}}$ is obtained from the Doppler broadening of the absorption line profiles. The examples of absorption line profiles measured in pure H_2 gas are plotted in figure 1. The rotational temperature (T_{rot}) is evaluated from the relative population of the monitored rotational states. These parameters of the afterglow plasma are routinely measured in SA-CRDS experiment [24]. On the basis of these measurements we conclude that for afterglow plasmas in the SA-CRDS the kinetic and rotational temperature of ions are equal to the temperature of the buffer gas (T_{He}) and to the wall temperature (T_{wall}) of the discharge tube, i.e. $T = T_{\text{wall}} = T_{\text{He}} = T_{\text{rot}} = T_{\text{kin-ion}}$ (for details see [24, 26]). The thermal equilibrium applies separately to the para- H_3^+ and ortho- H_3^+ nuclear spin manifolds, but at temperatures above 80 K, when normal hydrogen is used, the para to ortho ratio of H_3^+ is also close to the thermodynamic equilibrium value, as shown by studies [24, 26].

The electron temperature T_e was not measured in the present study. The thermalization of electrons in afterglow plasma was studied and discussed in our previous studies (see e.g. [24]). In the afterglow plasma electrons are cooled in collisions with He atoms. At typical He densities the characteristic time of the electron cooling is below 10 μs , but the electron temperature

can rise due to superelastic collisions with excited (metastable) neutral He or Ar atoms or H_2 molecules produced in the discharge. These excited particles, He metastables in particular, are removed by Penning ionization of Ar and H_2 . At the Ar and H_2 densities used in the present study, the characteristic time for Penning ionization is well below 100 μs , see table A1 in appendix. We directly observed fast cooling of electrons by monitoring visible light emission from the plasma in early afterglow. The calculations described in [24] indicate that at low gas temperatures near 77 K the electron temperature can be slightly elevated, but that at higher gas temperatures it is nearly equal to the He temperature, $T_{\text{He}} = T_e$. Hence, we assume thermal equilibration in afterglows in He/Ar/ H_2 gas mixtures, i.e. that $T = T_{\text{wall}} = T_{\text{He}} = T_{\text{rot}} = T_{\text{kin-ion}} = T_e$.

3. Afterglow ion-kinetic and recombination processes

Numerical models of the relevant ion kinetic processes are used to set the best conditions for the experiment and to analyze the recombination during the afterglow. The key reactions are listed in table A1 of appendix. The composition of the plasma at the end of the microwave pulse is difficult to ascertain and hence the calculations were performed for many sets of different initial conditions, such as the relative densities of He^+ ions and metastable helium atoms. The optimal partial pressures of He, Ar, and H_2 were then selected so that the afterglow plasma was dominated by H_3^+ ions within 150 μs after the end of the discharge and that the undesired species He^+ and He^m were sufficiently depleted at that time. The calculated characteristic time constants are listed in table A1 of the appendix. The initial transition time interval of 150 μs is excluded from the analysis of plasma decay in order to obtain rate coefficients of recombination processes.

The analysis of the afterglow decay of the ion and electron densities assumes that the plasma is quasineutral and that the spatial distribution is given by the fundamental diffusion mode. The first assumption is justified since the Debye length is small compared to the dimensions of the discharge tube. The second assumption is not critical since diffusive losses are small in this set of experiments. In the following, to keep the equations simple, we will omit losses due to ambipolar diffusion, but they are included in the actual data analysis.

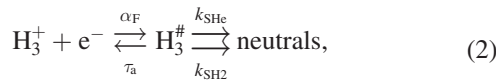
Several recombination processes contribute to the ion loss during the afterglow:

- (i) Binary dissociative recombination with electrons:



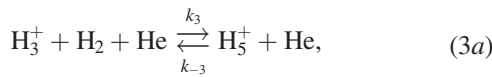
where α_{bin} is the rate coefficient of binary dissociative recombination.

- (ii) The second recombination mechanism postulates the formation of highly excited $\text{H}_3^{\#}$ complexes that can either decay by autoionization or can be stabilized (rendered incapable of autoionizing) in collision with He or H_2 :



where α_F is the rate coefficient for the formation of $\text{H}_3^\#$, τ_a is the autoionization time constant, and k_{SHe} and k_{SH_2} are the binary rate coefficients for collisional stabilization of $\text{H}_3^\#$ in collision with He and H_2 , leading eventually to neutral products. We assume that the autoionization time constant τ_a is much shorter than the overall recombination time scale and that hence only a very small fraction of H_3^+ ions will be bound in complexes at any time. In this approximation we exclude collision induced ionization by He or H_2 or electrons. This is certainly a highly simplified model and the nature of the complexes remains nebulous.

- (iii) The third route to recombination consists of formation of H_5^+ ions by three-body association of H_3^+ with H_2 and subsequent recombination of H_5^+ ions with electrons:



where k_3 is the rate coefficient of the three-body association reaction leading to formation of H_5^+ cluster ions, k_{-3} is the rate coefficient of the reverse reaction (collisional induced dissociation), and α_5 is the recombination rate coefficient of H_5^+ . We assume that k_3 and k_{-3} do not substantially differ from those for the three-body association reaction of H_3^+ with two H_2 [45, 46]. At temperatures greater than 300 K the fractional concentration of H_5^+ is very small, but it rises rapidly at low temperatures and below ≈ 240 K it becomes so large that no accurate information on H_3^+ recombination can be extracted from the data for $[\text{H}_2] > 10^{15} \text{ cm}^{-3}$.

For processes (1)–(3b) we can write following balance equations:

$$\frac{d[\text{H}_3^+]}{dt} = -(\alpha_{\text{bin}} + \alpha_F)[\text{H}_3^+]n_e + \frac{1}{\tau_a}[\text{H}_3^\#] - k_3[\text{H}_2][\text{He}][\text{H}_3^+] + k_{-3}[\text{He}][\text{H}_5^+], \quad (4)$$

$$\frac{d[\text{H}_3^\#]}{dt} = \alpha_F[\text{H}_3^+]n_e - \frac{1}{\tau_a}[\text{H}_3^\#] - k_{\text{SHe}}[\text{He}][\text{H}_3^\#] - k_{\text{SH}_2}[\text{H}_2][\text{H}_3^\#], \quad (5)$$

$$\frac{d[\text{H}_5^+]}{dt} = -\alpha_5[\text{H}_5^+]n_e + k_3[\text{H}_2][\text{He}][\text{H}_3^+] - k_{-3}[\text{He}][\text{H}_5^+], \quad (6)$$

where n_e is the electron number density and square brackets denote number densities of the corresponding species. The number densities of $\text{H}_3^\#$ and H_5^+ can be rewritten in steady-state approximation using equations (5) and (6) as:

$$[\text{H}_3^\#] = \frac{\alpha_F n_e [\text{H}_3^+]}{\frac{1}{\tau_a} + k_{\text{SHe}}[\text{He}] + k_{\text{SH}_2}[\text{H}_2]}, \quad (7)$$

$$\begin{aligned} [\text{H}_5^+] &= \frac{k_3[\text{H}_2][\text{He}][\text{H}_3^+]}{k_{-3}[\text{He}] + \alpha_5 n_e} = K_C \frac{[\text{H}_2][\text{H}_3^+]}{1 + \frac{\alpha_5 n_e}{k_{-3}[\text{He}]}} \\ &= R[\text{H}_3^+] \leq K_C[\text{H}_2][\text{H}_3^+] = [\text{H}_5^+]_{\text{LTE}}, \end{aligned} \quad (8)$$

where $K_C = k_3/k_{-3}$ (in units of cm^3) is the chemical equilibrium constant (see [47]). The index LTE indicates density of H_5^+ ions corresponding to local thermodynamic equilibrium. In the recombining plasma the ratio $R = [\text{H}_5^+]/[\text{H}_3^+]$ is smaller than $K_C[\text{H}_2]$ because the H_5^+ ions recombine much faster than H_3^+ . We express this by introducing a factor $\xi \leq 1$ so that $R = \xi K_C[\text{H}_2]$. This factor depends on conditions in discharge and afterglow plasma and has to be obtained from the numerical model. Quasineutrality implies that $n_e = [\text{H}_3^+] + [\text{H}_5^+]$ and hence:

$$[\text{H}_3^+] = \frac{n_e}{1 + R}. \quad (9)$$

By summing equations (4) and (6) and by using equation (7) to substitute $[\text{H}_3^\#]$ we get:

$$\frac{dn_e}{dt} = - \left(\alpha_{\text{bin}} + \alpha_F \frac{k_{\text{SHe}}[\text{He}] + k_{\text{SH}_2}[\text{H}_2]}{\frac{1}{\tau_a} + k_{\text{SHe}}[\text{He}] + k_{\text{SH}_2}[\text{H}_2]} \right) [\text{H}_3^+]n_e - \alpha_5[\text{H}_5^+]n_e. \quad (10)$$

We define the three-body recombination rate coefficients for He and H_2 assisted recombination (K_{He} and K_{H_2} , respectively) as:

$$K_{\text{He}} = \alpha_F k_{\text{SHe}} \tau_a, \quad (11)$$

$$K_{\text{H}_2} = \alpha_F k_{\text{SH}_2} \tau_a. \quad (12)$$

In terms of the three-body rate coefficients equation (10) then becomes:

$$\begin{aligned} \frac{dn_e}{dt} &= - \left(\alpha_{\text{bin}} + \alpha_F \frac{K_{\text{He}}[\text{He}] + K_{\text{H}_2}[\text{H}_2]}{\alpha_F + K_{\text{He}}[\text{He}] + K_{\text{H}_2}[\text{H}_2]} \right. \\ &\quad \left. + \alpha_5 \xi K_C[\text{H}_2] \right) [\text{H}_3^+]n_e. \end{aligned} \quad (13)$$

The quantity measured in SA-CRDS experiment is the number density of H_3^+ ions and it is convenient to use equation (9) and to replace n_e by $[\text{H}_3^+]$. From (13) we obtain:

$$\begin{aligned} \frac{d[\text{H}_3^+]}{dt} &= - \left(\alpha_{\text{bin}} + \alpha_F \frac{K_{\text{He}}[\text{He}] + K_{\text{H}_2}[\text{H}_2]}{\alpha_F + K_{\text{He}}[\text{He}] + K_{\text{H}_2}[\text{H}_2]} \right. \\ &\quad \left. + \alpha_5 \xi K_C[\text{H}_2] \right) [\text{H}_3^+]^2 \end{aligned} \quad (14)$$

and the effective recombination rate coefficient $\alpha_{\text{eff-ion}}$:

$$\alpha_{\text{eff-ion}} = \alpha_{\text{bin}} + \alpha_F \frac{K_{\text{He}}[\text{He}] + K_{\text{H}_2}[\text{H}_2]}{\alpha_F + K_{\text{He}}[\text{He}] + K_{\text{H}_2}[\text{H}_2]} + \alpha_5 \xi K_C[\text{H}_2]. \quad (15)$$

If we include term for losses due to ambipolar diffusion (up to now omitted) then equation (14) can be written in the more compact form:

$$\frac{d[\text{H}_3^+]}{dt} = -\alpha_{\text{eff-ion}}[\text{H}_3^+]^2 - \frac{[\text{H}_3^+]}{\tau_D}. \quad (16)$$

The first term on the right side of equation (16) corresponds to the recombination losses and the second term accounts for losses due to the ambipolar diffusion characterized by the time constant τ_D . The dependence of $\alpha_{\text{eff-ion}}$ on $[\text{He}]$ and $[\text{H}_2]$ is characterized by the parameters α_{bin} , α_F , K_{He} , K_{H_2} , and $\alpha_5 \xi K_C$. In equation (15) an upper limit of the third term (for $\xi = 1$) at a given temperature and $[\text{H}_2]$ can be calculated from the known values of α_5 and K_C . The actual value of $\alpha_5 \xi K_C [\text{H}_2]$ can be estimated from the numerical kinetic model.

In the low density limit ($[\text{He}]$ and $[\text{H}_2] \rightarrow 0$) equation (15) reduces to:

$$\alpha_{\text{eff-ion}} = \alpha_{\text{bin}} + K_{\text{He}}[\text{He}] + K_{\text{H}_2}[\text{H}_2] + \alpha_5 \xi K_C [\text{H}_2] \quad (17)$$

and $\alpha_{\text{eff-ion}}$ increases linearly with $[\text{He}]$ and $[\text{H}_2]$. The coefficients K_{He} and K_{H_2} are three-body recombination rate coefficients in units of $\text{cm}^6 \text{s}^{-1}$. Here we can see the reason for definition of K_{He} and K_{H_2} by formulas (11) and (12). In the high-density limit equation (15) reduces to:

$$\alpha_{\text{eff-ion}} = \alpha_{\text{bin}} + \alpha_F + \alpha_5 \xi K_C [\text{H}_2] \quad (18)$$

and $\alpha_{\text{eff-ion}}$ saturates if the last term describing H_5^+ recombination is small which will be true at higher temperatures because K_C falls off rapidly with increasing temperature [47, 48]. The saturation limit is approached when nearly all H_3^+ are stabilized in collisions with He or H_2 rather than suffering autoionization.

In principle, the three-body recombination rate coefficients can be obtained from linear fits of data in the low pressure limit using equation (17). In practice, it was found preferable to obtain these parameters by fitting measured values of $\alpha_{\text{eff-ion}}$ to equation (15).

4. Experimental data and results

The experiments were performed either in pure H_2 (pressures from 150 to 350 Pa) or in He/Ar/ H_2 mixtures (He pressures from 900 to 2700 Pa). No dependence of the measured effective recombination rate coefficient on argon number density in the range of $5 \times 10^{13} - 10^{15} \text{ cm}^{-3}$ was observed. From data similar to those in figure 2 the effective recombination rate coefficients $\alpha_{\text{eff-ion}}$ at particular partial densities of He and H_2 were determined at temperatures 240–340 K. The upper temperature limit is given by design limits of the discharge tube while the lower temperature limit is set by the increasing formation of H_5^+ ions. The dependences of the effective recombination rate coefficient $\alpha_{\text{eff-ion}}$ on $[\text{H}_2]$ measured at 240 K, 273 K, 300 K and 340 K are plotted in panels (a)–(d) of figure 3, respectively. At all four temperatures the helium buffer gas pressures were 900 Pa and 1800 Pa.

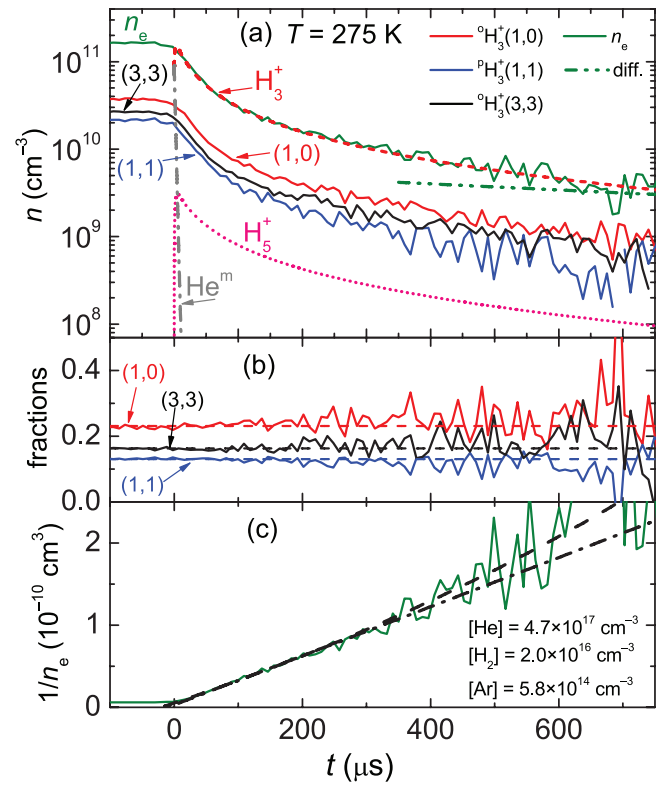


Figure 2. Decay of the ion densities during the afterglow measured in SA-CRDS at 275 K. Panel (a): The densities of H_3^+ ions in the para (1, 1), ortho (1, 0), and ortho (3, 3) rotational states measured in a He/Ar/ H_2 mixture at 275 K ($[\text{He}] = 4.7 \times 10^{17} \text{ cm}^{-3}$, $[\text{H}_2] = 2.0 \times 10^{16} \text{ cm}^{-3}$ and $[\text{Ar}] = 5.8 \times 10^{14} \text{ cm}^{-3}$). Normal hydrogen ($^n\text{H}_2$) was used in this experiment. The electron density n_e is obtained as a sum of densities of ions in ortho and para states under the assumption of thermal equilibrium. Calculated evolutions of H_3^+ , H_5^+ , and He^m densities are indicated as dashed, dotted and dot-dashed lines, respectively. The double dot-dashed line indicates the slow decay due to ambipolar diffusion, as obtained from fits to experimental data. Panel (b): The relative populations of para (1, 1), ortho (1, 0), and ortho (3, 3) states of H_3^+ . The dashed lines show the corresponding relative populations in thermal equilibrium at 275 K. Panel (c): The reciprocal electron number density, $1/n_e$. The dashed line through the data represents a fit that includes both recombination and diffusion, while the dot-dashed straight line is a simple linear fit during the first 400 μs .

In figure 3 the dashed lines represent fits to the data by equation (15). The maximal contributions of H_5^+ , assuming chemical equilibrium between H_3^+ and H_5^+ , are indicated by short dashed lines (LTE_{H_5}) in figure 3. In these calculations the value of $\alpha_5 = 2 \times 10^{-6} \text{ cm}^3 \text{s}^{-1}$ was taken from [36, 49] and the equilibrium constant K_C was calculated using the enthalpy and entropy changes $\Delta H_0 = -6.9$ [kcal mol^{-1}] and $\Delta S_0 = -17.4$ [cal $\text{K}^{-1} \text{mol}^{-1}$] of Hiraoka [47]. The full lines (M_{H_5}) indicate the somewhat smaller contributions of H_5^+ ions calculated from the full kinetic model.

Panel (a) of figure 4 shows a comparison of the data measured at 240 K, 273 K, 300 K and 340 K at 900 Pa in He/Ar/ H_2 mixtures, together with the calculated contributions (LTE_{H_5}) from H_5^+ . We have added the calculated H_5^+ contribution at 210 K to demonstrate that it becomes too large for a

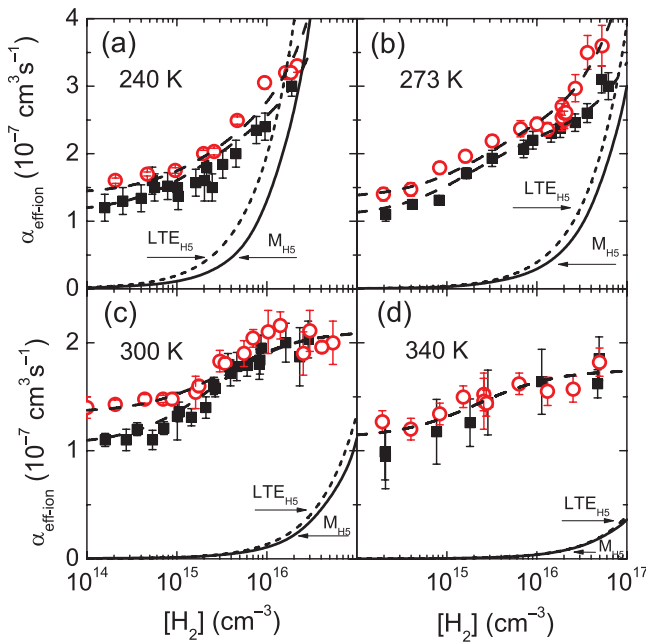


Figure 3. Effective recombination rate coefficients $\alpha_{\text{eff-ion}}$ at different H_2 densities and temperatures of 240 K (panel (a)), 273 K (panel (b)), 300 K (panel (c)) and 340 K (panel (d)). The two data sets measured at He pressures of 900 Pa and 1800 Pa are distinguished by squares and open circles, respectively. The dashed lines are fits to the data by equation (15). The short dashed lines (LTE_{H_5}) represent $\alpha_5 K_{\text{C}}[\text{H}_2]$, i.e. the upper limit of the contribution from H_5^+ recombination while the full lines (M_{H_5}) indicate the smaller and more realistic H_5^+ contributions obtained from the kinetic model.

reliable determination of the three-body coefficients. No data were taken at 210 K. The figure 4 also includes $\alpha_{\text{eff-ion}}$ data measured in pure H_2 at 240 K and 273 K for comparison with the data of Amano obtained in experiments with pure H_2 [30]. Note that as rate of ternary association reaction (3) leading to formation of H_5^+ ions depends on product of $[\text{He}][\text{H}_2]$ (in He/Ar/ H_2 mixture) or on product of $[\text{H}_2][\text{H}_2]$ (in pure H_2), the formation of H_5^+ will be slower in pure H_2 than in He/Ar/ H_2 mixture (see results of model of chemical kinetics in panel (b) of figure 4). For additional details on data obtained at 300 K see also figures 3 and 4 of [31]. Panel (b) of figure 4 illustrates how the contributions add up to the observed $\alpha_{\text{eff-ion}}$ at different H_2 densities. In this example, the temperature was 240 K, and the He pressure was 900 Pa. It is apparent from the figure that the $\alpha_{\text{eff-ion}}$ data fit by equation (15) (the dotted line) with $\xi = 0$, i.e. with exclusion of the term accounting for H_5^+ formation, falls short of reproducing the experimental data at high $[\text{H}_2]$, but that adding the contribution from H_5^+ improves the fit.

By fitting the measured values plotted in figure 3 using equation (15) we obtained α_{F} , α_{bin} , K_{H_2} and K_{He} for particular temperatures. The fit was done in the whole probed range of $[\text{H}_2]$ and only the values of $\alpha_{\text{eff-ion}}$ measured in the mixture of He/Ar/ H_2 were used in the fit. Figure 5 shows the binary rate coefficients α_{bin} , α_{F} , sum of $(\alpha_{\text{bin}} + \alpha_{\text{F}})$, and also α_{bin} measured in earlier SA-CRDS, AISA and FALP experiments in He/Ar/ H_2 mixtures using hydrogen ($^1\text{H}_2$) as precursor gas for formation of H_3^+ [22, 26]. Note that the previous studies were focused

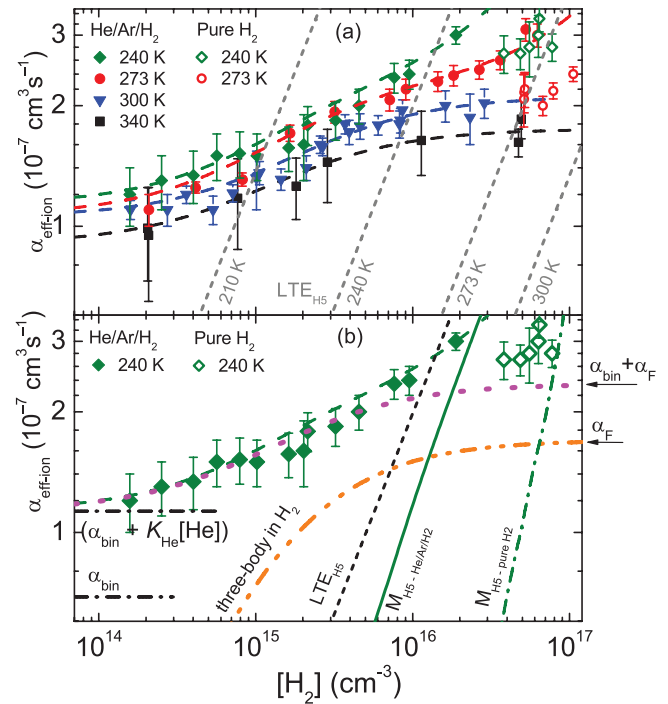


Figure 4. Panel (a): The dependences of $\alpha_{\text{eff-ion}}$ on $[\text{H}_2]$ measured at the indicated temperatures in He/Ar/ H_2 mixtures at a He pressure of 900 Pa (full symbols). The values measured in pure H_2 at 240 K and 273 K are plotted by open symbols. The dashed lines through the data are fits by equation (15). The short-dashed straight lines (LTE_{H_5}) are the upper limits of the H_5^+ contributions $\alpha_5 K_{\text{C}}[\text{H}_2]$ at indicated temperatures, using $\alpha_5 = 2 \times 10^{-6} \text{ cm}^3 \text{ s}^{-1}$ from [36, 49] and K_{C} from [47]. Panel (b): Breakdown of $\alpha_{\text{eff-ion}}$ into contributions from particular recombination processes.

The dotted line is calculated ignoring the contribution from H_5^+ recombination (i.e. using equation (15) with $\xi = 0$). The double-dot dashed line denoted ‘three-body in H_2 ’ shows the contribution of the three-body H_2 assisted recombination in pure H_2 . The full line ($M_{\text{H}_5-\text{He/Ar/H}_2}$) represents the contribution from the formation and recombination of H_5^+ ions in He/Ar/ H_2 mixtures obtained from the numerical model for 240 K and 900 Pa of He. The dot-dashed line ($M_{\text{H}_5-\text{pure H}_2}$) represents the contribution arising from the formation and recombination of H_5^+ ions as given by the model of chemical kinetics for pure H_2 gas.

on binary recombination rate coefficients α_{bin} [20, 21, 33]. The values measured by Amano [30] in a stationary afterglow experiment with pure H_2 shown in figure 5 are close to the sum $(\alpha_{\text{bin}} + \alpha_{\text{F}})$ and to the values obtained in the present set of experiments with pure H_2 .

The agreement with the data of Amano is particularly noteworthy. This otherwise excellent experiment gave values by factor of 3 higher than the currently accepted value of binary recombination rate coefficient α_{bin} [3]. That experiment marked the end of the confusing period when the recombination of H_3^+ in the ground vibrational state was claimed to be very slow [27]. We emphasize that the recombination coefficients measured by Amano are quite accurate, but that they do not represent the binary recombination rate coefficients. The saturation of the three-body channel explains why that experiment did not show a pressure dependence of the measured recombination rate coefficients. Although the very high

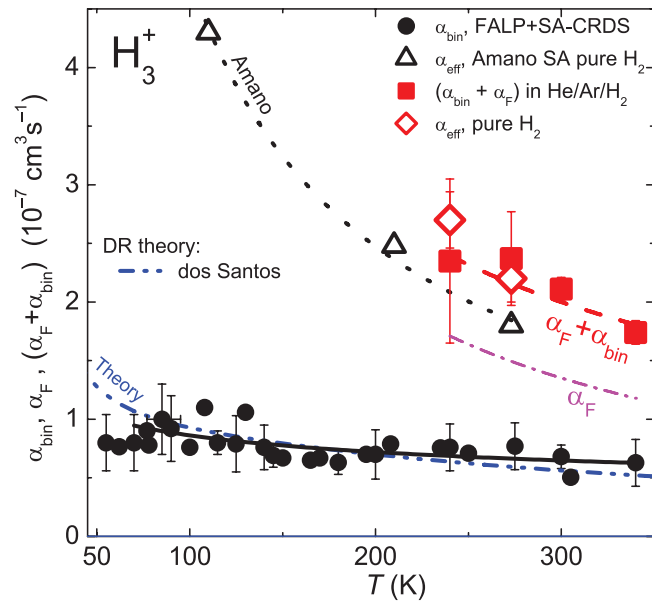


Figure 5. Temperature dependences of α_{bin} , α_{F} , and their sum ($\alpha_{\text{bin}} + \alpha_{\text{F}}$). The diamonds and squares indicate ($\alpha_{\text{bin}} + \alpha_{\text{F}}$) measured in pure H_2 and in $\text{He}/\text{Ar}/\text{H}_2$ mixture, respectively. The fit of the data (dashed line) gives the temperature dependence: $(\alpha_{\text{bin}} + \alpha_{\text{F}}) = (2.0 \pm 0.4) \times 10^{-7} (T/300 \text{ K})^{-(0.81 \pm 0.30)} \text{ cm}^3 \text{ s}^{-1}$. The filled circles indicate the values of α_{bin} for H_3^+ ions in $\text{He}/\text{Ar}/\text{H}_2$ mixtures that were obtained in several stationary and flowing afterglow experiments (for details see [22, 26]). The full line indicates the dependence $\alpha_{\text{bin}} = (6.5 \pm 1.4) \times 10^{-8} (T/300 \text{ K})^{-(0.26 \pm 0.07)} \text{ cm}^3 \text{ s}^{-1}$ obtained by fitting α_{bin} data at temperatures 80–340 K. Included are the present data and data from [22, 26]. The dependence of α_{F} on temperature (dot-dashed line) was obtained by subtracting α_{bin} (full line) from the sum of ($\alpha_{\text{bin}} + \alpha_{\text{F}}$) (dashed line). The rate coefficients measured by Amano [30] in pure H_2 , assumed to be due to binary recombination only, are plotted as open triangles for comparison. The dotted line indicates a fit to Amano's data: $\alpha_{\text{Amano}} = 1.7 \times 10^{-7} (T/300 \text{ K})^{-0.94} \text{ cm}^3 \text{ s}^{-1}$. The theoretical temperature dependence of the binary rate coefficient of dissociative recombination of H_3^+ ions calculated by Fonseca dos Santos *et al* [12] is plotted by a double dot-dashed line denoted Theory.

electron densities in the experiments of Amano lead to a more rapid plasma decay which leaves less time for H_5^+ formation, H_5^+ may nevertheless contribute at the lowest temperatures.

The obtained values of the three-body rate coefficients K_{H_2} and K_{He} of H_2 and He assisted recombination were almost independent on temperature in probed temperature range with the mean value of $K_{\text{He}} = (2.7 \pm 0.5) \times 10^{-25} \text{ cm}^6 \text{ s}^{-1}$ and $K_{\text{H}_2} = (9.4 \pm 1.3) \times 10^{-23} \text{ cm}^6 \text{ s}^{-1}$ at 240–340 K. On the other hand, the sum of $\alpha_{\text{bin}} + \alpha_{\text{F}}$ is increasing with decreasing temperature (see full squares in figure 5) in agreement within experimental error with the increase of the value of $\alpha_{\text{eff-ion}}$ measured in pure H_2 between 273 K and 240 K. Note that at 240 K the values of $\alpha_{\text{eff-ion}}$ measured in pure H_2 may have been slightly enhanced by the formation of H_5^+ ions (see the result of chemical kinetics model in panel (b) of figure 4). The measured values of K_{H_2} and K_{He} are shown in figure 6, together with K_{He} data obtained in our previous stationary and flowing afterglow experiments (for details see compilation in [34]). For comparison we include recently measured three-body

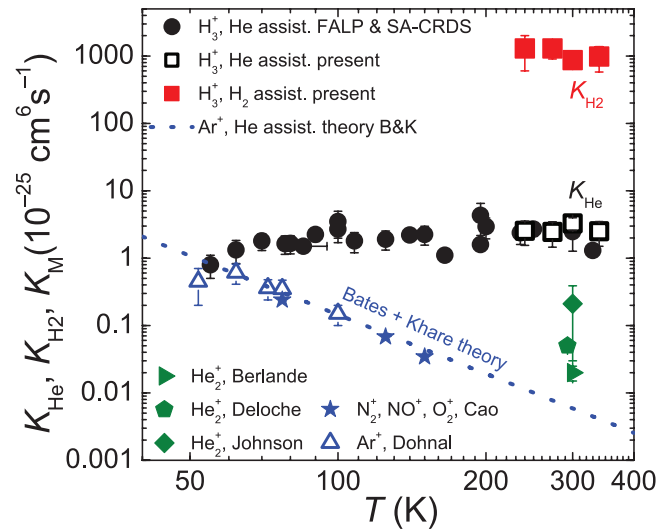


Figure 6. Temperature dependences of the three-body rate coefficients K_{H_2} (closed squares) and K_{He} (open squares) of H_2 and He assisted recombination of H_3^+ ions. Closed circles: K_{He} of H_3^+ ions obtained in our previous experiments [21, 23, 24, 34]. Open triangles: Three-body recombination rate coefficients of He-assisted collisional radiative recombination K_{HeAr^+} of Ar^+ ions measured in a Cryo-FALP II experiment [50]. Filled stars: $K_{\text{He-CRR}}$ as measured by Cao *et al* [51] for a mixture of atmospheric ions in He. Dotted line: Theoretical dependence of Bates and Khare [32] scaled for Ar^+ ions in He by the reduced mass. Full triangle, pentagon and diamond indicate three-body rate coefficients measured for He_2^+ ions in helium by Berlande [52], Deloche [53] and Johnson [54], respectively.

recombination rate coefficients K_{HeAr^+} of He-assisted three-body collisional radiative recombination of atomic Ar^+ ions (He-CRR) [50] and earlier data for several molecular ions measured in helium by Cao *et al* [51]. The data of Berlande [52], Deloche [53], and Johnson [54] are for He_2^+ ion in helium. The Ar^+ data and those of Cao *et al* are very close to the theoretical values (indicated by a dotted line) of Bates and Khare [32], scaled for atomic Ar^+ ions in He by the reduced mass [50]. At the higher temperatures the present values of K_{He} and K_{H_2} for H_3^+ are much larger than those predicted by the Bates and Khare theory and do not show a measurable dependence on temperature for the range of 240–340 K.

5. Summary and conclusions

We have studied the recombination of H_3^+ ions with electrons at temperatures from 240 K to 340 K in pure H_2 and in $\text{He}/\text{Ar}/\text{H}_2$ mixtures at pressures from 600 Pa up to 2700 Pa using a stationary afterglow SA-CRDS apparatus. The measured recombination rate coefficients $\alpha_{\text{eff-ion}}$ are found to initially increase with $[\text{He}]$ and $[\text{H}_2]$ and then to saturate. The accessible temperature range was limited to $T > 240 \text{ K}$ because at used gas densities the abundance of fast recombining H_5^+ ions increases sharply at lower temperatures. The formation of H_5^+ does make a contribution at higher temperatures [47] but it is not the main cause of the density dependences observed for $[\text{H}_2] < 10^{16} \text{ cm}^{-3}$, as had been surmised by us and others

Table A1. The reactions considered in the model of the formation and destruction of H_3^+ ions.

No.	Reaction	Rate coefficient [cm^3s^{-1}], [cm^6s^{-1}]	Characteristic reaction time [μs]	Reference
R1	$\text{He}^+ + 2 \text{He} \rightarrow \text{He}_2^+ + \text{He}$	1×10^{-31}	250	[62]
R2	$\text{He}^+ + \text{H}_2 \rightarrow \text{H}^+ + \text{He} + \text{H}$ (83%) $\rightarrow \text{H}_2^+ + \text{He}$ (17%)	1.1×10^{-13}	900	[63]
R3	$\text{He}^m + \text{He}^m \rightarrow \text{He}_2^+ + \text{e}^-$	5×10^{-9}	2000	[64]
R4	$\text{He}^m + \text{Ar} \rightarrow \text{Ar}^+ + \text{He} + \text{e}^-$	7×10^{-11}	30	[61]
R5	$\text{He}^m + \text{H}_2 \rightarrow \text{H}_2^+ + \text{He} + \text{e}^-$ (90%) $\rightarrow \text{HeH}^+ + \text{H} + \text{e}^-$ (10%)	3.2×10^{-11}	3	[65, 66]
R6	$\text{HeH}^+ + \text{H}_2 \rightarrow \text{H}_3^+ + \text{He}$	1.5×10^{-9}	0.07	[63]
R7	$\text{He}_2^+ + \text{Ar} \rightarrow \text{Ar}^+ + 2 \text{He}$	2×10^{-10}	10	[62]
R8	$\text{Ar}^+ + \text{H}_2 \rightarrow \text{ArH}^+ + \text{H}$ (85%) $\rightarrow \text{H}_2^+ + \text{Ar}$ (15%)	8.6×10^{-10}	0.1	[67]
R9	$\text{ArH}^+ + \text{H}_2 \rightarrow \text{H}_3^+ + \text{Ar}$	1.5×10^{-9}	0.07	[68]
R10	$\text{H}^+ + \text{He} + \text{He} \rightarrow \text{HeH}^+ + \text{He}$	9×10^{-32}	300	[69]
R11	$\text{H}^+ + \text{H}_2 + \text{H}_2 \rightarrow \text{H}_3^+ + \text{H}_2$	3×10^{-29}	300	[70]
R12	$\text{H}^+ + \text{H}_2 + \text{He} \rightarrow \text{H}_3^+ + \text{He}$	3×10^{-29}	20	estimate ^a
R13	$\text{H}_2^+ + \text{Ar} \rightarrow \text{ArH}^+ + \text{H}$	2.3×10^{-9}	1	[71]
R14	$\text{H}_2^+ + \text{H}_2 \rightarrow \text{H}_3^+ + \text{H}$	2.1×10^{-9}	0.05	[71]
R15	$\text{H}_3^+ + \text{H}_2 + \text{He} \rightarrow \text{H}_5^+ + \text{He}$	2×10^{-30}	250	estimate ^b
R16	$\text{H}_3^+ + \text{H}_2 + \text{H}_2 \rightarrow \text{H}_5^+ + \text{H}_2$	2×10^{-30}	5000 ^c	[46]
R17	$\text{H}_5^+ + \text{H}_2 \rightarrow \text{H}_3^+ + \text{H}_2 + \text{H}_2$	3×10^{-12}	30 ^d	[46, 47]
R18	$\text{H}_5^+ + \text{He} \rightarrow \text{H}_3^+ + \text{H}_2 + \text{He}$	3×10^{-12}	2	estimate ^e
R19	$\text{H}_5^+ + \text{e}^- \rightarrow \text{products}$	2×10^{-6}	5	[49]
R20	$\text{e}^- + \text{He}$ (elastic cooling)	7.3×10^{-13}	7	[24] ^f

Comments: The reaction rate coefficient for reaction (Ri) is denoted as k_i .

^a It is assumed that $k_{12} = k_{11}$.

^b k_{15} was assumed to be the same as k_{16} .

^c The reaction rate coefficient for reaction (R16) was extrapolated to 300 K from the values measured by Johnsen *et al* [46] in the temperature range of 156–210 K as $k_{16} = 2 \times 10^{-30}(T/300 \text{ K})^{-2.9} \text{ cm}^3 \text{ s}^{-1}$.

^d The rate coefficient for reaction (R17) was calculated as $k_{17} = k_{16}/K_C$, where the equilibrium constant K_C was taken from [47].

^e It is assumed that $k_{18} = k_{17}$.

^f The effective rate coefficient for elastic cooling of electrons was calculated for 300 K, for details see [24].

Note: The rate coefficients are for 300 K if available. The characteristic reaction times are calculated for $[\text{He}] = 2 \times 10^{17} \text{ cm}^{-3}$, $[\text{Ar}] = 5 \times 10^{14} \text{ cm}^{-3}$, $[\text{H}_2] = 1 \times 10^{16} \text{ cm}^{-3}$, $[\text{He}^m] = n_e = 10^{11} \text{ cm}^{-3}$. The rate coefficients for the reactions of H_2^+ are given for ions with vibrational excitation $v \leq 1$.

[31, 55]. Our results provide a more detailed picture of recombination in hydrogen containing afterglows and to some extent explain the discrepancies between earlier afterglow studies of H_3^+ recombination. It is also clear that models of hydrogen discharges, for instance those used in spectroscopy should include three-body in addition to binary H_3^+ recombination. The fast three-body H_2 assisted recombination process can also influence processes in H_2 rich ionospheres of large planets, e.g. Jupiter and Jupiter-like planets, in regions where $[\text{H}_2] > 10^{14} \text{ cm}^{-3}$ [56–58], and may be important for chemistry of gas giant exoplanets. The formula given by equation (15) can be used to calculate effective recombination rate coefficients for the conditions encountered in a particular application, regardless of whether or not our simplified complex model is valid.

The proposed complex formation model considers two parallel recombination processes: Binary recombination (characterized by α_{bin}) and three-body recombination proceeding via formation (characterized by α_{F}) of long-lived highly excited

$\text{H}_3^{\#}$ and subsequent stabilization in collision with atomic He or molecular H_2 . This model reproduces the measured dependence of $\alpha_{\text{eff-ion}}$ on $[\text{He}]$ and $[\text{H}_2]$ in terms of the parameters α_{bin} , α_{F} , K_{He} , and K_{H_2} . The present values of α_{bin} agree well with those obtained in our previous afterglow experiments (see e.g. [20–22, 26, 33]), those obtained in storage ring experiments [14–16] and with theoretically predicted values [12, 13]. The value of α_{F} is in the covered temperature range nearly the same as that measured in our previous experiment at 300 K [31].

It is striking but not unexpected that K_{He} is larger by factor of 100 than one would predict from the theory of Bates and Khare [32], and that the mean value of $K_{\text{H}_2} = (9.4 \pm 1.3) \times 10^{-23} \text{ cm}^6 \text{ s}^{-1}$ at 240–340 K is higher by another factor of 1000. The theory of Bates and Khare [32] is strictly applicable only to atomic ions recombining in atomic gases. We have discussed possible mechanisms of the three-body He assisted recombination in several of our previous papers [20, 21, 31, 33] and some aspects of the problem have

been discussed by Johnsen and Guberman in [7]. Possible routes to complex formation may be electron capture by rotational excitation of the ion core into Rydberg states with low electronic angular momentum l , followed by collisional l -mixing that increases the lifetime. Stabilization in collisions with He or H₂ may involve formation of excited (H₃-He)[#] or (H₃-H₂)[#] and subsequent dissociation. The current studies cannot shed much more light on such details, but more could probably be learned from spectroscopic observations, such as those of Amano and Chan in deuterium afterglows [59], who observed long-lived D₃ molecules with above-thermal energies. It is still not quite clear whether or not long-lived H₃[#] molecules are formed in binary electron-H₃⁺ collisions. They were observed in early merged-beam experiments [60] but not in later storage ring experiments.

There are still many open questions concerning H₃⁺ recombination in plasmatic experiments, e.g. the effect of other third bodies on the measured recombination rate, the influence of electron number density and the seeming absence of electron assisted collisional radiative recombination at low temperatures [24]. These issues should be addressed in future experiments.

Acknowledgments

This work was partly supported by Czech Science Foundation projects GACR 14-14649P, GACR P209/12/0233 and GACR 15-15077S and by Charles University in Prague projects GAUK 692214, GAUK 572214, UNCE 204020/2012 and SVV 260 090.

Appendix. The model of chemical kinetics

A model of chemical kinetics is employed to calculate the chemical evolution of the afterglow plasma at given conditions. The reactions that are most important for the formation and destruction of H₃⁺ ions in a mixture of He/Ar/H₂ are summarized in table A1. The number density of metastable helium atoms He^m at the beginning of the afterglow was assumed to be the same as the electron number density, [He^m] = n_e . This assumption is based on experimental study described in [61]. The rate coefficients listed in table A1 are for 300 K. For some reactions we had to extrapolate the measured temperature dependences found in literature to 300 K. For some associative reactions in He buffer we used rate coefficients measured for H₂ (reactions (R12) and (R15)).

References

- [1] Oka T 2006 *Proc. Natl Acad. Sci. USA* **103** 12235
- [2] Crabtree K N, Indriolo N, Kreckel H, Tom B A and McCall B J 2011 *Astrophys. J.* **729** 15
- [3] Larsson M and Orel A E 2008 *Dissociative Recombination of Molecular Ions* (Cambridge: Cambridge University Press)
- [4] Larsson M 2012 *Phil. Trans. R. Soc. A* **370** 5118
- [5] Oka T 2012 *Phil. Trans. R. Soc. A* **370** 4991
- [6] Oka T 2015 *EPJ Web Conf.* **84** 06001
- [7] Johnsen R and Guberman S L 2010 *Advances in Atomic, Molecular, and Optical Physics* vol 59 ed E Arimondo et al (New York: Academic) pp 75–128
- [8] Smith D and Španěl P 1993 *Int. J. Mass Spectrom.* **129** 163
- [9] Michels H H and Hobbs R H 1984 *Astrophys. J.* **286** L27
- [10] Bates D, Guest M and Kendall R 1993 *Planet. Space Sci.* **41** 9
- [11] Kokoouline V, Greene C H and Esry B D 2001 *Nature* **412** 891
- [12] Fonseca dos Santos S, Kokoouline V and Greene C H 2007 *J. Chem. Phys.* **127** 124309
- [13] Jungen C and Pratt S T 2009 *Phys. Rev. Lett.* **102** 023201
- [14] McCall B J et al 2003 *Nature* **422** 500
- [15] Kreckel H et al 2005 *Phys. Rev. Lett.* **95** 263201
- [16] Wolf A et al 2006 *Phil. Trans. R. Soc. A* **364** 2981
- [17] Tom B A et al 2009 *J. Chem. Phys.* **130** 031101
- [18] Petrigani A et al 2011 *Phys. Rev. A* **83** 032711
- [19] Kreckel H, Petrigani A, Novotný O, Crabtree K, Buhr H, McCall B J and Wolf A 2012 *Phil. Trans. R. Soc. A* **370** 5088
- [20] Glosík J, Korolov I, Plašil R, Novotný O, Kotrík T, Hlavenka P, Varju J, Mikhailov I A, Kokoouline V and Greene C H 2008 *J. Phys. B: At. Mol. Opt.* **41** 191001
- [21] Glosík J, Plašil R, Korolov I, Kotrík T, Novotný O, Hlavenka P, Dohnal P, Varju J, Kokoouline V and Greene C H 2009 *Phys. Rev. A* **79** 052707
- [22] Rubovič P, Dohnal P, Hejduk M, Plašil R and Glosík J 2013 *J. Phys. Chem. A* **117** 9626
- [23] Varju J, Hejduk M, Dohnal P, Jílek M, Kotrík T, Plašil R, Gerlich D and Glosík J 2011 *Phys. Rev. Lett.* **106** 203201
- [24] Dohnal P, Hejduk M, Varju J, Rubovič P, Roučka Š, Kotrík T, Plašil R, Glosík J and Johnsen R 2012 *J. Chem. Phys.* **136** 244304
- [25] Dohnal P, Hejduk M, Varju J, Rubovič P, Roučka Š, Kotrík T, Plašil R, Johnsen R and Glosík J 2012 *Phil. Trans. R. Soc. A* **370** 5101
- [26] Hejduk M, Dohnal P, Rubovič P, Kálosi Á, Plašil R, Johnsen R and Glosík J 2015 *J. Chem. Phys.* **143** 044303
- [27] Adams N G, Smith D and Alge E 1984 *J. Chem. Phys.* **81** 1778
- [28] Plašil R, Glosík J, Poterya V, Kudrna P, Ruzs J, Tichý M and Pysanenko A 2002 *Int. J. Mass Spectrom.* **218** 105
- [29] Leu M T, Biondi M A and Johnsen R 1973 *Phys. Rev. A* **8** 413
- [30] Amano T 1990 *J. Chem. Phys.* **92** 6492
- [31] Dohnal P, Rubovič P, Kálosi Á, Hejduk M, Plašil R, Johnsen R and Glosík J 2014 *Phys. Rev. A* **90** 042708
- [32] Bates D R and Khare S P 1965 *Proc. Phys. Soc.* **85** 231
- [33] Glosík J, Plašil R, Kotrík T, Dohnal P, Varju J, Hejduk M, Korolov I, Roučka Š and Kokoouline V 2010 *Mol. Phys.* **108** 2253
- [34] Johnsen R, Rubovič P, Dohnal P, Hejduk M, Plašil R and Glosík J 2013 *J. Phys. Chem. A* **117** 9477
- [35] Glosík J, Plašil R, Poterya V, Kudrna P, Tichý M and Pysanenko A 2001 *J. Phys. B: At. Mol. Opt.* **34** L485
- [36] Glosík J, Novotný O, Pysanenko A, Zakouřil P, Plašil R, Kudrna P and Poterya V 2003 *Plasma Sources Sci. Technol.* **12** S117
- [37] Romanini D, Kachanov A, Sadeghi N and Stoeckel F 1997 *Chem. Phys. Lett.* **264** 316
- [38] Macko P, Bánó G, Hlavenka P, Plašil R, Poterya V, Pysanenko A, Votava O, Johnsen R and Glosík J 2004 *Int. J. Mass Spectrom.* **233** 299
- [39] Hlavenka P, Plašil R, Bánó G, Korolov I, Gerlich D, Ramanlal J, Tennyson J and Glosík J 2006 *Int. J. Mass Spectrom.* **255/256** 170
- [40] Hlavenka P, Korolov I, Plašil R, Varju J, Kotrík T and Glosík J 2006 *Czech. J. Phys.* **56** B749
- [41] Glosík J, Hlavenka P, Plašil R, Windisch F, Gerlich D, Wolf A and Kreckel H 2006 *Phil. Trans. R. Soc. A* **364** 2931

- [42] Hejduk M, Dohnal P, Varju J, Rubovič P, Plašil R and Glosík J 2012 *Plasma Sources Sci. Technol.* **21** 024002
- [43] Lindsay C M and McCall B J 2001 *J. Mol. Spectrosc.* **210** 60
- [44] Rothman L *et al* 2009 *J. Quant. Spectrosc. Radiat. Transfer* **110** 533
- [45] Paul W, Lcke B, Schlemmer S and Gerlich D 1995 *Int. J. Mass Spectrom.* **149/150** 373
- [46] Johnsen R, Huang C M and Biondi M A 1976 *J. Chem. Phys.* **65** 1539
- [47] Hiraoka K 1987 *J. Chem. Phys.* **87** 4048
- [48] Novotný O, Plašil R, Pysanenko A, Korolov I and Glosík J 2006 *J. Phys. B: At. Mol. Opt. Phys.* **39** 2561
- [49] MacDonald J A, Biondi M A and Johnsen R 1984 *Planet. Space Sci.* **32** 651
- [50] Dohnal P, Rubovič P, Kotřík T, Hejduk M, Plašil R, Johnsen R and Glosík J 2013 *Phys. Rev. A* **87** 052716
- [51] Cao Y S and Johnsen R 1991 *J. Chem. Phys.* **94** 5443
- [52] Berlande J, Cheret M, Deloche R, Gonfalone A and Manus C 1970 *Phys. Rev. A* **1** 887
- [53] Deloche R, Monchicourt P, Cheret M and Lambert F 1976 *Phys. Rev. A* **13** 1140
- [54] Johnson A W and Gerardo J B 1971 *Phys. Rev. Lett.* **27** 835
- [55] Gougousi T, Johnsen R and Golde M 1995 *Int. J. Mass Spectrom.* **149/150** 131
- [56] Badman S, Branduardi-Raymont G, Galand M, Hess S, Krupp N, Lamy L, Melin H and Tao C 2015 *Space Sci. Rev.* **187** 99
- [57] Barrow D and Matcheva K I 2011 *Icarus* **211** 609
- [58] Menager H, Barthlemy M and Lilensten J 2010 *Astron. Astrophys.* **509** A56
- [59] Amano T and Chan M 2000 *Phil. Trans. R. Soc. A* **358** 2457
- [60] Yousif F B, Van der Donk P J T, Orakzai M and Mitchell J B A 1991 *Phys. Rev. A* **44** 5653
- [61] Glosík J, Bánó G, Plašil R, Luca A and Zakouřil P 1999 *Int. J. Mass Spectrom.* **189** 103
- [62] Ikezoe Y, Matsuoka S, Takebe M and Viggiano A 1987 *Gas Phase Ion-Molecule Reaction Rate Constants* (Tokyo: The Mass Spectroscopy Society)
- [63] Anicich V G 2003 *An Index of the Literature for Bimolecular Gas Phase Cation-Molecule Reaction Kinetics* (Pasadena, CA: Jet Propulsion Laboratory)
- [64] Urbain X 1999 *Dissociative Recombination, Theory, Experiment and Applications IV* ed M Larsson *et al* (Singapore: World Scientific) p 131
- [65] Lindinger W, Schmeltekopf A L and Fehsenfeld F C 1974 *J. Chem. Phys.* **61** 2890
- [66] Martin D W, Weiser C, Sperlein R F, Bernfeld D L and Siska P E 1989 *J. Chem. Phys.* **90** 1564
- [67] Bedford D and Smith D 1990 *Int. J. Mass Spectrom.* **98** 179
- [68] Villinger H, Futrell J H, Howorka F, Duric N and Lindinger W 1982 *J. Chem. Phys.* **76** 3529
- [69] Chatterjee B K and Johnsen R 1990 *J. Chem. Phys.* **93** 5681
- [70] Plašil R, Zymak I, Jusko P, Mulin D, Gerlich D and Glosík J 2012 *Phil. Trans. R. Soc. A* **370** 5066
- [71] Glosík J 1994 *Int. J. Mass Spectrom.* **139** 15

Monitoring the removal of excited particles in He/Ar/H₂ low temperature afterglow plasma at 80–300 K

Kálosi Á., Dohnal P., Augustovičová L., Roučka Š., Plašil R., Glosík J.

Eur. Phys. J.-Appl. Phys. **75(2)**, 24707, 2016.

Monitoring the removal of excited particles in He/Ar/H₂ low temperature afterglow plasma at 80–300 K[★]

Ábel Kálosi¹, Petr Dohnal¹, Lucie Augustovičová², Štěpán Roučka¹, Radek Plašil¹, and Juraĵ Glosík^{1,a}

¹ Department of Surface and Plasma Science, Faculty of Mathematics and Physics, Charles University in Prague, 18000 Prague, Czech Republic

² JILA, University of Colorado and National Institute of Standards and Technology, 80309-0440 Boulder, Colorado, USA

Received: 30 November 2015 / Received in final form: 14 January 2016 / Accepted: 20 January 2016
© EDP Sciences 2016

Abstract. Stationary afterglow (SA) experiments with cavity ring down absorption spectrometer (cw-CRDS) have been used to study recombination of H₃⁺ ions with electrons. To characterize the plasma during the afterglow we monitored the time evolution of density of He₂ excited dimers (*a*³Σ_u⁺) in plasmas in pure helium and in helium with small admixture of Ar and H₂. By monitoring the plasma decay and its dependence on [H₂] and [Ar] in the afterglow in pure He and in He/Ar/H₂ mixture we estimated the rate of plasma thermalization in the temperature range of 80–300 K. The inferred deexcitation rate coefficients for reaction of helium metastable atoms with H₂ were $(0.9 \pm 0.3) \times 10^{-10} \text{ cm}^3 \text{ s}^{-1}$, $(1.9 \pm 0.2) \times 10^{-10} \text{ cm}^3 \text{ s}^{-1}$ and $(2.7 \pm 0.2) \times 10^{-10} \text{ cm}^3 \text{ s}^{-1}$ at 80 K, 140 K and 300 K, respectively. The effective recombination rate coefficients for H₃⁺ were evaluated from the decay of the electron number density. We propose the lower estimate for the saturation of the effective recombination rate coefficient in H₃⁺ and D₃⁺ dominated plasma.

1 Introduction

Recombination of H₃⁺ ions with electrons at low temperature is important for theoretical physics, physical chemistry, plasma physics, and it is of special interest for astrophysics, because H₃⁺ is the most abundantly produced molecular ion in the Universe [1] that plays a key role in the chemistry of the interstellar medium [2]. Because of its importance, it was studied many times, but there were many discrepancies in the results [3]. The binary recombination of H₃⁺ ions was studied in merged electron-ion beam experiments [4,5] and in several afterglow experiments [3,6–9]. In afterglow experiments used for studies of H₃⁺ recombination the helium buffer gas is used to inhibit diffusive losses and to thermalize the electrons. Hydrogen is the precursor gas for H₃⁺ formation, and argon is added to remove undesired He metastable atoms created during the discharge [3,8]. Some experiments were carried out also in pure H₂ [10–12]. Using stationary afterglow (SA) and flowing afterglow with Langmuir probe (FALP) experiments we recently demonstrated that recombination in H₃⁺ dominated low temperature plasmas depends on the pressure of the ambient gas. We observed that already at He pressures of 100–2000 Pa, the ion losses

due to binary and ternary recombination processes are comparable. This is an unexpected result since the generally accepted classical theory of Bates and Khare [13] predicts such effects at pressures at least by three orders of magnitude higher. To study the ternary recombination processes the afterglow experiments have to be carried out over a large scale of pressures and for various compositions of gases. Because of the dependence of H₃⁺ recombination process on many parameters, the afterglow plasma has to be characterized very precisely. It is essential to create experimental conditions at which the afterglow plasma is in thermal equilibrium characterized by the temperature of the buffer gas.

This paper presents the results of the study of plasma thermalization at conditions used for the study of H₃⁺ recombination at low temperature and high pressures. The plasma thermalization was monitored by measuring the relative populations of molecular He₂ metastables and excited states of atomic Ar in the temperature range of 80–300 K. We also present and summarize the results of the measurements of binary and ternary rate coefficients of H₃⁺ recombination in afterglow plasmas.

2 Experimental

The experiments were performed using a stationary afterglow apparatus combined with continuous wave

^a e-mail: juraj.glosik@mff.cuni.cz

[★] Contribution to the topical issue “6th Central European Symposium on Plasma Chemistry (CESPC-6)”, edited by Nicolas Gherardi, Ester Marotta and Cristina Paradisi

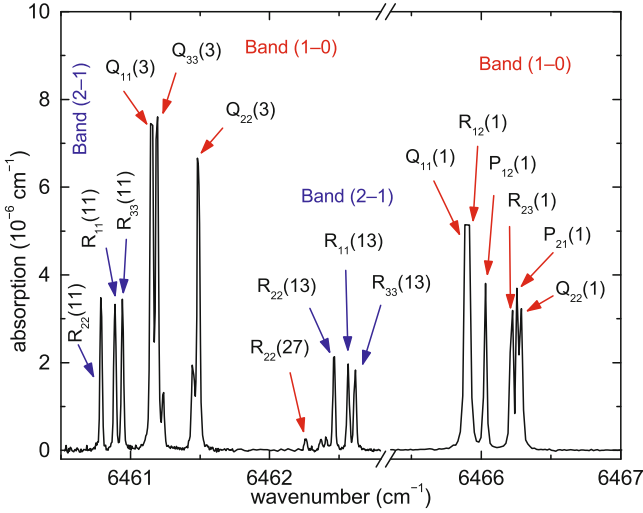


Fig. 1. Observed absorption spectrum of He₂ in the near-infrared spectral region: 6460.5–6467 cm⁻¹. The absorption lines belong to the (1–0) and (2–1) vibrational bands of the $b^3\Pi_g$ – $a^3\Sigma_u^+$ system. The measurement was performed during the discharge at 80 K in a He/Ar/H₂ mixture ($8 \times 10^{17}/10^{14}/2 \times 10^{14}$ cm⁻³). The lines are labelled with the corresponding quantum numbers $\Delta J_{F'F''}(N'')$, where $F = 1$ for $J = N + 1$, $F = 2$ for $J = N$, and $F = 3$ for $J = N - 1$ and the prime and double prime denote the upper and lower state, respectively.

cavity ring down spectrometer (SA-CRDS), for detailed description see e.g., references [14,15]. In the experiments the plasma is formed in a pulsed microwave discharge (2.45 GHz, 5–15 W) in a mixture of He/Ar/H₂ (typical composition $\sim 10^{17}/10^{14}/10^{14}$ cm⁻³), in a mixture of He/Ar ($\sim 10^{17}/10^{13}$ cm⁻³), in pure He ($\sim 10^{17}$ cm⁻³), or in pure H₂ ($\sim 10^{16}$ cm⁻³). Only normal H₂ was used in the experiments. Two fiber-coupled distributed feedback (DFB) laser diodes (1529.55 nm and 1546.92 nm) and a tunable external-cavity laser diode (Sacher TEC 500, 1380–1520 nm) were used as light sources. An example of the measured spectra is shown in Figure 1. The lines are labelled according to the notation used in reference [16].

By synchronizing the ring down acquisition with the microwave pulse, time resolved spectroscopy can be achieved with time resolution commensurate with the ring down time (typically ~ 32 μ s).

3 Theoretical calculations

The measured absorption lines were fitted by a Voigt profile and the obtained line positions (ν_{exp}) are listed in Table 1 together with calculated theoretical values (ν_{calc}). In the calculations we used an effective Hamiltonian for $^3\Sigma$ and $^3\Pi$ states [17] with matrix elements from reference [18] including selection rules and symmetry restrictions [19]. Note that the matrix elements listed in reference [18] are for the $^3\Sigma^-$ state. The matrix elements for the $^3\Sigma^+$ state are the same, except that f is replaced by e and e is replaced by f. The spectroscopic constants for $v = 0$ and $v = 1$ vibrational states of $a^3\Sigma_u^+$ and $b^3\Pi_g$ were

taken from reference [16], while those for the $v = 2$ vibrational state of $b^3\Pi_g$ were partly taken from reference [20] and partly set to be the same as for the $v = 1$ state.

To obtain the number densities of different states of He₂ we followed the procedure described by Tokaryk et al. [21]. We used potential energy curves for $a^3\Sigma_u^+$ and $b^3\Pi_g$ electronic states calculated by Yarkony [22] as an input into the program Level by Le Roy [23] for calculation of energy levels. The bound-states wavefunctions corresponding to the quantum numbers v and N were obtained as solutions of the Schrödinger equation using Numerov-Cooley methods [24,25] as implemented in reference [26]. The wavefunctions were then used together with the transition dipole moment function μ_{\perp} [22] connecting the given electronic states to calculate appropriate Einstein coefficients $A_{v'N'J' \rightarrow v''N''J''}$. A set of rotational line strength (Hönl-London) factors $S_{N'J',N''J''}$ [27] for an allowed $^3\Pi - ^3\Sigma$ transition in Hund's case (b) with a given $N = N'$ (or N'') when normalized obey a sum rule $\sum S_{N'J',N''J''} = 6(2N + 1)$, with the sum over all $\Delta N = N' - N''$ and over the different components J' and J'' . The calculated values of Einstein coefficients for a list of selected transitions are shown in Table 1.

The number density n_{He_2} of a particular state of He₂ was then determined using formula [28]:

$$n_{\text{He}_2} = 8\pi c \nu^2 \frac{2J'' + 1}{2J' + 1} \frac{\sqrt{2\pi}\sigma_D}{A_{v'N'J' \rightarrow v''N''J''}} \xi \text{ [cm}^{-3}\text{]}, \quad (1)$$

where c is speed of light (in units of cm s⁻¹), ξ (cm⁻¹) is the absorption coefficient at the centre of the Doppler broadened absorption line (described by standard deviation σ_D (cm⁻¹)), $A_{v'N'J' \rightarrow v''N''J''}$ (s⁻¹) is the Einstein coefficient for spontaneous emission of a photon with wavenumber ν (cm⁻¹), and J' and J'' are the rotational quantum numbers of the upper and lower state, respectively. At 80 K, the obtained number densities of the $v = 0$, $N = 1$, $J = 0$ $a^3\Sigma_u^+$ state of He₂ during the discharge were on the order of 10^9 cm⁻³ in 900 Pa of pure He and on the order of 10^7 cm⁻³ in a mixture of He/Ar/H₂. For example at $8 \times 10^{17}/1 \times 10^{14}/2 \times 10^{14}$ cm⁻³ and measured absorption coefficient at the centre of the absorption line $\xi = 3.2 \times 10^{-6}$ cm⁻¹ (corresponding to R₂₃(1) transition in Fig. 1), the obtained number density of $v = 0$, $N = 1$, $J = 0$ $a^3\Sigma_u^+$ state of He₂ is 1.1×10^7 cm⁻³.

4 Results and discussion

One necessary condition for measuring a recombination rate coefficient of H₃⁺ in SA-CRDS experiments is that the afterglow plasma has to be free from excited particles that may in superelastic collisions heat the electrons. It has been observed many times that in an afterglow plasma in He the presence of excited neutrals can be suppressed by a small admixture of a reactant gas which removes He and He₂ metastables by Penning ionization [29,30]. The time evolutions of the relative populations of He₂ (transitions Q₂₂(1) and R₂₂(27) originating from the

Table 1. Measured transitions (ν_{exp}) belonging to the (1–0) and (2–1) vibrational bands of the He₂ $b^3\Pi_g - a^3\Sigma_u^+$ system compared to the calculated values (ν_{calc}). The estimated error of the measurement is $5 \times 10^{-3} \text{ cm}^{-1}$. The calculated Einstein coefficients of spontaneous emission A are also listed.

band	transition	$\nu_{\text{exp}}(\text{cm}^{-1})$	$\nu_{\text{calc}}(\text{cm}^{-1})$	A (10^4 s^{-1})	band	transition	$\nu_{\text{exp}}(\text{cm}^{-1})$	$\nu_{\text{calc}}(\text{cm}^{-1})$	A (10^4 s^{-1})
(2–1)	R ₂₂ (15)	6459.925	6459.918	13.8	(2–1)	R ₂₂ (13)	6462.464	6462.460	13.7
(2–1)	R ₁₁ (15)	6460.028	6460.024	13.9	(2–1)	R ₁₁ (13)	6462.565	6462.564	13.7
(2–1)	R ₃₃ (15)	6460.074	6460.072	13.9	(2–1)	R ₃₃ (13)	6462.615	6462.616	13.8
(2–1)	R ₂₂ (11)	6460.788	6460.785	13.5	(1–0)	Q ₁₁ (1) ^c	6465.886	6465.890	9.6
(2–1)	R ₁₁ (11)	6460.888	6460.886	13.6	(1–0)	R ₁₂ (1) ^d	6465.917	6465.919	3.0
(2–1)	R ₃₃ (11)	6460.943	6460.943	13.6	(1–0)	P ₁₂ (1)	6466.027	6466.026	6.1
(1–0)	Q ₁₁ (3)	6461.151	6461.154	11.3	(1–0)	R ₂₃ (1)	6466.216	6466.217	4.0
(1–0)	Q ₃₃ (3)	6461.190	6461.192	10.7	(1–0)	P ₂₁ (1)	6466.260	6466.261	5.0
(1–0)	P ₃₂ (3)	6461.234	6461.236	1.9	(1–0)	Q ₂₂ (1)	6466.289	6466.290	3.1
(1–0)	R ₂₃ (3) ^a	6461.446	6461.444	1.0	(1–0)	R ₂₂ (21)	6533.661	6533.666	8.2
(1–0)	P ₂₁ (3) ^b	6461.460	6461.456	1.0	(1–0)	R ₁₁ (21)	6533.765	6533.760	8.4
(1–0)	Q ₂₂ (3)	6461.488	6461.488	10.1	(1–0)	R ₃₃ (21)	6533.806	6533.811	8.2
(1–0)	R ₂₂ (27)	6462.260	6462.251	8.2	(1–0)	R ₂₂ (5)	6536.518	6536.518	7.2
(1–0)	R ₁₁ (27)	6462.369	6462.360	8.2	(1–0)	R ₁₁ (5)	6536.598	6536.599	7.5
(1–0)	R ₃₃ (27)	6462.407	6462.411	8.2	(1–0)	R ₃₃ (5)	6536.694	6536.694	7.2

^aBlended with P₂₁(3); ^bblended with R₂₃(3); ^cblended with R₁₂(1); ^dblended with Q₁₁(1).

$a^3\Sigma_u^+(v = 0)$ electronic state) measured during the discharge and the afterglow in pure He are shown in Figure 2a. The decrease of the densities of both states is very slow and it is clear that highly excited He₂ are present even 1 ms after switching off the discharge. This is consistent with previously observed slow decrease of the electron temperature in He afterglow [30]. Detailed description of the processes involving atomic and molecular metastables in He buffered plasmas is given e.g., in reference [21].

Excited He and He₂ metastables can be removed from the afterglow plasma by adding Ar to the He buffer gas. The removal of metastable particles from the afterglow plasma by adding Ar leads to a decrease in electron temperature [30]. In the present study we observed the removal of He₂ and excited Ar ($3s^23p^5(^2P_{1/2}^{\circ})3d^2[3/2]^{\circ}$, $J = 2$) on a microsecond scale in the He/Ar/H₂ mixture (see Fig. 3). This is substantially faster than the time scale of the electron density decrease in a plasma that is dominated by the recombination of H₃⁺ ions at similar conditions (see Fig. 2b).

As there are several allowed transitions from the $3s^23p^5(^2P_{1/2}^{\circ})3d^2[3/2]^{\circ}$, $J = 2$ excited state of argon to lower states with corresponding Einstein A coefficients on the order of 10^6 s^{-1} [32] the lifetime of the $3s^23p^5(^2P_{1/2}^{\circ})3d^2[3/2]^{\circ}$, $J = 2$ state will be on the order of hundreds of nanoseconds or lower. As can be seen from Figure 3a, the $3s^23p^5(^2P_{1/2}^{\circ})3d^2[3/2]^{\circ}$, $J = 2$ excited state of argon survives in the He/Ar mixture ($4.1 \times 10^{17}/2.1 \times 10^{13} \text{ cm}^{-3}$) after switching off the discharge substantially longer than what would have been expected from its lifetime. This indicates that another source of excitation energy is present as the energy difference between the $3s^23p^5(^2P_{1/2}^{\circ})3d^2[3/2]^{\circ}$, $J = 2$ state and the ground state of argon is more than 14 eV. The most likely source of this

energy are helium metastable atoms that are produced in the discharge. In the afterglow the helium metastable atoms are removed by Penning ionization of argon. With the rate coefficient $k_{\text{PI}} = 7 \times 10^{-11} \text{ cm}^3 \text{ s}^{-1}$ [33] and $[\text{Ar}] = 2.1 \times 10^{13} \text{ cm}^{-3}$ the characteristic reaction time for Penning ionization of Ar by helium metastable atoms is $\approx 700 \mu\text{s}$, i.e., similar to the time constant of the decay of the $3s^23p^5(^2P_{1/2}^{\circ})3d^2[3/2]^{\circ}$, $J = 2$ excited state of argon in the afterglow plasma as shown by the dashed line in Figure 3a. At conditions used in H₃⁺ recombination studies [31,34] the $3s^23p^5(^2P_{1/2}^{\circ})3d^2[3/2]^{\circ}$, $J = 2$ state of argon is quickly removed from the afterglow (full line in Fig. 3a) indirectly hinting that also the helium metastable atoms are being destroyed.

We have performed several measurements of time evolutions of the absorption signals proportional to the number densities of the $3s^23p^5(^2P_{1/2}^{\circ})3d^2[3/2]^{\circ}$, $J = 2$ state of argon and the $a^3\Sigma_u^+(v = 0)$, $N = 1$ state of He₂ in the discharge and in the afterglow plasma at different $[\text{Ar}]$ and $[\text{H}_2]$. The results obtained at 140 K are plotted in Figure 4. As can be seen from Figure 4, the decay of the absorption signal is faster with increasing $[\text{H}_2]$. Similar dependence on $[\text{Ar}]$ was also observed. We have evaluated the measured decay curves by fitting them with a single exponential decay. The dependences of the reciprocal values $1/\tau$ of the measured time constants τ of the exponential decays on $[\text{H}_2]$ are plotted in the insert of Figure 4. The measured time constants for given states of Ar and He₂ are the same within the experimental errors in the probed range of $[\text{Ar}]$ and $[\text{H}_2]$ (for details see the insert of Fig. 4) indicating that metastable helium atoms probably serve as precursors for the creation of both He₂ and the $3s^23p^5(^2P_{1/2}^{\circ})3d^2[3/2]^{\circ}$, $J = 2$ state of Ar in the afterglow. The corresponding rate coefficient for destruction of

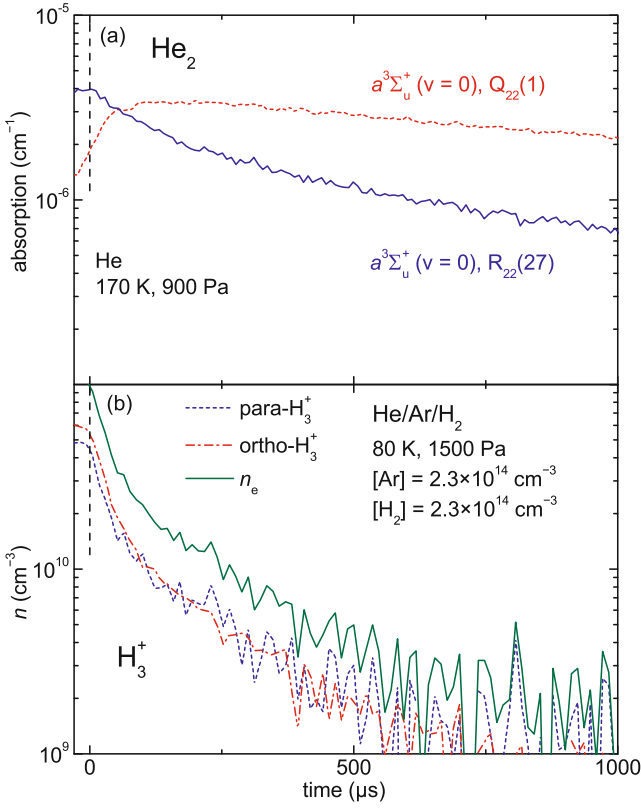


Fig. 2. (a) Time evolution of the absorption in the afterglow plasma measured at 170 K in 900 Pa of pure He using the transitions originating from the ground vibrational state (transitions $Q_{22}(1)$ and $R_{22}(27)$) of the $a^3\Sigma_u^+$ electronic state of the He_2 molecule. The upper state belongs to the first vibrational state of the $b^3\Pi_g$ electronic state of He_2 . Unlike the $R_{22}(27)$ transition, we were not able to measure at the centre of the $Q_{22}(1)$ absorption line as the absorption was too strong, exceeding the limits of our spectrometer. The displayed time evolution of absorption was therefore measured slightly off the centre of the line (at 6466.362 cm^{-1} instead of 6466.289 cm^{-1}). The zero time is set at the beginning of the afterglow. (b) Time evolution of number densities of ortho- H_3^+ and para- H_3^+ ions measured in the afterglow plasma at 80 K in a He/Ar/ H_2 mixture ($1.4 \times 10^{18}/2.3 \times 10^{14}/2.3 \times 10^{14}\text{ cm}^{-3}$). The electron number density (n_e) is calculated under the assumption of plasma quasineutrality and thermal population of states [31].

helium metastable atoms (states 2^1S and 2^3S) in collisions with H_2 at 140 K evaluated from the slope of the linear fit to the data in the insert of Figure 4 is $k_M(140\text{ K}) = (1.9 \pm 0.2) \times 10^{-10}\text{ cm}^3\text{ s}^{-1}$. Similar analysis was also done for values obtained at 80 K and 300 K with resulting rate coefficients of $k_M(80\text{ K}) = (0.9 \pm 0.3) \times 10^{-10}\text{ cm}^3\text{ s}^{-1}$ and $k_M(300\text{ K}) = (2.7 \pm 0.2) \times 10^{-10}\text{ cm}^3\text{ s}^{-1}$. These values are close to the values reported in the literature [36–38]. Based on the measurements shown in Figure 4 we can estimate the densities of Ar and H_2 that are needed to remove the excited particles from the afterglow within 100 μs after switching off the discharge as required for our studies of recombination of H_3^+ ions (see Fig. 3).

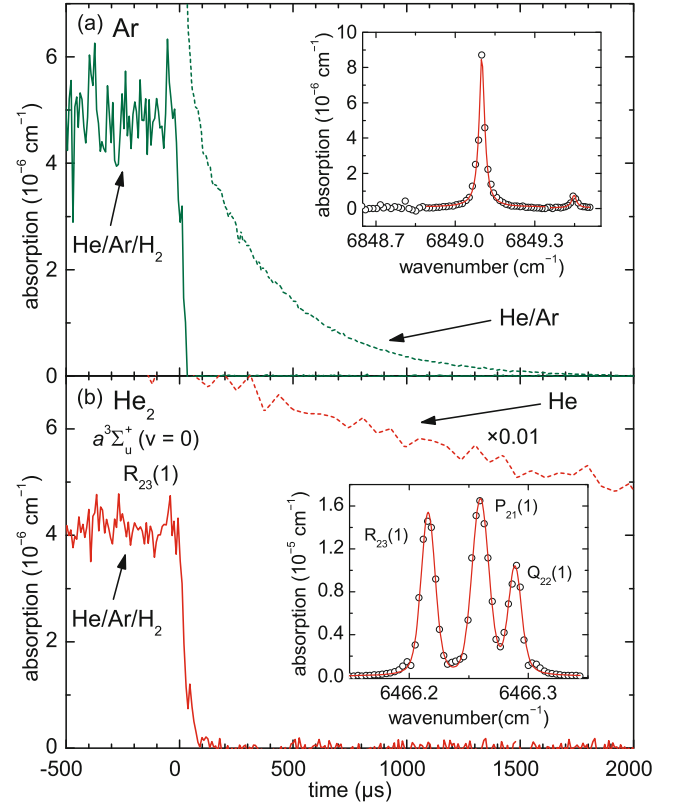


Fig. 3. (a) Time evolution of the absorption at the centre of an Ar absorption line (transition $3s^23p^5(^2P_{1/2}^o)3d^2[3/2]^o, J = 2 \rightarrow 3s^23p^5(^2P_{1/2}^o)4f^2[5/2], J = 3; 6849.099\text{ cm}^{-1}$ [32, 35]). The full and dashed lines denote the data measured at 80 K in a He/Ar/ H_2 mixture ($8.3 \times 10^{17}/3.4 \times 10^{14}/2.7 \times 10^{14}\text{ cm}^{-3}$) and in a He/Ar mixture ($4.1 \times 10^{17}/2.1 \times 10^{13}\text{ cm}^{-3}$), respectively. Note that in He/Ar the characteristic reaction time for Penning ionization of Ar by helium metastable atoms is $\approx 700\text{ }\mu\text{s}$ (with $k_{PI} = 7 \times 10^{-11}\text{ cm}^3\text{ s}^{-1}$ [33]). The insert shows the corresponding absorption line profile. (b) Time evolution of the absorption at the centre of a He_2 absorption line (transition $R_{23}(1)$ in the (1–0) vibrational band of the $b^3\Pi_g - a^3\Sigma_u^+$ system). The full and dashed lines denote the data obtained at 80 K in a He/Ar/ H_2 mixture ($7.6 \times 10^{17}/2.9 \times 10^{14}/2.5 \times 10^{14}\text{ cm}^{-3}$) and in pure He ($8.1 \times 10^{17}\text{ cm}^{-3}$) (scaled by a factor of 0.01 to fit into the figure), respectively. The insert shows the corresponding absorption line profiles.

In the present experiments using He/Ar/ H_2 gas mixtures we measured the decay of H_3^+ ion density (decay curve) by monitoring absorption of three states ((1,1) of para- H_3^+ and (1,0) and (3,3) of ortho- H_3^+ , for details on notation see Ref. [39]). The kinetic temperature of H_3^+ ions ($T_{\text{kin-ion}}$) was measured from the Doppler broadening of the absorption line profiles [31]. The rotational temperature (T_{rot}) and the ratio of densities of para- H_3^+ to ortho- H_3^+ were determined from measured partial populations of ions in the lowest rotational states of the vibrational ground state of H_3^+ [31]. On the basis of our measurements we conclude that for the afterglow plasmas in He/Ar/ H_2 in the SA-CRDS experiments the $T_{\text{kin-ion}}$ and T_{rot} of ions are

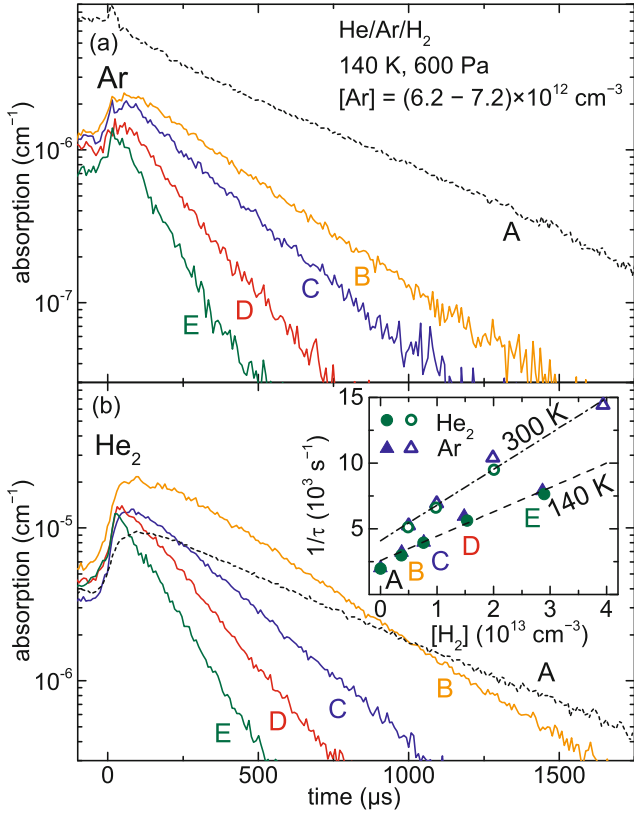


Fig. 4. (a) Time evolutions of the absorption coefficient measured at the centre of an argon absorption line (transition $3s^23p^5(2^2P_{1/2}^o)3d^2[3/2]^o, J = 2 \rightarrow 3s^23p^5(2^2P_{1/2}^o)4f^2[5/2], J = 3$; 6849.099 cm^{-1} [32,35]) in the discharge and the afterglow plasma, at $[\text{He}] = 3.1 \times 10^{17} \text{ cm}^{-3}$, $[\text{Ar}] \approx 6.7 \times 10^{12} \text{ cm}^{-3}$, and different densities of H_2 , capital letters A, B, C, D, and E indicate $[\text{H}_2] = 0, 3.8, 7.6, 15,$ and $29 \times 10^{12} \text{ cm}^{-3}$, respectively. The time is set to zero at the beginning of the afterglow. (b) Time evolutions of the absorption coefficient measured slightly off the centre of an He_2 absorption line (transition $\text{R}_{23}(1)$, measured at 6466.196 cm^{-1} instead of 6466.216 cm^{-1} , because of too high absorption at the centre of the absorption line) in the discharge and the afterglow plasma, at the same conditions as in panel (a). Inset: The $[\text{H}_2]$ dependences of the measured pseudo-first-order rate coefficients (reciprocal time constants $1/\tau$) of the exponential decays displayed in panels (a) (full triangles) and (b) (full circles). Capital letters A–E indicate corresponding $[\text{H}_2]$. For comparison the values of the same rate coefficients measured at 300 K and $[\text{He}] = 2.2 \times 10^{17} \text{ cm}^{-3}$ and $[\text{Ar}] = 7 \times 10^{12} \text{ cm}^{-3}$ for Ar (open triangles) and He_2 (open circles) are also plotted. The dashed and dot-dashed straight lines are fits to the measured pseudo-first-order rate coefficients at 140 K and 300 K, respectively.

equal to the temperature of the helium buffer gas (T_{He}) and the wall temperature (T_{wall}) of the discharge tube, i.e., we can write: $T = T_{\text{wall}} = T_{\text{He}} = T_{\text{rot}} = T_{\text{kin-ion}}$ (for details see Ref. [31]). The electron temperature T_e was not measured in the present study (see discussion in Ref. [31]). At He densities typical for the present experiments the estimated characteristic time of the electron cooling in collisions with He atoms is below $10 \mu\text{s}$.

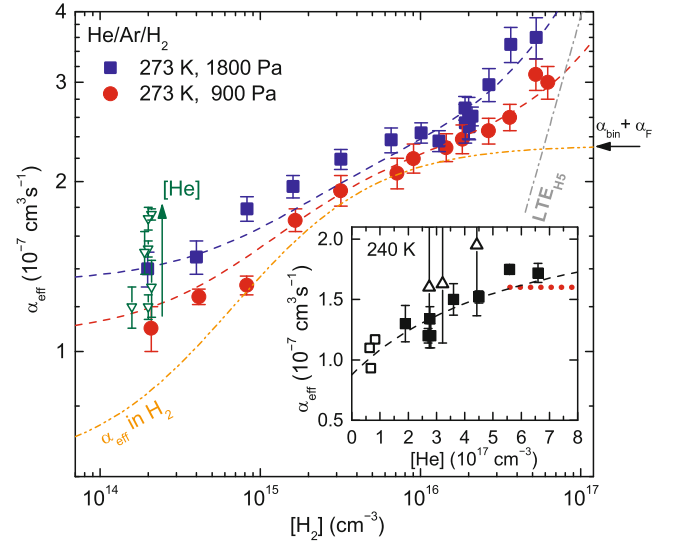


Fig. 5. Dependences of α_{eff} on $[\text{H}_2]$ measured at 273 K (the data were adapted from Ref. [12]). The dashed lines are fits to the data by equation (4) extended by the term accounting for H_5^+ formation. The double dot dashed line (α_{eff} in H_2) denotes the effective recombination rate coefficient α_{eff} that would have been measured in pure H_2 . The dot-dashed straight line (LTE_{H_5}) is the calculated upper limit of the contribution from H_5^+ formation (see Refs. [11,12]). The open triangles indicate the data measured in this experiment at fixed $[\text{H}_2] \approx 2 \times 10^{14} \text{ cm}^{-3}$ and different values of $[\text{He}]$, the arrow indicates the increase of α_{eff} with increasing $[\text{He}]$. Inset: Measured dependence of α_{eff} on $[\text{He}]$ (full squares) at 240 K compared to the values obtained in our previous SA (open squares) and FALP (open triangles) experiments [7]. The dashed line denotes the fit to the data by equation (4). The dotted line denotes the values measured by MacDonald [6] in neon at $[\text{Ne}] = 5.6 \times 10^{17} - 8 \times 10^{17} \text{ cm}^{-3}$.

An example of ion density decay curves of para- H_3^+ and ortho- H_3^+ measured at 80 K in a mixture of He/Ar/H₂ is plotted in Figure 2b. Because of the fast removal of He and He_2 metastables and Ar excited states in the used He/Ar/H₂ mixture (see Fig. 3) we can expect that the afterglow plasma dominated by H_3^+ recombination is in thermal equilibrium. From the measured decrease of ion densities during the afterglow the effective binary recombination rate coefficient α_{eff} can be calculated [31]. In systematic studies of dependence of α_{eff} on $[\text{He}]$ and $[\text{H}_2]$ we obtained dependences $\alpha_{\text{eff}}(T, [\text{He}], [\text{H}_2])$. Examples of typical data are plotted in Figure 5.

To understand the measured dependences $\alpha_{\text{eff}}(T, [\text{He}], [\text{H}_2])$, we propose a model where we consider binary recombination process:



where α_{bin} is the rate coefficient of binary dissociative recombination. We also consider ternary neutral assisted recombination, where we postulate formation of highly excited $\text{H}_3^\#$ “complexes” that can either decay by

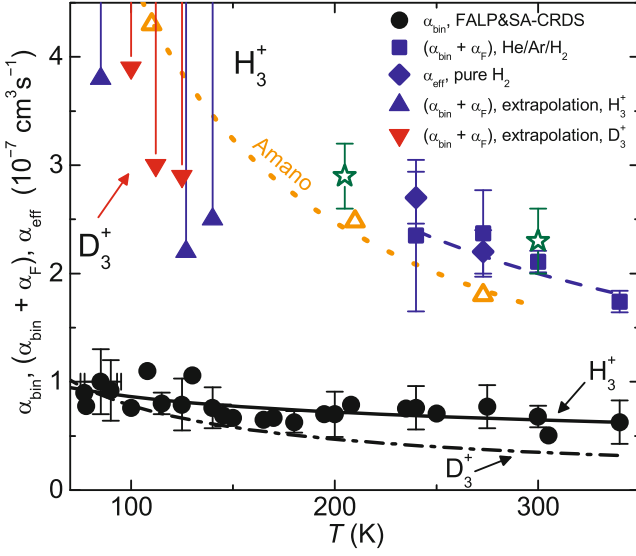
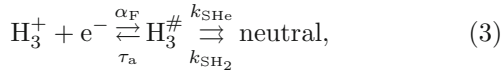


Fig. 6. Binary rate coefficient α_{bin} and the sum of $(\alpha_{\text{bin}} + \alpha_{\text{F}})$ characterizing the recombination of H_3^+ in low temperature plasmas. The lowest boundary estimates of $(\alpha_{\text{bin}} + \alpha_{\text{F}})$ (filled up-triangles) were obtained from the maxima of measured linear dependences of α_{eff} of H_3^+ ions on $[\text{He}]$. The filled down-triangles denote the lowest boundary estimates of $(\alpha_{\text{bin}} + \alpha_{\text{F}})$ obtained for D_3^+ (compilation of data from Ref. [40]). The open triangles indicate values of α_{eff} measured by Amano [10] in pure H_2 gas. The dotted line is a fit to Amano's values: $\alpha_{\text{Amano}} = 1.7 \times 10^{-7} (T/300 \text{ K})^{-0.94} \text{ cm}^3 \text{ s}^{-1}$. The stars show the values of α_{eff} obtained by Leu et al. [9] in high pressure stationary afterglow experiments. The diamonds and squares denote the values of α_{eff} measured by Glosík et al. [12] in pure H_2 gas and in a mixture of $\text{He}/\text{Ar}/\text{H}_2$ with $[\text{H}_2] > 2 \times 10^{16} \text{ cm}^{-3}$, respectively, these values are fitted by the dashed line [12]. The full and dot dashed lines are the fits to the values of α_{bin} of H_3^+ (full circles) and D_3^+ ions (only the fit is indicated, the data were taken from Ref. [41]), respectively.

autoionization or can be stabilized in collisions with He or H_2 :



where α_{F} is the binary rate coefficient for formation of $\text{H}_3^{\#}$, τ_a is the autoionization time constant, and k_{SHe} and k_{SH_2} are the binary rate coefficients for stabilization of $\text{H}_3^{\#}$ in collisions with He and H_2 , respectively. By writing the balance equations and by introducing $K_{\text{He}} = \alpha_{\text{F}} k_{\text{SHe}} \tau_a$ and $K_{\text{H}_2} = \alpha_{\text{F}} k_{\text{SH}_2} \tau_a$ we can obtain for α_{eff} (for details see Ref. [12]):

$$\alpha_{\text{eff}} = \alpha_{\text{bin}} + \alpha_{\text{F}} \frac{K_{\text{He}}[\text{He}] + K_{\text{H}_2}[\text{H}_2]}{\alpha_{\text{F}} + K_{\text{He}}[\text{He}] + K_{\text{H}_2}[\text{H}_2]}. \quad (4)$$

At high $[\text{He}]$ and/or $[\text{H}_2]$ densities the measured α_{eff} saturates at a value of $\alpha_{\text{eff}} = (\alpha_{\text{bin}} + \alpha_{\text{F}})$. In the low density limit ($[\text{He}]$ and $[\text{H}_2] \rightarrow 0$) equation (4) reduces to linear dependence $\alpha_{\text{eff}} = \alpha_{\text{bin}} + K_{\text{He}}[\text{He}] + K_{\text{H}_2}[\text{H}_2]$. The measured $\alpha_{\text{eff}}(T, [\text{He}], [\text{H}_2])$ are fitted by formula (4) extended

by the term accounting for formation of H_5^+ ions and their consequent recombination [12]. From the fits of data measured over a sufficiently broad range of He and H_2 densities the values of α_{bin} , α_{F} , K_{He} , and K_{H_2} can be determined. The obtained values of the binary recombination rate coefficient α_{bin} and the values of $(\alpha_{\text{bin}} + \alpha_{\text{F}})$ are shown in Figure 6.

Under our present experimental conditions at temperatures below 240 K the losses of H_3^+ ions due to the formation of H_5^+ dominate at high $[\text{He}]$ and $[\text{H}_2]$ over losses due to the ternary recombination, and from the measured dependence of α_{eff} on $[\text{He}]$ (see insert in Fig. 5) only a lower limit for the value of $(\alpha_{\text{bin}} + \alpha_{\text{F}})$ can be estimated. In Figure 6 we included these lower limits obtained in our experiments with H_3^+ at low temperatures. For comparison we also plotted lower limits obtained for D_3^+ from the compilation of data measured in our previous experiments [40]. The ternary recombination rate coefficients K_{He} and K_{H_2} and their temperature dependence (in the range of 240–340 K) are discussed in our previous publication (see Ref. [12]).

5 Conclusion

We have studied plasma thermalization during the afterglow using a stationary afterglow apparatus equipped with CRDS absorption spectrometer (SA-CRDS) from 77 K up to 340 K in pure He, and in He/Ar and He/Ar/ H_2 gas mixtures. We confirmed our previous conclusions that at conditions used in our studies of H_3^+ recombination the afterglow plasma is thermalized. The present values of α_{bin} and $(\alpha_{\text{bin}} + \alpha_{\text{F}})$ are consistent with our previous data. Further experiments in pure H_2 at higher electron densities are required to obtain $(\alpha_{\text{bin}} + \alpha_{\text{F}})$ and K_{H_2} at temperatures below 240 K.

This work was partly supported by Czech Science Foundation projects GACR 15-15077S, GACR 14-14649P, and by Charles University Grant Agency project GAUK 692214. We would like to thank Professor Rainer Johnsen for fruitful discussions.

References

1. T. Oka, Proc. Natl. Acad. Sci. USA **103**, 12235 (2006)
2. T.J. Millar, Plasma Source. Sci. Technol. **24**, 043001 (2015)
3. M. Larsson, A.E. Orel, *Dissociative Recombination of Molecular Ions* (Cambridge University Press, Cambridge, 2008)
4. H. Kreckel et al., Phys. Rev. Lett. **95**, 263201 (2005)
5. B.J. McCall et al., Nature **422**, 500 (2003)
6. J.A. Macdonald, M.A. Biondi, R. Johnsen, Planet. Space Sci. **32**, 651 (1984)
7. J. Glosík, R. Plašil, I. Korolov, T. Kotrík, O. Novotný, P. Hlavenka, P. Dohnal, J. Varju, V. Kokouline, C.H. Greene, Phys. Rev. A **79**, 052707 (2009)
8. N.G. Adams, D. Smith, E. Alge, J. Chem. Phys. **81**, 1778 (1984)

9. M.T. Leu, M.A. Biondi, R. Johnsen, *Phys. Rev. A* **8**, 420 (1973)
10. T. Amano, *J. Chem. Phys.* **92**, 6492 (1990)
11. P. Dohnal, P. Rubovič, Á. Kálosi, M. Hejduk, R. Plašil, R. Johnsen, *J. Glosík, Phys. Rev. A* **90**, 042708 (2014)
12. J. Glosík, P. Dohnal, P. Rubovič, Á. Kálosi, R. Plašil, Š. Roučka, R. Johnsen, *Plasma Source. Sci. Technol.* **24**, 065017 (2015)
13. D.R. Bates, S.P. Khare, *Proc. Phys. Soc.* **85**, 231 (1965)
14. P. Macko, G. Bánó, P. Hlavenka, R. Plašil, V. Poterya, A. Pysanenko, O. Votava, R. Johnsen, *J. Glosík, Int. J. Mass Spectrom.* **233**, 299 (2004)
15. D. Romanini, A.A. Kachanov, N. Sadeghi, F. Stoeckel, *Chem. Phys. Lett.* **264**, 316 (1997)
16. C. Focsa, P.F. Bernath, R. Colin, *J. Mol. Spectrosc.* **191**, 209 (1998)
17. J.M. Brown, E.A. Colbourn, J.K.G. Watson, F.D. Wayne, *J. Mol. Spectrosc.* **74**, 294 (1979)
18. C.R. Brazier, R.S. Ram, P.F. Bernath, *J. Mol. Spectrosc.* **120**, 381 (1986)
19. L. Augustovičová, V. Špirko, W.P. Kraemer, P. Soldán, *MNRAS* **435**, 1541 (2013)
20. M.L. Ginter, *J. Mol. Spectrosc.* **18**, 321 (1965)
21. D.W. Tokaryk, R.L. Brooks, J.L. Hunt, *Phys. Rev. A* **48**, 364 (1993)
22. D.R. Yarkony, *J. Chem. Phys.* **90**, 7164 (1989)
23. R.J. Le Roy, LEVEL 7.7: A Computer Program for Solving the Radial Schrodinger Equation, University of Waterloo Chemical Physics Research Report CP-661, 2005
24. B. Numerov, *Trudy Glavnoi Rossiskoi Astrofizicheskoj Observatorii* **2**, 188 (1923)
25. J.W. Cooley, *Math. Comp.* **15**, 363 (1961)
26. L. Augustovičová, V. Špirko, W.P. Kraemer, P. Soldán, *Astron. Astrophys.* **553**, A42 (2013)
27. J.K.G. Watson, *J. Mol. Spectrosc.* **252**, 5 (2008)
28. L.S. Rothman et al., *J. Quant. Spectrosc. Radiat. Transfer* **60**, 665 (1998)
29. R. Plašil, I. Korolov, T. Kotřík, P. Dohnal, G. Bánó, Z. Donkó, J. Glosík, *Eur. Phys. J. D* **54**, 391 (2009)
30. I. Korolov, R. Plašil, T. Kotřík, P. Dohnal, O. Novotný, J. Glosík, *Contrib. Plasma Phys.* **48**, 461 (2008)
31. M. Hejduk, P. Dohnal, P. Rubovič, Á. Kálosi, R., Plašil, R. Johnsen, *J. Glosík, J. Chem. Phys.* **143**, 044303 (2015)
32. W.L. Wiese, J.M. Bridges, R.L. Kornblith, D.E. Kelleher, *J. Opt. Soc. Am.* **59**, 1206 (1969)
33. J. Glosík, G. Bánó, R. Plašil, A. Luca, P. Zakouřil, *Int. J. Mass Spectrom.* **189**, 103 (1999)
34. P. Dohnal, M. Hejduk, J. Varju, P. Rubovič, Š. Roučka, T. Kotřík, R. Plašil, J. Glosík, R. Johnsen, *J. Chem. Phys.* **136**, 244304 (2012)
35. P. Palmeri, E. Biémont, *Phys. Scr.* **51**, 76 (1995)
36. M.H. Nayfeh, C.H. Chen, M.G. Payne, *Phys. Rev. A* **14**, 1739 (1976)
37. W. Lindinger, A.L. Schmeltekopf, F.C. Fehsenfeld, *J. Chem. Phys.* **61**, 2890 (1974)
38. A.L. Schmeltekopf, F.C. Fehsenfeld, *J. Chem. Phys.* **53**, 3173 (1970)
39. C.M. Lindsay, B.J. McCall, *J. Mol. Spectrosc.* **210**, 60 (2001)
40. P. Dohnal, M. Hejduk, P. Rubovič, J. Varju, Š. Roučka, R. Plašil, J. Glosík, *J. Chem. Phys.* **137**, 194320 (2012)
41. P. Rubovič, P. Dohnal, M. Hejduk, R. Plašil, J. Glosík, *J. Phys. Chem. A* **117**, 9626 (2013)

**Binary and ternary recombination of H_2D^+ and HD_2^+ ions with
electrons at 80 K**

Dohnal P., Kálosi Á., Plašil R., Roučka Š., Kovalenko A., Rednyk S., Johnsen R.,
Glosík J.

Phys. Chem. Chem. Phys. **18(34)**, 23549, 2016.



Cite this: *Phys. Chem. Chem. Phys.*, 2016, **18**, 23549

Binary and ternary recombination of H_2D^+ and HD_2^+ ions with electrons at 80 K

Petr Dohnal,^a Ábel Kálosi,^a Radek Plašil,^a Štěpán Roučka,^a Artem Kovalenko,^a Serhiy Rednyk,^a Rainer Johnsen^b and Juraj Glosík^{*a}

The recombination of deuterated trihydrogen cations with electrons has been studied in afterglow plasmas containing mixtures of helium, argon, hydrogen and deuterium. By monitoring the fractional abundances of H_3^+ , H_2D^+ , HD_2^+ and D_3^+ as a function of the $[\text{D}_2]/[\text{H}_2]$ ratio using infrared absorption observed in a cavity ring down absorption spectrometer (CRDS), it was possible to deduce effective recombination rate coefficients for H_2D^+ and HD_2^+ ions at a temperature of 80 K. From pressure dependences of the measured effective recombination rate coefficients the binary and the ternary recombination rate coefficients for both ions have been determined. The inferred binary and ternary recombination rate coefficients are: $\alpha_{\text{binH}_2\text{D}}(80 \text{ K}) = (7.1 \pm 4.2) \times 10^{-8} \text{ cm}^3 \text{ s}^{-1}$, $\alpha_{\text{binHD}_2}(80 \text{ K}) = (8.7 \pm 2.5) \times 10^{-8} \text{ cm}^3 \text{ s}^{-1}$, $K_{\text{H}_2\text{D}}(80 \text{ K}) = (1.1 \pm 0.6) \times 10^{-25} \text{ cm}^6 \text{ s}^{-1}$ and $K_{\text{HD}_2}(80 \text{ K}) = (1.5 \pm 0.4) \times 10^{-25} \text{ cm}^6 \text{ s}^{-1}$.

Received 14th June 2016,
Accepted 3rd August 2016

DOI: 10.1039/c6cp04152c

www.rsc.org/pccp

1 Introduction

Recombination of H_3^+ ions with electrons has been studied for over sixty years (see *e.g.* reviews by Larsson and Ore¹ and Johnsen and Guberman,² and references therein). The process is very fundamental and is of high importance for astrophysics, molecular chemistry and for understanding recombination processes in hydrogen-containing plasmas. Because of the high abundance of hydrogen in the universe it is not surprising that H_3^+ is the most abundantly produced molecular ion in the universe³ and that it plays a key role in the chemistry of the interstellar medium.⁴ If HD molecules are present in a H_3^+ containing plasma then they very efficiently react with H_3^+ to form H_2D^+ , HD_2^+ and finally also D_3^+ . H_2D^+ and HD_2^+ have been detected in the interstellar medium^{5,6} together with many other deuterated molecules.⁷ Models of interstellar chemistry contain all four isotopologues of H_3^+ .^{8,9} The degree of deuteration depends on physical conditions, the $[\text{D}]/[\text{H}]$ ratio (see *e.g.* paper by Brünken *et al.*¹⁰) and on the rate coefficients of the involved ion–molecule reactions.¹¹ The observed densities of *ortho*- and *para*- H_2D^+ have been also used to estimate the age of cloud core forming Sun-like stars.¹⁰ Dissociative recombination of H_3^+ , H_2D^+ , HD_2^+ and D_3^+ ions plays an essential role in such models.¹² The most advanced theoretical calculations predict recombination rate coefficients of different isotopologues of

H_3^+ and they also predict dependences on rotational excitation of the recombining ions and on temperature.^{13–15} The recombination rate coefficients of H_3^+ and D_3^+ ions have been measured many times (see *e.g.* reviews by Larsson and Ore¹ and Rubovič *et al.*¹⁶) but much less is known about those of H_2D^+ and HD_2^+ at low temperatures. The recombination rate coefficients of H_2D^+ and HD_2^+ were measured in CRYRING experiment^{17,18} and the relative cross sections, branching ratios and observed dependence of measured recombination rate on rotational excitation were reported by Test Storage Ring group.^{19,20} The cross sections for HD_2^+ recombination with electrons were also obtained in merged beams experiment by Mitchell *et al.*²¹ In all these experiments, the internal excitation of recombining ions was not known.

There are two main groups of experimental techniques used for recombination studies: merged beams including storage rings (see discussion and history in a book by Larsson and Ore¹) and plasma afterglow experiments – stationary afterglow (SA) and flowing afterglow (FA).^{22–24} The advantage of storage ring experiments is high energy-resolution, high accuracy, broad collision energy range and the possibility to analyse neutral products. The disadvantage is the possibility of high and poorly known rotational excitation of stored ions.^{25,26} In afterglow experiments multiple collisions with neutral particles efficiently remove the rotational and vibrational excitation of the probed species, but it is often difficult to produce a single ion species that can be studied in isolation. This is the reason why recombination of H_2D^+ and HD_2^+ ions has not been studied previously in afterglow experiments. To study the recombination of H_2D^+ and HD_2^+ ions and to measure the corresponding recombination rate coefficients in afterglow plasma one may

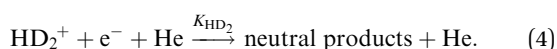
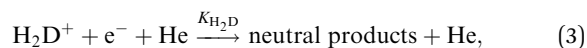
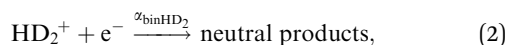
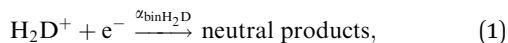
^a Department of Surface and Plasma Science, Faculty of Mathematics and Physics, Charles University in Prague, Prague, Czech Republic.

E-mail: juraj.glosik@mff.cuni.cz; Fax: +420 284 685 095; Tel: +420 951 552 224

^b Department of Physics and Astronomy, University of Pittsburgh, Pittsburgh, Pennsylvania 15260, USA

carry out experiments using H₂/D₂ gas mixtures in order to form H₂D⁺ and HD₂⁺ ions. Actually, H₃⁺ and D₃⁺ ions are also formed in such a case. To obtain recombination rate coefficients of H₂D⁺ and HD₂⁺ ions it is necessary to monitor absolute densities of all four ion species during the afterglow. One further problem in afterglow experiments is the possible occurrence of ternary neutral or electron assisted recombination processes.^{2,27} On the other hand, this makes it possible to obtain rate coefficients of ternary recombination processes.^{27–29} Those are particularly important in H₃⁺ dominated plasmas, where very fast He and H₂ assisted ternary recombination has recently been observed.^{30,31} Therefore, agreement between the results from various experiments was obtained only when ternary He and H₂ assisted recombination of H₃⁺ ions was included in the data analysis.^{27,30,31} Fast helium-assisted ternary recombination was also observed for D₃⁺ ions.³⁰

The present study is devoted to the experimental determination of binary ($\alpha_{\text{binH}_2\text{D}}$, α_{binHD_2}) and ternary ($K_{\text{H}_2\text{D}}$, K_{HD_2}) recombination rate coefficients of H₂D⁺ and HD₂⁺ ions at 80 K for the following processes:



2 Experiment

The experiments were performed using a stationary afterglow (SA) apparatus equipped with continuous wave cavity ring-down absorption spectrometer (CRDS).^{23,32–34} In the present SA-CRDS experiments a plasma is produced by a microwave discharge (2.5 GHz, 4–15 W) in a He/Ar/H₂/D₂ gas mixture (typical concentrations 10¹⁷/10¹⁴/10¹⁴/10¹⁴ cm⁻³). The discharge tube (silica glass, inner diameter 1.3 cm) is cooled by liquid nitrogen; the actual tube temperature is in the range 77–90 K. The discharge is switched on for 2–2.5 ms and then switched off for around 2–4 ms to let the plasma decay. Argon is added to the gas to remove He metastable atoms and molecules by Penning ionization and to increase the rate of the plasma relaxation after switching off the discharge (for discussion see paper by Kálosi *et al.*³⁵). Helium ions and metastables created in the discharge are rapidly converted to a mixture of H₃⁺, H₂D⁺, HD₂⁺ and D₃⁺ ions by a sequence of Penning ionization and ion–molecule reactions (for details on the kinetics of formation see ref. 36–38).

We used several laser diodes with linewidth < 5 MHz as light sources covering the transitions probed in the present study (see Table 1). Examples of measured time evolutions of absolute and relative populations of ions in plasma are shown in Fig. 1.

Table 1 Transitions used in present study. The numbers in parentheses at each transition are vibrational quantum numbers of the upper state, (ν_1, ν_2, ν_3) for H₂D⁺ and HD₂⁺, and (ν_1, ν_2) for H₃⁺ and D₃⁺. All the listed transitions originate in the ground vibrational state of the ion. Rotational quantum numbers are $J_{K_a K_c}$ for H₂D⁺ and HD₂⁺, and J_G for H₃⁺ and D₃⁺. For details on notations see paper by Asvany *et al.*³⁹ The listed wavenumbers were measured in the present study

Ion	$\tilde{\nu}$ (cm ⁻¹)	Transition
H ₂ D ⁺	6459.037	(0,2,1) 2 ₀₂ ← 1 ₁₁
H ₂ D ⁺	6466.532	(0,2,1) 1 ₁₁ ← 0 ₀₀
H ₂ D ⁺	6491.349	(0,2,1) 2 ₁₂ ← 1 ₀₁
HD ₂ ⁺	6466.935	(1,2,0) 1 ₀₁ ← 1 ₁₀
HD ₂ ⁺	6535.953	(1,0,2) 2 ₁₂ ← 1 ₀₁
HD ₂ ⁺	6536.316	(1,0,2) 1 ₁₁ ← 0 ₀₀
H ₃ ⁺	6807.288	(0,3 ⁺) 2 ₃ ← 3 ₃
D ₃ ⁺	6848.505	(0,3 ¹) 3 ₂ ← 2 ₂

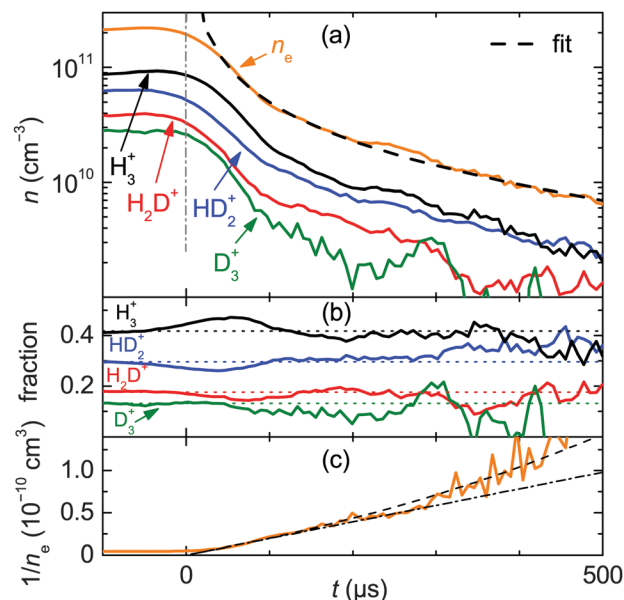


Fig. 1 Decay of the densities of H₃⁺, H₂D⁺, HD₂⁺ and D₃⁺ ions measured in SA-CRDS experiment at 80 K in He/Ar/H₂/D₂ gas mixture (4.5 × 10¹⁷/1.0 × 10¹⁴/4.5 × 10¹³/5.5 × 10¹³ cm⁻³). The zero of the time axis is the time when the microwave discharge switches off. Panel (a): The absolute densities of H₃⁺, H₂D⁺, HD₂⁺ and D₃⁺ ions, $n_e = [\text{H}_3^+] + [\text{H}_2\text{D}^+] + [\text{HD}_2^+] + [\text{D}_3^+]$. Panel (b): The relative populations (fractions $f_{\text{H}_3^+}$, $f_{\text{H}_2\text{D}^+}$, $f_{\text{HD}_2^+}$ and $f_{\text{D}_3^+}$) of H₃⁺, H₂D⁺, HD₂⁺ and D₃⁺ ions. Panel (c): The reciprocal electron number density, $1/n_e$. The dashed line through the data represents a fit that includes both recombination and diffusion, while the dot-dashed straight line is a simple linear fit during the first 300 μs.

The CRDS data yield the ion densities assuming that the afterglow plasma is in thermal equilibrium which has to be proved. In our previous studies we monitored the approach to equilibrium of afterglow plasmas in He/Ar, He/Ar/H₂ and He/Ar/D₂ gas mixtures.^{35,40,41} The kinetic temperature of ions ($T_{\text{kin-ion}}$) was obtained from Doppler broadening of measured absorption lines. The rotational temperature of ions (T_{rot}) was determined by measuring relative populations of the lowest rotational states.⁴¹ The electron temperature (T_e) was estimated by monitoring the losses due to the ambipolar diffusion.^{29,41,42}

Because excited particles can heat the electrons in super-elastic collisions, we also monitored the presence of the ground and the first vibrational state of the $a^3\Sigma_u^+$ electronic state of $(\text{He}_2)^*$ and the $3s^23p^5(^2P_{1/2}^0)3d^2[3/2]^0$ state of $(\text{Ar})^*$ during the afterglow. The population of these excited particles is coupled to the presence of He^m formed in the discharge.³⁵ In parallel FALP experiments we also studied the relaxation in afterglow plasma in $\text{He}/\text{Ar}/\text{H}_2$ gas mixtures by using a Langmuir probe.^{29,41} The rapid relaxation of the electron temperature was confirmed by measuring the temperature dependence of the ternary rate coefficient of collisional radiative recombination (CRR) of Ar^+ ions with electrons in He/Ar gas mixture.²⁹

The data on plasma relaxation obtained in the present study are in agreement with results of our previous studies and they support the assumption that the afterglow plasma in the SA-CRDS in the $\text{He}/\text{Ar}/\text{H}_2/\text{D}_2$ gas mixture at typical concentrations of $10^{17}/10^{14}/10^{14}/10^{14} \text{ cm}^{-3}$ is thermalized (well within 100 μs after switching off the discharge) and various temperatures have a common value (within $\pm 10 \text{ K}$) given by the temperature of the discharge tube (T_{wall}), *i.e.*, that $T = T_{\text{wall}} = T_{\text{rot}} = T_{\text{kin-ion}} = T_e$. The measured relative populations of *ortho*- and *para*- H_2D^+ (and HD_2^+) were also according to the thermodynamic equilibrium at given temperature.

3 Data analysis

In the data analysis we assume, in agreement with experimental data, that relative number density of ions (fraction) $f_{\text{H}_3} = [\text{H}_3^+]/([\text{H}_3^+] + [\text{H}_2\text{D}^+] + [\text{HD}_2^+] + [\text{D}_3^+])$ and the corresponding values of $f_{\text{H}_2\text{D}}$, f_{HD_2} and f_{D_3} are constant during the plasma decay (see example of data in the panel (b) of Fig. 1). The assumption is made for experiments using the $\text{He}/\text{Ar}/\text{H}_2/\text{D}_2$ gas mixture at typical concentrations of $10^{17}/10^{14}/10^{14}/10^{14} \text{ cm}^{-3}$. The loss rate of the electron density n_e in a recombination dominated afterglow plasma with H_3^+ , H_2D^+ , HD_2^+ and D_3^+ ions can be written in the form:

$$\frac{\partial n_e}{\partial t} = -(\alpha_{\text{effH}_3}[\text{H}_3^+] + \alpha_{\text{effH}_2\text{D}}[\text{H}_2\text{D}^+] + \alpha_{\text{effHD}_2}[\text{HD}_2^+] + \alpha_{\text{effD}_3}[\text{D}_3^+])n_e - \frac{n_e}{\tau_{\text{RD}}}, \quad (5)$$

where α_{effH_3} , $\alpha_{\text{effH}_2\text{D}}$, α_{effHD_2} and α_{effD_3} are the effective recombination rate coefficient for ions H_3^+ , H_2D^+ , HD_2^+ and D_3^+ , respectively. The subscript *eff* here indicates that the recombination rate coefficients are effective coefficients that contain contributions from both binary and ternary recombination processes, as was observed previously for H_3^+ and for D_3^+ ions.³⁰ The term n_e/τ_{RD} describes losses due to ambipolar diffusion and due to conversion to H_5^+ and its isotopologues.⁴³ If we assume quasineutrality of plasma, *i.e.* $n_e = ([\text{H}_3^+] + [\text{H}_2\text{D}^+] + [\text{HD}_2^+] + [\text{D}_3^+])$, then the overall effective recombination rate coefficient $\alpha_{\text{eff}\Sigma}$ is given by equation:

$$\alpha_{\text{eff}\Sigma} = \alpha_{\text{effH}_3}f_{\text{H}_3} + \alpha_{\text{effH}_2\text{D}}f_{\text{H}_2\text{D}} + \alpha_{\text{effHD}_2}f_{\text{HD}_2} + \alpha_{\text{effD}_3}f_{\text{D}_3}. \quad (6)$$

Note that under the assumption of constant relative populations of ions (constant fractions) the value of $\alpha_{\text{eff}\Sigma}$ is constant

during the plasma decay. The balance eqn (5) can then be written in the simple form:

$$\frac{\partial n_e}{\partial t} = -\alpha_{\text{eff}\Sigma}n_e^2 - \frac{n_e}{\tau_{\text{RD}}}. \quad (7)$$

The overall effective recombination rate coefficient $\alpha_{\text{eff}\Sigma}$ depends on temperature and on the plasma composition which depends on $[\text{He}]$, $[\text{H}_2]$ and $[\text{D}_2]$. By measuring the time evolutions of the ion densities $[\text{H}_3^+]$, $[\text{H}_2\text{D}^+]$, $[\text{HD}_2^+]$ and $[\text{D}_3^+]$ at fixed $[\text{He}]$, $[\text{H}_2]$ and $[\text{D}_2]$ the value of $\alpha_{\text{eff}\Sigma}$ can be determined using eqn (7) as described in ref. 42. In the text we will use fractions $F_{\text{D}_2} = [\text{D}_2]/([\text{H}_2] + [\text{D}_2])$ to express partial density of D_2 . If $\alpha_{\text{eff}\Sigma}$ for several ionic compositions (fractions f_{H_3} , $f_{\text{H}_2\text{D}}$, f_{HD_2} and f_{D_3}) are measured at fixed $[\text{He}]$ and temperature then the effective recombination rate coefficients α_{effH_3} , $\alpha_{\text{effH}_2\text{D}}$, α_{effHD_2} and α_{effD_3} can be inferred. By measuring the dependence of these effective rate coefficients on $[\text{He}]$ and F_{D_2} the binary and the ternary recombination rate coefficients for particular ions can be obtained.

4 Results

The dependences of $\alpha_{\text{eff}\Sigma}$ on F_{D_2} measured at three different buffer gas pressures are shown in Fig. 2, panel (a). The dependences of the ion compositions on F_{D_2} were measured for all three pressures. Examples of f_{H_3} , $f_{\text{H}_2\text{D}}$, f_{HD_2} and f_{D_3} as a function of F_{D_2} measured at helium pressure of 500 Pa are plotted in Fig. 2, panel (b). Using $\text{He}/\text{Ar}/\text{H}_2$ and $\text{He}/\text{Ar}/\text{D}_2$ gas mixtures we obtained α_{effH_3} and α_{effD_3} for H_3^+ and D_3^+ , respectively. These values are in very good agreement with our previous values (the empty symbols in Fig. 2, panel (a))^{16,30}. In data analysis we subtracted the appropriate contributions due to H_3^+ and D_3^+ recombination from the measured $\alpha_{\text{eff}\Sigma}$; $\alpha_{\text{effR}} = (\alpha_{\text{eff}\Sigma} - \alpha_{\text{effH}_3}f_{\text{H}_3} - \alpha_{\text{effD}_3}f_{\text{D}_3})$. As follows from the eqn (6) the remaining α_{effR} is the pure contributions from the recombination of H_2D^+ and HD_2^+ ions; $\alpha_{\text{effR}} = (\alpha_{\text{effH}_2\text{D}}f_{\text{H}_2\text{D}} + \alpha_{\text{effHD}_2}f_{\text{HD}_2})$. To obtain $\alpha_{\text{effH}_2\text{D}}$ and α_{effHD_2} we made a least square fit to the dependence of α_{effR} on F_{D_2} with $\alpha_{\text{effH}_2\text{D}}$ and α_{effHD_2} as free parameters. In other approach, we used instead of actual values of $\alpha_{\text{eff}\Sigma}$ a linear approximation given by the fit to the dependence of $\alpha_{\text{eff}\Sigma}$ on F_{D_2} as shown by dashed lines in panel (a) of Fig. 2. The resulting values of $\alpha_{\text{effH}_2\text{D}}$ and α_{effHD_2} from both these approaches were close to each other with lower statistical errors in the latter approach.

The evaluated $\alpha_{\text{effH}_2\text{D}}$ and α_{effHD_2} for H_2D^+ and HD_2^+ are plotted in Fig. 3. Assuming a linear dependence on helium density, $\alpha_{\text{effH}_2\text{D}} = \alpha_{\text{binH}_2\text{D}} + K_{\text{H}_2\text{D}}[\text{He}]$ and similarly $\alpha_{\text{effHD}_2} = \alpha_{\text{binHD}_2} + K_{\text{HD}_2}[\text{He}]$, the binary ($\alpha_{\text{binH}_2\text{D}}$, α_{binHD_2}) and the ternary ($K_{\text{H}_2\text{D}}$, K_{HD_2}) recombination rate coefficients were obtained from the dependence of $\alpha_{\text{effH}_2\text{D}}$ and α_{effHD_2} on $[\text{He}]$ as shown in Fig. 3: $\alpha_{\text{binH}_2\text{D}}(80 \text{ K}) = (7.1 \pm 4.2) \times 10^{-8} \text{ cm}^3 \text{ s}^{-1}$, $\alpha_{\text{binHD}_2}(80 \text{ K}) = (8.7 \pm 2.5) \times 10^{-8} \text{ cm}^3 \text{ s}^{-1}$, $K_{\text{H}_2\text{D}}(80 \text{ K}) = (1.1 \pm 0.6) \times 10^{-25} \text{ cm}^6 \text{ s}^{-1}$ and $K_{\text{HD}_2}(80 \text{ K}) = (1.5 \pm 0.4) \times 10^{-25} \text{ cm}^6 \text{ s}^{-1}$. The corresponding values for H_3^+ and D_3^+ are in agreement with those measured previously in the same experimental setup: $\alpha_{\text{binH}_3}(80 \text{ K}) = (10.1 \pm 1.4) \times 10^{-8} \text{ cm}^3 \text{ s}^{-1}$, $\alpha_{\text{binD}_3}(80 \text{ K}) = (9.2 \pm 1.7) \times 10^{-8} \text{ cm}^3 \text{ s}^{-1}$, $K_{\text{H}_3}(80 \text{ K}) = (1.5 \pm 0.2) \times 10^{-25} \text{ cm}^6 \text{ s}^{-1}$

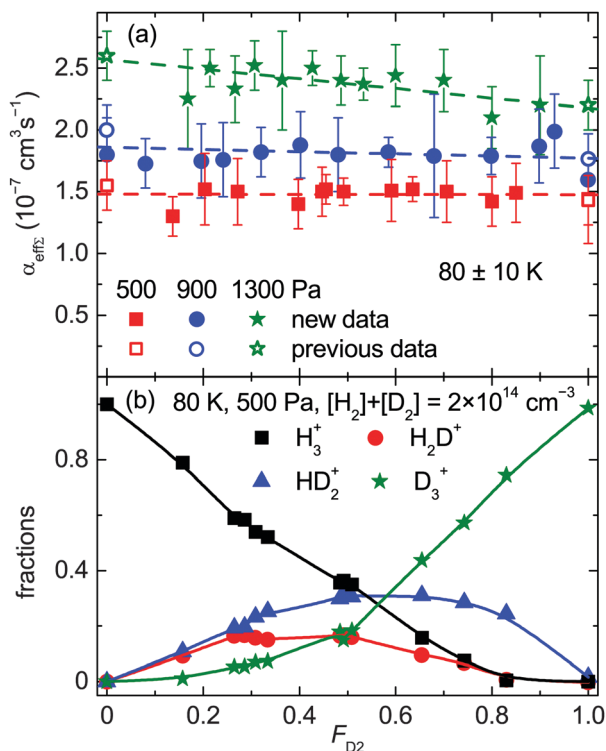


Fig. 2 Panel (a): The dependence of α_{eff} on fraction $F_{D_2} = [D_2]/([H_2] + [D_2])$ measured at 80 ± 10 K and three different He pressures. The dashed lines are linear fits to the data. The empty symbols denote previously measured values of effective recombination rate coefficient for H_3^+ and D_3^+ .³⁰ Panel (b): The measured dependences of the relative populations (fractions) $f_{H_3^+}$, $f_{H_2D^+}$, $f_{HD_2^+}$ and $f_{D_3^+}$ of H_3^+ , H_2D^+ , HD_2^+ and D_3^+ on F_{D_2} . The plotted data were obtained at a temperature of 80 K and a pressure of 500 Pa. The argon density was $[Ar] = 2 \times 10^{14} \text{ cm}^{-3}$ and $([H_2] + [D_2]) = 2 \times 10^{14} \text{ cm}^{-3}$.

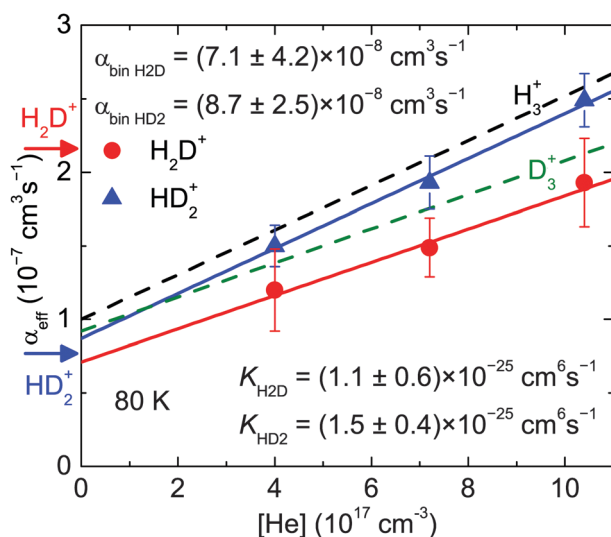


Fig. 3 The dependence of α_{eff,H_2D} and α_{eff,HD_2} on $[He]$. The full lines are linear fits to the data used to obtain the binary and the ternary recombination rate coefficients of H_2D^+ and HD_2^+ . The dashed lines denoted H_3^+ and D_3^+ are linear fits to the α_{eff,H_3} and α_{eff,D_3} taken from papers by Varju *et al.*⁴⁶ and Johnsen *et al.*³⁰ The arrows indicate the values of binary recombination rate coefficients obtained in theoretical calculations for H_2D^+ and HD_2^+ .¹³

and $K_{D_3}(80 \text{ K}) = (1.2 \pm 0.2) \times 10^{-25} \text{ cm}^6 \text{ s}^{-1}$.^{16,30} The errors are statistical errors. The systematic error of the measurement is estimated to be less than 10%. The binary recombination rate coefficients measured at 80 K are within experimental error almost the same for all four isotopologues indicating that there is no strong isotopic effect. The obtained values are in good agreement with the theoretical calculations of Jungen and Pratt¹⁵ (the actual thermal rate coefficients can be calculated from the cross sections published in ref. 44) and in the case of HD_2^+ also with calculations by Pagani *et al.*¹³ We did not observe a substantial difference between binary recombination rate coefficients of H_2D^+ and HD_2^+ that was predicted by Pagani *et al.*¹³ Improved quantum mechanical calculations are clearly needed. The results of the CRYRING experiments (inferred by extrapolating the 300 K values published in ref. 18 and 45 to 80 K by using $T^{-0.5}$ temperature dependence) are approximately two times larger than the values presented here, but the CRYRING experiments were done without *in situ* determination of the internal excitation of the recombining ions. The measured three body recombination rate coefficients of H_2D^+ and HD_2^+ are similar to those previously obtained for H_3^+ and D_3^+ ions.³⁰

5 Conclusions

This is the first low temperature experimental study on binary recombination of H_2D^+ and HD_2^+ with *in situ* determined populations of recombining ions, including rotational excitation. A similar methodology to obtain recombination rate coefficients for a mixture of ions was used in previous study on *ortho*- and *para*- H_3^+ recombination with electrons.⁴⁶ As the presented results depend on the assumption that there are no additional strong pressure dependences below the experimental pressures, experiments performed at low temperature in low-pressure environment with good control over rotational populations of H_2D^+ and HD_2^+ ions are desirable as a verification in the future. We hope that the presented results will help improve astrochemical models and will give new impulse for quantum mechanical calculations. Further studies of H_2D^+ and HD_2^+ recombination over broader temperature range are in progress.

Acknowledgements

This work was partly supported by Czech Science Foundation projects GACR 14-14649P, GACR 15-15077S, GACR P209/12/0233, and by Charles University in Prague Project No. GAUK 692214.

References

- M. Larsson and A. E. Orel, *Dissociative Recombination of Molecular Ions*, Cambridge University Press, Cambridge, 2008.
- R. Johnsen and S. L. Guberman, in *Dissociative Recombination of H_3^+ Ions with Electrons: Theory and Experiment*, ed. E. Arimondo, P. R. Berman and C. C. Lin, Academic Press, 2010, ch. 3, vol. 59, pp. 75–128.
- T. Oka, *Proc. Natl. Acad. Sci. U. S. A.*, 2006, **103**, 12235–12242.
- T. J. Millar, *Plasma Sources Sci. Technol.*, 2015, **24**, 043001.

- 5 J. Tennyson and S. Miller, *Spectrochim. Acta, Part A*, 2001, **57**, 661–667.
- 6 B. Parise, A. Belloche, F. Du, R. Güsten and K. M. Menten, *Astron. Astrophys.*, 2011, **526**, A31.
- 7 T. J. Millar, *Astron. Geophys.*, 2005, **46**, 2.29–2.32.
- 8 A. Das, L. Majumdar, S. K. Chakrabarti and D. Sahu, *New Astron.*, 2015, **35**, 53–70.
- 9 T. Albertsson, D. A. Semenov, A. I. Vasyunin, T. Henning and E. Herbst, *Astrophys. J., Suppl. Ser.*, 2013, **207**, 27.
- 10 S. Brünken, O. Sipilä, E. T. Chambers, J. Harju, P. Caselli, O. Asvany, C. E. Honingh, T. Kamiński, K. M. Menten, J. Stutzki and S. Schlemmer, *Nature*, 2014, **516**, 219–221.
- 11 H. Roberts, E. Herbst and T. J. Millar, *Astron. Astrophys.*, 2004, **424**, 16.
- 12 H. Roberts, E. Herbst and T. J. Millar, *Astrophys. J., Lett.*, 2003, **591**, L41.
- 13 L. Pagani, C. Vastel, E. Hugo, V. Kokoouline, C. H. Greene, A. Bacmann, E. Bayet, C. Ceccarelli, R. Peng and S. Schlemmer, *Astron. Astrophys.*, 2009, **494**, 623–636.
- 14 S. Fonseca dos Santos, V. Kokoouline and C. H. Greene, *J. Chem. Phys.*, 2007, **127**, 124309.
- 15 C. Jungen and S. T. Pratt, *Phys. Rev. Lett.*, 2009, **102**, 023201.
- 16 P. Rubovič, P. Dohnal, M. Hejduk, R. Plašil and J. Glosík, *J. Phys. Chem. A*, 2013, **117**, 9626–9632.
- 17 S. Datz, M. Larsson, C. Stromholm, G. Sundström, V. Zengin, H. Danared, A. Källberg and M. af Ugglas, *Phys. Rev. A: At., Mol., Opt. Phys.*, 1995, **52**, 2901–2909.
- 18 V. Zhaunerchyk, R. D. Thomas, W. D. Geppert, M. Hamberg, M. Kaminska, E. Vigren and M. Larsson, *Phys. Rev. A: At., Mol., Opt. Phys.*, 2008, **77**, 034701.
- 19 L. Lammich, D. Strasser, H. Kreckel, M. Lange, H. B. Pedersen, S. Altevogt, V. Andrianarijaona, H. Buhr, O. Heber, P. Witte, D. Schwalm, A. Wolf and D. Zajfman, *Phys. Rev. Lett.*, 2003, **91**, 143201.
- 20 D. Strasser, L. Lammich, H. Kreckel, M. Lange, S. Krohn, D. Schwalm, A. Wolf and D. Zajfman, *Phys. Rev. A: At., Mol., Opt. Phys.*, 2004, **69**, 064702.
- 21 J. B. A. Mitchell, C. T. Ng, L. Forand, R. Janssen and J. W. McGowan, *J. Phys. B: At. Mol. Phys.*, 1984, **17**, L909.
- 22 T. Amano, *J. Chem. Phys.*, 1990, **92**, 6492–6501.
- 23 P. Macko, G. Bánó, P. Hlavenka, R. Plašil, V. Poterya, A. Pysanenko, O. Votava, R. Johnsen and J. Glosík, *Int. J. Mass Spectrom.*, 2004, **233**, 299–304.
- 24 R. Plašil, I. Korolov, T. Kotrík, P. Dohnal, G. Bánó, Z. Donko and J. Glosík, *Eur. Phys. J. D*, 2009, **54**, 391–398.
- 25 H. Kreckel, M. Motsch, J. Mikosch, J. Glosík, R. Plašil, S. Altevogt, V. Andrianarijaona, H. Buhr, J. Hoffmann, L. Lammich, M. Lestinsky, I. Nevo, S. Novotny, D. A. Orlov, H. B. Pedersen, F. Sprenger, A. S. Terekhov, J. Toker, R. Wester, D. Gerlich, D. Schwalm, A. Wolf and D. Zajfman, *Phys. Rev. Lett.*, 2005, **95**, 263201.
- 26 A. Petrigiani, S. Altevogt, M. H. Berg, D. Bing, M. Grieser, J. Hoffmann, B. Jordon-Thaden, C. Krantz, M. B. Mendes, O. Novotný, S. Novotny, D. A. Orlov, R. Repnow, T. Sorg, J. Stützel, A. Wolf, H. Buhr, H. Kreckel, V. Kokoouline and C. H. Greene, *Phys. Rev. A: At., Mol., Opt. Phys.*, 2011, **83**, 032711.
- 27 J. Glosík, I. Korolov, R. Plašil, O. Novotný, T. Kotrík, P. Hlavenka, J. Varju, I. A. Mikhailov, V. Kokoouline and C. H. Greene, *J. Phys. B: At., Mol. Opt. Phys.*, 2008, **41**, 191001.
- 28 J. Glosík, R. Plašil, T. Kotrík, P. Dohnal, J. Varju, M. Hejduk, I. Korolov, Š. Roučka and V. Kokoouline, *Mol. Phys.*, 2010, **108**, 2253–2264.
- 29 P. Dohnal, P. Rubovič, T. Kotrík, M. Hejduk, R. Plašil, R. Johnsen and J. Glosík, *Phys. Rev. A: At., Mol., Opt. Phys.*, 2013, **87**, 052716.
- 30 R. Johnsen, P. Rubovič, P. Dohnal, M. Hejduk, R. Plašil and J. Glosík, *J. Phys. Chem. A*, 2013, **117**, 9477–9485.
- 31 J. Glosík, P. Dohnal, P. Rubovič, Á. Kálosi, R. Plašil, Š. Roučka and R. Johnsen, *Plasma Sources Sci. Technol.*, 2015, **24**, 065017.
- 32 P. Hlavenka, R. Plašil, G. Bánó, I. Korolov, D. Gerlich, J. Ramanlal, J. Tennyson and J. Glosík, *Int. J. Mass Spectrom.*, 2006, **255–256**, 170–176.
- 33 P. Hlavenka, I. Korolov, R. Plašil, J. Varju, T. Kotrík and J. Glosík, *Czech. J. Phys.*, 2006, **56**, B749–B760.
- 34 J. Glosík, P. Hlavenka, R. Plašil, F. Windisch, D. Gerlich, A. Wolf and H. Kreckel, *Philos. Trans. R. Soc., A*, 2006, **364**, 2931–2942.
- 35 Á. Kálosi, P. Dohnal, L. Augustovičová, Š. Roučka, R. Plašil and J. Glosík, *Eur. Phys. J.: Appl. Phys.*, 2016, **75**, 24707.
- 36 K. Giles, N. G. Adams and D. Smith, *J. Phys. Chem.*, 1992, **96**, 7645–7650.
- 37 M. Fárnik, S. Davis, M. A. Kostin, O. L. Polyansky, J. Tennyson and D. J. Nesbitt, *J. Chem. Phys.*, 2002, **116**, 6146–6158.
- 38 D. Gerlich, F. Windisch, P. Hlavenka, R. Plašil and J. Glosík, *Philos. Trans. R. Soc., A*, 2006, **364**, 3007–3034.
- 39 O. Asvany, E. Hugo, F. Müller, F. Kühnemann, S. Schiller, J. Tennyson and S. Schlemmer, *J. Chem. Phys.*, 2007, **127**, 154317.
- 40 M. Hejduk, P. Dohnal, J. Varju, P. Rubovič, R. Plašil and J. Glosík, *Plasma Sources Sci. Technol.*, 2012, **21**, 024002.
- 41 M. Hejduk, P. Dohnal, P. Rubovič, Á. Kálosi, R. Plašil, R. Johnsen and J. Glosík, *J. Chem. Phys.*, 2015, **143**, 044303.
- 42 P. Dohnal, M. Hejduk, J. Varju, P. Rubovič, Š. Roučka, T. Kotrík, R. Plašil, J. Glosík and R. Johnsen, *J. Chem. Phys.*, 2012, **136**, 244304.
- 43 O. Novotný, R. Plašil, A. Pysanenko, I. Korolov and J. Glosík, *J. Phys. B: At., Mol. Opt. Phys.*, 2006, **39**, 2561.
- 44 S. T. Pratt and C. Jungen, *J. Phys.: Conf. Ser.*, 2011, **300**, 012019.
- 45 M. Larsson, H. Danared, A. Larson, A. Le Padellec, J. R. Peterson, S. Rosén, J. Semaniak and C. Strömholm, *Phys. Rev. Lett.*, 1997, **79**, 395–398.
- 46 J. Varju, M. Hejduk, P. Dohnal, M. Jílek, T. Kotrík, R. Plašil, D. Gerlich and J. Glosík, *Phys. Rev. Lett.*, 2011, **106**, 203201.

**Stationary afterglow measurements of the temperature dependence
of the electron–ion recombination rate coefficients of H_2D^+ and HD_2^+
in He/Ar/ H_2 / D_2 gas mixtures at $T = 80\text{--}145$ K**

Plašil R., Dohnal P., Kálosi Á., Roučka Š., Johnsen R., Glosík J.

Plasma Sources Sci. Technol. **26(3)**, 035006, 2017.

Stationary afterglow measurements of the temperature dependence of the electron–ion recombination rate coefficients of H_2D^+ and HD_2^+ in He/Ar/ H_2 / D_2 gas mixtures at $T = 80\text{--}145\text{ K}$

Radek Plašil¹, Petr Dohnal¹, Ábel Kálosi¹, Štěpán Roučka¹,
Rainer Johnsen² and Juraj Glosík¹

¹Department of Surface and Plasma Science, Faculty of Mathematics and Physics, Charles University in Prague, Czech Republic

²Department of Physics and Astronomy, University of Pittsburgh, Pittsburgh, Pennsylvania 15260, United States of America

E-mail: radek.plasil@mff.cuni.cz

Received 31 October 2016, revised 20 December 2016

Accepted for publication 12 January 2017

Published 15 February 2017



CrossMark

Abstract

We report measurements of the binary and ternary recombination rate coefficients of deuterated isotopologues of H_3^+ . A cavity ring-down absorption spectrometer was used to monitor the fractional abundances of H_3^+ , H_2D^+ , HD_2^+ and D_3^+ during the decay of a plasma in He/Ar/ H_2 / D_2 mixtures. A dependence of the measured effective recombination rate coefficients on the helium buffer gas density was observed and hence both the binary and the ternary recombination rate coefficients for H_2D^+ and HD_2^+ were obtained in the temperature range 80–145 K.

Keywords: afterglow plasma, plasma relaxation, electron–ion recombination, binary recombination, three-body recombination, H_2D^+ , HD_2^+

(Some figures may appear in colour only in the online journal)

1. Introduction

Largely motivated by astrophysical applications, the recombination of the trihydrogen cation H_3^+ and its deuterated isotopologues H_2D^+ , HD_2^+ and D_3^+ with electrons has been investigated for nearly six decades (see e.g. [1–4]). H_3^+ ions in interstellar clouds are produced by cosmic ray ionization of the abundant molecular hydrogen, as was predicted [5, 6] long before these ions were actually observed in the interstellar medium in 1996 [7]. It is now commonly accepted that H_3^+ is the most abundantly produced molecular ion species in the Universe and that it plays a key role in the chemical evolution of the interstellar medium [6, 8]. HD molecules in the interstellar medium [9] lead to the formation of H_2D^+ , HD_2^+ and D_3^+ in a sequence of reactions starting from H_3^+ . Both H_2D^+ and HD_2^+ have now been detected in the interstellar medium [10–

12] and current models of the chemistry in interstellar molecular clouds incorporate all four isotopologues of H_3^+ [13–16]. The actual degree of deuteration depends on the physical conditions, on the [D]/[H] number density ratio, on the para/ortho ratio of H_2 and on the previous chemical evolution (see e.g. [17–20]). Binary dissociative recombination of H_3^+ , H_2D^+ , HD_2^+ and D_3^+ with electrons is an essential destruction mechanism for these ions [15, 16, 21] in the interstellar plasma. Recombination at low astrophysically relevant temperatures has also been studied theoretically for all four isotopologues of H_3^+ , including the dependence of the recombination rate coefficients on the nuclear spin states of the recombining ions [22–26]. For H_3^+ and D_3^+ ions these predictions have recently been confirmed by experiments (see e.g. [1, 27–31]).

Much less is known about the recombination rate coefficients of H_2D^+ and HD_2^+ at low temperatures, the subject of

this report. The cross section for HD_2^+ recombination was measured in a merged-beam experiment by Mitchell *et al* [32]. The recombination rate coefficients of H_2D^+ and HD_2^+ were also measured in CRYRING experiments [33, 34]. The relative cross sections, the product branching ratios and the dependence of recombination on rotational excitation were studied by the Test Storage Ring (TSR) group in Heidelberg [35, 36]. In beam experiments with H_3^+ ions the rotational temperature of the ions was probably high and not well known, but in the case of H_2D^+ and HD_2^+ , due to their dipole moment, it can be expected that the rotational temperature is considerably lower than that of H_3^+ . The recombination of H_2D^+ and HD_2^+ ions has not been studied previously in plasma afterglow experiments (with the exception of our recent study at 80 K [37]) because of the difficulty of producing plasmas that contain only a single ion species, either H_2D^+ or HD_2^+ .

Afterglow plasmas contain a significant density of neutral gas (the buffer gas) and, as an unavoidable consequence, recombination can also occur by three-body (or neutral-assisted) recombination [2, 38] in addition to the purely binary process that is of astrophysical interest. Recently, very fast neutral-assisted three-body recombination of H_3^+ and D_3^+ ions with electrons has been observed at low temperatures (50–340 K). The measured ternary recombination rate coefficients of He-assisted three-body recombination of H_3^+ and D_3^+ ions with electrons were found to be very large. The value measured at 300 K ($K_{\text{He}}(300\text{ K}) \approx 10^{-25} \text{ cm}^6 \text{ s}^{-1}$ [39]) exceeds by over two orders of magnitude the value expected on the basis of the Bates and Khare classical theory for atomic ions ($K_{\text{BK}}(300\text{ K}) \approx 10^{-27} \text{ cm}^6 \text{ s}^{-1}$) [40]. We will here use the term ternary recombination rate coefficients for the rate coefficients of neutral-assisted three-body recombination, without implying a particular mechanism. At temperatures from 77 K up to 340 K the measured ternary recombination rate coefficients of He-assisted three-body recombination for H_3^+ and D_3^+ ions slowly increase with temperature in contrast to the classical Bates and Khare theory [40], which predicts a negative temperature dependence of $K_{\text{BK}} \sim T^{-2.5}$.

The ternary recombination rate coefficient measured for H_2 -assisted three-body recombination of H_3^+ ions at 300 K ($K_{\text{H}_2}(300\text{ K}) \approx 9 \times 10^{-23} \text{ cm}^6 \text{ s}^{-1}$) [41] is even larger than that of the He-assisted process. It exceeds the classical Bates and Khare value by five orders of magnitude [38, 40]. As a consequence, three-body recombination already prevails over binary recombination at hydrogen pressures near 100 Pa (at 300 K). Although neutral-assisted recombination complicates the analysis of afterglow data, this process may have significant consequences for ionospheric applications, e.g. in the recombination of ions with electrons in ionospheres of Jupiter-like planets with a hydrogen atmosphere [42]. Also, mid-infrared laser lines have been observed in a hydrogen/rare gas discharge and it has been suggested that the mechanism for the population inversion involves ternary recombination of H_3^+ [43].

The unexpectedly fast three-body recombination process is probably one of the causes of the large discrepancies between earlier results of different afterglow experiments on

H_3^+ recombination [1, 41, 44–46]. Fast He-assisted three-body recombination was also observed for D_3^+ ions [47, 48]. The present study focuses on binary recombination of H_2D^+ and HD_2^+ ions but it includes a study of their three-body neutral-assisted recombination.

In the analysis of the present results we will, in agreement with prior experiments, assume that binary and three-body recombination processes add linearly, i.e. that an effective coefficient can be defined as $\alpha_{\text{effion}} = \alpha_{\text{binion}} + K_{\text{ion}}[\text{He}]$, where α_{binion} is the binary recombination rate coefficient of a particular ion and K_{ion} is the ternary rate coefficient of three-body recombination. The linear combination is known to become invalid at high He densities due to saturation [41]. We do not include electron-assisted three-body recombination [49, 50] in the data analysis.

This paper is organized as follows: section 2 briefly reviews the principal experimental methods used in recombination studies and describes the apparatus employed in the present studies. The question of thermalization of the plasma in a stationary afterglow in a He/Ar/ H_2 / D_2 gas mixture will be discussed in section 3. By thermalization we mean that the translational and internal states of the ions are those corresponding to the temperature of the ambient gas as well as to the electron temperature. In section 4 we describe our kinetic model of the plasma decay during the afterglow and discuss details of the data analysis. Section 5 presents experimental data and results, and compares them to those of other experiments and calculations.

2. Experiment

There are two distinct types of experimental techniques used in recombination studies (see discussion and history in [1, 2, 32]): merged-beam experiments including storage rings [1] and plasma afterglow experiments (e.g. stationary afterglow (SA) and flowing afterglow (FA) [1, 50–54]). Storage-ring experiments have high energy-resolution, high accuracy, a wide collision energy range, and yield information on neutral products [55]. Their disadvantage is the possibility of high and poorly known rotational excitation of the stored ions [27, 30]. The new Cryogenic Storage Ring (already working in Heidelberg) may be able to resolve the question of rotational excitation [56].

In an SA experiment, a plasma in a suitable gas mixture is produced in a pulsed discharge and the plasma decays after termination of the discharge. If the decay of the ion and electron densities is dominated by recombination of ions with electrons and by ambipolar diffusion then the rate coefficient of the electron–ion recombination at a well-defined temperature can be determined, provided that the ions and electrons in the afterglow plasma are quickly thermalized to the buffer gas temperature. During the microwave discharge the electron temperature can be high (several eV), and ions and neutrals can be highly excited. However, multiple collisions of ions and electrons with neutral particles efficiently thermalize the plasma. Experimental conditions have to be adjusted so that the thermalization time is short compared to the recombination

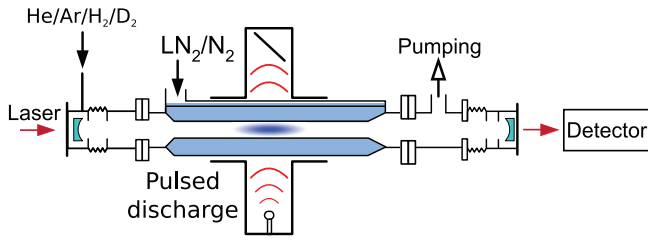


Figure 1. Stationary afterglow with the CRDS absorption spectrometer: SA-CRDS (not to scale). In the middle part of the silica discharge tube a discharge is periodically ignited in the microwave resonator (2.5 GHz, 4–15 W). A He/Ar/H₂/D₂ gas mixture is used to form a plasma containing H₃⁺, H₂D⁺, HD₂⁺ and D₃⁺ ions. The discharge tube is cooled by liquid nitrogen (LN₂) or its vapours.

time scale. For instance, long-lived helium atomic and molecular metastables are formed during the discharge and these can produce energetic electrons in superelastic collisions that transfer energy to the electron gas and slow down the thermalization of the electrons [53]. As is common practice, the metastables are destroyed in our experiments by adding a small amount of argon to the helium buffer gas [57]. In the present study the rate of removal of highly excited particles was monitored by a near infrared (NIR) absorption spectrometer (see discussion below).

The experimental setup (see figure 1) consists of SA apparatus in conjunction with a continuous wave cavity ring-down absorption spectrometer (cw CRDS) [52, 58–60]. The CRDS was used to determine the densities of the ion species. The plasma was produced in a silica glass discharge tube (inner diameter 1.3 cm) by a microwave discharge (2.5 GHz, 4–15 W) in a He/Ar/H₂/D₂ gas mixture with typical number densities $5 \times 10^{17}/10^{14}/10^{14}/10^{14} \text{ cm}^{-3}$. The discharge tube was cooled by vapours of liquid nitrogen; the actual tube temperature can be set within the range 77–300 K. The discharge was switched on for 2–2.5 ms and then switched off for around 4 ms to let the plasma decay. A modification of the cw-CRDS setup developed by Romanini *et al* [61] was employed in the construction of our spectrometer (see figure 1). In the CRDS spectrometer the laser light was modulated by the acousto-optic modulator and then injected through the highly reflective mirror (reflectivity over 99.98%) on one side, and photons exiting the cavity through the mirror on the other side were detected by an InGaAs avalanche photodiode [52]. The specific transitions and their measured wavenumbers used for measurements of H₃⁺, H₂D⁺, HD₂⁺ and D₃⁺ ion densities are listed in table 1. The Einstein A coefficients for the listed transitions of H₂D⁺ and HD₂⁺ were taken from [62], for H₃⁺ from [63] and for D₃⁺ from [64]. Their estimated uncertainty was less than 5% [65]. Several DFB laser diodes and an external cavity diode laser Sacher TEC 500 were used as light sources covering the transitions probed in the present study. The set laser wavelength was measured absolutely by a WA-1650 wavemeter.

The kinetic temperatures T_{kin} of the H₃⁺, H₂D⁺, HD₂⁺ and D₃⁺ ions were obtained from the Doppler broadening of particular absorption line profiles. Figure 2 shows examples

Table 1. Transitions used in the present study for measurement of ion densities and T_{kin} . The listed wavenumbers $\tilde{\nu}_0$ were obtained in the present study within an uncertainty of 0.003 cm^{-1} . The vibrational quantum numbers of the upper state are shown in parentheses in the third column as (v_1, v_2, v_3) for H₂D⁺ and HD₂⁺ and as (v_1, v_2) for H₃⁺ and D₃⁺. All transitions originate in the lowest vibrational state of the corresponding ion. The rotational quantum numbers are shown in the fourth column as J_{K_a, K_c} for H₂D⁺ and HD₂⁺ and J_G for H₃⁺ and D₃⁺. For details on spectroscopic notations see [58, 62].

Ion	$\tilde{\nu}_0 \text{ (cm}^{-1}\text{)}$	Transition
H ₂ D ⁺	6459.037	(0, 2, 1) 2 ₀₂ ← 1 ₁₁
H ₂ D ⁺	6466.532	(0, 2, 1) 1 ₁₁ ← 0 ₀₀
H ₂ D ⁺	6491.349	(0, 2, 1) 2 ₁₂ ← 1 ₀₁
HD ₂ ⁺	6466.935	(1, 2, 0) 1 ₀₁ ← 1 ₁₀
HD ₂ ⁺	6535.953	(1, 0, 2) 2 ₁₂ ← 1 ₀₁
HD ₂ ⁺	6536.316	(1, 0, 2) 1 ₁₁ ← 0 ₀₀
H ₃ ⁺	6807.288	(0, 3 ¹) 2 ₃ ← 3 ₃
D ₃ ⁺	6848.505	(0, 3 ¹) 3 ₂ ← 2 ₂

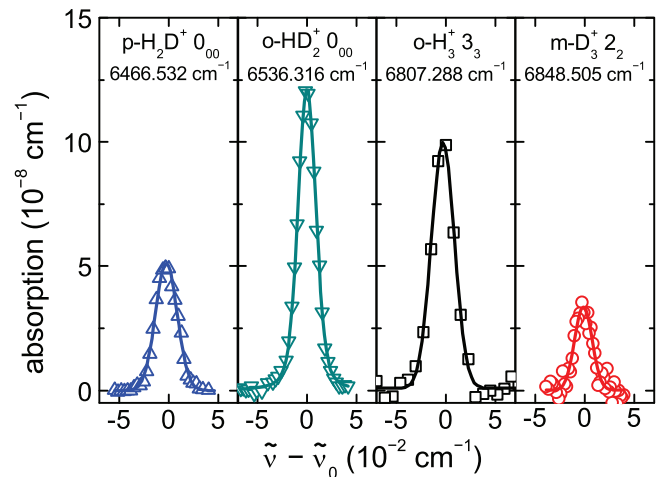


Figure 2. Examples of measured line profiles corresponding to the indicated quantum states of H₃⁺, H₂D⁺, HD₂⁺ and D₃⁺ ions, measured in experiments with discharge tube temperature $T_{\text{wall}} = 90 \text{ K}$ and at a pressure of 500 Pa. The lower states of the transitions and the measured central frequencies $\tilde{\nu}_0$ are indicated above the line profiles. In the example, the kinetic temperature of ions obtained from the fits is $T_{\text{kin}} = (85 \pm 10) \text{ K}$. The prefixes o-/p-/m- denote the nuclear spin state symmetry (ortho/para/meta) of particular ionic species.

of measured absorption lines corresponding to the lower rotational states 3₃, 0₀₀, 0₀₀ and 2₂ of the ground vibrational states of H₃⁺, H₂D⁺, HD₂⁺ and D₃⁺ ions, respectively (for notation see table 1). The fits indicate Doppler profiles of absorption lines.

Examples of measured time evolutions of the absolute ion densities during the discharge and during the afterglow are shown in the upper panel of figure 3. The electron density n_e is calculated under the assumption of quasineutrality of the plasma as a sum of the ion densities of all four ions, $n_e = [\text{H}_3^+] + [\text{H}_2\text{D}^+] + [\text{HD}_2^+] + [\text{D}_3^+]$. The relative population (fraction) $f_{\text{H}_3} = [\text{H}_3^+] / ([\text{H}_3^+] + [\text{H}_2\text{D}^+] + [\text{HD}_2^+] + [\text{D}_3^+])$ of H₃⁺, and the corresponding values of $f_{\text{H}_2\text{D}}$, f_{HD_2} and f_{D_3} of H₂D⁺, HD₂⁺ and D₃⁺ ions are shown in the middle panel

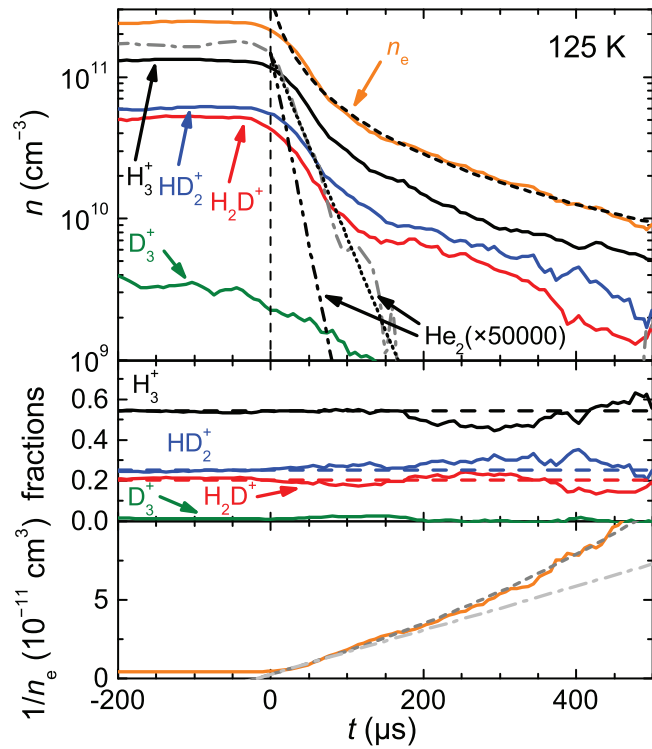


Figure 3. Time evolutions of the densities of H_3^+ , H_2D^+ , HD_2^+ and D_3^+ ions measured at 125 K in a He/Ar/ H_2 / D_2 gas mixture with densities $2.9 \times 10^{17}/2.1 \times 10^{14}/1.6 \times 10^{14}/4.5 \times 10^{13} \text{ cm}^{-3}$, $F_{\text{D}_2} = 0.22$. The time is set to zero at the beginning of the afterglow. Upper panel: The measured number densities of H_3^+ , H_2D^+ , HD_2^+ and D_3^+ ions and the electron number density n_e calculated as a sum of ionic number densities. The dashed line is a fit to the data that includes both diffusion and recombination losses. For comparison, we show the decay of the density of the $a^3\Sigma_u^+(N=1, J=0)$ excited state of He_2 (dash-dotted line) measured at 80 K and $[\text{He}] = 4.5 \times 10^{17} \text{ cm}^{-3}$, $[\text{Ar}] = 1 \times 10^{14} \text{ cm}^{-3}$, $[\text{H}_2] = 5 \times 10^{13} \text{ cm}^{-3}$, $[\text{D}_2] = 5 \times 10^{13} \text{ cm}^{-3}$. The measured $[\text{He}_2]$ is multiplied by a factor of 5×10^4 to fit in the figure. Using measured de-excitation rates published in [66] the calculated time decay of $[\text{He}_2]$ at two different conditions is also plotted (dotted line: 80 K, $[\text{Ar}] = 1 \times 10^{14} \text{ cm}^{-3}$, $[\text{H}_2] = 5 \times 10^{13} \text{ cm}^{-3}$, $[\text{D}_2] = 5 \times 10^{13} \text{ cm}^{-3}$; double-dot-dashed line: 125 K, $[\text{Ar}] = 2.1 \times 10^{14} \text{ cm}^{-3}$, $[\text{H}_2] = 1.6 \times 10^{14} \text{ cm}^{-3}$, $[\text{D}_2] = 4.5 \times 10^{13} \text{ cm}^{-3}$). See text for details. Middle panel: The relative populations $f_{\text{H}_3^+}$, $f_{\text{H}_2\text{D}^+}$, $f_{\text{HD}_2^+}$ and $f_{\text{D}_3^+}$ of the corresponding ions. The dashed lines denote the relative populations at the beginning of the afterglow. Lower panel: The plot of the reciprocal electron number density, $1/n_e$. The dashed line is the fit to the data that includes both the diffusion and the recombination losses. The dash-dotted straight line is a linear fit corresponding to the losses due to recombination only.

of figure 3. The evolution of the reciprocal electron number density $1/n_e$ is shown in the lower panel of figure 3. The linearity of the $1/n_e$ plot is characteristic of a recombination dominated afterglow plasma (see discussion below). Here and in the following text we will use the parameter $F_{\text{D}_2} = [\text{D}_2]/([\text{H}_2] + [\text{D}_2])$ to express the relative density of D_2 . The data in figure 3 were measured in a plasma with $F_{\text{D}_2} = 0.22$.

In order to infer the recombination rate coefficients of H_2D^+ and HD_2^+ ions it is necessary to measure simultaneously the densities of all four ion species. The accessible

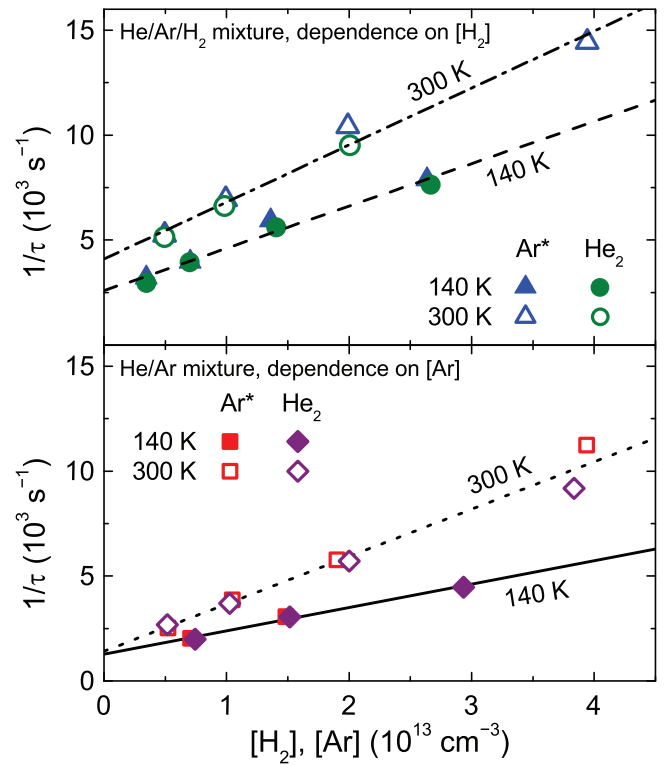


Figure 4. Dependences of the reciprocal time constants of exponential decays of He_2 and Ar^* number densities on $[\text{Ar}]$ and $[\text{H}_2]$ measured in the afterglow in He/Ar/ H_2 (upper panel) and He/Ar/ H_2 (lower panel) gas mixtures, respectively. Pressures of the neutral gas (He) were 600 Pa at 140 K and 900 Pa at 300 K. The argon number density was kept constant during the measurement of the $[\text{H}_2]$ dependences (upper panel): $[\text{Ar}] = 7 \times 10^{12} \text{ cm}^{-3}$ at 140 K and $[\text{Ar}] = 5 \times 10^{12} \text{ cm}^{-3}$ at 300 K.

temperature range is limited by the sensitivity of the CRDS and the strengths of available transitions to 80–145 K.

3. Characterization of the afterglow plasma

Ideally, one would like to determine the recombination rate coefficients of H_2D^+ and HD_2^+ ions separately in plasmas containing only a single ion species, but this is not possible in standard SA experiments. Hence, we varied the relative abundances of the two ion species by adjusting the $[\text{D}_2]/[\text{H}_2]$ ratio characterized by F_{D_2} and measured the effective recombination rate coefficients for several fractional abundances of all four H_3^+ isotopologues. This dependence on F_{D_2} was then analysed to deduce the individual rate coefficients.

The plasma was formed in a He/Ar/ H_2 / D_2 gas mixture with typical number densities of $5 \times 10^{17}/10^{14}/10^{14}/10^{14} \text{ cm}^{-3}$. During the discharge and in the early afterglow, the plasma contains ions, electrons and some highly excited particles (see, e.g. the detailed discussion in [67, 68]). The steady state is established typically within $\approx 100 \mu\text{s}$ after switching on the microwaves (see discussion, and for the case of H_3^+ , figures 4, 5 and 7, in [69]). When (after $\approx 2 \text{ ms}$) microwaves are switched off the electrons were very rapidly

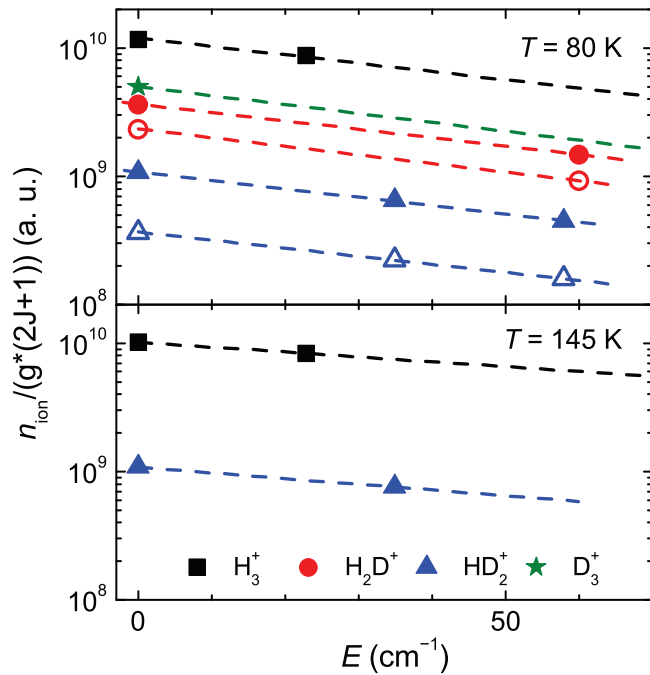


Figure 5. The Boltzmann plots. Upper panel: the data obtained at 80 K for H_3^+ , H_2D^+ , HD_2^+ and D_3^+ ions. The values measured for the H_3^+ (3_3) and D_3^+ (4_4) states with energies of 251.218 cm^{-1} and 254.964 cm^{-1} , respectively, are not shown in the figure but they are included in the fits. Open symbols denote values measured $100 \mu\text{s}$ after switching off the discharge. The values for H_2D^+ are multiplied by a factor of two for better readability (the slope of the lines carries information about the rotational temperature). Lower panel: The data obtained at 145 K for H_3^+ and HD_2^+ . The value measured for the H_3^+ (3_3) state is not shown but it is included in the fit. For all these ions the energies of the lowest allowed states were used as origins of the plots.

cooled in collisions with He atoms. At the He densities used in the present experiments ($[\text{He}] \approx 5 \times 10^{17} \text{ cm}^{-3}$) the time constant for this elastic cooling was below $10 \mu\text{s}$ (see table 2 in [31] and for a detailed calculation see [70]). Helium metastables (He^m) can heat electrons in superelastic collisions but they are removed by Penning ionization of Ar, H_2 or D_2 . To ascertain the rate of removal of the highly excited particles at the beginning of the afterglow and to characterize the afterglow plasma we monitored the decay of He_2 in the $a^3\Sigma_u^+(N=1, J=0)$ state and of Ar excited to the $(3s^23p^5(^2P_{1/2}^o)3d^2[3/2]^o; J=2)$ state. The population of these excited particles is coupled to the presence of He^m formed in the discharge [66]. The measurements were carried out in pure He, in He/Ar and in He/Ar/ H_2 in order to characterize the role of Ar and H_2 . The reciprocal values $1/\tau$ of the time constants of the decays of these excited states are plotted in figure 4. The time constants were measured at several experimental conditions as a function of Ar and H_2 densities for $[\text{Ar}]$ and $[\text{H}_2]$ up to $4 \times 10^{13} \text{ cm}^{-3}$. The observed linear dependences of $1/\tau$ on $[\text{Ar}]$ and $[\text{H}_2]$ (low-pressure limit) indicate that metastable atoms of helium He^m , which are the precursor of the highly excited He_2 and Ar^* are efficiently destroyed in collisions with Ar or H_2 . The rate

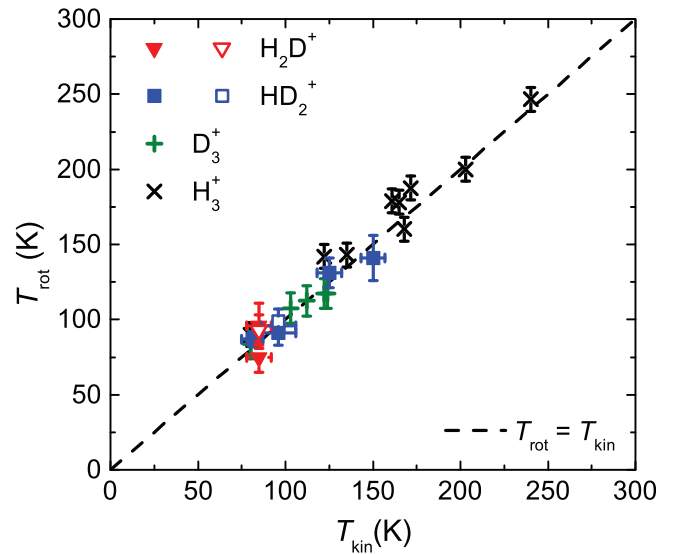


Figure 6. The thermalization of rotational excitation. The measured rotational temperatures (T_{rot}) versus measured kinetic temperature (T_{kin}) for H_3^+ , H_2D^+ , HD_2^+ and D_3^+ ions. Some values for H_3^+ and D_3^+ ions are from our previous experiments [31, 48, 75]. The open symbols denote values measured at a time of $100 \mu\text{s}$ in the afterglow. The dashed line indicates equality $T_{\text{rot}} = T_{\text{kin}}$ corresponding to thermal equilibrium. The plotted data were measured at the conditions used in the experiments for measurement of the recombination rate coefficients.

coefficients for the processes obtained from the plotted data were on the order of $0.1\text{--}1 \times 10^{-10} \text{ cm}^3 \text{ s}^{-1}$, typical for Penning ionization [71].

The measurements of the recombination rate coefficients were carried out in He/Ar/ H_2 / D_2 mixtures with typical densities $\approx 5 \times 10^{17}/10^{14}/10^{14}/10^{14} \text{ cm}^{-3}$. Here, the number densities of Ar and H_2 were much higher than those used in the measurements of the time constants τ (shown in figure 4). The upper panel of figure 3 compares the electron density decay to the measured and to the calculated He_2 ($a^3\Sigma_u^+(N=1, J=0)$) decay. The latter was calculated using the measured de-excitation rates of Kalosi *et al* [66]. The density of excited particles decayed with a time constant shorter than $\approx 50 \mu\text{s}$ while the electron density decayed for over $500 \mu\text{s}$ by more than a factor of 10, which is sufficient to obtain the recombination rate coefficients. The actual data analysis also included diffusion losses and resulted in more accurate recombination rate coefficients than those obtained from the linear part of $1/n_e$ plots (see lower panel of figure 3).

The ions and metastables created in the discharge in He/Ar/ H_2 / D_2 mixtures were rapidly converted by a sequence of Penning ionization and ion–molecule reactions to a mixture of H_3^+ , H_2D^+ , HD_2^+ and D_3^+ ions (for details on the kinetics of formation see [72–74]). Further collisions of H_3^+ , H_2D^+ , HD_2^+ and D_3^+ ions with He atoms and H_2 and D_2 molecules then thermalized their rotational states. To characterize the rotational excitation of ions during the discharge and during the afterglow we monitored the absolute densities of ions in

several lowest rotational states of the vibrational ground states of H_3^+ , H_2D^+ , HD_2^+ and D_3^+ ions. Similar studies for recombination of H_3^+ ions were made by Hejduk *et al* [69], who concluded that for $T > 77$ K, when normal hydrogen is used, the rotational temperature and also the para to ortho ratio of H_3^+ ions in the afterglow correspond to thermal equilibrium. In the present study the thermal population of rotational states for all four ions was also confirmed. Examples of Boltzmann plots for all four ions measured at 80 K and for H_3^+ and HD_2^+ at 145 K are shown in figure 5. For H_2D^+ and HD_2^+ ions the data shown were measured in the discharge and also in the early afterglow.

In the same experiments the kinetic temperature (T_{kin}) of ions was determined from the Doppler broadening of measured absorption lines. The relation between measured T_{rot} and T_{kin} is shown in figure 6.

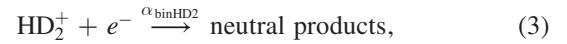
On the basis of the present studies we can conclude that ions H_3^+ , H_2D^+ , HD_2^+ and D_3^+ are thermalized during the afterglow (well within 100 μs after switching off the microwaves) and that their temperature is equal to that of the discharge tube (T_{wall}), i.e. that $T = T_{\text{wall}} = T_{\text{He}} = T_{\text{rot}} = T_{\text{kin}}$. The measured relative populations of ortho- and para- H_2D^+ and HD_2^+ are also in accordance with the thermodynamic equilibrium at a given temperature. We also reached the same conclusion for H_3^+ (D_3^+) dominated plasmas in SA-CRDS experiments at temperatures above 77 K when normal H_2 (D_2) was used [31, 48, 69, 75, 76].

Because of the very fast removal of excited He^m from the afterglow plasma we are confident that after a certain transition time (which is well within 100 μs) after switching off the microwaves [70] electrons are cooled in collisions with He atoms and that they are thermalized (i.e. they have a Maxwellian electron energy distribution function with $T_e = T_{\text{He}}$). To confirm this we rely on parallel FALP experiments and on modelling of the afterglow plasma in both FALP and SA-CRDS experiments. In the FALP experiment we studied the relaxation of the FA plasma in a He/Ar/ H_2 gas mixture using a Langmuir probe [45]. The rapid relaxation of the electron gas was also confirmed by measuring the temperature dependence of the rate coefficient of the electron-assisted three-body recombination of Ar^+ ions with electrons in a He/Ar gas mixture and also by monitoring the temperature dependence of the decay of plasma due to ambipolar diffusion [76, 77]. The agreement of the results for recombination of H_3^+ and D_3^+ ions from FALP and SA-CRDS experiments is significant because there are substantial differences in the parameters of the decaying plasmas. The large difference in the initial electron density of the afterglow plasmas in these two experiments gives a different time scale for the electron-density decay and different contributions of the three-body electron-assisted process. The consistency and agreement of results from SA-CRDS and FALP provides experimental evidence that in SA afterglow electrons are thermalized and $T_e = T_{\text{He}}$.

4. Data analysis

One complication in afterglow experiments arises from the contribution of three-body neutral- or electron-assisted recombination processes [2, 44, 78]. This can be important in low-temperature experiments because rate coefficients of three-body recombination processes usually have strong negative temperature dependence. The predicted dependence is $T^{-2.5}$ for neutral- and $T^{-4.5}$ for electron-assisted recombination [49, 79]. On the other hand, this makes it possible to study these three-body recombination processes and to measure their ternary rate coefficients. Recently we studied some three-body recombination processes using low-temperature versions of SA-CRDS and FALP experiments [4, 39, 44, 50, 77, 80]. These are particularly important in H_3^+ dominated plasmas, where very fast He- and H_2 -assisted three-body recombination has recently been observed [39, 41].

In the data analysis we assumed a quasineutral afterglow plasma consisting of H_3^+ , H_2D^+ , HD_2^+ and D_3^+ ions that recombine with electrons by binary and by neutral-assisted recombination processes. The assumption is made for experiments using the He/Ar/ H_2 / D_2 gas mixture at typical number densities of $5 \times 10^{17}/10^{14}/10^{14}/10^{14} \text{ cm}^{-3}$. In agreement with our previous studies and with present experimental data we consider the following recombination processes with the indicated recombination rate coefficients:



We assume, in agreement with experimental data, that the relative partial densities of ions (fractions) f_{H3} , f_{H2D} , f_{HD2} and f_{D3} are constant during the plasma decay (see the example of data in the middle panel of figure 3 and also data in [37]). Quasineutrality of plasma implies that the electron density $n_e = [\text{H}_3^+] + [\text{H}_2\text{D}^+] + [\text{HD}_2^+] + [\text{D}_3^+]$. The ionic fractions can be written as $f_{\text{H3}} = [\text{H}_3^+]/n_e$ and similarly for f_{H2D} , f_{HD2} and f_{D3} . For a recombination dominated afterglow plasma the balance equation for the electron density n_e can be written in the form:

$$\frac{\partial n_e}{\partial t} = -(\alpha_{\text{effH3}}[\text{H}_3^+] + \alpha_{\text{effH2D}}[\text{H}_2\text{D}^+] + \alpha_{\text{effHD2}}[\text{HD}_2^+] + \alpha_{\text{effD3}}[\text{D}_3^+])n_e - \frac{n_e}{\tau_{\text{RD}}}, \quad (9)$$

where α_{effH3} , α_{effH2D} , α_{effHD2} and α_{effD3} are the effective recombination rate coefficients for ions H_3^+ , H_2D^+ , HD_2^+ and

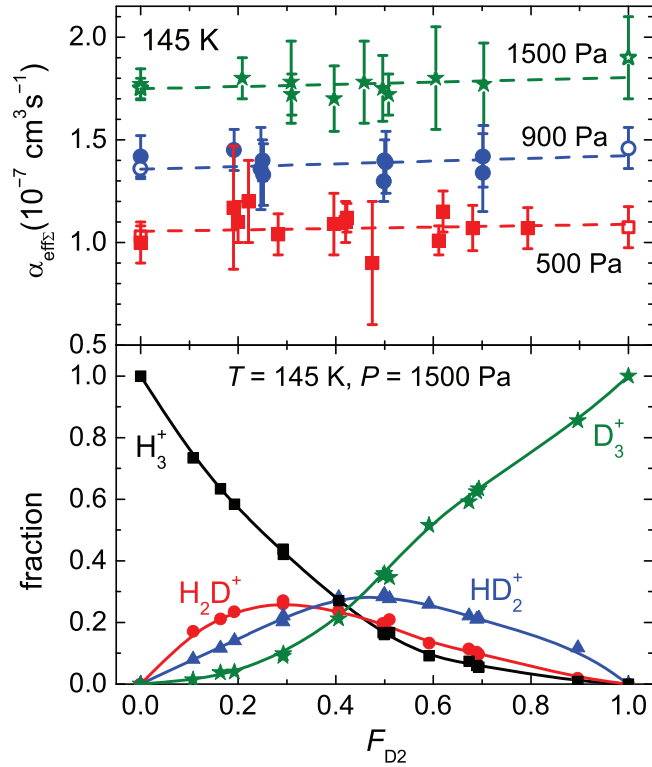


Figure 7. Upper panel: the dependence of the overall effective recombination rate coefficient $\alpha_{\text{eff}\Sigma}$ on F_{D_2} measured at 145 K and three different buffer gas pressures. The open symbols are values obtained for H_3^+ and D_3^+ taken from [39, 48, 84]. The dashed lines are linear fits to the data. Lower panel: the dependence of f_{H_3} , $f_{\text{H}_2\text{D}}$, f_{HD_2} and f_{D_3} on F_{D_2} measured at 145 K. The helium buffer gas pressure was 1500 Pa and $[\text{H}_2] + [\text{D}_2] = 1 \times 10^{14} \text{ cm}^{-3}$. The full lines are guiding for the eye only.

D_3^+ , respectively. The subscript eff here indicates that the recombination rate coefficients are effective rate coefficients, which can include contributions from binary and from three-body recombination processes, as was observed previously for H_3^+ and for D_3^+ ions [39]. The term n_e/τ_{RD} in equation (9) describes losses due to ambipolar diffusion and due to possible conversion to other ion species. Such loss processes can be the formation of H_3^+ -like ions and their consequent fast recombination. The actual value of the time constant τ_{RD} is given by the equation $1/\tau_{\text{RD}} = (1/\tau_{\text{D}} + 1/\tau_{\text{R}})$, where the time constants τ_{D} and τ_{R} describe the losses due to ambipolar diffusion and the losses due to fast recombination of H_3^+ type ions formed in three-body ion–molecule associative reactions [81–83]. By using in equation (9) the fractions instead of the ion densities the balance equation (9) can then be written in the simple form:

$$\frac{\partial n_e}{\partial t} = -\alpha_{\text{eff}\Sigma} n_e^2 - \frac{n_e}{\tau_{\text{RD}}}, \quad (10)$$

where we introduce the overall (summary) effective recombination rate coefficient $\alpha_{\text{eff}\Sigma}$:

$$\alpha_{\text{eff}\Sigma} = \alpha_{\text{effH}_3} f_{\text{H}_3} + \alpha_{\text{effH}_2\text{D}} f_{\text{H}_2\text{D}} + \alpha_{\text{effHD}_2} f_{\text{HD}_2} + \alpha_{\text{effD}_3} f_{\text{D}_3}. \quad (11)$$

Under the assumption of constant relative populations of ions (constant fractions) the value of $\alpha_{\text{eff}\Sigma}$ is constant during the decay of the afterglow plasma. The overall effective recombination rate coefficient $\alpha_{\text{eff}\Sigma}$ depends on the plasma temperature and on the plasma composition, which depends on densities $[\text{He}]$, $[\text{H}_2]$ and $[\text{D}_2]$. By measuring the time evolutions of the ion densities $[\text{H}_3^+]$, $[\text{H}_2\text{D}^+]$, $[\text{HD}_2^+]$ and $[\text{D}_3^+]$ at fixed $[\text{He}]$, $[\text{H}_2]$ and $[\text{D}_2]$ (see figure 3) the value of $\alpha_{\text{eff}\Sigma}$ can be determined. If $\alpha_{\text{eff}\Sigma}$ for several ionic compositions (fractions f_{H_3} , $f_{\text{H}_2\text{D}}$, f_{HD_2} and f_{D_3}) is measured at fixed $[\text{He}]$ and at fixed temperature then the specific effective recombination rate coefficients α_{effH_3} , $\alpha_{\text{effH}_2\text{D}}$, α_{effHD_2} and α_{effD_3} can be inferred.

In the data analysis we subtract the contributions due to H_3^+ and D_3^+ recombination from the measured $\alpha_{\text{eff}\Sigma}$ (see equation (11)) and express the remaining contribution (α_{effR}) due to H_2D^+ and HD_2^+ ions as:

$$\alpha_{\text{effR}} = \alpha_{\text{eff}\Sigma} - \alpha_{\text{effH}_3} f_{\text{H}_3} - \alpha_{\text{effD}_3} f_{\text{D}_3}. \quad (12)$$

Following equation (11) we can also write equation (12) in the form:

$$\alpha_{\text{effR}} = \alpha_{\text{effH}_2\text{D}} f_{\text{H}_2\text{D}} + \alpha_{\text{effHD}_2} f_{\text{HD}_2}. \quad (13)$$

Measurements of α_{effR} for different ion compositions then can be analysed to obtain effective recombination rate coefficients $\alpha_{\text{effH}_2\text{D}}$ and α_{effHD_2} . The observed dependence of the effective coefficients on helium density, as expressed by a linear sum:

$$\alpha_{\text{effion}} = \alpha_{\text{binion}} + K_{\text{ion}} [\text{He}], \quad (14)$$

then yields the binary and ternary contributions. The linear summation is valid only in the low-pressure limit. We have already observed saturation of α_{eff} given by the rate of formation of collisional complexes (see [41, 66]). We do not, therefore, include here a possible but unobserved electron-assisted three-body recombination. In our previous experiments on recombination of H_3^+ and D_3^+ ions with electrons, performed at a temperature of 80 K and with n_e differing by two orders of magnitude ($10^9 - 10^{11} \text{ cm}^{-3}$), we did not observe any substantial influence of the electron density on the measured recombination rate coefficients (for details see discussion in [31, 84]), although according to the theoretical calculation performed by Stevefelt for atomic ions [49], the recombination rate coefficient due to electron-assisted three-body recombination could be comparable to that due to dissociative recombination. We still do not have an explanation for this. It is possible that the theory describing this process has to be modified for molecular ions. At this point, it is important to emphasize that while in the case of recombination of H_3^+ and D_3^+ ions we have not seen electron-assisted three-body recombination, in studies of Ar^+ recombination the measured ternary rate coefficient of electron-assisted three-body recombination was in excellent agreement with theory; both experiments were carried out using our FALP apparatus [80].

5. Experimental data

From the measured evolutions of ion densities during the afterglow (see example in figure 3) we obtained the overall effective recombination rate coefficients $\alpha_{\text{eff}\Sigma}$ (see the example for three different pressures in the upper panel of figure 7) and fractions f_{H_3} , $f_{\text{H}_2\text{D}}$, f_{HD_2} and f_{D_3} . For all three pressures the dependences of the ion compositions on F_{D_2} were also measured. The examples of dependences of f_{H_3} , $f_{\text{H}_2\text{D}}$, f_{HD_2} and f_{D_3} on F_{D_2} measured at 145 K and a helium pressure of 1500 Pa are plotted in the lower panel of figure 7. The data shown in figure 7 indicate that the effective recombination rate coefficients do not change by much when the ion composition is varied, and this seems to be true at three different pressures. The previously measured values of α_{effH_3} and α_{effD_3} are plotted as open symbols in the upper panel of figure 7 [39, 48, 84]. The present values of $\alpha_{\text{eff}\Sigma}$ obtained for $F_{\text{D}_2} = 0$ and $F_{\text{D}_2} = 1$ are in good agreement with previous ones.

The dependence of the overall (summary) effective recombination rate coefficient $\alpha_{\text{eff}\Sigma}$ on the fraction $F_{\text{D}_2} = [\text{D}_2]/([\text{H}_2] + [\text{D}_2])$ were measured for temperatures 80 K, 125 K and 145 K. At every temperature, experiments were carried out for three different He pressures. Examples of α_{effR} as a function of F_{D_2} measured at 80 K and 125 K and two different He pressures are shown in figure 8. The values of α_{effR} were calculated from $\alpha_{\text{eff}\Sigma}$ using equation (12) and measured values of α_{effH_3} and α_{effD_3} adapted from [39, 48, 84] (see table 2).

The recombination rate coefficients $\alpha_{\text{effH}_2\text{D}}$ and α_{effHD_2} were deduced from the dependence of α_{effR} on F_{D_2} by calculating a least squares fit with $\alpha_{\text{effH}_2\text{D}}$ and α_{effHD_2} as free parameters and $f_{\text{H}_2\text{D}}$ and f_{HD_2} interpolated from the measured values. In a different approach, we used, instead of actual values of $\alpha_{\text{eff}\Sigma}$, a linear approximation given by the fit to the dependence of $\alpha_{\text{eff}\Sigma}$ on F_{D_2} , which is shown by dashed lines in the upper panel of figure 7. The values of $\alpha_{\text{effH}_2\text{D}}$ and α_{effHD_2} obtained in both these approaches are close to each other, with lower statistical errors in the latter one. Examples of evaluated effective recombination rate coefficients $\alpha_{\text{effH}_2\text{D}}$ and α_{effHD_2} for H_2D^+ and HD_2^+ ions for 80 K and 145 K are plotted in figure 9 as functions of the He density, together with values of α_{effH_3} and α_{effD_3} obtained in our previous FALP and SA-CRDS experiments [39, 48, 84]. Assuming a linear dependence on helium density (equation (14)), $\alpha_{\text{effH}_2\text{D}} = \alpha_{\text{binH}_2\text{D}} + K_{\text{H}_2\text{D}}[\text{He}]$ and similarly $\alpha_{\text{effHD}_2} = \alpha_{\text{binHD}_2} + K_{\text{HD}_2}[\text{He}]$, the binary $\alpha_{\text{binH}_2\text{D}}$ and α_{binHD_2} and the ternary $K_{\text{H}_2\text{D}}$ and K_{HD_2} recombination rate coefficients were obtained. For comparison, we also included in the lower panel of figure 9 the values of the effective recombination rate coefficients measured in the FALP experiment for Ar^+ ions in ambient helium [77], where we observed a very good agreement with the classical theory of Bates and Khare [40].

The measured binary recombination rate coefficients $\alpha_{\text{binH}_2\text{D}}$ and α_{binHD_2} are plotted in the upper panel of figure 10 together with theoretical dependences calculated by Pagani *et al* [24] and by Pratt and Jungen [26, 85]. The lower panel of figure 10 displays the binary recombination rate

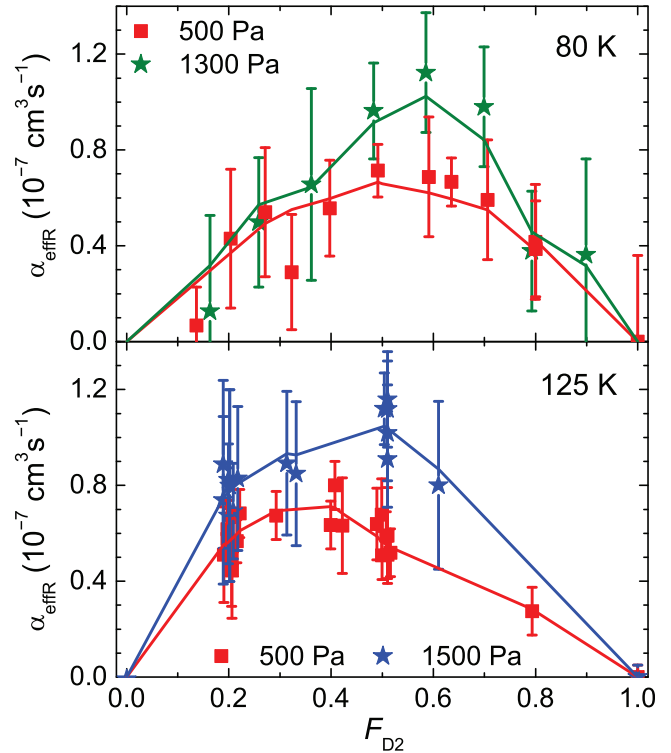


Figure 8. The dependence of $\alpha_{\text{effR}} = \alpha_{\text{effH}_2\text{D}}f_{\text{H}_2\text{D}} + \alpha_{\text{effHD}_2}f_{\text{HD}_2}$ on F_{D_2} obtained at 80 K for 500 Pa and 1300 Pa (upper panel) and at 125 K for 500 Pa and 1500 Pa (lower panel). The full lines are fits to the data using equation (13).

Table 2. The measured values of the binary (in units of $10^{-8} \text{ cm}^3 \text{ s}^{-1}$) and the ternary ($10^{-25} \text{ cm}^6 \text{ s}^{-1}$) recombination rate coefficients of H_2D^+ and HD_2^+ and corresponding values for H_3^+ and D_3^+ [39, 48, 84].

$T(\text{K})$	80 K	125 K	145 K
$\alpha_{\text{binH}_2\text{D}}$	7.1 ± 4.2	10.2 ± 5.0	6.5 ± 3.8
α_{binHD_2}	8.7 ± 2.5	8.3 ± 3.8	8.1 ± 2.8
α_{binH_3}	10.1 ± 1.4	8.0 ± 1.2	6.9 ± 1.0
α_{binD_3}	9.2 ± 1.7	7.9 ± 1.1	6.0 ± 1.0
$K_{\text{H}_2\text{D}}$	1.1 ± 0.6	1.2 ± 0.8	1.7 ± 0.8
K_{HD_2}	1.5 ± 0.4	1.6 ± 0.6	1.1 ± 0.7
K_{H_3}	1.5 ± 0.2	1.8 ± 0.2	1.4 ± 0.3
K_{D_3}	1.2 ± 0.2	2.2 ± 0.3	1.9 ± 0.2

coefficients α_{binH_3} and α_{binD_3} obtained in our previous FALP and SA-CRDS experiments [48, 84].

As can be seen from figure 10, the measured values of the binary recombination rate coefficients of H_2D^+ and HD_2^+ are the same within the error bars in the whole probed temperature range. We did not observe the substantial difference between $\alpha_{\text{binH}_2\text{D}}$ and α_{binHD_2} predicted by Pagani *et al* [24] (see also indication by arrows in figure 9). Nevertheless, the agreement between the values of the observed binary recombination rate coefficients and those predicted by the quantum mechanical calculations of Jungen and Pratt [26] (the actual thermal rate coefficients can be calculated from the cross sections published

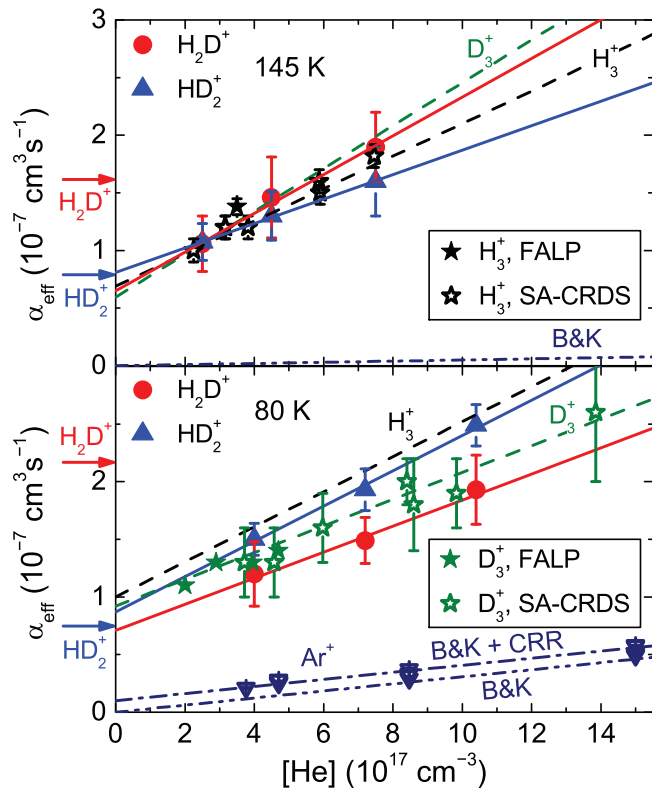


Figure 9. Upper panel: The dependence of α_{effH2D} and α_{effHD2} on $[\text{He}]$ measured at 145 K. The full lines are linear fits to the data used to obtain the binary and the three-body recombination rate coefficients of H_2D^+ and HD_2^+ . The dashed lines denoted H_3^+ and D_3^+ are linear fits to α_{effH3} and α_{effD3} taken from [39, 48, 84]. The arrows indicate the theoretical values of binary recombination rate coefficients for H_2D^+ and HD_2^+ [24]. The full and the open stars denote the values measured for H_3^+ in previous FALP [84] and SA-CRDS [76] experiments, respectively. The double-dot-dashed line labelled B&K shows the contribution to α_{eff} due to the helium-assisted three-body recombination calculated for Ar^+ ions in helium. The appropriate ternary recombination rate coefficient was taken from [40] and scaled for Ar^+ ions by the reduced mass ($K_{\text{Ar}}(145 \text{ K}) = 5 \times 10^{-27} \text{ cm}^6 \text{ s}^{-1}$). Lower panel: The dependence of α_{effH2D} and α_{effHD2} on $[\text{He}]$ measured at 80 K. These recombination rate coefficients were evaluated using data from [37] with the addition of several newly measured values of α_{eff} . The full and the open stars indicate the values of α_{effD3} obtained in the FALP [84] and SA-CRDS experiments [48], respectively. The open triangles are values of α_{eff} measured in the FALP experiment at 80 K for an Ar^+ ion in the helium buffer gas [77]. The double-dot-dashed line (B&K) denotes the contribution to α_{eff} due to helium-assisted three-body recombination calculated for Ar^+ ions in helium. The appropriate ternary recombination rate coefficient was taken from [40] and scaled for Ar^+ ions by the reduced mass ($K_{\text{Ar}}(80 \text{ K}) = 3.1 \times 10^{-26} \text{ cm}^6 \text{ s}^{-1}$). The dot-dashed line (B&K + CRR) includes, in addition to helium-assisted three-body recombination of Ar^+ ions with electrons, the contribution arising from electron-assisted three-body recombination. The corresponding α_{eff} was calculated using the ternary recombination rate coefficient from [49] ($K_{\text{E-CRR}} = 10^{-17} \text{ cm}^6 \text{ s}^{-1}$) and $n_e \approx 10^9 \text{ cm}^{-3}$.

in [85]) is good. In the case of HD_2^+ ions the measured binary recombination rate coefficients are very close to those calculated by Pagani *et al* [24] but their values for H_2D^+ are at least twice as high as α_{binH2D} determined in the present experiment.

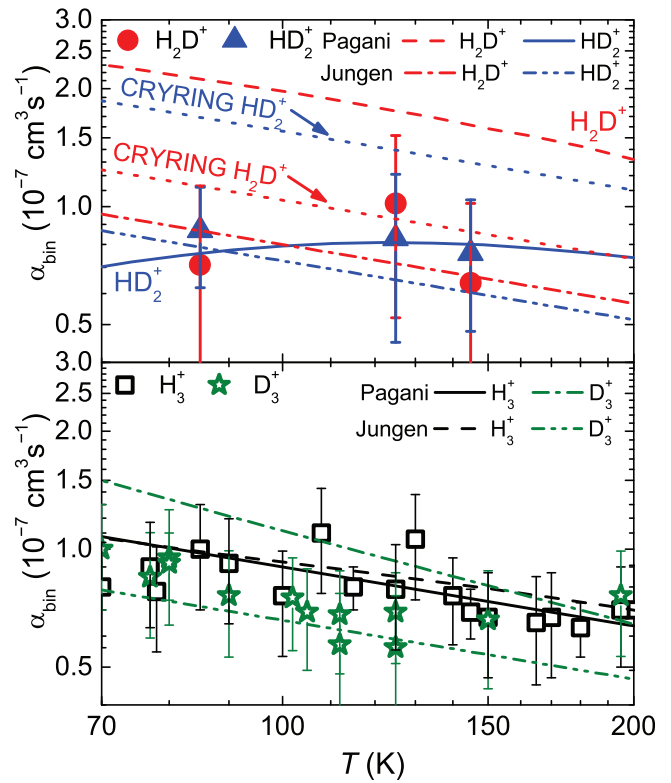


Figure 10. The temperature dependence of binary recombination rate coefficients of H_3^+ , H_2D^+ , HD_2^+ and D_3^+ ions with electrons. Upper panel: The temperature dependence of binary recombination rate coefficients for H_2D^+ and HD_2^+ ions obtained in this study. The dashed and the full lines denote the quantum mechanical calculations by Pagani *et al* [24] for H_2D^+ and HD_2^+ , respectively. The theoretical predictions of Jungen and Pratt [26, 85] for H_2D^+ (dot-dashed line) and for HD_2^+ (double-dot-dashed line) are also shown. The dotted lines labelled CRYRING denote the values obtained in the ion storage ring CRYRING at 300 K [34, 86] extrapolated to lower temperatures using a $T^{-0.5}$ dependence. Lower panel: The temperature dependence of binary recombination rate coefficients α_{binH3} and α_{binD3} for H_3^+ and D_3^+ ions adapted from [48, 84]. The full (H_3^+) and the dot-dashed (D_3^+) lines denote the theoretical calculations by Pagani *et al* [24]. The dashed and the double-dot-dashed lines denote the values calculated by Jungen and Pratt [26, 85] for H_3^+ and D_3^+ ions, respectively.

The ion storage ring experiment CRYRING reported at 300 K the values of $\alpha_{\text{binH2D}} = 6 \times 10^{-8} \text{ cm}^3 \text{ s}^{-1}$ [86] and $\alpha_{\text{binHD2}} = 9 \times 10^{-8} \text{ cm}^3 \text{ s}^{-1}$ [34], which are in reasonable agreement with our data, as shown in figure 10. Note that CRYRING experiments were done without *in situ* determination of the rotational excitation of recombining ions. For comparison we also included in the lower panel of figure 10 the calculated [24, 26, 85] and the measured [48, 84] values of α_{binH3} and α_{binD3} .

The measured values of the ternary recombination rate coefficients K_{H2D} and K_{HD2} of H_2D^+ and HD_2^+ ions are shown in figure 11, together with values obtained in our previous SA-CRDS and FALP experiments for H_3^+ [29, 31, 39, 45] and Ar^+ ions [77] and values obtained for different ions by other groups [67, 87–89]. The values of the ternary recombination rate coefficients previously obtained for D_3^+ are not shown but at temperatures above 80 K, they are very close to those of H_3^+ [39]. In

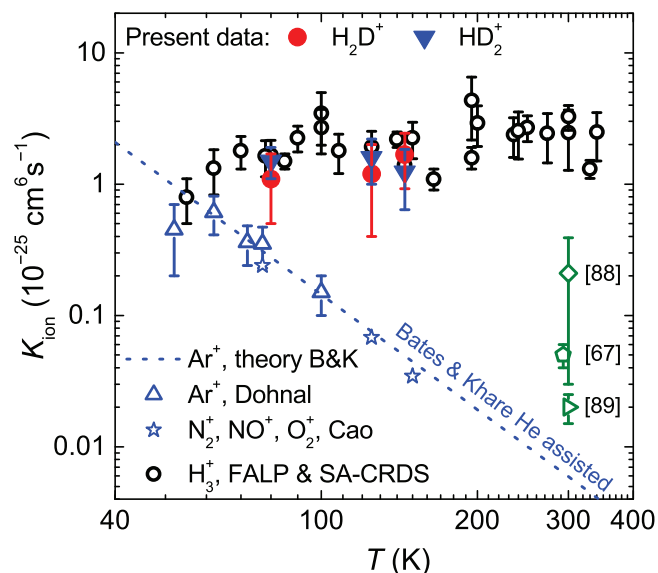


Figure 11. The temperature dependence of ternary recombination rate coefficients for helium-assisted three-body recombination of H_2D^+ (full circles) and HD_2^+ ions (full triangles). Values of ternary recombination rate coefficients of other ions are shown for comparison. Open circles: K_{H_3} of H_3^+ ions obtained in our previous experiments [29, 31, 39, 45]. Open triangles: ternary recombination rate coefficients K_{Ar} of He-assisted recombination of Ar^+ ions measured in a Cryo-FALP II experiment by Dohnal *et al* [77]. Open stars: K_{ion} as measured by Cao *et al* [87] for a mixture of atmospheric ions in He. Dotted line: theoretical dependence of Bates and Khare [40] scaled for Ar^+ ions in He by the reduced mass. The open triangle, pentagon and diamond on the right indicate the three-body rate coefficients measured for He_2^+ ions in helium by Berlande *et al* [88], Deloche *et al* [67] and Johnson *et al* [89], respectively.

the probed temperature range the values of the ternary recombination rate coefficients $K_{\text{H}_2\text{D}}$ and K_{HD_2} of H_2D^+ and HD_2^+ are similar to the values previously reported for H_3^+ and D_3^+ and substantially larger than the classical prediction for neutral-assisted recombination of atomic ions by Bates and Khare [40].

All the reported errors are statistical errors. The systematic error of the SA-CRDS experiment is estimated to be less than 10%.

6. Summary and conclusions

We have studied the recombination of H_2D^+ and HD_2^+ ions with electrons in the temperature range 80–145 K in a He/Ar/ H_2/D_2 gas mixture at pressures 500–1700 Pa using SA apparatus equipped with a CRDS absorption spectrometer. By measuring the time evolutions of the ion densities [H_3^+], [H_2D^+], [HD_2^+] and [D_3^+] at different gas densities [He], [H_2] and [D_2] (see figure 3), we were able to determine the binary ($\alpha_{\text{binH}_2\text{D}}$, α_{binHD_2}) and the ternary ($K_{\text{H}_2\text{D}}$, K_{HD_2}) recombination rate coefficients for H_2D^+ and HD_2^+ ions. The measured recombination rate coefficients are very close to the corresponding values previously obtained for H_3^+ and D_3^+ [39, 84] and there is reasonable agreement with ion storage ring data [34, 86] and some theoretical calculations [24, 26, 85]. We did not observe a substantial difference

between the binary recombination rate coefficients of H_2D^+ and HD_2^+ , which contradicts the prediction by Pagani *et al* [24]. The present results are summarized in figures 10 and 11, and in table 2. This set of experiments represents the first time $\alpha_{\text{binH}_2\text{D}}$ and α_{binHD_2} were measured for temperatures lower than 300 K and with *in situ* determined populations of recombining ions. The measured values of ternary recombination rate coefficients $K_{\text{H}_2\text{D}}$ and K_{HD_2} were close to those of H_3^+ and D_3^+ . We have previously offered an explanation of this fast three-body process [44, 45], but more advanced theoretical treatment is clearly needed.

A plasma is a complex multi-collisional environment and the inferred rate coefficients depend on the assumption that there are no unrecognized three-body processes. Further experiments performed with very low background pressure, and good control over rotational excitation, would provide a valuable test of our results.

The binary and ternary recombination rate coefficients reported in this paper are results of our long ongoing study of the recombination of H_3^+ ions and its isotopologues. We believe that these new data will help improve astrochemical models and lead to more accurate quantum mechanical calculations.

Acknowledgments

This work was partly supported by Czech Science Foundation projects GACR 14-14649P, GACR P209/12/0233 and GACR 15-15077S and by Charles University in Prague projects GAUK 692214, GAUK 572214, UNCE 204020/2012 and SVV 260 090.

References

- [1] Larsson M and Orel A E 2008 *Dissociative Recombination of Molecular Ions* (Cambridge: Cambridge University Press)
- [2] Johnsen R and Guberman S L 2010 *Dissociative Recombination of H_3^+ Ions with Electrons: Theory and Experiment* vol 59 (London: Academic) ch 3, pp 75–128
- [3] Smith D and Španěl P 1993 *Int. J. Mass Spectrom. Ion Process.* **129** 163–82
- [4] Glosík J, Plašil R, Kotrík T, Dohnal P, Varju J, Hejduk M, Korolov I, Roučka Š and Kokouline V 2010 *Mol. Phys.* **108** 2253–64
- [5] Herbst E and Klemperer W 1973 *Astrophys. J.* **185** 505–34
- [6] Oka T 2006 *Proc. Natl. Acad. Sci. USA* **103** 12235–42
- [7] Geballe T R and Oka T 1996 *Nature* **384** 334–5
- [8] Millar T J 2015 *Plasma Sources Sci. Technol.* **24** 043001
- [9] Watson W D 1973 *Astrophys. J., Lett.* **182** L73
- [10] Tennyson J and Miller S 2001 *Spectrochim. Acta A* **57** 661–7
- [11] Parise B, Belloche A, Du F, Güsten R and Menten K M 2011 *Astron. Astrophys.* **526** A31
- [12] Millar T J 2005 *Astron. Geophys.* **46** 2.29–2.32
- [13] Das A, Majumdar L, Chakrabarti S K and Sahu D 2015 *New Astron.* **35** 53–70
- [14] Albertsson T, Semenov D A, Vasyunin A I, Henning T and Herbst E 2013 *Astrophys. J., Suppl. Ser.* **207** 27
- [15] Sipilä O, Hugo E, Harju J, Asvany O, Juvela M and Schlemmer S 2010 *Astron. Astrophys.* **509** A98

- [16] Sipilä O, Caselli P and Harju J 2013 *Astron. Astrophys.* **554** A92
- [17] Brünken S et al 2014 *Nature* **516** 219–21
- [18] Roberts H, Herbst E and Millar T J 2004 *Astron. Astrophys.* **424** 16
- [19] Flower D R, Pineau des Forets G and Walmsley C M 2006 *Astron. Astrophys.* **449** 621–9
- [20] Ceccarelli C, Dominik C, Caux E, Lefloch B and Caselli P 2005 *Astrophys. J., Lett.* **631** L81
- [21] Roberts H, Herbst E and Millar T J 2003 *Astrophys. J., Lett.* **591** L41
- [22] Kokoouline V, Greene C H and Esry B D 2001 *Nature* **412** 891–4
- [23] Kokoouline V and Greene C H 2003 *Phys. Rev. A* **68** 012703
- [24] Pagani L, Vastel C, Hugo E, Kokoouline V, Greene C H, Bacmann A, Bayet E, Ceccarelli C, Peng R and Schlemmer S 2009 *Astron. Astrophys.* **494** 623–36
- [25] Fonseca dos Santos S, Kokoouline V and Greene C H 2007 *J. Chem. Phys.* **127** 124309
- [26] Jungen C and Pratt S T 2009 *Phys. Rev. Lett.* **102** 023201
- [27] Kreckel H et al 2005 *Phys. Rev. Lett.* **95** 263201
- [28] McCall B J et al 2003 *Nature* **422** 500–2
- [29] Varju J, Hejduk M, Dohnal P, Jílek M, Kotrčík T, Plašil R, Gerlich D and Glosík J 2011 *Phys. Rev. Lett.* **106** 203201
- [30] Petrigiani A et al 2011 *Phys. Rev. A* **83** 032711
- [31] Dohnal P, Hejduk M, Varju J, Rubovič P, Roučka Š, Kotrčík T, Plašil R, Glosík J and Johnsen R 2012 *J. Chem. Phys.* **136** 244304
- [32] Mitchell J B A, Ng C T, Forand L, Janssen R and McGowan J W 1984 *J. Phys. B: At. Mol. Phys.* **17** L909
- [33] Datz S, Larsson M, Stromholm C, Sundström G, Zengin V, Danared H, Källberg A and af Ugglas M 1995 *Phys. Rev. A* **52** 2901–9
- [34] Zhaunerchyk V, Thomas R D, Geppert W D, Hamberg M, Kaminska M, Vigrén E and Larsson M 2008 *Phys. Rev. A* **77** 034701
- [35] Lammich L et al 2003 *Phys. Rev. Lett.* **91** 143201
- [36] Strasser D, Lammich L, Kreckel H, Lange M, Krohn S, Schwalm D, Wolf A and Zajfman D 2004 *Phys. Rev. A* **69** 064702
- [37] Dohnal P, Kálosi Á, Plašil R, Roučka Š, Kovalenko A, Rednyk S, Johnsen R and Glosík J 2016 *Phys. Chem. Chem. Phys.* **18** 23549–53
- [38] Bates D R, Malaviya V and Young N A 1971 *Proc. R. Soc. A* **320** 437–58
- [39] Johnsen R, Rubovič P, Dohnal P, Hejduk M, Plašil R and Glosík J 2013 *J. Phys. Chem. A* **117** 9477–85
- [40] Bates D R and Khare S P 1965 *Proc. Phys. Soc.* **85** 231
- [41] Glosík J, Dohnal P, Rubovič P, Kálosi Á, Plašil R, Roučka Š and Johnsen R 2015 *Plasma Sources Sci. Technol.* **24** 065017
- [42] Badman S V, Branduardi-Raymont G, Galand M, Hess S L G, Krupp N, Lamy L, Melin H and Tao C 2015 *Space Sci. Rev.* **187** 99–179
- [43] Saykally R J, Michael E A, Wang J and Greene C H 2010 *J. Chem. Phys.* **133** 234302
- [44] Glosík J, Korolov I, Plašil R, Novotný O, Kotrčík T, Hlavenka P, Varju J, Mikhailov I A, Kokoouline V and Greene C H 2008 *J. Phys. B: At., Mol. Opt. Phys.* **41** 191001
- [45] Glosík J, Plašil R, Korolov I, Kotrčík T, Novotný O, Hlavenka P, Dohnal P, Varju J, Kokoouline V and Greene C H 2009 *Phys. Rev. A* **79** 052707
- [46] Dohnal P, Rubovič P, Kálosi Á, Hejduk M, Plašil R, Johnsen R and Glosík J 2014 *Phys. Rev. A* **90** 042708
- [47] Glosík J, Korolov I, Plašil R, Kotrčík T, Dohnal P, Novotný O, Varju J, Roučka Š, Greene C H and Kokoouline V 2009 *Phys. Rev. A* **80** 042706
- [48] Dohnal P, Hejduk M, Rubovič P, Varju J, Roučka Š, Plašil R and Glosík J 2012 *J. Chem. Phys.* **137** 194320
- [49] Stevefelt J, Boulmer J and Delpech J F 1975 *Phys. Rev. A* **12** 1246–51
- [50] Kotrčík T, Dohnal P, Rubovič P, Plašil R, Roučka Š, Opanasiuk S and Glosík J 2011 *Eur. Phys. J. Appl. Phys.* **56** 24011
- [51] Amano T 1990 *J. Chem. Phys.* **92** 6492–501
- [52] Macko P, Bánó G, Hlavenka P, Plašil R, Poterya V, Pysanenko A, Votava O, Johnsen R and Glosík J 2004 *Int. J. Mass Spectrom.* **233** 299–304
- [53] Plašil R, Korolov I, Kotrčík T, Dohnal P, Bánó G, Donko Z and Glosík J 2009 *Eur. Phys. J. D* **54** 391–8
- [54] Korolov I, Kotrčík T, Plašil R, Varju J, Hejduk M and Glosík J 2008 *Contrib. Plasma Phys.* **48** 521–6 ISSN 1521-3986
- [55] Novotný O et al 2014 *Astrophys. J.* **792** 132
- [56] O'Connor A P et al 2016 *Phys. Rev. Lett.* **116** 113002
- [57] Lindinger W, Schmeltekopf A L and Fehsenfeld F C 1974 *J. Chem. Phys.* **61** 2890–5
- [58] Hlavenka P, Plašil R, Bánó G, Korolov I, Gerlich D, Ramanlal J, Tennyson J and Glosík J 2006 *Int. J. Mass Spectrom.* **255–256** 170–6
- [59] Hlavenka P, Korolov I, Plašil R, Varju J, Kotrčík T and Glosík J 2006 *Czech. J. Phys.* **56** B749–60
- [60] Glosík J, Hlavenka P, Plašil R, Windisch F, Gerlich D, Wolf A and Kreckel H 2006 *Philos. Trans. R. Soc., A* **364** 2931–42
- [61] Romanini D, Kachanov A A, Sadeghi N and Stoekel F 1997 *Chem. Phys. Lett.* **264** 316–22
- [62] Asvany O, Hugo E, Müller F, Kühnemann F, Schiller S, Tennyson J and Schlemmer S 2007 *J. Chem. Phys.* **127** 154317
- [63] Neale L, Miller S and Tennyson J 1996 *Astrophys. J.* **464** 516
- [64] Tennyson J 2012 University College London private communication
- [65] Tennyson J 2016 University College London private communication
- [66] Kálosi Á, Dohnal P, Augustovičová L, Roučka Š, Plašil R and Glosík J 2016 *Eur. Phys. J. Appl. Phys.* **75** 24707
- [67] Deloche R, Monchicourt P, Cheret M and Lambert F 1976 *Phys. Rev. A* **13** 1140–76
- [68] Stevefelt J, Pouvesle J M and Bouchoule A 1982 *J. Chem. Phys.* **76** 4006–15
- [69] Hejduk M, Dohnal P, Varju J, Rubovič P, Plašil R and Glosík J 2012 *Plasma Sources Sci. Technol.* **21** 024002
- [70] Truncel D, Španěl P and Smith D 2003 *Chem. Phys. Lett.* **372** 728–32
- [71] Yencha A J 1984 *Penning Ionization and Related Processes* vol 5 (New York: Academic) p 197
- [72] Giles K, Adams N G and Smith D 1992 *J. Phys. Chem.* **96** 7645–50
- [73] Fárník M, Davis S, Kostin M A, Polyansky O L, Tennyson J and Nesbitt D J 2002 *J. Chem. Phys.* **116** 6146–58
- [74] Gerlich D, Windisch F, Hlavenka P, Plašil R and Glosík J 2006 *Philos. Trans. R. Soc., A* **364** 3007–34
- [75] Dohnal P, Hejduk M, Varju J, Rubovič P, Roučka Š, Kotrčík T, Plašil R, Johnsen R and Glosík J 2012 *Philos. Trans. R. Soc. A: Math. Phys. Eng. Sci.* **370** 5101–8
- [76] Hejduk M, Dohnal P, Rubovič P, Kálosi Á, Plašil R, Johnsen R and Glosík J 2015 *J. Chem. Phys.* **143** 044303
- [77] Dohnal P, Rubovič P, Kotrčík T, Hejduk M, Plašil R, Johnsen R and Glosík J 2013 *Phys. Rev. A* **87** 052716
- [78] Johnsen R 2015 *EPJ Web of Conf.* **84** 01003
- [79] Flannery M R 1991 *J. Chem. Phys.* **95** 8205–26
- [80] Kotrčík T, Dohnal P, Roučka Š, Jusko P, Plašil R, Glosík J and Johnsen R 2011 *Phys. Rev. A* **83** 032720
- [81] Novotný O, Plašil R, Pysanenko A, Korolov I and Glosík J 2006 *J. Phys. B: At., Mol. Opt. Phys.* **39** 2561

- [82] Glosík J, Novotný O, Pysanenko A, Zakouřil P, Plašil R, Kudrna P and Poterya V 2003 *Plasma Sources Sci. Technol.* **12** S117
- [83] Macdonald J A, Biondi M A and Johnsen R 1984 *Planet. Space Sci.* **32** 651–4
- [84] Rubovič P, Dohnal P, Hejduk M, Plašil R and Glosík J 2013 *J. Phys. Chem. A* **117** 9626–32
- [85] Pratt S T and Jungen C 2011 *J. Phys.: Conf. Ser.* **300** 012019
- [86] Larsson M, Danared H, Larson A, Le Padellec A, Peterson J R, Rosén S, Semaniak J and Strömholm C 1997 *Phys. Rev. Lett.* **79** 395–8
- [87] Cao Y S and Johnsen R 1991 *J. Chem. Phys.* **94** 5443–6
- [88] Berlande J, Cheret M, Deloche R, Gonfalone A and Manus C 1970 *Phys. Rev. A* **1** 887–96
- [89] Johnson A W and Gerardo J B 1971 *Phys. Rev. Lett.* **27** 835–8

**Overtone spectroscopy of N_2H^+ molecular ions—application of
cavity ring-down spectroscopy**

Kálosi A., Dohnal P., Shapko D., Roučka Š., Plašil R., Johnsen R., Glosík J.

J. Instrum. **12**, C10010, 2017.

18TH INTERNATIONAL SYMPOSIUM ON LASER-AIDED PLASMA DIAGNOSTICS
24–28 SEPTEMBER 2017
PRAGUE, CZECH REPUBLIC

Overtone spectroscopy of N_2H^+ molecular ions — application of cavity ring-down spectroscopy

Á. Kálosi,^a P. Dohnal,^{a,1} D. Shapko,^a Š. Roučka,^a R. Plašil,^a R. Johnsen^b and J. Glosík^a

^aDepartment of Surface and Plasma Science, Faculty of Mathematics and Physics, Charles University, V Holešovičkách 2, Prague, Czech Republic

^bDepartment of Physics and Astronomy, University of Pittsburgh, 3941 O'Hara St, Pittsburgh, Pennsylvania 15260, U.S.A.

E-mail: Petr.Dohnal@mff.cuni.cz

ABSTRACT: A stationary afterglow apparatus in conjunction with a laser absorption cavity ring-down spectrometer has been employed to observe absorption lines in the P- and R-branches of the (200) ← (000) and (21¹0) ← (01¹0) vibrational bands of the N_2H^+ molecular ion as a part of an ongoing study of the electron-ion recombination of N_2H^+ in afterglow plasmas. The probed absorption lines lie in the near-infrared spectral region around 1580 nm. The observed transition wavenumbers were fitted to experimental accuracy and improved molecular constants for the (200) vibrational state were obtained. The employed experimental technique enables probing of the translational, rotational and vibrational temperature of the studied ions as well as the determination of the number densities of different quantum states of the ion in discharge and afterglow plasma.

KEYWORDS: Plasma diagnostics - interferometry, spectroscopy and imaging; Lasers

¹Corresponding author.

Contents

1	Introduction	1
2	Experimental technique	2
2.1	Cavity ring-down spectrometer	2
2.2	Stationary afterglow	2
3	Results and discussion	3
4	Summary and conclusions	7

1 Introduction

The N_2H^+ molecular ion, being an important and abundant interstellar species, has been the subject of spectroscopic and electron-ion recombination studies since its first radio astronomical detection [1, 2]. It has been observed in a variety of interstellar environments [3–5] and serves as a versatile probe of N_2 and CO abundances and physical structure of dark clouds [6, 7]. In denser regions it is formed via proton transfer from H_3^+ and the main destruction mechanisms include proton transfer to CO and dissociative recombination with free electrons.

The dissociative recombination of N_2H^+ with electrons has been studied by Flowing Afterglow and Storage Ring techniques resulting in the determination of temperature dependence of its rate coefficient and branching ratios of the product channels and observation of emission spectra of electronically excited products. For an overview of the different experimental results see recent publications [8–10] and references therein. Only one spectroscopic determination of the decay of the N_2H^+ number density in an afterglow plasma has been carried out so far, which gave a surprisingly high value of the recombination rate coefficient [11]. Fully *ab initio* calculations have indicated that the inclusion of several types of vibronic coupling in the indirect recombination mechanism yields theoretical cross sections comparable to experimental data [12].

Detailed descriptions of the experimental work on spectroscopic studies of N_2H^+ are given in refs. [13, 14]. These include the observation of rotational transitions in excited vibrational states. N_2H^+ has a linear configuration in its ground electronic state. Its vibrational states will be represented in this paper by the symbol $(\nu_1\nu_2^l\nu_3)$, where ν_1 , ν_2 , and ν_3 indicate the numbers of vibrational quanta in its three normal modes: in the ν_1 N-H stretching vibration, the ν_2 bending vibration, and the ν_3 N-N stretching vibration, respectively. l is the quantum number associated with the vibrational angular momentum corresponding to the doubly degenerate bending mode. Extensive information on the excited vibrational states has been published [15].

The main aim of this study was to find suitable transitions of the N_2H^+ ion that could be used for the determination of number densities of the ground vibrational state and of the first excited vibrational state of N_2H^+ for further studies of its recombination with electrons in afterglow plasmas.

2 Experimental technique

The present experiments employ a cavity ring-down (CRD) laser absorption spectrometer in conjunction with a stationary afterglow (SA) apparatus. The following sections will give a brief description of the diagnostic technique and the apparatus. For more technical details see [16].

2.1 Cavity ring-down spectrometer

The design of the CRD spectrometer is based on the continuous wave modification developed by [17]. The radiation sources employed in our setup are either fiber-coupled distributed feedback diode lasers (DFB, typical linewidth of less than 10 MHz and optical output power higher than 10 mW) or an external cavity diode laser (ECDL, Sacher Lasertechnik, output power of 3 mW), with central wavelengths in the near-infrared spectral region around 1580 nm and 1450 nm, respectively. The active radiation source wavelength is measured by a Michelson interferometer-based wavemeter (EXFO WA-1650). The optical setup is divided into two almost identical parts for the two types of lasers. Each part consists of a free space optical isolator, an acousto-optic modulator, a pair of lenses, and a pinhole for spatial filtering and mode matching the laser beam into the cavity. Two plano-concave highly reflective mirrors (reflectivity $> 99.95\%$) form the optical resonator. The spacing of the mirrors is 75 cm and a typical ring-down time of the empty resonator is 32 μ s. The entry mirror is fitted with a piezoelectric transducer which in turn is modulated either by a triangular waveform or by a combination of a relatively low-amplitude sinusoidal waveform with a slowly varied voltage offset controlled by active feedback to achieve higher acquisition rate of the ring-down events. Photons exiting the cavity are detected by an avalanche photodiode. The detector is equipped by an optical bandpass filter centered at the used wavelengths to minimize background contributions from the discharge light emissions.

2.2 Stationary afterglow

The highly reflective mirrors of the CRD spectrometer are placed inside the stationary afterglow vacuum apparatus at both ends of a fused silica discharge tube with an inner diameter of 1.2 cm. The ions of interest are generated in a periodically switched microwave discharge inside a rectangular waveguide resonator. The neutral gas typically consists of several hundred Pascal of buffer gas (hydrogen or helium) with admixtures of reactants. The buffer gas is purified in the high pressure region by liquid nitrogen cooled cryotrap before passing through the mass flow meter. The flowing gas mixture is further purified in two other liquid nitrogen cooled cryotrap before entering the discharge tube. The 2.45 GHz magnetron based microwave generator is continuously operated at relatively low power of 8–20 W. Switching off the microwave power is achieved by an external high-voltage switch connected directly to the magnetron power supply. Typical discharge period is 4 ms with a 50% duty cycle. The ring-down signal acquisition is synchronized with the discharge pulses in order to achieve temporally resolved absorption measurements, sampled at 1.25 MHz sampling frequency by a 12-bit AD converter. Light emitted from the discharge can be monitored through a view port in the waveguide. The discharge tube itself is surrounded by an outer glass tube that can be closed off at both ends and filled with liquid nitrogen to make a cooling bath. Pre-cooled liquid nitrogen vapors from a heated reservoir can also be flowed through this surrounding volume to achieve stable discharge tube wall temperatures T_{wall} in the range of 77–300 K.

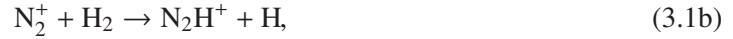
3 Results and discussion

In the present experiments H_2/N_2 and $\text{He}/\text{H}_2/\text{N}_2$ gas mixtures were utilized to produce N_2H^+ dominated low-temperature plasmas. In both hydrogen and helium buffered plasmas optimal reactant number densities were chosen to maximize the observed absorption signal. All the experiments were conducted at $T_{\text{wall}} = 300$ K with nitrogen vapors flowing through the surrounding volume to maintain stable temperature.

The first set of experiments, inspired by previous spectroscopic and recombination experiments of [11, 18], was conducted in gas mixtures of H_2 and N_2 with typical number densities of 10^{16} cm^{-3} and $10^{14} - 10^{15} \text{ cm}^{-3}$, respectively. When using $\text{He}/\text{H}_2/\text{N}_2$ gas mixtures, the typical number densities used in the experiments were $10^{17}/10^{14}/10^{14} \text{ cm}^{-3}$. The main reactions for formation of N_2H^+ at these conditions are:



and



where the second reaction is slightly more exothermic [19]. For more details on H_3^+ formation in H_2 buffered plasmas see [20]. Computer simulations of the chemical kinetics predict abundant production of N_2H^+ ions at typical experimental conditions. Special attention was paid to the presence of H_2O and NH_3 impurity molecules in the discharge. The amount of H_2O impurities was monitored using transition at 6804.401 cm^{-1} ($0, 2, 1$) $2_{02} \leftarrow (0, 0, 0)$ 3_{03} . The line position and intensity were taken from the HITRAN database [21]). The number density of water was found to be substantially lower than 10^{11} cm^{-3} . NH_3 reacts fast with the N_2H^+ ions forming NH_4^+ molecular ions [22]. We found that even if the NH_3 number density is as low as 10^{12} cm^{-3} the absorption signal from the N_2H^+ ions decreases by almost an order of magnitude. The NH_3 molecules are probably formed at the walls of the discharge tube. We used transitions at 6314.133 cm^{-1} and 6314.438 cm^{-1} (line positions and transition line strengths taken from the HITRAN database [21] and from ref. [23]) to monitor the actual density of NH_3 in the discharge tube. By changing the buffer gas flow and the H_2/N_2 ratio we were able to keep the NH_3 number density well below 10^{11} cm^{-3} .

The search for P-branch lines in the ν_1 first overtone band of N_2H^+ was initiated by simulating a stick spectrum from the spectroscopic parameters determined by [18] for the (200) state and [14] for the ground state. The rovibrational energy levels in units of cm^{-1} of these states relative to the ground state term value are expressed as follows:

$$T(\nu, J) = E(\nu, J)/hc = G_\nu + B_\nu [J(J+1)] - D_\nu [J(J+1)]^2 + H_\nu [J(J+1)]^3 \quad (3.2)$$

where ν and J represent the vibrational and rotational quantum numbers, respectively. The intensity of these rovibrational absorption lines can be expressed as (in accordance with the definitions used in the HITRAN database [24]):

$$S_\nu^N(T) = \frac{\tilde{\nu}_0}{Q_{\text{tot}}(T)} \frac{8\pi^3}{4\pi\epsilon_0 3hc} \left[\exp\left(-\frac{E_1}{k_B T}\right) - \exp\left(-\frac{E_2}{k_B T}\right) \right] S_R F(R_{12})^2 \quad (3.3)$$

where E_2 and E_1 are the upper and lower state energies, respectively, $\tilde{\nu}_0 = (E_2 - E_1)/(hc)$ is the transition wavenumber, h is the Planck constant, c is the speed of light in vacuum, Q_{tot} is the total

internal partition function, ϵ_0 is the vacuum permittivity, k_B is the Boltzmann constant, T is the temperature, S_R is the rotational intensity factor, F is the Herman-Wallis correction term and R_{12} is the transition moment of the vibrational band. For the rotational and Herman-Wallis factors we adapted the expressions found in [25]. The transition moment of the ν_1 first overtone band was computed by Vladimír Špirko¹ using the ab initio potential energy surface and dipole moment surface from ref. [26]. The integrated absorption coefficient (area of the absorption line) equals the line intensity multiplied by the number density of the absorbing molecules.

Figure 1 shows a section of the recorded spectrum, eight transitions in the P-branch of the ν_1 first overtone were observed from 6296 cm^{-1} to 6320 cm^{-1} . The measurements were later extended to the R-branch in the range from 6388 cm^{-1} to 6401 cm^{-1} in order to achieve higher sensitivity in the determination of the rotational temperature of the ions. Each line was fitted by a Gaussian line shape resulting in the determination of the transition wavenumbers and the translational temperature of the ions. In several cases where the absorption lines of interest were partially overlapped with strong lines of N_2 arising from transitions between excited electronic states, mostly in the case of R-branch lines [18], the lines were, in addition, fitted in a suitable section of the spectrum.

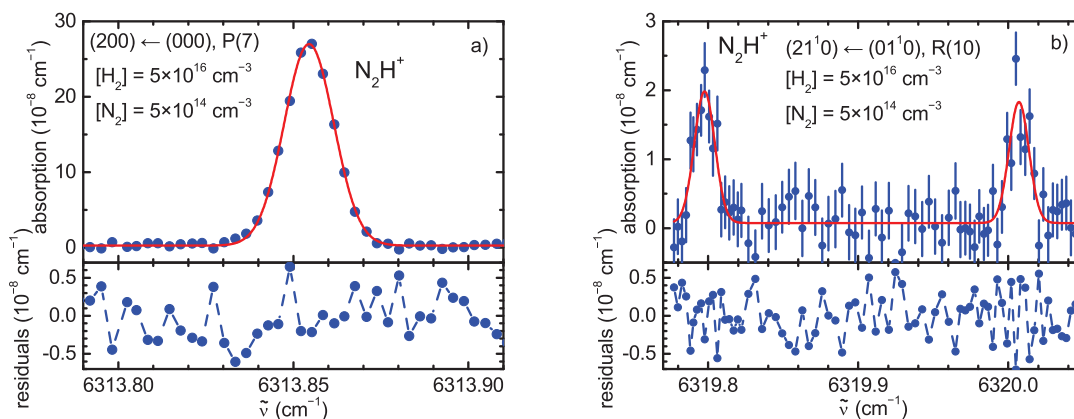


Figure 1. Panel (a): an example of the measured absorption spectra for a P-branch transition. The full line is the Gaussian fit to the data. The residuals of the fit are shown in the lower part of the figure. Panel (b): examples of measured transitions originating in the first vibrationally excited state of N_2H^+ . The full line is the Gaussian fit to the data. The residuals of the fit are shown below.

The measured transition wavenumbers are listed in table 1 and were fitted together with the data from [18] by a linear model in which the ground state parameters were fixed to the values given by [14]. The transition wavenumbers were weighted by the quoted uncertainties, in the case of the data from [18] a constant uncertainty was assumed given by the estimated experimental accuracy of 0.005 cm^{-1} quoted in the paper. The improved molecular parameters obtained for the upper vibrational state (200) are given in table 2.

The relatively high vibrational band strength of the transitions where ν_1 changes by two quanta enabled us to observe the $(21^1_0) \leftarrow (01^1_0)$ hot band that lies close to the ν_1 first overtone band. The energy levels of these states could be easily calculated using the effective energy expansion and

¹Private communication.

Table 1. The measured transition wavenumbers in the (200) \leftarrow (000) vibrational band of N_2H^+ ($\tilde{\nu}_{\text{exp}}$) compared to transition wavenumbers obtained by Sasada and Amano [18] and those calculated from the energy levels given by eq. (3.2). The spectroscopic constants for the lower state were taken from ref. [14] and for the upper state were obtained from the fit to the present data (see table 2 for details). The stars denote lines that were blended with those of N_2 and were not used in the fit. The difference between measured and calculated wavenumbers (Δ) is also shown. The numbers in parentheses are errors of the measurement in units of the last quoted digit.

transition	$\tilde{\nu}_{\text{exp}} (\text{cm}^{-1})$	$\tilde{\nu}_{\text{Sasada}} (\text{cm}^{-1})$	$\tilde{\nu}_{\text{calc}} (\text{cm}^{-1})$	$\Delta (10^{-4} \text{cm}^{-1})$
P(12)	6296.0276(2)		6296.0276	0
P(11)	6299.6940(2)		6299.6939	1
P(10)	6303.3097(2)		6303.3098	-1
P(9)	6306.8752(2)		6306.8753	-1
P(8)	6310.3902(2)		6310.3902	0
P(7)	6313.8544(2)		6313.8545	-1
P(6)	6317.2682(2)		6317.2681	1
P(5)	6320.6311(2)		6320.6310	1
R(19)	6388.0010(2)	6388.000(5)	6388.0009	1
R(20)	6390.0202(6)*	6390.007(5)	6390.0203	-1
R(21)	6391.9873(4)	6391.980(5)	6391.9872	1
R(22)	6393.9010(4)	6393.898(5)	6393.9016	-6
R(23)	6395.7635(5)	6395.759(5)	6395.7634	1
R(24)	6397.5723(6)*	6397.568(5)	6397.5726	-3
R(25)	6399.3291(4)	6399.327(5)	6399.3291	0
R(26)	6401.0331(9)	6401.029(5)	6401.0329	2

Table 2. The spectroscopic constants for the (200) vibrational state of the N_2H^+ ion. Values obtained in this study are compared with constants reported by Sasada and Amano [18] and Kabbadj et al. [15]. The numbers in the parentheses are errors in units of the last quoted digit.

	$G_{200} (\text{cm}^{-1})$	$B_{200} (\text{cm}^{-1})$	$D_{200} (10^{-6} \text{cm}^{-1})$
present	6336.68123(12)	1.5383702(14)	2.8933(22)
Sasada and Amano	6336.6775(39)	1.5383581(71)	2.875(fixed value)
Kabbadj et al.	6336.679	1.538368(14)	2.880(20)

molecular constants given in [15] as:

$$T(v, J) = G_v + B_v [J(J+1) - l^2] - D_v [J(J+1) - l^2]^2 + H_v [J(J+1) - l^2]^3. \quad (3.4)$$

When $v_2 = 1$, each rotational level is split into two sublevels that are characterized by the projection of the vibrational angular momentum onto the molecular axis and can also be labeled e and f depending on the parity of the wave function [27]. A single pair of lines of the (21¹0) \leftarrow (01¹0) hot band is plotted in panel (b) of figure 1 to compare the typical line intensity with that of the (200) \leftarrow (000) band. The measured transitions of the (21¹0) \leftarrow (01¹0) hot band are summarized in table 3.

Table 3. The measured transitions in the $(21^10) \leftarrow (01^10)$ hot band of N_2H^+ ($\tilde{\nu}_{\text{exp}}$) compared to transition wavenumbers calculated from equation (3.4) using the spectroscopic constants available in ref. [15]. The difference between measured and calculated wavenumbers (Δ) is also shown. The numbers in the parentheses are errors of the measurement in units of the last quoted digit. Upper indices e and f denote parity.

Transition	$\tilde{\nu}_{\text{exp}} \text{ (cm}^{-1}\text{)}$	$\tilde{\nu}_{\text{calc}} \text{ (cm}^{-1}\text{)}$	$\Delta \text{ (10}^{-4} \text{ cm}^{-1}\text{)}$
R(4) ^e	6303.7250(20)	6303.7231	19
R(4) ^f	6303.8142(5)	6303.8139	3
R(7) ^e	6311.9879(4)	6311.9881	-2
R(7) ^f	6312.1350(10)	6312.1371	-21
R(8) ^e	6314.6419(7)	6314.6420	-1
R(9) ^f	6317.2450(11)	6317.2454	-4
R(9) ^e	6317.4329(20)	6317.4341	-12
R(10) ^e	6319.7976(6)	6319.7979	-3
R(10) ^f	6320.0066(8)	6320.0071	-5

We recorded a set of absorption lines in the P-branch section of the spectrum including the hot band lines to create a Boltzmann plot (shown in figure 2) which can be used to evaluate the rotational temperature of the ions. Our first approach was to fit the ν_1 overtone lines separately in order to include the possibility of a difference in vibrational and rotational temperatures. The rotational temperature evaluated using states from the ground vibrational level using the Boltzmann plot is $T_{\text{rot}} = 356 \pm 8$ K, while the temperature of the discharge tube wall measured outside the microwave resonator was approximately 310 K. Assuming the same rotational temperature in both probed vibrational states and equal vibrational band strengths of the transitions, the resulting vibrational temperature is $T_{\text{vib}} = 340 \pm 10$ K in a very good agreement with the evaluated rotational temperature of the ions.

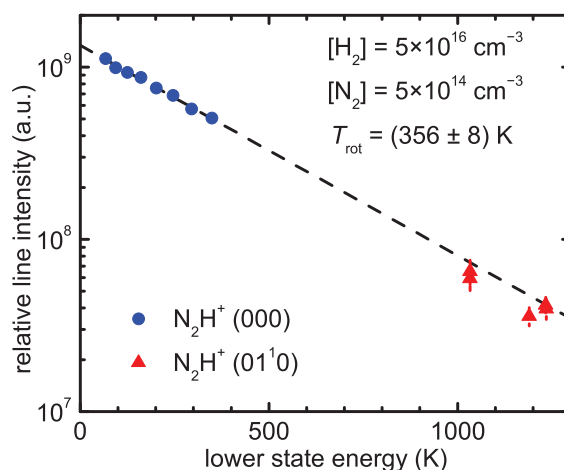


Figure 2. Boltzmann plot used for evaluation of the rotational temperature. The values obtained from the P-branch transitions originating in the ground vibrational state of the N_2H^+ ion are plotted as circles, whereas those from the first excited vibrational state are indicated by triangles. The dashed line denotes the fit to the data used for the determination of the rotational temperature.

We used several first overtone transitions from the ground state of the CO molecule (P(11), P(8), R(15) and R(16)) in the investigated frequency range to assess the systematic error of our wavenumber determination by comparing the measured values with the HITRAN database [21]. The estimated systematic error of our measurement is lower than $2 \times 10^{-4} \text{ cm}^{-1}$. The errors shown in table 1 and table 3 include both statistical and systematic errors.

The time dependence of the measured number density of the ions in the ground vibrational state of N_2H^+ in the discharge and early afterglow plasma is shown in the panel (a) of figure 3. The number density was evaluated assuming thermal population of states from the absorption on the P(6) line of the $(200) \leftarrow (000)$ vibrational band of N_2H^+ using equation (3.3) and $R_{12} = 0.0167$ Debye.² Panel (b) of figure 3 shows reciprocal plot of the ion number density n . Note that in recombination dominated plasma this plot is linear:

$$1/n = 1/n_0 + \alpha f_e(t - t_0) \quad (3.5)$$

where n_0 is the ion number density at $t = t_0$, α is the recombination rate coefficient and f_e is the ratio between the number densities of the electrons and probed ions. In our experimental setup the losses of charged particles by ambipolar diffusion are not negligible so equation (3.5) is valid only in the very early afterglow.

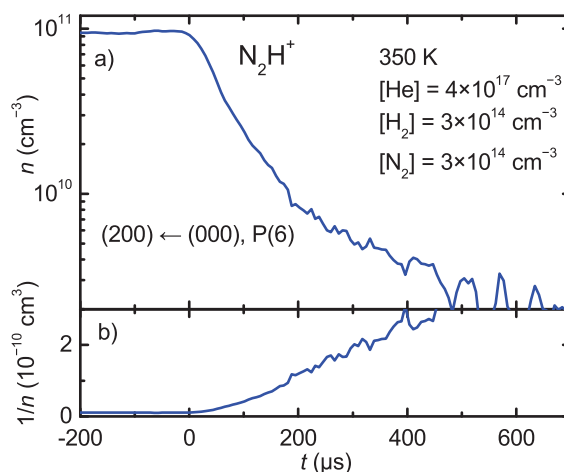


Figure 3. Panel (a): the time dependence of the overall number density of the N_2H^+ ions in the ground vibrational state calculated using equation (3.3) from the absorption on the P(6) line. The time is set to zero at the beginning of the afterglow. Panel (b): reciprocal plot of the ion number density.

4 Summary and conclusions

Using a stationary afterglow apparatus equipped with a cavity ring-down spectrometer we have probed several transitions belonging to the $(200) \leftarrow (000)$ and $(21^10) \leftarrow (01^10)$ bands of the N_2H^+ ion. In case of the ν_1 first overtone the transitions were probed in both P- and R-branches. The measured line positions shown in table 1 are in a very good agreement with previous experimental

²Špirko, private communication.

study by Sasada and Amano [18] and with theoretical calculations. The improved accuracy of our results in comparison with previous ones enabled us to calculate the spectroscopic constants of the (200) state (see table 2 for details). The observed transitions enable us to probe the translational, rotational and vibrational temperature of the ions as well as the number densities of different rotational and vibrational states of N_2H^+ . These results will be used in our ongoing study of N_2H^+ recombination with electrons.

Acknowledgments

We would like to thank Dr. Vladimír Špirko for calculating the transition dipole moment of the overtone transitions of N_2H^+ . This work was supported by Czech Science Foundation projects GACR 15-15077S, GACR 17-08803S, GACR 17-18067S and by Charles University project GAUK 1583517.

References

- [1] B.E. Turner, *U93.174 — A new interstellar line with quadrupole hyperfine splitting*, *Astrophys. J.* **193** (1974) L83.
- [2] S. Green, J.A. Montgomery and P. Thaddeus, *Tentative identification of U93.174 as the molecular ion N_2H^+* , *Astrophys. J.* **193** (1974) L89.
- [3] A. Dutrey, T. Henning, S. Guilloteau, D. Semenov, V. Pietu, K. Schreyer et al., *Chemistry in disks. 1. Deep search for N_2H^+ in the protoplanetary disks around LkCa 15, MWC 480 and DM Tau*, *Astron. Astrophys.* **464** (2007) 615 astro-ph/0612534.
- [4] F. Daniel, J. Cernicharo, E. Roueff, M. Gerin and M.L. Dubernet, *The excitation of N_2H^+ in interstellar molecular clouds. II. Observations*, *Astrophys. J.* **667** (2007) 980.
- [5] W.M. Schlingman, Y.L. Shirley, D.E. Schenk, E. Rosolowsky, J. Bally, C. Battersby et al., *The Bolocam Galactic Plane Survey. V. HCO^+ and N_2H^+ spectroscopy of 1.1 mm dust continuum sources*, *Astrophys. J.* **195** (2011) S14.
- [6] C. Qi, K.I. Öberg, S.M. Andrews, D.J. Wilner, E.A. Bergin, A.M. Hughes et al., *Chemical imaging of the CO snow line in the HD 163296 disk*, *Astrophys. J.* **813** (2015) 128.
- [7] M.L.R. van't Hoff, C. Walsh, M. Kama, S. Facchini and E.F. van Dishoeck, *Robustness of N_2H^+ as tracer of the CO snowline*, *Astron. Astrophys.* **599** (2017) A101.
- [8] V. Poterya, J.L. McLain, N.G. Adams and L.M. Babcock, *Mechanisms of electron-ion recombination of N_2H^+/N_2D^+ and HCO^+/DCO^+ ions: temperature dependence and isotopic effect*, *J. Phys. Chem. A* **109** (2005) 7181.
- [9] P.A. Lawson, D. Osborne and N.G. Adams, *Effect of isotopic content on the rate constants for the dissociative electron-ion recombination of N_2H^+* , *Int. J. Mass Spectrom.* **304** (2011) 41.
- [10] E. Vigren, V. Zhaunerchyk, M. Hamberg, M. Kaminska, J. Semaniak, M. af Ugglas et al., *Reassessment of the dissociative recombination of N_2H^+ at CRYRING*, *Astrophys. J.* **757** (2012) 34.
- [11] T. Amano, *The dissociative recombination rate coefficients of H_3^+ , HN_2^+ , and HCO^+* , *J. Chem. Phys.* **92** (1990) 6492.
- [12] S. Fonseca dos Santos, N. Douguet, V. Kokouline and A.E. Orel, *Scattering matrix approach to the dissociative recombination of HCO^+ and N_2H^+* , *J. Chem. Phys.* **140** (2014) 164308.

- [13] T. Amano, T. Hirao and J. Takano, *Submillimeter-wave spectroscopy of HN_2^+ and DN_2^+ in the excited vibrational states*, *J. Mol. Spectrosc.* **234** (2005) 170.
- [14] S. Yu, J.C. Pearson, B.J. Drouin, T. Crawford, A.M. Daly, B. Elliott et al., *Rotational spectroscopy of vibrationally excited N_2H^+ and N_2D^+ up to 2.7 THz*, *J. Mol. Spectrosc.* **314** (2015) 19.
- [15] Y. Kabbadj, T.R. Huet, B.D. Rehfuss, C.M. Gabrys and T. Oka, *Infrared spectroscopy of highly excited vibrational levels of protonated nitrogen, HN_2^+* , *J. Mol. Spectrosc.* **163** (1994) 180.
- [16] P. Macko, G. Bánó, P. Hlavenka, R. Plašil, V. Poterya, A. Pysanenko et al., *Afterglow studies of $H_3^+(v = 0)$ recombination using time resolved cw-diode laser cavity ring-down spectroscopy*, *Int. J. Mass Spectrom.* **233** (2004) 299.
- [17] D. Romanini, A.A. Kachanov, N. Sadeghi and F. Stoeckel, *CW cavity ring down spectroscopy*, *Chem. Phys. Lett.* **264** (1997) 316.
- [18] H. Sasada and T. Amano, *Observation of the $2v_1$ band of HN_2^+ with a 1.57 μm distributed feedback semiconductor laser*, *J. Chem. Phys.* **92** (1990) 2248.
- [19] N.G. Adams and L.M. Babcock, *Optical emissions from the dissociative electron recombination of N_2H^+ and HCO^+* , *J. Phys. Chem.* **98** (1994) 4564.
- [20] J. Glosík, P. Dohnal, P. Rubovič, Á. Kálosi, R. Plašil, Š. Roučka et al., *Recombination of H_3^+ ions with electrons in He/ H_2 ambient gas at temperatures from 240 K to 340 K*, *Plasma Sources Sci. Technol.* **24** (2015) 065017.
- [21] I.E. Gordon, L.S. Rothman, C. Hill, R.V. Kochanov, Y. Tan, P.F. Bernath et al., *The HITRAN2016 molecular spectroscopic database*, *J. Quant. Spectrosc. Ra.* **203** (2017) 3.
- [22] R.S. Hemsworth, J.D. Payzant, H.I. Schiff and D.K. Bohme, *Rate constants at 297° K for proton transfer reactions with NH_3 . Comparisons with classical theories and exothermicity*, *Chem. Phys. Lett.* **26** (1974) 417.
- [23] K. Sung, L.R. Brown, X. Huang, D.W. Schwenke, T.J. Lee, S.L. Coy et al., *Extended line positions, intensities, empirical lower state energies and quantum assignments of NH_3 from 6300 to 7000 cm^{-1}* , *J. Quant. Spectrosc. Ra.* **113** (2012) 1066.
- [24] M. Šimečková, D. Jacquemart, L.S. Rothman, R.R. Gamache and A. Goldman, *Einstein A-coefficients and statistical weights for molecular absorption transitions in the HITRAN database*, *J. Quant. Spectrosc. Ra.* **98** (2006) 130.
- [25] A. Maki, W. Quapp and S. Klee, *Intensities of hot-band transitions: HCN hot bands*, *J. Mol. Spectrosc.* **171** (1995) 420.
- [26] V. Špirko, O. Bludský and W.P. Kraemer, *Energies and electric dipole moments of the bound vibrational states of HN_2^+ and DN_2^+* , *Collect. Czech. Chem. Commun.* **73** (2008) 873.
- [27] J.M. Brown, J.T. Hougen, K.P. Huber, J.W.C. Johns, I. Kopp, H. Lefebvre-Brion et al., *The labeling of parity doublet levels in linear molecules*, *J. Mol. Spectrosc.* **55** (1975) 500.

**Stationary afterglow apparatus with CRDS for study of processes in
plasmas from 300 K down to 30 K**

Plašil R., Dohnal P., Kálosi Á., Roučka Š., Shapko D., Rednyk S., Johnsen R.,
Glosík J.

Rev. Sci. Instrum. **89**, 063116, 2018.

Stationary afterglow apparatus with CRDS for study of processes in plasmas from 300 K down to 30 K

R. Plašil,^{1,a)} P. Dohnal,¹ Á. Kálosi,¹ Š. Roučka,¹ D. Shapko,¹ S. Rednyk,¹
R. Johnsen,² and J. Glosík¹

¹Department of Surface and Plasma Science, Faculty of Mathematics and Physics, Charles University, Prague, Czech Republic

²Department of Physics and Astronomy, University of Pittsburgh, Pittsburgh, Pennsylvania 15260, USA

(Received 19 April 2018; accepted 28 May 2018; published online 15 June 2018)

A cryogenic stationary afterglow apparatus equipped with a near-infrared cavity-ring-down-spectrometer (Cryo-SA-CRDS) for studies of electron-ion recombination processes in the plasma at temperatures 30–300 K has been designed, constructed, tested, and put into operation. The plasma is generated in a sapphire discharge tube that is contained in a microwave cavity. The cavity and the tube are attached to the second stage of the cold head of the cryocooler system, and they are inserted to an UHV chamber with mirrors for CRDS and vacuum windows on both ends of the tube. The temperature of the discharge tube can be made as low as 25 K. In initial test measurements, the discharge was ignited in He/Ar/H₂ or He/H₂ gas mixtures and the density of H₃⁺ ions and their kinetic and rotational temperatures were measured during the discharge and afterglow. From the measured decrease in the ion density, during the afterglow, effective recombination rate coefficients were determined. Plasma relaxation was studied in He/Ar gas mixtures by monitoring the presence of highly excited argon atoms. The spectroscopic measurements demonstrated that the kinetic temperature of the ions is equal to the gas temperature and that it can be varied from 300 K down to 30 K. *Published by AIP Publishing.*
<https://doi.org/10.1063/1.5036834>

I. INTRODUCTION

Electron-ion recombination is one of the fundamental processes in plasma. Dependent on particular ion and on parameters of plasma, it can occur by a variety of mechanisms. From a kinetic point of view, recombination can be binary or multi-collisional proceeding via collisional complexes, e.g., ternary neutral-assisted (three-body, N-TBR, for a general discussion, see, e.g., Ref. 1) or electron-assisted (collisional radiative, E-CRR) recombination processes. In low-temperature plasmas containing molecular ions, the dominant binary recombination process is the dissociative recombination (DR) (see the recent review by Larsson and Orel²). In plasmas containing only atomic ions, recombination usually occurs by radiative recombination (RR).³ These processes have been studied, and their recombination rate coefficients have been measured in afterglow experiments for 70 years.^{2,4}

Rate coefficients for recombination of ions with electrons can be measured in two broad categories of experiments, the historically older plasma afterglows and the newer merged-beams and ion-storage-rings. Their basic principles have been reviewed extensively (see, e.g., Refs. 2 and 5). Only a very short overview of experimental techniques will be given here. A plasma afterglow technique is relatively simple and inexpensive, while the modern storage rings are large-scale, expensive, multi-user facilities (see short description below). Both techniques have their strengths and weaknesses. Examples

of afterglow techniques used for recombination studies are the stationary afterglow (SA) technique,^{4,6} flowing afterglow (FA),⁷ and flowing afterglow with Langmuir probe (FALP) technique.^{8–11} In the majority of these experiments, the ions are identified by using mass spectrometers. Only in some experiments, the recombining ions and their internal excitation are identified spectroscopically.^{12–15} The interpretation of afterglow plasmas, i.e., the decay of plasma subsequent to the removal of the ionization source, can be complicated by the occurrence of extraneous processes, and because they are carried out at relatively high neutral densities, they are not always free of third-body interactions. The latter has been found to be important in recombination studies of the H₃⁺ ions.^{16–19} Storage rings are free of many such complications since the gas densities are very low, but the absence of collisions also prevents thermalization of the internal degrees of freedom, e.g., rotational energy of the ions. In the afterglow methods, *in situ* optical absorption can be used to quantify internal states and to distinguish spin modifications of the ions, such as ortho- and para-H₃⁺.²⁰ Results obtained by the two measurement techniques have often agreed but sometimes differed in which case the disagreement often led to new insights. This is likely to continue.

Measurements at very low temperatures (or ion-electron collisions energies) are of particular interest for applications to cold astrophysical clouds. In part for that reason, new cryogenic ion storage-rings have been built and have recently become operative (CSR in Heidelberg²¹ and DESIREE in Stockholm²⁰). Afterglow studies have been carried out at temperature as low as 80 K, which is still higher than the temperatures of interest in astrophysics.

^{a)}Electronic mail: Radek.Plasil@mff.cuni.cz

In the analysis of the afterglow data, it is usually assumed that ions and electrons are in thermal equilibrium with neutrals (buffer gas) and that the temperatures of the electrons, ions, and atoms/molecules of the buffer gas are equal, $T_e = T_+ = T_{\text{gas}}$. In some afterglow experiments equipped with spectral diagnostics, the kinetic temperature of ions can be determined from the Doppler broadening of the absorption lines.²³ In FALP experiments, the electron energy distribution function and electron temperature can be measured by the Langmuir probe.^{24–26} In some SA and FALP experiments, the electron temperature was determined by monitoring the decrease in electron or ion densities due to the ambipolar diffusion.^{20,27}

In most of the afterglow experiments, recombination rate coefficients were measured at temperature of 300 K, and in some variable temperature FALP (VT-FALP), rate coefficients were measured in the range 80–600 K.^{28,29} Only in few experiments, it was possible to measure recombination rate coefficients at temperatures below 77 K. In recent CRYO-FALP II studies of recombination of H_3^+ ions, the minimal temperature was 60 K,²⁰ and in studies of E-CRR of Ar^+ ions, the minimal temperature was ~ 50 K.²⁷

As mentioned above, cross sections of binary recombination for several ions were measured also in merged beam experiments, including storage rings. For detailed reviews, see Refs. 2 and 5. Beam experiments can provide cross sections with very high energy resolution for binary recombination processes, and in some experiments, they can provide product distribution and kinetic energy of neutral products.² One advantage of beam experiments is that the ions are formed in a separate ion source so that the desired ion species can be preselected before being injected. Ternary recombination cannot be studied in beam experiments primarily because of the absence of third particles. A disadvantage of these experiments is that the excitation of some recombining ions is often unclear. It is sensitive to conditions in the ion source and also to relaxation/excitation in the ring (see, e.g., discussion for H_3^+ experiments in Ref. 30). TSR and CRYRING stopped operation a few years ago, and, as mentioned above, new cryogenic instruments (CSR and DESIREE) have been constructed and tested.³¹ These new instruments can reach temperatures down to liquid He temperatures.^{21,22} Recently, experiments on ion electron recombination were started at the main cooler storage ring (CSRm) at the Heavy Ion Research Facility at Lanzhou (HIRFL) accelerator facilities of the Institute of Modern Physics in Lanzhou, China.³²

The current studies of recombination processes are motivated by several factors:

- (I) The fundamental interest in binary electron ion interaction and recombination in particular.^{33–36}
- (II) The fundamental interest in multi-collisional recombination processes in low-temperature plasmas, including neutral-assisted three-body recombination (N-TBR)^{37,38} and electron-assisted collisional radiative recombination (E-CRR).^{27,39,40} Because of the very pronounced increase in the rate coefficients of the ternary recombination processes with decreasing temperature, it can be expected that at low temperatures, several recombination processes contribute to the removal of ions and electrons from plasmas.
- (III) Plasma modeling and need for particular temperature dependencies of recombination rate coefficients. The data are needed for modeling discharge plasmas, cold astrophysical plasmas, and plasmas for technological applications. Low temperature data are important for modelling of processes in cold interstellar medium and in ultra-cold plasmas. In astrophysics, recombination of H_3^+ , D_3^+ , H_2D^+ , and HD_2^+ ions with electrons and dependence on rotational excitation and on nuclear spin states (para and ortho) are of particular interest.^{41–43}
- (IV) The theoretical description of recombination processes at very low kinetic energies of the recombining particles and a comparison of measured binary and ternary recombination rate coefficients to calculated values.⁴⁴
- (V) The study of recombination in ultra-cold plasmas⁴⁵ and recombination studies in connection with formation of antihydrogen in ALPHA, ATRAP, and ATHENA experiments (see, e.g., Refs. 46–49).

To study recombination processes, at temperatures from 30 K to 100 K, where there are hardly any experimental data, and at electron and neutral number densities at which losses due to ternary recombination processes are comparable to binary recombination processes, we designed, constructed, and put into operation a new experimental apparatus—cryogenic stationary-afterglow with a near-infrared cavity-ring-down-spectrometer (Cryo-SA-CRDS) which can operate down to 30 K.

In the following, we present details on a newly constructed Cryo-SA-CRDS. Most technical problems have been successfully solved, and the apparatus has been tested. The first measurements focused on characterizing the plasma parameters and testing the CRDS detection of H_3^+ ions and gave very encouraging results.

II. APPARATUS SCHEMA, VACUUM, CRYOGENICS, AND PLASMA GENERATION

A. Overview

The apparatus is a cryogenic version of a stationary afterglow. The plasma is generated in a pulsed microwave discharge. The decay of the ion density in the afterglow plasma is measured, in this case, by optical absorption (Cavity Ring-Down Spectroscopy, CRDS). The decay of the ion density can then be analyzed to yield the recombination rate coefficient.

A sapphire discharge tube in which the plasma is formed is aligned along the axis of the cylindrical microwave cavity. The sapphire tube is on both sides axially extended by stainless steel bellows and tubes toward the mirrors of the CRDS. The tube, its extensions, mirrors, and the microwave resonator are placed in an UHV chamber (see Fig. 1). The working gas is only inside the sapphire tube and in tubes connected to it. The cavity of the microwave resonator is evacuated. The body of the resonator is attached to the second

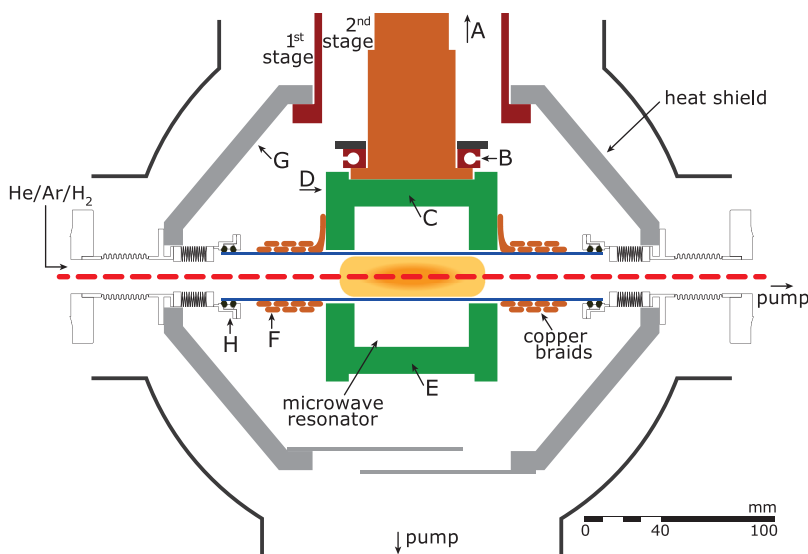


FIG. 1. Vacuum system including the sapphire discharge tube (blue in the figure), microwave resonator (green), and cooling system. Gas of the desired composition (e.g., He/Ar/H₂) enters the tube on one side, and it is continuously pumped out on the other side. The discharge tube is connected to the heat shield (made of EN AW 2030 Dural alloy) via vacuum bellows and is attached to the microwave resonator by silver-coated copper braids. The positions of the different temperature sensors are denoted by capital letters. See text for details. The red dashed line indicates the optical axis between the highly reflective mirrors of the CRDS optical resonator (not in the figure).

stage of a Sumitomo RDK 408S cold head. The sapphire tube is connected by copper braids to the microwave resonator. The bellows holding the sapphire tube are directly connected to the heat shield and through it to the first stage of the cold head.

The temperature of the middle section of the sapphire tube can be as low as 25 K. In the test measurements, the discharge was ignited in a He/Ar/H₂ or He/H₂ gas mixtures, and the H₃⁺ ion density and ion kinetic temperature were measured during the discharge and during the afterglow. The measurements indicated that for He densities higher than 10¹⁷ cm⁻³, the kinetic temperature of ions is equal to the gas temperature and can be varied from 300 K down to 30 K (see discussion below). From the measured decrease in the ion density, during the afterglow, effective recombination rate coefficients can be determined, assuming quasineutrality of the afterglow plasma.

B. Overall scheme and vacuum system

In order to produce cold plasmas, it is necessary to cool down the gas-filled discharge tube and to ignite the discharge. For operation at very low temperatures, it is necessary to put the discharge tube into a vacuum chamber for thermal insulation and also to maintain purity of the gases in the tube.

We calculated the optimal parameters of vacuum and cooling systems for various modifications of the experimental design. On the basis of calculations of the microwave resonator parameters, we decided to use a cylindrical TM₀₁₀ mode resonant cavity and to ignite the discharge in the sapphire tube (ID ≈ 2.5 cm and length of 20 cm) placed along the axis of the cavity. The tube made from monocrystalline sapphire was chosen because of its high thermal conductivity at low temperature.

During the measurements, the pressure in the discharge tube is in the order of hundreds of pascals and the gas flow through the discharge tube is in the order of 0.1 Pa m³ s⁻¹ (the actual flow velocity is ~1 m s⁻¹). A Pfeiffer® WKP 1000 A Roots pump is used to drive the buffer gas through the discharge tube. The buffer gas and the reactant gases are purified

prior to entering the discharge tube by passing them through liquid nitrogen cold traps. To minimize the heat losses, the outer vacuum chamber is pumped by a Pfeiffer TMH 071P turbomolecular pump to below 10⁻⁴ Pa.

C. Cryogenics

The microwave resonator is made of Dural alloy EN AW 6082. The resonator is located inside a vacuum chamber and is directly connected to the second stage of the cold head. Silver-coated copper braids are wrapped around the sapphire discharge tube and attached to the body of the microwave resonator facilitating heat transfer from the discharge tube. Because of possible large temperature gradients along the discharge tube and to account for thermal expansion, the discharge tube is connected to the vacuum system and to the heat shield via stainless steel vacuum bellows. A schematic view of the main vacuum chamber, discharge tube, and the cold head is shown in Fig. 1. A 3D view of the inside of the main vacuum chamber can be seen in Fig. 2. An actual photograph of the interior of a vacuum chamber of Cryo-SACRDS apparatus with the resonator, the heat shield (made of EN AW 2030 Dural alloy), discharge tube, and vacuum bellows is shown in Fig. 3. The temperature of the discharge tube can be regulated by changing the current through heating elements (3039-001 cartridge heaters from Cryo-Con®) installed in the upper part of the microwave resonator and on the second stage of the cold head. This allows us to effectively set the desired temperature and keep it stable within ±0.5 K during the measurements.

The temperatures of the different parts of the apparatus are measured by several types of temperature sensors. The temperature of the first and of the second stage of the cold head (A and B in Fig. 1, respectively) and of the upper part of the microwave resonator (C in Fig. 1) is monitored by LakeShore® DT-471-CU silicon diodes (stated precision in the temperature range below 100 K is 1.5 K). Different platinum resistance temperature detector (RTD) sensors from Cryo-Con are used: CP-100 on the upper part of the microwave resonator (D in Fig. 1) and XP-1K on the lower part of the microwave resonator

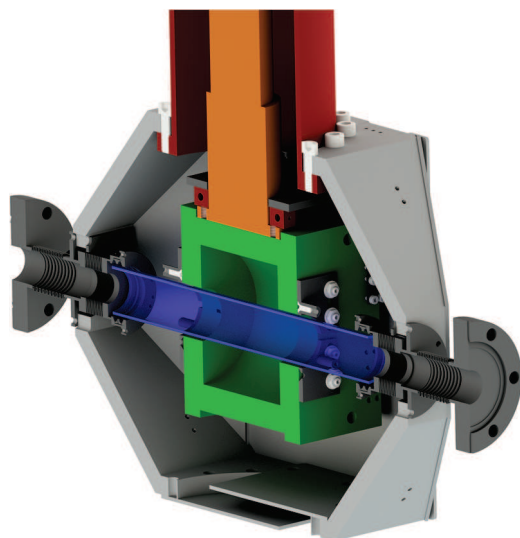


FIG. 2. 3D view. Schematic illustration of the inner section of the Cryo-SA-CRDS showing the sapphire discharge tube and its connection to the rest of the vacuum system, the microwave resonator, and the first and the second stage of the cold head. The components are drawn to scale. The sapphire tube is 20 cm long, and its inner diameter is 2.5 cm. The colour scheme is the same as in Fig. 1.

(E in Fig. 1), on the heat shield (G in Fig. 1), and on the discharge tube holder (H in Fig. 1). XP-100 RTD sensor is inserted between the copper braids that are wrapped around the discharge tube (F in Fig. 1). All platinum RTD sensors conform to IEC751 class B standards with maximal deviation from the calibration curve of 1.5 K for temperatures higher than 30 K.

The temperatures measured by different sensors during the cooling procedure are shown in panel (a) of Fig. 4. It takes more than four hours to cool down the discharge tube from room temperature to ≈ 30 K. Panel (b) of Fig. 4 shows the temperature rise of the apparatus after switching off the cold head. If required, the warming-up period can be shortened by switching on the installed heating elements, as demonstrated in panel (b) of Fig. 4.

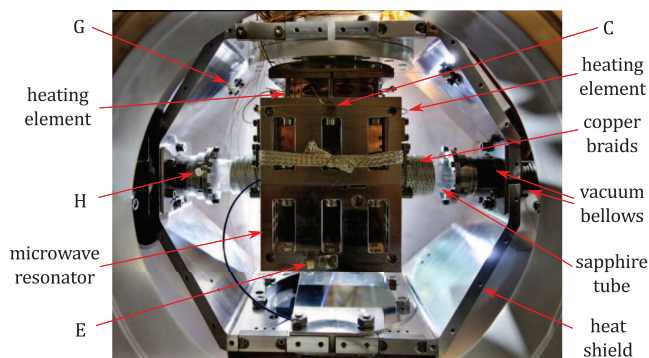


FIG. 3. A photograph of the inner section of the Cryo-SA-CRDS showing the sapphire discharge tube, copper braids, vacuum bellows, closed microwave resonator connected to the second stage of the cold head, part of the heat shield connected to the first stage of the cold head, and part of the main vacuum chamber. The positions of the temperature sensors are denoted by capital letters; for details, see the text. The position of the two heating elements is also indicated.

D. Microwave cavity

The basic design requirements for the cavity were to produce a nearly homogeneous column of plasma in a microwave discharge in the frequency range of 2.4–2.6 GHz. To keep the dimensions of the cavity small, we decided to use the TM_{010} mode of a cylindrical cavity (the convention for ordering of the mode indices is axial, radial, and azimuthal), which produces a homogeneous electric field on the axis. The plasma is contained in a coaxial sapphire tube passing through the cavity. This configuration has a long history of use for microwave plasma diagnostic (see, e.g., Refs. 50–54) and also for plasma generation as pioneered by Beenakker.^{55–58} The resonant frequency of a closed cavity containing a dielectric tube can be calculated analytically.⁵⁹ However, the influence of the holes for inserting the discharge tube and other possible modifications can only be estimated by the perturbation theory. We have used the equivalent circuit (EC) finite difference time domain (FDTD) method^{60,61} as implemented in the openEMS software⁶² to calculate the resonant frequencies of the cavity with an arbitrary geometry. Our numerical model included the cavity with the inserted discharge tube on a three-dimensional cylindrical mesh. The electromagnetic field was excited by applying a magnetic Gaussian pulse with a mean frequency of 2.5 GHz and 20 dB bandwidth of 0.4 GHz to an area near the cavity wall, which approximates the actual loop antenna (see Fig. 5). Perfectly matched layer boundary conditions were used outside of the cavity. After the excitation pulse, the time dependence of the electric field amplitude was recorded at a location close to the centre of the cavity. The resonant frequencies were then obtained by harmonic inversion of the signal^{63,64} implemented in the Harminv software.⁶⁵ We have chosen such a time step and mesh spacing that the numerically determined frequency for a cavity without holes agrees with the analytic model⁵⁹ within 1 MHz. Based on these calculations, we have chosen the inner radius of the cavity as 36.8 mm, which results in a resonant frequency of 2.479 GHz for a sapphire tube with outer radius of 12.6 mm and thickness of 1.3 mm and insertion holes with radius of 14 mm and length of 18 mm. The length of the cavity was chosen as 60 mm. Taking into account the uncertainty of the tube wall thickness of 0.1 mm, the cavity manufacturing tolerances of 0.2 mm, and possible deviation of the crystal c-axis from the tube axis up to 5° , we could predict the cavity resonant frequency to be in the range $f_{\text{calc}}(300 \text{ K}) = (2.475 \pm 0.050) \text{ GHz}$ at room temperature. The thermal contraction of the system [coefficients taken from page 176 of Ref. 66 for sapphire (a-axis) and from Ref. 67 for aluminum alloy (typical value)] and change in sapphire permittivity⁶⁸ cause frequency shifts of 7.4 and 12.2 MHz, respectively. Hence, the expected resonant frequency at temperatures between 20 and 50 K is $f_{\text{calc}}(30 \text{ K}) = (2.495 \pm 0.050) \text{ GHz}$. The actual measured resonant frequency was $f_{\text{meas}}(300 \text{ K}) = (2.434 \pm 0.001) \text{ GHz}$ at $T_H = 300 \text{ K}$ and $f_{\text{meas}}(30 \text{ K}) = (2.458 \pm 0.001) \text{ GHz}$ at $T_H = 30 \text{ K}$ which is in good agreement with the calculated values.

E. Microwave source

In order to ignite the microwave discharge inside a cavity of the microwave resonator made of solid aluminum block and

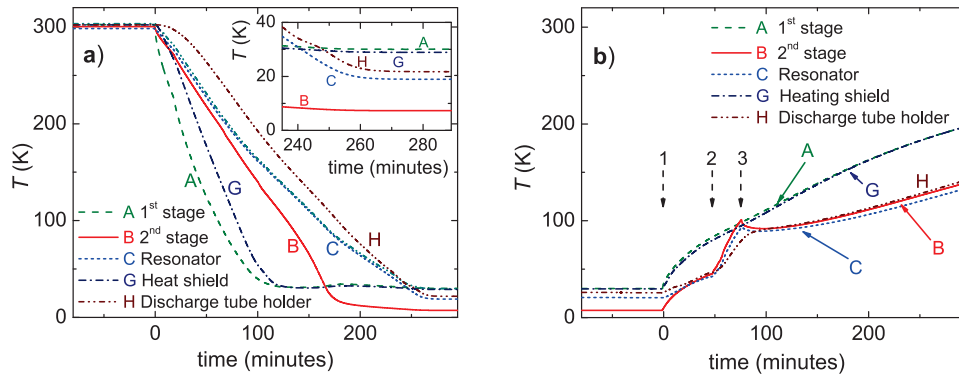


FIG. 4. Panel (a) Time evolution of the temperatures of different parts of the apparatus during the cooling procedure. For information on positions and types of different temperature sensors (denoted by capital letters), see the text. The inset shows detail at the lowest achievable temperatures. Time is set to zero at the beginning of the cooling procedure. Panel (b) Time evolution of the temperatures measured at different places after switching off the cold head and switching on and off the heating. Here, time is set to zero at the time when the cold head is switched off. The vertical dashed arrows denote the time of switching off the cold head (1), time at which the installed heating elements were switched on (2), and then off (3).

lacking any movable parts, we had to tune the frequency of the used microwave radiation to match the resonant frequency of the cavity of the microwave resonator. A microwave generator with amplifier was designed and constructed to obtain very fast shut-off of the discharge. Microwaves are generated by a solid-state SLSM5 synthesizer from Luff Research, Inc. and then amplified by a RCA2400H44CWB power amplifier from RFcore Co., Ltd. In combination with an absorptive PIN diode switch (SR-DA10-1S from Universal Microwave Components Corp.), microwave power ($P_{\mu w}$) of up to 25 W with a switch-off time below 1 μs can be obtained. The measured residual microwave power after switching off the PIN diode was ≈ 200 nW. Using the model of electron cooling described in Ref. 23 and assuming that this residual power

is absorbed by the electron gas (typical number density of $2 \times 10^{10} \text{ cm}^{-3}$ on axis, 2.4×10^{11} electrons in total), which is cooled by elastic collisions with helium ($P = 500 \text{ Pa}$, $T = 50 \text{ K}$), the equilibrium temperature of electrons will be approximately 0.10 K above the helium temperature. If we take into account the coulombic and inelastic (rotational excitation) collisions with H_3^+ , the calculated temperature difference drops to 0.07 K. Orders of magnitude higher power ($> 23 \mu W$) would be needed to heat the electrons by more than 10 K. The generator with short on/off time is necessary for studies of recombination and relaxation processes in a very early afterglow. The microwave frequency can be adjusted from 2.4 GHz to 2.6 GHz to effectively tune the system to the desired resonant frequency.

F. Optical diagnostics

A modification of continuous wave Cavity Ring-Down spectrometer (cw-CRDS) setup, developed originally by Romanini *et al.*,⁶⁹ was employed in the construction of our spectrometer. CRDS is a well-established technique for spectroscopy of weakly absorbing or transient species and a powerful tool for plasma diagnostics.^{70–75} In the CRDS, the laser light passes through the optical isolator to prevent back reflection to the laser and through the acousto-optic modulator (AA.MGAS80/A1 from AA Opto-Electronic) and is then injected into the optical cavity formed by two highly reflective mirrors (Layertec Laser Mirror 106978, reflectivity over 99.99%). The distance between the mirrors is 82 cm, and the characteristic time of the ring-down decay is $\approx 200 \mu s$. In order to periodically match the laser frequency to one of the optical cavity's TEM_{00} modes, one of the mirrors is positioned on a piezo transducer HPCh 150/15-8/3 from Piezomechanik GmbH. The photons exiting the optical cavity through the mirror on the other side are detected by an InGaAs avalanche photodiode,¹³ and the data acquisition is done via NI PCIe-6251 lab card (1.25 MS/s). A single mode distributed feedback (DFB) laser diode with central wavelength of 1381.60 nm and maximal output power of 20 mW (NTT Electronics NLK1E5GAAA) and an external cavity diode laser (ECDL) TEC500 from Sacher Lasertechnik GmbH (10 mW,

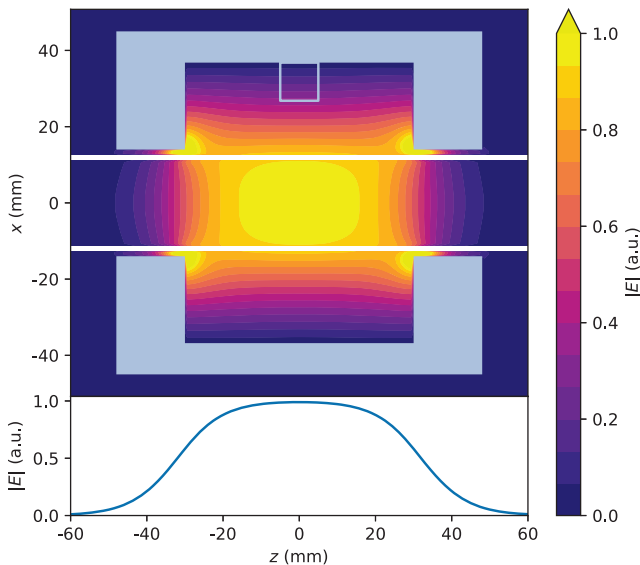


FIG. 5. The calculated amplitude of the electric field intensity in the resonator. The upper panel shows a 2D cut along the resonator axis (z-axis). The lower panel shows the amplitude of the electric field intensity along the resonator axis. The amplitude is normalized to unity in the centre of the cavity. The full width at half maximum of this curve is close to the actual cavity length. The electromagnetic field is formed by the loop in the upper part of the cavity; its location is indicated by the square in the upper part of the figure.

TABLE I. H_3^+ transitions used in the present study (ν_{present}) are compared to values ν_{expl} reported in Ref. 77. Transition wavenumbers calculated by Lindsay and McCall⁷⁸ from available experimental data (ν_{calc1}) and results of quantum mechanical calculations by Neale, Miller, and Tennyson⁷⁹ (ν_{calc2}) are also shown. Each transition is labeled with corresponding vibrational and rotational (J, G) quantum numbers. For further details on the spectroscopic notation, see Ref. 78. Energy of the lower levels E'' was taken from Ref. 78. The numbers in the parentheses are estimated errors of wavelength determination in the units of the last shown digit.

ν_{present} (cm ⁻¹)	ν_{expl} (cm ⁻¹)	ν_{calc1} (cm ⁻¹)	ν_{calc2} (cm ⁻¹)	Spin	E'' (cm ⁻¹)	Transition
6877.5538(12)		6877.546(35)	6877.553	p	169.296	$3v_2^1(1, 2) \leftarrow 0v_2^0(2, 2)$
7234.9729(12)		7234.967(9)	7234.977	o	315.342	$3v_2^1(4, 3) \leftarrow 0v_2^0(3, 3)$
7237.2978(5)	7237.277(17)	7237.302(25)	7237.314	p	64.123	$3v_2^1(2, 1) \leftarrow 0v_2^0(1, 1)$
7241.2623(5)	7241.235(17)	7241.249(9)	7241.283	o	86.959	$3v_2^1(2, 0) \leftarrow 0v_2^0(1, 0)$

1380–1520 nm) are used to probe the number densities of several low lying rotational states of H_3^+ ion in its ground vibrational state using the second overtone transitions listed in Table I. The laser wavelength is measured absolutely using an EXFO WA1650 wavemeter. By comparing the measured overtone transitions originating in the $\text{CO X } ^1\Sigma^+$ ground state and also the positions of several water transitions with those in HITRAN database,⁷⁶ we estimated the overall error of wavenumber determination to be lower than 5×10^{-4} cm⁻¹.

The discharge column length is estimated to be 6 cm. We made a 2D model in cylindrical coordinates of ion number density time and space evolution in discharge and afterglow plasma. Depending on parameters of the model, the systematic error of the number density (and consequently recombination rate coefficient) determination due to changes to discharge column length is at most 20%.

III. TESTS AND RESULTS

A. Kinetic and rotational temperature of the ions

To get further insight into the cooling of the gas mixture in the discharge tube, we determined the kinetic temperature (T_{kin}) of the H_3^+ ions by measuring the Doppler broadening of the absorption lines using second overtone transitions listed in Table I. Using our time-resolved Cavity Ring-Down Spectroscopy setup, we were able to monitor the time evolution of the kinetic temperature of the H_3^+ ions during the active discharge and in afterglow plasma. Examples of absorption line profiles measured at $T_{\text{C}} = 21$ K and $T_{\text{C}} = 96$ K in the discharge and during the early afterglow are shown in panels (a) and (b) of Fig. 6, respectively. As can be seen from the data plotted in Fig. 6, the measured kinetic temperature of H_3^+ ions is close to the temperature of the discharge tube holder (T_{H}). Because the temperature of ions is equilibrated in collisions with He atoms, we can conclude that under the experimental conditions, the temperature of the helium atoms in the tube is nearly equal to T_{H} . Important is also the observation that the temperature of the ions during the discharge is equal to the temperature of the ions during the afterglow within experimental uncertainty.

We have made systematic studies of the dependence of the kinetic temperature T_{kin} of the H_3^+ ions on helium pressure, on the partial pressures of Ar and H_2 , on the power of the microwave generator ($P_{\mu\text{w}}$), and on the length of microwave

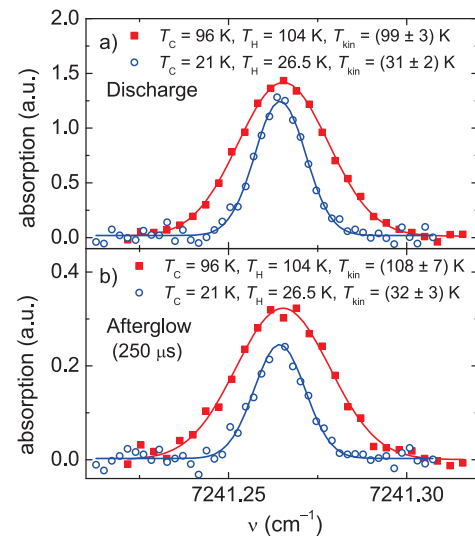


FIG. 6. Examples of H_3^+ absorption line profiles measured at $T_{\text{C}} = 21$ K ($[\text{He}] = 3.4 \times 10^{17}$ cm⁻³, $[\text{H}_2] = 1.0 \times 10^{14}$ cm⁻³) and $T_{\text{C}} = 96$ K ($[\text{He}] = 2.5 \times 10^{17}$ cm⁻³, $[\text{Ar}] = 1.7 \times 10^{14}$ cm⁻³, $[\text{H}_2] = 2.4 \times 10^{13}$ cm⁻³) during the discharge [panel (a)] and 250 μs in afterglow [panel (b)]. The corresponding kinetic temperatures T_{kin} of H_3^+ ions evaluated from the Doppler broadening of the H_3^+ absorption lines (transition $3v_2^1(2, 0) \leftarrow 0v_2^0(1, 0)$) are indicated in the figure. The discharge conditions were $P_{\mu\text{w}} = 9$ W, $D = 12.5\%$ for data obtained at $T_{\text{C}} = 21$ K and $P_{\mu\text{w}} = 14$ W, $D = 6.3\%$ for data obtained at $T_{\text{C}} = 96$ K.

pulse (on duty cycle D). We observed a substantial increase in T_{kin} with increasing $P_{\mu\text{w}}$ and duty cycle, as is shown in Fig. 7 for several combinations of $P_{\mu\text{w}}$ and D . However, for duty cycles lower than 13%, no substantial heating of the ions was observed even with the maximum microwave power allowed by our microwave generator ($P_{\mu\text{w}} = 25$ W). Short discharge pulses (where $T_{\text{kin}} \sim T_{\text{H}}$) were used in experiments where the recombination rate coefficient of H_3^+ ions was measured. For H_3^+ ions with thermal population of states at 30 K, 59.6% of the ions are in the para- H_3^+ (1,1) state, 39.9% in the ortho- H_3^+ (1,0) state, and less than 1% in the para- H_3^+ (2,2) state. These values were calculated from the H_3^+ energy levels and partition function published in Ref. 79. At $T_{\text{H}} = (32 \pm 1)$ K and $T_{\text{kin}} = (33 \pm 2)$ K, the second overtone transition of H_3^+ originating in the (2,2) state and readily observable at $T_{\text{H}} \approx 100$ K (see Table I for details) was not detected giving an upper limit of the number density of para- H_3^+ ions in the (2,2) state. Together with the measured number density of the para- H_3^+ ions in the (1,1) state, this enabled us to establish the upper

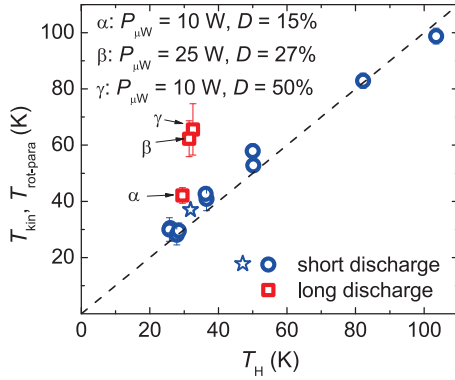


FIG. 7. The dependence of the measured kinetic temperature (T_{Kin}) of H_3^+ ions on the temperature T_{H} (temperature of the discharge tube holder, see Fig. 1). The kinetic temperatures are evaluated from the measured Doppler broadening of the absorption lines of H_3^+ ions (circles and squares). The star denotes the upper limit on the rotational temperature $T_{\text{rot-para}}$ obtained from the measured populations of two para-states [H_3^+ (1,1) and H_3^+ (2,2)]. The profiles of absorption lines were measured during the discharge. The values denoted by open circles and star were obtained in experiments with short discharge pulses (100–300 μs , less than 13% duty cycle) with microwave powers varying from $P_{\mu\text{w}} = 10$ W to 25 W. The values denoted by open squares were obtained with longer pulses and with duty cycles above 13%; the corresponding duty cycle (D) and microwave power ($P_{\mu\text{w}}$) are indicated. The dashed line indicates equality $T_{\text{Kin}} = T_{\text{H}}$.

limit of the rotational temperature of the para- H_3^+ ions ($T_{\text{rot-para}}$, denoted by star in Fig. 7). These results indicate that the rotational temperature of the para- H_3^+ ions is close to T_{H} and to the kinetic temperature of the ions.

B. Relaxation of the afterglow plasma

Here we will discuss the relaxation of the afterglow plasma in He/Ar and He/Ar/ H_2 gas mixtures. As has been discussed previously (see, e.g., Ref. 23), in order to obtain thermal rate coefficients for recombination of ions with electrons in a stationary afterglow experiment, the plasma should be thermalized and the electron and ion temperatures during the afterglow should be equal.

During the microwave discharge, the electrons are heated by the electric field and their temperature (T_e) is significantly higher than the kinetic temperature of the ions (T_{Kin}) and neutrals. After switching off the microwaves, T_e and T_{Kin} equilibrate due to elastic electron-neutral, ion-neutral, and electron-ion collisions. However, in He/Ar gas mixtures, some long-lived (metastable) excited He and Ar neutrals may survive into the afterglow and heat the electrons in superelastic collisions. For molecular ions, one further demands that the distribution of rotational and vibrational states of the recombining ions should be in thermal equilibrium at the kinetic temperature of the ions. In the case of H_3^+ ions, it is also important to know the relative populations of the two spin modifications (para and ortho), even if they are not in thermal equilibrium. The CRDS setup allows us to obtain the kinetic temperature of H_3^+ ions from the Doppler broadening of absorption line (see Sec. III A for details) as well as to infer the rotational temperature from the populations of different rotational states of H_3^+ .^{20,23} The relative abundances of the two nuclear spin states and their evolution during the afterglow plasma can be also monitored by CRDS.^{20,23}

As mentioned above, the crucial parameter for electron ion recombination in plasma is the electron temperature T_e . In low-temperature plasmas, it is in principle possible to measure T_e directly by a Langmuir probe (for details, see Ref. 25). The electron temperature can be indirectly determined by utilizing the steep temperature dependence of the electron-assisted ternary recombination (E-CRR) or from the measured rate of charged particles losses due to ambipolar diffusion.²⁰ Whereas the former method is applicable only for atomic ions (e.g., for Ar^+ ions^{11,80}), the latter ones sensitivity is limited and strongly depends on the quality of the evaluated data. In another approach, we monitored the relaxation of the afterglow plasma by probing the rate of removal of the highly excited particles (excited helium dimers and argon atoms) and its dependence on the Ar, H_2 , or D_2 number densities.^{81,82} This approach was used in the present study.

As a part of the tests of the new Cryo-SA-CRDS apparatus, we studied the time evolution of the number density of the $3s^23p^5(^2P_{3/2}^o)4p^2[3/2]J=2$ excited states of argon (we will use symbol $\text{Ar}^\#$ in the following text) in the discharge and afterglow plasma using the electronic transition $3s^23p^5(^2P_{3/2}^o)4p^2[3/2]J=2 \rightarrow 3s^23p^5(^2P_{3/2}^o)5s^2[3/2]J=2$ at 7230.922 cm^{-1} (see Ref. 83). The radiative lifetime of this state is shorter than 1 μs .⁸⁴ As can be seen from the data plotted in Fig. 8, at the used experimental conditions ($T_{\text{C}} = 58 \text{ K}$, $[\text{He}] = 6 \times 10^{17} \text{ cm}^{-3}$, and $[\text{Ar}] = 0.2 - 1.9 \times 10^{14} \text{ cm}^{-3}$), the excited $\text{Ar}^\#$ atoms survive in the plasma after switching off the discharge substantially longer than what would have been expected from the lifetime of $\text{Ar}^\#$. This indicates that

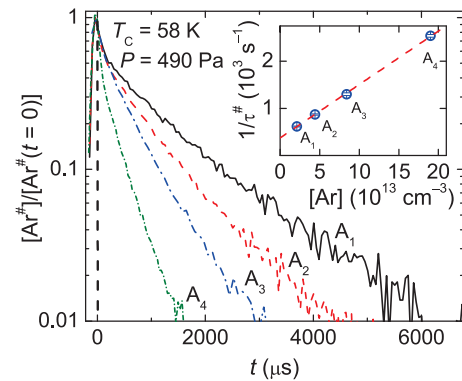


FIG. 8. Time evolution of the relative number densities of the $3s^23p^5(^2P_{3/2}^o)4p^2[3/2]J=2$ excited state of argon ($\text{Ar}^\#$) in afterglow plasma measured for different values of argon number densities denoted by A_1 , A_2 , A_3 , and A_4 ; the corresponding number densities of Ar are $2.1 \times 10^{13} \text{ cm}^{-3}$, $4.4 \times 10^{13} \text{ cm}^{-3}$, $8.4 \times 10^{13} \text{ cm}^{-3}$, and $1.9 \times 10^{14} \text{ cm}^{-3}$, respectively. The used transition was $3s^23p^5(^2P_{3/2}^o)4p^2[3/2]J=2 \rightarrow 3s^23p^5(^2P_{3/2}^o)5s^2[3/2]J=2$. Note that the radiative lifetime of the monitored state is shorter than 1 μs .⁸⁴ For better readability of the plot, the measured relative number density of excited argon atoms was divided (normalized) by the relative number density measured at the time of switching off the discharge. Time is set to zero at the beginning of the afterglow which is denoted by the vertical dashed line. The inset shows the dependence of measured reciprocal time constants $1/\tau^\#$ of the exponential decays on argon number density. The fast decay of the $\text{Ar}^\#$ number density in the early afterglow ($t < 200 \mu\text{s}$) is not considered in the fit. Under assumption of steady-state approximation, the slope of the plot corresponds to the overall rate coefficient of the removal of He^{m} in collisions with Ar from afterglow plasma including the Penning ionization and excitation transfer.

another source of excitation energy is present as the excitation energy of this electronic state is larger than 13 eV. The most likely sources of this energy are helium metastable atoms He^m (2^1S and 2^3S states) produced in the discharge.⁸⁵ The helium metastable atoms can, in superelastic collisions, transfer their energy to the electrons leading to the increase in the electron temperature. When Ar is added to the helium buffer gas, the helium metastable atoms are removed from the afterglow by the Penning ionization of argon and by the excitation transfer. This leads to the decrease in the measured time constant $\tau^\#$ of the exponential decays of $[\text{Ar}^\#]$ with $[\text{Ar}]$ (see Fig. 8 and its inset). Under the assumption of steady-state approximation, the corresponding overall rate coefficient for the removal of He^m from afterglow plasma (by the Penning ionization and excitation transfer) can be inferred from the plotted dependence of $1/\tau^\#$ on $[\text{Ar}]$ in the inset of Fig. 8, $k_{\text{Ar}}(T_C = 58 \text{ K}) = (1.0 \pm 0.2) \times 10^{-11} \text{ cm}^3 \text{ s}^{-1}$. Note that at 300 K, the rate coefficient for the Penning ionization of argon by helium metastable atoms is $k_{\text{PI}}(300 \text{ K}) = 7 \times 10^{-11} \text{ cm}^3 \text{ s}^{-1}$ (see Ref. 86). A similar set of experiments was performed by keeping the argon number density constant $[\text{Ar}] = 2 \times 10^{13} \text{ cm}^{-3}$ and changing $[\text{H}_2]$ in the range of $0.2 - 2 \times 10^{13} \text{ cm}^{-3}$. The evaluated rate coefficient for the removal of He^m in collisions with H_2 was then $k_{\text{H}_2}(T_C = 53 \text{ K}) = (6.1 \pm 1.3) \times 10^{-11} \text{ cm}^3 \text{ s}^{-1}$. The values of k_{H_2} obtained in the previous experiment⁸¹ were $k_{\text{H}_2}(80 \text{ K}) = (0.9 \pm 0.3) \times 10^{-10} \text{ cm}^3 \text{ s}^{-1}$, $k_{\text{H}_2}(140 \text{ K}) = (1.9 \pm 0.2) \times 10^{-10} \text{ cm}^3 \text{ s}^{-1}$, and $k_{\text{H}_2}(300 \text{ K}) = (2.7 \pm 0.2) \times 10^{-10} \text{ cm}^3 \text{ s}^{-1}$, i.e., k_{H_2} decreases with the decreasing temperature. A similar conclusion can be drawn based on data in Refs. 43 and 81 also for k_{Ar} . This emphasizes that for low-temperature recombination studies in helium afterglow plasmas, special attention has to be paid to ensure the effective removal of excited metastable particles.

C. Recombination study

In this section, we will demonstrate the capabilities of the Cryo-SA-CRDS apparatus for recombination studies on a test case of H_3^+ dominated plasma. We are aware that drawing meaningful conclusions about the recombination of H_3^+ at low temperatures will require large data sets. Those will be presented in a later publication.

Examples of observed time evolutions of H_3^+ number densities in afterglow plasmas measured at $T_C = 48 \text{ K}$ and $T_C = 119 \text{ K}$ are shown in Fig. 9. Our previous studies of H_3^+ recombination in the temperature range of 80–300 K have shown that the rotational temperature obtained separately from populations of rotational states within the ortho and para states manifolds is close to the temperature of the buffer gas. In the present study, we have also confirmed this observation for para- H_3^+ ions at 30 K. As shown, e.g., in Ref. 20, the thermal population of states within each nuclear spin states manifold is maintained even when the ratio between the para and ortho nuclear spin states number densities differs from the thermal equilibrium value.

To obtain the overall number density of H_3^+ ions, we first measured the relative population (para fraction, Pf_3) of the para- H_3^+ ions $Pf_3 = [\text{para-}\text{H}_3^+]/([\text{para-}\text{H}_3^+] + [\text{ortho-}\text{H}_3^+])$ at the given temperature. The number densities of all para- and

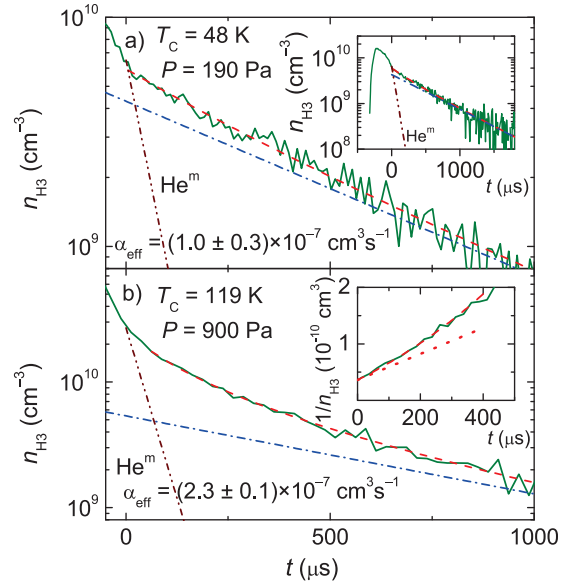


FIG. 9. Time evolutions of the number densities of the H_3^+ ions measured at two different temperatures. Panel (a): $T_C = 48 \text{ K}$, $P = 190 \text{ Pa}$, and $[\text{H}_2] = 3.4 \times 10^{14} \text{ cm}^{-3}$. Panel (b): $T_C = 119 \text{ K}$, $P = 900 \text{ Pa}$, $[\text{H}_2] = 5 \times 10^{13} \text{ cm}^{-3}$, and $[\text{Ar}] = 1.4 \times 10^{14} \text{ cm}^{-3}$. The dashed line is the fit to the data that includes both recombination and exponential losses. The dotted-dashed line denotes the exponential losses only. The double dotted-dashed lines show the calculated time evolutions of the relative density of He^m atoms, based on the overall rate coefficient of the Penning ionization and excitation transfer (see Refs. 43 and 81) and those obtained in this study [$k_{\text{Ar}}(T_C = 58 \text{ K}) = (1.0 \pm 0.2) \times 10^{-11} \text{ cm}^3 \text{ s}^{-1}$ and $k_{\text{H}_2}(T_C = 53 \text{ K}) = (6.1 \pm 1.3) \times 10^{-11} \text{ cm}^3 \text{ s}^{-1}$]. For simplicity, we assume that at $t = 0$, the density $[\text{He}^m]$ is equal to the measured ion density. The inset in panel (a) gives an overall view of the measured time evolution of the H_3^+ number density during the discharge and during the afterglow. The inset in panel (b) shows the time dependence of the reciprocal value ($1/n_{\text{H}_3}$) of the ion number density. Here the dashed line is again a fit that includes both recombination and exponential losses of charged particles, and the dotted line denotes appropriate recombination losses. The effective recombination rate coefficient α_{eff} evaluated from the presented data is written in each panel.

all ortho- H_3^+ ions were calculated from the measured number densities of the lowest para- H_3^+ ($J = 1, G = 1$) and the lowest ortho- H_3^+ ($J = 1, G = 0$) rotational states assuming a thermal population of states within each nuclear spin states manifold. The obtained relative fraction of the para nuclear spin states was then $Pf_3(T_C = 48 \text{ K}) = (0.45 \pm 0.02)$ and $Pf_3(T_C = 119 \text{ K}) = (0.49 \pm 0.02)$. The thermal equilibrium value of Pf_3 is ≈ 0.52 at 50 K and ≈ 0.49 at 120 K. To form an H_3^+ dominated plasma, we used normal hydrogen from a 300 K reservoir where the ratio between the number densities of the para and ortho nuclear spin states of H_2 is 1:3. At 50 K, the thermal equilibrium value for the ratio between the number densities of the para- and ortho- H_2 is approximately 3:1. By feeding ortho-enriched hydrogen at $T_C = 48 \text{ K}$, we probably shift the population of H_3^+ ions toward ortho- H_3^+ . Further measurements with different mixtures of ortho- and para- H_2 at various temperatures are needed to further quantify this effect.

The time evolutions of the H_3^+ ion number density displayed in panels (a) and (b) of Fig. 9 were calculated from the measured time evolution of the ortho ($J = 1, G = 0$) rotational state number density assuming thermal population of ortho and para nuclear spin states separately and using measured Pf_3 .

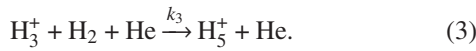
The dashed lines in Fig. 9 denote the fit of the measured overall H_3^+ ion number density n_{H_3} by the equation (assuming quasineutrality of plasma and that H_3^+ ions are dominant ionic species in the afterglow)

$$n_{\text{H}_3} = \frac{1}{\alpha_{\text{eff}}\tau \left(e^{\frac{t-t_0}{\tau}} - 1 \right) + \frac{1}{n_0} e^{\frac{t-t_0}{\tau}}}, \quad (1)$$

where α_{eff} is the effective recombination rate coefficient, n_0 is the H_3^+ ion number density at $t = t_0$ in the afterglow $n_0 = n_{\text{H}_3}(t = t_0)$, and τ is the time constant of the exponential losses of the charged particles

$$\frac{1}{\tau} = \frac{1}{\tau_{\text{D}}} + \frac{1}{\tau_{\text{R}}}, \quad (2)$$

where the time constant τ_{D} represents the losses of charged particles by ambipolar diffusion and τ_{R} is the time constant for losses of H_3^+ ions due to ion-neutral reactions. In the investigated temperature range, the main process in He/Ar/ H_2 gas mixtures is the formation of fast recombining H_3^+ ions in the three-body association of H_3^+ with H_2 and He,



The rate coefficient for this process at 80 K is $k_3 = (2.5 \pm 0.7) \times 10^{-29} \text{ cm}^6 \text{ s}^{-1}$ (see Ref. 87). Note that in the limit of negligible exponential losses ($\tau \rightarrow \infty$), Eq. (1) can be simplified as

$$\frac{1}{n_{\text{H}_3}} = \frac{1}{n_0} + \alpha_{\text{eff}}(t - t_0), \quad (4)$$

i.e., the reciprocal value of the measured ion number density increases linearly in time with the slope giving the value of α_{eff} .

Using the obtained rate coefficients for the Penning ionization and excitation transfer (see above) and those from Refs. 43 and 81, we calculated the expected decrease in the relative number density of He^{m} during the afterglow due to the Penning ionization and excitation transfer at $T_{\text{C}} = 48 \text{ K}$ and at $T_{\text{C}} = 119 \text{ K}$ [see panels (a) and (b) of Fig. 9]. Because we do not know the absolute value of the He^{m} density at the beginning of the afterglow, we set it arbitrarily equal to the ion number density for better comparison with H_3^+ ion density decays in Fig. 9. Previous studies performed in flowing afterglow²⁵ and stationary afterglow⁸⁸ plasmas have shown that the He^{m} number density after switching of the discharge is comparable to that of the electrons. Note that at the conditions of the present experiments, the calculated relative number density of He^{m} decays by more than order of magnitude within first 100 μs after switching off the discharge. The effective removal of the He^{m} particles on a time scale substantially shorter than that of the ion density decay is crucial for future recombination studies at low temperatures.

The effective recombination rate coefficients evaluated from the data in panels (a) and (b) of Fig. 9 were $\alpha_{\text{eff}}(T_{\text{C}} = 48 \text{ K}, \text{P}f_3 = 0.45) = (1.0 \pm 0.3) \times 10^{-7} \text{ cm}^3 \text{ s}^{-1}$ and $\alpha_{\text{eff}}(T_{\text{C}} = 119 \text{ K}, \text{P}f_3 = 0.49) = (2.3 \pm 0.1) \times 10^{-7} \text{ cm}^3 \text{ s}^{-1}$, respectively. The errors are statistical errors of the fits. It has been shown in previous studies^{16,17,19} that in the case of H_3^+

ion electron recombination, the value of the measured effective recombination rate coefficient is enhanced by collisions with buffer gas particles even at pressure of 100 Pa. The dependence of the measured α_{eff} on buffer gas number density (helium in our case) can be written as

$$\alpha_{\text{eff}} = \alpha_{\text{bin}} + K_{\text{He-TBR}}[\text{He}], \quad (5)$$

where α_{bin} is the binary recombination rate coefficient and $K_{\text{He-TBR}}$ is the ternary rate coefficient of He-assisted ternary recombination. The values of α_{bin} for 55 K and 125 K obtained in the recent Cryo-FALP II experiment⁸⁹ were $\alpha_{\text{bin}}(55 \text{ K}) = (8 \pm 3) \times 10^{-8} \text{ cm}^3 \text{ s}^{-1}$ (see Fig. 3 in Ref. 89) and $\alpha_{\text{bin}}(125 \text{ K}) = (8.2 \pm 2.0) \times 10^{-8} \text{ cm}^3 \text{ s}^{-1}$ [calculated from the dependence of α_{bin} on T from: Ref. 89 $\alpha_{\text{bin}} = (6.0 \pm 1.8) \times 10^{-8} (300/T)^{0.36 \pm 0.09} \text{ cm}^3 \text{ s}^{-1}$ that is valid in the temperature range of 80–300 K]. Similarly, the values of $K_{\text{He-TBR}}$ reported in the same experiment^{18,89} were $K_{\text{He-TBR}}(55 \text{ K}) = (8.0 \pm 3.0) \times 10^{-26} \text{ cm}^6 \text{ s}^{-1}$ and $K_{\text{He-TBR}}(125 \text{ K}) = (1.9 \pm 0.6) \times 10^{-25} \text{ cm}^6 \text{ s}^{-1}$. The corresponding effective recombination rate coefficients calculated from Eq. (5) using appropriate helium number density are then $\alpha_{\text{eff}}(55 \text{ K}, 190 \text{ Pa}) = (1.0 \pm 0.3) \times 10^{-7} \text{ cm}^3 \text{ s}^{-1}$ and $\alpha_{\text{eff}}(125 \text{ K}, 900 \text{ Pa}) = (1.8 \pm 0.4) \times 10^{-7} \text{ cm}^3 \text{ s}^{-1}$ which are in good agreement with values obtained in the present experiment. Note that in the Cryo-FALP II experiment,^{18,89} the actual value of $\text{P}f_3$ was not measured. It was later inferred from an extrapolation of the available experimental data that $\text{P}f_3(60 \text{ K}) = 0.45$ and $\text{P}f_3(125 \text{ K}) = 0.5$ (see in Ref. 20) which are in good agreement with the present values.

IV. CONCLUSION AND OUTLOOK

The primary purpose of this paper was to introduce a new experimental apparatus, designed to study electron-ion recombination at temperatures from 300 K down to 30 K, a temperature range of interest for applications in cold astrophysical clouds.

The apparatus was constructed, the discharge tube filled with He/Ar/ H_2 gas mixtures was successfully cooled down to 30 K, and Cryo-SA-CRDS was put into operation. In the test experiments, which included measurements of ion density evolutions and of the kinetic and the rotational temperature, the conditions optimal for recombination studies were determined. The first tests in H_3^+ dominated afterglow plasmas have demonstrated the performance and capabilities of new apparatus and support our expectation that the Cryo-SA-CRDS will be a powerful instrument for recombination studies at temperatures down to 30 K. The first application will be to H_3^+ ions with emphasis on nuclear spin state-specific electron ion recombination and then most likely to their isotopologues D_3^+ , H_2D^+ , and HD_2^+ .

ACKNOWLEDGMENTS

This work was partly supported by the Czech Science Foundation (Nos. GACR 15-15077S, GACR 17-08803S, and GACR 17-18067S) and by the Charles University (Projects Nos. GAUK 1583517 and GAUK 646218).

- ¹R. Johnsen and J. B. A. Mitchell, "Complex formation in electron-ion recombination of molecular ions," in *Advances in Gas Phase Ion Chemistry* (JAI Press, London, England, 1998), Vol. 3, pp. 49–80.
- ²M. Larsson and A. E. Orel, *Dissociative Recombination of Molecular Ions* (Cambridge University Press, Cambridge, 2008).
- ³D. R. Bates, A. E. Kingston, and R. W. P. McWhirter, *Proc. R. Soc. A* **270**, 155 (1962).
- ⁴M. A. Biondi and S. C. Brown, *Phys. Rev.* **76**, 1697 (1949).
- ⁵A. Florescu-Mitchell and J. Mitchell, *Phys. Rep.* **430**, 277 (2006).
- ⁶V. Poterya, J. Glosík, R. Plašil, M. Tichý, P. Kudrna, and A. Pysanenko, *Phys. Rev. Lett.* **88**, 044802 (2002).
- ⁷F. C. Fehsenfeld, E. E. Ferguson, and A. L. Schmeltekopf, *J. Chem. Phys.* **44**, 3022 (1966).
- ⁸D. Smith, N. G. Adams, A. G. Dean, and M. J. Church, *J. Phys. D: Appl. Phys.* **8**, 141 (1975).
- ⁹D. Smith and P. Španěl, *Int. J. Mass Spectrom. Ion Processes* **129**, 163 (1993).
- ¹⁰L. Lehfaoui, C. Rebrion-Rowe, S. Laub, J. B. A. Mitchell, and B. R. Rowe, *J. Chem. Phys.* **106**, 5406 (1997).
- ¹¹T. Kotrík, P. Dohnal, P. Rubovič, R. Plašil, Š. Roučka, S. Opanasiuk, and J. Glosík, *Eur. Phys. J. Appl. Phys.* **56**, 24011 (2011).
- ¹²T. Amano, *Astrophys. J. Lett.* **329**, L121 (1988).
- ¹³P. Macko, G. Bánó, P. Hlavenka, R. Plašil, V. Poterya, A. Pysanenko, O. Votava, R. Johnsen, and J. Glosík, *Int. J. Mass Spectrom.* **233**, 299 (2004).
- ¹⁴P. Hlavenka, R. Plašil, G. Bánó, I. Korolov, D. Gerlich, J. Ramanlal, J. Tennyson, and J. Glosík, *Int. J. Mass Spectrom.* **255-256**, 170 (2006).
- ¹⁵R. E. Rosati, R. Johnsen, and M. F. Golde, *J. Chem. Phys.* **119**, 11630 (2003).
- ¹⁶J. Glosík, I. Korolov, R. Plašil, O. Novotný, T. Kotrík, P. Hlavenka, J. Varju, I. A. Mikhailov, V. Kokoouline, and C. H. Greene, *J. Phys. B: At., Mol. Opt. Phys.* **41**, 191001 (2008).
- ¹⁷J. Glosík, R. Plašil, I. Korolov, T. Kotrík, O. Novotný, P. Hlavenka, P. Dohnal, J. Varju, V. Kokoouline, and C. Greene, *Phys. Rev. A* **79**, 052707 (2009).
- ¹⁸R. Johnsen, P. Rubovič, P. Dohnal, M. Hejduk, R. Plašil, and J. Glosík, *J. Phys. Chem. A* **117**, 9477 (2013).
- ¹⁹J. Glosík, P. Dohnal, P. Rubovič, Á. Kálosi, R. Plašil, Š. Roučka, and R. Johnsen, *Plasma Sources Sci. Technol.* **24**, 065017 (2015).
- ²⁰M. Hejduk, P. Dohnal, P. Rubovič, Á. Kálosi, R. Plašil, R. Johnsen, and J. Glosík, *J. Chem. Phys.* **143**, 044303 (2015).
- ²¹R. von Hahn, A. Becker, F. Berg, K. Blaum, C. Breitenfeldt, H. Fadil, F. Fellenberger, M. Froese, S. George, J. Gck, M. Grieser, F. Grussie, E. A. Guerin, O. Heber, P. Herwig, J. Karthein, C. Krantz, H. Kreckel, M. Lange, F. Laux, S. Lohmann, S. Menk, C. Meyer, P. M. Mishra, O. Novotný, A. P. O'Connor, D. A. Orlov, M. L. Rappaport, R. Repnow, S. Saurabh, S. Schippers, C. D. Schrter, D. Schwalm, L. Schweikhard, T. Sieber, A. Shornikov, K. Spruck, S. S. Kumar, J. Ullrich, X. Urbain, S. Vogel, P. Wilhelm, A. Wolf, and D. Zajfman, *Rev. Sci. Instrum.* **87**, 063115 (2016).
- ²²H. T. Schmidt, R. D. Thomas, M. Gatchell, S. Rosén, P. Reinhard, P. Lofgren, L. Brannholm, M. Blom, M. Bjorkhage, E. Backstrom, J. D. Alexander, S. Leontein, D. Hanstorp, H. Zettergren, L. Liljebj, A. Killberg, A. Simonsson, F. Hellberg, S. Mannervik, M. Larsson, W. D. Geppert, K. G. Rensfelt, H. Danared, A. Paál, M. Masuda, P. Halldén, G. Andler, M. H. Stockett, T. Chen, G. Kallersjö, J. Weimer, K. Hansen, H. Hartman, and H. Cederquist, *Rev. Sci. Instrum.* **84**, 055115 (2013).
- ²³P. Dohnal, M. Hejduk, J. Varju, P. Rubovič, Š. Roučka, T. Kotrík, R. Plašil, J. Glosík, and R. Johnsen, *J. Chem. Phys.* **136**, 244304 (2012).
- ²⁴I. Korolov, T. Kotrík, R. Plašil, J. Varju, M. Hejduk, and J. Glosík, *Contrib. Plasma Phys.* **48**, 521 (2008).
- ²⁵R. Plašil, I. Korolov, T. Kotrík, P. Dohnal, G. Bánó, Z. Donko, and J. Glosík, *Eur. Phys. J. D* **54**, 391 (2009).
- ²⁶I. Korolov, R. Plašil, T. Kotrík, P. Dohnal, O. Novotný, and J. Glosík, *Contrib. Plasma Phys.* **48**, 461 (2008).
- ²⁷P. Dohnal, P. Rubovič, T. Kotrík, M. Hejduk, R. Plašil, R. Johnsen, and J. Glosík, *Phys. Rev. A* **87**, 052716 (2013).
- ²⁸N. G. Adams, "Flowing afterglow studies of electron-ion recombination using Langmuir probes and optical spectroscopy," in *Dissociative Recombination*, NATO ASI Series (Series B: Physics) Vol. 313 (Springer, Boston, MA, 1998), pp. 49–80.
- ²⁹N. G. Adams, "Spectroscopic determination of the products of electron-ion recombination," in *Advances in Gas Phase Ion Chemistry* (JAI Press, London, England, 1993), Vol. 1, pp. 271–310.
- ³⁰A. Petrigani, S. Altevogt, M. H. Berg, D. Bing, M. Grieser, J. Hoffmann, B. Jordon-Thaden, C. Krantz, M. B. Mendes, O. Novotný, S. Novotny, D. A. Orlov, R. Repnow, T. Sorg, J. Stützel, A. Wolf, H. Buhr, H. Kreckel, V. Kokoouline, and C. H. Greene, *Phys. Rev. A* **83**, 032711 (2011).
- ³¹A. P. O'Connor, A. Becker, K. Blaum, C. Breitenfeldt, S. George, J. Gock, M. Grieser, F. Grussie, E. A. Guerin, R. von Hahn, U. Hechtfischer, P. Herwig, J. Karthein, C. Krantz, H. Kreckel, S. Lohmann, C. Meyer, P. M. Mishra, O. Novotný, R. Repnow, S. Saurabh, D. Schwalm, K. Spruck, S. Sunil Kumar, S. Vogel, and A. Wolf, *Phys. Rev. Lett.* **116**, 113002 (2016).
- ³²Z. Huang, W. Wen, X. Xu, H. Wang, L. Dou, X. Chuai, X. Zhu, D. Zhao, J. Li, X. Ma, L. Mao, J. Yang, Y. Yuan, W. Xu, L. Xie, T. Xu, K. Yao, C. Dong, L. Zhu, and X. Ma, in Proceedings of the 18th International Conference on the Physics of Highly Charged Ions (HCI-2016), Kielce, Poland, 11-16 September 2016 [*Nucl. Instrum. Methods Phys. Res., Sect. B*] **408**, 135 (2017)].
- ³³V. Kokoouline, A. Faure, J. Tennyson, and C. H. Greene, *Mon. Not. R. Astr. Soc.* **405**, 1195 (2010).
- ³⁴H.-K. Chung, B. J. Braams, K. Bartschat, A. G. Csaszr, G. W. F. Drake, T. Kirchner, V. Kokoouline, and J. Tennyson, *J. Phys. D: Appl. Phys.* **49**, 363002 (2016).
- ³⁵R. Čurík and C. H. Greene, *Phys. Rev. Lett.* **98**, 173201 (2007).
- ³⁶D. A. Little, K. Chakrabarti, J. Z. Mezei, I. F. Schneider, and J. Tennyson, *Phys. Rev. A* **90**, 052705 (2014).
- ³⁷D. R. Bates and S. P. Khare, *Proc. Phys. Soc.* **85**, 231 (1965).
- ³⁸L. P. Pitaevskii, *Sov. Phys. JETP* **15**, 919 (1962).
- ³⁹J. Stevefelt, J. Boulmer, and J. F. Delpech, *Phys. Rev. A* **12**, 1246 (1975).
- ⁴⁰S. X. Hu, *Phys. Rev. Lett.* **98**, 133201 (2007).
- ⁴¹O. Sipila, P. Caselli, and J. Harju, *Astron. Astrophys.* **554**, A92 (2013).
- ⁴²L. Pagani, C. Vastel, E. Hugo, V. Kokoouline, C. H. Greene, A. Bacmann, E. Bayet, C. Ceccarelli, R. Peng, and S. Schlemmer, *Astron. Astrophys.* **494**, 623 (2009).
- ⁴³R. Plašil, P. Dohnal, Á. Kálosi, Š. Roučka, R. Johnsen, and J. Glosík, *Plasma Sources Sci. Technol.* **26**, 035006 (2017).
- ⁴⁴V. S. Vorob'ev, *Phys. Plasmas* **24**, 073513 (2017).
- ⁴⁵T. C. Killian, *Science* **316**, 705 (2007).
- ⁴⁶M. Ahmadi, B. X. R. Alves, C. J. AU Baker, W. Bertsche, E. Butler, A. Capra, C. Carruth, C. L. Cesar, M. Charlton, S. Cohen, R. Collister, S. Eriksson, A. Evans, N. Evetts, J. Fajans, T. Friesen, M. C. Fujiwara, D. R. Gill, A. Gutierrez, J. S. Hangst, W. N. Hardy, M. E. Hayden, C. A. Isaac, A. Ishida, M. A. Johnson, S. A. Jones, S. Jonsell, L. Kurchaninov, N. Madsen, M. Mathers, D. Maxwell, J. T. K. McKenna, S. Menary, J. M. Michan, T. Momose, J. J. Munich, P. Nolan, K. Olchanski, A. Olin, P. Pusa, C. O. Rasmussen, F. Robicheaux, R. L. Sacramento, M. Sameed, E. Sarid, D. M. Silveira, S. Stracka, G. Stutter, C. So, T. D. Tharp, J. E. Thompson, R. I. Thompson, D. P. van der Werf, and J. S. Wurtele, *Nature* **541**, 506 (2016).
- ⁴⁷G. B. Andresen, M. D. Ashkezari, M. Baquero-Ruiz, W. Bertsche, P. D. Bowe, E. Butler, C. L. Cesar, S. Chapman, M. Charlton, A. Deller, S. Eriksson, J. Fajans, T. Friesen, M. C. Fujiwara, D. R. Gill, A. Gutierrez, J. S. Hangst, W. N. Hardy, M. E. Hayden, A. J. Humphries, R. Hydomako, M. J. Jenkins, S. Jonsell, L. V. Jørgensen, L. Kurchaninov, N. Madsen, S. Menary, P. Nolan, K. Olchanski, A. Olin, A. Povilus, P. Pusa, F. Robicheaux, E. Sarid, S. Seif el Nasr, D. M. Silveira, C. So, J. W. Storey, R. I. Thompson, D. P. van der Werf, J. S. Wurtele, and Y. Yamazaki, *Nature* **468**, 673 (2010).
- ⁴⁸G. Gabrielse, R. Kalra, W. S. Kolthammer, R. McConnell, P. Richerme, D. Grzonka, W. Oelert, T. Seifzick, M. Zielinski, D. W. Fitzakerley, M. C. George, E. A. Hessels, C. H. Storry, M. Weel, A. Müllers, J. Walz, and ATRAP Collaboration, *Phys. Rev. Lett.* **108**, 113002 (2012).
- ⁴⁹M. Amoretti, C. Amsler, G. Bonomi, A. Bouchta, P. Bowe, C. Carraro, C. L. Cesar, M. Charlton, M. J. T. Collier, M. Doser, V. Filippini, K. S. Fine, A. Fontana, M. C. Fujiwara, R. Funakoshi, P. Genova, J. S. Hangst, R. S. Hayano, M. H. Holzschleiter, L. V. Jørgensen, V. Lagomarsino, R. Landua, D. Lindelöf, E. L. Rizzini, M. Macri, N. Madsen, G. Manuzio, M. Marchesotti, P. Montagna, H. Pruiys, C. Regenfus, P. Riedler, J. Rochet, A. Rotondi, G. Rouleau, G. Testera, A. Variola, T. L. Watson, and D. P. van der Werf, *Nature* **419**, 456 (2002).
- ⁵⁰P. Rosen, *J. Appl. Phys.* **20**, 868 (1949).
- ⁵¹B. Agdur and B. Enander, *J. Appl. Phys.* **33**, 575 (1962).
- ⁵²J. L. Shohet and C. Moskowitz, *J. Appl. Phys.* **36**, 1756 (1965).
- ⁵³P. Lukác, *J. Phys. D: Appl. Phys.* **1**, 1495 (1968).
- ⁵⁴J. L. Shohet and A. J. Hatch, *J. Appl. Phys.* **41**, 2610 (1970).
- ⁵⁵C. I. M. Beenakker and P. W. J. M. Boumans, *Spectrochim. Acta, Part B* **33**, 53 (1978).
- ⁵⁶C. I. M. Beenakker, B. Bosman, and P. W. J. M. Bousman, *Spectrochim. Acta, Part B* **33**, 373 (1978).









- ⁵⁷N. Rait, D. W. Golightly, and C. J. Massoni, *Spectrochim. Acta, Part B* **39**, 931 (1984).
- ⁵⁸T. Ikeda and M. Danno, *IEEE J. Quantum Electron.* **31**, 1525 (1995).
- ⁵⁹S. Li, C. Akyl, and R. Bosisio, *IEEE Trans. Microw. Theory Tech.* **29**, 1041 (1981).
- ⁶⁰W. K. Gwarek, *IEEE Trans. Microwave Theory Tech.* **33**, 1067 (1985).
- ⁶¹A. Rennings, J. Mosig, C. Caloz, D. Erni, and P. Waldow, *J. Comput. Theor. Nanosci.* **5**, 690 (2008).
- ⁶²T. Liebig, A. Rennings, S. Held, and D. Erni, *Int. J. Numer. Model. Electron. Network. Dev. Field.* **26**, 680 (2013).
- ⁶³V. A. Mandelshtam and H. S. Taylor, *J. Chem. Phys.* **107**, 6756 (1997).
- ⁶⁴V. A. Mandelshtam, *Prog. Nucl. Magn. Reson. Spectrosc.* **38**, 159 (2001).
- ⁶⁵S. G. Johnson, "Harminv software," <https://github.com/stevenj/harminv>, 2018.
- ⁶⁶Y. S. Touloukian, R. K. Kirby, E. R. Taylor, and T. Y. R. Lee, "Thermophysical properties of matter—The TPRC data series. Volume 13. Thermal expansion—Nonmetallic solids," Technical Report No. ADA129116, Thermophysical and Electronic Properties Information Analysis Center, Lafayette, IN, 1977.
- ⁶⁷F. R. Schwartzberg, S. H. Osgood, R. D. Keys, and T. F. Kiefer, "Cryogenic OGENIC materials data handbook. Report No. 14," Technical Report No. PB-171809, Martin-Marietta Corp. Aerospace Div., Denver, 1964.
- ⁶⁸R. Shelby, J. Fontanella, and C. Andeen, *J. Phys. Chem. Solids* **41**, 69 (1980).
- ⁶⁹D. Romanini, A. Kachanov, N. Sadeghi, and F. Stoeckel, *Chem. Phys. Lett.* **264**, 316 (1997).
- ⁷⁰Y. Duan, C. Wang, S. T. Scherrer, and C. B. Winstead, *Anal. Chem.* **77**, 4883 (2005).
- ⁷¹C. Wang and J. Anal, *J. Anal. At. Spectrom.* **22**, 1347 (2007).
- ⁷²L. Tao, A. P. Yalin, and N. Yamamoto, *Rev. Sci. Instrum.* **79**, 115107 (2008).
- ⁷³S. C. Thakur, D. McCarren, J. Carr, Jr., and E. E. Scime, *Rev. Sci. Instrum.* **83**, 023508 (2012).
- ⁷⁴B. C. Lee, W. Huang, L. Tao, N. Yamamoto, A. D. Gallimore, and A. P. Yalin, *Rev. Sci. Instrum.* **85**, 053111 (2014).
- ⁷⁵D. Zhao, J. Guss, A. J. Walsh, and H. Linnartz, *Chem. Phys. Lett.* **565**, 132 (2013).
- ⁷⁶I. Gordon, L. Rothman, C. Hill, R. Kochanov, Y. Tan, P. Bernath, M. Birk, V. Boudon, A. Campargue, K. Chance, B. Drouin, J.-M. Flaud, R. Gamache, J. Hodges, D. Jacquemart, V. Perevalov, A. Perrin, K. Shine, M.-A. Smith, J. Tennyson, G. Toon, H. Tran, V. Tyuterev, A. Barbe, A. Császár, V. Devi, T. Furtenbacher, J. Harrison, J.-M. Hartmann, A. Jolly, T. Johnson, T. Karman, I. Kleiner, A. Kyuberis, J. Loos, O. Lyulin, S. Massie, S. Mikhailenko, N. Moazzen-Ahmadi, H. Muller, O. Naumenko, A. Nikitin, O. Polyansky, M. Rey, M. Rotger, S. Sharpe, K. Sung, E. Starikova, S. Tashkun, J. V. Auwera, G. Wagner, J. Wilzewski, P. Wcislo, S. Yu, and E. Zak, *J. Quant. Spectrosc. Radiat. Transfer* **203**, 3 (2017), hITRAN2016 Special Issue.
- ⁷⁷J. Mikosch, H. Kreckel, R. Wester, R. Plašil, J. Glosík, D. Gerlich, D. Schwalm, and A. Wolf, *J. Chem. Phys.* **121**, 11030 (2004).
- ⁷⁸C. Lindsay and B. J. McCall, *J. Mol. Spectrosc.* **210**, 60 (2001).
- ⁷⁹L. Neale, S. Miller, and J. Tennyson, *Astrophys. J.* **464**, 516 (1996).
- ⁸⁰T. Kotřík, P. Dohnal, S. Roučka, P. Jusko, R. Plašil, J. Glosík, and R. Johnsen, *Phys. Rev. A* **83**, 032720 (2011).
- ⁸¹Á. Kálosi, P. Dohnal, L. Augustovičová, Š. Roučka, R. Plašil, and J. Glosík, *Eur. Phys. J. Appl. Phys.* **75**, 24707 (2016).
- ⁸²J. Glosík, P. Dohnal, Á. Kálosi, L. D. Augustovičová, D. Shapko, Š. Roučka, and R. Plašil, *Eur. Phys. J. Appl. Phys.* **80**, 30801 (2017).
- ⁸³A. Kramida, Y. Ralchenko, and J. Reader, NIST atomic spectra database (ver. 5.5.2) (Online), Available <https://physics.nist.gov/asd> (13 March 2018), National Institute of Standards and Technology, Gaithersburg, MD, 2018.
- ⁸⁴J. B. Shumaker and C. H. Popenoe, *J. Opt. Soc. Am.* **57**, 8 (1967).
- ⁸⁵J. Glosík, J. Pavlík, M. Šícha, and M. Tichý, *Czech J. Phys.* **37**, 188 (1987).
- ⁸⁶J. Glosík, G. Bánó, R. Plašil, A. Luca, and P. Zakouřil, *Int. J. Mass Spectrom.* **189**, 103 (1999).
- ⁸⁷W. Paul, B. Lucke, S. Schlemmer, and D. Gerlich, *Int. J. Mass Spectrom. Ion Proc.* **149-150**, 373 (1995).
- ⁸⁸C.-G. Schregel, E. A. D. Carbone, D. Luggenholscher, and U. Czarnetzki, *Plasma Sources Sci. Technol.* **25**, 054003 (2016).
- ⁸⁹P. Rubovič, P. Dohnal, M. Hejduk, R. Plašil, and J. Glosík, *J. Phys. Chem. A* **117**, 9626 (2013).

Towards state selective recombination of H_3^+ under astrophysically relevant conditions

Dohnal P., Shapko D., Kálosi Á., Kassayová M., Roučka Š., Rednyk S., Plašil R.,
Hejduk M., Glosík J.

Faraday Discuss. **217**, 220–234, 2019.

Towards state selective recombination of H_3^+ under astrophysically relevant conditions

Petr Dohnal, *^a Dmytro Shapko, ^a Ábel Kálosi, ^a
Miroslava Kassayová,^a Štěpán Roučka, ^a Serhiy Rednyk, ^a
Radek Plašil, ^a Michal Hejduk ^b and Juraj Glosík ^a

Received 29th November 2018, Accepted 17th January 2019

DOI: 10.1039/c8fd00214b

We present studies on the thermalisation of H_3^+ ions in a cold He/Ar/ H_2 plasma at temperatures 30–70 K. We show that we are able to generate a rotationally thermalised H_3^+ ensemble with a population of rotational and nuclear spin states corresponding to a particular ion translational temperature. By varying the para- H_2 fraction used in the experiment we are able to produce para- H_3^+ ions with fractional populations higher than those corresponding to thermodynamic values. At 35 K, only the lowest rotational states of para and ortho H_3^+ are populated. This is the first step towards experimental studies of electron–molecular ion recombination processes with precisely specified quantum states at astrophysically relevant temperatures.

1 Introduction

As a key proton donor in the interstellar medium (ISM),¹ the trihydrogen cation has been attracting the attention of the astrophysical community for around half a century.^{1,2} Despite a long history of its observation in discharge experiments dating back to the beginning of the 20th century,³ we have only recently – in the last decade in fact – begun to understand how these ions dissociate after recombination with an electron, on a fundamental, quantum mechanical level.

As we understand it now, H_3^+ ions recombine in an “indirect process”, in which the ion captures an electron into a high-lying Rydberg state and the whole complex evolves towards dissociation *via* a cascade consisting of Rydberg states belonging to different nuclear configurations.⁴ This non-Born–Oppenheimer coupling between the electronic and H_3^+ vibrational degrees of freedom enhances the dissociative recombination (DR) cross section, and once taken into account

^aFaculty of Mathematics and Physics, Department of Surface and Plasma Science, Charles University, V Holešovičkách 2, 180 00 Praha 8-Libeň, Czech Republic. E-mail: petr.dohnal@mff.cuni.cz

^bDepartment of Chemistry, University of Oxford, Physical and Theoretical Chemistry Laboratory, South Parks Road, Oxford, OX1 3QZ, UK

accurately,⁵ puts the whole model in excellent agreement with results from storage ring experiments^{6,7} for collision energies below 0.2 eV – a range relevant to the chemistry of ISMs.

However, it was clear already at the time of publication of the experimental results that this picture is not complete. The storage ring experiments by Kreckel *et al.*⁶ and Larsson *et al.*⁷ were partially blind to the rotational temperature of the ions as they both operated at room temperature. As Petrigani *et al.*⁸ pointed out later, the distribution of the rotational states of the H_3^+ ions corresponded to 380_{-130}^{+50} K, which was hardly useful for the determination of thermal rate coefficients used in astrochemical models. This also imposed complications on verification of the theory, as it predicts a strong dependence of a DR probability on a rotational state of the ion.^{4,9}

The matter gets complicated further if one realises that a rotational state a H_3^+ ion can occupy is restricted by the arrangement of its nuclear spins. Since a spontaneous conversion of the nuclear spin states is forbidden, the population of the lowest rotational levels of the ground vibrational level is frozen once the ions are isolated. This also means that one has to consider two different species, para- H_3^+ (with one nuclear spin anti-parallel to the others) and ortho- H_3^+ (with all nuclear spins parallel) when discussing the rotational temperature. This becomes an eminent problem in astronomical evaluations of ISM temperatures, in which the temperature inferred from a ratio of para and ortho state populations of H_3^+ mismatches the nuclear spin excitation temperature evaluated from the populations of the lowest para and ortho states of H_2 : typically, one gets a lower temperature for an ensemble of H_3^+ ions.¹⁰

To make the situation even more confusing, the theory,⁹ the storage ring experiments¹¹ and our plasma experiments,^{12,13} all show that para- H_3^+ recombines with a higher rate coefficient than ortho- H_3^+ . So why are para-states populated more in interstellar clouds? Why does para- H_3^+ not disappear leaving ortho- H_3^+ behind? According to Crabtree *et al.*,^{14,15} answers to these questions can be obtained from measurements of how nuclear spins get scrambled in para/ortho- H_3^+ + para/ortho- H_2 collisions. In their analysis of the H_3^+ state population in a hydrogen discharge, they specify which para-ortho transitions are energetically allowed at low temperatures. Unfortunately, the interpretation of their measurements is complicated by presence of H_5^+ clusters and by a high electron temperature. In the work by Hejduk *et al.*,¹⁶ we showed how to circumvent these complications by using a He/Ar/ H_2 precursor gas mixture and the afterglow rather than the discharge plasma. The same measurements for even lower plasma temperatures are repeated here to illustrate the applicability of this method to actively controlling the nuclear spin state population of H_3^+ ions at cryogenic temperatures.

With the advent of cryogenic electrostatic storage rings,¹⁷ it may seem that the best thing to do for the problem of the H_3^+ DR is to wait until new measurements of the cross sections are carried out, this time with a low temperature distribution of rotational states. That may be true if one is interested only in two-body recombination processes, but Nature, fortunately, offers many other phenomena to study. In our previous papers,^{12,13,18} we speculated that plasma temperatures below 100 K should bring an enhancement of neutral or electron assisted three-body recombination processes – much to our surprise, we discovered they do not in the covered temperature range and at the used electron

number densities. For example, the recombination rate coefficient for ortho- H_3^+ is not affected by the electron-assisted three body recombination process at all and decreases to an extent that can not be explained by the rotational state density.¹² It is tempting to speculate that we are starting to observe quantum mechanical restrictions here and that temptation drives our effort to decrease the plasma temperatures further and further. However, such an endeavour would be pointless if we do not tackle some of the problems emerging at very low temperatures: for example, it turns out that Penning ionisation is suppressed¹⁹ or that hydrogen cluster growth is enhanced so that it makes the dissociative recombination of H_3^+ ions with electrons unobservable (as discussed below). We will have to find out how to circumvent these peculiarities in the future. The good news we are presenting here is that we manage to set an arbitrary, even thermal, distribution of rotational and nuclear-spin states of H_3^+ ions in our experiments, which is the first step towards state-resolved plasma experiments.

2 Experiment

The experimental setup consists of a cryogenic stationary afterglow apparatus in conjunction with a continuous wave cavity ring-down absorption spectrometer (Cryo-SA-CRDS). A detailed description of the experimental setup can be found in ref. 19. The spectrometer is used to determine the densities of the ion species. The plasma is produced in a discharge tube made of monocrystalline sapphire (inner diameter of ≈ 2.3 cm) by a microwave discharge (2.4–2.5 GHz, 4–25 W) in a He/Ar/ H_2 or He/ H_2 gas mixture with typical number densities of $5 \times 10^{17}/10^{14}/10^{14} \text{ cm}^{-3}$ or $5 \times 10^{17}/10^{14} \text{ cm}^{-3}$. The discharge tube is cooled by a closed cycle helium refrigerator enabling operation in a temperature range of 30–300 K. Our CRDS employs a modification of the continuous wave CRDS setup developed by Romanini *et al.*²⁰ The laser light is modulated by an acousto-optic modulator before entering the optical cavity of the CRDS. The optical cavity itself is formed by two plano-concave highly reflective mirrors (reflectivity over 99.99%). Photons exiting the cavity through the mirror on the other side are detected by an InGaAs avalanche photodiode.²¹ A DFB laser diode and an external cavity diode laser (Sacher TEC 500) were used as light sources covering H_3^+ second overtone transitions probed in the present study (see Table 1 for details). The wavelength of the probing laser was measured by an EXFO WA-1650 wavemeter.

Table 1 The second overtone transitions of H_3^+ used in the present study (ν_{present}). Each transition is labeled with corresponding vibrational and rotational (J,G) quantum numbers. For further details on the spectroscopic notation see ref. 25. Energies of the lower levels E'' were taken from ref. 25. The numbers in the parentheses are estimated wavelength determination errors in the units of the last shown digit. The spectral line intensities for particular states S were calculated using Einstein A coefficients from ref. 26 using the definition in ref. 27. The estimated error of the Einstein A coefficients and hence of the H_3^+ rotational state number density determination is lower than 5% (ref. 28)

$\nu_{\text{present}} [\text{cm}^{-1}]$	Spin	$E'' [\text{cm}^{-1}]$	Transition	$S [\text{cm}^{-1} (\text{mol cm}^{-2})^{-1}]$
6877.5538(12)	p	169.296	$3\nu_2^1(1,2) \leftarrow 0\nu_2^0(2,2)$	2.8×10^{-19}
7234.9729(12)	o	315.342	$3\nu_2^1(4,3) \leftarrow 0\nu_2^0(3,3)$	3.3×10^{-19}
7237.2978(5)	p	64.123	$3\nu_2^1(2,1) \leftarrow 0\nu_2^0(1,1)$	2.1×10^{-19}
7241.2623(5)	o	86.959	$3\nu_2^1(2,0) \leftarrow 0\nu_2^0(1,0)$	3.8×10^{-19}

The experiments are carried out in the following manner. The microwave discharge is ignited in a flowing precursor gas mixture and maintained for 200 μs . After this period, the microwave power is switched off to let the plasma decay. The concentrations of ions are observed spectroscopically throughout the discharge/decay sequence. The next microwave power pulse arrives after 3 ms. This flow of events is repeated until the desired statistical accuracy of the measured values is reached.

In the following text, we will denote the relative concentrations of para- H_2 hydrogen (p- H_2) and ortho- H_2 hydrogen (o- H_2) by $^{\text{p}}f_2$ and $^{\text{o}}f_2$, respectively. Similarly, ortho- H_3^+ will be abbreviated as $^{\text{o}}\text{H}_3^+$ and para- H_3^+ as $^{\text{p}}\text{H}_3^+$. A notation p- $\text{H}_3^+(\text{J},\text{G})$ or o- $\text{H}_3^+(\text{J},\text{G})$ will stand for a rotational state of para- H_3^+ or ortho- H_3^+ with rotational quantum numbers J and G. For hydrogen gas with a 300 K thermal population of nuclear spin states (“normal hydrogen”, n- H_2), $^{\text{p}}f_2 = 0.25$ and $^{\text{o}}f_2 = 0.75$. The symbol e- H_2 denotes para-enriched H_2 gas with $^{\text{p}}f_2$ between 0.25 and ≈ 0.995 . The highly para-enriched hydrogen gas is produced using a “para-hydrogen generator” that converts o- H_2 to p- H_2 on a paramagnetic surface (thermally dehydrated $\text{Fe}(\text{OH})\text{O}$, CAS number 20344-49-4), cooled down in a cryostat to temperatures 10–18 K.^{22,23} During the experiment, n- H_2 is liquefied in a catalyst container and the saturated vapour of the converted gas e- H_2 flows through an outlet tube connected to the Cryo-SA-CRDS apparatus. This configuration provides e- H_2 with a well-defined and constant value of $^{\text{p}}f_2$ equaling 0.995 ± 0.005 . This value was determined separately from the temperature dependence of the $\text{N}^+ + \text{H}_2$ reaction rate coefficient in an ion trap in a setup described in ref. 24. Note that the value of $^{\text{p}}f_2$ measured in our 22-pole ion trap experiment represents the maximal obtainable para state purity. As we have no means to determine $^{\text{p}}f_2$ *in situ* in the Cryo-SA-CRDS experiment, the actual value of $^{\text{p}}f_2$ could be lower. The flow of highly enriched p- H_2 gas can be set in the range of 2×10^{-4} to 4×10^{-2} $\text{Pa m}^3 \text{ s}^{-1}$ with few percent relative error by varying the temperature of the catalyst container, *i.e.*, by changing its vapour pressure. To achieve a desired value of $^{\text{p}}f_2$, the produced H_2 gas is mixed with an appropriate amount of normal hydrogen. When referring to e- H_2 without the admixture of n- H_2 thorough the text, we will use a “nominal” value of $^{\text{p}}f_2 = 0.995 \pm 0.005$ but as stated above the actual value of $^{\text{p}}f_2$ could be lower with the best estimate being $^{\text{p}}f_2 = 0.98 \pm 0.02$.

Absorption line profiles shown throughout the presented work are compiled from time dependent values of the spectral absorption coefficient averaged over the nominal discharge period at a given laser frequency. The term discharge in this work corresponds to the state when the microwave power is *on*, *i.e.* the first 200 microseconds of the discharge/afterglow cycle and the term “early discharge” corresponds to the first 50 microseconds of the discharge/afterglow cycle. We have to add that due to the very nature of the employed CRDS, values of the spectral absorption coefficient given at a nominal time parameter represent a non-linear average of the actual spectral absorption coefficient over the characteristic time of the ring-down signal. This means that each value assigned to a specific time contains information from the future development of the monitored species. We are currently working on a method that will allow us to combine the standard methods of fitting the inferred data to an afterglow chemical kinetics model with a simulation of our CRDS setup. Similarly, the term afterglow means values determined as the average of the nominal time period from 200 to 400 μs .

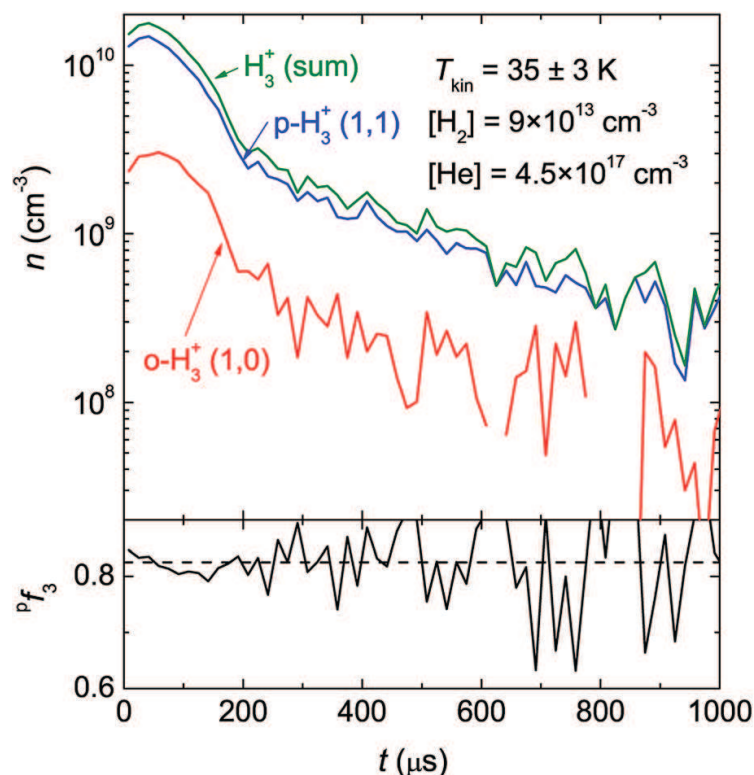


Fig. 1 Upper panel: The time evolution of the number densities of the two lowest rotational states of H_3^+ in the discharge and afterglow plasma measured at $T_{\text{kin}} = 35 \pm 3$ K and nominal $Pf_2 = 0.995 \pm 0.005$. Lower panel: The time evolution of $Pf_3 = [\text{p-H}_3^+]/([\text{p-H}_3^+] + [\text{o-H}_3^+])$. Time is set to zero at the beginning of the discharge. The discharge is switched off after 200 μs .

We also suspect that during the microwave power *on* phase, the discharge does not reach a steady state value of electron number density as can be seen from the drop of the temporal evolution of the inferred ion number densities, shown in Fig. 1 and 2. This premature termination of the discharge is apparently not caused only by the acquisition method (CRDS) itself but by a quality of the microwave resonator. Once the electron number density reaches a value high enough to shift a resonant frequency of the discharge set-up, the microwave power penetrating the resonator decreases and the discharge terminates. This effect needs to be closer examined in future work.

3 Results and discussion

In general, it is not safe to assume that in plasmatic environments the kinetic, rotational, and vibrational temperatures of the ions (T_{kin} , T_{rot} , and T_{vib}), the temperature of the neutral buffer gas T_{He} and the electron temperature T_e have the same value, either in the discharge or in the afterglow, as both discharge and afterglow are dynamic systems, exchanging energy with the surroundings – the microwave discharge pumps energy into the plasma, which has to be dissipated in the afterglow. Therefore, the determination of all the aforementioned temperatures is necessary. The kinetic temperature of the H_3^+ ions was measured from the Doppler broadening of the absorption lines and the rotational temperature was evaluated from the relative populations of different rotational

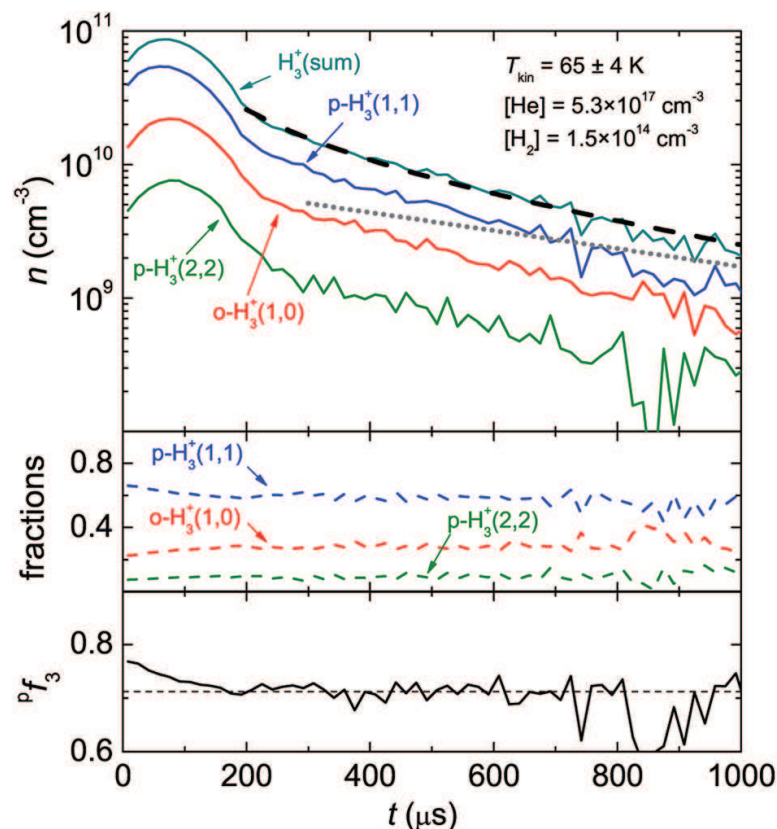


Fig. 2 Upper panel: The time evolution of the number densities of the three lowest rotational states of H_3^+ in the discharge and afterglow plasma obtained at $T_{\text{kin}} = 65 \pm 4$ K and nominal $p_f = 0.995 \pm 0.005$. The dashed line denotes the fit to the data by eqn (8) and the dotted line shows the fitted exponential losses of charged particles. Middle panel: the relative populations of the corresponding rotational states of H_3^+ . Lower panel: The time evolution of $p f_3 = [\text{p-H}_3^+]/([\text{p-H}_3^+] + [\text{o-H}_3^+])$. Time is set to zero at the beginning of the discharge.

states of the ground vibrational state of H_3^+ . In addition, we can define the nuclear spin temperature T_{op} :

$$T_{\text{op}} = \frac{E_{11} - E_{10}}{k_{\text{B}}} \frac{1}{\ln \frac{N_{10} g_{\text{p}} (2J_{11} + 1)}{N_{11} g_{\text{o}} (2J_{10} + 1)}} = \frac{E_{10} - E_{11}}{k_{\text{B}} \ln 2 \frac{N_{11}}{N_{10}}}, \quad (1)$$

where k_{B} is the Boltzmann constant and the rotational energies, rotational quantum numbers and number densities of the (J,G) states are marked as E_{JG} , J_{JG} and N_{JG} . Note that the nuclear spin state degeneracies for para (ortho) states are $g_{\text{p}} = 2$ ($g_{\text{o}} = 4$). In case of a thermal population of states $T_{\text{op}} = T_{\text{rot}}$.

We can also define the rotational temperature for the para ($T_{\text{rot-para}}$) and ortho ($T_{\text{rot-ortho}}$) nuclear spin states separately using the number densities of the two lowest ortho and para states of H_3^+ , respectively:

$$T_{\text{rot-para}} = \frac{E_{11} - E_{22}}{k_{\text{B}}} \frac{1}{\ln \frac{N_{22} g_{\text{p}} (2J_{11} + 1)}{N_{11} g_{\text{p}} (2J_{22} + 1)}} = \frac{E_{22} - E_{11}}{k_{\text{B}} \ln \frac{5N_{11}}{3N_{22}}}, \quad (2)$$

$$T_{\text{rot-ortho}} = \frac{E_{10} - E_{33}}{k_{\text{B}}} \frac{1}{\ln \frac{N_{33} g_{\text{o}} (2J_{10} + 1)}{N_{10} g_{\text{o}} (2J_{33} + 1)}} = \frac{E_{33} - E_{10}}{k_{\text{B}} \ln \frac{7N_{10}}{3N_{33}}}, \quad (3)$$

where the same notation as in eqn (1) is used for the $p\text{-H}_3^+(2,2)$ and $o\text{-H}_3^+(3,3)$ states.

Comparisons of the absorption line profiles for transitions from $p\text{-H}_3^+(1,1)$ and $o\text{-H}_3^+(1,0)$ states obtained in discharge at $T_{\text{kin}} = 35 \pm 3$ K with nominal $Pf_2 = 0.995 \pm 0.005$, and $Pf_2 = 0.25$ are plotted in upper and lower panels of Fig. 3. Absorption lines corresponding to ions in $p\text{-H}_3^+(2,2)$ and $o\text{-H}_3^+(3,3)$ states were undetectable within our experimental accuracy at this temperature because more than 98% of all the H_3^+ ions were in one of the two lowest rotational states. The population of $p\text{-H}_3^+$ in discharge with $n\text{-H}_2$, as evaluated from the absorption spectrum, was $Pf_3 = 0.462 \pm 0.014$ (bottom panel of Fig. 3). The corresponding nuclear spin temperature $T_{\text{op}} = 61 \pm 4$ K. On the other hand, under the same experimental conditions (temperature, buffer gas pressure, hydrogen number density) but using para enriched hydrogen (nominal $Pf_2 = 0.995 \pm 0.005$), the measured $p\text{-H}_3^+$ fraction was $Pf_3 = 0.832 \pm 0.016$ and $T_{\text{op}} = 14 \pm 2$ K. This means that we are able to change the fractional population of the $p\text{-H}_3^+(1,1)$ state from 46% up to 83% (with the majority of the remaining ions being in the $o\text{-H}_3^+(1,0)$ state) by changing the Pf_2 fraction in the injected H_2 gas.

The time evolution of the number densities of the $p\text{-H}_3^+(1,1)$ and $o\text{-H}_3^+(1,0)$ rotational states obtained at $T_{\text{kin}} = 35 \pm 3$ K, $[\text{He}] = 4.5 \times 10^{17} \text{ cm}^{-3}$ and $[\text{H}_2] = 9 \times 10^{13} \text{ cm}^{-3}$ with nominal $Pf_2 = 0.995 \pm 0.005$ is plotted in the upper panel of

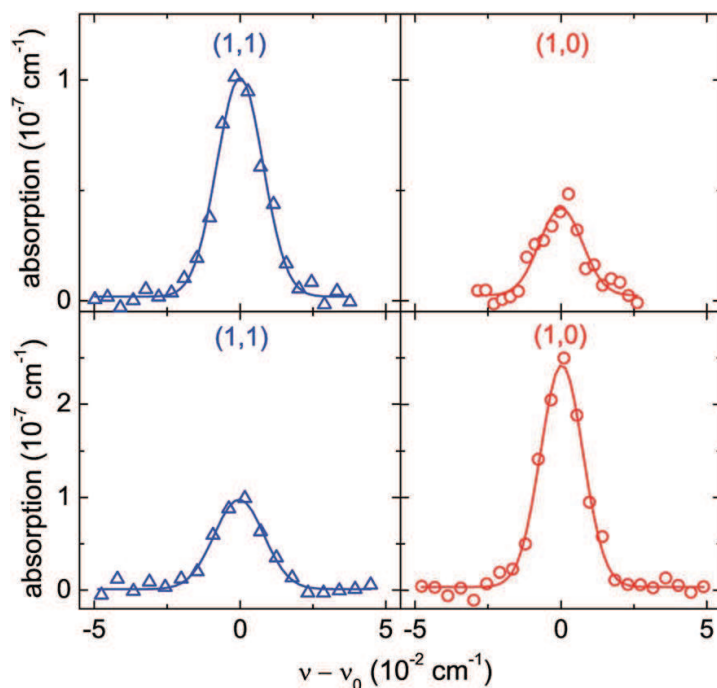


Fig. 3 Upper panel: The absorption line profiles measured in discharge for the lowest rotational states of H_3^+ , $o\text{-H}_3^+(1,0)$ and $p\text{-H}_3^+(1,1)$, at $[\text{He}] = 4.5 \times 10^{17} \text{ cm}^{-3}$, $[\text{H}_2] = 9 \times 10^{13} \text{ cm}^{-3}$ and $T_{\text{kin}} = 35 \pm 3$ K with para enriched H_2 (nominal $Pf_2 = 0.995 \pm 0.005$). ν_0 is the wavenumber of the corresponding transition from Table 1. The $p\text{-H}_3^+(2,2)$ and $o\text{-H}_3^+(3,3)$ states were not observed. Lower panel: The same as in the upper panel but normal H_2 gas ($Pf_2 = 0.25$) was used to produce H_3^+ ions. Note that the spectral line intensity S for the transition involving the $o\text{-H}_3^+(1,0)$ state is almost two times higher than that for the transition involving the $p\text{-H}_3^+(1,1)$ state. The resulting relative population of the $p\text{-H}_3^+(1,0)$ state with respect to all H_3^+ states is 0.462 ± 0.014 when using normal H_2 gas and 0.832 ± 0.016 with para enriched H_2 .

Fig. 1. The corresponding time dependence of the relative population of the p-H₃⁺(1,1) state is shown in the bottom panel of Fig. 1.

The absorption line profiles obtained in discharge with para enriched hydrogen (nominal $Pf_2 = 0.995 \pm 0.005$) at $T_{\text{kin}} = 56 \pm 4$ K and $T_{\text{kin}} = 65 \pm 4$ K are shown in Fig. 4. As in the previous case of $T_{\text{kin}} = 35$ K, the overtone transition from the o-H₃⁺(3,3) state was not observed with normal or with para enriched H₂ but the transition from the p-H₃⁺(2,2) rotational state was readily detected at both $T_{\text{kin}} = 56 \pm 4$ K and $T_{\text{kin}} = 65 \pm 4$ K. The nuclear spin temperature was evaluated to be $T_{\text{op}} = 18 \pm 2$ K for $T_{\text{kin}} = 56 \pm 4$ K and $T_{\text{op}} = 20 \pm 3$ K for $T_{\text{kin}} = 65 \pm 4$ K, so the ratio of the populations of the ortho and para states of H₃⁺ is far from the thermal equilibrium values at the given temperatures (the thermal equilibrium values are $Pf_3(56 \text{ K}) = 0.51$ and $Pf_3(65 \text{ K}) = 0.50$, respectively). On the other hand, the rotational temperatures evaluated from a pair of “para” states (1,1) and (2,2) are $T_{\text{rot-para}} = 52 \pm 2$ K at $T_{\text{kin}} = 56 \pm 4$ K and $T_{\text{rot-para}} = 60 \pm 3$ K at $T_{\text{kin}} = 65 \pm 4$ K. We showed in our previous works^{12,13} that the rotational temperature evaluated from “ortho” states ($T_{\text{rot-ortho}}$) is equal within experimental accuracy to T_{kin} at neutral gas temperatures above 80 K: this implies that, while the measured relative ratio of the number densities of H₃⁺ ions in the ortho and para nuclear spin states (mirrored in Pf_3 and T_{op}) is strongly non thermal, the relative populations of the states within the respective ortho and para state manifolds are in accordance with the thermal equilibrium value at a given temperature (T_{kin}).

The time evolution of the number densities of p-H₃⁺(1,1), o-H₃⁺(1,0) and p-H₃⁺(2,2) measured in the discharge and afterglow plasmas at $T_{\text{kin}} = 65 \pm 4$ K and

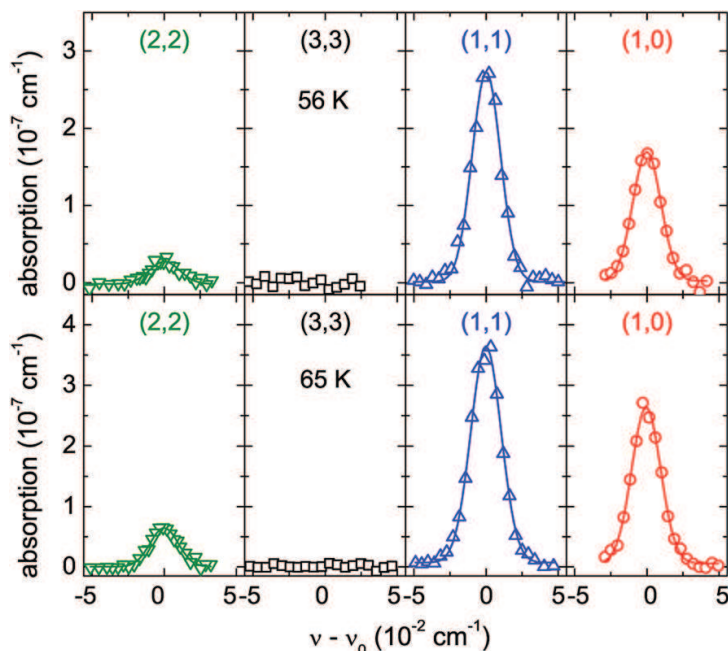


Fig. 4 Upper panel: The absorption line profiles measured in discharge for the three lowest rotational states of H₃⁺, ortho-H₃⁺(1,0), para-H₃⁺(1,1) and para-H₃⁺(2,2), at $T_{\text{kin}} = 56 \pm 4$ K at nominal $Pf_2 = 0.995 \pm 0.005$. ν_0 is the wavenumber of the corresponding transition from Table 1. The ortho-H₃⁺(3,3) state was not observed. $Pf_3 = 0.748 \pm 0.009$, $T_{\text{op}} = 18 \pm 2$ K, $T_{\text{rot-para}} = 52 \pm 2$ K. Lower panel: The absorption line profiles measured in discharge for the three lowest rotational states of H₃⁺: o-H₃⁺(1,0), p-H₃⁺(1,1) and p-H₃⁺(2,2), at $T_{\text{kin}} = 65 \pm 4$ K. The o-H₃⁺(3,3) state was not observed. $Pf_3 = 0.725 \pm 0.007$, $T_{\text{op}} = 20 \pm 3$ K, $T_{\text{rot-para}} = 60 \pm 3$ K.

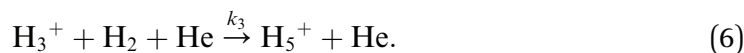
nominal $Pf_2 = 0.995 \pm 0.005$ is plotted in the upper panel of Fig. 2. The relative fractional populations of these states are shown in the middle panel of Fig. 2. The Pf_3 fraction (lower panel of Fig. 2) decreases by a few percent during the first 200 μs of the discharge and then does not substantially change, which is a condition necessary for future state selective recombination studies. $T_{\text{rot-para}}$ increases from 57 ± 2 K in the early discharge to 64 ± 4 K in the early afterglow plasma. The time decay of the overall number density of the H_3^+ ions (n_{H_3}) after switching off the discharge can be described by equation:

$$\frac{dn_{\text{H}_3}}{dt} = -\alpha_{\text{eff}}n_{\text{H}_3}n_e - \frac{n_{\text{H}_3}}{\tau} = -\alpha_{\text{eff}}n_{\text{H}_3}^2 - \frac{n_{\text{H}_3}}{\tau}, \quad (4)$$

assuming that H_3^+ is the dominant ionic species and that the plasma is quasi-neutral. Here α_{eff} is the effective recombination rate coefficient, n_e is the electron number density and τ is the time constant for the exponential losses of the charged particles:

$$\frac{1}{\tau} = \frac{1}{\tau_{\text{D}}} + \frac{1}{\tau_{\text{R}}}, \quad (5)$$

where τ_{D} is the time constant for losses of charged particles caused by ambipolar diffusion. The time constant τ_{R} represents H_3^+ losses by ion-neutral reactions, mainly by the formation of fast recombining H_5^+ ions in the three-body association of H_3^+ with H_2 and He:



As process (6) prevails over the reverse ‘‘collision induced dissociation’’ at low temperatures, the time constant for reaction losses is simply given by:

$$\frac{1}{\tau_{\text{R}}} = k_3[\text{H}_2][\text{He}]. \quad (7)$$

At 80 K the ternary reaction rate coefficient for process (6) is $k_3 = (2.5 \pm 0.7) \times 10^{-29} \text{ cm}^6 \text{ s}^{-1}$ (see ref. 29). Hence, the time constant for reaction losses is approximately 530 μs if $[\text{H}_2] = 1.5 \times 10^{14} \text{ cm}^{-3}$ and $[\text{He}] = 5 \times 10^{17} \text{ cm}^{-3}$ at this temperature.

The dashed line in the upper panel of Fig. 2 denotes the fit of the measured overall H_3^+ number density n_{H_3} by the analytical solution of eqn (4):

$$n_{\text{H}_3} = \frac{1}{\alpha_{\text{eff}}\tau \left(e^{\frac{t-t_0}{\tau}} - 1 \right) + \frac{1}{n_0} e^{\frac{t-t_0}{\tau}}}, \quad (8)$$

where n_0 is the number density of H_3^+ at $t = t_0$. The corresponding effective recombination rate coefficient is $\alpha_{\text{eff}} = (1.7 \pm 0.3) \times 10^{-7} \text{ cm}^3 \text{ s}^{-1}$. The cited errors are statistical errors of the fit.

In order to successfully determine the thermal recombination rate coefficients for ortho and para H_3^+ ions in the afterglow plasma, we have to make sure that several assumptions are valid:

- (1) H_3^+ is the dominant ion in the afterglow;

(2) It is possible to substantially change the ratio of the number densities of the ortho and para nuclear spin states of H_3^+ and this ratio is constant in the afterglow, or its time dependence is known with sufficient accuracy;

(3) The population of states within the nuclear spin state manifold is close to thermal equilibrium, *i.e.* the internal states of the o- H_3^+ and p- H_3^+ are thermalized to the temperature of the buffer gas: $T_{\text{rot-para}} = T_{\text{rot-ortho}} = T_{\text{kin}} = T_{\text{gas}}$;

(4) The electron temperature T_e is close to the temperature of the buffer gas;

(5) The populations of the excited vibrational states of H_3^+ are in accordance with the thermal equilibrium value at the given temperature.

The fulfilment of assumptions (2) and (3) was demonstrated in the previous text. We assume that the vibrational relaxation of H_3^+ ions is fast under the used experimental conditions for higher vibrational states^{30–32} but T_{vib} was not measured in the present experiments. Assumptions (1) and (4) have to be discussed in detail.

Although the falling edge of the microwave power pulse is much shorter than 1 μs , helium atoms excited by the discharge to metastable 2^1S and 2^3S states survive in the afterglow for a long enough time to transfer their internal energy to electrons in superelastic collisions increasing the electron temperature. As the radiative lifetimes of these states are orders of magnitude longer than the typical timescale of the experiment, it is necessary to ensure their fast removal from the afterglow. The helium metastable atoms can be destroyed *e.g.* in the Penning ionization³³ of argon and H_2 . In previous studies,^{19,34,35} we monitored the relaxation of the afterglow plasma by probing the rate of removal of the highly excited particles (excited argon atoms and helium dimers) from the afterglow and its dependence on $[\text{Ar}]$ or $[\text{H}_2]$. These measurements demonstrated that we can ensure the fast removal of excited particles from the plasma by a meticulous choice of reactant number densities at temperatures higher than approximately 45 K.

Unfortunately, the introduction of argon is not an efficient mechanism for the removal of the metastable atoms at temperatures below 45 K. At such low temperatures, the argon gas freezes on the walls of the discharge tube. Moreover, the rate coefficients for Penning ionization and the excitation transfer by the interaction of metastable helium atoms with H_2 or Ar decrease with decreasing temperature further complicating the experiments at low temperatures.

To describe the time evolution of the number densities of different species in the afterglow plasma, we use a numerical model of the chemical kinetics described *e.g.* in ref. 36. A comparison of a model prediction and measured data is shown in Fig. 5 for $T_{\text{kin}} = 65$ K. We modified the model from ref. 36 by adding state-to-state reaction rate coefficients for the o/p- $\text{H}_3^+ + \text{o/p-H}_2$ system from ref. 37. As can be seen in Fig. 5, the model of the chemical kinetics is in good agreement with the experimentally obtained time evolution of the p- H_3^+ and o- H_3^+ number densities. The model of the chemical kinetics also helps us to estimate the amount of H_5^+ ions produced in reaction (6) and their impact on the measured effective recombination rate coefficients. We can also employ the model of the chemical kinetics to predict the possible time evolution of $\text{P}f_3$ induced by different values of recombination rate coefficients for the recombination of p- H_3^+ and o- H_3^+ with electrons. Following the derivation in ref. 36 we can crudely estimate the number density of H_5^+ ions in the afterglow plasma using the steady state approximation:

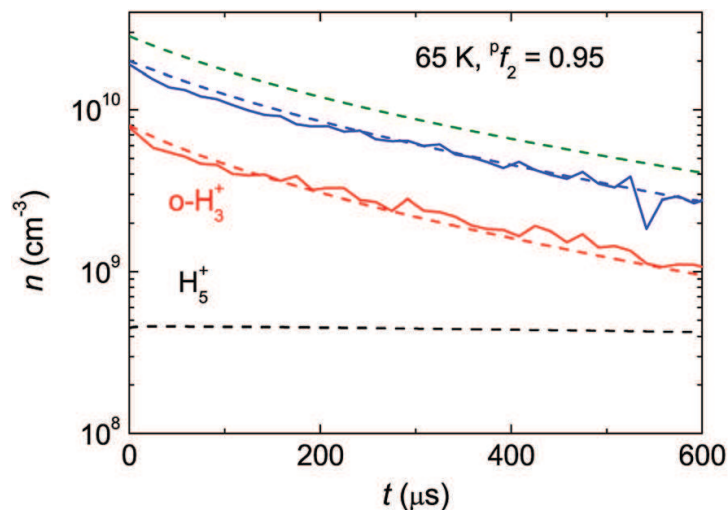


Fig. 5 The results of the model of the chemical kinetics (dashed lines) together with the actual measured time evolution of the p- H_3^+ and o- H_3^+ number densities obtained at $T_{\text{kin}} = 65 \pm 4$ K and nominal $Pf_2 = 0.995 \pm 0.005$. Parameters used in the model: $[\text{He}] = 5 \times 10^{17} \text{ cm}^{-3}$, $[\text{H}_2] = 1.5 \times 10^{14} \text{ cm}^{-3}$, $Pf_2 = 0.95$, $k_3 = 2.5 \times 10^{-29} \text{ cm}^6 \text{ s}^{-1}$ and the recombination rate coefficients for recombination of p- H_3^+ and o- H_3^+ with electrons were set as $\alpha_p = 1.7 \times 10^{-7} \text{ cm}^3 \text{ s}^{-1}$ and $\alpha_o = 0.2 \times 10^{-7} \text{ cm}^3 \text{ s}^{-1}$. Time is set to zero at the beginning of the afterglow.

$$[\text{H}_5^+] = \frac{k_3[\text{H}_2][\text{He}][\text{H}_3^+]}{k_{-3}[\text{He}] + \alpha_5 n_e}, \quad (9)$$

where k_{-3} is the rate coefficient for the reverse of reaction (6) and α_5 is the recombination rate coefficient of H_5^+ ions with electrons. Assuming $n_e = [\text{H}_3^+] + [\text{H}_5^+]$ and that the loss of H_5^+ ions by collision induced dissociation is negligible in comparison with losses due to their recombination with electrons, we get:

$$[\text{H}_5^+] = \frac{-1 + \sqrt{1 + \frac{4}{a}}}{2} [\text{H}_3^+], \quad (10)$$

where $a = \alpha_5 \tau_R [\text{H}_3^+]$. Using $\tau_R = 530 \mu\text{s}$, $\alpha_5 = 4 \times 10^{-6} \text{ cm}^3 \text{ s}^{-1}$ from ref. 38 and $[\text{H}_3^+] = 3 \times 10^{10} \text{ cm}^{-3}$, the estimated number density of H_5^+ ions is $[\text{H}_5^+] = 4.7 \times 10^8 \text{ cm}^{-3}$ (see the results of the chemical kinetics model in Fig. 5 for comparison).

The ability of the present experimental setup to control the ratio of the populations of the ortho and para nuclear spin states of H_3^+ is demonstrated in Fig. 6. The values of Pf_3 measured in discharge at $T_{\text{kin}} = 35 \pm 3$ K, $T_{\text{kin}} = 56 \pm 4$ K and $T_{\text{kin}} = 65 \pm 4$ K are plotted for different values of the relative fraction of p- H_2 . At $T_{\text{kin}} = 35$ K, the value of Pf_3 is given by the populations of the p- $\text{H}_3^+(1,1)$ and o- $\text{H}_3^+(1,0)$ states only. The obtained values of Pf_3 are compared to the Pf_2 and Pf_3 values expected for a thermal population of the states, and to the dependence of Pf_3 on Pf_2 calculated from the model of the chemical kinetics. As can be seen from the upper panel of Fig. 6, the values of Pf_3 measured in the early discharge at particular values of Pf_2 are not in agreement with the dependence of Pf_3 on Pf_2 calculated from the model of the chemical kinetics (lines in lower panel of Fig. 6). Note that in the discharge, H_3^+ ions are continuously produced in the reaction of H_3^+ with H_2 resulting in the ‘nascent’ Pf_3 fraction given by $Pf_{3,\text{nascent}}$ (dotted line

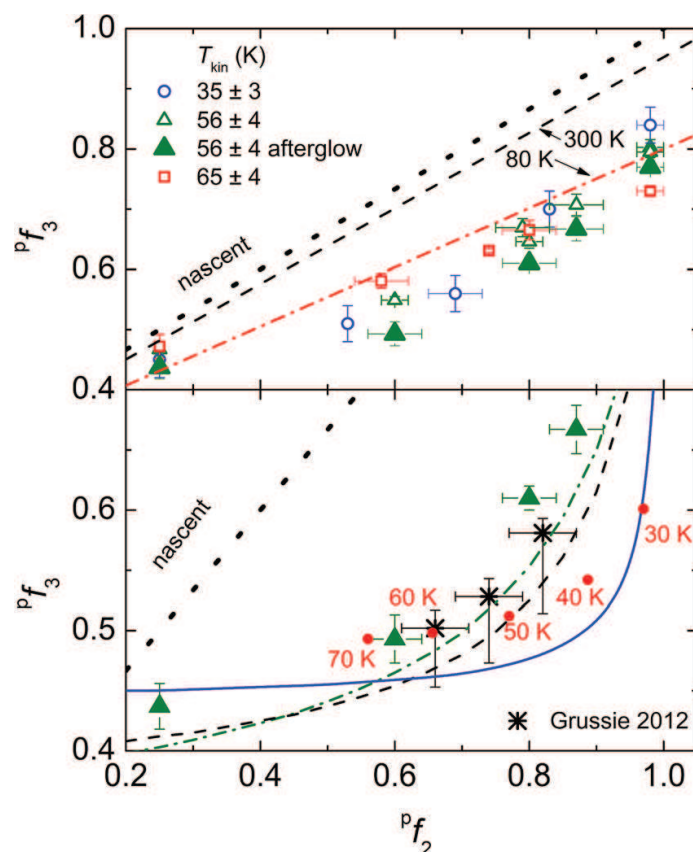


Fig. 6 Upper panel: The dependence of the measured Pf_3 ratios on the used nuclear spin composition of the H_2 gas in early discharge at $T_{kin} = 35 \pm 3$ K, $[He] = 5.0 \times 10^{17} \text{ cm}^{-3}$, $[H_2] = 9 \times 10^{13} \text{ cm}^{-3}$, at $T_{kin} = 56 \pm 4$ K, $[He] = 4.5 \times 10^{17} \text{ cm}^{-3}$, $[H_2] = 1.5 \times 10^{14} \text{ cm}^{-3}$, and at $T_{kin} = 65 \pm 4$ K, $[He] = 4.8 \times 10^{17} \text{ cm}^{-3}$, $[H_2] = 1.5 \times 10^{14} \text{ cm}^{-3}$, and in the afterglow plasma at $T_{kin} = 56 \pm 4$ K. Fits of the data obtained for the discharge plasma in ref. 16 at 80 K and 300 K are plotted as dash-dotted and dashed lines, respectively. The “nascent”⁴⁰ Pf_3 from $o/p-H_2^+ + o/p-H_2$ reactions is plotted as a dotted line. Lower panel: The values of Pf_3 obtained in the afterglow plasma at $T_{kin} = 56 \pm 4$ K are compared to data measured by Grussie *et al.*³⁹ using a 22-pole ion trap at a trap temperature of $T_{trap} = 54 \pm 1$ K, $T_{kin} = 62 \pm 3$ K, $T_{rot-para} = 69 \pm 4$ K and $Pf_2 = 0.66 \pm 0.05$; at $T_{trap} = 48 \pm 1$ K, $T_{kin} = 62 \pm 3$ K, $T_{rot-para} = 62 \pm 3$ K and $Pf_2 = 0.74 \pm 0.05$, and at $T_{trap} = 44 \pm 1$ K, $T_{kin} = 60 \pm 5$ K, $T_{rot-para} = 66 \pm 4$ K and $Pf_2 = 0.82 \pm 0.05$. The full circles denote the corresponding values of Pf_2 and Pf_3 in thermal equilibrium. The different lines denote the dependences of Pf_3 on Pf_2 calculated from the model of the chemical kinetics for 30 K (full line), 50 K (dashed line) and 60 K (dash-dotted line).

in Fig. 6). The values of Pf_3 obtained in the present experiment in an afterglow plasma at $T_{kin} = 56 \pm 4$ K are compared in lower panel of Fig. 6 to those measured by Grussie *et al.*³⁹ at $T_{kin} = 60 \pm 5$ K and at $T_{kin} = 62 \pm 3$ K in a 22-pole ion trap experiment (see the caption of Fig. 6 for further details). Although the values of Pf_3 measured in the afterglow plasma for particular Pf_2 values are lower than those obtained in discharge (compare the full and open triangles in the upper panel of Fig. 6) the agreement with the model of the chemical kinetics is not perfect. This could indicate that a small number of H_3^+ ions are still produced in the afterglow. This would be possible if the metastable helium atoms were not removed from the afterglow fast enough, leading to the creation of H_2^+ ions by the Penning ionization of H_2 . On the other hand, the thermal rate coefficients for the $o/p-H_3^+ + o/p-H_2$ collisional system employed in our chemical kinetics model were

calculated by Hugo *et al.*³⁷ based on a microcanonical approach using the Langevin model and conservation laws in the temperature range of 5–50 K. The actual values used in our calculations are those of Table 8 of ref. 37, fitted in temperature ranges of 5–20 K or up to 50 K, depending on the magnitude of the rate coefficients. For temperatures outside these ranges the extrapolated values based on the given functional forms lose their predictive power as can be seen from the comparison with the thermal values (full circles in the lower panel of Fig. 6). In other words, our model calculations for temperatures higher than 50 K come with a price of systematic uncertainties in the predicted values.

4 Summary

The Cryo-SA-CRDS apparatus was employed to study how the populations of the rotational and nuclear spin states of H_3^+ evolve in the discharge and afterglow plasma in the temperature range of 35–70 K. Both the rotational and the nuclear-spin state distributions were confirmed to not change significantly in the afterglow plasma. The distribution of the nuclear spin states can be varied by adjusting the fraction of para- H_2 in the precursor hydrogen gas, while the rotational state distribution within each nuclear spin manifold is governed within experimental uncertainty by the kinetic temperature of the ions. This behaviour can serve as a method for the preparation of a thermal ensemble of p- H_3^+ and o- H_3^+ ions, which is important for obtaining thermal recombination rate coefficients in the plasma. We have demonstrated that, although the nuclear spin temperature describing the ratio between the ortho and para H_3^+ states can substantially differ from the kinetic temperature of the H_3^+ ions, the rotational states within each ortho and para state manifold are populated in accordance with the thermal equilibrium at a given temperature. We have seen that only a few H_3^+ rotational states are populated in the studied temperature range. At $T_{\text{kin}} = 35$ K, the majority of H_3^+ ions are either in the p- $\text{H}_3^+(1,1)$ state or in the o- $\text{H}_3^+(1,0)$ state. We are thus able to prepare H_3^+ ions with a desired mixture of two quantum states of which up to 83% can be in the p- $\text{H}_3^+(1,1)$ state. This is crucial for future studies of the state selective recombination of H_3^+ ions with electrons performed at conditions relevant for astrochemistry. Nevertheless, prior to that, we still need to control the removal of metastable helium atoms from the afterglow plasma at temperatures below ≈ 50 K. We will address this issue in future work.

Conflicts of interest

There are no conflicts to declare.

Acknowledgements

This work was partly supported by the Czech Science Foundation (No. GACR 17-08803S and GACR 17-18067S) and by the Charles University (Projects No. GAUK 1583517 and GAUK 646218).

Notes and references

- 1 T. Oka, *Proc. Natl. Acad. Sci. U. S. A.*, 2006, **103**, 12235–12242.

- 2 M. Larsson, *Philos. Trans. R. Soc., A*, 2012, **370**, 5118–5129.
- 3 J. J. Thomson, *Proc. R. Soc. A*, 1913, **89**, 1–20.
- 4 V. Kokoouline, N. Douguet and C. H. Greene, *Chem. Phys. Lett.*, 2011, **507**, 1–10.
- 5 C. Jungen and S. T. Pratt, *Phys. Rev. Lett.*, 2009, **102**, 023201.
- 6 H. Kreckel, M. Motsch, J. Mikosch, J. Glosík, R. Plašil, S. Altevogt, V. Andrianarijaona, H. Buhr, J. Hoffmann, L. Lammich, M. Lestinsky, I. Nevo, S. Novotny, D. A. Orlov, H. B. Pedersen, F. Sprenger, A. S. Terekhov, J. Toker, R. Wester, D. Gerlich, D. Schwalm, A. Wolf and D. Zajfman, *Phys. Rev. Lett.*, 2005, **95**, 263201.
- 7 M. Larsson, N. Djuric, G. H. Dunn, A. Neau, A. M. Derkatch, F. Hellberg, S. Kalhori, D. B. Popovic, J. Semaniak, A. Larson and R. Thomas, *Dissociative Recombination of Molecular Ions with Electrons*, Boston, MA, 2003, pp. 87–94.
- 8 A. Petrigiani, S. Altevogt, M. H. Berg, D. Bing, M. Grieser, J. Hoffmann, B. Jordon-Thaden, C. Krantz, M. B. Mendes, O. Novotný, S. Novotny, D. A. Orlov, R. Repnow, T. Sorg, J. Stützel, A. Wolf, H. Buhr, H. Kreckel, V. Kokoouline and C. H. Greene, *Phys. Rev. A*, 2011, **83**, 032711.
- 9 S. Fonseca dos Santos, V. Kokoouline and C. H. Greene, *J. Chem. Phys.*, 2007, **127**, 124309.
- 10 T. Albertsson, N. Indriolo, H. Kreckel, D. Semenov, K. N. Crabtree and T. Henning, *Astrophys. J.*, 2014, **787**, 44.
- 11 B. A. Tom, V. Zhaunerchyk, M. B. Wiczer, A. A. Mills, K. N. Crabtree, M. Kaminska, W. D. Geppert, M. Hamberg, M. af Ugglas, E. Vigren, W. J. van der Zande, M. Larsson, R. D. Thomas and B. J. McCall, *J. Chem. Phys.*, 2009, **130**, 031101.
- 12 M. Hejduk, P. Dohnal, P. Rubovič, Á. Kálosi, R. Plašil, R. Johnsen and J. Glosík, *J. Chem. Phys.*, 2015, **143**, 044303.
- 13 P. Dohnal, M. Hejduk, J. Varju, P. Rubovič, Š. Roučka, T. Kotrík, R. Plašil, J. Glosík and R. Johnsen, *J. Chem. Phys.*, 2012, **136**, 244304.
- 14 K. N. Crabtree, C. A. Kauffman, B. A. Tom, E. Becka, B. A. McGuire and B. J. McCall, *J. Chem. Phys.*, 2011, **134**, 194311.
- 15 K. N. Crabtree, B. A. Tom and B. J. McCall, *J. Chem. Phys.*, 2011, **134**, 194310.
- 16 M. Hejduk, P. Dohnal, J. Varju, P. Rubovič, R. Plašil and J. Glosík, *Plasma Sources Sci. Technol.*, 2012, **21**, 024002.
- 17 R. von Hahn, A. Becker, F. Berg, K. Blaum, C. Breitenfeldt, H. Fadil, F. Fellenberger, M. Froese, S. George, J. Göck, M. Grieser, F. Grussie, E. A. Guerin, O. Heber, P. Herwig, J. Karthein, C. Krantz, H. Kreckel, M. Lange, F. Laux, S. Lohmann, S. Menk, C. Meyer, P. M. Mishra, O. Novotný, A. P. O'Connor, D. A. Orlov, M. L. Rappaport, R. Repnow, S. Saurabh, S. Schippers, C. D. Schröter, D. Schwalm, L. Schweikhard, T. Sieber, A. Shornikov, K. Spruck, S. Sunil Kumar, J. Ullrich, X. Urbain, S. Vogel, P. Wilhelm, A. Wolf and D. Zajfman, *Rev. Sci. Instrum.*, 2016, **87**, 063115.
- 18 R. Johnsen, P. Rubovič, P. Dohnal, M. Hejduk, R. Plašil and J. Glosík, *J. Phys. Chem. A*, 2013, **117**, 9477–9485.
- 19 R. Plašil, P. Dohnal, Á. Kálosi, Š. Roučka, D. Shapko, S. Rednyk, R. Johnsen and J. Glosík, *Rev. Sci. Instrum.*, 2018, **89**, 063116.
- 20 D. Romanini, A. Kachanov, N. Sadeghi and F. Stoeckel, *Chem. Phys. Lett.*, 1997, **264**, 316–322.

- 21 P. Macko, G. Bánó, P. Hlavenka, R. Plašil, V. Poterya, A. Pysanenko, O. Votava, R. Johnsen and J. Glosík, *Int. J. Mass Spectrom.*, 2004, **233**, 299–304.
- 22 E. Ilisca, *Prog. Surf. Sci.*, 1992, **41**, 217–335.
- 23 S. Yucel, *Phys. Rev. B: Condens. Matter Mater. Phys.*, 1989, **39**, 3104–3115.
- 24 I. Zymak, M. Hejduk, D. Mulin, R. Plašil, J. Glosík and D. Gerlich, *Astrophys. J.*, 2013, **768**, 86.
- 25 C. Lindsay and B. J. McCall, *J. Mol. Spectrosc.*, 2001, **210**, 60–83.
- 26 L. Neale, S. Miller and J. Tennyson, *Astrophys. J.*, 1996, **464**, 516.
- 27 L. Rothman, C. Rinsland, A. Goldman, S. Massie, D. Edwards, J.-M. Flaud, A. Perrin, C. Camy-Peyret, V. Dana, J.-Y. Mandin, J. Schroeder, A. Mccann, R. Gamache, R. Wattson, K. Yoshino, K. Chance, K. Jucks, L. Brown, V. Nemtchinov and P. Varanasi, *J. Quant. Spectrosc. Radiat. Transfer*, 1998, **60**, 665–710.
- 28 J. Tennyson, private communication, 2016.
- 29 W. Paul, B. Lucke, S. Schlemmer and D. Gerlich, *Int. J. Mass Spectrom. Ion Processes*, 1995, **149–150**, 373–387.
- 30 J. Kim, L. Theard and W. Huntress, *Int. J. Mass Spectrom. Ion Phys.*, 1974, **15**, 223–244.
- 31 C. R. Blakley, M. L. Vestal and J. H. Futrell, *J. Chem. Phys.*, 1977, **66**, 2392–2399.
- 32 T. Amano, *J. Chem. Phys.*, 1990, **92**, 6492–6501.
- 33 W. Lindinger, A. L. Schmeltekopf and F. C. Fehsenfeld, *J. Chem. Phys.*, 1974, **61**, 2890–2895.
- 34 Á. Kálosi, P. Dohnal, L. Augustovičová, Š. Roučka, R. Plašil and J. Glosík, *Eur. Phys. J.: Appl. Phys.*, 2016, **75**, 24707.
- 35 J. Glosík, P. Dohnal, Á. Kálosi, L. D. Augustovičová, D. Shapko, Š. Roučka and R. Plašil, *Eur. Phys. J.: Appl. Phys.*, 2017, **80**, 30801.
- 36 J. Glosík, P. Dohnal, P. Rubovič, Á. Kálosi, R. Plašil, Š. Roučka and R. Johnsen, *Plasma Sources Sci. Technol.*, 2015, **24**, 065017.
- 37 E. Hugo, O. Asvany and S. Schlemmer, *J. Chem. Phys.*, 2009, **130**, 164302.
- 38 J. A. Macdonald, M. A. Biondi and R. Johnsen, *Planet. Space Sci.*, 1984, **32**, 651–654.
- 39 F. Grussie, M. H. Berg, K. N. Crabtree, S. Gärtner, B. J. McCall, S. Schlemmer, A. Wolf and H. Kreckel, *Astrophys. J.*, 2012, **759**, 21.
- 40 K. N. Crabtree, N. Indriolo, H. Kreckel, B. A. Tom and B. J. McCall, *Astrophys. J.*, 2011, **729**, 15.

**Dissociative recombination of N_2H^+ ions with electrons in the
temperature range of 80–350 K**

Shapko D., Dohnal P., Kassayová M., Kálosi Á., Rednyk S., Roučka Š., Plašil R.,
Augustovičová L. D., Johnsen R., Špirko V., Glosík J.

J. Chem. Phys. **152(2)**, 024301, 2020.

Dissociative recombination of N_2H^+ ions with electrons in the temperature range of 80–350 K

Cite as: J. Chem. Phys. 152, 024301 (2020); doi: 10.1063/1.5128330

Submitted: 18 September 2019 • Accepted: 19 December 2019 •

Published Online: 8 January 2020



View Online



Export Citation



CrossMark

Dmytro Shapko,¹ Petr Dohnal,^{1,a)} Miroslava Kassayová,¹ Ábel Kálosi,¹ Serhiy Rednyk,¹ Štěpán Roučka,¹ Radek Plašil,¹ Lucie D. Augustovičová,² Rainer Johnsen,³ Vladimír Špirko,^{2,4} and Juraj Glosík¹

AFFILIATIONS

¹Faculty of Mathematics and Physics, Department of Surface and Plasma Science, Charles University, Prague, Czech Republic

²Faculty of Mathematics and Physics, Department of Chemical Physics and Optics, Charles University, Prague, Czech Republic

³Department of Physics and Astronomy, University of Pittsburgh, Pittsburgh, Pennsylvania 15260, USA

⁴Czech Academy of Sciences, Institute of Organic Chemistry and Biochemistry, Prague, Czech Republic

a)petr.dohnal@mff.cuni.cz

ABSTRACT

Recombination of N_2H^+ ions with electrons was studied using a stationary afterglow with a cavity ring-down spectrometer. We probed *in situ* the time evolutions of number densities of different rotational and vibrational states of recombining N_2H^+ ions and determined the thermal recombination rate coefficients for N_2H^+ in the temperature range of 80–350 K. The newly calculated vibrational transition moments of N_2H^+ are used to explain the different values of recombination rate coefficients obtained in some of the previous studies. No statistically significant dependence of the measured recombination rate coefficient on the buffer gas number density was observed.

Published under license by AIP Publishing. <https://doi.org/10.1063/1.5128330>

I. INTRODUCTION

N_2H^+ , an important interstellar ion, has been observed in different interstellar environments such as dark and translucent clouds,^{1,2} protostellar cores,³ and protoplanetary disks⁴ and is considered to play a role in the atmospheric chemistry of Titan.⁵ N_2H^+ serves as an important tracer for N_2 in dark clouds; therefore, detailed information on production and destruction processes of N_2H^+ could help with the prediction of N_2 abundance in this environment. N_2H^+ in the interstellar medium is mainly produced in proton transfer from H_3^+ to N_2 , and its main destruction mechanisms are proton transfer to CO and dissociative recombination with electrons.⁶

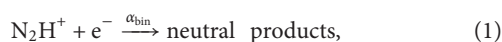
Due to the fundamental character of the process of recombination of N_2H^+ ions with electrons and because of its profound importance for the interstellar chemistry, the recombination of N_2H^+ ions has been studied for over 40 years,⁷ but the results of various

theoretical and experimental studies differed by almost an order of magnitude. Different experimental techniques were employed to obtain the value of the recombination rate coefficient for N_2H^+ recombination with electrons starting with the merged beam study of Mul and McGowan⁸ who reported a recombination rate coefficient $\alpha = 7.5 \times 10^{-7} \text{ cm}^3 \text{ s}^{-1}$ at 300 K (according to Refs. 7 and 9, this value has to be divided by a factor of two to correct for a calibration error). A substantially lower value at room temperature was obtained in the Flowing Afterglow Langmuir Probe (FALP) experiment of Smith and Adams ($1.7 \times 10^{-7} \text{ cm}^3 \text{ s}^{-1}$, see Refs. 10 and 11) and also in an early storage ring experiment CRYRING ($1.0 \times 10^{-7} \text{ cm}^3 \text{ s}^{-1}$, see Ref. 12). Later FALP experiments by Smith and Španel¹³ and by Poterya *et al.*¹⁴ reported slightly higher values of $2.4 \times 10^{-7} \text{ cm}^3 \text{ s}^{-1}$ and $2.8 \times 10^{-7} \text{ cm}^3 \text{ s}^{-1}$ at 300 K, respectively. A value of $2.1 \times 10^{-7} \text{ cm}^3 \text{ s}^{-1}$ was used by Rosati *et al.*¹⁵ to explain the emission spectra from N_2H^+ recombination in the flowing afterglow plasma at room temperature. This is in excellent agreement with

recent results from an ion storage ring experiment by Vigren *et al.*⁶ However, at the lower temperatures of interest to astrochemistry, the FALP and ion storage ring results differ by a factor of two at 100 K. In all these measurements, the internal excitation of the recombining ions was not known and, especially in the case of the ion storage ring experiments, the rotational population of N_2H^+ ions in the ring probably corresponded to a temperature of 300 K or higher.¹⁶ The only experimental study that probed the internal excitations of the recombining N_2H^+ ions was performed by Amano¹⁷ who reported a recombination rate coefficient $\alpha = 7 \times 10^{-7} \text{ cm}^3 \text{ s}^{-1}$ at 273 K, substantially higher than the corresponding FALP or ion storage ring results.

There are only a few theoretical studies of the dissociative recombination of N_2H^+ ions with electrons. The direct dissociative recombination process for N_2H^+ recombination with electrons at low collision energies is highly inefficient according to Hickman *et al.*¹⁸ and Talbi.¹⁹ Fonseca dos Santos *et al.*^{20,21} treated the indirect mechanism for dissociative recombination of N_2H^+ ions by considering several types of vibronic couplings through all vibrational modes of the molecular ion, but their results are up to a factor of two lower than the values from recent FALP and ion storage ring experiments and five times lower than the results of the absorption spectroscopy experiment by Amano.¹⁷ One of the aims of our study is to help resolve the discrepancies between theory and various experimental studies.

In low density environments, as in the interstellar medium or in ion storage rings, electron-ion recombination is a purely binary process,



where α_{bin} is the binary dissociative recombination rate coefficient. In the presence of an ambient gas (e.g., the helium buffer gas in the present experiments), the recombination can be enhanced by a three-body recombination process,²²



where K_{He} is the ternary recombination rate coefficient. Process (2) has been extensively studied for atomic ions^{23,24} and to some extent for molecules,^{23,25–28} and the experimental results at temperatures at or above 300 K mostly confirmed theoretical predictions^{22,29} with $K_{\text{He}} \approx 10^{-27} \text{ cm}^6 \text{ s}^{-1}$ at 300 K. On the contrary, recent studies on recombination of H_3^+ ions or their deuterated isotopologues with electrons in the helium buffer gas^{30–34} reported much faster ternary recombination with ternary recombination rate coefficients on the order of $10^{-25} \text{ cm}^6 \text{ s}^{-1}$ at 300 K. Even higher ternary recombination rate coefficients were obtained for H_3^+ ions in the H_2 buffer gas.^{35,36} This was taken as an indication that ternary recombination of H_3^+ (and its isotopologues) proceeds via dissociation of long-lived excited intermediate states.^{30,31} As the recombination of N_2H^+ ions with electrons is also governed by an indirect dissociative recombination process involving excited Rydberg states,²⁰ a three-body recombination might also contribute to the overall deionization of the N_2H^+ dominated plasma in ambient gas.

This paper describes an experimental study on recombination of N_2H^+ ions with electrons in the temperature range of 80–350 K with spectroscopic determination of number densities of different rotational and vibrational quantum states of recombining N_2H^+

ions. In addition, attention was paid to a possible dependence of the measured recombination rate coefficient on buffer gas number density.

II. EXPERIMENT

The recombination rate coefficients^{7,32} are measured in a stationary afterglow (SA) in conjunction with cavity ring-down spectroscopy (CRDS) to monitor the decay of the densities of different rotational and vibrational states of N_2H^+ ions. The plasma is generated in a pulsed microwave discharge in a fused silica tube (inner diameter $\approx 1.3 \text{ cm}$). The microwave generator is equipped with an external fast high-voltage switch to cut off the power to the magnetron within a fall time less than $30 \mu\text{s}$. A low microwave power in the range of 10–25 W, with $\approx 40\%$ duty cycle, is used to avoid excessive heating of the gas during the discharge. The discharge tube temperature (T_{tec}) is measured by a thermocouple outside of the discharge and can be varied between 80 and 350 K. As will be shown below, T_{tec} is within the error of the measurement equal to both kinetic temperature of the ions T_{kin} and rotational temperature T_{rot} . In the following text, we will use T_{tec} as a nominal temperature T describing the experiments. Liquid nitrogen or precooled nitrogen vapors are used as a coolant. The discharge is ignited in a helium buffer gas with admixtures of Ar, H_2 , and N_2 (with a typical composition of $10^{17}/10^{14}/10^{14}/10^{13} \text{ cm}^{-3}$) or in an H_2 buffer gas with an admixture of N_2 (typical density $[\text{H}_2] = (0.3\text{--}1) \times 10^{17} \text{ cm}^{-3}$, $[\text{N}_2] \sim 10^{13} \text{ cm}^{-3}$). Only “normal” hydrogen, where para and ortho nuclear spin manifolds are in equilibrium at 300 K and *para*- H_2 to *ortho*- H_2 ratio is 1/3, was used in these experiments. The time constants of processes of formation and relaxation of the N_2H^+ dominated afterglow plasma are discussed in the Appendix.

The main diagnostic technique is the time-resolved cavity ring down absorption spectroscopy in the continuous wave modification (cw-CRDS), based on the configuration described by Romanini *et al.*³⁷ For details on the present SA-CRDS setup used for studies of electron-ion recombination, see, e.g., Refs. 32 and 38–41. The vibrational states of N_2H^+ will be denoted here by the symbol $v_1 v_2 v_3$, where v_1 , v_2 , and v_3 indicate the numbers of vibrational quanta in their three normal modes, while l is the quantum number associated with the vibrational angular momentum corresponding to the doubly degenerate bending mode. The overtone transitions originating from the ground vibrational level (000) and from the first excited vibrational level (01¹0) of N_2H^+ were used to probe the time evolution of number densities of N_2H^+ ions in different rotational and vibrational states.

The transitions used in the present study are summarized in Table I. Ammonium transitions at $6314.1334 \text{ cm}^{-1}$ and $6314.4382 \text{ cm}^{-1}$ (line positions taken from HITRAN database⁴²) were scanned to estimate the amount of NH_3 produced in the discharge. NH_3 reacts rapidly ($k_{\text{NH}_3} = 2.3 \times 10^{-9} \text{ cm}^3 \text{ s}^{-1}$) with N_2H^+ ions forming NH_4^+ ions.⁴³ At the buffer gas and reactant number densities used, the measured number density of NH_3 during the experiments was less than $5 \times 10^{11} \text{ cm}^{-3}$. The corresponding characteristic time constant for formation of NH_4^+ in reaction of N_2H^+ with NH_3 is then at least $900 \mu\text{s}$. Our computer model of chemical kinetics predicts that, with $[\text{NH}_3] = 5 \times 10^{11} \text{ cm}^{-3}$, the number density of NH_4^+ ions will be below 3% of all ions in the recombination dominated early afterglow plasma.

TABLE I. List of the transitions in the (200)–(000) and (21¹0)–(01¹0) vibrational bands of N₂H⁺ (v_{exp}) that were used in the present study. The line positions were taken from Ref. 44. Note that there is a typing error in the third column of Table II in Ref. 44—there should be $B_{200} = 1.528 \text{ cm}^{-1}$ instead of 1.538 cm^{-1} in all rows in the table. The numbers in the parentheses are errors of the measurement in units of the last quoted digit. Each transition is denoted by the appropriate branch (P or R) and by the rotational quantum number of the lower state. Upper indices *e* and *f* denote parity.

Band	Transition	$v_{\text{exp}} \text{ (cm}^{-1}\text{)}$
(200)–(000)	P(8)	6310.3902(2)
(200)–(000)	P(7)	6313.8544(2)
(200)–(000)	P(6)	6317.2682(2)
(200)–(000)	P(5)	6320.6311(2)
(21 ¹ 0)–(01 ¹ 0)	R(9) ^f	6317.2450(11)
(21 ¹ 0)–(01 ¹ 0)	R(9) ^e	6317.4329(20)
(21 ¹ 0)–(01 ¹ 0)	R(10) ^e	6319.7976(6)

III. RESULTS AND DISCUSSION

The time dependent optical absorption signals are recorded during the discharge and during the afterglow. The measured absorbances are then converted to the number densities of N₂H⁺ ions in particular quantum states. The conversion makes use of recently calculated transition dipole moments (see Sec. IV and Ref. 45 for further details). The overall number density of N₂H⁺ is then calculated from these partial number densities under assumption of thermal population of states.

The time evolutions of the densities of N₂H⁺ ions in different rotational states of the ground vibrational state are plotted in the upper panel of Fig. 1. As can be seen from the middle panel of Fig. 1, the fractional populations of the measured rotational states do not change significantly in the afterglow. This does not necessarily imply that the recombination coefficients for different rotational states are the same since rotational relaxation is much faster than recombination at used experimental conditions.

In principle, rotational or vibrational excitation of the recombining N₂H⁺ ions could significantly affect the recombination rate coefficients, as was pointed out by Fonseca dos Santos *et al.*,²⁰ whose theoretical treatment, however, did not include such effects. The measurements reported here yield thermal recombination rate coefficients, and we carefully checked that the kinetic, rotational, and vibrational temperatures of the ions (T_{kin} , T_{rot} , and T_{vib}) and the temperature of the neutral buffer gas T_{He} have the same value in the afterglow plasma. The kinetic temperature of the N₂H⁺ ions was measured from the Doppler broadening of the absorption lines. At the used experimental number densities of the buffer gas, the pressure induced broadening is not negligible. We fitted the absorption lines by a Voigt profile. The corresponding pressure broadening coefficient B_p was determined from the dependence of the Lorentzian widths of the fitted Voigt profiles on helium number density. Pressure broadening coefficients B_p measured in the temperature range of 78–300 K in the helium buffer gas for the P(6) transition in the (200) ← (000) vibrational band are summarized in Table II. We assume that B_p for other transitions within the P branch are similar.

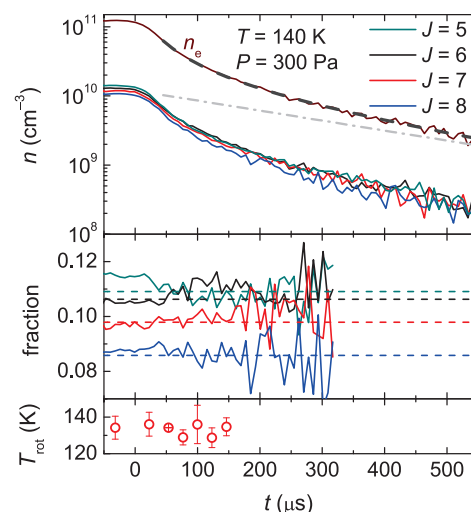


FIG. 1. Upper panel: time evolution of number densities of different rotational states of the ground vibrational state of N₂H⁺ ions during the discharge and the afterglow plasma. The electron number density n_e was calculated from the measured ion number densities under assumption of plasma quasineutrality and thermal population of states. Time is set to zero at the beginning of the afterglow. The dashed line denotes fit to the data by Eq. (5), and the dotted-dashed line represents fitted exponential losses of N₂H⁺ ions. The data were obtained at $T = 140 \text{ K}$, $T_{\text{kin}} = 139 \pm 6 \text{ K}$, $[\text{He}] = 1.5 \times 10^{17} \text{ cm}^{-3}$, $[\text{Ar}] = 2.5 \times 10^{14} \text{ cm}^{-3}$, $[\text{H}_2] = 5 \times 10^{14} \text{ cm}^{-3}$, and $[\text{N}_2] = 4 \times 10^{13} \text{ cm}^{-3}$. Middle panel: time evolution of the fractional populations of the different rotational states of N₂H⁺ ions in the discharge and the afterglow plasma. The dashed lines denote the corresponding values in thermal equilibrium at 140 K. Lower panel: time evolution of the rotational temperature of N₂H⁺ ions obtained from the relative populations of measured rotational states of the vibrational ground state of N₂H⁺.

The rotational temperature was evaluated from the measured relative populations of different rotational states of the ground vibrational state of N₂H⁺. As can be seen from the lower panel of Fig. 1, the rotational temperature measured in the discharge and early afterglow plasma is the same within experimental accuracy and is close to the discharge tube wall temperature T and to the kinetic temperature of the ions T_{kin} . The dependence of the rotational temperature measured in the discharge on the kinetic temperature of the ions is shown in Fig. 2. As can be seen from this figure, the rotational temperature of N₂H⁺ ions is close to the kinetic temperature in the whole studied temperature range.

In addition to the kinetic and rotational temperatures of the N₂H⁺ ions, we also estimated the vibrational temperature of the

TABLE II. Pressure broadening coefficients B_p measured for the P(6) transition in the (200) ← (000) vibrational band of N₂H⁺ in the helium buffer gas.

$T \text{ (K)}$	$B_p \text{ (} 10^{-21} \text{ cm}^{-1} \text{ cm}^3\text{)}$
78	6.2 ± 0.5
140	7.7 ± 0.6
200	8.9 ± 0.3
300	9.4 ± 0.5

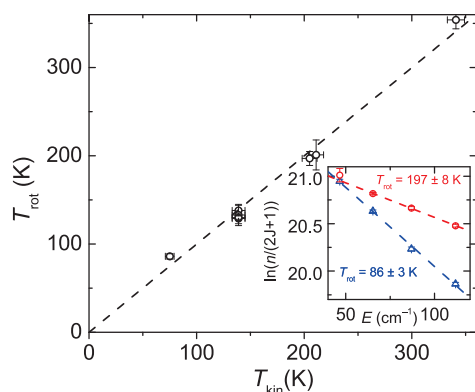


FIG. 2. Dependence of the rotational temperature measured during the discharge on kinetic temperature. All the displayed data were obtained in the helium buffer gas. Inset: an example of the Boltzmann plots used for determination of the rotational temperature obtained at $T = 200$ K and $T = 78$ K.

N_2H^+ ions from the number densities of different rotational states in the ground vibrational state (000) and the first excited vibrational state (01¹0) of N_2H^+ . As the energy difference between the (01¹0) state and the (000) ground state is according to Ref. 46 only ≈ 690 cm^{-1} , in thermal equilibrium at 300 K, almost 10% of all N_2H^+ ions are in this excited vibrational state. The time evolution of number densities of N_2H^+ ions in (000) and (01¹0) vibrational states obtained at $T = 300$ K in the discharge and afterglow plasma is shown in the upper panel of Fig. 3. Again, the relative population of the (01¹0) vibrational state is close to the thermal value at a given temperature both in the discharge and in the afterglow plasma. The dependence of vibrational temperature measured in the discharge

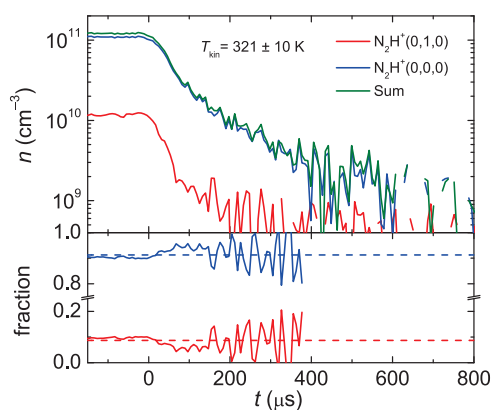


FIG. 3. An example of measured time evolutions of number densities of N_2H^+ ions in the ground and the first excited vibrational state. The lower panel shows the relative fractions of the vibrational states, and the dashed lines denote the corresponding fraction in thermal equilibrium at a temperature of 321 K. The particular vibrational state number densities were calculated from the measured number densities of the $J = 6$ rotational state of the ground vibrational state and of the $J = 9$ state of the (01¹0) vibrational state under the assumption of the same rotational temperature in both vibrational states.

on kinetic temperature of N_2H^+ ions is plotted in Fig. 4. At lower temperatures, the measured number density of the (01¹0) vibrational state decreases accordingly, and at 80 K, the absorption lines belonging to the (21¹0)–(01¹0) vibrational band of N_2H^+ were not visible at all. The vibrational temperature measured in the discharge is slightly higher than the corresponding kinetic temperature. Note that we are able to probe the number densities of only the two lowest vibrational states of N_2H^+ .

Based on the aforementioned measurements, we can safely assume that the rotational and vibrational populations of the recombining N_2H^+ ions are close to thermal ones given by the kinetic temperature of the ions that is in turn close to the discharge tube temperature T .

The electrons are heated by the electric field during the microwave discharge, and their temperature (T_e) is significantly higher than the kinetic temperature of the ions (T_{kin}) and neutrals. After switching off the microwaves, T_e and T_{kin} equilibrate due to elastic electron-neutral, electron-electron, and ion-neutral collisions.³² In helium buffered plasmas, the long-lived (metastable) 2¹S and 2³S states of He may survive into the afterglow and heat the electrons in superelastic collisions. In our previous studies,^{47–49} we monitored the relaxation of the afterglow plasma by probing the rate of removal of the highly excited particles (excited helium dimers and argon atoms) and its dependence on the Ar and H_2 number densities. These results indicate that, at the conditions used in the present study (number densities of Ar and H_2), the helium metastable atoms are removed from the afterglow plasma with a characteristic time constant lower than 30 μs after switching off the discharge.

If N_2H^+ is a dominant ionic species and taking into account quasineutrality of plasma, the time evolution of the number density of N_2H^+ ions $n_{\text{N}_2\text{H}}$ in the afterglow plasma can be described by the equation

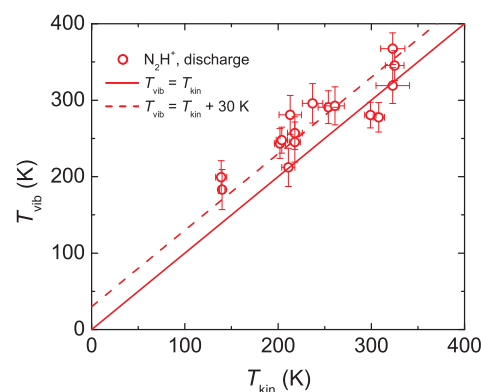


FIG. 4. Dependence of the measured vibrational temperature T_{vib} on kinetic temperature T_{kin} of the N_2H^+ ions measured in the discharge. The kinetic temperature was obtained from the Doppler broadening of the P(6) line of the (200) \leftarrow (000) vibrational band of N_2H^+ . It was assumed that the rotational temperature of (000) and (010) states is equal to T_{kin} . The vibrational temperature was then evaluated from the P(6) line of the (200) \leftarrow (000) vibrational band and from the R(9)^f line of the (210) \leftarrow (010) vibrational band of the N_2H^+ ion. The full line denotes equality of $T_{\text{vib}} = T_{\text{kin}}$, and the dashed line indicates $T_{\text{vib}} = T_{\text{kin}} + 30$ K. The displayed errors are statistical errors of the fits.

$$\begin{aligned}\frac{dn_{\text{N}_2\text{H}^+}}{dt} &= -\alpha_{\text{eff}}n_{\text{N}_2\text{H}^+}n_e - k_{\text{R}}n_{\text{N}_2\text{H}^+}[\text{R}] - \frac{n_{\text{N}_2\text{H}^+}}{\tau_{\text{D}}} \\ &= -\alpha_{\text{eff}}n_{\text{N}_2\text{H}^+}^2 - \frac{n_{\text{N}_2\text{H}^+}}{\tau}.\end{aligned}\quad (3)$$

Here, n_e is the electron number density, α_{eff} is the effective recombination rate coefficient, k_{R} is the rate coefficient for the reaction of N_2H^+ ions with impurities (e.g., NH_3) of number density $[\text{R}]$, and τ_{D} denotes the time constant of charged particle losses due to the ambipolar diffusion. τ represents the time constant of the exponential losses of the charged particles,

$$\frac{1}{\tau} = \frac{1}{\tau_{\text{D}}} + \frac{1}{\tau_{\text{R}}}, \quad (4)$$

where $1/\tau_{\text{R}} = k_{\text{R}}[\text{R}]$.

Equation (3) has an analytical solution in the form

$$n_{\text{N}_2\text{H}^+} = \frac{1}{\alpha_{\text{eff}}\tau\left(e^{\frac{t-t_0}{\tau}} - 1\right) + \frac{1}{n_0}e^{\frac{t-t_0}{\tau}}}, \quad (5)$$

where n_0 is the number density of N_2H^+ at time $t = t_0$.

The recombination rate coefficient is denoted here by the subscript eff—“effective” to account for a possible dependence of α_{eff} on the densities of the buffer or reactant gases. For example, at high buffer gas density (helium or H_2 in our case), the N_2H^+ ions can undergo both binary and three body recombination, and the effective recombination rate coefficient then has the form

$$\alpha_{\text{eff}} = \alpha_{\text{bin}} + K_{\text{M}}[\text{M}], \quad (6)$$

where $[\text{M}]$ is the number density of either helium or molecular hydrogen and K_{M} is the corresponding ternary recombination rate coefficient. The measured dependences of α_{eff} on $[\text{He}]$ or $[\text{H}_2]$ obtained at $T_{\text{kin}} = 325 \pm 10$ K and $T_{\text{kin}} = 350 \pm 15$ K, respectively, are plotted in Fig. 5. The helium number density was changed in the range of $(1-7) \times 10^{17} \text{ cm}^{-3}$. We did not observe any statistically significant enhancement of the measured α_{eff} with increasing $[\text{He}]$ at this temperature. The values of α_{eff} obtained in the hydrogen buffer gas ($[\text{H}_2] = (5-8) \times 10^{16} \text{ cm}^{-3}$) with an admixture of $(3-10) \times 10^{14} \text{ cm}^{-3}$ of N_2 at $T_{\text{kin}} = 350 \pm 15$ K are very close to those obtained in the helium buffer gas at $T_{\text{kin}} = 325 \pm 10$ K. A similar stationary afterglow experiment performed at 273 K in the hydrogen buffer gas ($[\text{H}_2] = (0.7-2.1) \times 10^{16} \text{ cm}^{-3}$, $[\text{N}_2] = (7-11) \times 10^{14} \text{ cm}^{-3}$) by Amano¹⁷ gave a value of the recombination rate coefficient $\alpha_{\text{eff}} = 7.0 \times 10^{-7} \text{ cm}^3 \text{ s}^{-1}$, almost two times higher than the values measured by us either in the helium or in the hydrogen buffer gas. On the other hand, recent FALP¹⁴ and ion storage ring⁶ values (open star and triangle in Fig. 5, respectively) are in a good agreement with our results. The dependence of the effective recombination rate coefficient on $[\text{He}]$ measured for H_3^+ ions at 300 K in different experiments (see Fig. 4, in Ref. 35 and references therein for details) is plotted for comparison. It is evident that the dependence of α_{eff} on $[\text{He}]$ is steeper for H_3^+ than for N_2H^+ ions.

At sufficiently large number densities of N_2 , N_4H^+ ions can be formed by three body association of N_2H^+ with N_2 and He,



Adams *et al.*¹¹ studied reaction (7) in their SIFT apparatus and obtained $k_{\text{N}_4\text{H}} = 2.8 \times 10^{-29} \text{ cm}^6 \text{ s}^{-1}$ at 80 K. As the binding energy

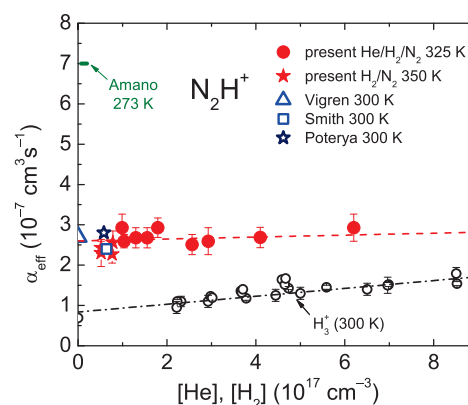


FIG. 5. Dependence of α_{eff} on $[\text{He}]$ measured at $T_{\text{kin}} = 325 \pm 10$ K in the helium buffer gas with $[\text{N}_2] = 3 \times 10^{14} \text{ cm}^{-3}$ and $[\text{H}_2] = 3 \times 10^{14} \text{ cm}^{-3}$. The values measured in the hydrogen buffer gas at $T_{\text{kin}} = 350 \pm 15$ K and $[\text{H}_2] = (3-10) \times 10^{14} \text{ cm}^{-3}$ are plotted as full stars. The data obtained in recent FALP^{13,14} and ion storage ring⁶ experiments at 300 K are plotted as squares, open stars, and triangles, respectively. The values of α_{eff} measured in different experiments for H_3^+ ions in the helium buffer gas at 300 K^{31,35,50} are plotted for comparison (for details, see Refs. 35; no distinction between different H_3^+ experiments is shown here). The dashed and the dashed-dotted lines are linear fits to the N_2H^+ and H_3^+ data, respectively. The arrow denoted “Amano” indicates values of α_{eff} obtained at 273 K by Amano in the hydrogen buffer gas ($[\text{H}_2] = 7 \times 10^{15} - 2 \times 10^{16} \text{ cm}^{-3} \text{ s}^{-1}$) with an admixture of N_2 .¹⁷

of N_4H^+ is relatively high (≈ 0.6 eV),⁵¹ we assume that the inverse reaction to reaction (7) has a negligible rate in the studied temperature range. Reaction (7) limits the number densities of He and N_2 that can be used in the experiments. The corresponding three body association reaction of N_2H^+ with H_2 and He is slow with a reaction rate coefficient at 80 K lower than $5 \times 10^{-30} \text{ cm}^6 \text{ s}^{-1}$ (see Ref. 11). The dependence of the measured α_{eff} on $[\text{N}_2]$ obtained at $T = 200$ K in the helium buffer gas ($[\text{He}] = (1-5) \times 10^{17} \text{ cm}^{-3}$, $[\text{H}_2] = (3-7) \times 10^{14} \text{ cm}^{-3}$, $[\text{Ar}] \approx 5 \times 10^{14} \text{ cm}^{-3}$) is plotted in Fig. 6. The dependence of the same data on $[\text{H}_2]$ is plotted in Fig. 7. As can be seen from Figs. 6 and 7, for $[\text{N}_2] < 10^{14} \text{ cm}^{-3}$, α_{eff} does not significantly change with $[\text{N}_2]$, $[\text{H}_2]$, or $[\text{He}]$. For $[\text{N}_2] > 10^{14} \text{ cm}^{-3}$, α_{eff} increases with increasing nitrogen number density. This is in qualitative agreement with the results of a computer model of the chemical kinetics (dashed line in Fig. 6) that predicts that, at higher nitrogen number densities, N_4H^+ cluster ions are formed in the three body association reaction (7). We evaluate α_{eff} from the time decay of N_2H^+ number density in the afterglow plasma assuming that it is equal to the electron number density. For $[\text{N}_2] > 10^{14} \text{ cm}^{-3}$, this assumption is no longer valid and it leads to an apparent increase in α_{eff} with $[\text{N}_2]$.

Aided by the model of chemical kinetics, we performed similar sets of measurements at $T = 80$ K and $T = 140$ K to ensure that the formation of cluster ions does not influence the measured value of the effective recombination rate coefficient. Unfortunately, as the formation of the N_4H^+ cluster ions is proportional to the product of $[\text{He}]$ and $[\text{N}_2]$, we were limited in the range of helium number density that could be used in present experiments, especially at the lowest temperatures. This in turn limited the precision

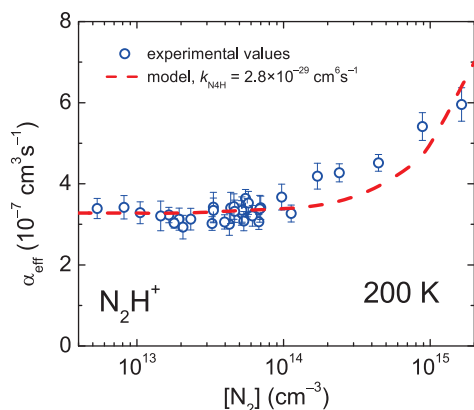


FIG. 6. Dependence of the measured effective recombination rate coefficient on $[N_2]$ obtained in the helium buffer gas at $T = 200 \pm 5$ K ($[He] = (1-5) \times 10^{17}$ cm^{-3} , $[H_2] = (3-7) \times 10^{14}$ cm^{-3} , $[Ar] \approx 5 \times 10^{14}$ cm^{-3}). The dashed line denotes the results of the model of the chemical kinetics fitted by the same procedure as experimental data. Parameters of the model: $T = 200$ K, $[He] = 1.9 \times 10^{17}$ cm^{-3} , $[H_2] = 5 \times 10^{14}$ cm^{-3} , and $[Ar] = 5 \times 10^{14}$ cm^{-3} .

of ternary recombination rate coefficient K_{He} determination. Similarly as for 325 K and 200 K, we did not observe any significant dependence of α_{eff} on helium number density at 140 K and 80 K, and given the complications mentioned above, only an upper estimate of K_{He} could be determined. These values are summarized in Table III and compared to the previously obtained ternary recombination rate coefficients for helium assisted recombination of H_3^+ ions.^{34,36} Note that the value of K_{He} predicted for helium ions in helium at 300 K is $K_{He} \approx 10^{-27}$ $cm^6 s^{-1}$ (see Ref. 22).

The binary recombination rate coefficients α_{bin} for recombination of N_2H^+ ions with electrons obtained in the temperature range of 80–350 K are plotted in Fig. 8. In the whole studied

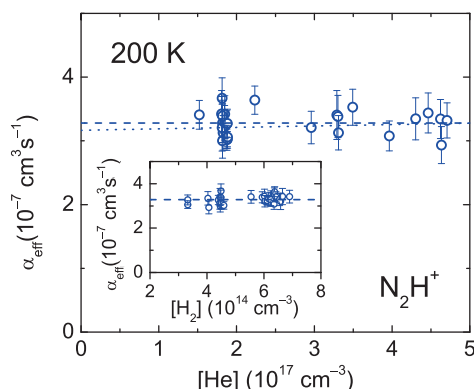


FIG. 7. Dependence of the measured effective recombination rate coefficient on $[He]$ for $[N_2] < 1.0 \times 10^{14}$ cm^{-3} obtained at $T = 200 \pm 5$ K, $T_{kin} = 217 \pm 9$ K, $T_{rot} = 197 \pm 8$ K, and $T_{vib} = 230 \pm 40$ K ($[He] = (1-5) \times 10^{17}$ cm^{-3} , $[H_2] = (3-7) \times 10^{17}$ cm^{-3} , $[Ar] \approx 5 \times 10^{14}$ cm^{-3}). The dotted line is a linear fit to the data, and the dashed line represents the average value of all displayed α_{eff} . Inset: dependence of α_{eff} on $[H_2]$. The plotted data are the same as in the main figure.

TABLE III. Values of K_{He} measured in the present experiment for N_2H^+ compared to those obtained for H_3^+ ions in the helium buffer gas.^{34,36} The numbers in parentheses in the first column denote the quoted temperature in the H_3^+ experiments. For comparison, the value predicted by Bates and Khare²² for helium ions in helium at 300 K is $K_{He-Bates} \approx 10^{-27}$ $cm^6 s^{-1}$.

T (K)	$K_{He}(N_2H^+)$ (10^{-25} $cm^6 s^{-1}$)	$K_{He}(H_3^+)$ (10^{-25} $cm^6 s^{-1}$)
78(80)	$1.8^{+2.9}_{-1.8}$	1.5 ± 0.2
140(145)	$0.1^{+1.7}_{-0.1}$	1.4 ± 0.3
200(200)	$0.2^{+0.5}_{-0.2}$	2.3 ± 0.9
325(300)	$0.2^{+0.6}_{-0.2}$	2.7 ± 0.5

temperature range, our results are in good agreement with the recent FALP experiment data by Poteyra *et al.*¹⁴ and for higher temperatures also with the latest ion storage ring data by Vigren *et al.*⁶ At lower temperatures, the apparent disagreement with ion storage ring results could probably be explained by possibly higher rotational temperatures of the ions in the ring. New generation of cryogenic storage rings such as CSR in Heidelberg⁵² will be able to address this issue. The measured values of α_{bin} do not follow $T^{-0.5}$ temperature dependence that is usual for ions recombining via a direct dissociative recombination process as, for example, in the case of O_2^+ ions.²⁴ For temperatures above 240 K, the obtained values of N_2H^+ binary recombination can be well described by a function $\alpha_{N_2H^+} = (2.81 \pm 0.04) \times 10^{-7} (T/300 K)^{-(0.81 \pm 0.10)}$ $cm^3 s^{-1}$, whereas

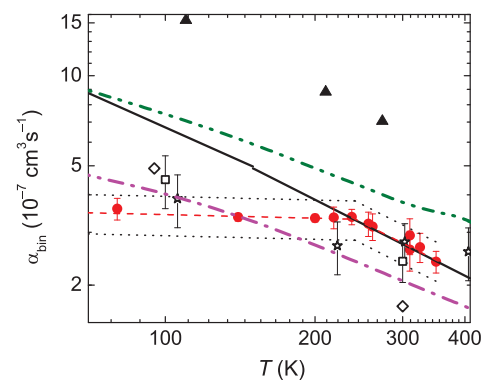


FIG. 8. Temperature dependence of the measured recombination rate coefficients of N_2H^+ (full circles, the value of α_{bin} at 350 K was obtained in the H_2 buffer gas, and for the rest of the data points, the helium buffer gas was used) compared to values obtained in previous experiments. Rhomboids: FALP,¹¹ squares: FALP,¹³ stars: FALP,¹⁴ triangles: stationary afterglow with absorption spectroscopy,¹⁷ full line: ion storage ring,⁶ and double-dot-dashed line: merged beams⁹ and recent theoretical calculations by Fonseca dos Santos²¹ (dotted-dashed line, the rate coefficient was calculated from the cross sections for the direct and indirect recombination processes in Ref. 21). The dashed line denotes fit to the data: $\alpha_{N_2H^+} = (2.81 \pm 0.04) \times 10^{-7} (T/300)^{-(0.81 \pm 0.10)}$ $cm^3 s^{-1}$ for $T > 240$ K and $\alpha_{N_2H^+} = (3.29 \pm 0.04) \times 10^{-7} (T/300)^{-(0.06 \pm 0.02)}$ $cm^3 s^{-1}$ otherwise. The dotted lines show 15% deviation from the fitted value (estimated systematic error of the measurement reflects mainly the uncertainty in the effective discharge column length and in the calculated vibrational transition moments).

at lower temperatures, the measured value of the binary recombination rate coefficient is almost independent of temperature with $\alpha_{\text{N}_2\text{H}^+} = (3.29 \pm 0.04) \times 10^{-7} (T/300 \text{ K})^{-(0.06 \pm 0.02)} \text{ cm}^3 \text{ s}^{-1}$. The mentioned errors are statistical errors of the fit.

Of particular note is the disagreement of the present data with the values obtained by Amano¹⁷ using infrared absorption spectroscopy in a stationary afterglow with the hydrogen buffer gas. Although we performed several measurements at $\approx 350 \text{ K}$ with the hydrogen buffer gas, we essentially obtained the same values of α_{eff} at that temperature as in the helium buffer gas. In the same paper, Amano also reported a very high recombination rate coefficient for H_3^+ ions in the hydrogen buffer gas.¹⁷ We were able to reproduce Amano's values for the H_3^+ recombination rate coefficient in the temperature range of 240–350 K using the same experimental setup as in the present study^{35,36} and explained the enhanced H_3^+ recombination rate by H_2 assisted three body recombination of H_3^+ ions. To obtain N_2H^+ number densities from the measured absorption spectra, Amano used transition dipole moments calculated by Botschwina⁵³ that are higher than those calculated in the present study. If we used the same transition dipole moments as Amano did, we would get a 40%–70% (depending on the actual level of theory Amano used from Ref. 53) larger value of the effective recombination rate coefficient. This largely but not fully resolves the difference between the values of α_{eff} obtained in present and Amano's¹⁷ experiment. At lower temperatures, the formation of cluster ions such as H_5^+ (see discussion in Ref. 36 on chemical kinetics of plasmas with high number densities of hydrogen) cannot be neglected. As Amano was probing time evolutions of ion number densities (as we do), the presence of any other ions than N_2H^+ in the afterglow would inevitably produce higher values of the measured effective recombination rate coefficient, but we cannot arrive at definite conclusions.

The recent quantum mechanical calculations by Fonseca dos Santos²¹ agree very well with our data at low temperatures (and are by a factor of two lower than the values obtained in the CRYRING experiment⁶), but at 300 K, they are almost 40% lower than the present data. This could indicate a possible dependence of the recombination rate coefficient on rotational or vibrational excitation of the N_2H^+ ions that is not included in the theory. In a very recent state selective study on recombination of HeH^+ ions with electrons, Novotný *et al.*⁵⁴ observed dependence of the measured recombination rate coefficient on rotational excitation of HeH^+ ions. The ions in higher rotational states recombined more than an order of magnitude faster than the rotational ground state [$\alpha_{\text{HeH}^+} (J = 0, 100 \text{ K}) \approx 2 \times 10^{-9} \text{ cm}^3 \text{ s}^{-1}$]. This corresponds to the previous ion storage ring experiment by Strömholm *et al.*⁵⁵ who reported a value of $\alpha_{\text{HeH}^+} (100 \text{ K}) \approx 8 \times 10^{-8} \text{ cm}^3 \text{ s}^{-1}$. The actual rotational population of HeH^+ ions in the study of Strömholm *et al.*⁵⁵ corresponded probably to the temperature of 300 K. A similar dependence of the recombination rate coefficient on rotational excitation of N_2H^+ ions could qualitatively explain the temperature dependence of the recombination rate coefficient obtained in our study. The comparison of our values with ion storage ring data measured by Vigen *et al.*⁶ also hints on a higher recombination rate coefficient for ions in higher rotational states—there is an excellent agreement around 300 K, where the rotational population of N_2H^+ corresponded to 300 K in both experiments. On the contrary, at 80 K, our recombination rate coefficients obtained with N_2H^+ rotational

TABLE IV. Vibrational transition moments $M_{\text{present}} = |\langle v_1'' v_2'' v_3'' | \mu_z | v_1' v_2' v_3' \rangle|$ of N_2H^+ (in Debye) calculated in the present study for two isotopes of nitrogen compared to those obtained by Botschwina⁵³ [$M_{\text{Botschwina}}$, CEPA-1(ED) level of theory]. The numbers in parentheses in the fourth column are the IR intensities of absorption in $\text{cm}^2 \text{ mol}^{-1}$ from Ref. 53. $M_{\text{Botschwina}}$ were calculated from these values using Eq. (2) in Ref. 56. Prime and double prime denote upper and lower states, respectively.

Transition	M_{present}		$M_{\text{Botschwina}}$ ($^{14}\text{N}_2\text{H}^+$)
	($^{14}\text{N}_2\text{H}^+$)	($^{15}\text{N}_2\text{H}^+$)	
$v_1'' v_2'' v_3'' \leftrightarrow v_1' v_2' v_3'$			
000 \leftrightarrow 000	3.4906 ^a	3.4910	
000 \leftrightarrow 200	0.0153	0.0157	0.0191(91.2)
100 \leftrightarrow 300	0.0256	0.0266	
000 \leftrightarrow 100	0.2432 ^b	0.2430	0.284(20 257)
01 ¹ 0 \leftrightarrow 21 ¹ 0	0.0153	0.0157	
02 ⁰ 0 \leftrightarrow 22 ⁰ 0	0.0153	0.0154	
01 ¹ 0 \leftrightarrow 11 ¹ 0	0.2430	0.2428	
001 \leftrightarrow 201	0.0147	0.0152	
02 ⁰ 0 \leftrightarrow 22 ² 0	0.0154	0.0154	

^aExperimental value from Ref. 57: $3.4 \pm 0.2 \text{ D}$.

^bExperimental value from Ref. 58: $0.23 \pm 0.02 \text{ D}$.

populations corresponding to 80 K are by a factor of two lower than the ion storage ring data with 300 K rotational populations of N_2H^+ ions.

IV. THEORETICAL CALCULATIONS

The electric dipole moments of N_2H^+ used in the present study for ion number density determination were calculated from the *ab initio* potential energy and electric dipole surfaces of Ref. 45 using the Suttcliffe-Tennyson Hamiltonian⁵⁹ for triatomic molecules. The calculated characteristics are found to be in a close agreement with their experimental counterparts that are available for low-lying vibrational states,^{57,58} thus ensuring reliability of the made predictions. The obtained vibrational transition moments M of N_2H^+ are summarized in Table IV. The calculated vibrational transition moments are almost 20% lower than those reported by Botschwina⁵³ and used by Amano¹⁷ in his absorption spectroscopy study of N_2H^+ recombination. As the evaluated number density of N_2H^+ is proportional to the inverse of M^2 , the value of the recombination rate coefficients obtained by Amano¹⁷ is overestimated by approximately 40%.

V. DISCUSSION OF ERRORS AND THEIR SOURCES

The errors quoted through this work are statistical errors. The systematic error of the measured recombination rate coefficients arises mainly from the uncertainty of the discharge column length (estimated as 10%) and from the uncertainty of the used vibrational transition moments. By comparing the calculated vibrational transition moments with those obtained experimentally in Refs. 57 and 58, we estimate the resulting systematic error of recombination rate coefficient determination to be lower than 5% and the overall systematic error to be lower than 15%.

VI. CONCLUSIONS

We have measured the recombination rate coefficient for recombination of N_2H^+ ions with electrons in the temperature range of 80–350 K using a stationary afterglow apparatus with a cavity ring-down spectrometer. In addition, the rotational and vibrational populations of N_2H^+ were monitored to ensure that the internal excitation of the recombining ions is in thermal equilibrium with the temperature of the buffer gas. Particular attention was given to possible influence of the neutral assisted three body recombination with electrons on the measured recombination rate coefficients. No statistically significant enhancement of the measured recombination rate coefficients with buffer gas density was observed in the studied temperature range giving an upper estimate on the ternary neutral assisted recombination rate coefficients for recombination of N_2H^+ ions with electrons. Essentially the same effective recombination rate coefficient was obtained for N_2H^+ ions in the hydrogen or helium buffer gas at $T_{kin} = 350 \pm 15$ K or $T_{kin} = 325 \pm 10$ K, respectively.

The binary recombination rate coefficient of N_2H^+ was found to be almost constant below 240 K: $\alpha_{N_2H^+} = (3.29 \pm 0.04) \times 10^{-7} (T/300 \text{ K})^{-(0.06 \pm 0.02)} \text{ cm}^3 \text{ s}^{-1}$. At higher temperatures, the obtained value of the binary recombination rate coefficient decreases with increasing temperature as $\alpha_{N_2H^+} = (2.81 \pm 0.04) \times 10^{-7} (T/300 \text{ K})^{-(0.81 \pm 0.10)} \text{ cm}^3 \text{ s}^{-1}$. We hope that our results will help improve models of interstellar chemistry involving N_2H^+ ions especially at low temperatures and will possibly give impulse for

enhancement of quantum mechanical calculations of the dissociative recombination rate coefficient for polyatomic ions.

ACKNOWLEDGMENTS

This work was partly supported by the Czech Science Foundation (Grant No. GACR 17-08803S) and by the Charles University (Project Nos. GAUK 1583517 and GAUK 646218) and IOCB (Grant No. RVO:61388963).

APPENDIX: MODEL OF CHEMICAL KINETICS

A model of chemical kinetics is employed to calculate the chemical evolution of the afterglow plasma at given conditions. The system of differential rate equations describing the number densities of each species is assembled from the appropriate set of chemical equations, which includes binary and ternary interactions among neutrals, ions, and electrons. Additionally, ambipolar diffusion of the charged species is represented as a first order chemical equation in the model. The system of differential equations is then solved using a multistep stiff equation solver implemented in the lsoda⁶⁰ routine. The reactions that are most important for the formation and destruction of N_2H^+ ions in a mixture of He/Ar/H₂/N₂ are summarized in Table V. The number density of metastable helium atoms He^m (2¹S and 2³S states) at the beginning of the afterglow was assumed to be the same as or lower than the electron

TABLE V. The most important reactions considered in the model of the formation and destruction of N_2H^+ ions. The reaction rate coefficients are for 300 K if not stated otherwise. The characteristic reaction times τ_{reaction} were calculated for $[He] = 2 \times 10^{17} \text{ cm}^{-3}$, $[H_2] = 5 \times 10^{14} \text{ cm}^{-3}$, $[Ar] = 5 \times 10^{14} \text{ cm}^{-3}$, $[N_2] = 5 \times 10^{13} \text{ cm}^{-3}$, $n_e = 1 \times 10^{11} \text{ cm}^{-3}$, $[NH_3] = 5 \times 10^{11} \text{ cm}^{-3}$, $[N] = 5 \times 10^{11} \text{ cm}^{-3}$, and $[H] = 5 \times 10^{11} \text{ cm}^{-3}$ from the appropriate reaction rate coefficient k and reactant number densities $[R]$ as $\tau_{\text{reaction}} = 1/(k[R])$ for two body reactions and similarly for the three body reactions. The rate coefficients for the reactions of H_2^+ are given for ions with vibrational excitation $v \leq 1$. The reaction rate coefficient for reaction R26 was obtained at 80 K.

No.	Reaction	Rate coefficient ($\text{cm}^3 \text{ s}^{-1}$, $\text{cm}^6 \text{ s}^{-1}$)	τ_{reaction} (μs)	References
R1	$He^m + H_2 \rightarrow H_2^+ + He + e^-$ 90% $\rightarrow HeH^+ + H + e^-$ 10%	3.2×10^{-11}	63	63 and 64
R2	$He^m + Ar \rightarrow Ar^+ + He + e^-$	7×10^{-11}	29	61
R3	$He^+ + He + He \rightarrow He_2^+ + He$	1×10^{-31}	250	65
R4	$He^+ + N_2 \rightarrow N^+ + N + He$ 60% $\rightarrow N_2^+ + He$ 40%	1.6×10^{-9}	13	66
R5	$HeH^+ + H_2 \rightarrow H_3^+ + He$	1.5×10^{-9}	1	67
R6	$HeH^+ + N_2 \rightarrow N_2H^+ + He$	1.70×10^{-9}	12	68
R7	$He_2^+ + Ar \rightarrow Ar^+ + He + He$	2×10^{-10}	10	65
R8	$He_2^+ + N_2 \rightarrow N_2^+ + He + He$	1.12×10^{-9}	18	69
R9	$Ar^+ + H_2 \rightarrow ArH^+ + H$ 85% $\rightarrow H_2^+ + Ar$ 15%	8.6×10^{-10}	3	70
R10	$Ar^+ + N_2 \rightarrow N_2^+ + Ar$	1.0×10^{-11}	2000	71
R11	$ArH^+ + H_2 \rightarrow H_3^+ + Ar$	1.5×10^{-9}	1	72
R12	$ArH^+ + N_2 \rightarrow N_2H^+ + Ar$	8.0×10^{-10}	25	72
R13	$H^+ + He + He \rightarrow HeH^+ + He$	9×10^{-32}	278	73
R14	$H^+ + H_2 + He \rightarrow H_3^+ + He$	3×10^{-29}	333	36

TABLE V. (Continued.)

No.	Reaction	Rate coefficient ($\text{cm}^3 \text{s}^{-1}$, $\text{cm}^6 \text{s}^{-1}$)	τ_{reaction} (μs)	References
R15	$\text{H}_2^+ + \text{Ar} \rightarrow \text{ArH}^+ + \text{H}$	2.3×10^{-9}	1	74
R16	$\text{H}_2^+ + \text{H}_2 \rightarrow \text{H}_3^+ + \text{H}$	2×10^{-9}	1	74
R17	$\text{H}_2^+ + \text{N}_2 \rightarrow \text{N}_2\text{H}^+ + \text{H}$	2×10^{-9}	10	75
R18	$\text{H}_3^+ + \text{N}_2 \rightarrow \text{N}_2\text{H}^+ + \text{H}_2$	1.8×10^{-9}	11	68
R19	$\text{H}_3^+ + \text{e}^- \rightarrow \text{products}$	1.10×10^{-7}	91	36 and 76
R20	$\text{H}_3^+ + \text{H}_2 + \text{He} \rightarrow \text{H}_5^+ + \text{He}$	2×10^{-30}	5000	36
R21	$\text{H}_3^+ + \text{NH}_3 \rightarrow \text{NH}_4^+ + \text{H}_2$	4.39×10^{-9}	456	77
R22	$\text{N}^+ + \text{H}_2 \rightarrow \text{NH}^+ + \text{H}$	3.7×10^{-10}	4	78 and 79
R23	$\text{N}_2^+ + \text{H}_2 \rightarrow \text{N}_2\text{H}^+ + \text{H}$	2×10^{-9}	1	80
R24	$\text{N}_2\text{H}^+ + \text{e}^- \rightarrow \text{products}$	2.8×10^{-7}	36	Present
R25	$\text{N}_2\text{H}^+ + \text{NH}_3 \rightarrow \text{NH}_4^+ + \text{N}_2$	2.3×10^{-9}	870	43
R26	$\text{N}_2\text{H}^+ + \text{N}_2 + \text{He} \rightarrow \text{N}_4\text{H}^+ + \text{He}$	2.8×10^{-29}	3571	11
R27	$\text{NH}_4^+ + \text{e}^- \rightarrow \text{products}$	1.4×10^{-6}	7	81
R28	$\text{N}_4\text{H}^+ + \text{e}^- \rightarrow \text{products}$	2×10^{-7}	50	Estimate

number density. This assumption is based on the experimental study described in Ref. 61. The reaction rate coefficients listed in Table V are for 300 K if not stated otherwise. For some associative reactions in the He buffer, we used rate coefficients measured for H_2 [reactions (R14) and (R20), see Ref. 36 for details]. Figure 9 shows the comparison between the measured and calculated time evolutions of N_2H^+ number densities in the afterglow plasma at 140 K. As the actual ionic composition of the plasma at the end of the discharge period is not known, we varied the initial conditions for number densities of different ionic species at the beginning of the afterglow. The results of the model of chemical kinetics show that N_2H^+ is a dominant ionic species in the afterglow within 200 μs after switching off the discharge. The only exception to this is when N^+

ions are present at the end of the discharge period in sufficient amounts (tens of percent). N^+ reacts rapidly with hydrogen (reaction R22) forming NH^+ , and in subsequent reactions with hydrogen, NH_4^+ ions are produced (for details on this particular reaction chain, see Ref. 62). During the experiments, we were searching for possible dependences of the measured effective recombination rate coefficient on reactant or buffer gas number densities (see Figs. 6 and 7). As the values of recombination rate coefficients of N_2H^+ obtained in this study did not change with reactant and buffer gas number densities varying by almost an order of magnitude, we assume that the number density of N^+ ions at the end of the discharge period was well below 10% of all ions.

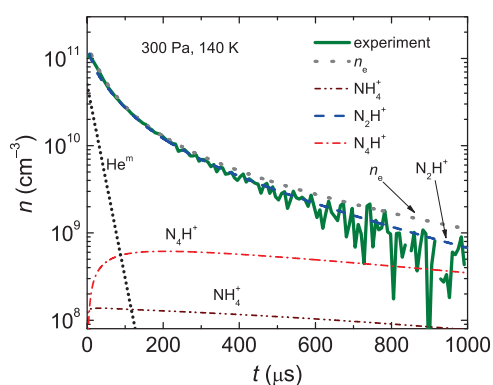


FIG. 9. Time evolution of the measured overall number density of N_2H^+ ions (full line) compared to the results obtained from the model of chemical kinetics. The data were obtained at $T = 140 \text{ K}$, $[\text{He}] = 1.5 \times 10^{17} \text{ cm}^{-3}$, $[\text{Ar}] = 2.5 \times 10^{14} \text{ cm}^{-3}$, $[\text{H}_2] = 5 \times 10^{14} \text{ cm}^{-3}$, and $[\text{N}_2] = 4 \times 10^{13} \text{ cm}^{-3}$ (same as in Fig. 1) and $[\text{NH}_3] = 5 \times 10^{11} \text{ cm}^{-3}$. $[\text{He}^m](t=0) = 1/3 n_e(t=0)$.

REFERENCES

- B. E. Turner, *Astrophys. J., Lett.* **193**, L83 (1974).
- B. E. Turner, *Astrophys. J.* **449**, 635 (1995).
- P. Caselli, C. M. Walmsley, A. Zucconi, M. Tafalla, L. Dore, and P. C. Myers, *Astrophys. J.* **565**, 344 (2002).
- D. E. Anderson, G. A. Blake, E. A. Bergin, K. Zhang, J. M. Carpenter, K. R. Schwarz, J. Huang, and K. I. Öberg, *Astrophys. J.* **881**, 127 (2019).
- V. Vuitton, R. V. Yelle, and M. J. McEwan, *Icarus* **191**, 722 (2007).
- E. Vigren, V. Zhaunerchyk, M. Hamberg, M. Kaminska, J. Semaniak, M. af Ugglas, M. Larsson, R. D. Thomas, and W. D. Geppert, *Astrophys. J.* **757**, 34 (2012).
- M. Larsson and A. E. Orel, *Dissociative Recombination of Molecular Ions*, Cambridge Molecular Science (Cambridge University Press, 2008).
- P. M. Mul and J. W. McGowan, *Astrophys. J., Lett.* **227**, L157 (1979).
- J. Brian and A. Mitchell, *Phys. Rep.* **186**, 215 (1990).
- D. Smith and N. G. Adams, *Astrophys. J., Lett.* **284**, L13 (1984).
- N. G. Adams, D. Smith, and E. Alge, *J. Chem. Phys.* **81**, 1778 (1984).
- W. Geppert, R. Thomas, J. Semaniak, A. Ehlerding, T. J. Millar, F. Österdahl, M. Af Ugglas, N. Djurić, A. Paal, and M. Larsson, *Astrophys. J.* **609**, 459 (2004).
- D. Smith and P. Španel, *Int. J. Mass Spectrom. Ion Processes* **129**, 163 (1993).

- ¹⁴V. Poterya, J. L. McLain, N. G. Adams, and L. M. Babcock, *J. Phys. Chem. A* **109**, 7181 (2005).
- ¹⁵R. E. Rosati, R. Johnsen, and M. F. Golde, *J. Chem. Phys.* **120**, 8025 (2004).
- ¹⁶A. Petrigiani, S. Altevogt, M. H. Berg, D. Bing, M. Grieser, J. Hoffmann, B. Jordon-Thaden, C. Krantz, M. B. Mendes, O. Novotný, S. Novotny, D. A. Orlov, R. Repnow, T. Sorg, J. Stützel, A. Wolf, H. Buhr, H. Kreckel, V. Kokoouline, and C. H. Greene, *Phys. Rev. A* **83**, 032711 (2011).
- ¹⁷T. Amano, *J. Chem. Phys.* **92**, 6492 (1990).
- ¹⁸A. P. Hickman, D. O. Kashinski, R. F. Malenda, F. Gatti, and D. Talbi, *J. Phys.: Conf. Ser.* **300**, 012016 (2011).
- ¹⁹D. Talbi, *Chem. Phys.* **332**, 298 (2007).
- ²⁰S. Fonseca dos Santos, N. Douguet, V. Kokoouline, and A. E. Orel, *J. Chem. Phys.* **140**, 164308 (2014).
- ²¹S. Fonseca dos Santos, V. Ngassam, A. E. Orel, and A. Larson, *Phys. Rev. A* **94**, 022702 (2016).
- ²²D. R. Bates and S. P. Khare, *Proc. Phys. Soc.* **85**, 231 (1965).
- ²³R. Deloche, P. Monchicourt, M. Cheret, and F. Lambert, *Phys. Rev. A* **13**, 1140 (1976).
- ²⁴P. Dohnal, P. Rubovič, T. Kotřík, M. Hejduk, R. Plašil, R. Johnsen, and J. Glosík, *Phys. Rev. A* **87**, 052716 (2013).
- ²⁵J. Berlande, M. Cheret, R. Deloche, A. Gonfalone, and C. Manus, *Phys. Rev. A* **1**, 887 (1970).
- ²⁶Y. S. Cao and R. Johnsen, *J. Chem. Phys.* **94**, 5443 (1991).
- ²⁷R. J. van Sonsbeek, R. Cooper, and R. N. Bhawe, *J. Chem. Phys.* **97**, 1800 (1992).
- ²⁸C.-G. Schregel, E. A. D. Carbone, D. Luggenöhlscher, and U. Czarnetzki, *Plasma Sources Sci. Technol.* **25**, 054003 (2016).
- ²⁹M. R. Flannery, *J. Chem. Phys.* **95**, 8205 (1991).
- ³⁰J. Glosík, I. Korolov, R. Plašil, O. Novotný, T. Kotřík, P. Hlavenka, J. Varju, I. A. Mikhailov, V. Kokoouline, and C. H. Greene, *J. Phys. B: At., Mol. Opt. Phys.* **41**, 191001 (2008).
- ³¹J. Glosík, R. Plašil, I. Korolov, T. Kotřík, O. Novotný, P. Hlavenka, P. Dohnal, J. Varju, V. Kokoouline, and C. H. Greene, *Phys. Rev. A* **79**, 052707 (2009).
- ³²P. Dohnal, M. Hejduk, J. Varju, P. Rubovič, Š. Roučka, T. Kotřík, R. Plašil, J. Glosík, and R. Johnsen, *J. Chem. Phys.* **136**, 244304 (2012).
- ³³P. Dohnal, Á. Kálosi, R. Plašil, Š. Roučka, A. Kovalenko, S. Rednyk, R. Johnsen, and J. Glosík, *Phys. Chem. Chem. Phys.* **18**, 23549 (2016).
- ³⁴R. Plašil, P. Dohnal, Á. Kálosi, Š. Roučka, R. Johnsen, and J. Glosík, *Plasma Sources Sci. Technol.* **26**, 035006 (2017).
- ³⁵P. Dohnal, P. Rubovič, Á. Kálosi, M. Hejduk, R. Plašil, R. Johnsen, and J. Glosík, *Phys. Rev. A* **90**, 042708 (2014).
- ³⁶J. Glosík, P. Dohnal, P. Rubovič, Á. Kálosi, R. Plašil, Š. Roučka, and R. Johnsen, *Plasma Sources Sci. Technol.* **24**, 065017 (2015).
- ³⁷D. Romanini, A. Kachanov, N. Sadeghi, and F. Stoeckel, *Chem. Phys. Lett.* **264**, 316 (1997).
- ³⁸P. Macko, G. Bánó, P. Hlavenka, R. Plašil, V. Poterya, A. Pysanenko, O. Votava, R. Johnsen, and J. Glosík, *Int. J. Mass Spectrom.* **233**, 299 (2004).
- ³⁹P. Hlavenka, I. Korolov, R. Plašil, J. Varju, T. Kotřík, and J. Glosík, *Czech J. Phys.* **56**, B749 (2006).
- ⁴⁰P. Hlavenka, R. Plašil, G. Bánó, I. Korolov, D. Gerlich, J. Ramanlal, J. Tennyson, and J. Glosík, *Int. J. Mass Spectrom.* **255**, 170 (2006).
- ⁴¹J. Glosík, P. Hlavenka, R. Plašil, F. Windisch, D. Gerlich, A. Wolf, and H. Kreckel, *Philos. Trans. R. Soc., A* **364**, 2931 (2006).
- ⁴²I. Gordon, L. Rothman, C. Hill, R. Kochanov, Y. Tan, P. Bernath, M. Birk, V. Boudon, A. Campargue, K. Chance, B. Drouin, J.-M. Flaud, R. Gamache, J. Hodges, D. Jacquemart, V. Perevalov, A. Perrin, K. Shine, M.-A. Smith, J. Tennyson, G. Toon, H. Tran, V. Tyuterev, A. Barbe, A. Császár, V. Devi, T. Furtenbacher, J. Harrison, J.-M. Hartmann, A. Jolly, T. Johnson, T. Karman, I. Kleiner, A. Kyuberis, J. Loos, O. Lyulin, S. Massie, S. Mikhailenko, N. Moazzen-Ahmadi, H. Müller, O. Naumenko, A. Nikitin, O. Polyansky, M. Rey, M. Rotger, S. Sharpe, K. Sung, E. Starikova, S. Tashkun, J. V. Auwera, G. Wagner, J. Wilzewski, P. Wcisło, S. Yu, and E. Zak, *J. Quant. Spectrosc. Radiat. Transfer* **203**, 3 (2017).
- ⁴³R. Hemsworth, J. Payzant, H. Schiff, and D. Bohme, *Chem. Phys. Lett.* **26**, 417 (1974).
- ⁴⁴Á. Kálosi, P. Dohnal, D. Shapko, S. Roučka, R. Plašil, R. Johnsen, and J. Glosík, *J. Instrum.* **12**, C10010 (2017).
- ⁴⁵V. Špirko, O. Bludský, and W. P. Kraemer, *Collect. Czech. Chem. Commun.* **73**, 873 (2008).
- ⁴⁶Y. Kabbadj, T. Huet, B. Rehffuss, C. Gabryns, and T. Oka, *J. Mol. Spectrosc.* **163**, 180 (1994).
- ⁴⁷Á. Kálosi, P. Dohnal, L. Augustovičová, S. Roučka, R. Plašil, and J. Glosík, *Eur. Phys. J.: Appl. Phys.* **75**, 24707 (2016).
- ⁴⁸J. Glosík, P. Dohnal, Á. Kálosi, L. Augustovičová, D. Shapko, Š. Roučka, and R. Plašil, *Eur. Phys. J.: Appl. Phys.* **80**, 30801 (2017).
- ⁴⁹R. Plašil, P. Dohnal, Á. Kálosi, Š. Roučka, D. Shapko, S. Rednyk, R. Johnsen, and J. Glosík, *Rev. Sci. Instrum.* **89**, 063116 (2018).
- ⁵⁰B. A. Tom, V. Zhaunerchyk, M. B. Wiczler, A. A. Mills, K. N. Crabtree, M. Kaminska, W. D. Geppert, M. Hamberg, M. af Ugglas, E. Vigren, W. J. van der Zande, M. Larsson, R. D. Thomas, and B. J. McCall, *J. Chem. Phys.* **130**, 031101 (2009).
- ⁵¹M. Meot-Ner and F. H. Field, *J. Chem. Phys.* **61**, 3742 (1974).
- ⁵²R. von Hahn, A. Becker, F. Berg, K. Blaum, C. Breitenfeldt, H. Fadil, F. Fellenberger, M. Froese, S. George, J. Göck, M. Grieser, F. Grussie, E. A. Guerin, O. Heber, P. Herwig, J. Karthein, C. Krantz, H. Kreckel, M. Lange, F. Laux, S. Lohmann, S. Menk, C. Meyer, P. M. Mishra, O. Novotný, A. P. O'Connor, D. A. Orlov, M. L. Rappaport, R. Repnow, S. Saurabh, S. Schippers, C. D. Schröter, D. Schwalm, L. Schweikhard, T. Sieber, A. Shornikov, K. Spruck, S. Sunil Kumar, J. Ullrich, X. Urbain, S. Vogel, P. Wilhelm, A. Wolf, and D. Zajfman, *Rev. Sci. Instrum.* **87**, 063115 (2016).
- ⁵³P. Botschwina, *Chem. Phys. Lett.* **107**, 535 (1984).
- ⁵⁴O. Novotný, P. Wilhelm, D. Paul, Á. Kálosi, S. Saurabh, A. Becker, K. Blaum, S. George, J. Göck, M. Grieser, F. Grussie, R. von Hahn, C. Krantz, H. Kreckel, C. Meyer, P. M. Mishra, D. Muell, F. Nuesslein, D. A. Orlov, M. Rimpler, V. C. Schmidt, A. Shornikov, A. S. Terekhov, S. Vogel, D. Zajfman, and A. Wolf, *Science* **365**, 676 (2019).
- ⁵⁵C. Strömholm, J. Semaniak, S. Rosén, H. Danared, S. Datz, W. van der Zande, and M. Larsson, *Phys. Rev. A* **54**, 3086 (1996).
- ⁵⁶P. Botschwina, *Chem. Phys.* **81**, 73 (1983).
- ⁵⁷M. Havenith, E. Zwart, W. Leo Meerts, and J. J. ter Meulen, *J. Chem. Phys.* **93**, 8446 (1990).
- ⁵⁸E. R. Keim, M. L. Polak, J. C. Owrtzky, J. V. Coe, and R. J. Saykally, *J. Chem. Phys.* **93**, 3111 (1990).
- ⁵⁹B. T. Sutcliffe and J. Tennyson, *Mol. Phys.* **58**, 1053 (1986).
- ⁶⁰A. C. Hindmarsh, "ODEPACK: A systematized collection of ODE solvers," in *Scientific Computing*, IMACS Transactions on Scientific Computation Vol. 1, edited by R. S. Stepleman (North-Holland, 1983), pp. 55–64.
- ⁶¹J. Glosík, G. Bánó, R. Plašil, A. Luca, and P. Zakouřil, *Int. J. Mass Spectrom.* **189**, 103 (1999).
- ⁶²S. Rednyk, Š. Roučka, A. Kovalenko, T. Tran, P. Dohnal, R. Plašil, and J. Glosík, *Astron. Astrophys.* **625**, A74 (2019).
- ⁶³W. Lindinger, A. L. Schmelteköpf, and F. C. Fehsenfeld, *J. Chem. Phys.* **61**, 2890 (1974).
- ⁶⁴D. W. Martin, C. Weiser, R. F. Sperlein, D. L. Bernfeld, and P. E. Siska, *J. Chem. Phys.* **90**, 1564 (1989).
- ⁶⁵Y. Ikezoe, S. Matsuoka, M. Takebe, and A. Viggiano, *Gas Phase Ion-Molecule Reaction Rate Constants Through 1986* (Maruzen Company, Ltd., 1987).
- ⁶⁶N. G. Adams and D. Smith, *J. Phys. B: At. Mol. Phys.* **9**, 1439 (1976).
- ⁶⁷D. K. Bohme, G. I. Mackay, and H. I. Schiff, *J. Chem. Phys.* **73**, 4976 (1980).
- ⁶⁸N. Adams and D. Smith, *Int. J. Mass Spectrom. Ion Phys.* **21**, 349 (1976).
- ⁶⁹W. Lindinger, F. C. Fehsenfeld, A. L. Schmelteköpf, and E. E. Ferguson, *J. Geophys. Res.* **79**, 4753, <https://doi.org/10.1029/ja079i031p04753> (1974).
- ⁷⁰D. Bedford and D. Smith, *Int. J. Mass Spectrom. Ion Phys.* **98**, 179 (1990).
- ⁷¹D. Smith and N. G. Adams, *Phys. Rev. A* **23**, 2327 (1981).
- ⁷²H. Villinger, J. H. Futrell, F. Howorka, N. Duric, and W. Lindinger, *J. Chem. Phys.* **76**, 3529 (1982).
- ⁷³B. K. Chatterjee and R. Johnsen, *J. Chem. Phys.* **93**, 5681 (1990).
- ⁷⁴J. Glosík, *Int. J. Mass Spectrom. Ion Phys.* **139**, 15 (1994).

⁷⁵J. K. Kim and W. T. Huntress, *J. Chem. Phys.* **62**, 2820 (1975).

⁷⁶P. Rubovič, P. Dohnal, M. Hejduk, R. Plašil, and J. Glosik, *J. Phys. Chem. A* **117**, 9626 (2013).

⁷⁷C. Praxmarer, A. Hansel, and W. Lindinger, *J. Chem. Phys.* **100**, 8884 (1994).

⁷⁸N. Adams and D. Smith, *Chem. Phys. Lett.* **117**, 67 (1985).

⁷⁹I. Zymak, M. Hejduk, D. Mulin, R. Plašil, J. Glosik, and D. Gerlich, *Astrophys. J.* **768**, 86 (2013).

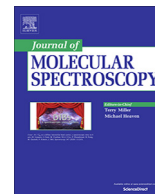
⁸⁰J. A. de Gouw, L. N. Ding, M. J. Frost, S. Kato, V. M. Bierbaum, and S. R. Leone, *Chem. Phys. Lett.* **240**, 362 (1995).

⁸¹E. Alge, N. G. Adams, and D. Smith, *J. Phys. B: At. Mol. Phys.* **16**, 1433 (1983).

**Cavity ring-down spectroscopy study of neon assisted recombination
of H_3^+ ions with electrons**

Shapko D., Dohnal P., Roučka Š., Uvarova L., Kassayová M., Plašil R., Glosík J.

J. Mol. Spectrosc. **378**, 111450, 2021.



Cavity ring-down spectroscopy study of neon assisted recombination of H_3^+ ions with electrons

Dmytro Shapko, Petr Dohnal*, Štěpán Roučka, Liliia Uvarova, Miroslava Kassayová, Radek Plašil, Juraj Glosík

Charles University, Faculty of Mathematics and Physics, Department of Surface and Plasma Science, V Holesovickach 2, CZ-18000 Prague 8, Czech Republic

ARTICLE INFO

Article history:

Received 21 January 2021

In revised form 9 March 2021

Accepted 11 March 2021

Available online 31 March 2021

Keywords:

Electron-ion recombination

H_3^+

Cavity ring-down spectroscopy

Einstein coefficients

ABSTRACT

A stationary afterglow apparatus with Cavity Ring-Down spectrometer was combined with electron number density measurement system to study the third-body assisted recombination of H_3^+ ions with electrons in neon gas at the temperature of 110 K. The measured ternary recombination rate coefficient $K_{\text{Ne}}(110 \text{ K}) = (1.8 \pm 0.2) \times 10^{-25} \text{ cm}^6 \text{ s}^{-1}$ is close to that obtained in helium buffered plasma. The applicability of the present experimental setup for Einstein coefficients determination is also discussed.

© 2021 Elsevier Inc. All rights reserved.

1. Introduction

The H_3^+ ion discovered by Thomson in 1911 [1] using an early form of mass spectrometry has been in the previous century a focus of many theoretical and experimental studies. In 1925 the formation of H_3^+ in a ion molecule reaction of H_2^+ with H_2 was described by Hogness and Lunn [2], whereas the equilibrium structure of H_3^+ ion as an equilateral triangle was established in the early thirties [3]. But it took nearly half a century until the absorption spectrum of this ion was experimentally observed by Oka in 1980 [4]. Prior to the laboratory or astrophysical detection, the H_3^+ ion was considered a crucial building block of the interstellar chemistry [5] as the most abundantly produced interstellar ion [6]. It was later detected in many astrophysical environments ranging from ionospheres of gas giants to interstellar gas clouds and towards the galactic centre [7–9]. Its key role in the cosmic chemistry is given by the ability to transfer a proton in ion molecule reactions as an universal proton donor [6,10].

Together with the abundance of the H_3^+ ion in the Universe and the variety of conditions that are available in space it makes H_3^+ the starting point for long reaction chains resulting in production of more complex molecules [11]. As a consequence, its dissociative recombination (DR) with electrons is one of the most important reactions in astrophysics [12] and has been studied for more than 70 years [13].

The value of the dissociative recombination rate coefficient of H_3^+ was a matter of heated debate and much controversy. During the turbulent history of H_3^+ recombination studies, until the early 2000s, the recombination rate coefficients obtained in ion storage rings experiments were close to $\approx 10^{-7} \text{ cm}^3 \text{ s}^{-1}$ (for 300 K) [14,15], while the values reported from afterglow experiments (stationary and flowing afterglows) were in a very broad range from 1.8×10^{-7} to $10^{-11} \text{ cm}^3 \text{ s}^{-1}$ [16–19]. To further complicate the overall picture, the theory predicted that there are no favourable potential energy curve crossings [20], which indicate a very small dissociative recombination rate coefficient. It was necessary to go beyond the Born–Oppenheimer approximation by invoking the Jahn–Teller mechanism with the latest theoretical calculations supporting the high value of the recombination rate coefficient [21,22]. Around the same time, the discovery of surprisingly fast three-body helium assisted recombination of H_3^+ ions by Glosik and coworkers [23] finally explained the results of various afterglow experiments. The obtained ternary recombination rate coefficients were almost two orders of magnitude larger than those predicted for atomic ions by the theory [24,25]. A similarly fast three-body helium assisted recombination was later observed for all deuterated isotopologues of H_3^+ [26–28] and even larger ternary recombination rate coefficients were reported for H_3^+ ions in H_2 buffered plasma [29,30]. There is no study on the third-body assisted recombination of H_3^+ ions with electrons with other third bodies than helium or hydrogen. MacDonald et al. [31] studied recombination of H_3^+ ions in neon buffered plasma but the covered

* Corresponding author.

E-mail address: petr.dohnal@mff.cuni.cz (P. Dohnal).

pressure range was too small to observe any dependence on the neon density.

Glosik and coworkers [23,32] pointed out that a long lived excited neutral molecule can be formed during the collision of H_3^+ ion with electron, with lifetimes on the order of tens of picoseconds. This is sufficiently long for this neutral molecule to undergo, at conditions typical for afterglow experiments, additional collisions with buffer gas particles. Unfortunately, there is no fully quantum mechanical study on third-body assisted recombination of H_3^+ ions.

In this paper we utilize the Cryogenic Stationary Afterglow apparatus equipped with a Cavity Ring-Down Spectrometer (Cryo-SA-CRDS) to study the recombination of H_3^+ ions with electrons in the neon buffered plasma. In the first part of the paper, the simultaneous measurements of electron and ion number densities in the afterglow plasma and the method for recombination rate coefficient determination will be described with H_3^+ in helium buffered plasma as a test case. In the second part of the paper this approach will be utilized for determination of ternary recombination rate coefficient for recombination of H_3^+ ions with electrons with neon as a third body.

2. Experiment

The Cryogenic Stationary Afterglow apparatus with a Cavity Ring Down Spectrometer (Cryo-SA-CRDS) was used in the present experiments. The simplified scheme of the apparatus is shown in Fig. 1 and a detailed description can be found in Ref. [33]. The main diagnostic technique is the continuous wave Cavity Ring-Down Spectroscopy (cw-CRDS) developed originally by Romanini et al. [34] which enables us to probe the time evolutions of the number densities of the studied ions in discharge and afterglow plasma.

The plasma is ignited in a discharge tube made of monocrystalline sapphire with an inner diameter ~ 2.5 cm and a length of 20 cm. The plano-concave mirrors (reflectivity 99.99% or better) of the CRD spectrometer are attached on each end of the discharge tube 82 cm apart. The tube material was chosen due to the high thermal conductivity of monocrystalline sapphire at low temperatures.

A distributed feedback (DFB) laser diode centered at 1381 nm was used as a light source to cover the second overtone transitions originating from the lowest energy para and from the two lowest energy ortho rotational states of H_3^+ . The light exiting the optical cavity is detected by an InGaAs avalanche photodiode. The wavelength is measured by EXFO WA-1650 wavemeter.

The H_3^+ ions are formed in the microwave discharge ignited either in a He/Ar/ H_2 or in a Ne/Ar/ H_2 mixture with typical composition $10^{17}/10^{14}/10^{14}$ cm^{-3} . The buffer gas flow velocity is ~ 1 m s^{-1} and the used gases are purified prior to entering the discharge tube by passing through liquid nitrogen cold traps. For details on the chemical kinetics in helium buffered plasmas containing argon and hydrogen see Ref. [30]. The formation of H_3^+ ions in neon buffered plasma will be discussed later.

The microwave resonator is made of two solid aluminium blocks and does not have any movable parts. To ignite the microwave discharge, it is necessary to tune the frequency of the microwave radiation to the resonant frequency of the microwave resonator cavity using the TM_{010} mode. A solid-state microwave source was built to produce microwave radiation in the frequency range of 2.4–2.6 GHz with a power of up to 20 W and a switching time of less than 1 μs (for details see Ref. [33]).

The discharge tube is connected by copper braids to the body of the microwave resonator that is attached to the Sumitomo RDK 408S cold head, which enables experiments in the temperature range of 30–300 K [33,35]. The discharge tube with the mirrors of the CRD spectrometer and the cold head are placed in an external vacuum chamber to provide thermal insulation. In order to minimize the heat losses, this vacuum chamber is pumped down to pressure below 10^{-4} Pa.

We added the time resolved microwave diagnostics to the Cryo-SA-CRDS for electron number density measurements. The method is based on tracing the changes of the resonance frequency of a resonator [36]. The shift of the resonance frequency of a cylindrical resonator is proportional to the electron number density n_e on the axis of the discharge tube of Cryo-SA-CRDS:

$$n_e = \Delta f_r f_r \frac{2\pi m_e}{e_0^2} \frac{\int_V E^2 dV}{\int_V J_0\left(\frac{2.405}{r_1} r\right) E^2 dV}, \quad (1)$$

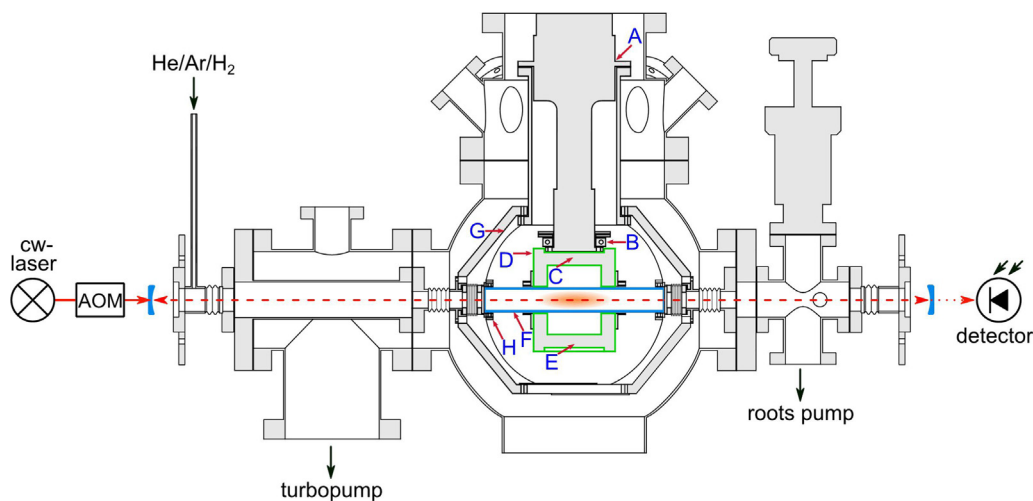


Fig. 1. The Cryogenic Stationary Afterglow apparatus in conjunction with a continuous wave Cavity Ring-Down absorption Spectrometer (Cryo-SA-CRDS). Temperature sensors are denoted by blue capital letters. The discharge tube is drawn as a dark blue frame. The microwave resonator is around the tube and shown by green frame. The Sumitomo RDK 408S cold head is placed above the microwave resonator. The laser light is controlled by the acousto-optic modulator (AOM) and goes through the first mirror, a discharge tube and the second mirror at the other side of the discharge tube and then to the detector. (For interpretation of the references to colour in this figure legend, the reader is referred to the web version of this article.)

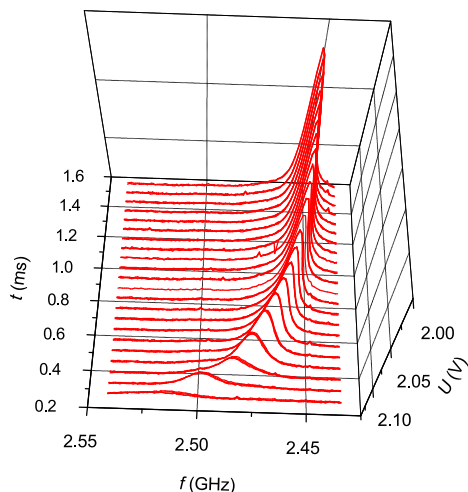


Fig. 2. Time evolution of the frequency response of resonant cavity obtained in helium buffered plasma at $T = 200$ K, $[\text{He}] = 3 \times 10^{17} \text{ cm}^{-3}$, $[\text{Ar}] = 2 \times 10^{14} \text{ cm}^{-3}$ and $[\text{H}_2] = 4.6 \times 10^{13} \text{ cm}^{-3}$. The frequency position of the center of each peak-like feature gives resonant frequency of the microwave resonator at a particular time in the afterglow and through Eq. (1) the electron number density.

where f_r is the resonance frequency, Δf_r is the shift in the resonance frequency caused by the plasma, E is the intensity of the high-frequency field in the resonator, V is the resonator volume, V_r is the volume of plasma tested, J_0 is the Bessel function of zeroth order, m_e and e_0 are the mass and charge of the electron and r_1 is the inner radius of the discharge tube, while r is a distance from the axis [37]. An equivalent circuit finite difference time domain method [38,39] as implemented in the openEMS software [40] was used to calculate the resonant frequencies of the cavity and other quantities in Eq. (1) based on the actual geometry of the cavity with the inserted discharge tube represented on a three-dimensional cylindrical mesh. The details of the calculations can be found in Ref. [33].

The aluminium body of the microwave resonator forms a cylindrical cavity (its rotational axis is coaxial with the optical axis) with two loop microwave antennas on opposite sides of it. The first antenna is used to transmit the microwave radiation both for ignition of the discharge (~ 20 W of input power) and for probing of the resonance frequency of the microwave cavity (~ 1 mW) while the second antenna is connected to the microwave power detector. The probing microwaves are generated using a SLSM5 synthesizer from Luff Research Inc in the frequency range of 2.4 GHz to 2.6 GHz and the entry of the microwaves into the resonator is controlled by a fast absorptive PIN diode switch (SR-DA10-1S from Universal Microwave Components Corp.).

In each discharge cycle the probing microwaves are set to a specific frequency and switched on for only ten microseconds at a chosen time relative to the onset of the discharge. In this way we are able to cover the time evolution of the resonance frequency of the resonant cavity in the afterglow plasma and at the same time ensure that the microwaves do not significantly influence the decay of the plasma in the afterglow. An example of the measured time evolution of the frequency response of the resonant cavity is shown in Fig. 2.

3. Results and discussion

3.1. Data analysis

The two second overtone transitions $3\nu_2^1(2,0) \leftarrow 0\nu_2^0(1,0)$ and $3\nu_2^1(2,1) \leftarrow 0\nu_2^0(1,1)$, which originate in the lowest rotational

states of H_3^+ with ortho and para nuclear spin state symmetry, respectively, were used in present study. The numbers in parentheses denote the rotational quantum number J and the quantum number $G = |K - l|$, where K is the quantum number for projection of the rotational angular momentum \vec{J} on the body-frame symmetry axis and l is the quantum number for vibrational angular momentum. For further details about symmetry and notation see Ref. [41]. The relevant rotational state number densities were calculated from measured absorbances using energies and Einstein coefficients from Ref. [42]. Based on previous studies that used the same or similar experimental setup and experimental conditions, [43,35] we can safely assume that the rotational states of H_3^+ are populated in accordance with the thermal equilibrium at a given temperature. Therefore, the number density of the H_3^+ ions presented through this text was determined under the assumption of thermal population of states using the strongest available transition $3\nu_2^1(2,0) \leftarrow 0\nu_2^0(1,0)$ from the measured number density of the ortho $\text{H}_3^+(1,0)$ state. The transition $3\nu_2^1(2,1) \leftarrow 0\nu_2^0(1,1)$ was used only to confirm thermal ratio of the ortho and para nuclear spin states.

The time evolution of the number density of H_3^+ ions in the afterglow plasma can be, assuming that there is no formation of H_3^+ ions in the afterglow, described by the formula:

$$\frac{dn_{\text{H}_3^+}}{dt} = -\alpha_{\text{eff}} n_{\text{H}_3^+} n_e - \frac{n_{\text{H}_3^+}}{\tau}, \quad (2)$$

where $n_{\text{H}_3^+}$ and n_e denote the H_3^+ ion number density and the electron number density, respectively and α_{eff} is the effective recombination rate coefficient. The subscript “eff” denotes the possible dependence of the measured recombination rate coefficient on the buffer gas number density [23]:

$$\alpha_{\text{eff}} = \alpha_0 + K_{\text{M}}[\text{M}], \quad (3)$$

where α_0 is the binary recombination rate coefficient appropriate for low density environments such as interstellar gas clouds and K_{M} is the ternary recombination rate coefficient with $[\text{M}]$ being the number density of the particular third body M. Symbol τ in Eq. (2) is the time constant that describes losses by the ambipolar diffusion and by ion-neutral reactions:

$$\frac{1}{\tau} = \frac{1}{\tau_{\text{D}}} + \frac{1}{\tau_{\text{R}}}, \quad (4)$$

where τ_{D} is the time constant for losses of charged particles by the ambipolar diffusion and the time constant τ_{R} represents the losses of H_3^+ ions by ion-neutral reactions. Under current experimental conditions (pressure, temperature, reactant number density) this term mainly arises from the formation of fast recombining H_5^+ ions in the three body association reaction of H_3^+ with H_2 and He or Ne (in helium or neon buffered plasma):



The main processes that influence the time evolution of the electron number density in afterglow plasma containing H_3^+ ions are the recombination with ions and the ambipolar diffusion:

$$\frac{dn_e}{dt} = -\alpha_{\text{eff}} n_{\text{H}_3^+} n_e - n_e \sum_i \alpha_i n_i - \frac{n_e}{\tau_{\text{D}}}, \quad (7)$$

where α_i and n_i are the recombination rate coefficients and number densities of ions other than H_3^+ present in the afterglow plasma. According to the model of chemical kinetics [30] in a helium buffered afterglow plasma at conditions used in present experiments these ions will be mainly H_5^+ .

The recombination rate coefficient for the studied ions can be, in principle, obtained by measuring the time evolutions of H_3^+ and electron number densities and by numerically solving a set of corresponding differential equation. This is possible even at conditions when the H_3^+ ions are not the dominant ionic species in the afterglow plasma. The main drawback of such an approach is that it is necessary to make assumptions about other processes in the afterglow. This is not a problem in a helium buffered plasma with admixtures of argon and hydrogen where conditions can be set, such as predominantly only H_3^+ and H_5^+ ions are present [30]. The corresponding set of differential equations then consists of only Eq. (2) for H_3^+ , Eq. (7) for electrons and equation:

$$\frac{dn_{\text{H}_5}}{dt} = -\alpha_5 n_{\text{H}_5} n_e - \frac{n_{\text{H}_5}}{\tau_{\text{DH}_5}} + \frac{n_{\text{H}_3}}{\tau_{\text{R}}}, \quad (8)$$

for H_5^+ ions, where n_{H_5} is their number density and α_5 is the corresponding recombination rate coefficient. In this case, $\tau_{\text{R}} = 1/(k_3[\text{H}_2][\text{He}])$ where k_3 is the reaction rate coefficient for the three body association reaction (5).

When the underlying chemical kinetics is not well known, as in the case of neon buffered plasmas, we opted for a direct integration of Eq. (2) yielding for H_3^+ number density in time t_i :

$$n_{\text{H}_3}(t_i) = n_{\text{H}_3}(t_0) e^{-\alpha_{\text{eff}} X(t_i) - \frac{1}{\tau} Y(t_i)}, \quad (9)$$

where $n_{\text{H}_3}(t_0)$ is the initial density of H_3^+ ions,

$$X(t_i) = \int_{t_0}^{t_i} n_e(t) dt, \quad (10)$$

and

$$Y(t_i) = t_i - t_0, \quad (11)$$

As $n_{\text{H}_3}(t_i)$, $X(t_i)$ and $Y(t_i)$ are measured quantities or may be calculated from the measured ones, we simply find the values of the parameters $n_{\text{H}_3}(t_0)$, α_{eff} and τ that fulfill Eq. (9) in the least square sense.

3.2. H_3^+ recombination in ambient helium gas

Guided by the model of the chemical kinetics [30], we have deliberately chosen the conditions so as to ensure that H_3^+ ions will be dominant in the helium buffered early afterglow plasma. Thus the H_3^+ number density obtained by the cavity ring-down spectrometry and the electron number density evaluated from the shift of the resonant frequency of the microwave resonator should be equal to each other within the uncertainty of the measurement at the beginning of the plasma decay.

Examples of the time evolution of the electron and H_3^+ number densities obtained in a helium buffered afterglow plasma at $T = 200$ K are shown in Fig. 3. Here and thorough the text the stated temperature was measured by sensor H in Fig. 1 i. e. at the discharge tube holder. As discussed in Ref. [33], and also confirmed in this study, the kinetic temperature of the H_3^+ ions obtained from the Doppler broadening of the absorption lines is very close to the one measured by this sensor. The data were obtained using different number densities of hydrogen gas and fitted using the integration method described above. The effective recombination rate coefficients obtained in this way are equal to each other within the statistical uncertainty of the fit even at conditions where the measured electron and ion number density are substantially affected by the formation of rapidly recombining H_5^+ ions in reaction (5).

The values of the binary and ternary recombination rate coefficients previously obtained for H_3^+ ions in the helium buffered

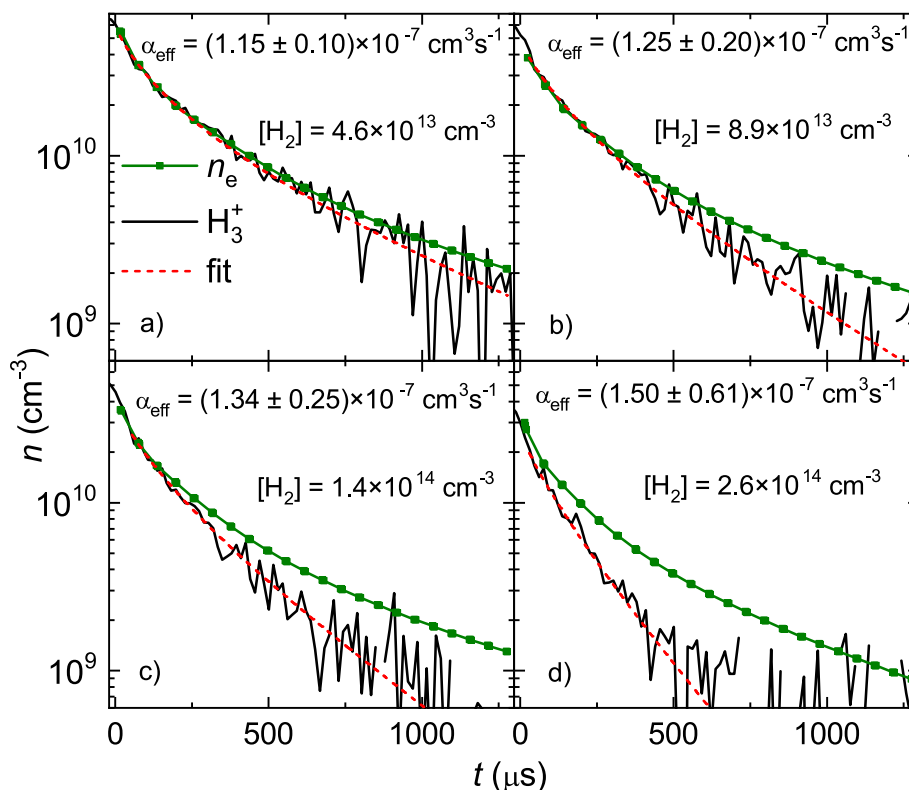


Fig. 3. Measured time evolutions of the electron (squares) and H_3^+ (full line) number densities in the helium buffered afterglow plasma at different number densities of hydrogen. The dashed line denotes fit of the data using Eq. (9). For details on the fitting procedure see in text. The obtained effective recombination rate coefficients are written in each panel and the displayed error is the statistical error of the fit. The experiments were performed at $T = 200$ K, $[\text{He}] = 3 \times 10^{17} \text{ cm}^{-3}$ and $[\text{Ar}] = 2 \times 10^{14} \text{ cm}^{-3}$ with $[\text{H}_2]$ in the range of 4.6×10^{13} to $2.6 \times 10^{14} \text{ cm}^{-3}$.

plasma at 200 K are $\alpha_0 = (6.9 \pm 2.0) \times 10^{-8} \text{ cm}^3 \text{ s}^{-1}$ and $K_{\text{He}} = (1.6 \pm 0.5) \times 10^{-25} \text{ cm}^6 \text{ s}^{-1}$, respectively [44,45]. By substituting these values into Eq. (3) we get $\alpha_{\text{eff}}(200 \text{ K}, [\text{He}] = 3 \times 10^{17} \text{ cm}^{-3}) = (1.17 \pm 0.25) \times 10^{-7} \text{ cm}^3 \text{ s}^{-1}$ in an excellent agreement with present values displayed in Fig. 3. We performed several measurements at $T = 115 \text{ K}$, $T = 150 \text{ K}$ and $T = 200 \text{ K}$ with $[\text{He}]$ in the range from 1×10^{17} to $3 \times 10^{17} \text{ cm}^{-3}$ and $[\text{H}_2]$ between 4×10^{13} and $5 \times 10^{14} \text{ cm}^{-3}$. The results show that simultaneous measurement of H_3^+ and electron number densities combined with the fitting procedure described above enables determination of reliable recombination rate coefficients even at conditions where the standard approach (e.g. $1/n_e$ plot [13]), relying on the studied ions being dominant in the afterglow, fails.

3.3. Determination of the A coefficient for the $3v_2^1(2,0) \leftarrow 0v_2^0(1,0)$ overtone transition

The ability of the present experimental setup to probe the time evolutions of both the electron number density and of the absorbance pertaining to the specific transition may be utilized in some cases to measure the corresponding absorption line strength. The mentioned model of the chemical kinetics [30] predicts that at low hydrogen number densities (e.g. for data plotted in panel a) of Fig. 3) the early afterglow plasma will be dominated by H_3^+ ions. Assuming thermal population of states and using the obtained electron number density as an estimate of the overall H_3^+ ion number density while taking into account the particular absorption line profile, one can calculate the Einstein A coefficient for the $3v_2^1(2,0) \leftarrow 0v_2^0(1,0)$ transition from the definition in Ref. [46] as:

$$A = \frac{S_{\text{abs}}}{n_e L} \frac{8\pi\nu^2 c Q(T)}{g_u} \frac{h c E_1}{e^{k_B T}} \sqrt{\frac{\pi}{4 \ln 2}} w = \frac{S_{\text{abs}}}{n_e} C_A [\text{s}^{-1}], \quad (12)$$

where S_{abs} is the absorbance measured at the centre of the Doppler broadened absorption line with full width at half maximum (FWHM) w in cm^{-1} , $\nu = 7241.245 \text{ cm}^{-1}$ is the transition wavenumber and $E_1 = 86.9591 \text{ cm}^{-1}$ is the energy of the lower state. $Q = 20.66$ is the partition function at $T = 200 \text{ K}$, c denotes the speed of light in cm s^{-1} , while h and k_B are the Planck and Boltzmann constants, respectively. The statistical weight of the upper state is $g_u = 20$ and $L = 6 \text{ cm}$ is the discharge column length. The upper and lower state energies and the partition function were taken from Ref. [47]. Fig. 4 shows the Einstein A coefficient calculated from Eq. (12) using the data plotted in panel a) of Fig. 3. The measured electron number density was linearly interpolated to get the same timescale for n_e and S_{abs} . The resulting $A_{\text{present}} = (8.7 \pm 0.5) \text{ s}^{-1}$ was calculated from the values in the first $600 \mu\text{s}$ of the afterglow and is in good agreement with the most recent theoretical value $A_{\text{theory}} = 9.0758 \text{ s}^{-1}$ [42].

3.4. Recombination of H_3^+ ions with electrons in neon buffer gas

In order to study the third-body assisted recombination of H_3^+ ions in the neon buffer gas, the discharge was periodically ignited in a mixture of Ne, Ar and H_2 with number densities in the range of $3 \times 10^{17} - 1.2 \times 10^{18} \text{ cm}^{-3}$ for neon, $5 \times 10^{13} - 2 \times 10^{14} \text{ cm}^{-3}$ for argon and $3 \times 10^{13} - 1 \times 10^{14} \text{ cm}^{-3}$ for hydrogen. There is one previous study of H_3^+ recombination in neon buffer gas performed at a gas temperature of 240 K using the stationary afterglow technique with the electron number density being measured by microwave diagnostics and with the mass spectrometric identification of recombining ions [31]. In that experiment, the neon number density was in the range of $5.6 - 8.0 \times 10^{17} \text{ cm}^{-3}$ and the hydrogen

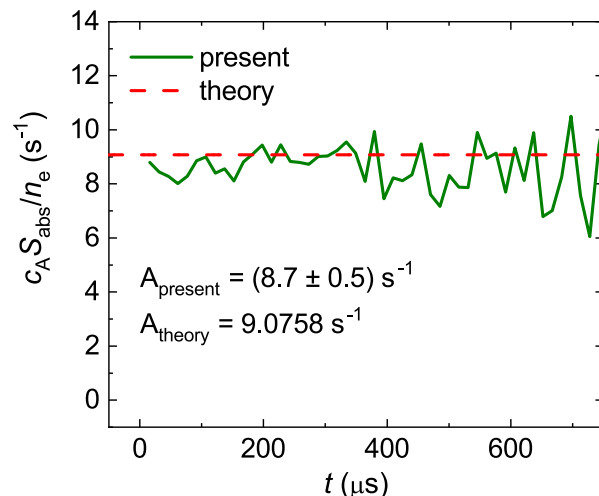


Fig. 4. The Einstein A coefficients for $3v_2^1(2,0) \leftarrow 0v_2^0(1,0)$ transition calculated using Eq. (12) for the data corresponding to the panel a) of Fig. 3 (full line). The dashed line denotes the theoretical value $A_{\text{theory}} = 9.0758 \text{ s}^{-1}$ from Ref. [42].

number density was $4 \times 10^{13} \text{ cm}^{-3}$. The recombination rate coefficient obtained in that study [31] was $\alpha = (1.6 \pm 0.3) \times 10^{-7} \text{ cm}^3 \text{ s}^{-1}$, a value very close to that obtained in the helium buffered plasmas at the same pressure and temperature [23,30]. They were unable to extend their measurements to lower temperatures as the plasma was increasingly dominated by H_5^+ ions. Note that the timescale of their experiment was on the order of tens of ms [48] while in our case it is on the order of hundreds of μs which is required to minimize the influence of H_5^+ ions formed in reaction (6).

In the present experiment the Ne^+ , Ar^+ and H_2^+ ions are produced in the discharge. A series of fast ion molecule reactions with hydrogen converts Ar^+ and H_2^+ ions to H_3^+ [30], while Ne_2^+ ions are formed in the three body association reaction:



At 80 K the three body reaction rate coefficient reported for reaction (13) by Johnsen et al. [49] is $k(\text{Ne}^+ \text{P}_{3/2}) = (12 \pm 3) \times 10^{-32} \text{ cm}^6 \text{ s}^{-1}$ and $k(\text{Ne}^+ \text{P}_{1/2}) = (3.5 \pm 1.8) \times 10^{-32} \text{ cm}^6 \text{ s}^{-1}$ for the two lowest fine structure states of neon ion. Ne_2^+ reacts with H_2 [50]:



The rate for reaction (14) obtained at 200 K is $1.1 \times 10^{-10} \text{ cm}^3 \text{ s}^{-1}$. While NeH^+ is the main product of reaction (14), other minority products (Ne_2H^+ and NeH_2^+) were also reported in Ref. [50]. These react further with H_2 with reaction rate coefficients $9.6 \times 10^{-11} \text{ cm}^3 \text{ s}^{-1}$ and less than $4.0 \times 10^{-13} \text{ cm}^3 \text{ s}^{-1}$, respectively. The main bottleneck for the production of H_3^+ is the reaction of NeH^+ with H_2 :



with a very low reaction rate coefficient of $2 \times 10^{-11} \text{ cm}^3 \text{ s}^{-1}$ [50]. At $[\text{H}_2] = 5 \times 10^{13} \text{ cm}^{-3}$, the characteristic time constant for reaction (15) will be 1 ms. Given the timescale of the present experiments, only negligible amount of the H_3^+ ions will be produced during the afterglow in process (15) and we do not take this production into account in the data analysis. As a consequence, the early afterglow plasma contains a mixture of ions: H_3^+ that was formed in discharge in ion molecule reactions involving Ar^+ , H_2^+ and H_2 , then NeH^+ pro-

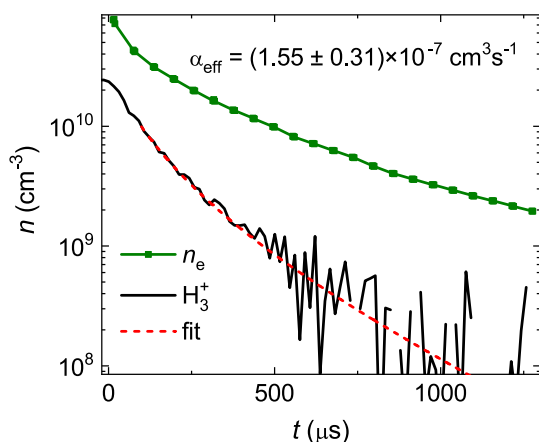


Fig. 5. Example of time evolution of electron (squares) and H_3^+ (full line) number densities measured in a neon buffered afterglow plasma at $T = 110$ K, $[\text{Ne}] = 6.3 \times 10^{17} \text{ cm}^{-3}$, $[\text{Ar}] = 5.4 \times 10^{13} \text{ cm}^{-3}$, $[\text{H}_2] = 1.0 \times 10^{14} \text{ cm}^{-3}$. Fit to the data using Eq. (9) is denoted by a dashed line and the obtained effective recombination rate coefficient is displayed in the figure.

duced from Ne_2^+ by reaction (14), and other minority ions like H_3^+ and NeH_2^+ .

An example of the time evolutions of the H_3^+ and electron number densities in a neon buffered plasma at $T = 110$ K is plotted in Fig. 5. As outlined in the discussion of the chemical kinetics above, H_3^+ is not a dominant ion species in the afterglow. In fact, it accounts for no more than one third of all ions. A similar behavior was observed for data obtained over the entire range of buffer gas and reactant number densities used in the experiment. We fitted the data by Eq. (9) and the resulting dependence of the measured effective recombination rate coefficients on the buffer gas number density is shown in Fig. 6. To obtain the binary and the ternary recombination rate coefficients we fitted this dependence with Eq. (3) yielding $\alpha_0(110 \text{ K}) = (7.0 \pm 1.7) \times 10^{-8} \text{ cm}^3 \text{ s}^{-1}$ and $K_{\text{Ne}}(110 \text{ K}) = (1.8 \pm 0.2) \times 10^{-25} \text{ cm}^6 \text{ s}^{-1}$. A fit of the effective recombination rate coefficients obtained for H_3^+ in helium buffer gas at 125 K is also plotted in the figure for comparison. As can be seen from Fig. 6 the obtained binary and ternary recombination

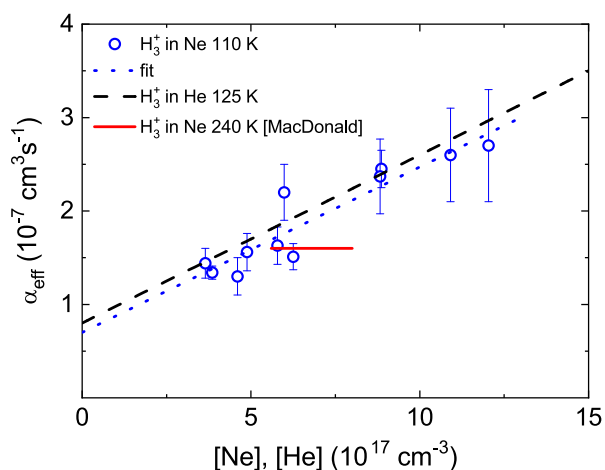


Fig. 6. The dependence of the effective recombination rate coefficients for recombination of H_3^+ ions with electrons on buffer gas number density obtained in the present study in neon buffer gas at 110 K (circles). The fit to the data by Eq. (3) is shown as a dotted line. The values are compared to those reported by Dohmal et al. [43] in helium buffer gas (dashed line) and by MacDonald et al. [31] in neon buffer gas at 240. K (full line).

rate coefficients are very close to those obtained in a helium buffered plasma using a similar experimental setup and conditions [43]. Bates and Khare [24] proposed that the recombination rate of atomic ions in ambient gas will be proportional to the reciprocal reduced mass of the positive ion-buffer gas atom system at low densities and temperatures. This would suggest that the ternary recombination rate coefficients for H_3^+ ions in helium and neon should differ by a factor of 1.5 which is consistent with our data when all uncertainties are taken into account. We note that the theory [24] fails to predict the magnitude of the H_3^+ ternary recombination rate in helium by several orders of magnitude at 300 K, so also this estimate should be taken with a grain of salt.

3.5. Uncertainties and their sources

The statistical uncertainty of the ion number density determination is on the order of 10^9 cm^{-3} , as evidenced by the scatter of the data in Figs. 3 and 5. The systematic uncertainty of the measured ion number density arises mainly from the uncertainty of the discharge column length (estimated as 10%) and from the uncertainties of the used vibrational transition moments that are estimated to be less than 5% [51]. The statistical uncertainty of the obtained electron number density is very small (comparable with the width of the corresponding line in Figs. 3 and 5), whereas the temporal resolution is $2.5 \mu\text{s}$. The systematic uncertainty of the electron number density measurement is largely determined by the precision of the determination of the resonant frequency of the empty cavity and is estimated to be less than $3 \times 10^8 \text{ cm}^{-3}$. The overall systematic uncertainty of the effective recombination rate coefficient determination is estimated to be 15%

4. Conclusions

We have combined a stationary afterglow apparatus equipped with a Cavity Ring-Down spectrometer with time resolved electron number density measurement based on the shift of the resonant frequency of the microwave resonator. The experimental setup was first tested on the recombination of H_3^+ ions in the helium buffer gas at conditions where the underlying ion formation processes were well known [30]. The results have shown that reliable recombination rate coefficients can be obtained even at conditions when the ions of interest are not the dominant ions in the afterglow plasma. The application of the present experimental setup for the determination of Einstein coefficients of observed transitions was demonstrated for the case of the $3v_2(2,0) \leftarrow 0v_2^0(1,0)$ second overtone transition yielding $A_{\text{present}} = (8.7 \pm 0.5) \text{ s}^{-1}$ in excellent agreement with the most recent theoretical prediction of $A_{\text{theory}} = 9.0758 \text{ s}^{-1}$ [42]. The third-body assisted recombination of H_3^+ ions with electrons in a neon gas was studied at $T = 110$ K and the obtained ternary recombination rate coefficient $K_{\text{Ne}}(110 \text{ K}) = (1.8 \pm 0.2) \times 10^{-25} \text{ cm}^6 \text{ s}^{-1}$ is close to the value measured in a helium buffered plasma.

Declaration of Competing Interest

The authors declare that they have no known competing financial interests or personal relationships that could have appeared to influence the work reported in this paper.

Acknowledgments

This work was partly supported by the Czech Science Foundation GACR 20-22000S and by Charles University projects GAUK 1162920, GAUK 646218.

References

- [1] J.J. Thomson, Rays of positive electricity, London, Edinburgh, Dublin Philos. Magaz. J. Sci. 21 (122) (1911) 225–249.
- [2] T.R. Hogness, E.G. Lunn, The ionization of hydrogen by electron impact as interpreted by positive ray analysis, Phys. Rev. 26 (1925) 44–55.
- [3] C.A. Coulson, The electronic structure of H_3^+ , Math. Proc. Cambridge Philos. Soc. 31 (2) (1935) 244–259.
- [4] T. Oka, Observation of the infrared spectrum of H_3^+ , Phys. Rev. Lett. 45 (1980) 531–534.
- [5] E. Herbst, W. Klemperer, The Formation and Depletion of Molecules in Dense Interstellar Clouds, Astrophys. J. 185 (1973) 505–534.
- [6] T. Oka, Interstellar H_3^+ , Proc. Natl. Acad. Sci. U.S.A. 103 (33) (2006) 12235–12242.
- [7] P. Drossart, J.-P. Maillard, J. Caldwell, S.J. Kim, J.K.G. Watson, S. Rednyk, W.A. Majewski, M. Hejduk, J. Tennyson, S. Miller, S.K. Atreya, J.T. Clarke, J.H. Waite, R. Wagoner, Detection of H_3^+ on Jupiter, Nature 340 (1989) 539–541.
- [8] T.R. Geballe, M.F. Jagod, T. Oka, Detection of H_3^+ Infrared Emission Lines in Saturn, Astrophys. J. Lett 408 (1993) L109.
- [9] L.M. Trafton, T.R. Geballe, S. Miller, J. Tennyson, G.E. Ballester, Detection of H_3^+ from Uranus, Astrophys. J. Lett. 405 (1993) 761.
- [10] T. Oka, Chemistry, astronomy and physics of H_3^+ , Philos. Trans. Royal Soc. A 370 (1978) (2012) 4991–5000.
- [11] D. Smith, P. Španel, Dissociative recombination of H_3^+ and some other interstellar ions: a controversy resolved, Int. J. Mass Spectrom. 129 (1993) 163–182.
- [12] W. Geppert, M. Larsson, Dissociative recombination in the interstellar medium and planetary ionospheres, Mol. Phys. 106 (16–18) (2008) 2199–2226.
- [13] M. Larsson, A.E. Orel, Dissociative Recombination of Molecular Ions, Cambridge Molecular Science, Cambridge University Press, 2008.
- [14] G. Sundström, J.R. Mowat, H. Danared, S. Datz, L. Broström, A. Filevich, A. Källberg, S. Mannervik, K.G. Rensfelt, P. Sigry, M. af Ugglas, M. Larsson, Destruction rate of H_3^+ by low-energy electrons measured in a storage-ring experiment, Science 263 (5148) (1994) 785–787.
- [15] B.J. McCall, A.J. Huneycutt, R.J. Saykally, N. Djuric, G.H. Dunn, J. Semaniak, O. Novotny, A. Al-Khalili, A. Ehlerding, F. Hellberg, S. Kalhori, A. Neau, R.D. Thomas, A. Paal, F. Österdahl, M. Larsson, Dissociative recombination of rotationally cold H_3^+ , Phys. Rev. A 70 (2004) 052716.
- [16] M.T. Leu, M.A. Biondi, R. Johnsen, Measurements of recombination of electrons with H_3^+ and H_5^+ ions, Phys. Rev. A 8 (1973) 413–419.
- [17] N.G. Adams, D. Smith, E. Alge, Measurements of dissociative recombination coefficients of H_3^+ , HCO^+ , N_2H^+ , and CH_5^+ at 95 and 300 K using the FALP apparatus, J. Chem. Phys. 81 (4) (1984) 1778–1784.
- [18] T. Amano, The dissociative recombination rate coefficients of H_3^+ , HN_2^+ , and HCO^+ , J. Chem. Phys. 92 (11) (1990) 6492–6501.
- [19] J. Glosik, O. Novotny, A. Pysanenko, P. Zakouril, R. Plasil, P. Kudrna, V. Poterya, The recombination of H_3^+ and H_5^+ ions with electrons in hydrogen plasma: dependence on temperature and on pressure of H_2 , Plasma Sources Sci. Technol. 12 (4) (2003) S117–S122.
- [20] H.H. Michels, R.H. Hobbs, Low-temperature dissociative recombination of $e + H_3^+$, Astrophys. J. Lett. 286 (1984) L27–L29.
- [21] V. Kokoouline, C.H. Greene, B.D. Esry, Mechanism for the destruction of H_3^+ ions by electron impact, Nature 412 (2001) 891–894.
- [22] C. Jungen, S.T. Pratt, Jahn-teller interactions in the dissociative recombination of H_3^+ , Phys. Rev. Lett. 102 (2009) 023201.
- [23] J. Glosik, I. Korolov, R. Plasil, O. Novotny, T. Kotrik, P. Hlavenka, J. Varju, I. Mikhailov, V. Kokoouline, C. Greene, Recombination of H_3^+ ions in the afterglow of a He–Ar– H_2 plasma, J. Phys. B–At. Mol. Opt. Phys. 41 (19) (2008) 191001.
- [24] D.R. Bates, S.P. Khare, Recombination of positive ions and electrons in a dense neutral gas, Proc. Phys. Soc. 85 (2) (1965) 231–243.
- [25] M.R. Flannery, Transport-collisional master equations for termolecular recombination as a function of gas density, J. Chem. Phys. 95 (11) (1991) 8205–8226.
- [26] J. Glosik, I. Korolov, R. Plasil, T. Kotrik, P. Dohnal, O. Novotny, J. Varju, S. Roucka, C. Greene, V. Kokoouline, Binary and ternary recombination of D_3^+ ions with electrons in He– D_2 plasma, Phys. Rev. A 80 (4) (2009) 042706.
- [27] P. Dohnal, A. Kálosi, R. Plašil, S. Roucka, A. Kovalenko, S. Rednyk, R. Johnsen, J. Glosik, Binary and ternary recombination of H_2D^+ and HD_2^+ ions with electrons at 80 K, Phys. Chem. Chem. Phys. 18 (34) (2016) 23549–23553.
- [28] R. Plašil, P. Dohnal, A. Kálosi, S. Roucka, R. Johnsen, J. Glosik, Stationary afterglow measurements of the temperature dependence of the electron–ion recombination rate coefficients of H_2D^+ and HD_2^+ in He/Ar/ H_2 / D_2 gas mixtures at $T = 80$ – 145 K, Plasma Sources Sci. Technol. 26 (3) (2017) 035006.
- [29] P. Dohnal, P. Rubovic, A. Kalosi, M. Hejduk, R. Plasil, R. Johnsen, J. Glosik, H_2 -assisted ternary recombination of H_3^+ with electrons at 300 K, Phys. Rev. A 90 (4) (2014) 042708.
- [30] J. Glosik, P. Dohnal, P. Rubovic, A. Kalosi, R. Plasil, S. Roucka, R. Johnsen, Recombination of H_3^+ ions with electrons in He/ H_2 ambient gas at temperatures from 240 K to 340 K, Plasma Sources Sci. Technol. 24 (6) (2015) 065017.
- [31] J.A. Macdonald, M.A. Biondi, R. Johnsen, Recombination of electrons with H_3^+ and H_5^+ ions, Planet. Space Sci. 32 (5) (1984) 651–654.
- [32] J. Glosik, R. Plasil, I. Korolov, T. Kotrik, O. Novotny, P. Hlavenka, P. Dohnal, J. Varju, V. Kokoouline, C. Greene, Temperature dependence of binary and ternary recombination of H_3^+ ions with electrons, Phys. Rev. A 79 (5) (2009) 052707.
- [33] R. Plašil, P. Dohnal, Á. Kálosi, Š. Roučka, D. Shapko, S. Rednyk, R. Johnsen, J. Glosik, Stationary afterglow apparatus with CRDS for study of processes in plasmas from 300 K down to 30 K, Rev. Sci. Instrum. 89 (6) (2018) 063116.
- [34] D. Romanini, A. Kachanov, N. Sadeghi, F. Stoeckel, CW cavity ring down spectroscopy, Chem. Phys. Lett. 264 (3) (1997) 316–322.
- [35] P. Dohnal, D. Shapko, A. Kálosi, M. Kassayová, S. Roucka, S. Rednyk, R. Plašil, M. Hejduk, J. Glosik, Towards state selective recombination of H_3^+ under astrophysically relevant conditions, Faraday Discuss. 217 (2019) 220–234.
- [36] S.C. Brown, D.J. Rose, Methods of measuring the properties of ionized gases at high frequencies. I. measurements of Q, J. Appl. Phys. 23 (7) (1952) 711–718.
- [37] M. Sicha, J. Gajdusek, S. Veprek, Comparison of microwave and probe methods of plasma diagnostics, Br. J. Appl. Phys. 17 (11) (1966) 1511–1514.
- [38] W.K. Gwarek, Analysis of an arbitrarily-shaped planar circuit a time-domain approach, IEEE Trans. Microw. Theory. Tech. 33 (10) (1985) 1067–1072.
- [39] A. Rennings, J. Mosig, C. Caloz, D. Erni, P. Waldow, Equivalent circuit (EC) FDTD method for the modeling of surface plasmon based couplers, J. Comput. Theor. Nanosci. 5 (2008) 690–703.
- [40] T. Liebige, A. Rennings, S. Held, D. Erni, openEMS – a free and open source equivalent-circuit (EC) FDTD simulation platform supporting cylindrical coordinates suitable for the analysis of traveling wave MRI applications, Int. J. Numer. Model. Electron. Networks Devices Fields 26 (6) (2013) 680–696.
- [41] K.N. Crabtree, B.J. McCall, On the symmetry and degeneracy of H_3^+ , J. Phys. Chem. A 117 (39) (2013) 9950–9958.
- [42] I.I. Mizus, A. Alijah, N.F. Zobov, L. Lodi, A.A. Kyuberis, S.N. Yurchenko, J. Tennyson, O.L. Polyansky, ExoMol molecular line lists – XX. A comprehensive line list for H_3^+ , Mon. Not. R. Astron. Soc. 468 (2) (2017) 1717–1725.
- [43] P. Dohnal, M. Hejduk, J. Varju, P. Rubovic, S. Roucka, T. Kotrik, R. Plasil, J. Glosik, R. Johnsen, Binary and ternary recombination of para- H_3^+ and ortho- H_3^+ with electrons: State selective study at 77–200 K, J. Chem. Phys. 136 (24) (2012) 244304.
- [44] P. Rubovic, P. Dohnal, M. Hejduk, R. Plašil, J. Glosik, Binary recombination of H_3^+ and D_3^+ ions with electrons in plasma at 50–230 K, J. Phys. Chem. A 117 (39) (2013) 9626–9632.
- [45] R. Johnsen, P. Rubovic, P. Dohnal, M. Hejduk, R. Plašil, J. Glosik, Ternary recombination of H_3^+ and D_3^+ with electrons in He– H_2 (D_2) plasmas at temperatures from 50 to 300 K, J. Phys. Chem. A 117 (39) (2013) 9477–9485.
- [46] L. Rothman, C. Rinsland, A. Goldman, S. Massie, D. Edwards, J.-M. Flaud, A. Perrin, C. Camy-Peyret, V. Dana, J.-Y. Mandin, J. Schroeder, A. McCann, R. Gamache, R. Wattson, K. Yoshino, K. Chance, K. Jucks, L. Brown, V. Nemtchinov, P. Varanasi, The HITRAN molecular spectroscopic database and HAWKS (HITRAN atmospheric workstaton): 1996 edition, J. Quant. Spectrosc. Radiat. Transf. 60 (5) (1998) 665–710.
- [47] L. Neale, S. Miller, J. Tennyson, Spectroscopic Properties of the H_3^+ Molecule: A New Calculated Line List, Astrophys. J. Lett. 464 (1996) 516.
- [48] J.A. Macdonald, M.A. Biondi, R. Johnsen, Electron temperature dependence of the dissociative recombination of Ne_3^+ ions with electrons, J. Phys. B: At. Mol. Phys. 16 (22) (1983) 4273–4280.
- [49] R. Johnsen, A. Chen, M.A. Biondi, Three-body association reactions of He^+ , Ne^+ , and Ar^+ ions in their parent gases from 78 to 300 K, J. Chem. Phys. 73 (4) (1980) 1717–1720.
- [50] N.G. Adams, D.K. Bohme, E.E. Ferguson, Reactions of He_2^+ , Ne_2^+ , Ar_2^+ , and rare-gas hydride ions with hydrogen at 200 K, J. Chem. Phys. 52 (10) (1970) 5101–5105.
- [51] Jonathan Tennyson, private communication, 2016.

Recombination of vibrationally cold N_2^+ ions with electrons

Uvarova L., Dohnal P., Kassayová M., Saito S., Rednyk S., Roučka Š., Plašil R.,
Glosík J.

Prepared for publication in *J. Geophys. Res. Atmos.*

1
2
3
4
5
6
7
8
9
10
11
12
13

Recombination of vibrationally cold N_2^+ ions with electrons

Liliia Uvarova¹, Petr Dohnal¹, Miroslava Kassayová¹, Serhiy Rednyk¹, Štěpán Roučka¹, Radek Plašil¹, Rainer Johnsen², Juraj Glosík¹

¹Faculty of Mathematics and Physics, Department of Surface and Plasma Science, Charles University, Prague, Czech Republic
²Department of Physics and Astronomy, University of Pittsburgh, Pittsburgh, Pennsylvania 15260, US

Key Points:

- electron-ion recombination
- N_2^+
- Cavity Ring-Down Spectroscopy

content...

Corresponding author: Petr Dohnal, petr.dohnal@mff.cuni.cz

Abstract

The recombination of vibrationally cold N_2^+ ions with electrons was studied in the temperature range of 140 – 250 K. A cryogenic stationary afterglow apparatus equipped with cavity ring-down spectrometer and microwave diagnostics was utilised to probe *in situ* the time evolutions of number densities of particular rotational and vibrational states of N_2^+ ions and of electrons. The obtained value of the recombination rate coefficient for the recombination of the vibrational ground state of N_2^+ with electrons is $\alpha_{\text{N}_2^+} = (2.95 \pm 0.50) \times 10^{-7} (300/T)^{(0.28 \pm 0.07)} \text{ cm}^3 \text{ s}^{-1}$.

Plain Language Summary

[enter your Plain Language Summary here or delete this section]

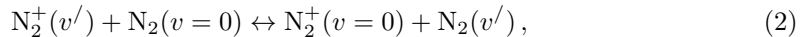
1 Introduction

Molecular nitrogen is the most abundant gas in the Earth atmosphere and also major component of the atmospheres of other solar system bodies such as Pluto (Krasnopolsky, 2020), Titan (Krasnopolsky, 2014) or Triton (Elliot et al., 2000). It is one of the main species in ices covering surfaces of trans-Neptunian objects (Young et al., 2020). As a result, N_2^+ is a main molecular ion in the Earth atmosphere (Lin & Ilie, 2022) as well as in the atmospheres of Titan (Lammer et al., 2000) and Triton (Yung & Lyons, 1990). It is also an important element in many technical and industrial processes (Sharma & Saikia, 2008; Morozov et al., 2016; Sakakura et al., 2019; Holcomb & Schucker, 2020) and in nitrogen containing plasmas. Dissociative recombination of N_2^+ ions with electrons,



is a key process in ionospheric modelling (Fox & Dalgarno, 1985; Sheehan & St.-Maurice, 2004; Fox, 2005) and has been for more than 70 years subject of many theoretical and experimental studies (Sheehan & St.-Maurice, 2004; Larsson & Orel, 2008).

Deionization of nitrogen plasma was studied in a seminal work by Biondi and Brown (Biondi & Brown, 1949) that served as stimulus for Bates to develop his theory of dissociative recombination (D. R. Bates, 1950). These early experiments were performed without identification of recombining ions and were characterized by strong pressure dependences of the measured recombination rate coefficients. The Biondi group added mass spectrometry to their stationary afterglow setup and reported values of recombination rate coefficient for N_2^+ at 300 K of $2.9 \times 10^{-7} \text{ cm}^3 \text{ s}^{-1}$ (Kasner & Biondi, 1965) and later $1.8 \times 10^{-7} \text{ cm}^3 \text{ s}^{-1}$ (Mehr & Biondi, 1969). The actual vibrational population of the recombining ions was not known. Zipf (Zipf, 1980) using laser induced fluorescence and similar conditions as those in Biondi's experiments reported 87 % of all N_2^+ ions in the ground vibrational state with the inferred value of the recombination rate coefficient for $\text{N}_2^+(v=0)$ being $2.2 \times 10^{-7} \text{ cm}^3 \text{ s}^{-1}$ and higher for $v=1$ and $v=2$ states. Johnsen pointed out (Johnsen, 1987) that the analysis of Zipf's data did not take into account the efficient resonant charge exchange process between N_2^+ ions and nitrogen molecules



and that the measured recombination rate coefficient reflected the high vibrational temperature (~ 1500 K) of the N_2^+ ions. Bates (D. Bates & Mitchell, 1991) reanalyzed Zipf's data with inclusion of charge exchange process (2) and suggested a corrected value of $2.6 \times 10^{-7} \text{ cm}^3 \text{ s}^{-1}$ for the vibrational ground state of N_2^+ at 300 K. The reanalysis also indicated that the value of the recombination rate coefficient would decrease with increasing vibrational excitation of the N_2^+ ions.

The FALP (Flowing Afterglow with Langmuir Probe) experiments by Mahdavi et al., Geoghegan et al. (Mahdavi et al., 1971; Geoghegan et al., 1991) and Canosa et al. (Canosa

et al., 1991) reported values of the recombination rate coefficient for N_2^+ ions at room temperature of $2.2 \times 10^{-7} \text{ cm}^3\text{s}^{-1}$, $2.0 \times 10^{-7} \text{ cm}^3\text{s}^{-1}$ and $2.6 \times 10^{-7} \text{ cm}^3\text{s}^{-1}$, respectively. The advantage of the FALP technique in comparison with stationary afterglow is that the studied ions are produced separately from the discharge and are thus with high probability in their vibrational ground state.

Cunningham and Hobson (Cunningham & Hobson, 1972) used shock tube to measure the temperature dependence of the recombination rate coefficient for the N_2^+ ions in the range of 700 – 2700 K. Despite the high temperatures used in the study, they claimed that the obtained results are for $v = 0$ state of N_2^+ and by extrapolating their data down to 300 K got value of $\alpha = 1.78 \times 10^{-7} \text{ cm}^3\text{s}^{-1}$. Mul and McGowan (Mul & McGowan, 1979) used the merged electron-ion beam technique and obtained the dependence of the recombination rate coefficient $\alpha = 3.6 \times 10^{-7}(T_e/300)^{(-0.5)} \text{ cm}^3\text{s}^{-1}$ for electron temperatures between 100 and 20 000 K (according to refs. (Brian & Mitchell, 1990; Larsson & Orel, 2008) this value should be divided by a factor of two due to calibration error). The internal excitation of the recombining ions was not known. In another merged electron-ion beam study Noren et al. (Noren et al., 1989) employed a radiofrequency ion trap source that could be utilized to control the number of collisions that the ions undergo prior to their injection to the beam line. The obtained value of the recombination rate coefficient for vibrationally cold ions was $0.4 \times 10^{-7} \text{ cm}^3\text{s}^{-1}$, substantially lower than values reported in afterglow experiments, and increased when number of collisions in the ion source decreased – i. e. for vibrationally excited ions. Sheehan et al. in their excellent review (Sheehan & St.-Maurice, 2004) speculated that instead of vibrational quenching, the ions became vibrationally reactivated due to collisions in the ion source. On the other hand, Mitchell (Florescu-Mitchell & Mitchell, 2006) suggested that possible calibration error could explain results of Noren et al. (Noren et al., 1989).

The merged electron-ion beam study of Sheehan et al. (Sheehan & St.-Maurice, 2004) and the ion storage ring experiment CRYRING (Peterson et al., 1998) reported practically identical cross sections for recombination of N_2^+ ions with electrons in a broad energy range. The corresponding recombination rate coefficients for the temperature of 300 K were $1.5 \times 10^{-7} \text{ cm}^3\text{s}^{-1}$ and $1.75 \times 10^{-7} \text{ cm}^3\text{s}^{-1}$, respectively. The latter study also probed vibrational populations of the recombining ions with 46% percent of all N_2^+ ions in the $v = 0$ state, 27% in $v = 1$, 10 % in $v = 2$, and 16% in $v = 3$ state.

Despite the breadth of the available experimental data, the reported values of recombination rate coefficients differ by a factor of two or more at 300 K and there are no experiments with vibrationally cold ions performed for temperatures below 300 K. The majority of the studies, with notable exception of merged electron-ion beam experiment by Noren et al. (Noren et al., 1989), also hint that the recombination rate coefficient decreases with increasing vibrational excitation of the recombining ions (for further discussion see ref. (Sheehan & St.-Maurice, 2004). Unfortunately, of all the studies that were able to determine the vibrational populations of the recombining N_2^+ ions, none was conducted with overwhelming majority of ions in the vibrational ground state.

Dissociative recombination of N_2^+ ions with electrons was extensively studied by Guberman (Guberman, 1991, 2007, 2012, 2013, 2014) using multichannel quantum defect approach (MQDT). His calculations have shown that at elevated temperatures the $v = 0$ state of N_2^+ will recombine with electrons substantially faster than the excited states. At 300 K the predicted ratio between the values of the recombination rate coefficients for the two lowest vibrational states of N_2^+ is less than 1.5 and decreasing with decreasing temperature.

Little (Little et al., 2014) used the framework of the R matrix theory to obtain the recombination rate coefficients for several low lying vibrational states of N_2^+ . This approach was later refined by Abdoulanziz et al. (Abdoulanziz et al., 2021) by taking into account higher kinetic energies of incoming electrons and more vibrational levels of the target molecular ion. Their calculations confirmed Guberman’s results (Guberman, 2014) that $v = 0$

88 state of N_2^+ recombines faster than the vibrationally excited states but the ratio between
 89 recombination rate coefficients for $v = 0$ and $v = 1$ states is predicted to be more than 4 at
 90 the temperature of 300 K and does not significantly change with decreasing temperature.
 91 The obtained absolute value of the recombination rate coefficient for $v = 0$ is also higher
 92 than that from MQDT theory (Guberman, 2014) while the value for the $v = 1$ state is
 93 substantially lower.

94 In this paper we present the results of experimental study on recombination of the
 95 vibrational ground state of N_2^+ ions with electrons performed in the temperature range of
 96 140 – 250 K.

97 2 Experiment

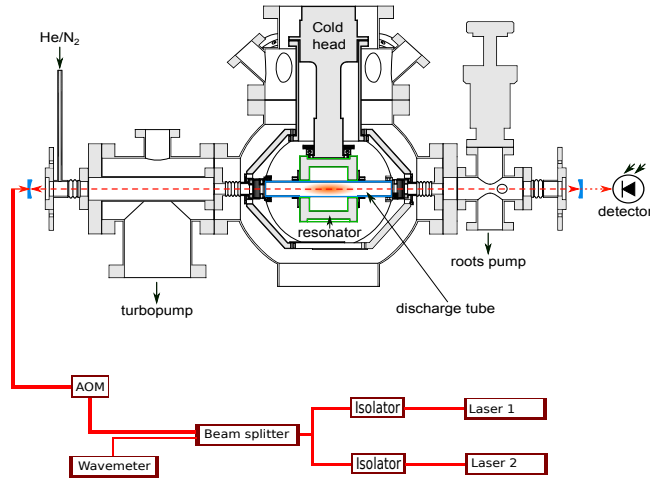


Figure 1. A scheme of the Cryogenic Stationary Afterglow with Cavity Ring-Down Spectrometer (Cryo-SA-CRDS) apparatus. The microwave resonator (green in the figure) is connected to the discharge tube via copper braids. A cold head of the close cycle helium refrigerator Sumitomo RDK 408S is attached to the microwave resonator enabling operating the discharge tube in the temperature range of 30 – 300 K. The laser is switched on and off by passing through an acousto-optic modulator (AOM) and then passes through mode matching optics (not in the figure) before entering the optical cavity formed by two highly reflective plano-concave mirrors. The light leaking through the cavity is collected by an avalanche photodiode.

98 A Cryogenic Stationary Afterglow apparatus with Cavity Ring Down Spectrometer
 99 (Cryo-SA-CRDS) was used in present experiments. The simplified scheme of the experi-
 100 mental setup is shown in Figure 1 and its detailed description can be found e.g. in refs.
 101 (Plašil et al., 2018; Shapko et al., 2021) so only a short overview will be given here. The
 102 gas of the required composition enters the discharge tube on one side and is pumped by a
 103 roots pump on the other side. The plasma is produced in a sapphire discharge tube with
 104 an inner diameter of 2.5 cm and a length of 20 cm by a microwave discharge in a prepared
 105 gas mixture. The discharge tube is cooled by a closed cycle helium refrigerator enabling
 106 operation in the temperature range of 30-300 K. The Cavity Ring-Down Spectrometer based
 107 on an approach developed by Romanini et al. (Romanini et al., 1997) is used to monitor
 108 the time evolutions of the number densities of ions in particular rotational (and vibrational)
 109 state. The optical cavity consists of two highly reflective plano-concave mirrors with a re-
 110 flectivity greater than 99.99 %. The light that leaves the cavity through the second mirror
 111 is detected by an InGaAs avalanche photodiode. For the experiment with N_2^+ ions we used

Table 1. List of transitions of the ${}^2\Sigma_g^+ - {}^2\Pi_u$ Meinel system of N_2^+ used in present study. v'' and v' denote the vibrational quantum number of the lower and upper state, respectively. The transition wavenumbers ν were taken from ref. (dan Wu et al., 2007) for transitions originating in the ground vibrational state of N_2^+ and from ref. (Benesch et al., 1980) for the $\nu = 1$ state. For details on spectroscopic notation see in ref. (dan Wu et al., 2007). Lines denoted by asterisk were overlapping to some degree with nearby lines of N_2 .

Transition	v''	v'	ν (cm^{-1})
$R_{11}(8.5)$	1	3	12358.082
$R_{11}(9.5)$	1	3	12358.354
$Q_{22}(11.5)$	1	3	12358.426
$Q_{22}(9.5)$	1	3	12370.692*
$Q_{21}(18.5)$	1	3	12374.848*
$Q_{22}(10.5)$	0	2	12726.047*
$P_{21}(10.5)$	0	2	12731.879
$Q_{22}(9.5)$	0	2	12731.981
$R_{22}(17.5)$	0	2	12737.000
$P_{21}(9.5)$	0	2	12737.428
$Q_{22}(8.5)$	0	2	12737.524
$P_{21}(8.5)$	0	2	12742.591
$Q_{22}(7.5)$	0	2	12742.675
$P_{22}(3.5)$	0	2	12747.298*
$P_{21}(7.5)$	0	2	12747.370
$Q_{22}(6.5)$	0	2	12747.436

112 optical system consisting of two lasers (L785P090 with central wavelength of 785 nm and
 113 L808P030 centred at 808 nm) covering transitions in the Meinel system of $\text{N}_2^+ {}^2\Sigma_g^+ - {}^2\Pi_u$
 114 originating in the ground and the first vibrational state of the ion. The transitions used in
 115 the present study are listed in Table 1. The Einstein A coefficients for transitions between
 116 different vibronic levels were taken from ref. (Qin et al., 2017) and the state to state line
 117 intensities were calculated following refs. (Rothman et al., 1998; Hansson & Watson, 2005)
 118 using Hönl-London factors from ref. (Earls, 1935), spectroscopic constants from ref. (dan
 119 Wu et al., 2007) and transition wavenumbers published in refs. (Benesch et al., 1980; dan
 120 Wu et al., 2007). The wavelength is measured absolutely by WA-1650 wavemeter.

121 The time evolution of the electron number density in the afterglow plasma is determined
 122 by tracing the changes of the resonant frequency of the microwave resonator. For details see
 123 ref. (Shapko et al., 2021). The N_2^+ ions are formed in a pulsed microwave discharge (10 W,
 124 period of 3 ms, discharge on for few hundred μs) ignited in a He/ N_2 mixture with a typical
 125 composition of $10^{17}/10^{14} \text{ cm}^3$. The buffer gas flow velocity is $\sim \text{ms}^{-1}$ and the used gases are
 126 purified prior to entering the discharge tube by passing through liquid nitrogen cold traps.
 127 Our previous study (Plašil et al., 2018) has shown that for H_3^+ ions in helium buffer gas the
 128 kinetic T_{kin} and the rotational T_{rot} temperature of the ions in the discharge tube is within
 129 the error of the measurement equal to the temperature given by the temperature sensor
 130 positioned on the stainless-steel holder of the discharge tube. Here and in the following
 131 text, this temperature will be denoted as T_H .

132 3 Data analysis

The values of the recombination rate coefficients were obtained from the measured time evolutions of the electron and ion number densities using procedure described in detail in

ref. (Shapko et al., 2021). If N_2^+ ions are no longer formed in the afterglow plasma, the time evolution of their number density can be described by formula:

$$\frac{dn_{N_2}}{dt} = -\alpha n_{N_2} n_e - \frac{n_{N_2}}{\tau}, \quad (3)$$

where n_{N_2} and n_e are the number densities of N_2^+ ions and of electrons, α is the recombination rate coefficient and τ is the time constant for the losses of N_2^+ ions by ambipolar diffusion and by reactions (ion-molecule reaction, three-body association reaction, etc.):

$$\frac{1}{\tau} = \frac{1}{\tau_D} + \frac{1}{\tau_R}, \quad (4)$$

here τ_D is the time constant of ambipolar diffusion losses and τ_R describes reaction losses. At experimental conditions in the present experiments (temperature, pressure, reactant number density) this term is given mainly by the formation of N_4^+ ions in the three-body association reaction of N_2^+ with N_2 and He:



133 The value of the rate coefficient for reaction (5) was determined by Anicich [Anicich et al.,
134 1999] to be higher than $2 \times 10^{-29} \text{ cm}^3\text{s}^{-1}$ at 300 K.

By directly integrating equation (3) we get for N_2^+ number density in time t_i in the afterglow:

$$n_{N_2}(t_i) = n_{N_2}(t_0) e^{-\alpha X(t_i) - \frac{1}{\tau} Y(t_i)}, \quad (6)$$

where $n_{N_2}(t_0)$ is the initial number density of N_2^+ ions,

$$X(t_i) = \int_{t_0}^{t_i} n_e(t) dt, \quad (7)$$

and

$$Y(t_i) = t_i - t_0, \quad (8)$$

135 As $n_{N_2}(t_i)$, $X(t_i)$ and $Y(t_i)$ are measured in present experiments (or may be calculated from
136 the measured quantities), we find the parameters $n_{N_2}(t_0)$, α and τ that fulfil equation (6)
137 in the least square sense.

138 As has been shown by Shapko et al. (Shapko et al., 2021), by measuring at the same
139 time both electron and ion number densities, reliable recombination rate coefficients can
140 be evaluated even at conditions when the studied ions are not dominant in the afterglow
141 plasma. Moreover, as both sides of equation (3) depend linearly on the N_2^+ number density,
142 if no N_2^+ ions are produced in the afterglow, the data analysis is very robust with respect
143 to possible systematic errors in N_2^+ number density determination.

144 4 Uncertainties and their sources

145 The statistical uncertainty of the ion number density determination is on the order of
146 $1 \times 10^8 \text{ cm}^{-3}$, and its systematic uncertainty, arising mainly from the uncertainty in the
147 discharge column length (estimated as 10%) and in the used vibrational transition moment.
148 While the statistical uncertainty of the electron number density is very small, the systematic
149 uncertainty is largely given by the precision of the determination of the resonant frequency
150 of the empty cavity and is estimated to be less than $1 \times 10^8 \text{ cm}^{-3}$. The overall systematic
151 uncertainty of the effective recombination rate coefficient determination is estimated to be
152 15%.

153

5 Results and Discussion

154

155

156

157

158

An example of measured absorption line profiles is shown in Figure 2. The $P_{21}(10.5)$ and $Q_{22}(9.5)$ lines of the ${}^2\Sigma_g^+ - {}^2\Pi_u(0-2)$ band of N_2^+ are accompanied by a N_2 line around 12371.75 cm^{-1} . For recombination rate coefficient determination, only those N_2^+ lines that were not overlapping with N_2 lines were used. In this we were aided by the list of wavelengths and relative intensities of molecular nitrogen transitions reported in ref. (Western et al., 2018).

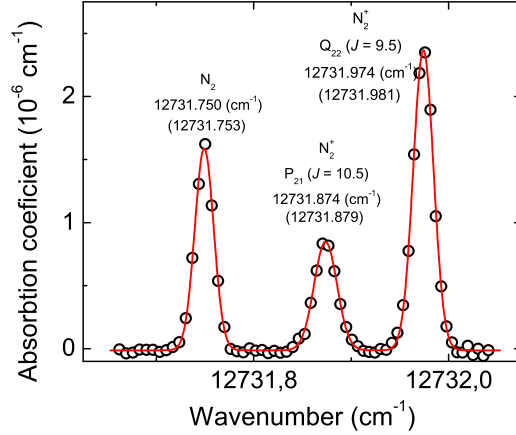


Figure 2. Example of spectra measured around 12732 cm^{-1} in discharge plasma. Each line is labeled by the name of corresponding species (N_2 or N_2^+), spectroscopic notation of the transition and the measured central wavelength. The numbers in parentheses are wavenumbers from refs. (dan Wu et al., 2007; Western et al., 2018). The data were obtained at $T_{\text{H}} = 209 \text{ K}$, $[\text{He}] = 7 \times 10^{16} \text{ cm}^{-3}$ and $[\text{N}_2] = 7 \times 10^{14} \text{ cm}^{-3}$.

159

160

161

162

163

164

165

166

167

168

The total number density of N_2^+ ions in $v = 0$ or $v = 1$ state was determined from the population of single state **meaning unclear!!** under the assumption of thermal populations of rotational levels pertaining to each vibrational state. The dependence of relative number densities of N_2^+ ions in different rotational states of the vibrational ground state on rotational energy measured at $T_{\text{H}} = 140 \pm 5 \text{ K}$ is plotted in Figure 3. The statistical weight of each state was taken into account. The obtained rotational temperature was $T_{\text{rot}} = 136 \pm 5 \text{ K}$, a value very close to T_{H} . As the number density of the probed rotational states of vibrationally excited N_2^+ ions was very low, we assumed that the populations of rotational states for N_2^+ ($v = 1$) are in accordance with thermal equilibrium at a given temperature.

169

170

171

172

173

174

175

176

177

178

An example of absorption line profiles for transitions originating in the ground and the first excited vibrational states of N_2^+ is shown in Figure 4. It is evident that the majority of the ions is in the ground vibrational state. Under assumption of thermal population of rotational energy levels in $v = 1$ state, only 1.5 % of all N_2^+ ions are in the first vibrationally excited state. By changing the experimental conditions (discharge power, reactant and buffer gas number densities) we were able to slightly increase the relative population of the $v = 1$ state. The highest fraction was obtained when neon buffer gas was used instead of helium – around 3 % of all ions were in $v = 1$ state. The measured recombination rate coefficient at such conditions $\alpha(200 \text{ K}) = (3.0 \pm 0.3) \times 10^{-7} \text{ cm}^3\text{s}^{-1}$ is very close to that obtained with lower vibrational excitation of the recombining ions. In the following

179

text, only the results of experiments conducted in helium buffer gas and with the lowest vibrational excitation of the ions will be presented.

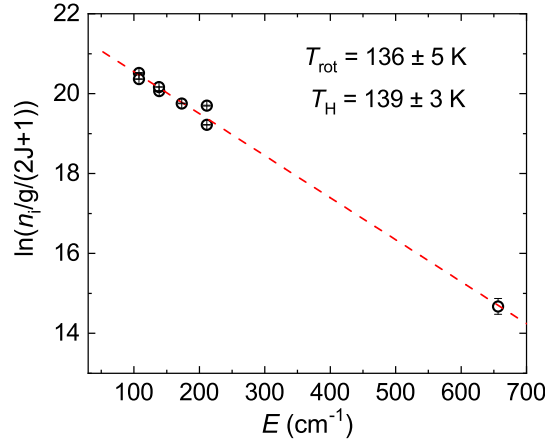


Figure 3. The dependence of the relative number densities of N_2^+ ions in different rotational states of the ground vibrational state on the energy of given state (Boltzmann plot). The data were obtained in discharge plasma. The obtained rotational temperature $T_{\text{rot}} = 136 \pm 5$ K is very close to the temperature of the discharge tube holder $T_{\text{H}} = 139 \pm 3$ K. The helium and N_2 number densities were $1 \times 10^{17} \text{ cm}^{-3}$ and $5.5 \times 10^{14} \text{ cm}^{-3}$, respectively.

180

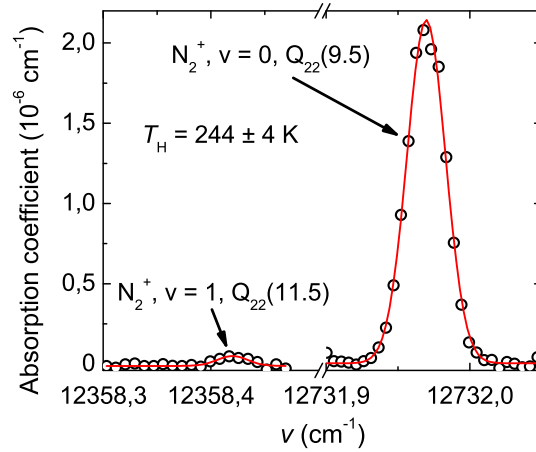
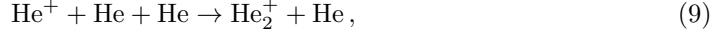


Figure 4. Comparison of absorption line profiles of two lines originating in the ground and the first excited vibrational state of N_2^+ . The data were obtained in discharge at temperature of the discharge tube holder $T_{\text{H}} = 244 \pm 4$ K, $[\text{He}] = 5.8 \times 10^{16} \text{ cm}^{-3}$ and $[\text{N}_2] = 1 \times 10^{15} \text{ cm}^{-3}$. The calculated amount of vibrationally excited N_2^+ in the discharge is 1.5 % of all N_2^+ ions.

Typical time evolutions of electron and N_2^+ number densities measured in afterglow plasma are shown in Figure 5. The measured number density of N_2^+ ions is lower than the

electron number density and the relative fraction of N_2^+ with respect to all ions decreases at later times in the afterglow. Part of this behavior is due to the formation of N_4^+ ions in the three-body association reaction of N_2^+ with helium and molecular nitrogen (5). In order to minimize the influence of process (5) on plasma decay we had to keep the helium buffer gas density quite low – below $1 \times 10^{17} \text{ cm}^{-3}$. At such conditions the He^+ ions formed in the discharge are not converted sufficiently fast to He_2^+ ions in three-body association reaction:

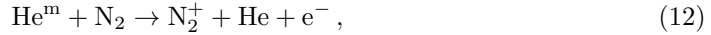


and may remain in the afterglow plasma. The value of the rate coefficient for reaction (9) was reported to be $1 \times 10^{-31} \text{ cm}^6\text{s}^{-1}$ at 300 K (Ikezoe et al., 1987). After switching off the discharge, He^+ ions are quickly removed from the afterglow plasma by a fast ion-molecule reaction with N_2 :



181 Reaction (10, 11) slightly favours production of N^+ ions over N_2^+ (Lane, 1986). A subsequent
 182 three-body association reaction of N^+ ions with helium and N_2 then leads to formation of
 183 N_3^+ ions. The reported experiments were aided by a model of chemical kinetics that included
 184 the main processes influencing charged particles in afterglow plasma. The model is further
 185 described in Appendix A.

A crucial parameter for recombination studies is the electron temperature. In helium buffered stationary afterglow plasma, metastable electronic states of helium (2^1S and 2^3S) are formed in the discharge and can in superelastic collisions transfer energy to electrons thus increasing the electron temperature (Plašil et al., 2009). In present experiments, the helium metastable atoms He^m are removed from the afterglow plasma by Penning ionization of N_2 :



186 We estimated the reaction rate coefficient for Penning ionization of N_2 in collisions with
 187 helium metastable atoms (12) from the increase of electron and N_2^+ number densities in
 188 the early afterglow at given temperature and N_2 number densities. As the time evolution
 189 of the number density of the helium metastable atoms was not directly measured and we
 190 have to roughly estimate the electron and ion loss processes in early afterglow, such an
 191 approach is inherently burdened by a large systematic error. The inferred reaction rate
 192 coefficients for Penning ionization of N_2 by helium metastable atoms were $k^m(140K) =$
 193 $(3_{-1.5}^{+3}) \times 10^{-11} \text{ cm}^3\text{s}^{-1}$ and $k^m(250K) = (5_{-2.5}^{+5}) \times 10^{-11} \text{ cm}^3\text{s}^{-1}$. This is in reasonable
 194 agreement with previous measurement by Lindinger et al. (Lindinger et al., 1974) who
 195 reported a value of $k^m(300K) = 7 \times 10^{-11} \text{ cm}^3\text{s}^{-1}$.

196 In our study of N_2^+ recombination we kept the number density of N_2 sufficiently high to
 197 ensure that helium metastable atoms are removed from the afterglow plasma within 100 μs
 198 after switching off the discharge. The data obtained within the first 200 μs of the afterglow
 199 are excluded from the data analysis.

200 The values of recombination rate coefficients obtained in the temperature range of 140
 201 – 250 K are plotted in Figure 6 and compared to the results from previous experimental
 202 and theoretical studies. Our results are in an excellent agreement with recent theoretical
 203 predictions for N_2^+ ($v = 0$) by Abdoulanziz et al. (Abdoulanziz et al., 2021). The values of
 204 recombination rate coefficient obtained by other groups who also monitored the vibrational
 205 state of recombining ions are substantially lower than our data. In all these experiments a
 206 large fraction of ions was vibrationally excited. This indicates, in agreement with analysis
 207 by Bates et al. (D. Bates & Mitchell, 1991) and Sheehan et al. (Sheehan & St.-Maurice,
 208 2004) that the recombination process is less efficient for vibrationally excited ions than for
 209 the ground vibrational state of N_2^+ . A summary of previous studies that probed populations
 210 of vibrational levels of N_2^+ ions is given in Table 2.

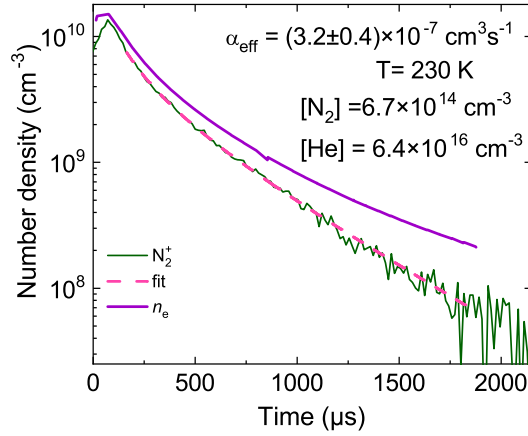


Figure 5. Time evolution of the measured electron and N_2^+ number densities obtained at 230 K. The buffer gas and reactant number densities were: $[He] = 6.4 \times 10^{16} \text{ cm}^{-3}$ and $[N_2] = 6.7 \times 10^{14} \text{ cm}^{-3}$. The dashed line denotes fit of the data by equation (6). The N_2^+ number density was calculated from the absorbance at the center of the $Q_{22}(9.5)$ transition of the ${}^2\Sigma_g^+ - {}^2\Pi_u(0-2)$ band of N_2^+ under assumption of thermal population of rotational states. Time is set to zero at the beginning of the afterglow.

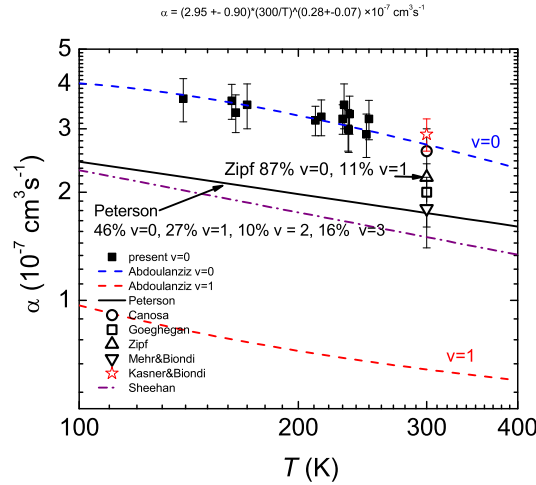


Figure 6. The dependence of N_2^+ recombination rate coefficient on temperature. Present data (full squares) are compared to the results of recent quantum mechanical calculations by Abdoulanziz et al. (Abdoulanziz et al., 2021) for particular vibrational states (dashed lines denoted $v = 0$ and $v = 1$). Values obtained in previous experiments by Peterson (Peterson et al., 1998), Sheehan (Sheehan & St.-Maurice, 2004), Zipf (Zipf, 1980), Canosa (Canosa et al., 1991), Kasner (Kasner & Biondi, 1965), Mehr (Mehr & Biondi, 1969) and Goeghegan (Geoghegan et al., 1991) are plotted as full line, dash-dotted line, up triangle, circle, star, down triangle and open square, respectively.

By taking together available experimental data from Table 2. We can make an estimate of recombination rate coefficient for higher vibrational states. As the available state resolved experimental data are very scarce, we were unable to calculate the recombination rate

Table 2. Comparison of values of recombination rate coefficient for N_2^+ ions obtained present and in previous experiments with available information on N_2^+ vibrational excitation. The recombination rate coefficients from refs. (Peterson et al., 1998; Sheehan & St.-Maurice, 2004) are stated to be valid for electron temperature T_e lower than 1200 K. The present data were obtained in the temperature range of 140 – 250 K.

Reference	$v = 0$	$v = 1$	$v = 2$	$v = 3$	α (10^{-7} cm ³ s ⁻¹)
(Peterson et al., 1998) ^a	46%	27%	10%	16%	$(1.75 \pm 0.09) \times (T_e/300)^{-0.30}$
(Sheehan & St.-Maurice, 2004) ^b	65.1%	21.1%	8.4%	3.5%	$(1.5 \pm 0.23) \times (T_e/300)^{-0.38}$
(Zipf, 1980)	87%	11%	2%		2.2 at 300 K
Present ^c	98.5%	1.5%			$(2.95 \pm 0.50) \times (T/300)^{-0.28}$

^aindicated rate coefficient was recalculated by Sheehan et al. (Sheehan & St.-Maurice, 2004) to be $\alpha = (1.50 \pm 0.23) \times (T_e/300)^{-0.39} \times (10^{-7}$ cm³s⁻¹)

^b vibrational populations were estimated based on the calculations in ref. (Noren et al., 1989).

^c fit of the data plotted in Figure 6.

coefficient for particular state with sufficient precision. Instead, we fitted the recombination rate coefficients from Table 2 by following equation:

$$\alpha(f_0, f_1, f_2, f_3, T) = \alpha_{v=0}(T)f_0 + \alpha_{v>0}(T)(f_1 + f_2 + f_3), \quad (13)$$

where $\alpha(f_0, f_1, f_2, f_3, T)$ are the recombination rate coefficients from Table 2, f_i are the fractional vibrational populations of N_2^+ ions for given vibrational state with $v = i$, $\alpha_{v=0}$ is the recombination rate coefficient for the ground vibrational state and $\alpha_{v>0}$ is the effective recombination rate coefficient for N_2^+ ions with $v > 0$.

The value of recombination rate coefficient reported by Zipf et al. (Zipf, 1980) was obtained at 300 K. We extrapolated this value to 250 K using temperature dependence observed by Mehr et al. (Mehr & Biondi, 1969) which is exactly the same as in the one measured in merged electron-ion beam experiment by Sheehan et al. (Sheehan & St.-Maurice, 2004).

In the fitting procedure we used the present experimental data in place of $\alpha_{v=0}$ as majority of the ions were in $v = 0$ state. The resulting effective recombination rate coefficient was $\alpha_{v>0} = (4 \pm 4) \times 10^{-8}$ cm³s⁻¹ at 250 K. As in all experiments listed in Table 2 the majority of vibrationally excited ions were in $v = 1$ state, we assume that the obtained value will be close to the recombination rate coefficient for that state. The theoretical calculations by Abdoulanziz et al. (Abdoulanziz et al., 2021) predicted value of $\alpha_{v=1} = 6.8 \times 10^{-8}$ cm³s⁻¹ for the first excited vibrational state of N_2^+ . This is in a good agreement with our results.

6 Summary

We have studied the recombination of N_2^+ ions, predominantly in their ground vibrational state, with electrons in the temperature range of 140 – 250 K. The results are in good agreement with the most recent quantum mechanical calculations (Abdoulanziz et al., 2021). By comparing our data to the recombination rate coefficients obtained by other groups with higher vibrational excitation of N_2^+ ions, we inferred that N_2^+ ions in the first excited vibrational state recombine with electrons less efficiently than the ions in the vibrational ground state. The recommended value of recombination rate coefficient for recombination of N_2^+ ($v=1$) ions with electrons is $\alpha_{v=1} = (4 \pm 4) \times 10^{-8}$ cm³s⁻¹ at 250 K.

We hope that our results will help to improve models of nitrogen containing planetary ionospheres.

238 **Acknowledgments**

239
240 This work was partly supported by the Czech Science Foundation (GACR 20-22000S,
241 GACR 22-059358) and by the Charles University (GAUK 337821, GAUK 332422).

242 **Appendix A APPENDIX A: MODEL OF CHEMICAL KINETICS**

243 A kinetic model was used in the experiment for prediction of the chemical evolution of
244 the afterglow plasma with conditions similar to the experiment. The model was based on
245 the set of reaction equations of binary or ternary interactions of ions, electrons and neu-
246 trals with corresponding rate coefficients. The model also included the ambipolar diffusion
247 with corresponding time of the charged particles losses. Differential equations of the kinetic
248 model were solved by using an equation solver implemented in lsoda routine (Hindmarsh,
249 1983). The chemical reactions used in the kinetic model are summarizing in Table 1. The
250 temperature for the reaction rate coefficients stated in Table 1 is 300 K if not stated other-
251 wise.

252 Based on experimental study by Glosík et al (Glosík et al., 1999), we have presumed,
253 that the number density of metastable helium atoms He^m for both 2^1S and 2^3S states was
254 the same or lower than the electron number density at the beginning of the afterglow.

255 The actual ionic composition at the beginning of the afterglow was not known – with
256 the exception of N_2^+ ions and of electrons that were probed in the experiment. Various
257 initial compositions of ions were tried for the kinetic model, until we came to an agreement
258 with the experiment.

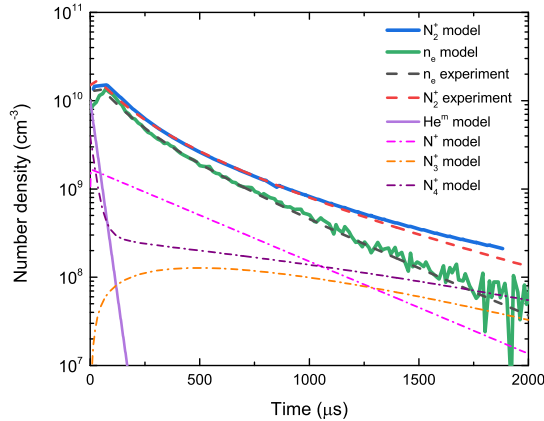


Figure A1. The time evolution of the measured number densities of N_2^+ and electrons and of the number densities obtained from the model of chemical kinetics at $T = 230$ K. Time is set to zero at the beginning of the afterglow.

259 The comparison between the measured number densities of N_2^+ and of electrons and
260 number densities obtained from kinetic model of the afterglow is shown in Figure 1. Both,
261 the kinetic model as well as the measured data were obtained at temperature $T = 230$ K.
262 The kinetic model shows that N_2H^+ is a dominant ionic species within $250 \mu\text{s}$ after switching
263 off the discharge in good agreement with the measures data.

Table A1. The most important reactions for formation and destruction of N_2H^+ ions included in the model of chemical kinetics. The ambipolar diffusion losses were calculated for $T = 230$ K. The characteristic reaction times were calculated using the formula: $\tau = 1/k[R]$, where k is the rate coefficient of the reaction, $[R]$ is the neutral reactant number density for the two body reactions and the product of the neutral reactant number densities for the three body reactions. The number densities used in the model were $[He] = 6.4 \times 10^{16} \text{ cm}^{-3}$ and $[N_2] = 6.7 \times 10^{14} \text{ cm}^{-3}$.

No.	Reaction	Rate coefficient [cm^{-3}], [cm^6s^{-1}]	Characteristic reaction time [s]	Reference
R1	$He^m + N_2 \rightarrow N_2^+ + He + e^-$	6.1×10^{-11}	2.45×10^{-5}	(Lindinger et al., 1974)
R2	$He^+ + He + He \rightarrow He_2^+ + He$	1.0×10^{-31}	2.44×10^{-3}	(Glosik et al., 2015)
R3	$He_2^+ + N_2 \rightarrow N_2^+ + He + He$	1.12×10^{-9}	1.33×10^{-6}	(Lindinger et al., 1974)
R4	$N^+ + N_2 + He \rightarrow N_3^+ + He$	4.0×10^{-29}	5.83×10^{-4}	Estimate
R5	$N^+ + N_2 + N_2 \rightarrow N_3^+ + N_2$	8.6×10^{-30}	2.59×10^{-1}	(Hwang et al., 1996)
R6	$He^+ + N_2 \rightarrow N^+ + He + N$	8.4×10^{-10}	1.77×10^{-6}	(Lane, 1986)
R7	$He^+ + N_2 \rightarrow N_2^+ + He$	6.6×10^{-10}	2.26×10^{-6}	(Lane, 1986)
R8	$N_2^+ + N_2 + He \rightarrow N_4^+ + He$	1.9×10^{-29}	1.23×10^{-3}	(Anicich et al., 2000)
R9	$N_2^+ + N_2 + N_2 \rightarrow N_4^+ + N_2$	8.0×10^{-29}	2.78×10^{-2}	(Anicich et al., 2000)
R10	$N_2^+ + e^- \rightarrow N + N$	3.5×10^{-7}	1.90×10^{-4}	Present data
R11	$N_3^+ + e^- \rightarrow N_2 + N$	6.5×10^{-7}	1.03×10^{-4}	(Zhaunerchyk et al., 2007)
R12	$N_4^+ + e^- \rightarrow N_2 + N_2$	2.6×10^{-6}	2.56×10^{-5}	(Adams et al., 2009)

References

264

- 265 Abdoulanziz, A., Argentin, C., Laporta, V., Chakrabarti, K., Bultel, A., Tennyson, J.,
 266 ... Mezei, J. Z. (2021). Low-energy electron impact dissociative recombination and
 267 vibrational transitions of N_2^+ . *Journal of Applied Physics*, 129(5), 053303.
 268 Adams, S. F., DeJoseph, C. A., & Williamson, J. M. (2009). Formation and electron-ion
 269 recombination of N_4^+ following photoionization in near-atmospheric pressure N_2 . *The*
 270 *Journal of Chemical Physics*, 130(14), 144316.
 271 Anicich, V. G., Milligan, D. B., Fairley, D. A., & McEwan, M. J. (2000). Termolecular
 272 ion-molecule reactions in titan's atmosphere, i: Principal ions with principal neutrals.
 273 *Icarus*, 146(1), 118-124.
 274 Bates, D., & Mitchell, J. (1991). Rate coefficients for $N_2^+(v)$ dissociative recombination.
 275 *Planetary and Space Science*, 39(9), 1297-1300.
 276 Bates, D. R. (1950, May). Dissociative recombination. *Phys. Rev.*, 78, 492-493.
 277 Benesch, W., Rivers, D., & Moore, J. (1980, Jul). High resolution spectrum of the N_2^+
 278 meinel system to 11 250 Å. *J. Opt. Soc. Am.*, 70(7), 792-799.
 279 Biondi, M. A., & Brown, S. C. (1949, Dec). Measurement of electron-ion recombination.
 280 *Phys. Rev.*, 76, 1697-1700.
 281 Brian, J., & Mitchell, A. (1990). The dissociative recombination of molecular ions. *Physics*
 282 *Reports*, 186(5), 215-248.
 283 Canosa, A., Gomet, J. C., Rowe, B. R., & Queffelec, J. L. (1991). Flowing afterglow langmuir
 284 probe measurement of the $N_2^+(v=0)$ dissociative recombination rate coefficient. *The*
 285 *Journal of Chemical Physics*, 94(11), 7159-7163.
 286 Cunningham, A. J., & Hobson, R. M. (1972). Dissociative recombination at elevated tem-
 287 peratures. iv. N_2^+ dominated afterglows. *Journal of Physics B: Atomic and Molecular*
 288 *Physics*, 5(12), 2328-2331.
 289 dan Wu, Y., wen Ben, J., Li, L., juan Zheng, L., qin Chen, Y., & hua Yang, X. (2007).
 290 Study of (2, 0) band of $A_u^2 - X_g^{2+}$ system of N_2^+ by optical heterodyne detected velocity
 291 modulation spectroscopy. *Chinese Journal of Chemical Physics*, 20(3), 285-290.

- 292 Earls, L. T. (1935). Intensities in ${}^2\Pi - {}^2\Sigma$ transitions in diatomic molecules. *Phys. Rev.*,
293 48, 423–424.
- 294 Elliot, J., Strobel, D., Zhu, X., Stansberry, J., Wasserman, L., & Franz, O. (2000). The
295 thermal structure of triton’s middle atmosphere. *Icarus*, 143(2), 425–428.
- 296 Florescu-Mitchell, A., & Mitchell, J. (2006). Dissociative recombination. *Physics Reports*,
297 430(5), 277–374.
- 298 Fox, J. L. (2005). Effects of dissociative recombination on the composition of planetary
299 atmospheres. *Journal of Physics: Conference Series*, 4, 32–37.
- 300 Fox, J. L., & Dalgarno, A. (1985). The vibrational distribution of N_2^+ in the terrestrial
301 ionosphere. *Journal of Geophysical Research: Space Physics*, 90(A8), 7557–7567.
- 302 Geoghegan, M., Adams, N. G., & Smith, D. (1991). Determination of the electron-ion
303 dissociative recombination coefficients for several molecular ions at 300 k. *Journal of*
304 *Physics B: Atomic, Molecular and Optical Physics*, 24(10), 2589–2599.
- 305 Glosík, J., Bánó, G., Plašil, R., Luca, A., & Zakouřil, P. (1999). Study of the electron ion
306 recombination in high pressure flowing afterglow: recombination of $NH_4^- + (NH_3)_2^+$.
307 *International Journal of Mass Spectrometry*, 189(2), 103–113.
- 308 Glosík, J., Dohnal, P., Rubovič, P., Kálosi, Á., Plašil, R., Roučka, Š., & Johnsen, R. (2015,
309 nov). Recombination of H_3^+ ions with electrons in He/ H_2 ambient gas at temperatures
310 from 240 k to 340 k. *Plasma Sources Science and Technology*, 24(6), 065017.
- 311 Guberman, S. L. (1991). Dissociative recombination of the ground state of N_2^+ . *Geophysical*
312 *Research Letters*, 18(6), 1051–1054.
- 313 Guberman, S. L. (2007). Role of excited core rydberg states in dissociative recombination.
314 *The Journal of Physical Chemistry A*, 111(44), 11254–11260.
- 315 Guberman, S. L. (2012). Spectroscopy above the ionization threshold: dissociative recombi-
316 nation of the ground vibrational level of N_2^+ . *The Journal of chemical physics*, 137(7),
317 074309.
- 318 Guberman, S. L. (2013). The vibrational dependence of dissociative recombination: Cross
319 sections for N_2^+ . *The Journal of Chemical Physics*, 139(12), 124318.
- 320 Guberman, S. L. (2014). The vibrational dependence of dissociative recombination: Rate
321 constants for N_2^+ . *The Journal of Chemical Physics*, 141(20), 204307.
- 322 Hansson, A., & Watson, J. (2005). A comment on hönl-london factors. *Journal of Molecular*
323 *Spectroscopy*, 233, 169–173.
- 324 Hindmarsh, A. C. (1983). *ODEPACK, A Systematized Collection of ODE Solvers* (Vol. 1;
325 R. S. Stepleman, Ed.). North-Holland.
- 326 Holcomb, J. D., & Schucker, A. (2020). Helium plasma skin regeneration: Evaluation of skin
327 tissue effects in a porcine model and comparison to nitrogen plasma skin regeneration.
328 *Lasers in Surgery and Medicine*, 52(1), 23–32.
- 329 Hwang, H. H., Olthoff, J. K., Van Brunt, R. J., Radovanov, S. B., & Kushner, M. J. (1996).
330 Evidence for inelastic processes for N_3^+ and N_4^+ from ion energy distributions in He/ N_2
331 radio frequency glow discharges. *Journal of Applied Physics*, 79(1), 93–98.
- 332 Ikezoe, Y., Matsuoka, S., Takebe, M., & Viggiano, A. (1987). *Gas phase ion-molecule*
333 *reaction rate constants through*. Maruzen Company Ltd.,
- 334 Johnsen, R. (1987). Microwave afterglow measurements of the dissociative recombination
335 of molecular ions with electrons. *International Journal of Mass Spectrometry and Ion*
336 *Processes*, 81, 67–84.
- 337 Kasner, W. H., & Biondi, M. A. (1965). Electron-ion recombination in nitrogen. *Phys.*
338 *Rev.*, 137, A317–A329.
- 339 Krasnopolsky, V. A. (2014). Chemical composition of titan’s atmosphere and ionosphere:
340 Observations and the photochemical model. *Icarus*, 236, 83–91.
- 341 Krasnopolsky, V. A. (2020). A photochemical model of pluto’s atmosphere and ionosphere.
342 *Icarus*, 335, 113374.
- 343 Lammer, H., Stumtner, W., Molina-Cuberos, G., Bauer, S., & Owen, T. (2000). Nitrogen
344 isotope fractionation and its consequence for titan’s atmospheric evolution. *Planetary*
345 *and Space Science*, 48(6), 529–543.

- 346 Lane, K. R. (1986). *Flowing afterglow studies of gas-phase anionic transition-metal chem-*
 347 *istry (nucleophilic addition, bond energies, oxidation, carbonyls).*
- 348 Larsson, M., & Orel, A. E. (2008). *Dissociative recombination of molecular ions.* Cambridge
 349 University Press.
- 350 Lin, M.-Y., & Ilie, R. (2022). A review of observations of molecular ions in the earth's
 351 magnetosphere-ionosphere system. *Frontiers in Astronomy and Space Sciences*, 8.
- 352 Lindinger, W., Schmeltekopf, A. L., & Fehsenfeld, F. C. (1974). Temperature dependence
 353 of de-excitation rate constants of He(2^3S) by Ne, Ar, Xe, H₂, N₂, O₂, NH₃, and CO₂.
 354 *The Journal of Chemical Physics*, 61(7), 2890-2895.
- 355 Little, D. A., Chakrabarti, K., Mezei, J. Z., Schneider, I. F., & Tennyson, J. (2014).
 356 Dissociative recombination of N₂⁺: An ab initio study. *Phys. Rev. A*, 90, 052705.
- 357 Mahdavi, M. R., Hasted, J. B., & Nakshbandi, M. M. (1971). Electron-ion recombination
 358 measurements in the flowing afterglow. *Journal of Physics B: Atomic and Molecular*
 359 *Physics*, 4(12), 1726-1737.
- 360 Mehr, F. J., & Biondi, M. A. (1969). Electron temperature dependence of recombination
 361 of O₂⁺ and N₂⁺ ions with electrons. *Phys. Rev.*, 181, 264-271.
- 362 Morozov, I. A., Mamaev, A. S., Osorgina, I. V., Lemkina, L. M., Korobov, V. P., Belyaev,
 363 A. Y., ... Sherban, M. G. (2016). Structural-mechanical and antibacterial proper-
 364 ties of a soft elastic polyurethane surface after plasma immersion N₂⁺ implantation.
 365 *Materials Science and Engineering: C*, 62, 242-248.
- 366 Mul, P. M., & McGowan, J. W. (1979). Merged electron-ion beam experiments. III. temper-
 367 ature dependence of dissociative recombination for atmospheric ions NO⁺, O₂⁺, N₂⁺.
 368 *Journal of Physics B: Atomic and Molecular Physics*, 12(9), 1591-1601.
- 369 Noren, C., Yousif, F. B., & Mitchell, J. B. A. (1989). Dissociative recombination and
 370 excitation of N. *J. Chem. Soc., Faraday Trans. 2*, 85, 1697-1703.
- 371 Peterson, J. R., Le Padellec, A., Danared, H., Dunn, G. H., Larsson, M., Larson, A., ...
 372 van der Zande, W. J. (1998). Dissociative recombination and excitation of N₂⁺: Cross
 373 sections and product branching ratios. *The Journal of Chemical Physics*, 108(5),
 374 1978-1988.
- 375 Plašil, R., Korolov, I., Kotrik, T., Dohnal, P., Bano, G., Donko, Z., & Glosík, J. (2009).
 376 Non-maxwellian electron energy distribution function in He, He/Ar, He/Xe/H₂ and
 377 He/Xe/D₂ low temperature afterglow plasma. *Eur. Phys. J. D*, 54(2), 391-398.
- 378 Plašil, R., Dohnal, P., Kálosi, Roučka, Š., Shapko, D., Rednyk, S., ... Glosík, J. (2018).
 379 Stationary afterglow apparatus with crds for study of processes in plasmas from 300
 380 k down to 30 k. *Rev. Sci. Instrum.*, 89, 063116.
- 381 Qin, Z., Zhao, J., & Liu, L. (2017). Radiative transition probabilities for the main diatomic
 382 electronic systems of N₂, N₂⁺, NO, O₂, CO₂⁺, CO⁺, CN₂⁺, C₂ and H₂ produced in
 383 plasma of atmospheric entry. *Journal of Quantitative Spectroscopy and Radiative*
 384 *Transfer*, 202, 286-301.
- 385 Romanini, D., Kachanov, A., Sadeghi, N., & Stoeckel, F. (1997). Cw cavity ring down
 386 spectroscopy. *Chemical Physics Letters*, 264(3), 316-322.
- 387 Rothman, L., Rinsland, C., Goldman, A., Massie, S., Edwards, D., Flaud, J.-M., ...
 388 Varanasi, P. (1998). The hitran molecular spectroscopic database and hawks (hi-
 389 tran atmospheric workstation): 1996 edition. *Journal of Quantitative Spectroscopy*
 390 *and Radiative Transfer*, 60(5), 665-710.
- 391 Sakakura, T., Murakami, N., Takatsuji, Y., Morimoto, M., & Haruyama, T. (2019). Con-
 392 tribution of discharge excited atomic N, N₂, and N₂⁺ to a plasma/liquid interfacial
 393 reaction as suggested by quantitative analysis. *ChemPhysChem*, 20(11), 1467-1474.
- 394 Shapko, D., Dohnal, P., Roučka, Š., Uvarova, L., Kassayová, M., Plašil, R., & Glosík, J.
 395 (2021). Cavity ring-down spectroscopy study of neon assisted recombination of H₃⁺
 396 ions with electrons. *J. Mol. Spectrosc.*, 378, 111450.
- 397 Sharma, M., & Saikia, B. (2008). Discharge conditions and emission spectroscopy of N₂
 398 and N₂⁺ active species in a variable power dc pulsed plasma used for steel nitriding.
 399 *Ind. Jour. of Pure and App. Physics*, 46, 463-370.
- 400 Sheehan, C. H., & St.-Maurice, J.-P. (2004). Dissociative recombination of N₂⁺, O₂⁺, and

- 401 NO⁺: Rate coefficients for ground state and vibrationally excited ions. *Journal of*
402 *Geophysical Research: Space Physics*, 109(A3).
- 403 Western, C. M., Carter-Blatchford, L., Crozet, P., Ross, A. J., Morville, J., & Tokaryk,
404 D. W. (2018). The. *Journal of Quantitative Spectroscopy and Radiative Transfer*,
405 219, 127-141.
- 406 Young, L. A., Braga-Ribas, F., & Johnson, R. E. (2020). Chapter 6 - volatile evolution and
407 atmospheres of trans-neptunian objects. In D. Prialnik, M. A. Barucci, & L. A. Young
408 (Eds.), *The trans-neptunian solar system* (p. 127-151). Elsevier.
- 409 Yung, Y. L., & Lyons, J. R. (1990). Triton: Topside ionosphere and nitrogen escape.
410 *Geophysical Research Letters*, 17(10), 1717-1720.
- 411 Zhaunerchyk, V., Geppert, W. D., Vigrén, E., Hamberg, M., Danielsson, M., Larsson, M.,
412 ... Österdahl, F. (2007). Dissociative recombination study of N₃⁺: Cross section and
413 branching fraction measurements. *The Journal of Chemical Physics*, 127(1), 014305.
- 414 Zipf, E. C. (1980). The dissociative recombination of vibrationally excited N₂⁺ ions. *Geo-*
415 *physical Research Letters*, 7(9), 645-648.